



ALT`23

INTERNATIONAL CONFERENCE

Advanced Laser Technologies

BOOK OF ABSTRACTS

September 18-21, 2023

SAMARA, RUSSIA



УДК 535.21; 535.23; 535.33; 535.37
ББК 22.343.4; 22.344; 22.345

Abstracts of the 30th International Conference on Advanced Laser Technologies – 2023. – 276 с.

The book contains abstracts of ALT`23 conference reports devoted to fundamental and applied aspects of innovative laser technologies, laser-matter interaction, biomedical photonics, laser systems and materials, laser diagnostics and spectroscopy, nonlinear and terahertz photonics. The book contains abstracts of plenary, invited, oral and poster presentations. The official language of the conference is English.

ALT`23 Conference Book of Abstracts are on the conference website
<https://altconference.org/proceedings>

ISBN 978-5-6050309-0-4



9 785605 030904 >

© The Russian Academics of Sciences, 2023
© Prokhorov General Physics Institute
of Russian Academics of Sciences, 2023
© Samara National Research University, 2023
© ООО "МЕКОЛ", 2023

BOOK OF ABSTRACTS

ALT'23

The 30th International Conference on Advanced Laser Technologies

September 18-21, 2023 / Samara, Russia



Contents

Organizers and Sponsors	4
Program and Organizing Committees	5
Plenary Speakers	7
SECTION LM. Laser–Matter Interaction	11
SECTION B. Biomedical Photonics	70
SECTION LS. Laser Systems and Materials	136
SECTION LD. Laser Diagnostics and Spectroscopy	183
SECTION N. Nonlinear and Terahertz Photonics	218
SECTION P. Photonics in Quantum Technologies	251



Organizers and Sponsors



A.M. Prokhorov General Physics Institute of the Russian Academy of Sciences (GPI RAS)



Samara National Research University



Department of Physical Sciences of the Russian Academy of Sciences



Institute of Spectroscopy of the Russian Academy of Sciences (ISAN)



Center of Laser Technology and Material Science



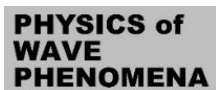
Lomonosov Moscow State University



National Research Nuclear University MEPhI (Moscow Engineering Physics Institute)



FRC "Crystallography and Photonics" of the Russian Academic of Science



Physics of Wave Phenomena journal



"Polarus" LLC



Quanttelecom LLC



Volga document LLC



Conference Chairman

Ivan SHCHERBAKOV (Russia)

Program Committee Chair

Vitaly KONOV (Russia)

Victor SOIFER (Russia)

International Program Committee

Mukhsin ASHUROV (Republic of Uzbekistan)

Ekaterina BARMINA (Russia)

Elena BIBIKOVA (Russia)

Aladar CZITROVSKY (Hungary)

Boris DENKER (Russia)

Sergey GARNOV (Russia)

Mikhail GLYAVIN (Russia)

Leonid GOLOVAN (Russia)

Pavel KASHKAROV (Russia)

Nikolay KAZANSKIY (Russia)

Sergey KLIMENTOV (Russia)

Victor KOTLYAR (Russia)

Yuri KULCHIN (Russia)

Mahesh KUMAR (India)

Sandeep KUMAR (India)

Vladimir MAKAROV (Russia)

Tofiq MAMMADOV (Republic of Azerbaijan)

Ashok Kumar MISHRA (India)

Beat NEUENSCHWANDER (Switzerland)

Kyung Hyun PARK (Korea)

Alexander PRIEZZHEV (Russia)

Alexander SHKURINOV (Russia)

Nishant TRIPATHI (Russia)

Valery TUCHIN (Russia)

Vadim VEIKO (Russia)

Igor VLASOV (Russia)

Victor ZADKOV (Russia)

Irina ZAVESTOVSKAYA (Russia)

Dan ZHU (China)

Organizing Committee Chair

Vladimir PUSTOVOY (Russia)

Vladimir PAVELYEV (Russia)



Plenary Speakers



10.24412/cl-35039-2023-23-8-8

P-I

Prof. Vladimir Pavelyev

*Samara University, Samara, Russia***Title:** Control of characteristics of high-power terahertz laser beams by methods of diffractive optics**Abstract**

Technologies for silicon and diamond transmissive diffractive microoptics have been developed [1-6]. Silicon and diamond diffractive optical elements (DOE) for focusing terahertz laser beam [1-3] as well for formation of terahertz laser beam with predetermined mode composition [4] and polarization state [5] have been manufactured and experimentally investigated. Developed technologies are based on lithographic etching [1,4,5] and laser ablation [2,3]. The experiments were carried out at a wavelength of 130-150 μm using the Novosibirsk Free Electron Laser [6].

The generation of power terahertz beams with pre-given characteristics paves the way for the development of new applications. In [7] it was shown that the diffraction of a generated Bessel beam [4] by a periodic two-dimensional grating in the Talbot planes results in the formation of periodic gratings of annular microbeams. Another application was demonstrated in [8], where beams with orbital angular momentum generated by the DOEs described in [4] were used to excite vortex surface plasmon polaritons propagating along a cylindrical conductor for a distance of up to 150 mm.

In this talk, the fabrication of photonic elements for far terahertz and millimeter ranges is considered. Perspectives of 3D printing application [9] for the fabrication of photonic crystals in terahertz and millimeter ranges are considered. Besides, technologies for reflective terahertz free-form optics fabrication are considered [10].

The experiments were carried out at the Novosibirsk Free Electron Laser Facility, which is part of “the Siberian Synchrotron and Terahertz Radiation Center”..



P-II



Prof. Igor Nabiev

University of Reims Champagne-Ardenne, Reims, France
National Research Nuclear University MEPhI, Moscow, Russia

Title: Nanophotonic detection of tumor markers and micrometastases with conjugates of single-domain antibodies and quantum dots

Abstract

To improve cancer prognosis, early detection of the disease is one of the main purposes in diagnostic approaches. In this regard, the rapidly progressing field of nanotechnology is considered a powerful tool in cancer diagnostic and therapeutic applications. The use of nanophotonic materials brings an improvement of signal-to-noise ratios in detection and greater penetration depths for the treatment of deep-seated tumours [1-3]. Quantum dots (QDs) with broad absorption spectra and narrow emission bands are the excellent nanophotonic labels for FRET applications. They have a quantum yield close to 100%; high single- and two-photon molar extinction coefficients, and photoresistance. To ensure cell specificity, QDs are normally bound to recognition molecules, such as antibodies, aptamers or peptides. Single-domain antibodies (sd-Abs) are the smallest antibody fragments capable of binding their antigens, they diffuse much better into tissues than full-size Abs. Because of these advantages, we have conjugated QDs to sd-Abs in a highly oriented fashion, with all antigen binding sites facing outwards, which considerably increases the nanoprobe sensitivity and possible therapeutic use in oncology and demonstrated their advantages in cancer cell imaging and the micrometastases detection [3].

The possibility of increasing the Forster resonance energy transfer (FRET) efficiency is emerging in sensing and diagnostics. Light-matter coupling in microcavities leads to the formation of two new “hybrid” light-matter (polaritonic) states, instead of the two original molecular and electromagnetic field energy states. A strong coupling between light and matter can be controlled by fine tuning the electromagnetic modes of the microresonator; it has been also demonstrated that strong coupling can modulate both distance and efficiency of FRET [4].

We have developed an adjustable unstable $\lambda/2$ Fabry-Perot microresonator with a convex metal mirror [5] satisfying the flat-parallelism conditions at least at one point of the convex mirror and minimises the adjustable mode volume of the confined electromagnetic field with the nm-accuracy.

The strong light-matter coupling between the optical modes of a tuneable microcavity and the excitonic transitions of two closely located donor and acceptor molecules have shown that the energy states and relaxation pathways of the systems with strong dipole-dipole interaction can be altered by strong coupling of their exciton transitions to the cavity photon [6]:

(1) We have demonstrated a significant increase in the efficiency of energy transfer from the donor to the acceptor exciton reservoir, which tends to be unity inside the microcavity.

(2) We have shown the polariton-assisted energy state inversion and energy flow alteration thus demonstrating the so-called “carnival effect”, where the donor and acceptor reverse their roles.

We speculate that these findings will pave the way to new applications of strong coupling in optically controlled FRET-based sensing and diagnostics with the ultra-small conjugates of sdAbs and QDs.



P-III



Prof. Igor Vlasov
Prokhorov General Physics Institute of the Russian Academy of Sciences, Moscow, Russia

Title: Diamond nanothermometer

Abstract

Future progress in studying intracellular thermodynamics needs an instrumentation revolution allowing local control of thermogenesis at micro/nanoscale, control of heat dissipation and heat energy conversion to other electrochemical energy types [1]. Nanodiamonds hosting temperature-sensing centers constitute a closed thermodynamic system. Such a system prevents direct contact of the temperature sensors with the environment making it an ideal environmental insensitive nanosized thermometer. A new design of a diamond nanothermometer, based on a luminescent nanodiamond embedded into the inner channel of a glass submicron pipette is reported [2]. All-optical detection of temperature, based on spectral changes of the emission of “silicon-vacancy” (SiV) centers with temperature, is used.

Further, combining a heater and a thermometer in one unit allows one to implement ultra-local hot spot control inside living cells. For this purpose, we use a single polycrystalline diamond particle containing SiV centers. Due to the presence of amorphous carbon at its intergranular boundaries such a particle is an efficient light absorber and, when illuminated by a laser, becomes a local heat source. Thus, the designed device is capable of operating in two modes. At higher laser power, it operates as the local heater and thermometer simultaneously. At low laser excitation this device does not produce heating and operates solely as a thermometer.

The first examples of successful application of a diamond nanothermometer/nanoheater are presented. In particular:

- (1) the possibility of measuring high temperature gradients (up to 20 oC/ μ m) with submicron spatial resolution is demonstrated [2];
- (2) the significant heat release of isolated mouse brain mitochondria (up to 22 oC) during total uncoupling of transmembrane potential is revealed [3];
- (3) the local heating of 11-12 °C next to individual HeLa cells and neurons, isolated from the mouse hippocampus, is shown to change the intracellular distribution of the calcium ion concentration [4].

This work was supported by Russian Science Foundation, grant No 23-14-00129 .



LASER-MATTER INTERACTION



10.24412/cl-35039-2023-23-12-12

LM-I-1

Laser-induced micro-plasma ablation recent progress and future prospects

**V.P. Veiko, A.A. Samochvalov, M.M. Sergeev, V.A. Rymkevich
G.K. Kostyuk, A.A. Petrov, V.A. Shkuratova, R.A. Zakoldaev**

*ITMO University, St. Petersburg, Russia,
vadim.veiko@mail.ru*

Scientific and applied interest in laser plasma (LP) has not faded away for a long time. LP is essentially a "converter" of laser energy into other radiation ranges, forms of matter and motion. This is confirmed by such LP applications as soft X-ray generation, laser jet propulsion, nanoparticles synthesis, deposition of thin films, impact hardening of metals, etc. However, in this work, the main attention is paid to a relatively new type of LP and its specific applications, namely, the plasma formed during laser ablation of a strongly absorbing target in a full contact with a solid medium transparent to a laser radiation.

This kind of LP will be called "compressed laser-induced microplasma ablation" (CLIMPA). CLIMPA is, in essence, a "focused" bunch of excited particles (electrons, ions, atoms and molecules), and its temporal and spatial parameters are completely determined by the parameters of the laser beam and the properties of the target substance and transparent medium, as well as the size of the gap between them. Transparent material, limiting the expansion of the LP, is under the influence of a controlled CLIMPA and it becomes possible for its precise and efficient processing

Previously, the use of the CLIMPA methods for fabricating a number of optical elements on the surface of fused quartz, such as microlens arrays, diffraction gratings, phase optical elements (POEs) etc., has already been reported [1, 2]. At this stage, one of the most pressing issues in optics is the creation of structured light beams, which opens up new possibilities in various problems of optical measurements, as well as in a number of tasks in the processing of thin films. Structured light beams can be obtained using phase-polarization optical elements (PPOE) on birefringent materials. However, the CLIMPA method has not yet been applied to the processing of such crystalline materials, since they are subject to brittle thermomechanical fracture.

The report describes an essence of the CLIMPA method, its parameters, regimes and examples of its application for fabrication of PPOEs, which provide generation and multiplexing of vortex beams. We used CLIMPA for multisectoral binary phase plates (MBPPs) and a birefringent spiral phase retarder (BSPR) fabrication. Fabricated on fused silica plates MBPPs successfully multiplexed Gaussian beam to the scalar vortex beam superposition. Fabricated on an Iceland spar plate BSPR was used to generate radially and azimuthally polarized vector vortex beams [3, 4]. High speed fabrication of MBPPs and BSPR was no more than 10 minutes to fabricate 8 mm² samples. Fabricated components were tested in the schemes with He-Ne (633 nm) and fiber (1.06 μm) lasers.

The CLIMPA method has all advantages of laser processing - flexibility, accuracy, simplicity, single-stage, ease of automation, etc., and it is able to provide energy-efficient and relatively simple production of POEs with high productivity. Extension of the CLIMPA method to new wavelengths of laser radiation (up to 10.6 μm in the IR region and up to 193 nm in the UV), to short pulse durations (up to psec and fsec), and the use of new targets, including chemically active ones, as well as a more detailed study of the CLIMPA mechanism, can significantly expand the range of processed materials and possible applications [5, 6].

[1] Veiko V.P., Volkov S.A., Zakoldaev R.A., Sergeev M.M., *Laser-induced microplasma as a tool for microstructuring transparent media // Quantum Electronics. – 2017. – V. 47. – №. 9. – P. 842-848.*

[2] Zakoldaev R.A., Kostyuk G.K., Rymkevich V.S., Koval V.V., Sergeev M.M., Veiko V.P., Yakovlev E.B., Sivers A.N. *Fast Fabrication of Multilevel Phase Plates Used for Laser Beam Correction // Journal of Laser Micro Nanoengineering - 2017, Vol. 12, No. 3, pp. 281-285*

[3] Shkuratova V.A., Rymkevich V. S., Kostyuk G. K., Sergeev M.M., *Laser-induced microplasma as effective tool for phase elements fabrication on amorphous and crystalline materials // Journal of Laser Micro Nanoengineering. – 2018. – V. 13. – №. 3. – P. 211-215.*

[4] Kostyuk G.K., Shkuratova V.A., Petrov A.A., Sergeev M.M. *Birefringent phase masks for laser beams shaping during laser material processing at imaging plane, June 2022, Optical Engineering 61(06)*

[5] Gresko V.R., Rymkevich V.S., Samokhvalov A.A., Veiko V.P. et al, *CO₂ laser-induced micro-plume treatment of silicon: technique and application // Optical and Quantum Electronics - 2019, Vol. 51, No. 12, pp. 397*

[6] Rymkevich V.S., Sergeev M.M., Zakoldaev R.A. *Laser microplasma as a spot tool for glass processing: focusing conditions // Journal of Materials Processing Technology - 2021, Vol. 292, pp. 117061*

LM-I-3

Laser plasma source of powerful unipolar THz pulses

D.Gorlova, A. Savel'ev

Faculty of Physics, Lomonosov Moscow State University, 119991, Leninskie gory 1 bld.62, Moscow, Russia
gorlova.da14@physics.msu.ru

Generation of THz radiation in the interaction of laser pulse with intensity $\sim 5 \cdot 10^{18}$ W/cm² with a controlled preplasma, created by an additional laser pulse interacting with a 16 μm polymer film target, was studied. The mechanism of generation of THz radiation in the frequency range 1-5 THz was found to be coherent transition radiation (CTR) of accelerated electrons traversing the rear plasma-vacuum boundary. The THz radiation yield is well correlated with the simultaneously measured relativistic electrons' yield (Fig.1). Integral THz radiation energy reaches ~ 0.1 mJ in the 1-5 THz spectral range, corresponding to 0.2% laser-to-THz conversion efficiency, and increases linearly with laser pulse energy. Temporal envelope of the THz pulse was studied numerically using the CTR theory and experimentally with Michelson interferometric measurements, confirming close to unipolar pulse structure (Fig.2).

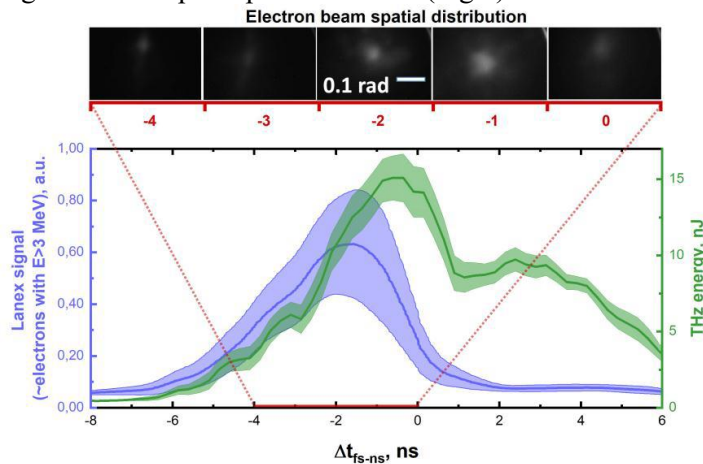


Fig.1. Dependences of the THz radiation energy and LANEX screen signal (\sim number of electrons with energy $E > 3$ MeV) on the delay between the main pulse and the prepulse. The inset shows a typical electron beam spatial profile in the delay range from -4 to 0 ns.

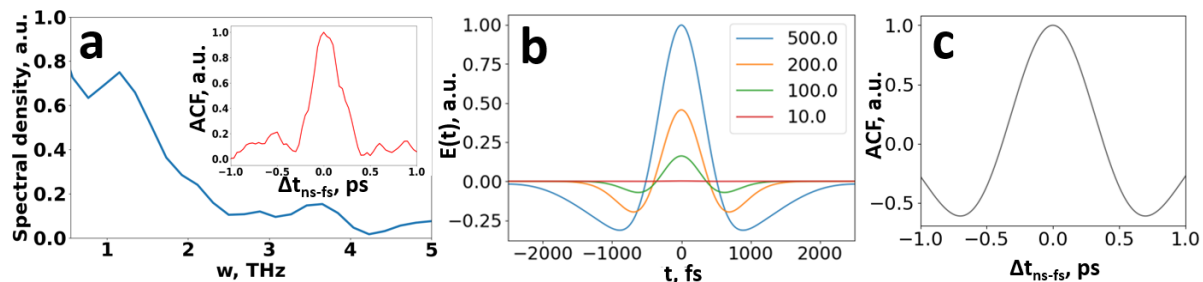


Fig.2. Experimentally measured THz radiation power spectral density (a) and corresponding autocorrelation function (shown in the inset) for the delay -1 ns (a), numerically calculated THz pulse shape for delay -1 ns and different preplasma cloud characteristic sizes (shown in the graph, in mkm) (b) and autocorrelation function of (b) for 500 mkm preplasma size.

We also considered scaling of the proposed scheme toward multi TW and PW laser systems. Numerical simulations indicate maintained level of THz radiation efficiency for the optimized schemes and parameters.

[1] D. Gorlova, I. Tsymbalov, R. Volkov, and A. Savel'ev. Transition radiation in the thz range generated in the relativistic laser—tape target interaction. *Laser Physics Letters*, 19(7):075401(2022).

[2] Д. А. Горлова, И. Н. Цымбалов, К. А. Иванов, и А. Б. Савельев. Генерация терагерцевого излучения с экстремальными параметрами с использованием мультитераваттного лазерного пучка. *Квантовая электроника*, 53(3):259–264 (2023).



LM-I-4

Final surface and subsurface structures formed as a result of laser action

N.A. Inogamov^{1,3}, V.A. Khokhlov¹, Yu.V. Petrov^{1,4}, V.V. Zhakhovskiy^{2,3}, S.I. Ashitkov³, S.A. Romashevskiy³, D.S. Sitnikov³, K.V. Khishchenko³, Yu.R. Kolobov⁵, S.S. Manokhin⁵, I.V. Nelasov⁵, S.V. Fortova⁶, E.A. Perov^{3,6}, V.V. Shepelev⁶

- 1- *L.D. Landau Institute for Theoret. Physics, RAS, 142432, Mosc. Reg., Chernogolovka, Ak. Semenova, 1A*
 2- *N.L. Dukhov All-Russia Research Institute of Automatics, 127055, Moscow, Sushchevskaya, 22*
 3- *Joint Institute for High Temperatures, RAS, 125412, Moscow, Izhorskaya st. 13 Bd.2*
 4- *The Moscow Institute of Physics and Technology, 141701, Mosc. Reg., Dolgoprudny, Institutskiy per., 9*
 5- *Institute of Problems Chem. Phys. RAS, 142432, Moscow Region, Chernogolovka, Ak. Semenova, 1*
 6- *Institute of Computer Aided Design of the RAS, 123056, Moscow, 2 Brestskaya st, 19/18*
naulinogamov@gmail.com

The physics of processes caused by action of a laser is discussed. The influence of laser parameters on these processes is considered: pulse duration (fs [1-5], ps [1-5], subns [1,2], ns [1,2]), absorbed energy ($\sim 0.1-10$ J/cm² [1-6] appropriate to the technological applications), wavelength (from optical [1-6] to soft [7,8] and hard X-rays [9-11]), spot radius ($0.1-10^3$ μm [3,12-15]), metals and dielectrics. Conclusions are made concerning the characteristics of the plume (including during ablation into a liquid) [1,2,5,16,17], laser shocks [3,4,6,10,18-23], the random structures that arise on the surface [8,11,24] and in the volume (changes in crystalline structure [6]) of the target. Effects on homogeneous, film and layered objects are investigated. Typical initial plasma temperatures are ~ 1 eV for nanosecond pulses acting through liquid to metal or semiconductor [1,2,5] targets and up to \sim few tens of eV in the case of femtosecond pulses [6] acting through air near threshold ($\sim 10-100$ J/cm², $\sim 10^{14-15}$ W/cm²) of optical breakdown of air. Applications related to laser shock peening [3,4,6,19-21], optoacoustics, and nanoparticle production [1,2,5,16,17] are described.

- [1] Petrov et al., Hydrodynamic phenomena induced by laser ablation of metal into liquid, *Applied Surface Science*, **492**, 285-297, (2019).
 [2] Petrov et al., Condensation of laser-produced gold plasma during expansion and cooling in a water environment, *Contrib. Plasma Phys.*, **59**(6), e201800180, (2019).
 [3] Shepelev et al., Attenuation and inflection of initially planar shock wave generated by femtosecond laser pulse, *Optics and Laser Technology* **152**, 108100, (2022).
 [4] Inogamov et al., Laser Shock Wave: The Plasticity and Thickness of the Residual Deformation Layer and the Transition from the Elastoplastic to Elastic Propagation Mode, *JETP Letters*, **115**, 71-78, (2022).
 [5] Inogamov et al., Dynamics of Gold Ablation into Water, *JETP*, **127**, (1), 79-106, (2018).
 [6] Khokhlov et al., Melting of Titanium by a Shock Wave Gener. by an Intense Femtosec. Laser Pulse, *JETP Letters*, **115**, 523-530, (2022).
 [7] Inogamov et al., Hydrodyn. driven ultrashort laser pulse: simul. and opt. pump-X-ray probe exper., *Appl. Phys. B*, **119**, 413-419, (2015).
 [8] Ishino et al., Study of damage structure formation on aluminum film targets by picosecond soft X-ray laser ablation around threshold region, *Applied Physics A*, **124**, 649, 8pp., (2018).
 [9] Albertazzi et al., Dynamic fracture of tantalum under extreme tensile stress, *Sci. Adv.*, **3**: e1602705, (2017).
 [10] Makarov et al., Direct imaging of shock wave splitting in diamond at Mbar pressures, arXiv:2207.01719
 [11] Kohmura et al., Nano-structuring of multi-layer material by single x-ray vortex pulse with femtosecond duration, *Appl. Phys. Lett.*, **112**, 123103, (2018).
 [12] Inogamov and Zhakhovskii, Formation of Nanojets and Nanodroplets by an Ultrashort Laser Pulse at Focusing in the Diffraction Limit, *JETP Lett.*, **100** (1), 4-10, (2014).
 [13] Inogamov et al., Jet Formation in Spallation of a Metal Film from a Substrate under the Action of a Femtosecond Laser Pulse, *JETP*, **120** (1), 15-48, (2015).
 [14] Inogamov et al., Solitary Nanostructures Produced by Ultrashort Laser Pulse, *Nanoscale Res. Lett.*, **11**, 177 (13 pp.), (2016).
 [15] Wang et al., Laser-Induced Translative Hydrodynamic Mass Snapshots: Noninvasive Characterization and Predictive Modeling via Mapping at Nanoscale, *Phys. Rev. Applied*, **8** (4), 044016, 17 pp., (2017).
 [16] Inogamov et al., Hydrodynamic and molecular-dynamics modeling of laser ablation in liquid: from surface melting till bubble formation, *Opt Quant Electron.* **52**, 63, 24 pp., (2020).
 [17] Inogamov et al., Physical Processes Accompanying Laser Ablation in Liquid, *JETP Letters*, **115**, 16-22, (2022).
 [18] Ashitkov et al., Behavior of Al near an ultimate theor. strength in experim. with femtosec. laser pulses, *JETP Lett.* **92**, 516-520. (2010).
 [19] Zhakhovskii and Inogamov, Elastic-plastic phenomena in ultrashort shock waves, *JETP Lett.* **92**, 521-526, (2010).
 [20] Zhakhovskiy et al., Single two-zone elastic-plastic shock waves in solids, *Phys. Rev. Lett.* **107**, 135502, (2011).
 [21] Inogamov et al., Superelasticity and the Propagation of Shock Waves in Crystals, *JETP Letters*, **93** (4), 226-232, (2011).
 [22] Demaske et al., Ultrashort shock waves in Nickel induced by femtosecond laser pulses, *Phys. Rev. B* **87**, 054109, (2013).
 [23] Perriot et al., Evolution of elastic precursor and plastic shock wave in copper via molecular dynamics simulations, *J. Phys.: Conf. Ser.* **500**, 172008, (2014).
 [24] Ashitkov et al., Formation of nanostructures under femtosecond laser ablation of metals, *Quantum Electronics*, **45** (6), 547-550, (2015).

[10.24412/cl-35039-2023-23-15-15](https://doi.org/10.24412/cl-35039-2023-23-15-15)

LM-I-5

Photothermal applications of laser-synthesized nanomaterials

A. Popov¹*1- National research nuclear University (MEPhI), Moscow, Russia**email address: aapopov1@mephi.ru*

Pulsed laser ablation in liquids is a very powerful and versatile physical technique for the synthesis of colloidal nanoparticles (NPs), having a number of unique features including an exceptional purity of the NPs surface, high colloidal stability without using of any ligands and unusual surface chemistry. The method of laser ablation profits from a natural generation of nanoclusters under irradiation of a solid target by laser pulses in various liquids. Among many useful types of the laser-synthesized NPs, a class of light-absorbing colloidal nanomaterials is especially interesting as it has lots of practical applications in biomedicine, renewable energy and photocatalysis. Here we present our recent results in laser ablative synthesis of NPs having high optical absorption in visible and near-infrared spectral ranges. Optical and structural properties of the laser-synthesized NPs based on alternative plasmonic materials (transitional metal nitrides and lanthanoid borides) and MXenes will be discussed. Moreover, an assessment of the NPs in photothermal therapy, photoacoustic visualization and solar energy harvesting will be also presented.

LM-I-6

Laser ablation synthesis and assembly of multicomponent nanostructures in liquids

N.V. Tarasenko, V.G. Kornev, A.A. Nevar, M.I. Nedelko, N.N. Tarasenko

B. I. Stepanov Institute of Physics, National Academy of Sciences of Belarus

68-2 Nezalezhnasti Ave., 220072 Minsk, Belarus

n.tarasenko@ifanbel.bas-net.by

In recent years, development of plasma-assisted methods in liquids towards their application in material processing and nanotechnology has been a relevant topic of modern research. Among the plasma-induced approaches, laser-assisted methods are among the most studied due to its simplicity and versatility as well as dependence of the nanomaterials characteristics on the laser parameters that opens up possibilities for the controlled formation of nanoparticles (NPs) of a given size and composition. Moreover, in plasma-liquid systems, plasma exists, as a rule, in a non-equilibrium state, contains various highly reactive particles, and thus is well suited for the synthesis of composite nanomaterials such as hybrid, alloyed, and doped ones. Apart from the controlled synthesis, of interest is also to develop the methods of assembly and deposition of the forming nanomaterials into ordered structures for their further practical application. In this paper, we discuss the capabilities of laser ablation plasma approaches for synthesis and assembly of multicomponent nanostructures with a control over their composition, structure and morphology. The relationship between the NPs structure and experimental parameters revealed in the present work allowed proposing several novel laser assisted schemes suitable for the synthesis of NPs of alloys (Ge-Sn) [1], compounds (SiC, ZnO, CuO) [2,3], doped (ZnO:Nd) [4] nanocrystals and hybrid (ZnO/C, Si-Ag, Si-Cu and Si-Ag-Au) [5,6] structures. Furthermore, several schemes for the one-pot synthesis and assembly of the forming NPs are discussed. As one of the promising approaches, application of the electric field to the target and substrate during laser ablation in liquids has been shown to be capable both of varying the nanoparticles morphology and of their simultaneous deposition into ordered hierarchical nanostructures on the counter electrode. The morphology variation has been shown to be achieved by the changing the polarity and strength of the applied external electric field. For example, ZnO nanoflowers or nanodiscs can be formed depending on the polarity of the electrical field applied to the target, while in the case of Cu ablation in water nanowires or nanorods were produced. Moreover, in the case of Cu ablation in water, changing the polarity allows also to vary the CuO:Cu₂O ratio in the nanomaterial. The Raman, XRD and FTIR results proved the formation of metal oxides phases. For further formation of heterostructures, a two-step combined laser-discharge approach was developed shown to be capable of preparation of CuO/ZnO nanoheterostructures. In the proposed scheme, preliminarily, plasma assisted deposition of ZnO film on the ITO substrate was performed using the developed technique based on atmospheric pressure dc discharge plasma. The plasma-assisted electrolysis ensured the ZnO thin film electrodeposition with a good adhesion to the ITO substrate. The deposited ZnO/ITO sample was further used as a substrate for CuO deposition during electric field-assisted laser ablation in liquid. At this stage, the heterogeneous CuO/ZnO nanocomposite structures were formed. The achieved uniform nanomaterial distribution of the formed heterogeneous nanostructures as well as developed surface is beneficial for the different practical applications.

The work was supported by the National Academy of Sciences of Belarus under project Convergence 2.2.05 and by the Belarusian Foundation for Fundamental Researches under Grants F23RNF-156 and F22SRBG-008.

[1] N.N. Tarasenko, N.V. Tarasenko, V.V. Pankov, Preparation of Germanium-Tin Alloy Nanoparticles by Laser-Assisted Techniques in Liquid, *Intern. J. of Nanoscience*, vol. 18, p.1940049 (2019).

[2] N. Tarasenko, V. Kornev, M. Rzhetski, E. Lutsenko, S. Chakrabarti, T. Velusamy, D. Mariotti, N. Tarasenko Fabrication of luminescent silicon carbide nanoparticles by pulsed laser synthesis in liquid, *Applied Physics A*, vol. 128, (2022).

[3] N. Tarasenko, E. Shustava, A. Butsen, A. Kuchmizhak, S. Pashayan, S. Kulnich, N. Tarasenko, Laser-assisted fabrication and modification of copper and zinc oxide nanostructures in liquids for photovoltaic applications, *Appl. Surface Science* vol. 554, 149570 (2021).

[4] N. Tarasenko, V. Kornev, A. Ramanenka, R. Li, N. Tarasenko Photoluminescent neodymium-doped ZnO nanocrystals prepared by laser ablation in solution for NIR-II fluorescence bioimaging *Heliyon*, vol.8, p.e09554, (2022).

[5] N. Tarasenko, et al Synthesis of ZnO/C Nanocomposites via Liquid-Assisted Laser Ablation in an Applied Electric Field for Supercapacitor Applications, *ACS Appl. Nano Mater.*, vol.6, p.5918 (2023).

[6] N. Tarasenko, et al Laser Synthesis and Optical Properties of Hybrid Silicon Nanostructures for Photothermal Conversion of Solar Radiation *J. of Appl. Spectroscopy*, vol 90, p. 253, (2023).



10.24412/cl-35039-2023-23-17-17

LM-I-7

Laser-induced extreme state of matter in silicon: the way to create and to diagnose

Fedor Potemkin

119991, Russia, Moscow, Faculty of Physics, Leninskie Gory, bld.1/62

potemkin@physics.msu.ru

The field of silicon photonics is a rapidly developing area of research due to the fact that modern microelectronics are primarily based on silicon, making the development of photonic circuits in semiconductors crucial [1]. Silicon's small band gap (~ 1.1 eV) and high number of free electrons also limit the use of commercially available lasers. Moreover, due to the presence of a sufficiently large number of free electrons, even when exposed to ultra-short laser pulses with a wavelength greater than 1100 nm, microplasma is efficiently generated, which effectively increases the laser impact area, leading to a drop in the deposited energy density (DED).

In the first part of this study, the way to control and to increase the DED inside the silicon sample has been proposed. Mid-IR (more than 4 μm) ultrashort laser pulse excitation is one the most convenient way to increase the deposited energy density which is enough for bulk microstructuring of silicon [2]. Two- and three- photon absorption cross section in silicon becomes negligible in mid-IR that leads to field-driven laser energy absorption localization in space.

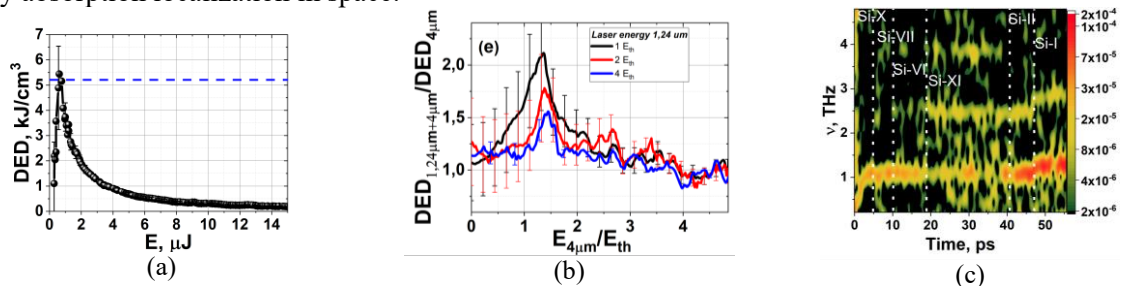


Fig.1 (a) DED into the bulk Si as a function of laser energy of tightly focused ($\text{NA}=0.86$) mid-IR ($\lambda=4,6 \mu\text{m}$) femtosecond ($\tau=160$ fs) laser pulse. Blue dashed line indicates the DED threshold for micromodification formation. (b) DED into the bulk Si under two color excitation by a pair of tightly focused ($\text{NA}=0.5$) mid-IR ($\lambda=4,6 \mu\text{m}$) and near-IR femtosecond laser pulses as a function of mid-IR laser pulse energy compared to single pulse mid-IR excitation. (c) Intensity map of changes in the frequency of coherent phonons in silicon, depending on the delay between the pump and probe mid-IR ($\lambda=4,6 \mu\text{m}$) laser pulses.

Using tightly focused ($\text{NA}=0.86$) mid-IR ($\lambda=4,6 \mu\text{m}$) femtosecond ($\tau=160$ fs) laser pulse excitation the DED more than 5 kJ/cm^3 was achieved that allow to modify the bulk Si in single pulse regime (see Fig.1 a). It was demonstrated that adding the near-IR laser field at the wavelength of $1,24 \mu\text{m}$ with the energy much less than the plasma formation threshold energy makes it possible to weaken the numerical aperture of the focusing optics down to $0,5$ as well as to increase the DED value up to 8 kJ/cm^3 (see Fig.1 b).

Such a huge impact on the silicon makes it possible to create the extreme state of matter inside it and the phase transitions can be occurred. Thus, in the second part of this study the dynamics of the impact of mid-IR-range ($\lambda=4.6 \mu\text{m}$) femtosecond laser pulses on bulk silicon under tight focusing conditions ($\text{NA} = 0.5$) was reconstructed for the first time. Initially, the femtosecond pulse energy is absorbed by the laser-induced plasma, with a lifetime of approximately $160\text{--}320$ fs (depending on the laser pulse energy). The energy transfer from the plasma to the atomic subsystem occurs on a sub-ps timescale, which generates a shock wave and excites coherent phonons on a sub-ps scale. The shift of atoms in the lattice at the front of the shock wave results in a cascade of phase transitions ($\text{Si-X} \Rightarrow \text{Si-VII} \Rightarrow \text{Si-VI} \Rightarrow \text{Si-XI} \Rightarrow \text{Si-II}$), leading to a change in the phonon spectra of silicon [3] (see Fig.1 c).

This work in part of phase transitions investigations was supported by Russian Science Foundation (Project № 23-73-00039) and Russian Foundation for Basic Research (Project № 21-32-70021) in part of research on phonons.

[1] Bogaerts, W.; Chrostowski, L. Silicon Photonics Circuit Design: Methods, Tools and Challenges. Laser Photonics Rev. 12, 1700237 (2018).

[2] Mareev, E.; Pushkin, A.; Migal, E.; Lvov, K.; Stremoukhov, S. Single-shot femtosecond bulk micromachining of silicon with mid-IR tightly focused beams. Sci. Rep. 12, 7517 (2022).

[3] Mareev, E.; Obydenov, N.; Potemkin, F. Dynamics of the Femtosecond Mid-IR Laser Pulse Impact on a Bulk Silicon. Photonics, 10, 380 (2023).



LM-I-8

Light-matter coupling in optical microcavities

M.C. Houghton¹, K. Kurassova², N.A. Toropov^{1,2}, F. Vollmer¹

1- University of Exeter, Exeter, UK, EX4 4QD

2- ITMO University, St. Petersburg, Russia, 197101

nikita.a.toropov@gmail.com

In this contribution, we discuss two aspects of light-matter interaction in optical microcavities: first – when microcavities are decorated with plasmonic nanostructures and used as biosensors; second – when microcavities are doped with fluorescent nanocrystals.

First aspect is related to biosensing with optical microcavities. Light circulating in such cavities forms whispering gallery modes (WGMs), which have extremely high quality-factors. High Q-factors make such cavities unsurpassed instruments for single-molecule sensing. In this work, we developed the idea of whispering gallery modes for single-molecule biosensing via decorating them with plasmonic nanoparticles. Despite high Q-factors, WGMs have comparatively big effective mode volume reducing sensitivity; in turn, plasmonic structures can concentrate energy of WGMs in a tiny area; this leads to a better sensitivity of WGM biosensors. Conventionally, WGMs used for biosensing can be excited with lasers and prism couplers, typical power levels are ~0.01–0.1 mW. In our latest work we extended this range, that showed us that molecules attached to such biosensors may strongly interact with plasmonic nanoparticles, showing strong nonlinear response of the sensors; in addition, we proposed to use a newly discovered phenomena for single-molecule absorption spectrometers.

In the second part of the talk, we will discuss light-matter interaction inside microcavities. Such cavities were made of polymers with added semiconductor nanocrystals via a microfluidics technique. Upon excitation of nanocrystals fluorescence in such cavities, there were observed its lifetime shorting by 100 of times in comparison with fluorescence of same nanocrystals in solutions. This is discussed in terms of the Purcell effect. The second part of this work was supported by the Russian Science Foundation (Project 22-72-10057).

Ultrafast conductivity control by femtosecond lasers

D. Boschetto¹

1- Laboratoire d'Optique Appliquée, ENSTA Paris, Ecole Polytechnique, CNRS, Institut Polytechnique de Paris, Palaiseau, France

Main author email address: Davide.Boschetto@ensta.fr

The field of materials science and nanoelectronics has been revolutionized by the ability to control conductivity through femtosecond laser pulse irradiation, presenting promising opportunities for progress in multiple disciplines. The capacity to induce rapid and transient alterations in the electrical properties of materials has unlocked a wide range of possibilities in optoelectronics, photonics, and information processing. The utilization of femtosecond laser pulses enables precise manipulation of material conductivity, providing exceptional control over their electronic characteristics. This technique offers a distinct advantage compared to conventional methods by allowing rapid modulation of conductivity within femtosecond time scale [1-3]. The ultra-fast timescale facilitates dynamic manipulation of electrical properties, opening the possibility to innovative applications in areas such as ultrafast electronics, high-speed data processing, and advanced photonic devices.

During this talk, we will highlight recent advancements in manipulating material conductivity through the use of femtosecond laser pulses, with a specific emphasis on the interesting phenomenon of photoinduced reduction of conductivity by targeting localized states with a specific pump photon energy [3]. We will focus in particular on incommensurate crystals, which are characterized by a lattice mismatch leading to the presence of localized states that affect the overall conductivity of the crystal. We will demonstrate how targeted excitation can selectively promote electrons to occupy these localized states, offering a means to control and reduce the conductivity of the crystal.

The experimental findings are supported by Density Functional Theory calculations, together with a time-dependent simulation using rate equations and a two-temperature model. These investigations reveal that the conductivity reduction occurs as photoexcited electrons become trapped in the localized energy state of vanadium clusters, which are formed due to the incommensurability of the layered crystal structure.

[1] G. Lantz et al., "Ultrafast evolution and transient phases of a prototype out-of-equilibrium Mott- Hubbard material." *Nature Communications* 8, 13917 (2017).

[2] N. Yoshikawa et al., "Ultrafast switching to an insulating-like metastable state by amplitudon excitation of a charge density wave." *Nature Physics* 17, 909 (2021).

[3] M. Lejman et al., "Ultrafast photoinduced conductivity reduction by bonding orbital control in an incommensurate crystal." *Submitted*.

LM-I-10

Properties of a terahertz holographic axicon fabricated by laser ablation of a black diamond

M. Komlenok¹, V. Pavelyev^{2,3}, B. Knyazev, A. Bolshakov¹, V. Konov¹

*1- Prokhorov General Physics Institute of the Russian Academy of Sciences,
38 Vavilova St., Moscow, 119991, Russian Federation*

2- Samara National Research University, 34 Moskovskoye Shosse, Samara, 443086, Russian Federation

*3- IPSI RAS - Branch of the FSRC "Crystallography and Photonics" RAS, 151 Molodogvardeyskaya St., Samara,
443001, Russian Federation*

komlenok@nsc.gpi.ru

The use of high-power sources of terahertz radiation requires durable and highly efficient optics. Silicon diffractive optical elements have a low coefficient of thermal conductivity and high reflective losses (51%) in comparison with diamond elements. However, large plates of optical grade polycrystalline diamond are expensive for the fabrication of terahertz optics and, moreover, are difficult in direct precise processing, even if laser technologies are used for these purposes. In the case of using high-performance IR lasers, a breakdown occurs in the bulk of the diamond [1]. Here, we propose to use the so-called "black" diamond to create optical elements operating in the terahertz range. It is distinguished by transparency in the far infrared range and the presence of developed boundaries between crystallites, which should prevent self-focusing of laser radiation in the bulk. Usually this material is used as a heat sink, and also has a cheap production cost due to fast synthesis. In this work, we report on the fabrication of holographic axicon for powerful THz radiation by structuring of the surface of "black" diamond with the disk Yb:YAG laser (Dausinger + Giesen GmbH, $\lambda = 1030$ nm, $\tau = 1$ ps, $f = 200$ kHz), which provides high productivity of ablation to create a maximum relief depth of about 100 μm on a plate with a diameter of 20 mm. Under the optimized irradiation condition, the necessary relief with piecewise continuous profile (fig. 1) was formed by the moving of the laser beam over the diamond surface by a galvanic XY scanner. The results of the testing of the fabricated axicon on the Novosibirsk free electron laser at a wavelength of 141 μm showed good agreement between experimental and calculated optical properties. The experimental and calculated cross sections of Bessel beam at the distance of 120 mm from the axicon are shown in fig. 2a and c, respectively. The perfect beam, which is formed in the focal plane when Bessel beam is focused by a lens, demonstrates a homogeneous narrow ring (fig. 2b) according to the numerical calculation (fig. 2d). The obtained result demonstrates the high potential of the proposed approach for production of high-efficient complex optical elements based on the "black" diamond to control the powerful THz radiation.



Fig.1. Optical image of the fabricated diamond axicon.

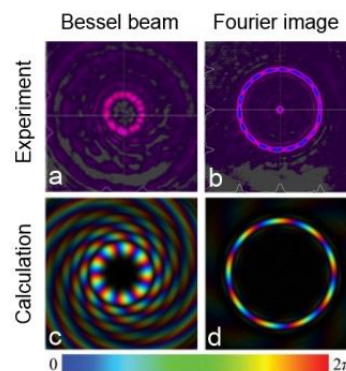


Fig.2. Intensity distribution for Bessel beam: (a) experiment, (c) calculation. Perfect vortex beams: (b) experiment, (d) calculation.

[1] T.V. Kononenko, P.A. Pivovarov, A.A. Khomich, R.A. Khmel'nitskii, and V.I. Konov, Effect of absorbing coating on ablation of diamond by IR laser pulses. Quantum Electronics vol. 48 (3), pp. 244-250, (2018).

LM-I-11

Laser synthesis of gold and carbon chains in liquid media

**K. Ashikkalieva¹, V. Kononenko¹, N. Arutyunyan¹, E. Akhlyustina², E. Zavedeev¹,
A. Vasiliev^{3,4}, V. Konov¹**

1- Prokhorov General Physics Institute of the Russian Academy of Sciences, Moscow, Russia

2- National Research Nuclear University "MEPhI", Moscow, Russia

3-National Research Centre "Kurchatov Institute", Moscow, Russia

4- FRSC Crystallography and Photonics RAS, Moscow, Russia

Main author email address: kuralay.physics@mail.ru

Ultrashort intense pulses are known to cause processes of nonlinear multiphoton and avalanche ionization in liquid [1]. This initiates structural transformations in liquid media, leading to occurrence radically new compounds and structures (molecules, nanoparticles of different shape, chains etc.). However general physical regularities of laser synthesis in liquid media have been studied, the problem of controlling morphology and sizes of the synthesized structures is not well understood. In particular, the most important problem is to control the shape of synthesized structures by changing the irradiation conditions (the number of laser pulses, pulse duration and repetition rate). Here, we report on synthesizing gold and carbon chains under multiple laser irradiation of liquid solutions.

The materials under study were hydrochloroauric acid (HAuCl₄) aqueous solutions (5×10^{-4} mol/L) and colloid solutions of graphite microparticles in ethanol (0.4 mg/ml). The gold ion solutions were irradiated with femtosecond (fs) irradiation of Ti-sapphire laser "Spectra Physics" ($\tau=120$ -fs, $\lambda=800$ nm, $f=1$ kHz). The graphite colloid solutions were treated with picosecond (ps) irradiation of hybrid laser "Huaray-Olive-1064-40" ($\tau=10$ -ps, $\lambda=1064$ nm, $f=10$ kHz). The solutions were irradiated at a fixed pulse energy ($E = 800$ μ J and $E = 16$ μ J for fs- and ps-pulses, respectively) by varying the number of laser pulses. Optical absorption spectra in the range from UV to near-IR were measured with a double-beam spectrophotometer Perkin Elmer Lambda 950. The morphology of synthesized nanostructures was studied by analyzing their images obtained in a transmission electron microscope (TEM).

It was found that high-intensity femtosecond pulses along with single gold nanoparticles caused formation of numerous elongated (chain) particles [2]. As TEM shows, individual gold nanoparticles can have triangle and round shape, whereas chain structures (up to several nanometers in length) can have linear or dendrite structure. The synthesis of chain structures depended on the pulse number: the maximum concentration of gold chains are observed at the pulse number $N \approx N_{cr} = 4 \times 10^5$; under further irradiation the chains almost completely disappeared. Apparently, elongated nanostructures disintegrated into individual nanoparticles due to the melting and evaporation processes. The thermal disintegration of gold chains during multiple fs-laser irradiation was accompanied with their repeated formation upon switching off the laser (cooling the liquid).

According to the preliminary experiment on picosecond irradiation of pure ethanol, in spectra of the irradiated liquid there were no distinguishable absorption peaks attributed to linear carbon chains (polyynes). This means that ethanol is likely to be resistant to laser irradiation in the range of the processing parameters studied ($E=20$ μ J, $N \leq 4 \times 10^7$). This is why ethanol was chosen as a solvent for graphite microparticles. It has been found that optical absorption spectra of the ps-irradiated graphite solutions contain a set of lines (216–297 nm), which are corresponding to polyynes. Among synthesized linear carbon chains there were short (C₆H₂, C₈H₂) and longer (C₁₀H₂, C₁₂H₂, C₁₄H₂) ones. It has been found that absorption lines in the spectra become clearly distinguished at $N > 2 \times 10^6$. Further increase in the number of laser pulses causes the rise in intensity of the absorption peaks related to the polyynes.

This work was supported by the Russian Science Foundation (project no. 19-12-00255-P).

[1] V. Kononenko, K. Ashikkalieva, N. Arutyunyan, et al., Femtosecond laser-produced plasma driven nanoparticle formation in gold aqueous solution, *Journal of Photochemistry & Photobiology, A: Chemistry*, vol. 426, P.113709 (2022)

[2] K. Ashikkalieva, V.Kononenko, N. Arutyunyan, et al., Laser Synthesis of Gold Nanochains from Hydrochloroauric Acid Aqueous Solutions, *Physics of Wave Phenomena*, vol. 31, pp. 44–50, (2023)

LM-I-13

Influence of high-energy laser irradiation on structural and phase transformations in aluminum-lithium alloys during laser welding

A.G. Malikov

*Khristianovich Institute of Theoretical and Applied Mechanics SB RAS, Novosibirsk
smalik@ngs.ru*

Laser welding is widely recognized as an advanced technology for joining materials using a high-power, high-density energy laser beam. Laser welding offers several advantages, such as high speed, high precision, a small heat-affected zone, no need for vacuum chambers, flexibility, and the ability to automate the process. The process of laser welding involves several physical phenomena, including the interaction of the laser with the material, multiple reflections of the laser radiation inside the vapor-gas channel, phase transitions, liquid and gas flow, and heat and mass transfer. In aerospace and rocket engineering, the main method for joining alloys is riveting, but this method has several disadvantages. Riveting technology is characterized by high labor intensity, and the process is accompanied by significant noise and vibration that can be harmful to humans, industrial buildings, and structures.

Currently, riveting is being replaced by welding as a leading technology in the field. According to estimates by VIAM, the transition to third-generation Al-Li alloys with a replacement of riveted joints with welded ones will result in a weight reduction of aircraft structures (Il-112V, SSJ-New) up to 25% [1-2]. However, there is a problem related to the static-mechanical characteristics (tensile strength, yield strength, and elongation) of laser-welded joints, which are directly related to the structural and phase changes of the original material as a result of laser processing. These characteristics remain low, constituting only 50-80% of the original alloy values [3]. The complexity of these processes is due to the simultaneous occurrence of a significant number of physical and chemical processes involving liquid, solid, and gaseous phases, as well as high temperatures and complex hydrodynamic and thermal flows.

This work is for the first time aimed at solving a complex scientific problem associated with achieving maximum static mechanical characteristics of permanent laser welded joints new class of materials - Al-Li alloys of the third generation. This became possible by controlling the structure and phase composition of the weld as a result of optimizing the process of laser exposure and for the first time used to control the evolution of the structural-phase composition of the weld of aluminum alloys, through the use of a modern independent diagnostic method: synchrotron radiation diffractometry, on a “megascience” class facility. The influence of the energy parameters of laser action on the change in the structure and phase composition of the weld material depending on the alloying system and the thermophysical properties of aluminum-lithium alloys of the third generation is shown. It is also shown that the subsequent optimization of post-heat treatment in the form of hardening and artificial aging makes it possible to obtain the strength of laser welded joints at the level of the strength of the base material.

The research was carried out with the support of a grant from the Russian Science Foundation № 23-79-00037, <https://rscf.ru/project/23-79-00037/>.

[2] Malikov A., Orishich A., Bulina N., Karpov E., Sharafutdinov M. Effect of post heat treatment on the phase composition and strength of laser welded joints of an Al-Mg-Li alloy, *Materials Science and Engineering A*. 2019, vol. 765. Art. 138302 (8 p.).

[3] Malikov A., Orishich A., Vitoshkin I., Bulina N., Karpov E., Gutakovskii A., Batsanov S., Ancharov A., Tabakaev R. Effect of the structure and the phase composition on the mechanical properties of Al-Cu-Li alloy laser welds, *Materials Science and Engineering: A*. 2021, vol. 809. Art. 140947 (16 p.).

[1] Malikov A., Golyshev A., Vitoshkin I. Current Trends in Laser Welding and Additive Technologies (Review), *Applied Mechanics and Technical Physics*, vol. 64, pp. 36-59, (2023).



LM-I-14

Phase composition and tribological characteristics of surface layers of multicomponent iron-based alloys after laser modification in air

S.I. Yaresko¹, A.T. Kozakov², A.V. Sidashov³

¹Samara Branch of P.N. Lebedev Physical Institute of the Russian Academy of Sciences, 221 Novo-Sadovaya Str., Samara 443011, Russia

²Research Institute of Physics, Southern Federal University, 194 Stachki Ave., Rostov-on-Don 344090, Russia

³Rostov State Transport University, 2 Narodnogo Opolcheniya Sq., Rostov-on-Don 344038, Russia

E-mail address: yarsi54@gmail.com

The studies results of the surface layers of tool carbon (W1-7, W1-9), alloyed (DIN 150Cr14) and heat-resistant (M2, T8) steels performed by electrochemical analysis, Auger spectroscopy and XPS in combination with ion profiling after laser treatment in air are presented. For laser treatment (LT), an ytterbium quasi-continuous fiber laser with a power of up to 130 W and a pulsed Nd glass laser with a pulse energy of up to 70 J were used. The phase composition and structure of oxide films formed on the surface of multicomponent iron-based alloys after the LT were investigated, the structure of the oxide-metal interface was established, the thickness of fully oxidized layers and the thickness of the transition layer located at the boundary with an basic steel volume was determined. For tool carbon steels, the transition layer containing FeO and iron atoms is located most deeply, then a layer of Fe₃O₄ oxide is followed and, finally, an outer layer consisting of a mixture of FeO and Fe₂O₃ oxides is located near the surface (Fig. 1). The thicknesses of fully oxidized layers for W1-7 and W1-9 steels reach 100 nm. The total thickness of the oxide layer together with the transition layer is 225.0 nm. For T8 alloy steel, iron oxides and oxide of alloying elements are present in the surface layer, with tungsten and vanadium oxides located closer to the surface. The maximum thickness of the oxidized surface layer of FeO is 126 nm, the thicknesses of the oxide layers WO₃, V₂O₅, V₂O₃ are 97 nm, 90 nm, 126 nm, respectively. Selective enrichment of the surface with tungsten and vanadium atoms was found, leading to hardening of the intergrain boundaries and the appearance of a local hardened layer at a depth of 90 nm.

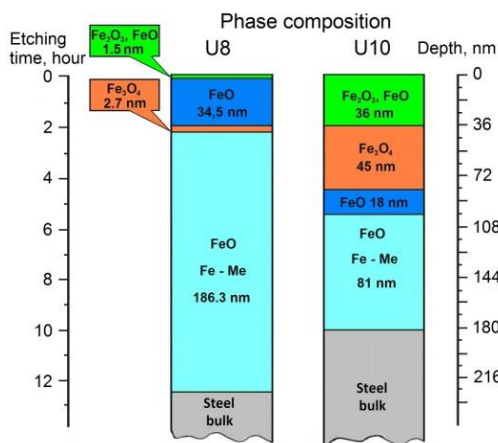


Fig. 1. Location diagram and thickness of oxide layer on W1-7 and W1-9 steel surface

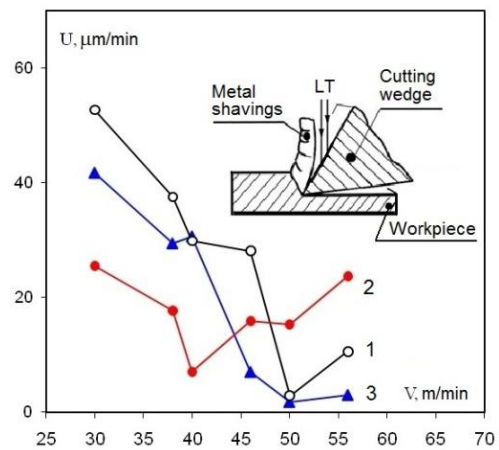


Fig. 2. Wear rate U ($\mu\text{m}/\text{min}$) of a tool made of T8 steel: 1 – without LT; 2 – LT in air; 3 – LT in the Ar medium

It is shown that the presence of Fe₂O₃ and Fe₃O₄ oxides provides a higher wear resistance of the W1-9 steel surface after LT during nanotribo tests. For high-speed steel T8, the presence of oxides on the surface after LT affects its frictional properties and determines the stable flow of the cutting process and the stable operation of the tool (Fig. 2).

Kozakov A.T. is grateful for the financial support the Ministry of Science and Higher Education of the Russian Federation (State assignment in the field of scientific activity 2023 r. №FENW-2023-0014).

LM-I-15

Optical anisotropy of 2D and 3D metal nanoparticle ensembles induced by optical and mechanical treatments

I.A. Gladskikh, D.R. Dadadzhanov, D.A. Kafeeva, T.A. Vartanyan

ITMO University, Kronverksky Pr. 49, bldg. A, St. Petersburg, 197101, Russia

Main author email address: 138020@mail.ru

In this work two alternative approaches for development of polarization-dependent systems based on anisotropic ensembles of plasmonic nanoparticles were proposed.

The first approach involves the phenomenon of longitudinal plasmon resonance of uniaxially oriented nanorod assemblies in polymer matrices. Polyvinyl alcohol is often chosen as a polymer matrix, since films are fairly easy to obtain with conventional drying, they are transparent in the visible range, have a low glass transition temperature, and the amount of possible stretching depends on the length of the molecules. The alignment of the nanorods in this case is carried out by heating the film to a softening temperature while simultaneously subjecting it to tensile stress. In this process, the nanorods in contact with the polymer chains interlock and reach the final orientational position parallel to the stretching direction. It turns out that the degree of orientation of the nanorods is directly proportional to the degree of stretching of the film.

The second approach is proposed to obtain anisotropic metasurface by modifying thin metal layers using powerful linearly or circular polarized laser radiation. The method consists in spectral hole burning in the inhomogeneously broadened spectra of silver nanostructures. Under the action of laser radiation, resonant nanoparticles are heated and, depending on the intensity of heating, change their shape and/or size, and also lose mass due to evaporation.

Both methods lead to corresponding changes in the absorption spectra (Fig. 1). The measured extinction spectra (Fig. 1a) confirm that unstretched composite films have isotropic optical properties, since both longitudinal and transverse modes can be excited regardless of the polarization state of the incident light. This is due to the random orientation of the rods, which averages their individual anisotropy. Stretched films, on the other hand, are optically anisotropic at the macroscale due to the uniform orientation of metal nanorods caused by stretching so the longitudinal and transverse surface plasmon resonance modes can only be excited by light polarized parallel and perpendicular to the stretching axis of the film, respectively.

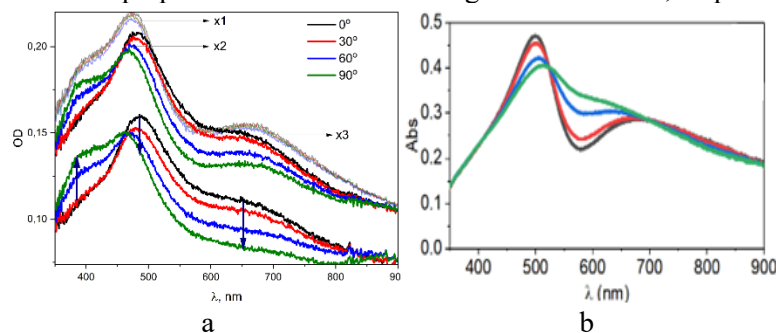


Fig. 1. Extinction spectra of silver nanorods in stretched polymer film (a) and irradiated granular silver film by 532 nm pulsed laser (b) in polarized light.

Laser irradiation of granular silver films also led to formation of metasurfaces with strong linear (Fig. 1b) or circular dichroism at the wavelengths close to laser wavelength depending on laser polarization. The action of polarized radiation on anisotropic particles depends not only on their size and shape, but also on their orientation. Therefore, the spectral dips after laser irradiation are not the same for different probe polarisation. The greatest changes are observed when the polarization of probe beam coincides with laser polarization. The study was supported by the Russian Science Foundation grant No. 21-72-10098, <https://rscf.ru/en/project/21-72-10098/>.

LM-I-16

Laser synthesis of linear carbon structures for develop of new optics devices

A. Kucherik¹, A. Osipov¹, V. Samyshkin¹, A. Abramov¹, A. Lelekova, A. Povolotskiy²

1 - Department of Physics and Applied Mathematics, Stoletov Vladimir State University, 600000 Gorkii street, Vladimir, Russia

*2 - Institute of Chemistry, St. Petersburg State University, 198504, Ulianovskaya str. 5, St. Petersburg, Russia
kucherik@vlsu.ru*

Carbon is one of the widespread materials having multiple allotropic forms. Carbon-based nanostructures include nanotubes, fullerenes, onion-structures, linear chains of carbon etc. The variety of nanostructured forms of carbon opens an opportunity to tailor electronic and optical properties of carbon-based devices for a variety of perspective applications. However, the mass production of nanostructured carbon for industrial applications would require technologies of controllable synthesis large volumes of specific carbon allotropes characterised by a high stability.

Here we study stable elongated carbon chains synthesized by the laser ablation technique in a colloidal solution [1]. The mechanical stabilisation of carbyne is achieved due to the electron bonding of carbon chains to gold nanoparticles (NPs) [2]. When deposited on a substrate, the stabilized chains demonstrate straight parts whose lengths significantly exceed the theoretical limit for a free stable monoatomic carbon chain. The high-resolution transmission electron microscopy (HR TEM) of our samples shows straight linear carbon chains of the lengths that sometimes exceed 5 nm. The time-resolved photoluminescence (TRPL) spectra show that the radiative life-time of the observed transitions is of the order of 1 ns, that is similar to the data reported for excitons in CNTs. The exciton radiative lifetime decreases with the decrease of the length of the chain. We refer to the Su-Schrieffer-Heeger model [3] to argue that the transition that dominates low temperature PL spectra is based on the edge electronic states that form the HOMO-LUMO pair in carbon chains stabilized by gold NPs.

The study was carried out using the equipment of the interregional multispecialty and interdisciplinary center for the collective usage of promising and competitive technologies in the areas of development and application in industry/mechanical engineering of domestic achievements in the field of nanotechnology (Agreement No. 075-15-2021-692 of August 5, 2021). This work was also partially supported by the framework of the state task of VISU FZUN-2020-0013 and RSF-grant 23-12-20004.

[1] A. Kucherik, S.M Arakelian et al Two-stage laser-induced synthesis of linear carbon chains, *Quantum Electronics* 46, 627 (2016).

[2] S. Kutrovskaya, I. Chestnov et al Electric field assisted alignment of monoatomic carbon chain, *Scientific Reports* 10(1) (2020)

[3] W. P. Su, J. R. Schrieffer, and A. J. Heeger, Solitons in polyacetylene, *Phys. Rev.Lett.* 42, 1698 (1979).



Intracellular trafficking using plasmon resonance in silver and gold nanoparticles with arbitrary shape

D.R. Dadadzhanov¹, N.S. Petrov¹, E.S. Smirnova¹, T.A. Vartanyan¹

*1- International Research and Educational Center for Physics of Nanostructures,
ITMO University, 49 Kronverksky pr., St. Petersburg 197101, Russia*

Email: daler.dadadzhanov@gmail.com

Silver and gold metal nanoparticles find widespread applications in various fields such as targeted drug delivery, photothermal and photodynamic cancer therapies, optical coherence tomography, immunoassays, and biosensing. Extensive research focuses on the use of nanoparticles to investigate physiological structures and cellular functions both in vitro and in vivo. The interest in metal nanoparticles stems from their unique optical and catalytic properties, which are influenced by the size and shape of the particles obtained [1]. The optical properties of metallic nanoparticles are determined by the excitation of localized surface plasmon resonance. This phenomenon occurs when electromagnetic radiation interacts with collective vibrations of conduction electrons within the nanoparticle. Understanding the impact of physicochemical properties such as shape, size, surface charge, surface chemistry, and cytotoxicity of nanoparticles on endocytosis, cell uptake, and cell survival is crucial for diagnosing and treating various disorders in living systems [2, 3]. The optical properties of silver and gold nanoparticles were investigated through experimental and numerical approaches with a focus on endocytosis. The experimental study examined the impact of nutrient medium (RPMI 1640 and dMEM) on gold and silver nanoparticles produced via pulsed laser ablation and chemical methods. It was observed that silver nanoparticles obtained through laser ablation displayed certain solubility and stability, whereas nanoparticles synthesized chemically with citric acid exhibited instability and were prone to aggregation, resulting in the loss of their characteristic plasmon resonance peak.

To simulate the vesicle formation during the endocytosis of plasmonic nanoparticles, a protein shell derived from bovine serum albumin (BSA) was utilized. The formation of the shell was validated by the displacement of the plasmon resonance towards longer wavelengths in comparison to pure nanoparticles, indicating the conjugation of the nanoparticle surface with the protein. In the case of silver nanoparticles obtained through both laser ablation and chemical methods, a maximum shift of 7 nm was observed, surpassing that of gold nanoparticles synthesized chemically (3 nm) or via laser ablation (5 nm). The experimental findings were further supported by numerically calculated results using COMSOL Multiphysics.

This work was supported by the Russian Science Foundation (Project 22-72-10057)

[1] Kelly K.L. et al. The optical properties of metal nanoparticles: The influence of size, shape, and dielectric environment // Journal of Physical Chemistry B. American Chemical Society, 2003. Vol. 107, № 3. P. 668–677.

[2] Ding L. et al. Size, Shape, and Protein Corona Determine Cellular Uptake and Removal Mechanisms of Gold Nanoparticles // Small. Wiley-VCH Verlag, 2018. Vol. 14, № 42.

[3] Kettler K. et al. Cellular uptake of nanoparticles as determined by particle properties, experimental conditions, and cell type // Environ Toxicol Chem. 2014. Vol. 33, № 3. P. 481–492.

LM-I-18**Structured optothermal traps****A. Mayorova, S. Kotova, N. Losevsky, S. Samagin, E Razueva***Lebedev Physical Institute, Samara Branch, 221, Novo-Sadovaya, Samara, 443011, Russian Federation**mayorovaal@smr.lebedev.ru*

Optothermal traps are an actively developing manipulation technique [1]. In such traps, a sharply focused laser beam not only creates optical power, but also forms a temperature gradient and, accordingly, convection currents, due to which the capture and movement of microobjects occurs. The advantages of optothermal traps are the ability to use lower laser radiation powers (from tenths to several tens of milliwatts) compared to optical traps and to effectively capture objects of various morphologies, shapes, and sizes (from nanometers to tens of micrometers) from relatively large distances.

The authors of [2] for the first time formed a structured optothermal trap in the shape of a light ring. We implemented optothermal traps of more complex shapes: triangle and square boundaries, Archimedes spiral, double contours, lattices of zeros, including those with a vortex component [3, 4]. The report demonstrates the capabilities of structured optothermal traps for the formation of various configurations of micron and submicron objects, their dynamic rearrangement and fixing objects on a substrate.

The scheme of the experimental setup included a DPSS laser with a wavelength of 0.53 μm , a spatial light modulator (SLM) HOLOEYE PLUTO-2-NIR-011, which forms a structured light beam. A microobjective (40x) focused the beam into a given plane, forming a structured (vortex) optical trap. The total observation power in the working area ranged from 10 mW to 100 mW. The convection component of the trap was formed by using an OC 13 light filter absorbing at a wavelength of 0.53 μm as the bottom of the cell with samples. As manipulation microobjects, we used latex microparticles from 2 to 6 μm , submicron silver particles, and yeast cells suspended in distilled water.

The capture of micro- and nano-objects in determined configurations, the movement of micro-objects along the boundaries of the light contour were demonstrated. It was found that the angular velocity of particles along light boundary of optothermal traps is significantly higher than in optical traps.

SLM provides the ability to change the configuration of the generated intensity distributions in a given plane in real time due to the rapid replacement of one phase mask supplied to the modulator for another. In this way, the configurations of captured ensembles of particles can also be rearranged. We also proposed a simple efficient method for fixing micro- and nanoobjects in a given configuration at the bottom of a cell by adding albumin to the cell with samples and briefly increasing the laser power. Typical power values were 60-130 mW depending on albumin concentration. The technique may be of interest for fixing objects of biological origin.

[1] P. Kollipara, Z. Chen, Y. Zheng, Optical Manipulation Heats up: Present and Future of Optothermal Manipulation, *ACS nano*, 17(8), pp. 7051-7063, (2023).

[2] E. Flores-Flores, S. Torres-Hurtado, R. Páez, U. Ruiz, G. Beltrán-Pérez, S. Neale, ... and R. Ramos-García, Trapping and manipulation of microparticles using laser-induced convection currents and photophoresis, *Biomedical optics express*, 6(10), 4079-4087, (2015).

[3] S. Kotova, A. Korobtsov, N. Losevsky, A. Mayorova and S. Samagin, Manipulation of microparticles using combined optical traps, *Journal of Quantitative Spectroscopy and Radiative Transfer*, 268, pp. 107641, (2021).

[4] S. Kotova, N. Losevsky, A. Mayorova, Y. Razueva, and S. Samagin, Structured Optothermal Traps, *Bulletin of the Russian Academy of Sciences: Physics*, 86(12), pp. 1434-1437, (2022).

LM-I-19

Machine learning and multiparametric investigation of laser ablation in liquid for the synthesis of nanoparticles

Vincenzo Amendola

University of Padova, Department of Chemical Sciences, Via Marzolo 1, 35131 Padova - ITALY

Main author email address: vincenzo.amendola@unipd.it

In recent years, laser ablation in liquid (LAL) made a whole library of nanomaterials available for integration in green emerging technologies.[1-3] However, the achievement of a specific type of nanocrystals by LAL has been until now a rather empirical endeavour based on changing synthesis parameters and characterizing the products. Here we started from the bibliographic analysis on LAL of Cu-based nanocrystals, to identify the relevant synthesis features and lead to the predetermination of the optimal conditions for producing Cu-based nanoparticles with defined copper oxidation state. First, single features and their combinations were screened by linear regression analysis to find the best correlation with experimental output and identify an equation for predicting LAL results. Then, machine learning algorithms were exploited to unravel cross correlations between features which are hidden to the linear regression analysis. This approach is of general applicability to any other nanomaterial and can help understanding the origin of the chemical pathways of nanomaterials generated by LAL, ultimately providing a rational guideline for the conscious predetermination of synthetic parameters toward the desired compounds.

[1] V. Amendola et al., Room-Temperature Laser Synthesis in Liquid of Oxide, Metal-Oxide Core-Shells, and Doped Oxide Nanoparticles, Chem. Eur. J., 26, 9206 – 9242 (2020).

[2] E.V. Barmina et al.; Laser ablation and fragmentation of Boron in liquids, Optics Laser Tech. 155, 108393 (2022).

[3] A.A. Popov, Z. Swiatkowska-Warkocka, S.M. Klimentov, T.E. Itina, A.V. Kabashin et al.; Laser-Ablative Synthesis of Ultrapure Magneto-Plasmonic Core-Satellite Nanocomposites for Biomedical Applications, Nanomaterials, 12, 649 (2022).

Precision laser technologies for optical instrumentation

V. Bessmetlsev, V. Korolkov, A. Dostovalov, S.A. Babin

IA&E SB RAS, Koptuyuga ave.1, 630090, Novosibirsk, Russia

Main author email address: victork@iae.nsk.su

The development of new laser technologies and equipment for its implementation is aimed not only at increasing the resolution and productivity of the micro-/nano-processing, but also at increasing an accuracy, including both spatial localization and compliance with a given degree of transformation of the processed material, given parameters. Over the past decades, the IA&E SB RAS has been developing areas of applied research related to the fundamental and engineering foundations of precision laser technologies focused on the problems of optical instrumentation.

To improve the quality and speed characteristics, a complementary scanning principle is used, in which a fast galvanoscanner with a short-focus lens and a small recording field is used to obtain a high scanning speed and a minimum point in focus, and a full recording field is obtained due to the precise movement of the microprocessing object and software-hardware docking fields.

The advent of pico- and femtosecond lasers with a high average power caused a sharp surge in research on the micromachining of various materials, including brittle ones, providing a new quality of processing. However, when trying to increase the productivity of processing at micron and more depths of micromachining by increasing the energy per pulse or the number of pulses in a pack, the resulting thermal and hydrodynamic effects significantly worsen roprocessing object and software-hardware docking fields.

For processing fragile materials, such as glass, quartz, semiconductor materials, raster scanning technologies have been developed within the contour of the zone of the removed material, which take into account the length of the processing line, the overlap of focused spots and the pulse energy. When forming deep microchannels to obtain high-quality walls, the direction of microchannel processing is taken into account. The technology used has made it possible to increase the productivity of micromachining of brittle materials by several times and improve the quality of processing. the quality of processing materials with low thermal conductivity and a tendency to form microcracks.

The technology of femtosecond laser modification of transparent materials makes it possible to perform precision surface micromachining of the surface of various optical elements, for example, to increase the transmission of nonlinear optical crystals with a high refractive index and high optical losses due to Fresnel reflection. We present the results on the development of antireflection microstructures on the surface of a GaSe crystal, demonstrating an increase in transmission from 65% to 80% in case of fs laser inscription of microstructures on one side and up to 94% in case of micromachining on both sides. Based on the surface profile of a single crater measured by atomic force microscopy, the transmission spectra for GaSe with the microstructures are numerically calculated that is in a good agreement with the experimental data.

The report also considered a technological complex created for piece and small-scale production of diffractive and micro-optical elements based on laser technologies in combination with vacuum-plasma technologies and optical methods of product control. The complex includes a system for magnetron sputtering of thin films, a circular laser system [1] for resistless thermochemical writing of microstructures on chromium films [2], an X-Y system [3] for laser lithography on a photoresist, reactive ion etching systems, optical profilometers and diffractometers. The experience of using this equipment for the manufacture of microstructured optical elements of various types is discussed.

The equipment of the Central Research Center "Spectroscopy and Optics" of the IA&E SB RAS and Core Facilities VTAN NSU were used in the research. The work was supported by the Russian Science Foundation grant (No. 21-72-20162).

[1] A.G. Poleshchuk, V.P. Korolkov, V.V. Cherkashin, S. Reichelt, and J. Burge "Polar-coordinate laser writing systems: error analysis of fabricated DOEs", Proc. SPIE 4440, pp. 161-172 (2001).

[2] V.P. Veiko, V.P. Korolkov, A.G. Poleshchuk, D.A. Sinev, E.A. Shakhno, Laser technologies in micro-optics. Part 1. Fabrication of diffractive optical elements and photo-masks with amplitude transmission, Optoelectronics, Instrumentation and Data Processing, vol. 53(5), pp. 474-483 (2017).

[3] <https://heidelberg-instruments.com/product/dwl-66-laser-lithography-system/>

LM-I-21

High-speed integrated optics on the base of fluorinated and composite polymer materials

V.I. Sokolov, V.Ya. Panchenko

*Federal Research Center «Crystallography and Photonics», Russian Academy of Sciences,
Moscow, Leninsky ave. 59*

email: visokol@rambler.ru

New optical materials on the base of amorphous fluorine-containing polymers are of great interest for integrated optics and photonics due to their high optical transparency, low refractive index, low index dispersion, chemical and environmental stability, manufacturability. We present the review of new results concerning synthesis of these materials using high-pressure (15 – 16 MPa) technique, development of advanced laser technologies for fabrication of various waveguide elements of integrated photonic circuits, new methods for measuring optical parameters of thin-film polymer light-guiding structures, which were realized in the Federal Research Center «Crystallography and Photonics» recently. These elements include multimode and single-mode polymer waveguides, splitters and directional couplers, waveguide Mach-Zhender interferometers, narrowband waveguide filters with submicron Bragg gratings, optical multiplexers and demultiplexers for DWDM optical fiber networks as well as high – speed optical bus on printed circuit board (PCB) for micro-processor computing systems, Fig. 1.

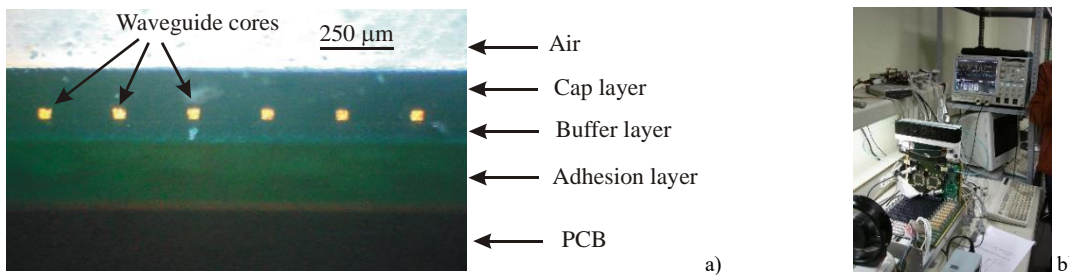


Fig. 1. Array of fluorinated polymer waveguides on PCB (a), electro-optical PCB with high-speed optical bus in computer frame (b).

We report also the results concerning development of active photonic devices: high – speed optical waveguide modulators based on fluorine-containing polymer with electrooptic chromophores in the side-chain, and compact optical waveguide amplifiers for telecommunication C – band 1530 – 1565 nm. The amplifiers include single-mode polymer waveguide with embedded fluorinated nanocrystals NaYF₄/Yb/Er/Ce possessing enhanced photoluminescence in down-conversion around 1550 nm when pumped by 980 nm laser diode, Fig. 2.

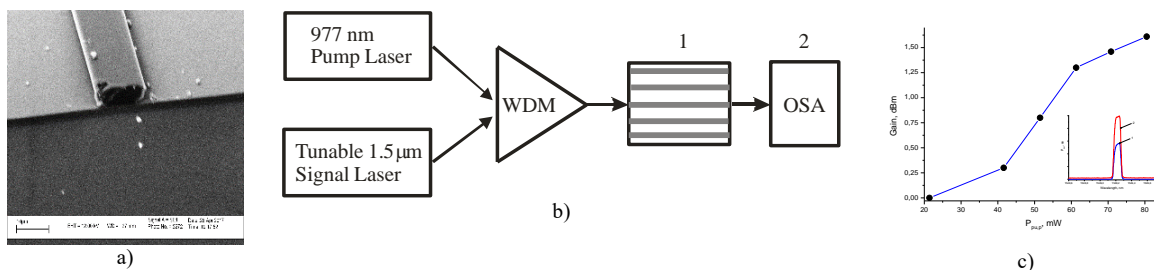


Fig. 2. SEM microphotograph of polymer waveguide with embedded NaYF₄/Yb/Er/Ce nanocrystals on Si/SiO₂ waver. Waveguide width is 8 μm (a). Scheme for measuring optical gain. WDM – wavelength division multiplexer, 1 – array of polymer waveguides, 2 - optical spectrum analyser (b). Gain coefficient in the waveguide amplifier of length $L = 12$ mm at $\lambda = 1535$ nm versus 980 nm pump power P_{pump} . The inset shows the input (1) and output (2) signal spectra at 1535 nm for pump power 85 mW.

The investigations were supported by the Russian Foundation for Basic Research.

LM-I-22

THz quantum cascade lasers with resonant two-photon design

**R.A. Khabibullin^{1,2,3*}, D.V. Ushakov⁴, A.A. Afonenko⁴, D.S. Ponomarev¹, M.A. Ladugin²,
A.A. Marmalyuk², S.V. Morozov⁵, V.I. Gavrilenko⁵**

1- V.G. Mokerov Institute of ultra-high frequency semiconductor electronics of RAS, Moscow, Russia

2- Moscow Institute of Physics and Technology, Dolgoprudny, Russia

3- Ioffe Institute, St. Petersburg, Russia

4- Belarusian State University, Minsk, Belarus

5- Institute for Physics of Microstructures of RAS, Nizhny Novgorod, Russia

khabibullin@isvch.ru

The scheme of laser transitions of the proposed two-photon design is based on five electron levels. This design works due to electron tunneling from the injector level 1' to the upper laser level 5, two sequential laser transitions (5 – 4 and 4 – 3) with an energy of 14.9 meV (3.6 THz) and depletion of the lower laser level 3 due to tunneling to the extractor level 2 and resonant emission of an optical phonon. In this case, the "intermediate" level 4 simultaneously plays the role of the lower laser level for the first optical transition and the upper laser level for the second optical transition. The operating voltage on one active module is close to the sum of two radiation energies and the energy of a longitudinal optical phonon $2 \cdot \hbar\omega_{\text{THz}} + \hbar\omega_{\text{LO}}$.

An optimized two-photon design was developed using the balanced equation method [1,2] and grown by MOVPE technique with 10 μm active region thickness. The fabricated QCLs with Au-Au double metal waveguide based on grown structures show an excellent growth robustness, as all MOVPE-grown structures (6 wafers) demonstrate laser generation. The maximum operation temperatures of fabricated lasers are equal to 90-100 K. The light-current characteristics have two shoulders in the experimental curves (see Fig. 1), which corresponds to the two-photon nature of the proposed design. The fabricated QCLs have a lasing frequency of 3.6 THz (see Fig. 2), which completely coincides with the target frequency. At high currents the generation shifts to 3.7 THz. This effect can be explained by increasing the energy separation between lasing levels 5-4 (the first THz photon) at high electric fields.

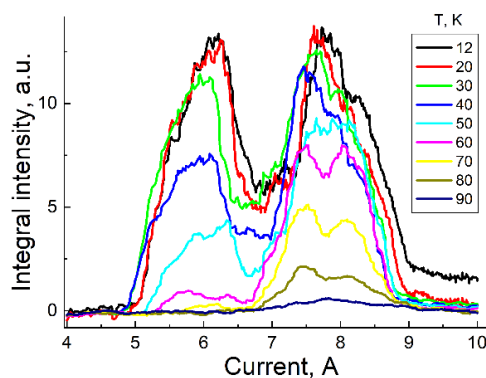


Fig. 1. Pulsed current-voltage and light-current characteristics of MOVPE-grown THz QCLs with two-photon design.

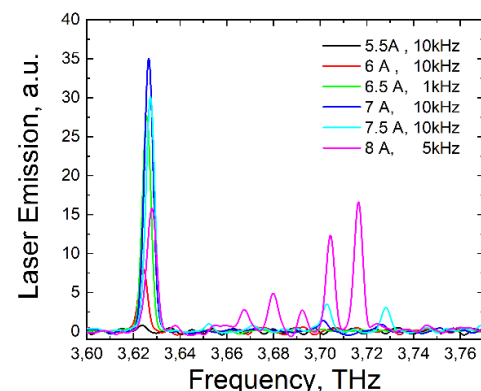


Fig. 2. Emission spectra of MOVPE-grown THz QCLs with two-photon design.

This study was partially supported by the Russian Science Foundation project no. 21-72-30020 and the Ministry of Science and Higher Education of the Russian Federation in the scope of the government assignment (Agreement 075-03-2023-106 13.01.2023).

[1] D. V. Ushakov, A. A. Afonenko, A. A. Dubinov, V. I. Gavrilenko, O. Yu. Volkov, N. V. Shchavruk, D. S. Ponomarev, R. A. Khabibullin, "Balance-equation method for simulating terahertz quantum-cascade lasers using a wave-function basis with reduced dipole moments of tunnel-coupled states," *Quantum Electronics*, vol. 49, pp. 913–918, (2019).

[2] D. Ushakov, A. Afonenko, R. Khabibullin, D. Ponomarev, V. Aleshkin, S. Morozov, A. Dubinov, "HgCdTe-based quantum cascade lasers operating in the GaAs phonon Reststrahlen band predicted by the balance equation method," *Opt. Express*, vol. 28, pp. 25371–25382, (2020).



LM-I-23

Holographic security signs based on LIPSS: physics and technology

V.P Veiko, M.K. Moskvina, E.V. Prokofiev, G.V Odintsova

*ITMO University, St. Petersburg, Russia
vadim.veiko@mail.ru*

Holographic security signs are an integral part of many industrial sectors, serving the purpose of protecting products against counterfeiting. However, the problem of counterfeiting is always relevant and requires improvement of protection methods. To effectively counter counterfeiters, the methods of protection must be ahead of the curve, anticipating fraudulent techniques and adapting to evolving technologies and counterfeit strategies. As the development progresses, the problem of creating security signs on products not only remains unresolved but also advances into the high technologies. This is because simple solutions are being circumvented and counterfeited through various methods. In terms of protective diffraction signs, computer calculation methods allow us to determine the necessary reliefs for the implementation of optical effects: both shape and color, kinematics, etc. However, there is a problem to achieve efficient writing that would enable to integrate all known identification features and new technical solutions into a single sign. These issues are addressed in detail in this report. The aim was to investigate the feasibility of creating high-quality holographic security signs by laser-induced periodic surface structures (LIPSS). The physical peculiarities of the LIPSS formation method and its application for creation of holographic protective signs of different degrees of complexity are discussed. Additionally, this work presents a set of visual security features for holographic signs implemented by LIPSS.

The base of realization of holographic security signs is the diffraction of white light on the LIPSS matrix with different spatial directions. A new method is presented that makes it possible to achieve control by the orientation of the LIPSS by coordinated dynamic changes in direction and type polarization with the scanning trajectory of the laser beam. Coordinated parameter adjustments allow the formation of complex diffraction grating configurations. This method opens new possibilities for the direct laser writing of holographic protective signs, on metal products ensuring durability, visual appeal, and function.

LM-I-25

Photovoltaic tweezers on the base of diffusion structures LiNbO₃:Cu**S. Shandarov¹, A. Kolmakov¹, R. Anisimov¹, A. Temereva¹, K. Mambetova¹, E. Komov¹***1- Tomsk State University of Control Systems and Radioelectronics, 40 Lenin Avenue, Tomsk 634050, Russia**stanislavshandarov@gmail.com*

Strong inhomogeneous evanescent electric fields generated above the surface of lithium niobate crystals due to photovoltaic effect are successfully used to realization of optical tweezers [1,2]. The advantages of photovoltaic tweezers over the other optical manipulators consist of possibility for repeated using of mono-crystal substrates as well as in minimization of an overheating for captured objects at the expense of application the low-power radiation [3]. The lithium niobate crystals doped by photovoltaic impurities such as Fe [1,3] and Cu [2] are usually used in the capacity of substrate for the photovoltaic manipulation of nanoparticles. The surface character of evanescent electric fields used for realization of photovoltaic tweezers makes it attractive to apply diffusion doping of lithium niobate substrate by photovoltaic impurities [2,4].

In this work we present the results of experimental realization of the technology of diffusion doping of X- and Z-cut congruent lithium niobate crystals by copper and the results of studying their photorefractive and photovoltaic properties, which determine the effectivity of aggregation of dielectric nanoparticles on the surface of the fabricated LiNbO₃:Cu samples. The process of copper diffusion into the substrates involved deposition of the Cu films with thickness of 400 nm on the related polished surface by thermal evaporation in a vacuum. The diffusion carried out at temperatures of 1000 °C and 600 °C for the samples with X- and Z-orientation respectively during the time from 5 h to 9 h.

To obtain the concentration distribution for copper ions existing in the LiNbO₃ lattice in Cu⁺ and Cu²⁺ charge states the dependences of absorption coefficients on the depth from the X- and Z-surfaces for the light with the wavelengths of 532 and 808 nm respectively were experimentally investigated. It was established that these dependences characterized by nonmonotonic behavior. In addition, the positions of maxima for concentration of Cu⁺ and Cu²⁺ might be differ. Because of that, we have theoretically considered the formation of dynamic photorefractive gratings by a high-contrast interference pattern of writing laser beams in an X-cut plate of LiNbO₃:Cu crystal with two different gaussian distributions for concentration of Cu⁺ and Cu²⁺ ions on the base of approach described in Ref. 4. The theoretical modeling for distribution of electric field of the photorefractive dynamic hologram on the depth from the X-surface in the crystal as well as of an evanescent field above the one is performed.

The experimental study of time evolution for diffraction effectivity of dynamic photorefractive holograms in the LiNbO₃:Cu crystal allow us to estimate of Glass constant of diffusion layer for laser wavelength of 532 nm as well as to determine the optimal conditions for aggregation of dielectric nanoparticle on its surface.

This study was funded by the Ministry of Science and Higher Education of the Russian Federation in the framework of the state assignment for 2023-2025 (job-order FEWM-2023-0012).

[1] J. Villarroel, H. Burgos, Á. García-Cabañes, M. Carrascosa, A. Blázquez-Castro A., and F. Agulló-López, Photovoltaic versus optical tweezers, *Opt. Express*, vol. 19, pp. 24320-24330 (2011).

[2] K.M. Mambetova, S.M. Shandarov, A.I. Tatyannikov, and S.V. Smirnov, Aggregation of dielectric nanoparticles on the X-cut of LiNbO₃ crystal by electric field of photorefractive holograms, *Russian Physics Journal*, vol. 62, pp. 658-663, (2019).

[3] A. Blázquez-Castro, A. García-Cabañes, M. Carrascosa, Biological applications of ferroelectric materials, *Appl. Phys. Rev.*, vol. 5, pp. 041101 (2018).

[4] K.M. Mambetova, S.M. Shandarov, L.N. Orlikov, S.I. Arestov, S.V. Smirnov, L.Ya. Serebrennikov, and V.A. Krakovskii, Formation of dynamic photorefractive gratings in a LiNbO₃:Cu surface-doped crystal, *Optics and Spectroscopy*, vol. 126, pp. 781-786 (2019).

LM-I-26

Promising phase-changing materials for neuromorphic devices and memory elements

A.V. Kiselev, A.A. Burtsev, V.V. Ionin, N.N. Eliseev, A.A. Nevzorov, V.A. Mikhalevsky,

A.A. Lotin

ILIT RAS — Branch of FSRC “Crystallography and Photonics” RAS, 1, Svyatoozerskaya Str., 140700, Shatura, Moscow Region, Russia

Main author email address: lotin_82@mail.ru

Non-volatile photonic memory and neuro-inspired computing are promising technologies that can enhance data storage and processing capabilities [1]. Photonic memory devices offer high operational speed and non-volatility, while neuro-inspired computing integrates processing and storage into a single cell [2]. Phase-change photonics is the conjunction between phase-change materials (PCMs) and nanophononics, which enables integrated photonic circuits (PICs) with novel functionalities [3]. Chalcogenide alloys based on germanium telluride (GeTe, Ge₂Sb₂Te₅) are the most mature and widely used materials for optical data storage and electric non-volatile memory devices. These alloys have rapid amorphization and crystallization rates, along with a distinct property contrast between their crystalline and amorphous phases [4].

The research presented in this study demonstrates stable multilevel reversible phase transitions in thin films of chalcogenide alloys, as well as an optical synapse prototype based on a planar waveguide with a chalcogenide cell [5]. The optical transmission and reflection coefficients of Ge₂Sb₂Te₅ (GST) thin films, which change dynamics during nano- and femtosecond laser radiation-induced phase transitions, are studied. The authors propose a predictive model based on the thermokinetic approach, which allows the qualitative and quantitative determination of the of the crystalline phase and the depth of its occurrence in the GST film [6]. Experimental methods including Raman spectra, XRD and TEM were used to validate the model. The modelling and experimental results can be used to optimize the duration, shape and spatial distribution of laser pulses to control the state of PCM-based devices.

- [1] W. Zhang, R. Mazzarello, M. Wuttig and E. Ma. Designing crystallization in phase-change materials for universal memory and neuro-inspired computing. *Nature Reviews Materials*, 4, pp. 150–168 (2019).
- [2] M. Wuttig, H. Bhaskaran, & T. Taubner, T. Phase-change materials for non-volatile photonic applications. *Nature photonics*, 11, 8, 465-476 (2017)
- [3] F. Brücknerhoff-Plückelmann, J. Feldmann, C.D Wright, H. Bhaskaran, & W.H. Pernice (2021). Chalcogenide phase-change devices for neuromorphic photonic computing. *Journal of Applied Physics*, 129, 151103 (2021)
- [4] P. Guo, A. M. Sarangan and I. Agha. A Review of Germanium-Antimony-Telluride Phase Change Materials for Non-Volatile Memories and Optical Modulators. *Applied Sciences*. 9, 3, 530 (2019).
- [5] V. V. Ionin, A. V. Kiselev, N. N. Eliseev, V. A. Mikhalevsky, M. A. Pankov, A. A. Lotin, Multi-level reversible laser-induced phase transitions in GeTe thin films. *Applied Physics Letters*, 117, 011901 (2020).
- [6] A.A. Nevzorov, V.A. Mikhalevsky, A.V. Kiselev, A.A. Burtsev, N.N. Eliseev, V.V. Ionin, & A.A. Lotin. Controlling optical properties of GST thin films by ultrashort laser pulses series impact. *Optical Materials*, 141, 113925 (2023)

LM-O-1

Modeling of laser fragmentation of nanoparticles as wave process**P. S. Kuleshov^{1,2}, E. V. Barmina³, G. A. Shafeev³***1-P. I. Baranov Central Institute of Aviation Motors, Russia**2-Moscow Institute of Physics and Technology, Russia**3-Prokhorov General Physics Institute, Russian Academy of Sciences, Russia**barminaev@gmail.com*

In this presentation we would like to familiarize our colleagues with current investigations of the development of NPs laser fragmentation model based on the theory of wave processes in soft matter. It is suggested that laser fragmentation of metallic nanoparticles in liquids leads to decrease of their size due to formation of capillary waves on the molten nanoparticle and their further interference with deformation waves. The dependencies of the size of secondary clusters and the degree of their size dispersion on the size of the initial nanoparticles are proposed. A minimal size of the initial particle which can be dispersed is determined. The necessary conditions for particle dispersion are formulated. The values of the most probable sizes of fragmentation particles and the dispersion of their size distributions are analytically obtained [1]. Experimental data on laser fragmentation of Au and Al [2,3] nanoparticles are corroborated by the derived model.

We thank our industrial partner Pokkels LLC for providing innovative technical solutions.

[1] P. S. Kuleshov and V. D. Kobtsev, Distribution of aluminum clusters and their ignition in air during dispersion of aluminum nanoparticles in a shock wave, *Combustion, Explosion, and Shock Waves*, vol. 56(5), pp. 566-575, (2020).

[2] N. A. Kirichenko, I. A. Sukhov, G. A. Shafeev and M. E. Shcherbina, Evolution of the distribution function of Au nanoparticles in a liquid under the action of laser radiation, *Quantum Electronics*, vol. 42(2), p. 175, (2012).

[3] V.V. Smirnov, M.I. Zhilnikova, E.V. Barmina, G.A. Shafeev, V. D. Kobtsev, S. A. Kostitsa and S. M. Pridvorova, *Chemical Physics Letters*, vol. 763, p. 138211, (2021).



Laser ablation and fragmentation of nanoparticles in liquid, electrostatic and magnetic fields

A. Chernikov, D. Kochuev, A. Voznesenskaya, R. Chkalov, D. Abramov, K. Khorkov

Institute of Applied Mathematics, Physics and Computer Science, Vladimir State University, Gorky Street, 87, 600000, Vladimir, Russia

email address: khorkov@vlsu.ru

In this paper we present the results of various techniques for laser ablation and fragmentation of nanoparticles. Ablative synthesis was carried out on the developed experimental stands using liquid and gas media. During ablation in liquid media, the materials obtained were in the state of colloidal solutions. At the end of the ablation process, the target was removed from the resulting solution. If necessary, nanoparticles were selected, as well as fragmentation of the resulting material to achieve the necessary properties of the colloidal system (particle dispersion, chemical and phase composition) [1,2].

Materials obtained during ablation in a gas medium were deposited on the surface of the substrates under the action of an electrostatic or magnetic field [3]. To change the chemical composition of the compounds obtained, or to preserve the state of the initial substance, appropriate gas media were used, including with different percentages. The obtained nanoparticles MoS₂, WS₂, ZnS, ZnSe, Al₂O₃, Ti, Fe, Fe₂O₃ were analyzed using electron microscopy, Raman spectroscopy, X-ray diffraction analysis and other methods.

The experiments were carried out on a laser robotic complex based on the Yb:KGW femtosecond laser system (Avesta Ltd.), generating pulses with a duration of 280 fs at a wavelength of 1030 nm with a repetition frequency of 10 kHz and a maximum pulse energy of 150 μJ. This complex has a modular structure, which allows the use of various additional nodes included in the optical schemes of exposure and processing of materials by femtosecond laser radiation.

A complex of studies of the physicochemical properties of nanoparticles allowed us to evaluate their characteristics such as shape and size, morphology and surface composition. The optical properties of the obtained colloidal solutions were investigated by spectrophotometry. The obtained data are necessary to make a decision on the most appropriate ways of using nanoparticles and possible adjustment of the parameters of the method of production. Schemes for photothermal response of synthesized colloidal solutions have been developed. The dependences of temperature change on time during irradiation of colloidal solutions, as well as the change in the transmission of laser radiation by colloidal solutions during irradiation are presented.

The study of the processes of formation of nanoparticles was carried out at the expense of the grant of the Russian Science Foundation No. 22-79-10348. Preparation and analysis of samples was carried out within the framework of the state assignment of the Ministry of Science and Higher Education of the Russian Federation, subject FZUN-2020-0013.

[1] Kurilova, U.E., Chernikov A.S., Kochuev D.A. et al., Physical and Biological Properties of Layers with Nanoparticles Based on Metal Chalcogenides and Titanium Synthesized by Femtosecond Laser Ablation and Fragmentation in Liquid, *Journal of Biomedical Photonics & Engineering*, vol., 9(2), 020301, (2023)

[2] Chernikov A.S., Tselikov G.I., Gubin M.Y. et al. Tunable optical properties of transition metal dichalcogenide nanoparticles synthesized by femtosecond laser ablation and fragmentation, *Journal of Materials Chemistry C*, vol. 11(10), pp. 3493-3503 (2023).

[3] Chernikov A.S., Kochuev D.A., Voznesenskaya A.A. et al. Synthesis of spherical zinc sulfide nanoparticles produced by femtosecond laser ablation and deposited on a silicon substrate under the action of an electrostatic field, *Journal of Physics: Conference Series*, vol. 2077(1), 012002 (2021).



LM-O-3

Advanced optical manipulation with structured laser beams

A. Porfirev^{1,2}, S. Khonina^{1,2}, D. Porfirev^{1,2}, S. Karpeev^{1,2}

1- Samara National Research University, Samara, Russia

2- Image Processing Systems Institute of RAS—Branch of the FSRC “Crystallography and Photonics” RAS, Samara, Russia

porfirev.alexey@gmail.com

Now structured laser beams with predetermined intensity, phase, and/or polarization distributions are widely used for implementation of holographic optical tweezers (HOTs) - modifications of the conventional optical tweezers, for the invention of which Ashkin was awarded the Nobel Prize in Physics in 2018. The OT is an all-optical technology that allows one to three-dimensionally confine and guide nano- and microscale objects trapped at the focus of a laser Gaussian beam. HOTs made it possible to shape complex optical traps and allow one not only to carry out parallel trapping of a set of micro-objects [1] but also to carry out such types of optical non-contact manipulation as the rotation of micro-objects [2], moving them along the desired complex three-dimensional trajectories [3], as well as moving along linear trajectories in the direction of the laser source, i.e. allow realizing simple forms of pulling(tractor) laser beams [4]. It is the inhomogeneous structure of the intensity, phase, or polarization of such optical traps that makes it possible to carry out such types of manipulation.

Here, we proposed new techniques for shaping of structured laser beams with the desired two and three-dimensional structure of the intensity distribution. The techniques are based on the use of classical and diffractive optical elements. The shaped multiple optical traps, polygon laser beams, and clusters of rotating beams with autofocusing and transformation properties were used for demonstration of simultaneous trapping of multiple (up to a thousand) light-absorbing particles in air (see Figs. 1 and 2). The trapping of such particles is possible due to the so-called photophoretic (PP) forces pushing the trapped strongly absorbing particles away from areas of relatively high intensity [5]. The demonstrated HOTs do not require an active control of location or orientation of the generated optical traps for implementation of multiple laser trapping and guiding of the particles. Only a control of the initial power of the laser source generating optical traps is used in some cases. The proposed HOTs can be used for solving of the problem of passive all-optical sorting of airborne particles and their guiding along curvilinear trajectories. This work was supported by the Russian Science Foundation grant No. 22-12-00041.

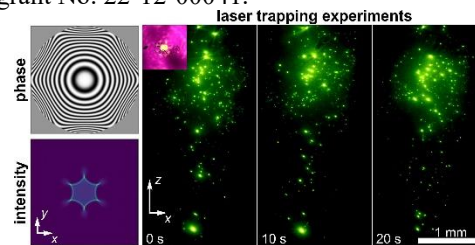


Figure 1. Laser trapping of multiple light-absorbing particles in air with a polygonal laser beam.

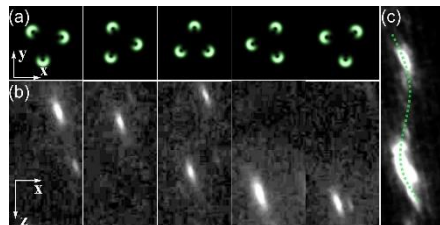


Figure 2. Laser guiding of a light-absorbing particle in air with a rotating laser beam: (a) transverse intensity distributions of the beam, (b) motion stages of the guided particle, (c) particle trajectory.

[1] D. G. Grier, A revolution in optical manipulation, *Nature*, vol. 424, pp. 810-816 (2003).

[2] M. Padgett, R. Bowman, Tweezers with a twist, *Nat. Photonics*, vol. 5, pp. 343 (2011).

[3] J.A. Rodrigo and T. Alieva, Freestyle 3D laser traps: tools for studying light-driven particle dynamics and beyond, *Optica*, vol. 2, pp. 812-815 (2015).

[4] S. Sukhov and A. Dogariu, Negative nonconservative forces: optical “tractor beams” for arbitrary objects, *Phys. Rev. Lett.*, vol. 107, pp. 203602 (2011).

[5] H. Horvath, “Photophoresis-a forgotten force?” *KONA Powder Part. J.*, vol. 31, pp. 181–199 (2014).

LM-O-4

Structured laser beams for polarization-sensitive laser material processing

S. Khonina¹, N. Ivliev¹, S. Syubaev², A. Porfirev¹

1- Image Processing Systems Institute of RAS—Branch of the FSRC “Crystallography and Photonics” RAS, Samara, Russia

2- Far Eastern Federal University, Vladivostok, Russia

khonina@ipsiras.ru

After their first demonstration sixty years ago, lasers were envisaged to be ideal tools for material processing. In 1967, Peter Houldcroft demonstrated the first experiments in gas-assisted laser cutting with a 300W CO₂ gas laser. Since that, a lot of progress in the development and commercialization of laser material processing systems has been achieved, especially regarding the thickness of the processed samples and the processing velocity. Currently, structured laser beams are increasingly used for material processing. Structured laser beams are known as spatially amplitude, phase, and polarization modulated laser radiation shaped with the help of classical optical elements, diffractive optical elements, metasurfaces, or structured screens [1]. These laser beams make it possible to control the morphology of structures formed on the surface and in the volume of materials both at the nano- and micro-levels. For example, polarization makes it possible to set the orientation of laser-induced periodic surface structures (LIPSSs) [2]. Even more opportunities arise when using structured laser radiation in the processing of polarization-sensitive materials, such as various azopolymers and chalcogenide glasses (CGs) [3]. Multilayer structures based on CGs and azopolymers are promising optically sensitive materials used for dynamic systems of optical conversion and signal transmission, data recording, and storage. Such materials are able to change their structure under the influence of illuminating laser radiation - not only depending on the amplitude but also the polarization of the radiation. Recent studies have shown the high sensitivity of such materials to both transverse and longitudinal components of the light field. Their joint consideration should provide an unprecedented level of control over the profiles of nano- and microstructures formed in polymers, which is necessary for the creation of various elements of planar and three-dimensional micro-optics and components of nanophotonics. Here we demonstrate some examples of laser processing of thin metal and polymer films with vector laser beams with the predetermined polarization distributions (see Fig. 1). We use laser beams shaped with the help of such elements as *q*-plates of different orders and depolarizers. In addition, we demonstrate polarization-sensitive direct laser patterning of azopolymer thin films with vortex beams and the realization of spiral-shaped mass transfer. This work was financially supported by Russian Science Foundation (grant No. 21-79-20075).

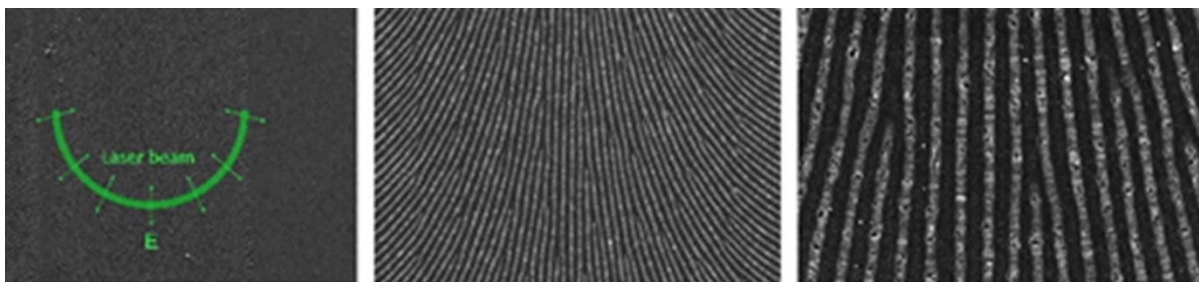


Figure 1. LIPSSs with radial symmetry formed on the surface of titanium films using cylindrically polarized laser beams with an intensity distribution in the form of a semicircle.

[1] A. Forbes, M. de Oliveira, M. R. Dennis, Structured light, *Nat. Photonics*, vol. 15, pp. 253-262 (2021).

[2] W. H. Duff and L. V. Zhigilei, Computational study of cooling rates and recrystallization kinetics in short pulse laser quenching of metal targets, *J. Phys.: Conference Series*, vol. 59, pp. 413 (2007).

[3] Z. Sekkat, S. Kawata, Laser nanofabrication in photoresists and azopolymers, *Laser Photon. Rev.*, vol. 8, pp. 1–26 (2014).

LM-O-5

Femtosecond pulses inscription of fiber Bragg gratings with phase shift by motion velocity modulation

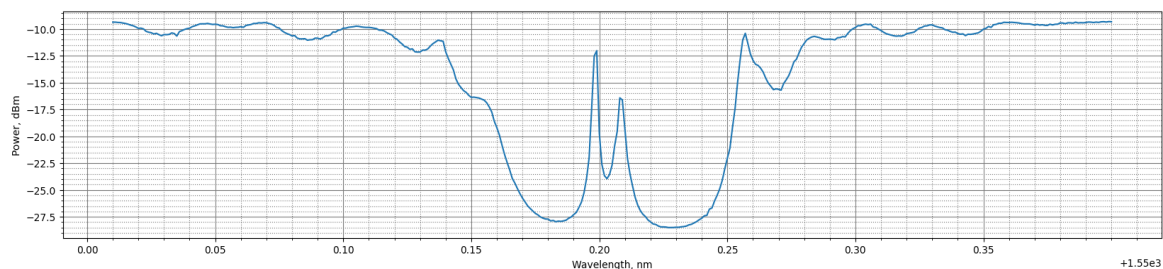
A. Shikin¹, A. Smirnov¹, O. Butov¹

*1- Kotelnikov Institute of Radioengineering and Electronics, Russian Academy of Sciences, 11-7 Mokhovaya St., Moscow 125009, Russia
artem.shikin@phystech.edu*

Single-frequency fiber lasers are important for modern sensorics and optical telecommunications [1-3]. One of the ways to create such device is to fabricate a Bragg grating, containing a phase shift. When phase shift is equal to integer number of light waves plus one half, it favors to generation single longitudinal mode with. [4-6]. This results in a low level of phase noise and a narrow emission spectrum.

FBG can be fabricated either by UV-light or femtosecond laser pulses. To form a phase shift, one needs to modify existing set-up or to do special post-processing. The latter usually demonstrates poor precision and therefore fabrication of phase shift simultaneous with inscription is preferred. Mask-based processes require careful design of the mask and limited to mask parameters [7]. Though some attempts to overcome this problem were made. Femtosecond point-by-point inscription is more flexible. To form a phase shift using additional piezo-positioner was suggested. Alternative way was to control the shutter of acousto-optic modulator [8,9]. Both methods have good precision in single-pass mode, but struggle in multi-pass.

We demonstrate fabrication of phase-shift in controllable manner by modulating nanopositioner velocity. In combination with technology of synchronization with oscillator firing [10] it allows to fabricate FBG with phase shifts in multi-pass mode. We also present FBG with π -shift in erbium-doped fiber. A laser based on this resonator demonstrates linewidth less than 1 kHz.



- [1] V. Mizrahi, D. J. DiGiovanni, R. M. Atkins, S. G. Grubb, Y.-K. Park, and J.-M. Delavaux, *J. Lightwave Technol.* 11(12), 2021–2025 (1993).
- [2] V. Stepanov, A. A. Zhirmov, O. Chernutsky, K. I. Koshelev, A. B. Pnev, A. I. Lopunov, and O. V. Butov, *Sensors* 20(22), 6431 (2020).
- [3] V. Yatseev, A. Zotov, and O. Butov, *Results Phys.* 19, 103485 (2020).
- [4] N. Groothoff, J. Canning, T. Ryan, K. Lyytikainen, and H. Inglis, *Opt. Express* 13(8), 2924–2930 (2005).
- [5] W. Loh and R. Laming, *Electron. Lett.* 31(17), 1440–1442 (1995).
- [6] O. V. Butov, A. A. Rybaltovskiy, M. Y. Vyatkin, A. Bazakutsa, S. Popov, Y. K. Chamorovskiy, and K. M. Golant, 2017 Progress In Electromagnetics Research Symposium-Spring (PIERS), 1594–1597 (2017).
- [7] Gribaev, A. I., Pavlishin, et al., *Optical and Quantum Electronics*, 48, 1 (2016).
- [8] Burgmeier, J., Waltermann, C., Flachenecker, G., and Schade, W., *Optics Letters*, 39 (3), 540 (2014)
- [9] Wolf, A., Dostovalov, et al., *Optics Laser Technology*, 101, 202 (2018)
- [10] Przhiialkovskii, D. V. and Butov, O. V., *Results in Physics*, 30, 104902 (2021)

Optical nanosensing enabled by advanced laser technologies

Yu. Borodaenko¹, V. Puzikov¹, S. Khonina², A. Porfirev², A. Kuchmizhak^{1,3}

1- Institute of Automation and Control Processes, Far Eastern Branch, Russian Academy of Science, 5 Radio Str., Vladivostok 690041, Russia

2- Image Processing Systems Institute of RAS – Branch of the FSRC “Crystallography and Photonics” RAS, Samara, Russia

3- Pacific Quantum Center, Far Eastern Federal University, Vladivostok, Russia

alex.iacp.dvo@mail.ru

Resonant coupling of optical radiation to specially designed nanostructures provides multiple pathways for realization of diverse chemo- and biosensors pushing forward development of highly productive and advanced fabrication technologies. Applications direct laser-assisted technologies for production of such functional nanostructures allows to addresses modern demands regarding morphology/composition controllability and fabrication yield. At the same time, fabrication of rationally designed hybrid nanostructures made of dissimilar materials such as typical plasmon-active metals and low-loss semiconductors is still challenging. Here, we summarize our recent efforts in production of such metal-semiconductor nanostructures using two promising laser-assisted fabrication strategies: laser-induced period surface structuring (LIPSS) in functionalizing solutions and laser ablation in liquids (LAL). In particular, LIPSS patterning of monocrystalline Si with a visible-range femtosecond-laser pulses in isopropanol containing precursor noble-metal salts was found to yield in formation of deep-subwavelength nanograting with an extremely short period down to 70 nm and high-aspect-ratio nano-trenches loaded with controllable amount of plasmonic nanoparticles [1]. In its turn, LAL technology with inexpensive nanosecond lasers was used to produce diverse hybrid Au@Si [2], Ag@Si [3] and Au@TiO₂ [4] nanoparticles. Certain applications of the produced hybrid nanostructures for advanced optical nanosensing of molecular species and metal ions, light-to-heat conversion and labeling are also discussed [5].

This work was partially supported by Russian Science Foundation (grant. 21-79-20075)

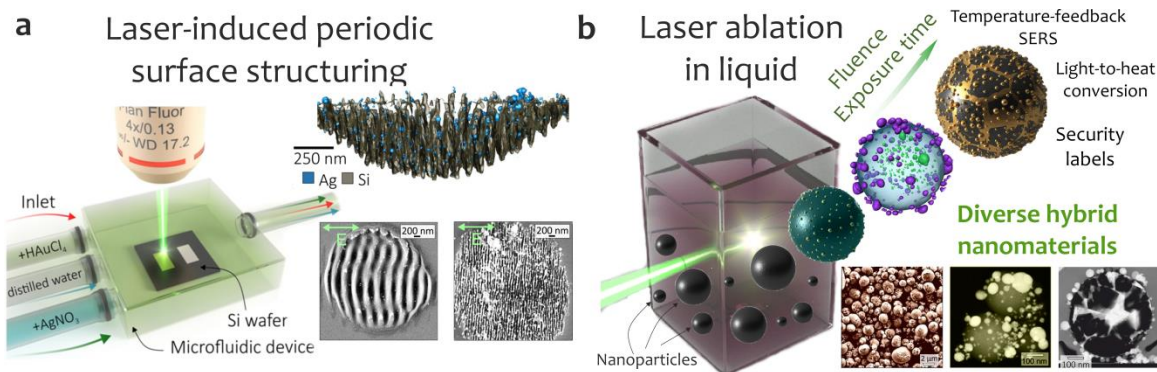


Fig .1. Schematically illustrated advanced laser technologies used for production of hybrid metal-semiconductor nanostructures: (a) laser-induced period surface structuring (LIPSS) in functionalizing solutions and (b) Laser ablation in liquids.

[1] Y. Borodaenko, S. Syubaev, E. Khairullina, I. Tumkin, S. Gurbatov, A. Mironenko, E. Mitsai, A. Zhizhchenko, E. Modin, E. L. Gurevich, A.A. Kuchmizhak. On-Demand Plasmon Nanoparticle-Embedded Laser-Induced Periodic Surface Structures (LIPSSs) on Silicon for Optical Nanosensing. *Advanced Optical Materials* vol. 10, 2201094 (2022).

[2] S. Gurbatov, V. Puzikov, D. Storozhenko, E. Modin, E. Mitsai, A. Cherepakhin, A. Shevlyagin, A.V. Gerasimenko, S.A. Kulinich, A. Kuchmizhak, Multigram-Scale Production of Hybrid Au-Si Nanomaterial by Laser Ablation in Liquid (LAL) for Temperature-Feedback Optical Nanosensing, Light-to-Heat Conversion, and Anticounterfeit Labeling, *ACS Applied Materials & Interfaces* vol. 15, 3336–3347 (2023)

[3] Ag-Decorated Si Microspheres Produced by Laser Ablation in Liquid: All-in-One Temperature-Feedback SERS-Based Platform for Nanosensing. S. Gurbatov, V. Puzikov, E. Modin, A. Shevlyagin, A. Gerasimenko, E. Mitsai, S.A. Kulinich, A. Kuchmizhak. *Materials* vol. 15, 8091 (2022).

[4] S.O. Gurbatov, E. Modin, V. Puzikov, P. Tonkaev, D. Storozhenko, A. Sergeev, N. Mintcheva, S. Yamaguchi, N.N. Tarasenko, A. Chuvilin, S. Makarov, S.A. Kulinich, A. A Kuchmizhak, Black Au-Decorated TiO₂ Produced via Laser Ablation in Liquid, *ACS Applied Materials & Interfaces*, vol. 13, 6522–6531 (2021).

[5] A Laser-Printed Surface-Enhanced Photoluminescence Sensor for the Sub-Nanomolar Optical Detection of Mercury in Water. Y. Borodaenko, S. Gurbatov, E. Modin, A. Chepak, M. Tutov, A. Mironenko, A. Kuchmizhak. *Chemosensors* vol. 11, 307 (2023).



LM-O-7

Laser-induced processes in lithium battery materials, studied by micro-Raman spectroscopy

D. Pelegov, A. Ryabin, A. Nikiforov

Ural Federal University, 19 Mira street, Ekaterinburg, 620002, Russian Federation

Main author email address: dmitry.pelegov@urfu.com

Today, lithium battery market is a crucial element for three major industries: automotive, portable electronics and energy generation/distribution. The fast-growing popularity of electric vehicles, renewables, and smart grids resulted in the boom of lithium battery gigafactories all around the world, raising the question of proper quality control tools ensuring the desired quality of the produced products at newly established production lines. Raman Spectroscopy is an industry-friendly, prompt, and inexpensive method to control the quality of various lithium battery materials. But since Raman spectroscopy uses laser irradiation and in the most cases the laser beam is focused on the spot with a sub-micron diameter, the study of laser-induced processes became of the great value.

In this work the laser-induced degradation for main electrode materials is reviewed in brief and discussed in details for LiFePO_4 (LFP) [1] and Mn-doped $\text{Li}_4\text{Ti}_5\text{O}_{12}$ (Mn-LTO) [2]. For popular cathode material LFP we have revealed the variation of the decomposition pathways and products. For anode material Mn-LTO we report about fast and slow induced degradation processes, and laser ablation of degradation processes (Fig. 1). The obtained results let us to conclude about non-thermal amorphization and melting processes due to electronic system excitation by intraband transitions with the following covalent bond destabilization. The key role of imperfections in laser-induced decomposition is discussed.

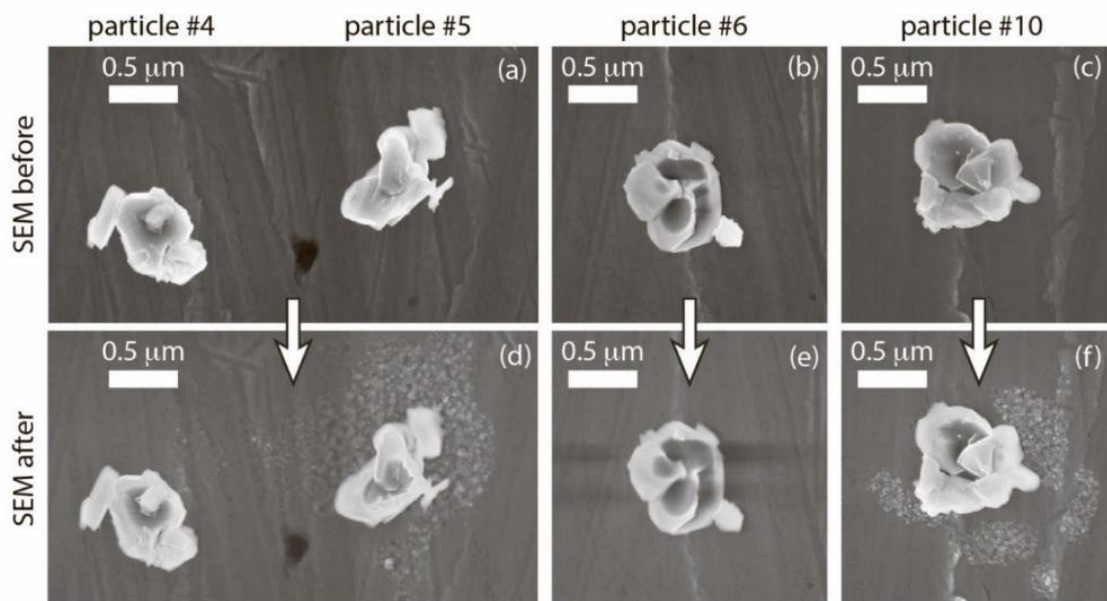


Fig. 1. SEM images of Mn-LTO particle before (first row) and after (second row) the repeated action of focused laser irradiation during Raman spectra measurements. The image is taken from [2].

The research was funded by the Russian Science Foundation (project no. 22-22-00350, <https://rscf.ru/project/22-22-00350>).

[1] A. Ryabin and D. Pelegov, An ambiguity of laser-induced degradation in LiFePO_4 and advantages of single-particle approach to Raman spectroscopy. *J Raman Spectrosc*, 53, 1625–1634 (2022).

[2] A. Nikiforov, D. Kuznetsov, R. Nasara, K. Govindarajan, S. Lin, D. Pelegov, Fast and Slow Laser-Stimulated Degradation of Mn-Doped $\text{Li}_4\text{Ti}_5\text{O}_{12}$, *Batteries*, 8, 251 (2022).



LM-O-8

Laser-assisted synthesis of electrode materials

E. Khairullina, A. Levshakova, I. Tumkin, M. Panov, A. Manshina

St Petersburg University, 7/9 Universitetskaya Emb., St Petersburg 199034, Russia

e.khayrullina@spbu.ru

Enzyme-free electrochemical sensors are a rapidly advancing class of devices that hold significant potential for applications in biomedical diagnostics and environmental monitoring. These sensors offer a key advantage of high sensitivity, achieved through direct electron transfer from the analyte to the electrode's electrocatalytic active center, eliminating the need for mediators or enzymes. Notably, enzyme-free sensors exhibit enhanced stability and reliability compared to their enzyme-based counterparts, overcoming limitations associated with enzyme denaturation and degradation, ensuring a longer shelf life.

This study focuses on the development of laser-based approaches for synthesizing working electrodes specifically designed for enzyme-free detection of diverse analytes. Laser synthesis methods offer distinct advantages over traditional techniques, including scalability and precise localization, enabling the fabrication of electrodes with custom geometries on substrates of arbitrary shapes. The combination of laser synthesis with wet chemistry approaches allows for the creation of a wide range of composite systems with improved sensing characteristics, such as heightened sensitivity and extended detectable concentration ranges.

Specific emphasis is placed on two methodologies: laser-induced deposition solution (LCLD) and laser activation of dielectric surfaces followed by copper deposition. These approaches enable the localized formation of metallic structures on dielectric surfaces. Optimization of laser exposure conditions, development of techniques for synthesizing materials with superior adhesion and electrical conductivity, and methods for surface modification to enhance electrochemical activity towards the target analyte are explored. The electrocatalytic activity towards the target analytes is evaluated using cyclic voltammetry and amperometry techniques. Additionally, the study comprehensively investigates the effects of common interfering impurities and examines the long-term stability of the sensory properties.

Authors express their gratitude to the Russian Science Foundation (Project № 23-29-00493). The authors would also like to thank the SPbSU Nanotechnology Interdisciplinary Centre, the Centre for Physical Methods of Surface Investigation, the Centre for Optical and Laser Materials Research, and the Centre for X-ray Diffraction Studies.



LM-O-9

Laser deposition of electrically conductive structures from a deep eutectic solvent on dielectric substrates

D. Shestakov¹, L. Logunov²

1- Department of Physical Electronics and Technology, Saint Petersburg Electrotechnical University "LETI", 197376 Saint Petersburg, Russia

2- School of Physics and Engineering, ITMO University, Lomonosova, 9, Saint- Petersburg, 191002, Russia

Main author email address: dsshstakov@stud.etu.ru

Local metallization of dielectrics is an important practical task; inkjet and laser sintering have been developed in industry today. Inkjet printing allows to obtain very low electrical resistance by using Ag-based inks, but it requires high-precision equipment and post-processing (annealing), moreover it has speed limitation of printing and high cost of ink.[1].

The second method is laser sintering, this method is the simplest compared to others. Nanoparticles are sintered on the surface by laser action. The characteristics of the resulting structures depend on the laser parameters (power, scanning speed, focal spot diameter, etc.) and on deposited films containing nanoparticles. This method makes it possible to obtain conductors with low resistivity, but requires the preliminary synthesis of nanoparticles and ink creation, and substrate covering with thin film formation of inks [2].

We investigate laser induced chemical deposition method, it is a promising way to template-free metallization methods. The method makes it possible to create metal structures locally on the surface in the zone of laser radiation focus. The advantages of the method include simplicity, low consumption of reagents, the ability to control the shape and size of structures by an optical scheme, low cost of reagents, and environmental friendliness. The maximum scanning speed was 18 mm/s with a resistivity 0.5 Ω mm²/m. We have developed a new method for obtaining thin films of deep eutectic solutions, which made it possible to achieve such results [3].

In this work, we have created films for various applications, such as: a heating element, a transparent conductive electrode, a large solid film, high-precision electrical circuit (Fig. 1).

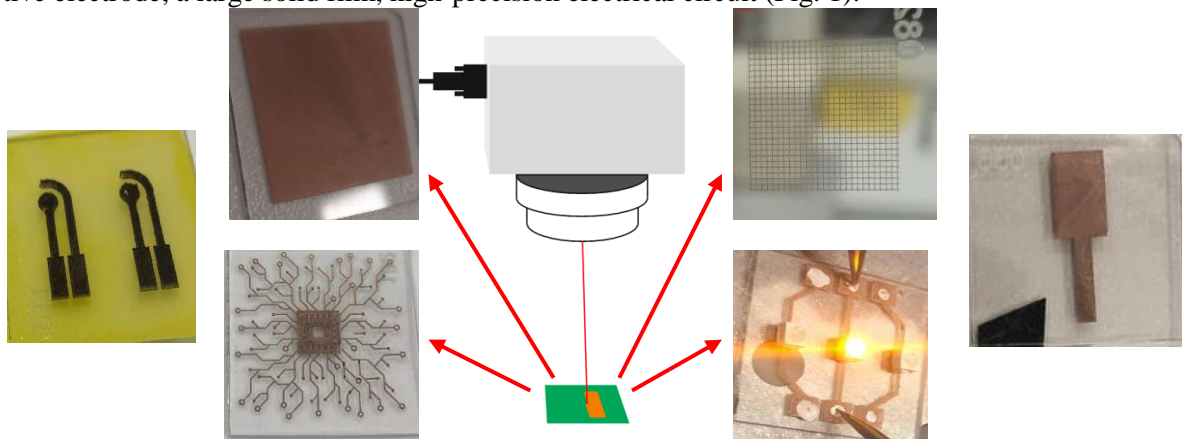


Fig 1. Examples of various applications Cu films.

Acknowledgments

This work was done with the financial support of the Russian Science Foundation (Project No. 390313)

- [1] Beedasy, V., & Smith, P. J. (2020). Printed electronics as prepared by inkjet printing. *Materials*, 13(3), 704.
- [2] Gao, D., & Zhou, J. G. (2019). Designs and applications of electrohydrodynamic 3D printing. *International journal of bioprinting*, 5(1).
- [3] Shestakov, D. S., Shishov, A. Y., Mesh, M. V., Tumkin, I. I., Makarov, S. V., & Logunov, L. S. (2022). Copper Grid/ITO Transparent Electrodes Prepared by Laser Induced Deposition for Multifunctional Optoelectronic Devices. *Bulletin of the Russian Academy of Sciences: Physics*, 86(1), S201-S206.

Laser-integration of metal-organic framework on thermoplastic polyurethane for robust flexible electronics

Tuan-Hoang Tran¹, R. Gulyaev¹, A.S. Garcia Balza¹, R.D. Rodriguez¹, E.S. Sheremet¹

*1- Tomsk polytechnic university, Lenina avenue, 30, 634050, Tomsk, Russia.
Cungbinh9327@gmail.com*

Metal-organic framework (MOF) has gained tremendous interest in scientific and industrial communities thanks to its porous and uniform structure, tunable pore sizes and well-defined molecular adsorption site properties. MOF has been used in catalysis, gas storage, chemical sensors, biomedicine[1]. Flexible electronics allows to continuously monitor different parameters of human body. The intrinsically brittle and rigid attribute of MOFs is mechanically incompatible with flexible electronics, leading to potential challenges in constructing MOF-based flexible devices[2]. Laser technologies are one of the promising ways to create robust integration of MOFs into flexible polymer in designated patterns, which is critical for flexible electronics. Herein, we report the integration of zeolitic imidazolate framework (ZIF-8) into thermoplastic polyurethane (TPU) by laser irradiation. It has been found that after laser irradiation the sample color changed from white to black (see Fig. 1a) and sample became conductive with the resistance of about 300 Ω .

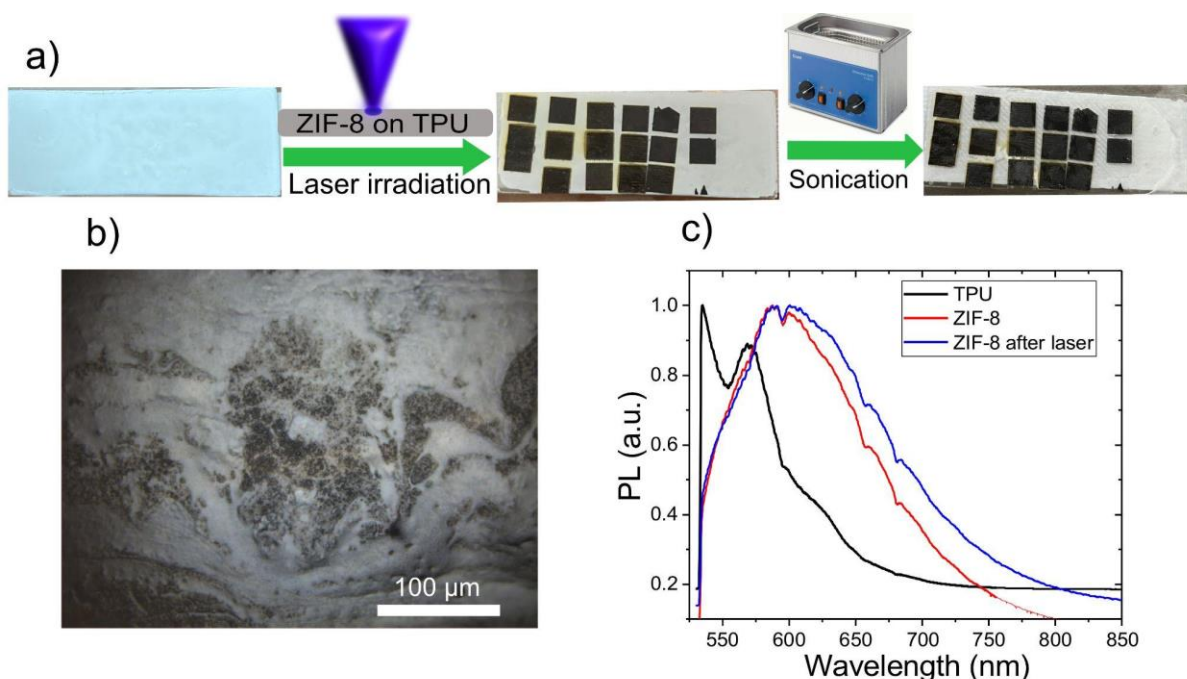


Fig. 1 a) The laser irradiation of ZIF-8 on TPU and sonication process, b) Optical image of ZIF-8 after laser irradiation, c) photoluminescence (PL) spectra of TPU substrate, ZIF-8 before and after laser irradiation.

ZIF-8 is well integrated into TPU after laser irradiation because even after 10 mins of sonication, the unirradiated ZIF-8 was almost removed from the TPU surface, nevertheless the laser-irradiated ZIF-8 is still on the surface (see Fig. 1c). Interestingly, we found that ZIF-8 survived after laser ablation due to the presence of almost the same PL peak. Overall, we demonstrated that laser-irradiated ZIF-8 on TPU is promising material for robust flexible electronics.

The work was supported by Russian Science Foundation grant № 23-42-00081.

1. Ding M, Cai X, Jiang H-L. Improving MOF stability: approaches and applications. *Chem Sci*. 2019;10: 10209–10230.
2. Ling W, Liew G, Li Y, Hao Y, Pan H, Wang H, et al. Materials and techniques for implantable nutrient sensing using flexible sensors integrated with metal-organic frameworks. *Adv Mater*. 2018;30: 1800917.

LM-O-11

Usage of the metal silicide formation reactions for direct thermochemical laser writing

R. Kuts, D. Belousov, V. Korolkov

*Institute of Automation and Electrometry of the Siberian Branch of the Russian Academy of Sciences, Koptyug Ave., 1,
Novosibirsk, Russia, 630090
r.i.kuts@mail.ru*

The paper considers development of the new technology of direct thermochemical laser writing from the point of view of increasing the spatial resolution, reducing technological steps and simplifying the technology through the use of thin metal films coated with a thin capping layer of amorphous silicon. During laser action, the multilayer film material is heated to temperatures at which different phases of metal silicides are formed [1], which have optical and chemical properties different from those of the metal oxide that is formed during thermochemical writing on a pure metal film.

This new approach has been implemented for widely used chromium films [2, 3]. It is shown that the resulting chromium silicides compound layer is highly stable when treated with a selective chromium etchant based on $K_3Fe(CN)_6$ in comparison with chromium oxide, which is formed in the standard thermochemical technology. This provides several advantages of the proposed technology: firstly, an increase in the selectivity of etching makes it possible to reduce the effect of overetching on the quality of manufactured elements. Secondly, the proposed multilayer film material has a sharp writing energy threshold, which can be used for high-contrast writing of structures with a size smaller than the wavelength [4]. Third, during the formation of silicide, the reflection coefficient of a two-layer film increases monotonically with an increase in the beam power in a wide power range. This makes it possible to carry out high-precision control of the written structures before selective etching. This will significantly increase the yield of suitable products in practical applications.

This research was funded by Russian Science Foundation, grant No. 22-79-00049.

- [1] S. Chen et al, Laser-induced formation of titanium silicides, *Surface and Interface Analysis*, vol. 28/1, pp 200-203, (1999).
[2] S.D. Poletaev, Laser ablation of thin films of molybdenum for the fabrication of contact masks elements of diffractive optics with high resolution, *Proc. of ITNT-2015, CEUR Workshop Proceedings*, vol. 1490, pp. 82-89, (2015).
[2] L. Kotsedi, Z. Nuru, et. al., Femtosecond laser surface structuring and oxidation of chromium thin coatings: black chromium, *Appl. Surf. Sci.*, vol. 321, pp. 560-565, (2014).
[4] R. Kuts, et al. "Increasing the spatial resolution of direct laser writing by using a non-Gaussian intensity distribution in the writing laser spot, *Proc. SPIE*. vol. 12318, 123180O, (2022).

Laser synthesis of ruby nanoparticles for photo-conversion of solar spectrum

K.O. Aiyzyhy^{*1}, E.V. Barmina¹, I.I. Rakov¹, G.A. Shafeev¹

1- Prokhorov General Physics Institute of the Russian Academy of Sciences, Vavilova str. 38, 119991 Moscow, Russia

**aiyzyhy@phystech.edu*

Solar radiation is used by plants for photosynthesis. The most demanded part for the efficient proliferation of land plants (embryophytes) is in the red range of the spectrum from 600 nm to 780 nm [1]. This is especially true for land plants grown in greenhouses in terrestrial areas of risky agriculture [2,3]. However, the fraction of radiation in this range of the solar spectrum is rather small. Therefore, the photoconversion of solar radiation to the red region is highly desirable to increase the photosynthetic efficiency factor. Existing coatings based on semiconductors (CdS, CdSe) or organic dyes convert solar radiation to the red region. However, these coatings are not stable under sunlight and are rapidly degraded. Ruby-based materials can become an alternative to these converters, since ruby has a high photostability and is characterized by strong photoluminescence near 695 nm.

In this work ruby particles at various Cr³⁺ (2 - 10%) content were obtained by laser heating of a mixture of industrial Al₂O₃ and Cr₂O₃ micro-powders in air. The mixture was exposed to quasi-continuous wave radiation of a Nd:YAG laser with wavelength of 1064 nm modulated at frequency of 200 kHz by 1.5 μs pulses. The estimated diameter of the laser spot was 100 μm, average power of the laser radiation was 15 W, which corresponds to power density of 150 kW/cm² on the surface of the mixture. Laser-heated ruby grains have average size of 0.5-1 μm. Further laser fragmentation of these grains in isopropanol was applied to reduce their size. The same laser source was used for fragmentation: Q-switch mode, the repetition rate of laser pulses of 10 kHz, pulse duration of 10 ns, and the energy per pulse of 2 mJ. Data from dynamic light scattering shows that ruby nanoparticles with average size of 310 nm formed after laser fragmentation. Laser-fragmented nanoparticles of ruby were incorporated into a free-standing film of fluoropolymer LF-32. This type of polymer is widely used for greenhouses coatings. Photoluminescence map of the nano-composite of fluoropolymer LF-32 with nanoparticles of ruby (Fig. 1) comprised both photoluminescence peaks of LF-32 (350-550 nm) and photoluminescence peaks of ruby in the vicinity of 700 nm. Thus, coatings based on ruby nanoparticles are a promising replacement for existing materials for greenhouse coatings.

This work was supported by a grant of the Ministry of Science and Higher Education of the Russian Federation (075-15-2022-315) for the organization and development of a world-class research center "Photonics" and scholarship of the President of the Russian Federation for young scientists and graduate students (SP- 1006.2021.1). We thank our industrial partner Pokkels LLC for providing innovative technical solutions.

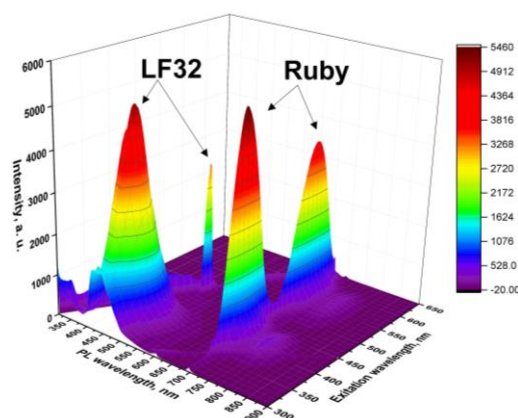


Fig. 1. Luminescence map of ruby nanoparticles in fluoropolymer matrix.

- [1] S. B. Powles, Photoinhibition of Photosynthesis Induced by Visible Light, Annual review of plant physiology, vol. 35, pp. 15-44, (1984).
- [2] A. V. Simakin et al., Photoconversion fluoropolymer films for the cultivation of agricultural plants under conditions of insufficient insolation, Applied Sciences, vol. 10, №22, p. 8025, (2020).
- [3] S. V. Gudkov et al., Development and application of photoconversion fluoropolymer films for greenhouses located at high or polar latitudes, Journal of Photochemistry and Photobiology B: Biology, vol. 213, p. 112056, (2020).



LM-O-16

Fundamental and applied aspects of radiation degradation in solid state electronics materials in the light of modern radiation physics concepts

B. L. Oksengendler^{1,2}

¹*Institute of Materials Science, Academy of Sciences of the Republic of Uzbekistan, Tashkent, 100084 Uzbekistan*

²*Institute of Physics and Technology, Ural Federal University, Yekaterinburg, 620078, Russia*

e-mail: oksengendlerbl@yandex.ru

Radiation physics and related technologies of the 21st century, combining both phys-chemical and structural properties of materials and objects with strong non-equilibrium, demonstrate the manifestation and interpretation of many unusual non-linear effects (see Fig.). This is especially evident in the case of high-intensity irradiation of various nature under the conditions of radiation in a special energy spectrum (synchrotron, lasers, high-current electron accelerators, et. al.). Accounting for five different channels of energy transfer from radiation to matter (elastic scattering, ionization, heat release, elastic and shock waves) makes it difficult to see the number of new unusual combinations of radiation response, the study of which at the present stage, however, is possible using the concept of “COMPLEXITY”. Among the various characteristics of irradiated objects, the hierarchy of their structure plays a very special significance, which is fundamentally important for objects of both inanimate and living nature. The peculiarity of including objects of a hierarchical structure in the analysis of radiation effects leads to a new situation - the involvement of the ideas of cybernetics in radiation physics. The solution of these problems required both new theoretical approaches and modification of traditional Radiation Solid State Physics schemes. This range of issues has received a certain solution in relation to objects of inanimate and living nature in a series of our publications, some of which are given below [1-5]. It is essential that all the considered effects (radiation degradation of materials and devices, Corona virus inactivation, laser materials degradation, radiation segregation, Fobos-Grunt space vehicle failure and others) fit well within the framework of only three paradigms (see fig.)

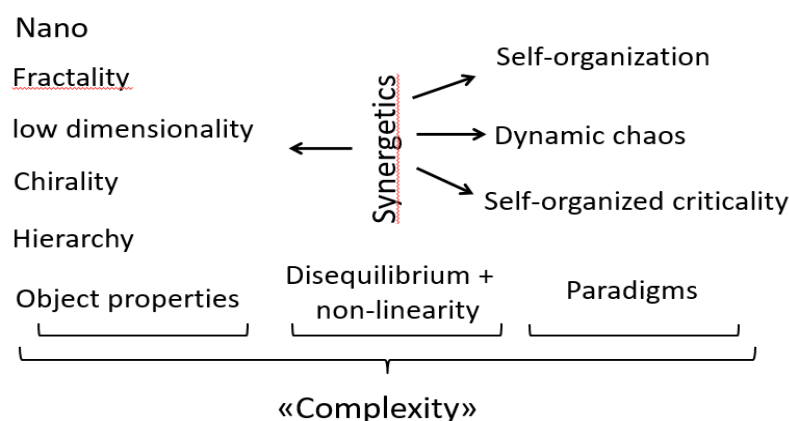


Figure. Generalized scheme for the concept of “Complexity”

[1] S.E. Maksimov, B.L. Oksengendler, N. Yu. Turaev, J. Surf. Invest. vol.7, p.333 (2013).

[2] M.Kh.Ashurov, I.A. Shcherbakov, B.L. Oxengendler, Abst. Int. Conf. ALT-29, Moscow, p.137 (2022).

[3] B.L. Oksengendler, A.F. Zatsepin, N.N. Turaeva, S.Kh. Suleimanov, N.N. Nikiforova, J. Surf. Invest. vol.16 (3), p.364 (2022).

[4] B.L. Oksengendler, A.Kh. Ashirmetov, N.N. Turaeva, N.N. Nikiforova, S.X. Suleymanov, Nucl. Instr. Meth. B. vol.512 (4), p. 66 (2022).

[5] B.L. Oksengendler, F.A. Iskandarova, A.F. Zatsepin, N.N. Nikiforova, S.Kh. Suleimanov, N.N. Turaeva, J. Surf. Invest. vol.17 (1), p.31 (2023).



LM-O-17

Application of scaling laws to describe laser cladding of metal-ceramic coatings

A.A. Golyshev

Khristianovich Institute of Theoretical and Applied Mechanics SB RAS, Novosibirsk

alexgol@itam.nsc.ru

Additive manufacturing (AM) represent one of the fastest growing technologies nowadays [1]. Various methods and materials for additive manufacturing are created every year.

Defining parameters that characterize the physical processes occurring during additive manufacturing allows to control the behavior of the melt pool. It was shown in [2] that by controlling the geometry of the melt pool, one can directly establish the relationship between the specified parameters and the microstructure and, thus, formulate analytical equations that can be used in optimizing the additive manufacturing process. Introducing dimensionless parameters into these equations using the Π -theorem simplifies physical models and reveals dependencies between physical quantities. This method has been successfully applied in hydrodynamics, biology, biomechanics [3], nuclear physics [4], and laser technologies [5-6].

Introduction of variable combinations into analytical equations allows, firstly, to reduce the number of parameters that need to be studied when using AT, and secondly, to more accurately determine the processes occurring during AT. [7].

In this work, the direct metal deposition (DMD) method of laser cladding is used. This method involves feeding the deposited powder mixture through a nozzle coaxially to the laser beam.

During the experiments, a powder mixture of titanium alloy Ti64 and silicon carbide (SiC) with different ceramic concentrations of 0%, 10%, and 20% by weight was deposited. Single tracks were formed from the metal-ceramic powder mixture with SiC concentrations of 0%, 10%, and 20% wt. at different laser parameters. It was shown that the geometric dimensions of the tracks, regardless of the ceramic concentration, are determined by two dimensionless parameters - normalized enthalpy B and Peclet number Pe - and can be described by a single dependence. It was demonstrated that the found laws are valid both when depositing onto a metallic substrate and onto a metal-ceramic layer (Ti64 - 10% wt. SiC).

The research was carried out with the support of a grant from the Russian Science Foundation № 21-79-10213, <https://rscf.ru/project/21-79-10213/>.

[1] Altıparmak S.C., Xiao B. A market assessment of additive manufacturing potential for the aerospace industry, *Journal of Manufacturing Processes*, vol. 68, pp. 728-738, (2021).

[2] Malikov A., Golyshev A., Vitoshkin I. Current Trends in Laser Welding and Additive Technologies (Review), *Applied Mechanics and Technical Physics*, vol. 64, pp. 36-59, (2023).

[3] Buckingham E. On physically similar systems; Illustrations of the use of dimensional equations, *Phys. Rev.*, vol. 4, pp. 345, (1914).

[4] Pelz P.F., Vergé A. Validated biomechanical model for efficiency and speed of rowing, *J. Biomech.*, vol. 47, pp. 3415-3422, (2014).

[5] Rubenchik A.M., King W.E. Wu S.S. Scaling laws for the additive manufacturing, *J. Materials Process. Technol.*, vol. 257, pp. 234-243, (2018).

[6] Golyshev A. Standardization of Laser-Oxygen Cutting Based on Surface Roughness Criteria, *Metal Processing (technology, equipment, tools)*, vol. 1, pp. 16-21, (2016).

[7] Golyshev A., Orishich A. Microstructure and mechanical characterization of ti6al4v-b4c metal ceramic alloy, produced by laser powder-bed fusion additive manufacturing, *The International Journal of Advanced Manufacturing Technology*, vol. 109, pp. 579-588, (2020).

LM-O-18

Resonances of coherent population trapping in cells with pairs of alkali atoms, detected by the Ramsey method

G.V. Voloshin¹, A.N. Litvinov¹, K.A. Barantsev¹, Ammosov A.P.¹, A.S. Kuraptsev¹, I.M. Sokolov¹

*1- Peter the Great St.Petersburg Polytechnic University, 195251, St.Petersburg, Russia
gavrilyvsh@gmail.com*

The interaction of bichromatic laser radiation with the media of alkali atoms under certain conditions leads to the appearance of the effect of coherent population trapping [1, 2]. This phenomenon is resonant in nature with respect to the frequency difference between the two radiation components. The width of such resonances turns out to be much smaller than the width of the natural absorption line, which largely determines the possibility of using this phenomenon in such areas as quantum frequency standards, optical magnetometers, high-resolution spectroscopic devices, devices for recording and storing quantum information, and the development of lasers without inversion.

Recently, the method of detecting CPT resonances by means of pulsed pumping (the Ramsey method) has become widespread [3]. The width of the resonances, with this method, is determined solely by the temporal characteristics of the pulse sequences and can be made much smaller than the width of the CPT resonance detected by continuous radiation.

The cause of the CPT phenomenon is the destructive interference of two quantum excitation channels. For this reason, in the theoretical description of this phenomenon, simple three- and four-level models of atoms are often used [4, 5]. However, it is known that taking into account the “real” multilevel structure of alkali atoms in describing CPT excitation under certain conditions leads to significantly different qualitative results [6].

In this work, on the basis of the semiclassical theory of the interaction of light and matter using the density matrix method in the Wigner representation with respect to the translational degrees of freedom of atoms, a mathematical model of the interaction of pulsed bichromatic laser radiation with the resonant medium of alkali atoms is constructed, taking into account the non-zero temperature of the ensemble and the real (magnetic) structure of atomic levels. Based on this model, the contours of CPT resonances detected by two pulses separated in time by a dark pause are calculated. The calculation results are compared with experiments [7, 8]. The dependence of the shape of the resonances on various parameters of the atomic medium and laser pumping is analyzed.

This work was financially supported by the Theoretical Physics and Mathematics Advancement Foundation “BASIS” (Leader grant no. 21-1-1-36-1) and the Russian Science Foundation (grant no. 21-72-10004).

- [1] G. Alzetta, A. Gozzini, L. Moi, G. Orriols, An experimental method for the observation of r.f. transitions and laser beat resonances in oriented Na vapour, *Nuovo Cim. B*, vol. 36(1), p. 5 (1976).
- [2] E. Arimondo and G. Orriols, Nonabsorbing atomic coherences by coherent two-photon transitions in a three-level optical pumping, *Lett. Nuovo Cim.*, vol. 17(10), p. 333 (1976).
- [3] N.F. Ramsey, A New Molecular Beam Resonance Method, *Phys. Rev.*, vol. 76, p. 996 (1949).
- [4] G.V. Voloshin, K.A. Barantsev, E.N. Popov et al., The Effect of the Hyperfine Structure of an Excited Level on the Shape of the Coherent Population Trapping Resonance under Ramsey Interrogation in an Optically Dense Medium, *J. Exp. Theor. Phys.*, vol. 129, pp. 1–8 (2019).
- [5] G.V. Voloshin, K.A. Barantsev and A.N. Litvinov, Line shape and light shift of coherent population trapping resonance under Ramsey interrogation in 'hot' atoms in an optically dense medium, *Quantum Electron.*, vol. 52, p. 108 (2022).
- [6] G. Kazakov, B. Matisov, I. Mazets, G. Mileti, J. Delporte, Pseudoresonance mechanism of all-optical frequency-standard operation, *Phys. Rev. A.*, vol. 72, 063408 (2005).
- [7] G.S. Pati, F.K. Fatemi, M. Bashkansky, S.M. Shahriar, Optical Ramsey interference and its performance in D1 line excitation in rubidium vapor for implementation of a vapor cell clock, *Proc. SPIE 7949, Advances in Slow and Fast Light IV*, 794910 (2011).
- [8] Z. Warren, M. S. Shahriar, R. Tripathi, G. S. Pati, Pulsed coherent population trapping with repeated queries for producing single-peaked high contrast Ramsey interference, *Journal of Applied Physics*, vol. 123, 053101 (2018).

High efficient laser method of powder production

Yu.Chivel

*1- Additive Technologies Lab , 22019 Minsk, Belarus
Merphotonics , 42100 Saint Etienne, France*

email address: yuri-chivel@mail.ru

A process of laser gas atomization has been developed [1] to obtain a spherical metal powder with a particle size of 30-100 μm using laser beams of conical geometry.

A process is presented for obtaining a spherical powder in a wide size range of 50 nm - 100 μm , in which a continuous optical discharge in laser cavity [2] with a temperature of 20 kK is formed using conical laser beams in an inert gas flow, into which the material is introduced in the form of a wire or a powder flow. Particle condensation is strongly and rapidly quenched by the inert gas flow, resulting in high supersaturation.

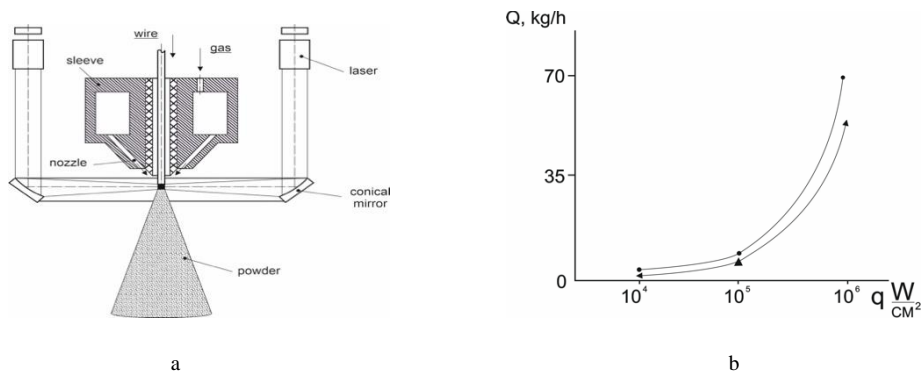


Fig.1 a - System for laser gas atomization; b- Productivity of the powder production process depending on the power density of laser radiation. * - evaporation of eight 1 mm wires; ▲ - optical atomization of 2 mm wire.

The efficiency of the proposed laser method for producing powders is up to 0.5 kg/kWh at an electric power of 16 kW, while the existing, most efficient methods of plasma and gas spraying provide an efficiency of no better than 0.1-0.25 kg/h kW. The method can be used to obtain powders from various materials - metals, ceramics, plastics, suspensions.

The process of formation of nanoparticles by means of inert gaseous condensation of metal vapors obtained by laser evaporation of a micropowder flow of 40–60 μm with a particle concentration of 10^4 – 10^6 cm^{-3} has been studied. The resulting nanoparticles with a size of 20-50 nm are collected in the form of conglomerates up to 100 nm in size. The productivity of the process reaches 0.2 kg/kWh.

1. Yu.Chivel . New approach to powder production using conical laser beams // In: Proceedings WORLD PM 22 , 5371750, Lyon (2022).
- 2 . Yu.Chivel .Continuous optical discharge in laser cavity // Tech. Phys. Journ., **86**, pp.150 -152 (2016).

LM-O-20

Investigation of the short pulse laser ablation of porous silicon targets with molecular dynamics simulation.

M. Grigoryeva^{1,2}, I. Kutlubulatova^{1,2}, A. Kanavin¹, V. Timoshenko^{1,2,3}, and I.N. Zavestovskaya^{1,2}

1- P. N. Lebedev Physical Institute of the Russian Academy of Sciences, 53 Leninskiy Prospekt, Moscow 199991, Russian Federation

2- National Research Nuclear University MEPHI (Moscow Engineering Physics Institute), 31 Kashirskoe shosse, Moscow 115409, Russian Federation

3- Lomonosov Moscow State University, GSP-1 Leninskie Gory, Moscow 119991, Russian Federation

grigorevams@lebedev.ru

The interaction of high-power laser radiation with matter is represented by a complex of processes, such as absorption of light by electrons, diffusion of hot electrons, thermionic emission, heat transfer by hot electrons to the lattice, heating of the crystal lattice, detachment of atoms or ions from the lattice, interaction of radiation with detached particles, cooling and recrystallization [1,2]. Taking into account all the processes leads to difficulties in the creation of a universal laser ablation model, and the effects caused by the above mentioned processes are often studied separately [3].

The laser ablation of a silicon (Si) target was widely studied because of the great practical importance of Si-based nanomaterials [4–6]. The modeling has been mostly performed for single-crystalline Si (c-Si), while interaction with a nano-structured substrate, such as porous silicon (PS), may be of particular interest. In this work, we simulated the ablation of PS substrates with various degrees of porosity and pore size under laser radiation with wavelengths in ultraviolet (UV), visible and infrared (IR) spectral ranges and various fluences using a one-temperature molecular dynamics model. The number of ablated atoms and ablation threshold are calculated.

It is found that for UV and visible irradiation an increase of the porosity to 80% leads to a 1.5-3 times decrease of the ablation threshold compared to the bulk silicon. For IR irradiation, the maximum drop in the ablation threshold was observed for the porosity of 60-65%. In addition, a decrease of pores size from 5 to 1 nm leads to the ablation threshold drop almost 40%.

Despite the reduction of the ablation threshold, the ablation rate of PS substrates is significantly lower than that of crystalline targets. Reducing the ablation threshold can be important in the laser ablation synthesis of nanoparticles due to lowering the laser requirements for the ablation. However, a decrease in the ablation rate with an increase in porosity leads to the need to optimize the treatment regimes and the initial porous target for each specific synthesis process.

This work was financially supported by Ministry of Science and Higher Education of Russian Federation (project No 075-15-2021-1347).

[1] D. von der Linde and K. Sokolowski-Tinten, The physical mechanisms of short-pulse laser ablation, *Applied Surface Science*, vol.154 (1), pp. 1-10, (2000)

[2] S. Amoroso, R. Bruzzese, N. Spinelli, R. Velotta, M. Vitiello, X. Wang and L. Lanotte, Generation of silicon nanoparticles via femtosecond laser ablation in vacuum, *Applied Physics Letters*, vol. 84, pp. 4502–4504, (2004)

[3] M.E. Povarnitsyn, T.E. Itina, M. Sentis, K.V. Khishchenko and P.R. Levashov, Material decomposition mechanisms in femtosecond laser interactions with metals, *Physical Review B*, vol. 75, pp. 235414, (2007)

[4] Y.F. Zhang, Y.H. Tang, N. Wang, D.P. Yu, C.S. Lee, I. Bello and S.T. Lee, Silicon nanowires prepared by laser ablation at high temperature, *Applied Physics Letters*, vol. 72, pp. 1835-1837, (1998)

[5] S. Barcikowski, A. Hahn, A.V. Kabashin and B.N. Chichkov, Properties of nanoparticles generated during femtosecond laser machining in air and water, *Applied Physics A*, vol. 87, pp. 47-55, (2007)

[6] A.V. Kabashin, P. Delaporte, A. Pereira, D. Grojo, R. Torres, T. Sarnet and M. Sentis, Nanofabrication with Pulsed Lasers, *Nanoscale Research Letters*, vol. 5, pp. 454-463, (2010)

LM-O-21

Laser cavitation in liquid hydrocarbons at a high pulse repetition rate

E.V. Zavedeev, V.V. Kononenko, K.K. Ashikkalieva, N.R. Arutyunyan, V.I. Konov

*Prokhorov General Physics Institute of the Russian Academy of Sciences, 38 Vavilova St., Moscow, 119991, Russian Federation
vitali.kononenko@nsc.gpi.ru*

Optical breakdown in liquids is quite complex process which includes a number of fast dynamic components: from the formation of a dense nonequilibrium plasma to cavitation. In solutions, suspensions, and even in pure liquids the chemically “pure” synthesis of various nanomaterials and nanocomposites can be realized at laser intensity exceeding $\sim 10^{13}$ W/cm². Physical and chemical rearrangement of the structure of molecules proves possible due to the highest degree of the liquid ionization (up to 10^{22} cm⁻³ and higher), which initiates many new effects from laser exposure.

The experiments presented are stimulated by a study of laser synthesis of linear carbon chains in liquid hydrocarbons. We describe the main laws of the formation and evolution of a cavitation bubble, which inevitably occurs during an avalanche optical breakdown in liquid hydrocarbons (in hexane and in ethyl alcohol). The main attention is paid to the effects of interplay of this bubble with the laser beam and the features of cavitation that develops when using laser sources with a high pulse repetition rate (up to 500 kHz), which, in turn, is caused by the need to increase the productivity of laser synthesis of polyines.

The ionization and breakdown of liquids were carried out in a cuvette using intense picosecond (~ 10 ps) radiation emitted by a Huaray Olive-1064-40 laser (wavelength of 1064 nm). The focusing aperture was NA=0.27. Using optical microscopy, the cavitation process was traced (Fig. 1a). At pulse repetition rates $> \sim 10$ kHz, a tendency was found for formation of single relatively large (up to ~ 100 μ m) superbubble instead of multiple microbubbles (Fig. 1b). An even more interesting effect is that the formed superbubble remains for a long time (up to minutes) inside the beam caustic (in front of the laser waist), thus blocking the light focusing and stopping laser synthesis. Possible mechanisms of the described processes are discussed.

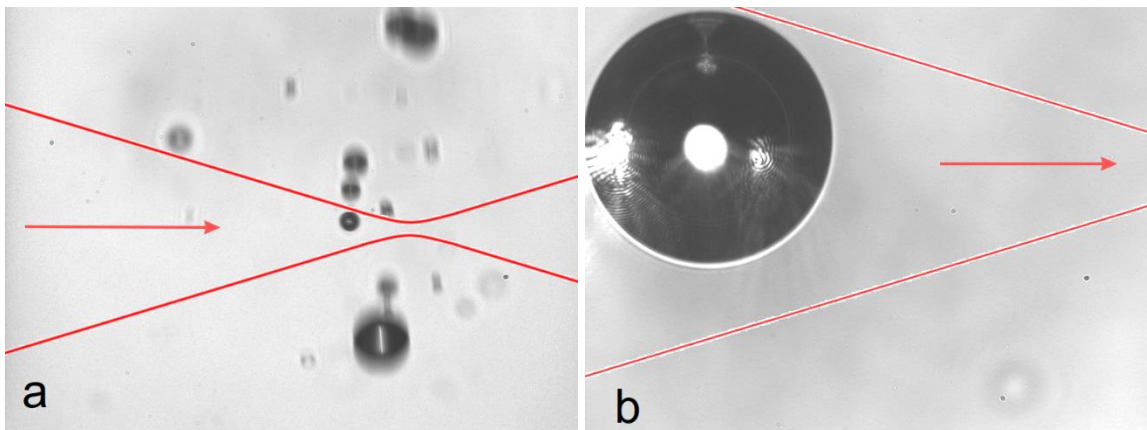


Fig. 1. Optical microscopy of laser cavitation in hydrocarbons: a) “normal” cavitation; b) formation of superbubble. The light was propagating from left to right, red lines indicate an approximate boundaries of the laser caustic.

This work was supported by the Russian Science Foundation (project no. 19-12-00255-P).

Laser-induced fragmentation of solid and porous Si nanoparticles in colloidal solutions using molecular dynamics

S.Yu. Lukashenko¹, I.A. Kutlubulatova^{1,2}, M.S. Grigoryeva¹, V.A. Dimitreva², D.S. Ivanov¹, A.P. Kanavin¹, V.Yu. Timoshenko^{1,2,3}, and I.N. Zvestovskaya^{1,2}

¹ P. N. Lebedev Physical Institute of Russian Acad. Sci., Leninskiy Pr. 53, 119991 Moscow, Russia

² MEPHI, Institute of Engineering Physics for Biomedicine (PhysBio), 115409 Moscow, Russia

³ Lomonosov Moscow State University, Leninskie Gory 1, 119234 Moscow, Russia

email address: stas.lukashenko@mail.ru

Silicon nanoparticles (NPs), due to their high biocompatibility and non-toxicity, are widely used in biomedical technologies [1, 2]. In this case, it is crucial to utilize homogeneous colloidal solutions of nanoparticles with controlled properties. The laser ablation method has emerged as a powerful technique for nanoparticle synthesis. However, controlling the size distribution of the resulting particles has proven challenging [3]. Therefore, subsequent fragmentation of NPs using pulsed laser radiation is often employed to achieve the desired particle characteristics. Nevertheless, the understanding of the underlying mechanisms involved in this process is severely limited. In our work, we use molecular dynamics (MD) modeling to study the mechanism of silicon NP fragmentation under the action of short-pulse laser radiation.

We conducted large-scale parallel MD simulations of the interaction between a 270 fs laser pulse and the colloid solution model at an incident fluence of approximately (1 – 10) J/cm², with a wavelength of 800 nm. The irradiated volume was represented by a water cube measuring (100 x 100 x 100) nm, in which three solid or three porous nanoparticles of sizes (30, 20, 10) nm were submerged. The simulation accounted for the complete absorption of a Gaussian laser pulse by the NPs, as well as subsequent processes including heating, phase transition, vaporization, nucleation, and aggregation.

We present the kinetics of dispersion of primary NPs and condensation of silicon atoms into secondary NPs. The fragmentation thresholds for solid and porous NPs are estimated and compared. We also discuss the features that can occur during laser ablation of NPs in colloidal solutions of high concentration. The study aims to contribute for revealing the mechanisms involved in laser fragmentation of NPs and to develop experimental conditions for generating NPs with desired properties.

This work was financially supported by Ministry of Science and Higher Education of Russian Federation (project No 075-15-2021-1347).

[1] M. Nikzamir, A. Akbarzadeh, Y. Panahi, "An overview on nanoparticles used in biomedicine and their cytotoxicity", *Journal of Drug Delivery Science and Technology* 61, 102310-102316 (2021).

[2] L.T. Canham, *Handbook of Porous Silicon*, Cham: Springer. 2018.

[3] D. Zhang, B. Gökce, S. Barcikowski, *Laser Synthesis and Processing of Colloids: Fundamentals and Applications Chem. Rev.* 117, 3990–4103 (2017).

Pressure recoil behavior in picosecond laser metal interaction: MD simulation

D.S.Ivanov¹, A.A.Samokhin^{2*}

1-P. N. Lebedev Physical Institute of Russian Acad. Sci., Leninskiy Pr. 53, 119991 Moscow, Russian Federation

2- Prokhorov General Physics Institute of the Russian Academy of Sciences, st.Vavilova 38, Moscow, 119991 Russian Federation

Main author email address: asam40@mail.ru*

The numerical method combining Molecular Dynamic (MD) with Two Temperature Model (TTM) [1] is used to describe ps laser pulse interaction with thick Al film. Thus, the MD-TTM method described the laser-induced non-equilibrium phase transition with atomic precision, whereas accounts on the effect of free carriers (conduction band electrons) in the continuum. The Al target heating due to 30 ps laser pulses is simulated up to the states where the pressure recoil P_r can probably exceed the critical pressure P_c for liquid-vapor phase transition. However, this exceeding does not necessarily exclude surface evaporation or subcritical explosive boiling processes since pressure P_s and temperature T_s at the irradiated surface can be lower than its critical values. The performed investigations shed light on the real critical parameter's values for Al (and most of metals) that are not yet well defined experimentally and theoretically.

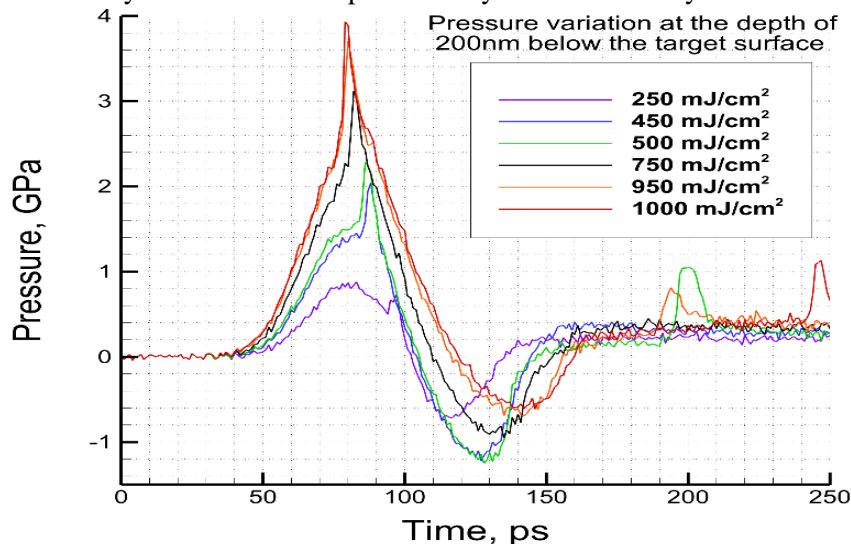


Fig. 1: Evolution of pressure at 200 nm depth below the surface for a range of fluences.

From Fig.1 one can see how small vaporization peak appears on the thermoacoustic pressure signal maximum and grows at higher fluence E with displacing at earlier times. Another somewhat delayed pressure peaks visible at $t = 200$ ps, 195 ps and 245 ps for $E = 500$ mJ/cm², 950 mJ/cm² and 1000 mJ/cm² are due to the cavitation effect which is well known for longer time scales [2] and is probably responsible [3] for the delayed effects mentioned in [4,5]. The situation needs further investigation as well as the problem of metal-dielectric transition during laser ablation [3].

[1]D.S. Ivanov et al., Experimental and Theoretical Investigation of Periodic Nanostructuring of Au with UV Laser Near the Ablation Threshold, *Phys. Rev. Appl.* 4, 064006 (2015).

[2] V.I. Vovchenko, S.M.Klimentov, P.A. Pivovarov, et al. Effect of submillisecond radiation of the erbium laser on absorbing liquid. *Bull. Lebedev Phys. Inst.* 34, 325–328 (2007).

[3] A.A. Samokhin, P.A.Pivovarov, , E.V. Shashkov, et al. On the Metal–Nonmetal Transition under Nanosecond Laser Ablation. *Phys. Wave Phen.* 29, 204–209 (2021).

[4]A.V. Pakhomov, M.S. Thompson, D.A. Gregory, Laser-induced phase explosions in lead, tin and other elements: microsecond regime and UV-emission, *J. Phys. D: Appl. Phys.* 36, 2067 (2003).

[5] J.H. Yoo, S.H. Jeong, R. Greif, and R.E. Russo, Explosive change in crater properties during high power nanosecond laser ablation of silicon, *J. Appl. Phys.* 88, 1638 (2000)



LM-P-1

Modelling of the temperature field during continuous source laser treatment

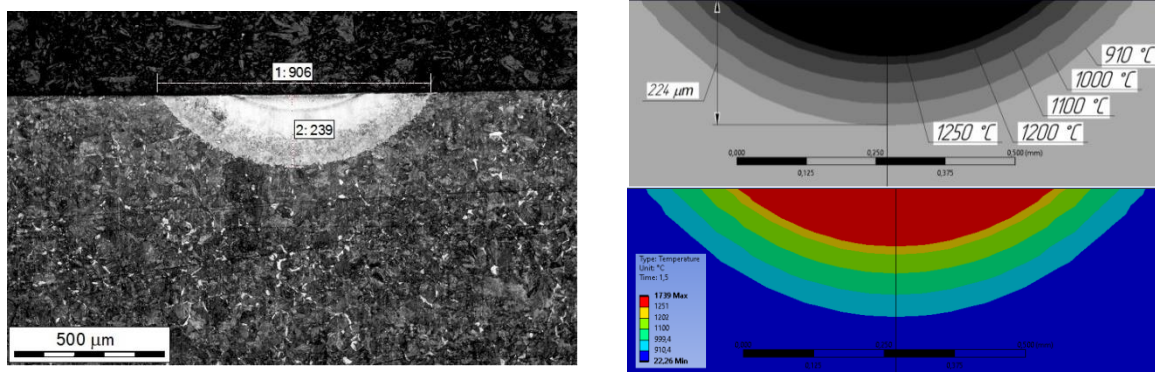
S.I. Yaresko¹, S.N. Balakirov¹, I.A. Antoshin²

¹Samara Branch of P.N. Lebedev Physical Institute of the Russian Academy of Sciences,
221 Novo-Sadovaya Str., Samara 443011, Russia

²Samara State Technical University, 244 Molodogvardeyskaya Str., Samara 443100, Russia

E-mail address: ilyaantoshin16@mail.ru

The determination of the temperature field during the hardening treatment of parts by a moving laser source was realized by the finite element method (FE) in a 3D-formulation using the ANSYS Workbench software product and Moving Heat module. The developed parametric mathematical model makes it possible to describe the laser treatment (LT) of samples of various sizes made of materials with different thermo physical properties, using laser radiation (LR) of various power levels, beam diameter and scanning speed of the laser beam. The type of analysis is Transient Thermal with automatic selection of the number of sub-steps. The size of the FE mesh for the basic material was set to 0.5 mm, for the LT zone – 0.05 mm with a gradient decrease of the size of the FE. The depth of the laser hardening zone (LHZ) in the model was estimated taking into account the fact that the temperature of the end of the austenitic transformation shifts to higher temperatures [1]. For the class of steels under consideration, the temperature shift is assumed equal to 110°C. The heating source was modeled by supplying a Heat Flux in the form of a round spot of LR with a normal radiation intensity distribution. In the model, this was realized in the form of three circles nested into each other, with the ratio of intensity of LR in them corresponding to the normal distribution. To reduce the calculation time, the property of symmetry with a plane of model symmetry along the trajectory of LR motion was used. The verification of model was conducted with the following fixed parameters: the beam diameter was 1.7 mm; the intensity distribution of LR was constructed as follows: 68.26 % of the LR power was distributed in the area of a circle with a diameter of 0.56 mm, 27.18 % – in a circle with a diameter of 1.12 mm, 4.28 % – in a circle with a diameter of 1.7 mm.



on the left - the result of measuring the depth of the LHZ in the cross section, on the right - the results of the calculation
Fig. 1. Comparison of the LHZ depth according to metallography data and according to the FE method calculation for the AISI A290C1M steel after LT ($P=100$ W; $V=5$ mm/s)

The developed FE model of calculating the temperature field during laser heating by a moving concentrated source was used to calculate the temperature field for the laser treatment of AISI E3310, A290C1M, 4140, 5135 steels and chrome vanadium cast iron at variations in the power and scanning speed of the laser beam (Fig. 1). The discrepancy between the experimental and calculated values of the LHZ depth at the laser treatment does not exceed 14 %.

Thus, the FE model of calculating the temperature field of the LHZ of structural steels can be used to predict the LHZ depth and to develop a technology of hardening laser treatment from the point of view of assigning of a specific material's LT mode.

[1] A.G. Grigoryants, I.N. Shiganov, A.I. Misyurov. Technological processes of laser processing (Publishing House of Bauman Moscow State Technical University, 2006)



LM-P-2

Controlling, optimizing, and scaling the microstructure features by laser treatment under an auxiliary graphite layer

X. Egorova¹, A. Sidorova¹, K. Rozanov¹, D. Sinev¹

1- Institute Laser Technology, University ITMO, Kronverksky avenue 49, St. Petersburg, 197101, Russia

Main author email address: x_egorova@itmo.ru

Titanium-based materials are highly valued in industries that require a combination of strength and light weight. For components requiring increased wear resistance (such as drills, gears, knives, pistons, etc.), surface hardness and strength are required, while the core requires toughness and ductility, although increasing the hardness of an alloy often reduces its toughness and ductility. In many cases, the simultaneous achievement of high hardness and ductility is not required for the entire structure. This balance of mechanical properties can be achieved using laser technology to form structures with various chemical compositions and microstructures.

During laser irradiation, the heated area on the metal surface is quickly cooled down by the surrounding cold metal, which contributes to efficient heat removal and rapid cooling. This specific approach to laser processing involves complex thermal cycling and rapid solidification, resulting in certain structural features. Numerous hardening methods, including laser surface modification [1,2] and laser cladding [3, <https://doi.org/10.32620/act.2020.6.07>] were used to increase the hardness of titanium materials.

In this work, the main attention is paid to the study of the dependence of the microstructure on laser exposure during the formation of structures of different sizes. The results obtained establish a correlation between the laser parameters and the resulting microstructure, which makes it possible to optimize and control its characteristics.

This study reveals aspects of the dependence of the microstructure on laser exposure during the formation of structures of different scales. The relationships found between laser parameters and microstructural characteristics make it possible to optimize and control the desired microstructural features. Thus, the results are expected to be applied to industry, helping to improve production efficiency, create materials with individual properties and develop innovative products.

This research was supported by Priority 2030 Federal Academic Leadership Program. The authors also express their gratitude to the Faculty of Physics and Technology at ITMO University for supporting students' scientific and research projects.

[1] H. Soyama and F. Takeo, Effect of Various Peening Methods on the Fatigue Properties of Titanium Alloy Ti6Al4V Manufactured by Direct Metal Laser Sintering and Electron Beam Melting, *Materials*, 13 (10), 2216, (2020).

[2] M. Jamesh, S. Kumar, T.S.N. Sankara Narayanan, Effect of Thermal Oxidation on Corrosion Resistance of Commercially Pure Titanium in Acid Medium. *J. of Mater Eng and Perform* 21, 900–906 (2012).

[3] H. Zhao, C. Zhao, W. Xie et al, Research Progress of Laser Cladding on the Surface of Titanium and Its Alloys. *Materials*.16 (8), 3250, (2023).



LM-P-3

Instabilities and ablation under laser melting of powder layers

Yu. Chivel

*Additive Technologies Lab ,220019 Minsk,Belarus
Merphotonics,42100 Saint Etienne,France*

email address: yuri-chivel@mail.ru

The ejected liquid droplets, spatter, can be seen during the selective laser melting process in many cases. This is not considered as a deviation from the technological regime and it is perceived as inevitable. But it is not so. Particulate emissions lead to defects in the layers, the outer surface geometry violations and may even cause damage of the power optics because the particles have velocities of several meters per second. At keyhole regime [1] ($q \geq 3 \text{ MW} / \text{cm}^2$), under intense evaporation, the main cause of spatter is vapor recoil pressure [1]. But as experiments show, particle emissions are also observed in the absence of evaporation [2,3] in conduction regime. In addition some instabilities of the melting process also lead to defects and catastrophic decline in the accuracy and quality of products.

Process of melting of the thick metal powder layers in the absence of an evaporation was investigated under temperature control. Ejection of dispersed particles from the overheated melt has been observed and investigated. Also ejection of very fine green powder particles can be observed [3,4] due to gas heating in the porous structure before melting. Mechanisms of the melt penetration into loose powder bed have been determined. Instability of the contact surface between the melt and powder revealed by in experiment has been studied and is defined as the Rayleigh - Taylor instability [5] of the boundary between the powder layer and the melt layer.

Numerical simulation of the Rayleigh - Taylor instability suggest that instability develops starting from small scale passing to the large-scale structure.

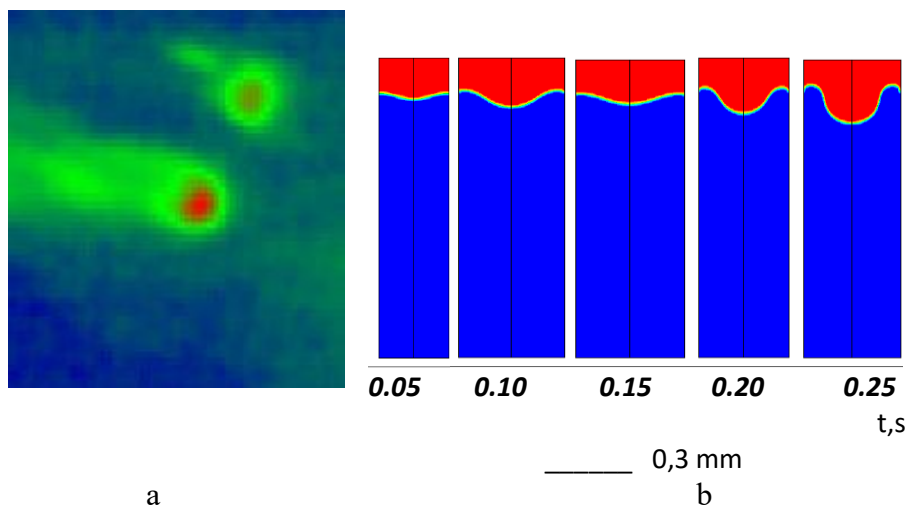


Fig. 1 (a) Image of the melting process when scanning with droplet release. Powder CoCr. P= 80W, Scan speed – 100 mm/s.
(b) - The development of Rayleigh Taylor instability for 0,3 mm mode, viscosity of powder – 0.5 Pa s.

References.

- 1.Ly, A.M. Rubenchik, S.A. Khairallah, G. Guss, M.J. Matthews, Scientific Reports 7(1),4085 (2017)
- 2.Chivel Yu., Petrushina M., Smurov I., Appl. Surf. Sci., 254, 820 (2007)
- 3.Chivel Yu., Physics Procedia, 41, 897 (2013)
- 4.Gusarov A., Smurov I., Proceedings SMT - 26; Lyon, 51(2012).
- 5.Chandrasekhar S., Hydrodynamic and Hydromagnetic Stability, Oxford Press(1961) p.505.



Femtosecond laser modification of ZnO:Ag thin films

V. Gresko¹, V. Smirnova¹, M. Sergeev¹, A. Dolgopolov¹

1- ITMO University, St. Petersburg, Russia

vrgresko@itmo.ru

ZnO thin films due to their physical properties are often used as photosensitive elements and layers of various optoelectronic devices, including photodetectors [1]. The addition of silver nanoparticles to the composition of films can significantly increase the sensitivity of sensors in a certain spectral wavelength range due to the phenomenon of localized plasmon resonance, as well as increase the conductivity of the material [2]. Laser radiation is a very convenient tool for a fast, highly efficient and at the same time easily implemented method of local modification of film properties with the possibility of their correction in real time. By selecting the radiation parameters, it is possible to influence the ZnO matrix itself or the metal nanoparticles contained in it. Thanks to this, it is possible to observe various mechanisms of laser action, as well as the properties of the modified material.

In this work, we studied the effect of femtosecond laser radiation on the optical and electrical properties of composite ZnO films with silver nanoparticles. The radiation wavelength (515 nm) was close to the plasmon resonance of nanoparticles. The surface of the samples was processed at different values of the pulse duration, radiation power, pulse repetition rate, and radiation polarization. The optical and electrical characteristics of the films have been studied. A change in the position of the plasmon resonance peak was observed, as well as a change in the electrical conductivity of the material.

This work was supported by the Russian Science Foundation (project no. 19-79-10208).

[1] Ahmed A. A. et al. Eco-friendly ultrafast self-powered p-Si/n-ZnO photodetector enhanced by photovoltaic-pyroelectric coupling effect //Ceramics International. – T. 48. – №. 11. – C. 16142-16155, (2022).

[2] Tzeng S. K., Hon M. H., Leu C. Improving the performance of a zinc oxide nanowire ultraviolet photodetector by adding silver nanoparticles //Journal of the Electrochemical Society. – T. 159. – №. 4. – C. H440, (2012).



LM-P-5

UV spectral characteristics of colloidal gold nanoparticles obtained by Nd:YAG pulsed laser ablation in tetrahydrofuran

P. Kazakevich¹, S. Yaresko¹

1- Samara Branch of P.N. Lebedev Physical Institute of the Russian Academy of Sciences (SB LPI), 221, Novo-Sadovaya, Samara, 443011, Russian Federation

pavvel.v.k@gmail.com

Pulsed laser ablation in liquid (PLAL) method makes it possible to create metal-carbon nanostructures if organic solvents are chosen as liquids, which are an ideal carbon source for the formation of carbon layers. However, experimental studies often lack data on the absorption of a colloid in the UV region, although due to σ - σ^* and π - π^* electronic transitions, carbon nanoparticles may have absorption bands in the ultraviolet part of the spectrum [1].

The aim of this work is to identify absorption bands in the UV region of the spectrum responsible for the absorption of carbon in a colloid of gold nanoparticles during laser ablation of a Au target by Nd:YAG laser radiation in a tetrahydrofuran (THF) medium, as well as to consider the subsequent interaction of the colloid with 266 nm radiation.

PLAL method by Nd:YAG laser radiation with a pulse duration of 250 ps was used to obtain gold nanoparticles (NPs) in THF. Single pulse energy is 0.3 mJ. Laser fluence on the surface of the samples was $\sim 1.0 \text{ J/cm}^2$. Subsequent irradiation of the colloid was carried out through the side of a 10 mm quartz cell with unfocused radiation from an LCS_DTL-382QT laser with a wavelength of 266 nm, a repetition rate 2 kHz, a pulse duration and energy of 7 ns and $<4 \mu\text{J}$, respectively. A gold (99.99%) plate 0.5 mm thick was exposed to irradiation in H₂O and THF media. The liquid layer thickness above the sample surface is 20 mm.

Picoseconds Nd:YAG laser ablation of a gold target in THF leads to the formation of two absorption bands in the UV, visible, and near-IR regions of the spectra (Fig.1 green line). The absorption band with a maximum around 280 nm is characteristic of the carbon particles formation, while the shift to 570 nm and broadening of the SPR band of gold NPs indicates the deposition of carbon particles around the metal core.

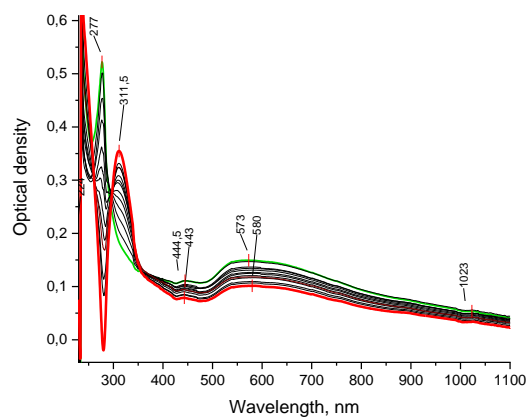


Fig. 1. Dynamics of changes in the UV-Vis THF Au NPs colloid absorption spectra under irradiation at 266 nm. Irradiation time 137 minutes.

Subsequent interaction of the Au NP colloid, obtained by PLAL in THF, with 266 nm radiation leads to a shift of the absorption band in the UV region from 280 nm up to 312 nm, which may be due to the process of absorption of modified solvent molecules on the surface of carbon-metal particles (Fig. 1. red line).

[1] Llamas-Jansa; C. Jäger; H. Mutschke; Th. Henning. Far-ultraviolet to near-infrared optical properties of carbon nanoparticles produced by pulsed-laser pyrolysis of hydrocarbons and their relation with structural variations, *Carbon* **45**(7), pp. 1542–1557, (2007)

Photothermal response of colloidal solutions based on substoichiometric molybdenum oxide

A. Chernikov, D. Kochuev, R. Chkalov, D. Abramov, K. Khorkov

*Institute of Applied Mathematics, Physics and Computer Science, Vladimir State University,
Gorky Street, 87, 600000, Vladimir, Russia*

email address: khorkov@vlsu.ru

In this paper, we present the results of measuring the photosensitized properties of colloidal solutions of nanoparticles based on substoichiometric molybdenum oxide. These solutions were obtained using the techniques of femtosecond laser ablation and fragmentation of molybdenum disulfide in liquid [1, 2]. The experiments were carried out on a laser robotic complex based on the Yb:KGW femtosecond laser system (Avesta Ltd.), generating pulses with a duration of 280 fs at a wavelength of 1030 nm with a repetition frequency of 10 kHz and a maximum pulse energy of 150 μ J.

Measurement of the photosensitivity properties of colloidal systems was carried out on this laboratory stand. We used laser radiation from a continuous diode laser source with a wavelength of 800 nm and an average laser radiation power of 1 W. The use of this laser radiation source is determined based on the spread of application in the areas of therapy, in view of the good permeability of body tissues by radiation with a wavelength of about 800 nm. A collimated laser beam with a cross section in the form of a parallelepiped with sides of 1x3.5 mm was directed to the surface of a quartz test tube for spectrophotometry of the QS grade, 5 ml in volume, with a wall thickness of 1 mm. The investigated colloidal solution was contained inside the quartz test tube. The attenuated laser beam leaving the test tube was measured with a power meter. Registration of thermal processes was carried out by a thermal imaging camera from the surface of the wall of a quartz test tube. The spectral sensitivity range of a thermal imaging camera is 8-12 μ m. Measurement of photosensitivity characteristics was carried out during the time required to reach the maximum temperature in the zone of exposure to the laser beam. During the measurement, the time to reach the maximum temperature was recorded, as well as the transmitted laser radiation.

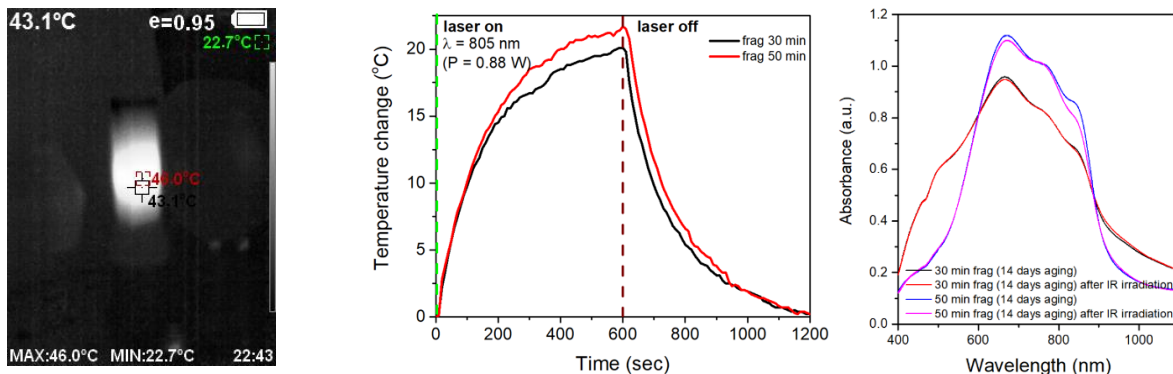


Fig. 1. Time dependence of temperature change during irradiation of colloidal solutions by cw IR laser (805 nm, $P = 0.88$ W); image with thermal imaging camera; absorption spectra of colloidal solutions obtained by laser fragmentation for 30 and 50 minutes in ethanol (black and blue lines) and after IR laser irradiation for 10 minutes (805 nm) (pink and red lines).

The study of the processes of formation of nanoparticles was carried out at the expense of the grant of the Russian Science Foundation No. 22-79-10348. a

[1] Kurilova, U.E., Chernikov A.S., Kochuev D.A. et al., Physical and Biological Properties of Layers with Nanoparticles Based on Metal Chalcogenides and Titanium Synthesized by Femtosecond Laser Ablation and Fragmentation in Liquid, *Journal of Biomedical Photonics & Engineering*, vol. 9(2), 020301, (2023)

[2] Chernikov A.S., Tselikov G.I., Gubin M.Y. et al. Tunable optical properties of transition metal dichalcogenide nanoparticles synthesized by femtosecond laser ablation and fragmentation, *Journal of Materials Chemistry C*, vol. 11(10), pp. 3493-3503 (2023).

The way of the second wave in photonic crystal with PT-symmetry periodic longitudinal and linear transverse modulation

T.A.Khudaiberganov¹, I.A.Sidnihin¹, S.M.Arakelian¹

*1- Department of Physics and Applied Mathematics, Vladimir State University named after A. G. and N. G. Stoletovs, 87 Gorkii st., 600000 Vladimir, Russia
e-mail address: thomasheisenberg@mail.ru*

In non-Hermitian physics, systems with parity-time (PT) symmetry are of interest, since this type of symmetry, under certain conditions, preserves the integrals of motion, in particular energy. This discovery belongs to Bender [1]. This fields of research is of great interest in photonics, quantum mechanics, and topological protected states [2]. Photonic crystals can used as a convenient platform for studying the properties of PT-symmetric systems. Photonic crystals are inhomogeneous optical materials, which are presence of spatial periodic modulation of the permittivity with a period of the order of the wavelength of light. Topological photonics doing the possibility of realizing stable transport phenomena, which, together with non-Hermitian physics, could cause new effects. It has been observed that dimerization results in improved light retention in the defective waveguide [3].

Consider a photonic crystal with modulation of the real and imaginary parts given by the following expression [4]:

$$\varepsilon(x, z) = U_0(\cos(\Lambda(z)x) + i\gamma\sin(\Lambda(z)x)), \quad (1)$$

here U_0 and $U_0\gamma$ – is modulation amplitudes of gains and losses in a photonic crystal, $\Lambda(z)$ – is modulation period of the photonic crystal lattice, which depends linearly on the z coordinate as

$$\Lambda(z) = \Lambda_0(1 + az) \quad (2)$$

This PT-symmetry photonic crystal are shown in Fig.1a. The type of spatial modulation of the permittivity is shown in Fig. 1b.

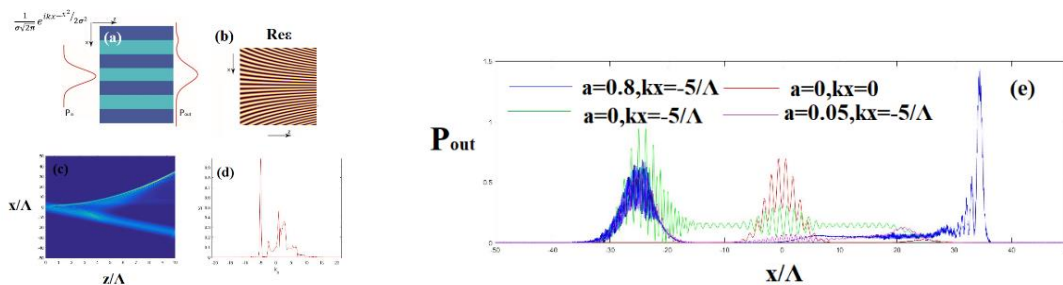


Figure 1 – (a) Sketch a PT-symmetry photonic crystal with a slow increase in the period of the crystal; (b) the shape of the permittivity of photonic crystal; (c) The shape of the intensity distribution over the photonic crystal; (d) the spectrum of the signal at the output of the photonic crystal, according to the x-coordinate wavenumbers k_x ; (e) The shape of the intensity distribution over the photonic crystal at the output of the photonic crystal.

When the PT-symmetry is broken, the transmission spectrum of the photonic crystal (in the direction of modulation, i.e. along the x-axis) becomes asymmetric, see Fig.1d (which implies unidirectional light propagation). The asymmetry of the transmission spectrum leads to the fact that for the Gaussian pulse, the wave components directed towards the best signal transmission prevail over the $-k_x$ component. This leads to the propagation of the wave energy towards the negative gradient of the imaginary part of the permittivity, i.e. arise x-component Poynting vector. For a transversely incident modulation pulse of a photonic crystal, a secondary wave arises when the PT symmetry is broken. It spreads at an angle to the main signal. The tangent of the angle of this wave is determined by the ratio of the gradients of the propagation constants of the x and z components. For the case of modulation according to the relation (2), the secondary wave propagates along a more difficult trajectory. Moreover, if the secondary wave in the usual case $a = 0$, see Fig. 1e, is weak compared to the main signal, then when incident at an angle such that the x-component of the wave vector of the secondary wave falls into resonance with the transmission spectrum of the photonic crystal, then it will be amplified many times over and will even dominate the main signal, see Fig.1e.

[1] Bender C M, Boettcher S Phys. Rev. Lett. 80 5243 (1998).

[2] Mandal S. et al. Nonreciprocal transport of exciton polaritons in a non-Hermitian chain. PRL. – 2020. v. 125. №. 12. – P. 123902.

[3] T. Eichelkraut, R. et.al., Mobility transition from ballistic to diffusive transport in non-Hermitian lattices Nat. Commun., 4, 2533.

[4] Makris K. G. et al. Wave propagation through disordered media without backscattering and intensity variations //Light: Science & Applications. – v. 6. – №. 9. – P. e17035-e17035. 2013.

LM-P-8

Fast and efficient technique for fabricating highly reactive electrode material using laser deposition from DES

A.S. Levshakova¹, E.M. Khairullina¹, A. Yu. Shishov¹, I.I. Tumkin¹, A.A. Manshina¹

1- Institute of Chemistry, Saint Petersburg University, SPbU, 7/9 Universitetskaya nab., St. Petersburg 199034, Russia

Main author email address: sashkeens@gmail.com

The development of advanced techniques for the production of metallic conductive structures on dielectric substrates is crucial for a wide range of applications, including flexible electronics, sensors, and modern devices. This necessitates the fabrication of prototypes and complex conductive structures, sometimes with three-dimensional morphology. In this study, a novel approach employing laser deposition of metals from deep eutectic solvents (DES) is investigated, replacing traditional aqueous or alcoholic solutions. DESs are mixtures of substances with a lower melting point than the precursors, enabling efficient metal deposition [1].

By incorporating DES in the laser-assisted metal deposition method, significant improvements have been achieved. The deposition rate has been notably enhanced, simplifying the technique by eliminating the need for cuvettes. This advancement has demonstrated the capability to rapidly and effectively metallize a broad range of metals. Figure 1a illustrates the schematic representation of the single-step method, while Figures 1b and 1c depict photographs and an image, respectively, of the fabricated nickel electrodes.

To showcase the applicability of the resulting metal micropatterns, electrochemical studies were conducted. These structures were utilized as working electrodes for non-enzymatic glucose sensing and the detection of other biologically important analytes, as demonstrated in Figure 1d.

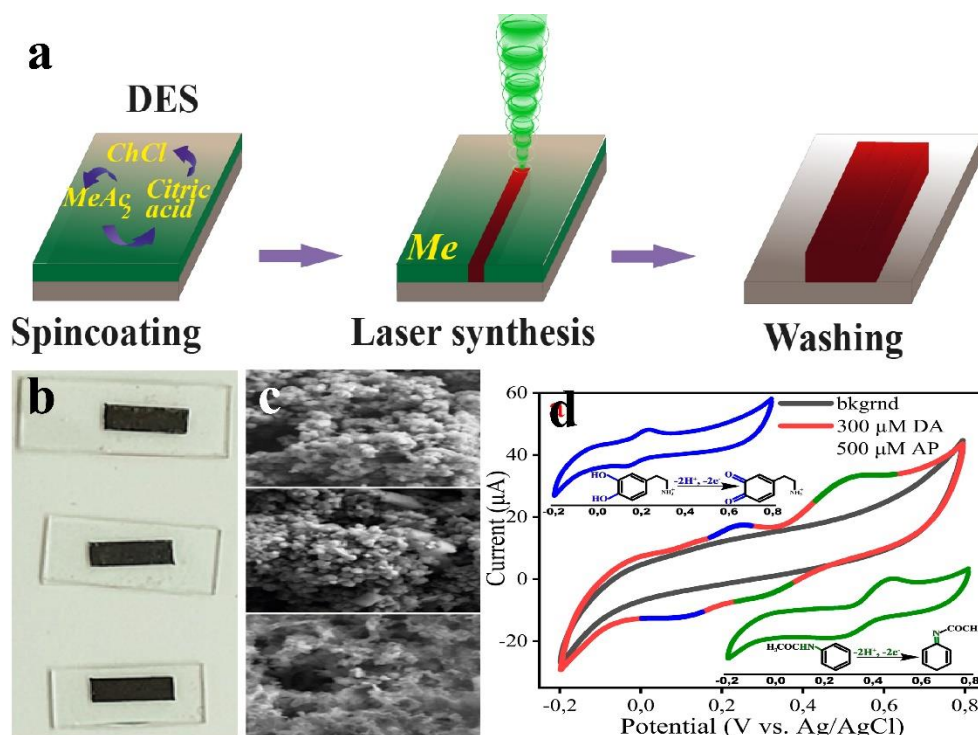


Figure 1. a) Process scheme, b) Electrode photographs c) SEM images of electrodes d) samples CV regarding the enzyme-free determination of dopamine and paracetamol.

[1] E. L. Smith, A. P. Abbott and K. S. Ryder, Chem. Rev., 2014, 114, 11060–11082

[2] Khairullina E. M. et al, New J. Chem, 45, 46, 21896, 2021;

[3] Levshakova A. S. et al, Mater. Lett., 308, 131085, 2022.

This work was supported by RSF № 23-49-10044.



10.24412/cl-35039-2023-23-63-63

LM-P-9

Bulk domains growth created by femtosecond laser in magnesium doped lithium niobate

B. Lisjikh¹, M. Kosobokov¹, A. Efimov¹, D. Kuznetsov¹, V. Shur¹

1- Institute of Natural Sciences and Mathematics, Ural Federal University 620002, Ekaterinburg, Russia

boris.lisikh@urfu.ru

One of the most important reasons for application of the ferroelectric crystals in nonlinear optics is related to creation of precise stable periodical domain structure for efficient frequency conversions based on quasi-phase matching. The irradiation by femtosecond laser is the only method which allows to create the periodical domain patterns both, at the surfaces and in the bulk [1,2].

The crystals of lithium niobate LiNbO₃ family are the most popular objects of the domain engineering due to their outstanding electro-optical and nonlinear optical properties. The MgO-doped lithium niobate (MgO:LN) is the most attractive due to higher optical damage threshold and lower value of the threshold field for polarization reversal as compare to usual congruent LN.

Here we used Yb-doped fiber laser system TETA-10 (Avesta, Russia) emitting pulses in TEM₀₀ mode at the 1030 nm wavelength with energies from 0.7 to 6.7 μJ in filamentation regime, duration 240 fs, repetition frequency 100 kHz. The 1-mm thick plates of single-domain MgO:LN cut perpendicular to the polar axis were mounted at the motorized table to carry out point-by-point irradiation focused at depths of 200-800 μm below Z- polar surface.

Three methods have been used for imaging of the microtracks and domains: (1) optical microscopy (Olympus BX-61, Olympus, Japan), (2) confocal Cherenkov-type second harmonic generation microscopy (CSHG) (Ntegra Spectra, NT-MDT, Russia) and (3) scanning electron microscopy (EVO LS 10, Carl Zeiss, Germany) after selective chemical etching.

It was shown that the irradiation led to formation of ferroelectric domains localized at the microtracks represented the modified crystal areas in the crystal bulk (Fig. 1a). In proper range of the pulse energy the domains grew from the microtracks to the polar surface towards the irradiation source (Fig. 1b, c). The typical for LN hexagonal shape was obtained for domains which reached the polar surface. The domain growth is attributed to polarization reversal under the action of pyroelectric field during the sample cooling after termination of pulsed irradiation [3,4].

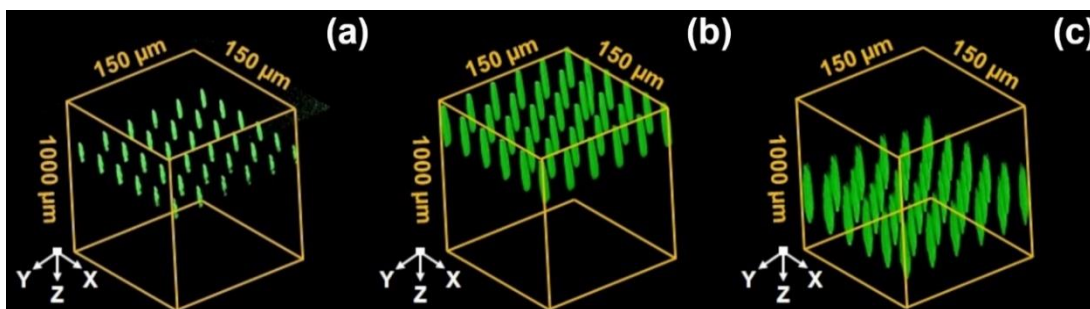


Fig. 1. 3D reconstructions by CSHG of ferroelectric domains in the bulk: (a) depth 400 μm, pulse energy 2.7 μJ; (b) depth 200 μm, pulse energy 4 μJ; (c) depth 800 μm, pulse energy 6.7 μJ.

The obtained results can be used for development of the domain engineering methods without application of the electric field in various ferroelectric crystals.

This research was funded by the Ministry of Science and Higher Education of the Russian Federation (Ural Federal University Program of Development within the Priority-2030 Program).

- [1] J. Imbrock, D. Szalek, S. Laubrock, H. Hanafi, and C. Denz, Thermally assisted fabrication of nonlinear photonic structures in lithium niobate with femtosecond laser pulses, *Optics Express*, vol.30., pp.39340-39352 (2022).
- [2] Y. Chen, C. Yang, S. Liu, S. Wang, N. Wang, Y. Liu, Y. Sheng, R. Zhao, T. Xu, and W. Krolikowski, Optically induced nonlinear cubic crystal system for 3D quasi - phase matching, *Advanced Photonics Research*, vol.3, p.2100268 (2022).
- [3] V. Ya. Shur, M. S. Kosobokov, A. V. Makaev, D. K. Kuznetsov, M. S. Nebogatikov, D. S. Chezganov, and E. A. Mingaliev, Dimensionality increase of ferroelectric domain shape by pulse laser irradiation, *Acta Materialia*, vol.219, p.117270 (2021).
- [4] B. I. Lisjikh, M. S. Kosobokov, A. V. Efimov, D. K. Kuznetsov, V. Ya. Shur, Thermally assisted growth of bulk domains created by femtosecond laser in magnesium doped lithium niobate, *Ferroelectrics*, vol.604, pp.47-52 (2023).

LM-P-10

Laser method of relief formation on the surface of steel to protect against biofouling in the aquatic environment

**M.A. Mikhalevich¹, E.A. Davydova¹, I.A. Filatov¹, A.A. Novopashin¹, A. Peltek¹,
A.V. Shmalko², G.V. Odintsova¹**

1 - ITMO University, Kronverksky Pr. 49, bldg. A, St. Petersburg, 197101, Russia

2 - Interdisciplinary Nanotechnology Resource Center of Science Park, St. Petersburg State University, ul. Ulyanovskaya 1, St. Petersburg, 198504, Russia

mikhalevich@itmo.ru

Currently, the problem of unwanted surface's fouling in aquatic environment is widespread in industry. Various methods of protection against biofouling exist, including hydropneumatic cleaning, application of anti-fouling coatings and laser microstructuring. The last one of the methods is an environmentally friendly preventive treatment that does not require additional resources.

This paper examined the influence of surface wettability characteristics and surface geometry parameters on the quantitative level of biofouling of stainless steel samples placed in a dynamic aquatic environment. A fiber ytterbium nanosecond laser source with a wavelength of 1064 nm was chosen as the processing tool, as steel has an absorption peak at the specified wavelength and this laser system is commercially available. Optical and scanning electron microscopy, profilometry, and the lying-drop method were used to evaluate the morphology of structures and wettability state. The quantitative level of biofouling was assessed using chemical indicators based on resazurin and resorufin. In the process of hydrophobization of the investigated surfaces for the adsorption of organic compounds after laser treatment, the samples were preserved for a long time in air under normal conditions.

In this paper, we studied the biomimetic structure of the rose formed by laser radiation parameters that conform to the treatment mode above the evaporation limits, and also the structure of which the laser radiation parameters are in the range of values below the evaporation limits. During the experiment, samples were placed in aquariums with a dynamic aquatic environment created by electric immersion pumps. The water for placing the samples was taken at the place with the highest proportion of microorganisms in the Leningrad region[1]. The samples were in the dynamic environment for 1-4 weeks, after which their surfaces were investigated for level of biofouling and wettability.

This study tested the hypothesis of changes in the level of biofouling depending on the obtained relief and surface wettability state. A decrease in the level of biofouling was revealed in samples with hydrophobic periodic relief obtained by laser structuring and prolonged exposure to air.

This research was supported by Priority 2030 Federal Academic Leadership Program.

[1] Polyak Yu.M. et al. Monitoring of the Gulf of Finland Baltic Sea: Impact of anthropogenic factors on biogeochemical processes in the coastal zone // Problems of ecological monitoring and modeling of ecosystems. - 2018. - T. 29. - №. 2. - C. 99-117.

LM-P-11

Double depolarizer for controllable laser writing surface relief gratings in chalcogenide glasses

A. Porfirev¹, S. Khonina¹, N. Ivliev¹, D. Porfirev¹

1-Image Processing Systems Institute of RAS—Branch of the FSRC “Crystallography and Photonics” RAS, Samara, Russia

porfirev.alexey@gmail.com

It is well known that in the interferometric approach widely used for recording of surface relief gratings (SRGs) the interference of two laser beams creates light field with periodically changed intensity distribution. The polarization distribution of the generated light field is also periodical. For example, in the case of right-handed and left-handed circular polarizations of the interfering laser beams, the polarization vector of the formed light field continuously rotates from 0 to 180 degrees. However, a Gaussian or uniform laser beam with such a non-uniform polarization distribution can be shaped without any interferometric setup. The so-called depolarizers, patterned microretarder arrays can be used for transformation of the polarization distribution of a linearly polarized Gaussian laser beam and allow one to generate complex vector beams. In our recent work [1], we showed a possibility of fabrication of SRGs in chalcogenide glasses (CGs) thin films using the structured laser radiation formed with a liquid crystal polymer (LCP) depolarizer transforming uniform linear polarization distribution into space variant polarization distribution. The photoionization process underlying the processing of such materials strongly depends on the local polarizations of the transversal and the longitudinal laser electric field components [2]. The photo-induced mass transport, a lateral redistribution of amorphous material under illumination by the near-bandgap light, is one of the fundamental physical phenomena used for laser patterning of CGs [3].

In this work, we propose to use two depolarizers to control the period of the polarization modulation of the transformed light field. The angle of the fast axis of each depolarizer is increased by 2 degree and the retardation has a periodic variation between 250 nm and 300 nm across each consecutive 25 μm strip [4]. The period is controlled by turning the axis of one depolarizer relative to the axis of the other. This allowed us to change the period of the fabricated SRGs in the range from 1 to 3 μm (see Fig. 1). This work was financially supported by Russian Science Foundation (grant No. 22-79-10007).

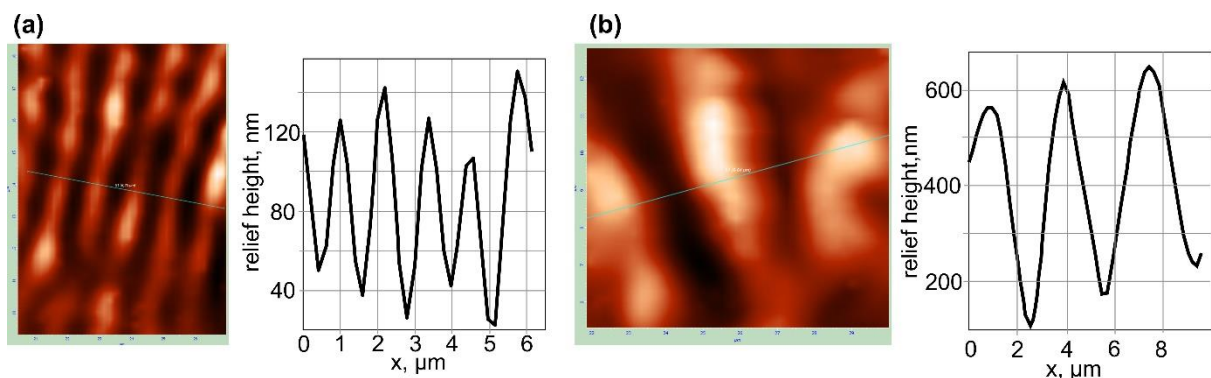


Figure 1. Examples of SRGs fabricated with the help of two depolarizer with different orientations of their axes. The atomic force microscopy images and the cross-sections of the fabricated reliefs for period of 1 (a) and 3 (b) μm are shown.

[1] A.P. Porfirev, S. N. Khonina, N.A. Ivliev, D.P. Porfirev, Laser processing of chalcogenide glasses using laser fields with a spatially varying polarization distribution, submitted to Optics and Laser Technology (2023).

[2] J. Wätzel, J. Berakdar, Spatiotemporal delay in photoionization by polarization-structured laser fields, Phys. Rev. A, vol. 103, pp. 063107 (2021).

[3] E. Achimova, A. Stronski, V. Abaskin, A. Meshalkin, A. Paiuk, A. Prisacar, P. Oleksenko, G. Triduh, Direct surface relief formation on As₂S₃-Se nanomultilayers in dependence on polarization states of recording beams, Opt. Mater., vol. 47, 566-572 (2015).

[4] https://www.thorlabs.com/newgrouppage9.cfm?objectgroup_id=8043

Pressure pulses generated in metals during picosecond laser ablation

S.I.Kudryashov¹, P.A.Pivovarov², V.I.Prikloński³, A.A.Samokhin^{2*}, S.Ph.Umanskaya¹,
N.V.Chernega¹

1- P. N. Lebedev Physical Institute of Russian Acad. Sci., Leninskiy Pr. 53, 119991 Moscow, Russian Federation

2- Prokhorov General Physics Institute of the Russian Academy of Sciences, st.Vavilova 38, Moscow, 119991 Russian Federation

3- Faculty of Physics Lomonosov Moscow State University, 1 Leninskie Gory, bldg. 2, Moscow, 119234 Russian Federation

Main author* email address: asam40@mail.ru

The behavior of pressure pulses generated in a metal during picosecond laser ablation is analyzed. The contribution to the formation of such pulses is due to the thermoacoustic and evaporative mechanisms, as well as possible explosive boiling or metal-insulator transition and accompanying hydrodynamic effects. For shorter pulses in this range, the main role is played by the thermoacoustic mechanism, which is realized at a subcritical change in the density of the condensed medium. Analytical and numerical estimates show that, for a certain duration of picosecond exposure, the stationary evaporation regime can be achieved in the region where the evaporation pressure does not yet exceed the contribution from the thermoacoustic mechanism. In this case, in contrast to the nanosecond exposure [1], the change in the main mechanisms of pressure generation with increasing laser intensity may not be accompanied by a sharp change in the pressure increase due to surface evaporation. This behavior is compared with the experimental data obtained on monitoring the recoil pressure in lead and aluminum targets irradiated with 30 ps laser pulses ($\lambda=532$ nm) in the intensity range $I<90$ GW/cm². These data do not show noticeable manifestations of delayed effects after the action of a laser pulse, which were discussed in [2-5] for different laser pulse duration and materials. Questions about observing the effects of explosive boiling or metal-dielectric transition in such a regime of exposure and monitoring also remain open, in particular, due to the limitations of the resolution of pressure sensors. To detect and study such effects, the nanosecond exposure mode is more optimal. Revealing the features of laser ablation of metals due to the presence of a critical liquid-vapor transition point is necessary to clarify the possibility of their use in order to obtain experimental information about the parameters of this point, which continue to be poorly defined for most metals.

[1] A.A. Samokhin, P.A. Pivovarov, Effect of the Metal–Nonmetal Transition on the Pressure Pulse in Laser Ablation of Mercury. *Phys. Wave Phen.* 30, 364–369 (2022).

[2] A.V. Pakhomov, M.S. Thompson, D.A. Gregory, Laser-induced phase explosions in lead, tin and other elements: microsecond regime and UV-emission, *J. Phys. D: Appl. Phys.* 36, 2067 (2003).

[3] V.I. Vovchenko, S.M.Klimentov, P.A. Pivovarov, et al. Effect of submillisecond radiation of the erbium laser on absorbing liquid, *Bull. Lebedev Phys. Inst.* 34, 325–328 (2007).

[4] A.A. Samokhin, P.A.Pivovarov, , E.V. Shashkov, et al. On the Metal–Nonmetal Transition under Nanosecond Laser Ablation, *Phys. Wave Phen.* 29, 204–209 (2021).

[5] A.A. Samokhin, N.N. Il'ichev, A.V. Sidorin, P.A. Pivovarov, Delayed effects in laser ablation, Abstract book of International Conference on Advanced Laser Technologies (ALT) (2022)

LM-P-13

Laser-ablative synthesis of alternative plasmonic nanomaterials for biomedical applications

M.S. Savinov¹, A.A. Popov¹, G.V. Tikhonowski¹, I.V. Zelepukin^{1,2}, A.I. Pastukhov³, S.M. Klimentov¹, A.V. Kabashin^{1,3}

1- MEPhI, Institute of Engineering Physics for Biomedicine (PhysBio), Moscow, Russia

2- Shemyakin-Ovchinnikov Institute of Bioorganic Chemistry of Russian Academy of Sciences, Moscow, Russia

3- Aix-Marseille University, CNRS, LP3, Marseille, France

email: MSSavinov@mephi.ru

The field of nanotechnology plays an increasingly important role in the development of new diagnostic and therapeutic approaches for cancer treatment. Among them, targeted photothermal therapy (PTT) and related photoacoustic imaging (PAI) are among the most promising methods. These techniques are based on the selective heating of nanoparticles (NPs), localized in tumor, by external light radiation. Plasmonic nanomaterials and especially gold (Au) NPs are widely used in PTT and PAI. One major drawback of the classical plasmonic NPs is related to the spectral position of their plasmonic feature. For example, small spherical Au NPs (5-50 nm) have plasmonic peak around 520-540 nm, which is far from the biological tissue transparency window located between 650 and 950 nm. This spectral mismatch problem can be solved by using an engineered Au-based nanostructures, which however have several major limitations. There is another solution to the plasmonic mismatch problem, which implies application of alternative plasmonic materials, such as TiN, ZrN, HfN, etc. These NPs look much more promising for PTT than traditional plasmonic materials due to several factors, including spectral position of their plasmonic peak in the window of relative tissue transparency combined with their low cost and high availability.

However, synthesis of colloidal solution of these NPs, suitable for biomedical applications, is challenging. Traditional synthesis methods are based on approaches of colloidal chemistry, which often results in NPs surface contamination and related reduced biocompatibility. An alternative laser-based technology for the colloidal nanomaterials synthesis is pulsed laser ablation in liquids (PLAL). This method makes possible synthesis of stable colloidal solutions of clean NPs with controllable physico-chemical properties. The unique surface purity of the laser-synthesized nanomaterials, as well as the high productivity and simplicity of this method, have led to a wide application of PLAL-synthesized NPs in multiple biomedical applications.

Here, we present our recent results on laser synthesis of alternative plasmonic NPs based on TiN and ZrN, their surface modification and biological assessment as sensitizers of PTT and contrast agents for PA imaging.

This study was supported by the Russian Science Foundation (project no. 22-72-00015).



LM-P-15

Study of migration of elements on the metal surfaces after laser shock peening

E. Surmenko, P. Ustinov, T. Sokolova, D. Bessonov

1- Saratov State Technical University, 77 Polytechnicheskaya st., 410054, Saratov, Russia

surmenko@vandex.ru

Laser shock peening is an enough well-known technology of surface material treating. The treated surface is previously covered by non-transparent layer (paint) and transparent layer (water). The energy of the laser pulse is absorbed by the non-transparent layer, which leads to its heating, evaporation and the formation of a high-temperature plasma bounded on one side by the surface of the material, and on the other, by a transparent layer that restrains the spread of the plasma temperature. Due to the limited volume, the gas pressure rises sharply to high values and passes into the metal, creating a shock wave in it, which leads to the appearance of compressive stresses in the material. If these stresses exceed the elastic Hugoniot limit, then the material plastically deformed. Residual stress states strengthen the surface layer of radiated metals.

The non-transparent layer serves as protection against direct contact of the sample surface with laser-induced plasma, and also helps to match the surface properties for interaction with laser radiation, regardless of the actual properties of the sample. Direct interaction of the sample surface with plasma leads in most cases to the formation of a metal melt on the surface. That is why when making peening it is important to control the absorption of paint on the surface and, in the same time, to study fractions and chemical elements migration in the laser action zone.

The paper describes the study of chemical composition of the steel and aluminum alloys before and after laser shock peening. The samples were treated with Nd:YAG-laser ($\lambda=1.06 \mu\text{m}$), pulse repetition rate 25 Hz, speed 900 m/s, power 24 W. Three types of paints were used and different number of peening passes.

The estimation of chemical composition of surface was studied by LIBS-method (laser induced breakdown spectroscopy). The diffusion of paints and migration of elements of the substrate was observed layer-by-layer way with the aid of scanning sampling – three times from the same sampling path.

It was found out that the very surface layer is always depleted with Mn. This trend is common for almost all the studied samples metals and paints. At the same time Ti shows local maximum for some paints. Some other trends and their comparative analysis are presented in the work.

LM-P-16

Development of technologies for laser thin-layer surface modification of products made of stainless chromium-nickel steels

P. Ustinov¹ I. Rodionov E. Surmenko D. Bessonov T. Sokolova

1- Saratov State Technical University, 77 Polytechnicheskaya st., 410054, Saratov, Russia

azenrod@gmail.com

The purpose of this work is to develop a technology for creating a thin-layer hardening layer from a finely dispersed tungsten carbide powder.

Along with many advantages, stainless steel also has disadvantages, such as insufficient wear resistance and hardness. One way to solve this problem is to create a hardened layer using laser processing. This process is one of the most effective methods for restoring coatings with increased wear resistance. Laser cladding consists in applying a coating to the surface of the workpiece by melting the base and filler material. Since the base does not melt much, the properties of the coating mainly depend on the properties of the filler material. Finely dispersed tungsten carbide powder with a fineness of 1 μm , which is widely used in various industries, was chosen as the deposited filler material[1,2].

To conduct the study, a plate made of stainless steel grade 12X18H10T with a size of 150 × 20 mm was used as a prototype. A layer of graphite paste was applied to the surface of the sample to create a bonding layer, over which a layer of fine tungsten carbide powder about 100-200 micrometers thick was spread.

For the experiments, a RAYLOGIC V12 6040 laser unit was used. This unit has a continuous radiation method, the active element is carbon dioxide CO₂, and the power is 30 W.

During the experiment, the surface treatment modes were changed, the main ones being the radiation power, processing speed, and line density.

To study the surface of the samples before and after processing, the PMT-3M hardness tester was used to study the microhardness of the surface and spectral analysis using the Spektr-2000 installation.

The results of measuring the microhardness showed that the upper layers of the surface of the samples were strengthened by 2-3.5 times from the initial microhardness index. When conducting a qualitative spectral analysis, a significant increase in the content of tungsten in the structure of the surface of the samples at a depth of up to 60 μm was revealed.

[1] Krasnova E.V., Morgunov Yu.A., Saushkin B.P., Shandrov B.V. Development of applied scientific research in mechanical engineering in Russia. *Ekonomika v promyshlennosti = Economics in industry*. 2021;14(3):274–287. (In Russ.)

[2] Kolomiytsev E.V. Corrosion-fatigue resistance of tee joints of steel 12Kh18N10T and methods for its challenge. *Avtomaticheskaya svarka = Automatic welding*. 2012;(12): 41–43. (In Russ.)



BIOMEDICAL

PHOTONICS

B-I-1

One-shot laser-pulse modification of Au and Au@SiO₂ nanoparticles of various shapes and morphology

N. Khlebtsov^{1,2}, V. Khanadeev^{1,3}, A. Simonenko^{1,2}, O. Grishin², L. Dykman¹

1- Institute of Biochemistry and Physiology of Plants and Microorganisms, Saratov Scientific Centre of the Russian Academy of Sciences (IBPPM RAS), 13 Prospect Entuziastov, Saratov 410049, Russia

2- Saratov State University, 83 Ulitsa Astrakhanskaya, Saratov 410012, Russia

3 -Saratov State University of Genetics, Biotechnology, and Engineering named after N. I. Vavilov

e-mail: khlebtsov@ibppm.ru

Gold and hybrid SiO₂@Au / Au@SiO₂ nanoparticles are widely used in laser biomedical applications as photothermal, sensoric, bioimaging, and therapeutic agents due to their favorable near-field and far-field optical properties based on localized plasmon resonance (PR). However, laser radiation can cause a change in the shape and size of plasmonic nanoparticles thus resulting in an unwanted reduction of their photothermal and photodynamic efficiency due to a drastic alteration of optical properties. Most previously reported experiments were carried out with bulk colloids where different particles were irradiated by different numbers of laser pulses thus making it difficult accurately evaluate the laser power photomodification (PM) threshold. Here, we examine the one-shot nanosecond laser-pulse PM of bare and silica-coated gold nanoparticles moving in a capillary flow [1]. Four types of gold nanoparticles, including nanostars, nanoantennas, nanorods, and SiO₂@Au nanoshells were fabricated for PM experiments. To evaluate the changes in the particle morphology under laser irradiation, we combine measurements of extinction spectra with electron microscopy. A quantitative spectral approach is developed to characterize the laser power PM threshold in terms of normalized extinction parameters: $PM_{factor} = [q(0) - q(F)]/[q(0) - q(F_{max})]$, $q(F) = A(F, PR)/A(F, 550)$, where $A(F, PR)$ is the extinction of particles at PR wavelength after PM treatment with the fluence value F ; $A(F, 550)$ is the extinction value at the wavelength of the short-wavelength maximum in the region of 500-600 nm (if it exists), or is the extinction value at the wavelength of 550 nm, if there is no maximum in this region. The experimentally determined PM threshold increases in series: nanorods, nanoantennas, nanoshells, and nanostars. An important observation is that even a thin silica shell significantly increases the photostability of gold nanorods (Fig. 1). The developed methods and reported findings can be useful for the optimal design of plasmonic particles and laser irradiation parameters in various biomedical applications of functionalized hybrid nanostructures.

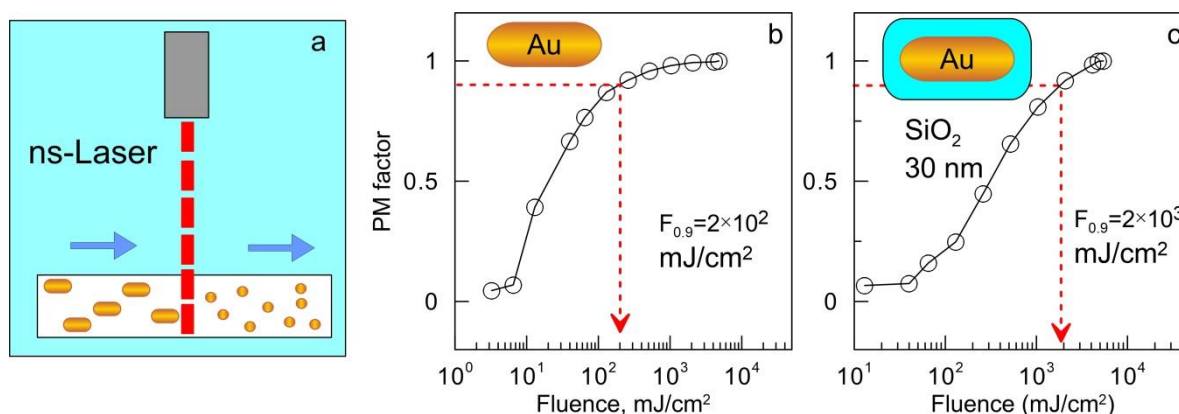


Fig. 1. Scheme of pulsed laser irradiation of nanoparticles moving in a capillary (a) and photomodification factor as a function of fluence for bare (b) and silica-coated (c) gold nanorods. A 30-nm silica coating increases the 90%-PM fluence threshold from 200 to 2000 mJ/cm².

This work was supported by the Russian Scientific Foundation (project No. 19-14-00077).

[1] Khanadeev V., Simonenko A., Grishin O., Khlebtsov N. One-shot laser-pulse modification of bare and silica-coated gold nanoparticles of various morphologies. *Nanomaterials*, vol. 13, 1312 (2023).



B-I-2

Laser-ablated Si and Si/Ag nanoparticles in biophotonics: biocompatibility, bioimaging, and photothermal therapy

**S. Zobotnov¹, D. Shuleiko¹, V. Nesterov^{1,2}, O. Sokolovskaya¹, L. Golovan¹, A. Khilov³,
D. Kurakina³, E. Sergeeva³, P. Agrba⁴, A. Balashova⁴, M. Kirillin³**

1- Lomonosov Moscow State University, Faculty of Physics, 1/2 Leninskie Gory, Moscow, 119991, Russia

2- Moscow Institute of Physics and Technology, 9 Institutskiy Per., Dolgoprudny, 141701, Russia

3- Institute of Applied Physics RAS, 46 Uljanov St., Nizhny Novgorod, 603950, Russia

4- N.I. Lobachevsky State University of Nizhny Novgorod, 23 Gagarin Ave., Nizhny Novgorod, 603950, Russia

zobotnov@physics.msu.ru

Silicon nanoparticles (SiNPs) are successfully used in various biomedical applications due to their low toxicity and biodegradability [1, 2].

In this paper we study the possibility of employment of laser-ablated SiNPs in biophotonics. The particles are formed by femtosecond (1250 nm, 150 fs) and picosecond (1064 nm, 34 ps) laser ablation of monocrystalline and porous silicon targets in various liquids: water, ethanol, liquid nitrogen, and aqueous ethanol solution with silver nitrate. In the latter case, it is possible to decorate the SiNPs surface with silver particles of several nanometers in size (Si/Ag) [3].

As a result of the ablation, SiNPs suspensions were fabricated with the nanoparticles mean size varying from 25 to 120 nm depending on the parameters of laser pulses (energy, duration, and number), the targets used, and the buffer liquids.

An analysis of the measured values of the scattering and absorption coefficients of the prepared SiNPs suspensions showed that such nanosystems have high potential as contrast agents in optical coherence tomography. This assumption was confirmed by experiments on contrasting structural inhomogeneities of agar gel with the embedded SiNPs.

A numerical experiment of a photothermal therapy process with the SiNPs embedded into a human subcutaneous basal cell carcinoma showed that it is possible to select irradiation parameters (633 nm, 60–200 mW) that provide hyperthermia of the entire tumor without significant overheating the surrounding healthy tissues. A real experiment on heating was carried out with a phantom simulating the optical properties of human skin and made on the basis of agar gel, lipofundin, and red ink. It was confirmed that the administration of the SiNPs on the phantom increases its heating under equivalent irradiation conditions (660 nm, 410 mW/cm²) compared with the phantom without nanoparticles. Additionally, the decorated Si/Ag nanoparticles are of interest for further research as agents for photothermal therapy, since the silver inclusions, according to the analysis of spectrophotometric data, provide resonant Mie absorption in the spectral range near 435 nm and may increase heating without increasing the mass concentration of the agents.

In vivo monitoring of the reaction of laboratory mice after administration the SiNPs was carried out using the "Open field" test, which makes it possible to estimate the general (locomotor) and exploratory animal activities. Low toxicity of SiNPs was shown for oral and topical administration, however, an increase in the stress level in the experimental groups relative to the control ones was revealed.

Thus, the biocompatible SiNPs formed by laser ablation in liquids are of undoubted interest for solving problems of biological tissues theranostics.

[1] M. d'Amora, M. Rodio, G. Sancataldo, et al., ACS Appl. Bio Mater., Laser-fabricated fluorescent, ligand-free silicon nanoparticles: scale-up, biosafety, and 3D live imaging of zebrafish under development, 2(1), 321–329, (2019).

[2] S.V. Zobotnov, A.V. Skobelkina, E.A. Sergeeva, et al., Nanoparticles produced via laser ablation of porous silicon and silicon nanowires for optical bioimaging, Sensors, 20(17), 4874, (2020).

[3] S.O. Gurbatov, V. Puzikov, E. Modin, et al., Materials, Ag-decorated Si microspheres produced by laser ablation in liquid: all-in-one temperature-feedback SERS-based platform for nanosensing, 15(22), 8091, (2022).

B-I-3

Visualization of complexes of upconversion nanoparticles with a photosensitizer in biological objects

V. I. Kochubey,^{1,2} A. M. Mylnikov,³ N. A. Navolokin,^{3,4,5} I. Yu. Yanina^{1,2}

¹- Saratov State University (National Research University), Institute of Physics, 83 Astrakhanskaya str., Saratov 410012, Russia

²- Tomsk State University (National Research University), Laboratory of laser molecular imaging and machine learning, 36 Lenin's av., Tomsk 634050, Russia

³- Saratov State Medical University, Department of Pathological Anatomy, 112 B Kazachaya str., Saratov 410012, Russia

⁴- Saratov State Medical University, Center for Collective Use of Experimental Oncology, Experimental Department, 112 B Kazachaya str., Saratov 410012, Russia

⁵- State Healthcare Institution "Saratov City Clinical Hospital No. 1 named after Yu.Ya. Gordeev", 19 Kholzunova st., Pathological Department, Saratov 410017, Russia

e-mail: irina-yanina@list.ru

Photodynamic therapy (PDT), has the potential to cure cancerous tissue with minimal side effects [1]. However, conventional PDT mostly uses visible (VIS) light range with the application of hydrophobic photosensitizers (PSs), which may not be sufficient in clinical practice, especially for deep-seated cancer cells, due to poor penetration of VIS wavelengths.

Upconversion nanoparticles (UCNPs) with unique optical properties are considered a promising platform for creating tumor markers that provide real-time optical visualization of tissues with high sensitivity and contrast, enabling them to be used for intraoperative diagnostics [2,3]. UCNPs are also promising platforms for enhancing the therapeutic response of cancer cells to PDT [4]. When coupled with UCNPs, the PSs in PDT are indirectly activated by near-infrared (NIR) excitation allowing for deeper tissue penetration and reduced attenuation. To achieve maximum performance, the up-converted emission peak of the UCNPs and the absorption band of the PSs must overlap significantly. However, the spectral mismatch between the up-converted emission maximum of UCNPs (predominantly in the green) and the absorption maximum of most available PSs (in the red) severely limits the therapeutic efficacy of current UCNP-PDT platforms.

In this paper, we present data on stable surface coating of the UCNPs with human serum albumin (HSA) and PS. The choice was based on the overlap of the NP luminescence and PS absorption bands.

We have been carried out studies on the visualization of nanoparticles in sections of rat organs and tumors by direct registration of a luminescent image. Samples of skin, organs and tumors were obtained surgically from rats with model liver cancer after intravenous injection of the NaYF₄:Yb,Er-HSA-PS complex.

Nanoparticles embedded in biological tissue are displayed as light spots whose size of which is determined by the size of the diffraction spot formed by the optical system. The images show a significant number of nanoparticles, both single and aggregated. UCNPs accumulate mainly in the spleen, as confirmed by histopathological analysis data. When the particles are injected intravenously twice, their maximum accumulation occurs in the tumor tissue. In general, no significant damage to organs, tissues, and erythrocytes was observed during particle accumulation. It can be concluded that the studied particles do not cause a pronounced toxic effect, and any changes that occur on the background of their introduction are reversible and not persistent.

We have proposed a promising complex for photodynamic therapy.

The study was supported by a grant Russian Science Foundation No. 21-72-10057, <https://rscf.ru/project/21-72-10057/>

[1] B. Güleriyüz, U. Ünal, M. Gülsoy, Near infrared light activated upconversion nanoparticles (UCNP) based photodynamic therapy of prostate cancers: An *in vitro* study, *Photodiagnosis Photodyn Ther.*, vol. 36, pp. 102616 (2021).

[2] A. Nadort, V. K. Sreenivasan, Z. Song, E. A. Grebenik, A. V. Nechaev, V. A. Semchishen, V. Y. Panchenko, A. V. Zvyagin, Quantitative imaging of single upconversion nanoparticles in biological tissue, *PLoS One*, vol. 8, no.5, pp. e63292-1-13 (2013).

[3] G. Dumlupinar, S. K. V. Sekar, C. N. Guadagno, J. S. Matias, P. Lanka, C. K.W. Kho, S. Andersson-Engels, Solid optical tissue phantom tools based on upconverting nanoparticles for biomedical applications, *J. Biomed. Opt.*, vol. 28, no.3, pp.036004-1-12 (2023).

[4] S. He, N. J. J. Johnson, V. A. N. Huu, Y. Huang, A. Almutairi, Leveraging Spectral Matching between Photosensitizers and Upconversion Nanoparticles for 808 nm-Activated Photodynamic Therapy, *Chem. Mater.*, 30, 12, 3991–4000 (2018).



B-I-5

VIS-NIR diffuse reflectance spectroscopy system with self-calibrating fiber-optic probe

V. Perekatova, A. Kostyuk, M. Kirillin, E. Sergeeva, D. Kurakina, O. Shemagina, A. Orlova, A. Khilov and I. Turchin

Federal Research Center A.V. Gaponov-Grekhov Institute of Applied Physics of the Russian Academy of Sciences, 603950 Ulyanov St., 46, Nizhny Novgorod, Russia

ilya340@mail.ru

Diffuse reflectance spectroscopy (DRS) is based on illuminating biological tissue with broadband light in the visible (VIS) and/or near infrared (NIR) spectrum region and detecting backscattered light at a given distance from the source. The recorded spectrum contains information on the absorption of various tissue chromophores (oxy- and deoxyhemoglobin, melanin, water, lipids), the concentration of which can be reconstructed by solving an inverse problem. One of the key points of successful reconstruction of tissue chromophores is taking into account the instrumental characteristics of the DRS system. Traditional ratiometric (or single-slope) approach based on the measurements with two source-detector distances (one source and two detectors or two sources and a single detector) allows for compensation of detector spectral sensitivity and the source brightness variations [1], but it does not allow compensating all transient functions of the source and detector. The self-calibrating approach proposed in [2] is based on symmetrical multi-distance measurements (at least four measurements with two sources and two detectors) and makes it possible to compensate for the instrumental contributions of the source and detector channels. Additionally, it is less sensitive to changes in the optical coupling between the optical sensor and tissue [3] in comparison to single-distance and single-slope approaches. In this paper, we present an experimental setup for VIS-NIR DRS with a fiber optic probe using a self-calibrating approach. To our knowledge, this is the first application of the self-calibration approach for the 460–1030 nm ultra-wideband (VIS-NIR) DRS. The stability of the self-calibrating and traditional single-slope approaches to instrumental perturbations were compared in phantom and in vivo studies on human palm, including attenuations in individual channels, fiber curving, and introducing optical inhomogeneities in the probe–tissue interface [4]. The self-calibrating approach demonstrated high resistance to instrumental perturbations introduced into the source and detection channels, while the single-slope approach showed resistance only to perturbations introduced into the source channels. The developed experimental setup has been employed successfully in the in vivo studies on rats to reveal the differences in dynamics of allo- and autografts physiological parameters (blood and water content, and oxygenation) [5].

There are many applications of DRS in biomedicine, among them the study of brain hemodynamics, diagnosis of skin diseases, assessing the tumor boundaries of various localizations, and many other applications.

The study was supported by Center of Excellence «Center of Photonics» funded by The Ministry of Science and Higher Education of the Russian Federation, Contract No. 075-15-2022-316

[1] F. Scholkmann, A. J. Metz, and M. Wolf, "Measuring tissue hemodynamics and oxygenation by continuous-wave functional near-infrared spectroscopy—how robust are the different calculation methods against movement artifacts?," *Physiological measurement* 35, 717 (2014).

[2] D. M. Hueber, S. Fantini, A. E. Cerussi, and B. B. Barbieri, "New optical probe designs for absolute (self-calibrating) NIR tissue hemoglobin measurements," in *Optical tomography and spectroscopy of tissue III*, (SPIE, 1999), 618-631.

[3] A. Sassaroli, G. Blaney, and S. Fantini, "Dual-slope method for enhanced depth sensitivity in diffuse optical spectroscopy," *JOSA A* 36, 1743-1761 (2019).

[4] V. Perekatova, A. Kostyuk, M. Kirillin, E. Sergeeva, D. Kurakina, O. Shemagina, A. Orlova, A. Khilov, I. Turchin, VIS-NIR Diffuse Reflectance Spectroscopy System with Self-Calibrating Fiber-Optic Probe: Study of Perturbation Resistance, *Diagnostics*, 13, 457 (2023).

[5] I. Turchin, V. Beschastnov, P. Peretyagin, V. Perekatova, A. Kostyuk, A. Orlova, N. Koloshein, A. Khilov, E. Sergeeva, M. Kirillin, M. Ryabkov, Multimodal Optical Monitoring of Auto- and Allografts of Skin on a Burn Wound, *Biomedicines*, 11, 351 (2023).

B-I-6**Time-resolved measurements of singlet oxygen phosphorescence in the solvents lacking hydrogen atoms. Application to the study of biologically important compounds****A. Krasnovsky, Jr.***, A. Benditkis*FRC of biotechnology RAS, Leninskii pr., 33, bld. 2, Moscow, 199071, Russia***phoal@mail.ru*

In solvents, molecules of which do not contain hydrogen atoms, the lifetime of singlet oxygen is known to reach several tens of milliseconds. Therefore, the use of these solvents is exceptionally efficient for studying the properties of singlet oxygen and measuring the intrinsic IR phosphorescence of singlet oxygen at 1270 nm, which is known to be the most reliable method for singlet oxygen detection. However, for phosphorescence measurements in these solvents, one needs a special equipment that allows recording slowly decaying phosphorescence under a very low rate of generation of singlet oxygen. We have recently succeeded in constructing such spectrometers for steady-state and time-resolved phosphorescence measurements that are based on the use of cw and pulsed diode lasers and LEDs [1]. For kinetic measurements, the methods of time-resolved photon counting and time-correlated single photon counting were applied with the accumulation and averaging of a phosphorescence signal after hundreds of thousands of exciting laser (LED) flashes. These set-ups open up new amazing research opportunities, some of which will be presented in our talk. For instance, the lifetimes of singlet oxygen have been measured in a range of solvents, in which hydrogen atoms are replaced by chlorine, fluorine or iodine. It was shown that in aerated solvents of this type singlet oxygen is quenched by dissolved triplet oxygen molecules and the quenching rate constants were determined. The spectrometers are very efficient for excitation of photosensitizers absorbing light in violet, blue and near ultraviolet regions. In particular, this allowed us to reveal the ability of phytofluene, which is the universal precursor of all natural colored carotenoids, to efficiently generate singlet oxygen. It was found that colored C40 carotenoids that are usually considered as strong quenchers of singlet oxygen, photosensitize its formation upon photoexcitation.

Application of these spectrometers to studies of chlorophylls and bacteriochlorophylls, which are rapidly destroyed under light will also be discussed.

This work was partially supported by the Russian Science Foundation, Project # 23-65-10005.

[1] A. Krasnovsky, A. Benditkis, A. Kozlov. *Biochemistry (Moscow)*, vol. 84, pp. 153-163 (2019) doi: 10.1134/S0006297919020068

[2] A. Ashikhmin, A. Benditkis, A. Moskalenko, A. Krasnovsky, *Biochemistry (Moscow)*, vol. 85, pp. 773-780 (2020) doi: 10.31857/S0320972520070052

[3] A. Benditkis, A., Kozlov, S. Goncharov, A. Krasnovsky, *J. Opt. Soc. Am. B*, vol. 38, 3410-3416 (2021); doi.org/10.1364/JOSAB.432684

[4] A. Ashikhmin, A. Benditkis, A. Moskalenko, A. Krasnovsky, *Biochemistry (Moscow)*, vol. 87, pp. 1169-1178. doi: 10.1134/S0006297922100108

[5] A. Benditkis A., Ashikhmin, A. Moskalenko, A. Krasnovsky, *Photosynth. Res.*, submitted



B-I-7

Optical evaluation of differences in the diffusion of probe molecules in normal and pathological human kidney tissues

M. Pinheiro¹, I. Carneiro^{2,3}, S. Carvalho⁴, R. Henrique^{2,5}, V. Tuchin^{6,7}, L. Oliveira^{1,8}

- 1- *Institute for Systems and Computer Engineering, Technology and Science (INESC TEC), Campus da FEUP, Rua Dr. Roberto Frias, 4200-465 Porto, Portugal*
- 2- *Department of Pathology and Cancer Biology and Epigenetics Group, Portuguese Oncology Institute of Porto, Rua Dr. António Bernardino de Almeida, 4200-072 Porto, Portugal*
- 3- *Department of Pathological, Cytological and Thanatological Anatomy, Polytechnic of Porto – School of Health (ESS), Rua Dr. António Bernardino de Almeida, 4200-072 Porto, Portugal*
- 4- *Department of Pathology, Santa Luzia Hospital (ULSAM), Estrada de Santa Luzia, 4904-858 Viana do Castelo, Portugal*
- 5- *Department of Pathology and Molecular Immunology, Porto University – Institute of Biomedical Sciences Abel Salazar, Rua de Jorge Viterbo Ferreira, n° 228, 4050-313 Porto, Portugal*
- 6- *Institute of Physics and Science Medical Center, Saratov State University, 83 Astrakhanskaya str., Saratov 410012, Russia*
- 7- *Laboratory of Laser Diagnostics of Technical and Living Systems, Institute of Precision Mechanics and Control of the FRC “Saratov Scientific Centre of the Russian Academy of Sciences,” 24 Rabochaya, Saratov 410028, Russia*
- 8- *Physics Department, School of Engineering, Polytechnic of Porto, Rua Dr. António Bernardino de Almeida n° 431, 4249-015 Porto, Portugal*

Main author email address: lmo@isep.ipp.pt

The application of kinetic spectroscopy and thickness measurements has been widely used to evaluate the diffusion properties of optical clearing agents (probe molecules) in tissues under treatment with solutions of different osmolarity [1]. Such methodology can be useful in various fields, such as dermatology, cosmetics or cryopreservation of organs and food products [2]. By performing those measurements from human colorectal mucosa tissues, in addition to discriminated diffusion properties in normal and pathological (adenocarcinoma) mucosa, it was possible to evaluate a higher mobile water content in the diseased tissue [3]. Since both the discriminated diffusion properties and different mobile water content in normal and diseased tissues can be used in diagnostic procedures, human kidney tissues, both normal and with chromophobe renal cell carcinoma (CRCC) were submitted to those measurements when under treatment with glycerol or sucrose solutions. It was found in this study that the characteristic diffusion coefficient of glycerol was 4.85×10^{-7} cm²/s in the normal kidney and 3.16×10^{-7} cm²/s in the CRCC kidney, while the characteristic diffusion coefficient of sucrose was 4.63×10^{-7} cm²/s in the normal kidney and 3.31×10^{-7} in the CRCC kidney. Apart from the discriminated diffusion properties of glycerol and sucrose in both tissues, it was also found that the CRCC kidney contains about 5% more mobile water than the normal kidney. Now that such difference in the mobile water content was found for two different cancers, it will be interesting to evaluate it as a function of cancer progression.

[1] I. Carneiro, S. Carvalho, R. Henrique, L. Oliveira and V. Tuchin, A robust ex vivo method to evaluate the diffusion properties of agents in biological tissues, *J. Biophotonics*, vol. 12, pp. e201800333 (2019).

[2] L. Oliveira and V. Tuchin, *The Optical Clearing Method: A New Tool for Clinical Practice and Biomedical Engineering* (Springer), Chapter 6, (2019).

[3] S. Carvalho, N. Gueiral, E. Nogueira, R. Henrique, L. Oliveira and V. Tuchin, Glucose diffusion in colorectal mucosa – a comparative study between normal and cancer tissues, *J. Biomed. Opt.*, vol. 22, pp. 091506 (2017).

B-I-8**Factors determining the increased sensitivity of cancer cells to the action of laser radiation in the blue region of the spectrum**

V. Plavskii, L. Plavskaya, O. Dudinova, A. Sobchuk, A. Svechko, R. Nahorny, A. Tretyakova, A. Mikulich, T. Ananich, S. Yakimchuk, I. Leusenko

B.I. Stepanov Institute of Physics of the National Academy of Sciences of Belarus, Minsk, Belarus

v.plavskii@ifanbel.bas-net.by

The objective of this work is comparative studies of the effectiveness of radiation of various wavelengths of the blue spectral region on cancer and untransformed cells in vitro, comparing the level of concentrations of endogenous photosensitizers and reactive oxygen species (ROS) in cells of these types, elucidation of the mechanism of antitumor activity of blue light and the reasons determining the higher sensitivity of cancer cells to the action of blue light.

The performed studies have shown the ability of radiation from laser and LED sources with a wavelength in the range of $\lambda = 405\text{--}465$ nm, in the range of energy doses of $1\text{--}15$ J/cm² to influence the metabolic activity of cancer cells (epithelioid carcinoma of the cervix HeLa) and normal untransformed cells (African green monkey kidney cells BGM). Comparative studies performed using semiconductor lasers and LEDs with a wavelength of 405 and 445 nm revealed the absence of fundamental differences in the biological effect of monochromatic radiation from laser sources and quasi-monochromatic radiation from LEDs. The most pronounced effect on the metabolic activity of cells is exerted by radiation with $\lambda = 405$ nm. The photobiological effect initiated by exposure to radiation with $\lambda = 445$ nm is significantly lower; radiation with $\lambda = 465$ nm has the least pronounced effect. Depending on the intensity of radiation and the energy dose, the light of the blue region of the spectrum can both stimulate the metabolic activity of cells (which is observed in a fairly narrow range of energy doses) and inhibit it. Moreover, the inhibitory effect increases with an increase in the energy dose of light exposure. At low energy doses of light exposure, the decrease in the metabolic activity of cells is not explained by their death, but is due to a change in the duration of individual phases of the cell cycle. However, at high energy doses, cell death, realized by the mechanism of necrosis and apoptosis, makes a significant contribution to the decrease in metabolic activity.

The main conclusion that follows from the performed studies is that at the same energy dose, the inhibitory effect of blue light is significantly more pronounced in relation to tumor cells than in relation to normal untransformed ones. It has been established that the biological effect of blue light is caused by reactions initiated by ROS due to the excitation of endogenous photosensitizers. The addition of ROS quenchers to the nutrient medium of cells before their irradiation can block the photobiological effect. It was shown for the first time that the contribution of various types of ROS (singlet oxygen, hydrogen peroxide, etc.) to the effects of cell inactivation depends on the time after the cessation of irradiation, which is associated with the launch of a wave of massive secondary ROS production in cells, and, above all, hydrogen peroxide. If, immediately after the cessation of exposure, the main intermediate determining the course of photobiological reactions in cells is singlet oxygen, then a day after the cessation of irradiation – hydrogen peroxide.

Using stationary and kinetic spectrofluorimetry methods, porphyrin components were registered for the first time in the fluorescence spectra of a suspension of living cells along with the flavin component. It has been shown that the level of porphyrin photosensitizers is approximately 2.5 times higher in tumor cells than in untransformed ones. The higher concentration of endogenous photosensitizers in cancer cells is the reason for the higher rate of their inactivation compared to normal cells. Based on a comparison of the absorption characteristics of flavin and porphyrin sensitizers, as well as data from chemiluminescence analysis and the biological effects of radiation with $\lambda = 405$ and 445 nm, it is concluded that the determining contribution to the formation of singlet oxygen in cells when exposed to radiation with $\lambda = 405$ nm is made by endogenous porphyrins, characterized by the most intense absorption in this area. The contribution of flavins is more pronounced under the action of radiation with $\lambda = 445$ nm, corresponding to the maximum in their absorption spectrum and the minimum absorption of endogenous porphyrins.



B-I-9

Physical features of laser multiwave action on biological tissues

**Andrei V. Belikov^{1,2}, Yulia V. Fedorova¹, Sergey N. Smirnov¹,
Anastasia D. Kozlova¹, Viktor Yu. Chuchin³**

1-ITMO University, 49 Kronverksky Pr., 197101, Saint Petersburg, Russia

2- Pavlov First St. Petersburg State Medical University, 6-8 L'va Tolstogo str., 197022, Saint Petersburg, Russia

3- Limited Liability Company «NPP VOLO», 4-6 17th line of V. Island, 199034, Saint Petersburg, Russia

Main author email address: avbelikov@gmail.com

The progress of laser medicine is associated not only with the development and implementation of new laser sources, but also with the search for new modes of operation of already known lasers. In this regard, it is very promising to use several wavelengths to action on biological tissues. For example, in neurosurgery, a dual-wavelength surgery system to resect brain tumors is very promising, where a continuous wave (CW) thulium (1.94 μm) laser applied before/during/after μs -pulsed Er:YAG ablation to maintain a blood free zone while retaining the high efficiency of Er:YAG ablation [1]. In dermatology, when vein sclerosis is used, the multiwave effect of pulsed dye and Nd:YAG lasers is used, in which the effect of dye laser radiation (0.585 μm) leads to an increase in the absorption of Nd:YAG laser radiation (1.064 μm) by the dermis, as a result of which the efficiency of destruction of veins by radiation of this laser increases [2]. In laser drug delivery, multiwave laser action can also be used, in which one wavelength, for example, an Er:YLF laser (2.81 μm) is used for biotissue microporation and drug delivery, and the other (0.656 \pm 10 μm) for photodynamic effect on the drug [3].

In this study, the problems of optical and thermophysical modeling of multiwave laser action in dermatology with laser treatment of blood vessels and in neurosurgery with laser interstitial therapy of malignant tumors will be touched upon. We will also represent experimental results of photodynamic treatment of fungus *Candida Albicans* by radiation of different visible wavelength.

Numerical optical and thermophysical models of human skin with and without telangiectasia have been developed. The possibility of using laser radiation with one wavelength to heat the skin with telangiectasia in order to convert hemoglobin in the blood of the vessel into methemoglobin and thereby control the optical properties of the skin, followed by exposure of the vessel to laser radiation with a second wavelength in order to coagulate it, is considered. The effect of methemoglobin concentration on the extinction coefficient and the degree of optical clearing of the skin was studied by numerical methods. It has been established that methemoglobin in the composition of the skin leads to its greatest optical clearing at wavelengths near 0.441 μm and 0.578 μm and maximizes the extinction coefficient at wavelengths near 0.629 μm and 1.105 μm . It has been demonstrated that the replacement of hemoglobin with methemoglobin leads to a change in the absorbed optical power in the skin layers, which can be used to control the optical properties of the skin when creating laser systems and technologies for the treatment of skin diseases, including laser sclerosis of telangiectasias.

Numerical optical and thermophysical models of a human brain tumor have been developed. The features of the effect of laser radiation with a wavelength of 0.98 μm and 1.56 μm on brain tumor (glioma) tissues are considered. It has been demonstrated that the combined effect of multiwave action on a brain tumor makes it possible to increase the efficiency of laser coagulation of the tumor.

In an experiment on a daily culture of the fungus *Candida Albicans*, the antimycotic activity of chlorine-containing photosensitizing drugs "Chloderm" and "Chloderm with hyaluronic acid" (Russia) was evaluated when exposed to radiation with wavelengths of 0.405, 0.450 and 0.656 \pm 10 μm . The high antimycotic activity of the studied drugs was demonstrated. The main mechanisms of the effect of radiation with the investigated wavelengths on the biotissues are discussed.

The research was supported by Russian Science Foundation (project No. 22-25-00468).

[1] N. Katta et al. Laser brain cancer surgery in a xenograft model guided by optical coherence tomography, *Theranostics*, vol. 9, No. 12, pp. 3555–3564, (2019).

[2] Trelles M. A. et al. Treatment of leg veins with combined pulsed dye and Nd: YAG lasers: 60 patients assessed at 6 months, *Lasers in surgery and medicine*, Vol. 42. – №. 9. – pp. 769-774, (2010).

[3] A. V. Belikov, S. N. Smirnov and A. D. Tavalinskaya, Laser Delivery and Spectral Study of a Chlorine-Containing Drug for the Treatment of Onychomycosis at Sequential Laser ($\lambda= 2810 \text{ nm}$) and Photodynamic ($\lambda= 656\pm 10 \text{ nm}$) Impact, *Optics and Spectroscopy*, pp.1-9, (2021).

B-I-10**Experimental substantiation of the prospects for the use of "blue" laser radiation with $\lambda=450$ nm for the effective removal of congenital giant pigmented nevi**

Podurar S.A.¹, Gorbatoва N.Ye.¹, Tertychny A.S.¹, Platonova A.D.¹, Sirotkin A.A.², Kuz'min G.P.², Tikhonovich O.V.², Kalachev Yu.L.², Varev_G.A.³

1- Research Institute of Emergency Pediatric Surgery and Traumatology, Moscow, Russia

2- Prokhorov General Physics Institute of the Russian Academy of Sciences, Moscow, Russia

3- Russian Engineering Club LLC, Tula, Russia

Main author email address: oligaperd@mail.ru

Currently, laser methods for the treatment of skin diseases are widely used and actively introduced into clinical practice due to the pronounced selectivity of the effect [1]. Pigmented nevi (PN) are pathological benign skin formations consisting of accumulations of melanocytes, cells containing the pigment melanin. The group of congenital giant pigmented nevi (CGPN) is a special psychological and medical problem associated with extensive damage to the skin and changes in the patient's appearance [2].

The existing numerous methods of treating CGPN are not effective enough or are accompanied by significant damage to tissue structures, and therefore are not always applicable due to the large amount of skin lesions with pigment formation [2].

The purpose of this work is to improve the results of treatment of CGPN by experimentally substantiating the possibility of using laser radiation with a wavelength (λ 450 nm) and developing a method for their effective removal in order to achieve a good clinical and aesthetic result of treatment. As a radiation source, we used a laser device based on the convergence of laser diodes with a total power of up to 10 W, a spot diameter of 0.6 to 1.5 mm, generating continuous and pulsed "blue" laser radiation $\lambda=450$ nm.

An in vivo experimental study was performed on the pigmented, black-brown skin of living laboratory rats. The skin was exposed to laser radiation in continuous and pulsed (0.5 sec) modes, with a distance between pulses of 0.5 sec, 0.25 and 0.1 sec, with a constant speed of a single scan of 0.5 cm per 1 second over the surface of the object. We used variable radiation power modes: 3.0 W, 6.0 W, 10.0 W.

During the experiment, visually determined macroscopic changes in the impact zones on the surfaces of these samples were studied, followed by a histological examination immediately after irradiation, as well as on days 4, 12, 30, and 90. Based on the results of an experimental study, a method for removing CGPN was developed based on the selective absorption of laser radiation with a wavelength of $\lambda=450$ nm by pigmented tissues, predominantly containing melanin and hemoglobin, which makes it possible to predict the depth of layer-by-layer removal of pigmented tissues and minimize damage to the underlying tissue structures, including the elements of the skin appendages located there. The optimal modes of "blue" ($\lambda=450$ nm) laser radiation for effective removal of CGPN were determined. A preliminary clinical study of the use of this method determined the prospect of its application.

[1] A. A. Sirotkin et al., "Optimization of selective photodestruction by laser radiation of the yellow-green range of capillary angiodyplasia of the skin," 2018 International Conference Laser Optics (ICLO), St. Petersburg, Russia, 2018, pp. 602-602, doi: 10.1109/LO.2018.8435420 [2] Podurar S.A., Gorbatoва N.E., Zolotov S.A., et al. Pigmented nevi in children, necessity and optimization of their treatment, Russian Journal of Pediatric Surgery. 2023; 27(1, Supplement): p. 142



B-I-11

Application of optical spectroscopy in minimally invasive surgery

**E. Potapova¹, V. Dremin^{1,2}, E. Zherebtsov³, K. Kandurova¹, V. Shupletsov¹,
A. Mamoshin^{1,4}, N. Polenov⁵, A. Dunaev¹**

1 - Research & Development Center of Biomedical Photonics, Orel State University, Orel 302026, Russia

2 - College of Engineering and Physical Sciences, Aston University, Birmingham B4 7ET, UK

3 - Optoelectronics and Measurement Techniques Unit, University of Oulu, Oulu 90570, Finland

4 - Orel Regional Clinical Hospital, Orel 302028, Russia

5 - The Research Institute of Obstetrics, Gynecology and Reproductology named after D.O. Ott, Saint Petersburg 199034, Russia

potapova_ev_ogu@mail.ru

Minimally invasive surgery (MIS) is a rapidly evolving field that requires the development of new technologies to provide diagnostic information about the condition of the organs being operated on. Optical spectroscopy methods offer information on metabolic processes, perfusion and morphological structure of tissues and can be combined with standard surgical instruments.

The team of the R&D Center of Biomedical Photonics (Orel State University) has been engaged in the development and implementation of optical spectroscopy devices for MIS for several years. This work presents the application of the developments for MIS in preclinical and clinical practice.

The techniques were developed to differentiate between healthy parenchyma of the liver and tumor during liver percutaneous biopsy using an optical fine needle probe compatible with standard Chiba 17.5G biopsy needles. Two optical biopsy systems were proposed: 1) multimodal optical percutaneous needle biopsy system including fluorescence spectroscopy (FS) and diffuse reflectance spectroscopy (DRS) channels [1]; 2) fluorescence lifetime optical biopsy based on a TCSPC approach [2]. In preclinical and clinical studies, high diagnostic accuracy was achieved in differentiating between healthy liver and tumor. The sensitivity and specificity of the multimodal biopsy system reached 0.90 and 0.95, and those of the fluorescence lifetime optical biopsy system reached 0.90 and 1.0 respectively. Parameters such as the fluorescence lifetime of metabolic co-enzymes of free NADH and protein-bounded NAD(P)H have great potential for distinguishing different types of cancer.

Obstructive jaundice is a group of diseases of the biliary system characterized by obstruction of the bile ducts leading to hepatocyte dysfunction and impaired functional state of the liver. The optical percutaneous needle biopsy system allows to record FS spectra of the liver of patients with obstructive jaundice during preoperative biliary drainage. Clinical studies demonstrated a statistically significant increase in the contribution of NAD(P)H, bilirubin, flavins and vitamin A fluorophores in the liver tissue of patients with obstructive jaundice. These parameters may be used as promising prognostic markers for determining the development of liver failure [3].

Laparoscopic myomectomy is the method for surgical treatment of symptomatic uterine myomas. A special probe was developed to record FS and laser Doppler flowmetry signals through laparoscopic accesses. We found that myomas have different blood supply and fluorescence levels depending on their growth intensity and size. The ability of laser Doppler flowmetry to assess endometrial perfusion is also demonstrated to investigate the effect of myomas of different types on endometrial tissue blood supply. The results obtained can be used to provide a better understanding of pathological processes in uterine leiomyomas, thus helping physicians to select treatment strategies [4].

Optical spectroscopy provides a wide range of diagnostic capabilities for clinical applications in a variety of MIS fields.

The study was supported by the Russian Science Foundation (project 21-15-00325).

[1] V. Dremin, E. Potapova, E. Zherebtsov, K. Kandurova, V. Shupletsov, A. Alekseyev, A. Mamoshin and A. Dunaev, Optical percutaneous needle biopsy of the liver: A pilot animal and clinical study, *Sci Rep.* 10(1), pp. 1–11 (2020).

[2] E. Zherebtsov, E. Potapova, A. Mamoshin, V. Shupletsov, K. Kandurova, V. Dremin, A. Abramov and A. Dunaev, Fluorescence lifetime needle optical biopsy discriminates hepatocellular carcinoma, *Biomed. Opt. Express*, 13(2), pp. 633–646 (2022).

[3] K. Kandurova, D. Sumin, A. Mamoshin and E. Potapova, Deconvolution of the fluorescence spectra measured through a needle probe to assess the functional state of the liver, *Lasers Surg. Med.* (2023) (in press).

[4] E. Potapova, N. Polenov, K. Zakuraeva, V. Krutikova, M. Yarmolinskaya and I. Kogan, Intraoperative Optical Diagnostics of Uterine Microcirculation during Myomectomy, *J. Biomed. Photonics Eng.* 9(1), p.10307 (2023).

B-I-12**Tissue optical clearing imaging: from in vitro to in vivo****Dan Zhu**

*Britton Chance Center for Biomedical Photonics - MoE Key Laboratory for Biomedical Photonics, Advanced Biomedical Imaging Facility-Wuhan National Laboratory for Optoelectronics, Huazhong University of Science and Technology, Wuhan, Hubei 430074, China.
dawnzh@mail.hust.edu.cn*

Biomedical optical imaging techniques provide powerful tools for observing biomedical tissue structural and functional information. However, the high scattering of biological tissues limits the penetration of light, and decreases imaging resolution and contrast as light propagates deeper into the tissue. Fortunately, novel tissue optical clearing technique provide a way for solving the above problem. This presentation will introduce some progress in tissue optical clearing imaging, i.e., in vitro tissue optical clearing methods for whole organs imaging; in vivo skull/skin optical clearing window for imaging structural and functional of cutaneous / cortical vascular and cells.

- [1] Y. Qi, T. Yu, J. Xu, P. Wan, Y. Ma, J. Zhu, Y. Li, H. Gong, Q. Luo, and D. Zhu, FDISCO: advanced solvent-based clearing method for imaging whole organs, *Science Advances*, 5(1), eaau8355 (2019).
- [2] J. Zhu, T. Yu, Y. Li, J. Xu, Y. Qi, Y. Yao, Y., P. Wan, Z. Chen, X. Li, H. Gong, Q. Luo, and D. Zhu, MACS: Rapid aqueous clearing system for three-dimensional mapping of intact organs, *Advanced Science*, 201903185 (2020).
- [3] C. Fang, T. Yu, T. Chu, W. Feng, F. Zhao, X. Wang, Y. Huang, Y. Li, P. Wan, W. Mei, D. Zhu, and P. Fei, Minutes-timescale 3D isotropic imaging of entire organs at subcellular resolution by content-aware compressed-sensing light-sheet microscopy, *Nature Communications*, 12(1):107 (2021).
- [4] J. Xu, Y. Li, Y. Yao, A. Xuan, J. Zhu, D. Li, T. Yu, and D. Zhu, Three-dimensional mapping reveals heterochronic development of the neuromuscular system in postnatal skeletal muscles. *Communication Biology*, 5(1): 1200 (2022).
- [5] D. Li, Z. Hu, H. Zhang, Q. Yang, L. Zhu, Y. Liu, T. Yu, J. Zhu, J. Wu, J. He, P. Fei, Wang Xi, Jun Qian, and D. Zhu, A Through-Intact-Skull (TIS) chronic window technique for cortical structure and function observation in mice, *eLight*, 2:15 (2022).
- [6] Y. Zhao, T. Yu, C. Zhang, Z. Li, Q. Luo, T. Xu, and D. Zhu, Skull optical clearing window for in vivo imaging of the mouse cortex at synaptic resolution, *Light: Science & Applications*, 7, 17153 (2018).
- [7] C. Zhang, W. Feng, Y. Zhao, T. Yu, P. Li, T. Xu, Q. Luo, and D. Zhu, A large, switchable optical clearing skull window for cerebrovascular imaging, *Theranostics*, 8(10): 2696-2708 (2018).



B-I-14

Motion correction of laser speckle imaging of blood flow

Xiaohu Liu¹, Liangwei Meng¹, Jinling Lu¹, Pengcheng Li^{1,2*}

1- Britton Chance Center for Biomedical Photonics and MoE Key Laboratory for Biomedical Photonics, Wuhan National Laboratory for Optoelectronics, Huazhong University of Science and Technology, China

2- Department of Biomedical Engineering, Hainan University, China

*Corresponding author: pengchengli@mail.hust.edu.cn

Laser speckle contrast imaging (LSCI) is widely used for mapping the blood flow speed of biological tissue. Since multiple speckle images are usually required to reconstruct a high-resolution and high SNR blood flow map, LSCI is highly sensitive to the motion artifacts. The blood flow perfusion obtained by LSCI during tissue motion is a mixture of the artifacts due to inter-frame image misalignment and intra-frame image blurring. It is of urgent importance to minimize the impact of motion when LSCI is put into practical use. Previous studies have mainly focused on correcting either the inter-frame or intra-frame artifact of global rigid motion. However, in practical biomedical applications, owing to the flexibility of biological tissues, the subjects often produce many non-rigid, spatially non-uniform movements, such as respiration, heartbeats, peristalsis of digestive organs. Such artifacts cannot be well corrected only with an estimation of global movement of tissues and rigid registration. In order to solve this problem, it is essential to accurately detect the heterogeneous local movements of biological tissues in the field of view and perform non-rigid registration. It is difficult to correct the local non-rigid motion only by using granular raw speckle images, especially in the tissue dominated by small blood vessels. We proposed a dual-wavelength imaging system to solve the problem that laser speckle images with graininess are difficult to be directly registered. Laser speckle images and corresponding tissue structure images are acquired simultaneously by a color CMOS camera under the illumination of 660 nm laser diode and a 470 nm light-emitting diode. The registration matrix is extracted from the tissue structure images registration process, which is then used to register the corresponding laser speckle images [1]. Considering the graininess of the speckle images, the application of the nearest neighbor interpolation method is proposed during registration to preserve the original speckle information, so as to avoid the overestimation of the blood flow speed. To further address the problem of overestimation of blood flow due to non-rigid tissue motion during the exposure of a single frame, we proposed a method that combines the strategy of heterogeneous regression analysis with the above dual-wavelength imaging, enabling the extraction of the true blood flow signal from the measured mixture LSCI signal.

[1] X. Liu, J. Wei, L. Meng, W. Cheng, X. Zhu, J. Lu and P. Li. Motion correction of laser speckle contrast imaging of blood flow by simultaneous imaging of tissue structure and non-rigid registration, *Optics and Lasers in Engineering*, Vol. 140, pp.106526, (2021)

Laser-optic methods for determining the relationship of microrheologic properties of blood, microcirculation parameters and endothelium function of patients suffering from socially important diseases

Priezzhev A.¹, Lugovtsov A.¹, Ermolinskiy P.¹, Gurfinkel Yu.², Diachenko P.³, Li Pengcheng⁴

¹*Faculty of Physics and ²Medical Research-Education Center of M.V. Lomonosov Moscow State University, Leninskie Gory 1/2, Moscow 119991, Russia*

³*N.G. Chernyshevsky Saratov State University, 83 ul. Astrakhanskaya, Saratov 410012, Russia*

⁴*Britton Chance Center for Biomedical Photonics and MoE Key Laboratory for Biomedical Photonics, Wuhan National Laboratory for Optoelectronics, Huazhong University of Science and Technology, China*

avp2@mail.ru

During the last few years, we have been developing new methods of quantitative assessment of microrheologic properties of blood, microcirculation parameters and endothelium function (EF). These methods include diffuse light scattering, laser tweezers, digital capillaroscopy and tonometry [1-3]. Currently we work on combining these methods with laser speckle contrast imaging (LSCI) technique, which we use for mapping the blood flow speed so far in the laboratory small animals [4-5]. Microcirculation parameters are studied using the Kapilyaroscanner-1 device (Russia) implementing artificial intelligence for digital image processing, which allows for estimating the number of red blood cells (RBC) in the capillaries [6]. Arterial stiffness and EF are determined by pulse tonometry using the Angiochek device (Russia). We characterize the microrheologic properties of blood by the intrinsic properties of RBC to reversibly aggregate and to deform in shear flow by measuring such parameters as aggregation index, aggregation rate, hydrodynamic strength of aggregates, paired aggregation and disaggregation forces, RBC deformability indices as functions of shear stress [7]. These measurements are performed *in vitro* in the samples of blood freshly drawn from healthy donors or patients suffering from socially important diseases. Digital capillaroscopy, tonometry and LSCI measurements are performed *in vivo*. Three groups of patients were formed for the study with the main diagnoses of atrial fibrillation (AF), coronary heart disease (CHD), and chronic heart failure (CHF). Statistical differences in parameters for different groups of patients were analyzed using the nonparametric statistical Mann-Whitney test ($p < 0.05$). The correlation between capillary blood velocity (CBV) with the number of RBC aggregates in the capillaries was calculated according to the Pearson coefficient of linear correlation. The results of the study showed a statistically significant correlation of measured parameters for the AF and CHF groups of patients. In percentage terms, the ratio of CBV in capillaries without aggregates to CBV in capillaries with aggregates for different groups of patients equals to 39.6% (AF); 46.9% (CHD); 46.4% (CHF). Based on these data we can conclude that there is a significant correlation between the presence of aggregates in the capillaries and a decrease in CBV in the examined patients. The analysis of the relationship between the number of aggregates in capillaries and EF in patients suffering from AF and CHD has showed that the impairment of EF is associated with an increase in the number of RBC aggregates in the capillaries of patients of both groups.

The study was financially supported by the Russian Science Foundation grant № 23-45-00027.

- [1] A. E. Lugovtsov, Y. I. Gurfinkel, P. B. Ermolinskiy, A. I. Maslyanitsina, L. I. Dyachuk, A. V. Priezzhev, Optical assessment of alterations of microrheologic and microcirculation parameters in cardiovascular diseases, *Biomedical Optics Express*, 10(8):3974–3986, (2019).
- [2] A. Maslyanitsyna, P. Ermolinskiy, A. Lugovtsov, A. Pigurenko, M. Sasonko, Yu. Gurfinkel, A. Priezzhev, Multimodal diagnostics of microrheologic alterations in blood of coronary heart disease and diabetic patients, *Diagnostics* 11, 76, (2021).
- [3] A.I. Maslyanitsyna, I.M. Kadanova, A.I. Neznanov, P.B. Ermolinskiy, Yu.I. Gurfinkel, L.I. Dyachuk, A.E. Lugovtsov, A.V. Priezzhev, Microrheologic properties of blood and capillary blood flow in case of arterial hypertension and type 2 diabetes mellitus: *in vitro* and *in vivo* optical assessment, *Complex Issues of Cardiovascular Diseases*, 9(2):53–63, (2020).
- [4] P.A. Dyachenko, D.A. Alexandrov, A.B. Bucharskaya, V.V. Tuchin, Speckle-contrast imaging of pathological tissue microhemodynamics in the development of various diabetes models, *Progress in Biomedical Optics and Imaging - Proceedings of SPIE*, 11457, (2020).
- [5] Jiachi Hong, Xuan Zhu, Jingling Lu, Pengcheng Li, Quantitative laser speckle auto-inverse covariance imaging for robust estimation of blood flow, *Optics Letters*, 46(10): 2505-2508, (2021).
- [6] Yu.I. Gurfinkel, O.V. Suchkova, M.L. Sasonko, A.V. Priezzhev, Implementation of digital optical capillaroscopy for quantifying and estimating the microvascular abnormalities in diabetes mellitus, *Proc. of SPIE Vol. 9917*, 991703-1, (2016).
- [7] A. Semenov, A. Lugovtsov, P. Ermolinskiy, K. Lee, A. Priezzhev, Problems of red blood cell aggregation and deformation assessed by laser tweezers, diffuse light scattering and laser diffractometry, *Photonics*, 9, 238, (2022).

B-I-16

Multimodal approach to the diagnosis of human skin cancer *in vivo*

E. Genina^{1,2}, I. Serebryakova^{1,2}, Y. Surkov^{1,2}, Y. Kuzinova³, E. Lazareva^{1,2}, O. Konopatskova³, V. Tuchin^{1,2,4}

1- Institution of Physics, Saratov State University, 83, Astrakhanskaya St., Saratov, 410012 Russia

2- Laboratory of Laser Molecular Imaging and Machine Learning, National Research Tomsk State University, 36, Lenin Ave., Tomsk, 634050 Russia

3- Department of Faculty Surgery and Oncology, Saratov State Medical University, 112, Bolshaya Kazachya St., Saratov, 410012 Russia

4- Institute of Precision Mechanics and Control, FRC "Saratov Scientific Centre of the Russian Academy of Sciences", 24, Rabochaya St., Saratov, 410028 Russia

eagenina@yandex.ru

Despite the development of medicine, cancer remains one of the most dangerous diseases nowadays. Many recent technological innovations have used physics principles, such as optics and coherent photonics, to improve early diagnostic and therapeutic procedures to reduce cancer incidence and mortality. In this study, the development of technologies for biomedical imaging of skin cancer is presented. Modern optical technologies combined with optical clearing of tissues based on reducing light scattering in tissues by partially replacing interstitial fluid with biologically compatible hyperosmotic immersion agents, increase the effectiveness of optical cancer diagnostics methods.

The study involved 60 neoplasms in 38 volunteers of both sexes (benign neoplasms was 13 and BCC was 47). A combination of high-resolution ultrasound examination and optical methods (Raman spectroscopy, optical coherence tomography (OCT), and backscattered diffuse reflectance spectroscopy) with biocompatible optical clearing agents was used for the study of basal cell carcinoma (BCC) and benign neoplasms in humans.

Texture analysis of pixel brightness changes within the area of interest in OCT images allowed us to differentiate various types of BCC, melanoma, and benign neoplasms (Fig. 1).

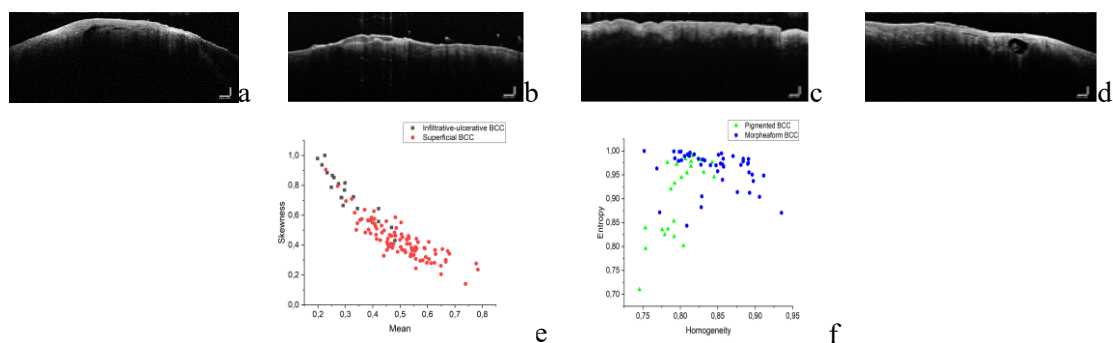


Fig. 1. OCT images of several types of BCC: a) Infiltrative-ulcerative, b) Superficial, c) Pigmented, and d) Morpheaform, and differentiation of these types using statistical parameters of texture analysis of OCT images:: e) Skewness and Mean and f) Entropy and Homogeneity.

Our results demonstrated the ability of these modalities to quantitatively assess tissue biochemical, structural, and physiological parameters that can be used to determine tissue pathology. This work was supported by the grant of RFBR # 20-52-56005.

B-I-17**Balanced detection spectral-domain optical coherence tomography with a single line-scan camera****Jun Zhang¹***1- School of Artificial Intelligence, Guilin University of Electronic Technology, Guilin 541004, China
junzhang@guet.edu.cn*

The spectral interferogram of Fourier domain Optical Coherence Tomography (FD-OCT) incorporates a direct current term (DC), an autocorrelation term (AC), which signifies the mutual interference from reflectors at varying depths of the sample [1], and a cross-correlation interference term (CC). Generally, the reference spectrum is subtracted from the interference spectrum, which acts as the background, in order to mitigate the DC and AC terms. These terms typically cause low frequency noise near the zero-delay line [2,3]. Moreover, balanced detection has been extensively utilized in Time-Domain OCT (TD-OCT) and Swept-Source OCT (SS-OCT) employing balanced photodetectors, providing a more effective approach to remove the DC and AC terms [4,5].

Recently, several balanced detection Spectral Domain OCT (BD-SD-OCT) techniques have been proposed. However, these come with drawbacks such as limited imaging speed, bulky and complex setups, signal loss, and an additional imbalance between the two channels [6,7].

In this study, we have developed a cost-effective and structurally simple dual balanced detection spectral-domain optical coherence tomography (SD-OCT) system. It uses a 4096-pixel single line-scan camera to both reduce auto-correlation (AC) artifacts and improve the signal-to-noise ratio (SNR) in SD-OCT. The system simultaneously detects two interference spectra—each in opposed-phase and incident on the spectrometer at different angles—using 2048 pixels per channel.

The developed dual balanced detection SD-OCT system demonstrated a direct current (DC) term suppression of 10 dB, an AC term suppression of 5-10 dB and SNR enhancement of 5.4 dB in comparison to unbalanced detection configuration.

In vivo imaging of human nail fold and retina also exhibited that the balanced detection SD-OCT technique proposed in this paper is able to suppress AC noise in *in vivo* imaging and acquire deeper layers of the tissue with more details.

The technique allows for a relatively simple structure, taking advantage of the high acquisition rate of the line-scan camera, and avoids crosstalk between the balanced detection spectra.

- [1] M. Wojtkowski, R. Leitgeb, A. Kowalczyk, T. Bajraszewski, and A. F. Fercher, *In vivo* human retinal imaging by Fourier domain optical coherence tomography, *J Biomed Opt*, 7(3), 457-463 (2002).
- [2] R. Leitgeb, C. K. Hitzenberger, and A. F. Fercher, Performance of fourier domain vs. time domain optical coherence tomography, *Optics Express*, 11(8), 889-894 (2003).
- [3] S. H. Yun, G. J. Tearney, J. F. de Boer, N. Iftimia, and B. E. Bouma, High-speed optical frequency-domain imaging, *Optics Express*, 11(22), 2953-2963 (2003).
- [4] J. Mo, M. de Groot, and J. F. de Boer, Focus-extension by depth-encoded synthetic aperture in Optical Coherence Tomography, *Opt Express*, 21(8), 10048-10061 (2013).
- [5] M. A. Choma, K. Hsu, and J. A. Izatt, Swept source optical coherence tomography using an all-fiber 1300-nm ring laser source, *J Biomed Opt*, 10(4), 44009 (2005).
- [6] J. Ai and L. V. Wang, Synchronous self-elimination of autocorrelation interference in Fourier-domain optical coherence tomography, *Opt Lett*, 30(21), 2939-2941 (2005).
- [7] M. G. Hyeon, H. J. Kim, B. M. Kim, and T. J. Eom, Spectral domain optical coherence tomography with balanced detection using single line-scan camera and optical delay line, *Optics Express*, 23(18), 23079-23091 (2015).



B-I-18

Laser spectroscopy biomedical data analysis and interpretation using machine learning

Yury V. Kistenev, Alexey V. Borisov, Viktor E. Skiba, Vladimir V. Prishcha, Denis A. Vrazhnov

Laboratory of laser molecular imaging and machine learning, Tomsk State University, Tomsk 634050, Russian Federation

Corresponding author email: yuk@iao.ru

An idea of using exhaled air and a carrier of important information for medical diagnostics is very attractive because such diagnostic method is fast, noninvasive, comfortable for patients. But implementation of this idea requires applications of effective methods of spectral data analysis, including a preprocessing, informative features extraction, and predictive data model creation and validation. We plan to present results of application of machine learning methods [1], including deep learning [2] in every step of spectral data analysis pipeline presented above.

The research was carried out with the support of a grant under the Decree of the Government of the Russian Federation No. 220 of 09 April 2010 (Agreement No. 075-15-2021-615 of 04 June 2021).

References

- [1] A. V. Borisov, A. G. Syrkina, D. A. Kuz'min, V. V. Ryabov, A. A. Boyko, O. Zaharova, V. S. Zasedatel', and Y. V. Kistenev, Application of machine learning and laser optical-acousticspectroscopy to study the profile of exhaled air volatile markers of acute myocardial infarction, *J. Breath Res.* **15** (2), 027104 (2021).
- [2] Yu. V. Kistenev, V. E. Skiba, V. V. Prishcha, D. A. Vrazhnov, and A. V. Borisov, Super-resolution reconstruction of noisy gas-mixture absorption spectra using deep learning, *J. Quant. Spectrosc. Radiat. Transfer* (2022). <https://doi.org/10.1016/j.jqsrt.2022.108278>

**B-I-19**

Deep-learning 4D live fluorescence microscopy advancing biomedical applications

Peng Fei¹*1- School of Optical and Electronic Information, Huazhong University of Science and Technology**Main author email address: feipeng@hust.edu.cn*

Many important biological phenomena, such as heartbeat, blood flow, organelle interactions, etc., often require rapid and high-resolution observations in 4-dimensional time-space. Current fluorescence microscopy imaging techniques are difficult to solve such challenges due to limited spatiotemporal resolution (limited optical throughput), and the measurements are either fast but inaccurate, or accurate but not fast. This presentation will describe how we combined new design in imaging optics with cutting-edge deep learning to increase the throughput of 3D fluorescence microscopy by 2 orders-of-magnitude and achieve ultra-high spatiotemporal resolution observations at both the tissue and single-cell levels. Our deep learning-enhanced light field and light-sheet microscopy techniques realize three-dimensional high-resolution imaging of millisecond-level biological dynamics, such as heartbeat and neural behavior, in freely-moving samples, as well as super-resolution visualization of the 3D interactions between various organelles in a living cell.



B-I-20

Optical and liquid biopsy in combination with machine learning for non-communicable diseases identification

L. Bartchenko¹, Yu. Khrisoforova¹, A. Matveeva¹, S. Al-Sammarræe¹, E. Typikova¹,
P. Lebedev², M. Skuratova³, I. Bratchenko¹

1- Samara National Research University, Samara, Russia

2- Samara state medical university, Samara, Russia

3- Samara regional clinical hospital named after VD Seredavin

Main author email address: iabratchenko@gmail.com

In modern world practice, promising diagnostic methods are emerging, such as "optical biopsy" [1] and "liquid biopsy" [2], which are used for specific diseases biomarkers detection in biological tissues and fluids. Optical methods have the potential to overcome the limitations of traditional methods of clinical analysis. One of the most promising methods of optical analysis (and optical biopsy) is a Raman spectroscopy, which can contribute to understanding of molecular basis of diseases and creation of new bioanalytical tools for the diagnosis of diseases. Since each type of biological tissue and biofluid has an individual molecular composition and, thus, a unique spectral profile resulting from the transition of a molecule from one vibrational-rotational state to another, a set of such individual states of functional groups of nucleic acids, proteins, lipids and carbohydrates makes it possible to characterize component composition of tissues, which ultimately makes it possible to isolate disease markers [3]. Along with the use of optical biopsy methods, it is possible to apply a supersensitive technique for analyzing biofluids based on surface-enhanced Raman spectroscopy, which will be most effective for detecting low concentrations of disease markers in biological fluids. In the last decade, the development of nanotechnology has led to the creation of promising tools for solving new problems in the study of various human diseases, which is especially important for effective and targeted treatment and a deeper fundamental understanding of the biochemistry of diseases [2].

In this study we demonstrate application of conventional Raman spectroscopy for the analysis of skin tissues and application of SERS for serum analysis to determine the presence of non-communicable diseases. In this study, the *in vitro* analysis of human serum was performed for more than 400 subjects, and more than 300 skin samples were analyzed *in vivo* for the detection of chronic heart failure (CHF), chronic heart failure and other non-communicable diseases. Analyzed groups separation based on deep learning was implemented using a separate one-dimensional convolutional neural network (CNN). Application of Raman spectroscopy to investigate the forearm skin has yielded the accuracy of 0.96, sensitivity of 0.94 and specificity of 0.99 in terms of identifying the target subjects with kidney failure. When classifying subjects by the presence of kidney failure using the PLS-DA method, the most informative Raman spectral bands are 1315 to 1330, 1450 to 1460, 1700 to 1800 cm^{-1} . The performed study demonstrates that for *in vivo* skin analysis, the conventional Raman spectroscopy can provide the basis for cost-effective and accurate detection of CHF and associated metabolic changes in the skin.

The results of the SERS data for CHF demonstrates that CNN significantly outperforms standard methods of analysis as projection on latent structures and allows for detection of CHF with 95-100% accuracy. By means of multivariate analysis, the informative spectral bands associated with the CHF during disease progression were identified. In addition, the analysis of the correlation between the serum spectral characteristics and urea, creatinine has made it possible to determine the spectral bands correlated with levels of creatinine and urea into the complex spectral characteristics of serum. In general, the reported approach may form the basis for monitoring the health status of CHF patients and find application in studying other pathological conditions of the human body [3]. Raman-based optical and liquid biopsy may be promising in non-communicable diseases identification, as it provides fast and rapid diagnosis.

[1] I Bratchenko, Y Khristoforova, L Bratchenko, et al. Optical biopsy of amelanotic melanoma with Raman and autofluorescence spectra stimulated by 785 nm laser excitation, Journal of Biomedical Photonics & Engineering, 7., pp. 020308, (2021).

[2] L.A. Bratchenko, S.Z. Al-Sammarræe, I.A. Bratchenko, et al. Analyzing the serum of hemodialysis patients with end-stage chronic kidney disease by means of the combination of SERS and machine learning, Biomedical Optics Express, 13., pp. 4926-4938, (2022).

[3] A Bratchenko, LA Bratchenko, YA Khristoforova, et al. Classification of skin cancer using convolutional neural networks analysis of Raman spectra, Computer Methods and Programs in Biomedicine, 219, 106755 (2022).

[10.24412/cl-35039-2023-23-89-89](https://doi.org/10.24412/cl-35039-2023-23-89-89)**B-I-21**

Autofluorescence in flow cytometry: multifarious capabilities for cells analysis

E. Shirshin

*M.V. Lomonosov Moscow State University, 119991, Leninskie gory 1/2, Moscow, Russia
eshirshin@gmail.com*

Flow cytometry is routinely used in biochemical and biophysical studies of cells, as well as in medical diagnostics. The mainstream modality is using fluorescent marker for selective labeling of cell structures and specific proteins, which allows for phenotyping, status assessment etc. In this context, autofluorescence is a non-desirable background signal, which should be avoided when analysing the cytometry data. On the other hand, autofluorescence contains information about endogenous fluorophores in cells, some of which are involved in important biochemical processes. Thus, potentially, autofluorescence analysis in flow cytometry experiments could yield important data for cells analysis. In this report, we will address the possibilities of autofluorescence in cells analysis using the flow cytometry setup.



B-I-22

Registration of low-intensity fluorescence in subcutaneous xenografts: from problems to their solutions

V. Zherdeva¹, A. Bogdanov Jr⁴, G. Abushinova^{3,1}, L. Maloshenok^{1,2},

1- Research Center of Biotechnology RAN, AN Bach Institute of Biochemistry, Moscow, Russian Federation

2- Vavilov Institute of General Genetics RAN, Moscow, Russian Federation

3- Moscow State University, Biology, Moscow, Russian Federation

4- UMASS Chan Medical School, Worcester, United States of America

vjerdeva@yandex.ru

Various strategies for imaging living cells altered by genome editing with CRISPR/Cas9 system have been implemented since discovery [1]. Catalytically inactive Cas9 (dCas9) has multiple applications with the most useful being the activation/repression of transcription [2]. The use of dCas9 may assist in mapping of genes within chromatin structure at the level of individual cells and intact tissue. The goal of our study was in developing and testing of dCas9 orthologs expressed under an inducible promoter to ensure regulated expression of chimeras in cells and in tumor animal models.

All chimeric constructs were cloned into 3d-generation lentiviral (LV) transfer vector FU-tet-o-hOct4 with Tet-On doxycycline (Dox) -regulated gene expression. dCas9 orthologs from *S. thermophilus* (Stt) and *N. meningitidis* (Nm) and fluorescent proteins (FP) were fused with 2 NLS at 1:1 ratio. A pair EGFP and mCherry were selected as FPs due to their potential to engage in emissive FRET. The obtained transfer vectors (FU-Tet-o-SttdCas9-EGFP and FU-Tet-o-NmdCas9-mCherry) were used for LV particles production and HEK293T and A549 cells transduction for establish clones expressing double chimeras (SttdCas9-EGFP and NmdCas9-mCherry, E9). Tumor xenografts were maintained in athymic mice that were given doxycycline via gavage followed by fluorescence imaging using a planar system.

Cells expressing Stt1 dCas9-EGFP and Nm dCas9-mCherry showed normal morphology with predominantly nuclear dual fluorescence. Before FP chimera induction with Dox there was no fluorescent signal noted in cells showing tight regulation of chimera expression. FP expression *in vivo* was observed 1 day post induction and fluorescent signal underwent a decrease during the course of 4-5 days if Dox was withdrawn. It was shown that the highest fluorescence signal in tumor xenografts was registered on the 3rd day after induction of chimeric protein expression. Subsequently fluorescence detection was carried out on the 3rd day. To improve the contrast, a 0.7 M solution of gadobutrol was used according to [4]. FI of red chimera expressed in tumor xenograft was amplified two-fold *in vivo* by applying 0.7 M gadobutrol due to the optical clearing (OC) of the skin. The MRI study reflected the perfusion of the tumor and coincided with the area of fluorescence.

Conclusion

The use of optical clearing approach enabled high-contrast imaging of dual (red and green fluorescent) chimeric dCas9- based proteins expression in tumor xenografts have been demonstrated. MR contrast agent gadobutrol improved both the intensity and contrast of FI as well as mapping of tumor perfusion by MRI.

Acknowledgement

The work of V. Zh., L.M., G.A. was supported by the grant of Russian Science Foundation № 22-14-00205 <https://rscf.ru/project/22-14-00205/>

The authors declare no competing financial interest.

References

- [1] Ma H. et al. 2015. Multicolor CRISPR labeling of chromosomal loci in human cells. *Proc. Natl. Acad. Sci. U. S. A.* 112: 3002–3007.
- [2] Gao Y. et al. 2016. Complex transcriptional modulation with orthogonal and inducible dCas9 regulators. *Nat. Methods.* 13:1043–1049.
- [3] Cawthorne C. et al. 2007. Comparison of doxycycline delivery methods for Tet-Inducible gene expression in a subcutaneous xenograft model. *J. Biomol. Tech.* 18:120–123.
- [4] Kazachkina NI, et al. 2021. Topical cutaneous gadobutrol application causes fluorescence intensity change in RFP-expressing tumor bearing mice. *J. Biomed Phot & Eng.* 7: 02030.
- [5] Maloshenok, L et al. 2023. Tet-Regulated Expression and Optical Clearing for *In Vivo* Visualization of Genetically Encoded Chimeric dCas9/Fluorescent Protein Probes. *Materials.* 3, 16, 940.

B-I-23**Non-invasive assessment of hemoglobin using spatial frequency domain imaging and machine learning approaches****B. Yakimov^{1,2}, K. Buiankin¹, G. Denisenko², I. Bardadin¹, E. Shirshin^{1,2}***1 – Faculty of Physics, M.V.Lomonosov Moscow State University, 1-2 Leninskie Gory, 119234 Moscow, Russia**2 – Laboratory of Clinical Biophotonics, Biomedical Science and Technology Park, Sechenov First Moscow State Medical University, Trubetskaya 8, Moscow 119048, Russia**Main author email address: bp.jakimov@physics.msu.ru*

Hemoglobin (Hb) is the main protein in the human blood, responsible for oxygen transport in the body, thus, the assessment of the total Hb concentration in the patient's blood is of high importance. Especially, correct estimation of Hb blood concentration is important to detect the decreased level of total hemoglobin (anemia), as it affects approximately ~30% of woman and children [1], while undiagnosed or improperly treated anemia can lead to adverse outcomes and significant reduction of the life quality [1].

The gold standard of total Hb blood quantitation is an invasive blood sampling followed by the analysis using flow-cytometry-based or staining-based procedures. This method is time-consuming (on the order of several hours), requires qualified medical staff for blood sampling, and could be painful for the patient, so non-invasive methods of blood Hb level assessment are in high demand.

It was recently demonstrated [2], that the Hb level could be assessed with ~15 g/L error (the Hb normal range is 130–160 g/L for adult males and 120–150 g/L for adult females) using simple RGB-imaging with a smartphone camera by the analysis of the color of fingernails. Indeed, fingernails are a promising tissue site for the optical Hb non-invasive assessment, as it does not contain any other visible chromophores, such as melanin, and are easily accessible to any imaging technique. Yet, the estimation error in the non-invasive Hb assessment using RGB-imaging does not meet clinical standards to readily translate this method to a clinic.

Here we explore whether advanced imaging techniques, such as spatial frequency domain imaging (SFDI), can superior simple RGB-imaging in the accuracy of Hb non-invasive assessment. As SFDI allows one not only to estimate relative changes in optical signal but quantitatively determine the values of the absorption and reduced scattering coefficients of tissues at the imaging wavelength, it surpasses the accuracy of other optical techniques and is a promising method for non-invasive Hb level assessment.

The work was supported by the Russian Science Foundation (grant No. 22-25-00759).

[1] E. Gayat et al. "Non-invasive measurement of hemoglobin: assessment of two different point-of-care technologies." *PloS one* 7.1 (2012): e30065.

[2] R. Mannino et al. "Smartphone app for non-invasive detection of anemia using only patient-sourced photos." *Nature communications* 9.1 (2018): 4924.



B-I-24

Enhancement of near field and local absorption in plasmonic nanoparticle-protein fluorescent complexes

A. Yakunin¹, S. Zarkov¹, Yu. Avetisyan¹, G. Akchurin^{1,2}, I. Meerovich³, A. Savitsky³, V. Tuchin^{1,2,4}

1- Institute of Precision Mechanics and Control, FRC "Saratov Research Centre of Russian Academy of Sciences,"
Rabochaya str. 24, Saratov, 410028, Russia

2- Saratov State University, Astrakhanskaya str. 83, Saratov, 410012, Russia

3- A.N. Bach Institute of Biochemistry, Research Center of Biotechnology of the Russian Academy of Sciences,
Leninsky Ave. 33, bld. 2, Moscow, 119071, Russia

4- Tomsk State University, Lenin's av. 36, Tomsk, 634050, Russia

e-mail: yakunin@iptmuran.ru

The phenomenon of localized surface plasmon resonance (LSPR) is caused by collective oscillations of conduction band electrons in the metal nanostructures under the influence of irradiating light. At present, this effect, which leads to a significant enhancement of the field in the vicinity of irradiated nanoparticles at resonant wavelengths, attracts increased attention of researchers and has found a wide variety of applications [1], ranging from technologies of local hyperthermia and plasmon photocatalysis to SERS and plasmon-enhanced fluorescence (PEF). Developing the study of the PEF of plasmon-protein fluorescent complexes [2], we present the results of calculations of the near-field enhancement in the vicinity of nanospheres synthesized from various materials - silver, gold, and copper. The solution of the problem of the distribution of the electric field during the irradiation of the nanosphere with an electromagnetic wave was carried out using both an analytical model (electrostatic approximation) and a finite element method implemented in the COMSOL software environment. The calculation models were verified in [3,4].

Since the fluorescence radiation power is proportional to the flux of exciting photons [5], it is of practical interest for the synthesis of efficient plasmon-protein fluorescent complexes to know the integral of the field amplification factor I_s in the vicinity of nanospheres. A comparative analysis of the obtained spectral dependences of I_s has shown that these dependences for nanospheres synthesized from various materials under study differ qualitatively and quantitatively from each other. However, their common feature is a certain correlation of I_s with the corresponding absorption cross section spectra of C_{abs} nanoparticles. As a result of the studies, it was found that for a certain combination of factors (optical properties of the metal, size of the nanosphere, wavelength of the incident radiation), such a correlation between the amplification of the excitation field of the fluorophore and the resonant absorption of radiation by the nanoparticle can play a negative role. This is due to the fact that the heating induced by light absorption in the vicinity of a nanoparticle can lead to an undesirable effect of fluorescence quenching, which was experimentally shown in [6]. In our work, we propose a composite criterion for assessing the quality of plasmon-protein fluorescent complexes, taking into account the influence of the induced temperature field, and present the results of evaluating the effectiveness of complexes focused on the use of fluorophores in the range from UV to near IR. The prospects for the use of complexes based on silver nanospheres are shown, and the conditions for the competitiveness of complexes based on cheap copper nanospheres in comparison with traditional complexes based on gold nanospheres are determined.

The research was carried out within the state assignment of Ministry of Science and Higher Education of the Russian Federation (theme No. 121022000123-8).

[1] E. Demishkevich et al., Synthesis Methods and Optical Sensing Applications of Plasmonic Metal Nanoparticles Made from Rhodium, Platinum, Gold, or Silver. *Materials*, vol. 16, art. 3342, (2023), <https://doi.org/10.3390/ma16093342>.

[2] S.V. Zar'kov et al., Interaction of laser radiation and complexes of gold nanoparticles linked with proteins, *Quantum Electronics*, vol. 51(1), pp. 52–63 (2021).

[3] A.N. Yakunin et al., Modeling of Laser-Induced Plasmon Effects in GNS-DLC-Based Material for Application in X-ray Source Array Sensors. *Sensors*, vol. 21, art. 1248, (2021), <https://doi.org/10.3390/s21041248>.

[4] A.N. Yakunin et al., Photoemission of Plasmonic Gold Nanostars in Laser-Controlled Electron Current Devices for Technical and Biomedical Applications. *Sensors*, vol. 22, art. 4127, (2022), <https://doi.org/10.3390/s22114127>.

[5] W. Deng et al., Metal-enhanced fluorescence in the life sciences: Here, now and beyond. *Physical Chemistry Chemical Physics*, vol. 15, pp. 15695–15708, (2013), <https://doi.org/10.1039/C3CP50206F>.

[6] J.V. Pellegrotti et al., Plasmonic Photothermal Fluorescence Modulation for Homogeneous Biosensing. *ACS Sens.*, vol. 1, is. 11, pp. 1351–1357, (2016), <https://doi.org/10.1021/acssensors.6b00512>.

B-I-25**Nonlinear optical microscopic imaging techniques and applications****Liwei Liu¹**

1- Key Laboratory of Optoelectronic Devices and Systems of Guangdong Province and Ministry of Education, College of Physics and Optoelectronic Engineering, Shenzhen University, No. 3688, Nanshan Avenue, Shenzhen 518060, China.

Main author email address: liulw@szu.edu.cn

Ensuring the health of individuals is a key imperative highlighted in the 14th Five-Year Plan for National Development. How to meet this demand presents a formidable challenge for scientists engaged in information science and related fields. Currently, the field of biomedical photonics has emerged as a branch of rapidly advancing information science, while also serving as an integral component of optical engineering and medical imaging. The rapid advancement and breakthroughs in this field are attributed to the support of optical imaging technology, particularly optical microscopic imaging technology.

In the past two decades, optical microscopic imaging technology has undergone rapid development and constant breakthroughs, providing a crucial tool for real-time dynamic observation of life systems and facilitating the transformation of optical microscopy from scientific research to clinical application. However, in the face of rapid technological development and increasing demand, it remains imperative to continuously explore and develop novel methods and technologies for addressing bottleneck issues encountered during practical applications of optical microscopic imaging, such as limited resolution, information acquisition, and imaging speed.

Our research group has conducted fundamental and applied research in the development and application of optical microscopic imaging technology for over a decade. The content encompasses a range of nonlinear optical microscopic imaging techniques, including fluorescence lifetime, two-photon excited fluorescence, second harmonic generation, stimulated Raman scattering, and others. These techniques enable imaging characterization at various levels spanning from molecules to cells, tissues, and in vivo. This report primarily presents the recent research endeavors of our research group in utilizing nonlinear optical microscopy imaging technology for biomedical applications.

B-I-26

Multi-parametric, high-resolution imaging of biological tissues relying on endogenous contrast

Zhiyi Liu

*State Key Laboratory of Modern Optical Instrumentation, College of Optical Science and Engineering; International Research Center for Advanced Photonics, Zhejiang University, Hangzhou, Zhejiang 310027, China
Email address: liuzhiyi07@zju.edu.cn*

Disease progression is associated with subtle changes in both cellular metabolism and extracellular matrix organization [1-3]; therefore, sensitive detection of these changes can lead to a better understanding of diseases. In this work, we use two-photon excited fluorescence (TPEF) and second harmonic generation (SHG) to acquire images from cells and collagen fibers, respectively, without the need for any exogenous labels. Based on these images, we have developed quantitative, multi-parametric measures, including optical redox ratio and mitochondrial clustering corresponding to cellular metabolic activity, as well as a series of metrics to represent collagen fiber orientation and organization. A combination of these quantitative metrics can provide systematic investigations of correlation between cells and matrix during progression of diseases. Figure 1 shows representative feature maps of collagen fibers, including orientation, waviness, alignment (represented by the variance metric) and local coverage within normal, benign and malignant cervical tissues. Different hues in maps among these three groups of samples are observed, indicating that the tumor progression alters the spatial characteristics of collagen fibers.

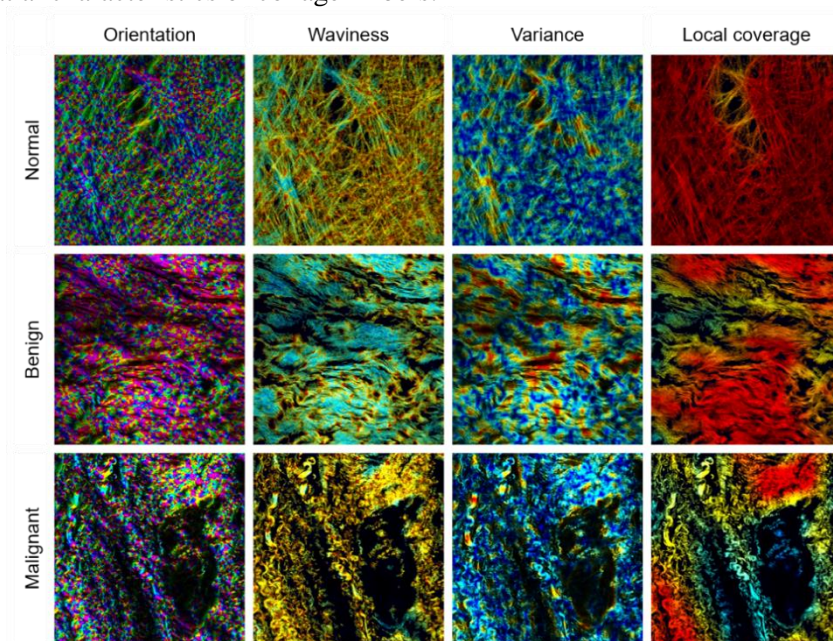


Figure 1. Representative maps of collagen fibers from normal, benign and malignant cervical tissues, revealing fiber features including orientation, waviness, alignment and local coverage.

Overall, this label-free, multi-parametric, high-resolution imaging method of biological tissues provides complementary insights into the functional and structural alterations in diseases, and offers opportunities to study interactions between cells and extracellular matrix as disease progresses.

- [1] Liu, Z. et al. Rapid three-dimensional quantification of voxel-wise collagen fiber orientation. *Biomed Opt Express* 6, 2294-2310 (2015).
- [2] Liu, Z. et al. Automated quantification of three-dimensional organization of fiber-like structures in biological tissues. *Biomaterials* 116, 34-47 (2017).
- [3] Liu, Z. et al. Mapping metabolic changes by noninvasive, multiparametric, high-resolution imaging using endogenous contrast. *Sci Adv* 4, eaap9302 (2018).

B-I-27**Analytical and numerical models for advancement of diffuse spectroscopic techniques**

M. Kirillin¹, D. Kurakina¹, V. Perekatova¹, V. Shishkova¹, A. Kostyuk¹, A. Khilov¹, I. Turchin¹, and E. Sergeeva¹

1- A.V. Gaponov-Grekhov Institute of Applied Physics RAS, 46 Uljanov St., Nizhny Novgorod, 603950, Russia

mkirillin@yandex.ru

Optical diffuse spectroscopy (ODS) is an efficient tool for non-invasive evaluation of biotissue chromophore content. Being based on reflectometry principles, it consists in wideband or wavelength-by-wavelength biotissue probing and calculation of basic chromophores concentrations from the reconstructed biotissue absorption and/or scattering spectra. For reconstruction of absorption and scattering spectra from the registered reflectance spectra one requires to employ a model of light propagation in tissue. Traditionally, for fast reconstruction, an analytical solution of the diffuse approximation of the radiative transfer equation in infinite medium is employed [1,2]. However, this approach suffers from its marginal applicability, especially for relatively small source-detector separation. Account for semi-infinite medium allows one to significantly increase the accuracy of the diffuse approximation model [3], however, such approach may provide some deviation at relatively small distances. Moreover, one should account that due to strong dispersion of the biotissue optical properties in the visible and NIR ranges, wideband measurements may result in different probing depth for different probing wavelength adding additional uncertainty to the measurement results. Moreover, generally one should account for different transfer functions of the different channels in the measurement setup, however, this problem could be overcome using so-called dual-slope method, that uses radiometric approach to diminish the effect of channel transfer functions [2].

This paper considers application of the analytical and numerical models in order to enhance the reconstruction in ODS. A refined analytical model is proposed based on diffuse approximation solution in a semi-infinite medium, which provides higher accuracy as compared to currently employed model [3]. The model was verified by the comparison with the results of extensive Monte Carlo simulations for source-detector separations corresponding to a real existing system [4,5] and biotissue optical properties typical for human skin. The effect of the superficial layer with different optical properties, mimicking stratum corneum and skin, is discussed, since it may affect the results obtained using model for a uniform medium. The Monte Carlo simulations for multi-layer geometry were also employed for estimation of typical probing depth spectra for different source detector separations, which also affects the accuracy of the chromophore content reconstruction [6].

The good agreement of the developed analytical model with the results of Monte Carlo simulations provides an ultimate opportunity for creating large datasets of synthetic data that could be successively employed for machine-learning based algorithms for chromophores concentrations reconstruction.

The authors acknowledge the support by Center of Excellence «Center of Photonics» funded by the Ministry of Science and Higher Education of the Russian Federation, Contract No. 075-15-2022-316.

[1] F. Larusson, S. Fantini, E.L. Miller. Hyperspectral image reconstruction for diffuse optical tomography, *Biomed Opt Express*, vol. 2, pp. 946-965 (2011)

[2] V. Perekatova, A. Kostyuk, M. Kirillin, E. Sergeeva, D. Kurakina, O. Shemagina, A. Orlova, A. Khilov and I. Turchin, VIS-NIR diffuse reflectance spectroscopy system with self-calibrating fiber-optic probe, *Diagnostics*, vol. 13, p. 457 (2023).

[3] T.J. Farrell, M.S. Patterson, B. Wilson, A diffusion theory model of spatially resolved, steady-state diffuse reflectance for the noninvasive determination of tissue optical properties in vivo, *Med Phys*, vol. 19, pp. 879-888 (1992)

[4] I. Turchin, V. Beschastnov, P. Peretyagin, V. Perekatova, A. Kostyuk, A. Orlova, N. Koloshein, A. Khilov, E. Sergeeva, M. Kirillin, M. Ryabkov, "Multimodal optical monitoring of auto and allografts of skin on a burn wound" *Biomedicines*, vol. 11, p. 351 (2023).

[5] A Orlova, Y Perevalova, K Pavlova, N Orlinskaya, A Khilov, D Kurakina, M. Shakhova, M. Kleshnin, E. Sergeeva, I. Turchin, M. Kirillin, *Diffuse Optical Spectroscopy Monitoring of Experimental Tumor Oxygenation after Red and Blue Light Photodynamic Therapy*, *Photonics* vol. 9, p. 19 (2022).

[6] D. Kurakina, V. Perekatova, E. Sergeeva, A. Kostyuk, I. Turchin, and M. Kirillin, "Probing depth in diffuse reflectance spectroscopy of biotissues: a Monte Carlo study." *Laser Physics Letters*, vol. 19, p. 035602 (2022).



B-I-28

A digital pathology technique based on Mueller matrix microscopy

Jiachen Wan, Haojie Pei, Yue Yao and Hui Ma

*Shenzhen International Graduate School, Tsinghua University, 518055, China
Email: mahui@tsinghua.edu.cn*

Digital pathology aims to assist pathologists during diagnostic process through the digitization of pathological slides followed by extraction of the diagnostic information. Mueller matrix microscopy is an emerging optical imaging method that is label-free and non-invasive, capable of revealing microstructural details at subcellular scale. It provides invaluable diagnostic information to pathologists that is otherwise unavailable through other non-polarization optical microscopy techniques.

Here we report a label-spreading method based on evaluating super-pixels from Mueller matrix microscopic images to represent their polarization features and propagating the pathologist's initial manual label of cancerous region to the entire field of view in finer detail, highlighting regions that share the same microstructural characteristic with pathologist's labeled region. A human-in-the-loop design is adopted which allows the pathologists to play a crucial role in supervising the label-spreading process by controlling essential model parameters and providing feedback on the label-spreading quality. After sufficient iterations, the label-spreading technique predicts all the potential candidates of cancerous regions and leads to substantial reduction in the diagnostic workload of doctors. In the meantime, the label-spreading process generates a vast amount of high-quality labeled image patches that will serve as invaluable data for other downstream tasks, particularly deep learning feature extractions of high resolution images in whole slide imaging (WSI). This technique is a key step towards realizing the assisted diagnostic application based on Mueller matrix microscopy, expanding the possibilities for other prospective applications in the future.

B-I-29**Raman Spectroscopy of body fluids for glioma diagnosis****O. Cherkasova^{1,2}, A. Samarinova³, D.A. Vrazhnov^{3,4}, Yu.V. Kistenev^{3,4}**

1- Institute of Automation and Electrometry, Siberian Branch of the Russian Academy of Sciences, 1 Academician Koptuyug Ave., 630090 Novosibirsk, Russia

2- Novosibirsk State Technical University, 20 Prospekt K. Marksa, 630073 Novosibirsk, Russia

3- Laboratory of Laser Molecular Imaging and Machine Learning, Tomsk State University, 36, Lenin Ave., 634050 Tomsk, Russia

4- V.E. Zuev Institute of Atmospheric Optics SB RAS, 1, Akademian Zuev Sq., 634055 Tomsk, Russia

o.p.cherkasova@gmail.com

The most commonly occurring malignant brain tumors are gliomas [1]. One reason for the poor outcome of glioma is a late-stage diagnosis, since most of the existing methods of noninvasive diagnostics, such as magnetic resonance imaging and computer tomography, are ineffective for diagnosing small-size tumors [2]. Tissue biopsies can be taken to study cellular and molecular composition. It is an invasive and traumatic procedure. Liquid biopsy provides the opportunity to detect cancer instead of a standard biopsy [3]. Control of glioma molecular markers in body fluids has a potential to become equivalent to studying glioma tissues [4]. It is important that similar molecular markers can appear in biofluids at the early stage, opening a way to an early diagnosis [5, 6].

Previously, we studied Raman spectra of mouse blood serum in the dynamics of the experimental glioblastoma U87 development [4, 7]. Groups of patients with glioma, with skull craniectomy defects (SCD), and healthy donors were studied. We used an inVia Reflex Raman spectrometer (Renishaw, UK), excitation wavelength 785 nm. A machine learning pipeline was used to analyze the Raman spectra of blood plasma and cerebrospinal fluid samples. It consists of the following main steps: 1) background subtraction and data normalization (dividing by the maximum value for proper comparison of spectra intensities); 2) principal component analysis was used to lower data dimensionality and remove noise; 3) support vector machine, random forest and XGboost methods were used to build predictive models; 4) ten-fold cross-validation procedure was applied to test models; 4) informative features selection and analysis.

It was shown that constructed prognostic models allow separating patients with glioma from healthy donors and from patients with SCD by the Raman spectra. The AUC is more than 0.9. The informative Raman shifts in the range of 1156-1200 and 1524-1584 cm^{-1} make the greatest contribution to the separation of groups. Thus, this study showed that Raman spectroscopy of human blood plasma and cerebrospinal fluid can be used for the diagnosis of glioma and allowing to monitor changes in the state of brain tissue during the development of glioblastoma.

The work was carried out within the framework of the budget project of the Institute of Automation and Electrometry SB RAS. The data analysis by D.V., Yu.K. was supported by the Ministry of Science and Higher Education of the Russian Federation (V.E. Zuev Institute of Atmospheric Optics of Siberian Branch of the Russian Academy of Sciences) and agreement № 075-15-2021-615 from 04.06.2021.

[1] Q.T. Ostrom, M. Price, C. Neff et al, CBTRUS Statistical Report: Primary Brain and Other Central Nervous System Tumors Diagnosed in the United States in 2015–2019. *Neuro-Oncology*, vol. 24, pp. v1–v95 (2022).

[2] M. Bulik, J. Jancalek, J. Vanicek et al, Potential of MR spectroscopy for assessment of glioma grading. *Clin. Neurol. Neurosurg.*, vol. 115, pp.146–153 (2013).

[3] S.N. Lone, S. Nisar, T. Masoodi et al, Liquid biopsy: A step closer to transform diagnosis, prognosis and future of cancer treatments, *Mol. Cancer*, vol. 21, pp. 79 (2022).

[4] D. Vrazhnov, A. Mankova, E. Stupak et al, Discovering Glioma Tissue through Its Biomarkers' Detection in Blood by Raman Spectroscopy and Machine Learning, *Pharmaceutics*, vol. 15, pp. 203 (2023).

[5] L. Ronvaux, M. Riva, A. Coosemans et al, Liquid Biopsy in Glioblastoma. *Cancers*, vol. 14, pp. 3394 (2022).

[6] O. Cherkasova, Y. Peng, M. Konnikova et al, Diagnosis of Glioma Molecular Markers by Terahertz Technologies, *Photonics*, vol. 8, pp. 22 (2021).

[7] O. Cherkasova, A. Mankova, D. Vrazhnov, Raman spectroscopy of blood plasma for cancer diagnosis, *Proc. SPIE*, vol. 12086, pp. 120861M (2021).



B-I-30

Microviscosity of a cell membrane and its implication for cancer treatment

L.E. Shimolina¹, A.A. Gulin², M.K. Kuimova³, I.N. Druzhkova¹, N.I. Ignatova¹, M.V. Gubina², A.E. Khlynova¹, E.V. Zagaynova¹ and M.V. Shirmanova¹

1- Privolzhsky Research Medical University, Minin and Pozharsky Square, 10/1, 603005 Nizhny Novgorod, Russia;

2- Semenov Federal Research Center for Chemical Physics, of the Russian Academy of Sciences, Kosygina Str. 4, 117977 Moscow, Russia;

3- Imperial College London, London SW7 2AZ, United Kingdom
Shirmanovam@mail.ru

Viscosity, a reciprocal of fluidity, plays an important role in the functioning of living cells.

The microviscosity of the plasma membrane determines the activity of transporters and receptors, biosynthesis and catalytic activity of membrane enzymes, permeability to substances and the rate of diffusion, and much more. Microviscosity of cell membranes depends primarily on their lipid composition, specifically on cholesterol content, the ratio of saturated and unsaturated fatty acids and the length of the phospholipid tails. Despite the multiple roles of the microviscosity in cells, its significance for the response to chemotherapy is not fully understood.

Here, we developed methodology to measure microviscosity of cancer cells membrane *in vitro* and *in vivo* and investigated the changes in microviscosity and lipid composition upon chemotherapy and acquisition of drug resistance.

Plasma membrane viscosity was monitored in live cancer cells and tumor xenografts using two-photon excited fluorescence lifetime imaging microscopy (FLIM) using the viscosity-sensitive probe BODIPY 2 [1, 2]. The probe is a fluorescent molecular rotor that possesses sensitivity to a local viscosity due to conformational mobility. Viscous environment restricts conformational change of the rotor, which results in the increase of its fluorescence lifetime. The lipid profile of membranes was analyzed using time-of-flight secondary ion mass spectrometry (ToF-SIMS). The effects of different clinical cytotoxic agents were examined, including oxaliplatin, 5-fluorouracil and paclitaxel.

Our results indicate that chemotherapy affects the state of the plasma membrane irrespective of the mechanism of the drug action. For example, oxaliplatin induces increase of microviscosity of membrane, while paclitaxel decreases it. In both cases, the changes are associated with alterations in lipid composition [3, 4]. The acquisition of chemoresistance was accompanied by modification of membrane lipids in ways that preserve the viscous properties unchanged upon further treatment.

Therefore, we conclude that the ability of cancer cells to tightly control microviscosity of the plasma membrane and maintain it at a constant level is crucial for cell survival upon chemotherapeutic interventions.

The study was supported by the Russian Science Foundation (Project No. 20-14-00111, continuation).

[1] L. Shimolina et al. Imaging tumor microscopic viscosity *in vivo* using molecular rotors. *Sci Rep.* 41097, (2017)

[2] L. Shimolina et al. Probing Metabolism and Viscosity of Cancer Cells using Fluorescence Lifetime Imaging Microscopy. *J. Vis. Exp.* 173 e62708, (2021)

[3] L. Shimolina et al. The Role of Plasma Membrane Viscosity in the Response and Resistance of Cancer Cells to Oxaliplatin. *Cancers*, 13, 6165, 2021

[4] L. Shimolina et al. Development of resistance to 5-fluorouracil affects membrane viscosity and lipid composition of cancer cells. *Methods Appl. Fluoresc.* 10 044008, (2022)

B-I-31**Multimodal collaborative tumor precision therapy
based on phototherapy****Siwen Li¹, Yueqing Gu²**

^{1,2} State Key Laboratory of Natural Medicines, Jiangsu Key Laboratory of Drug Screening, Department of Biomedical Engineering, School of Engineering, China Pharmaceutical University, No. 639 Longmian Avenue, Jiangning District, Nanjing 211198, China.

Corresponding author e-mail address: lsw@cpu.edu.cn

Abstract: Chemotherapy, radiotherapy and surgery are the main treatments in the field of tumor therapy, but they all have their own limitations. Phototherapy, including photodynamic therapy (PDT) and photothermal therapy (PTT), which relies on the conversion of light energy into chemical and thermal energy by phototherapeutic moieties to kill tumors, has been widely used in clinic as a non-invasive oncologic therapeutic modality. Besides, the biological effects in vivo of phototherapy can be combined with other strategies to achieve the purpose of synergistic treatment. In this study, we constructed a nanobiomaterial drug carrying system for multimodal combined precision treatment of solid tumor, which combined immunotherapy, gene therapy, chemotherapy and phototherapy to make each treatment cooperative and enhance tumor treatment including effective inhibition of tumor development, metastasis and recurrence. In vitro and in vivo experiments have shown that these tactics may provide a promising and pragmatic platform for clinical applications.

- [1] Yewen Zhai, Xiaorong He, Ying Li, Ran Han, Yuying Ma, Peng Gao, Zhiyu Qian, Yueqing Gu*, Siwen Li*. A splenic-targeted versatile antigen courier: iPSC wrapped in coalescent erythrocyte-liposome as tumor nanovaccine. *Science Advances*, 2021, 7(35).
- [2] Tian Xu, Yuying Ma, Qinling Yuan, Huixin Hu, Xinkai Hu, Zhiyu Qian, Rolle Janiqua Kyiesha, Yueqing Gu*, Siwen Li*. Enhanced Ferroptosis by Oxygen-Boosted Phototherapy Based on a 2-in-1 Nanoplatform of Ferrous Hemoglobin for Tumor Synergistic Therapy. *ACS Nano*, 2020, 14(3): 3414-3425.
- [3] Yuying Ma, Jinnan Zhang, Yalan Rui, Rolle Janiqua, Tian Xu, Zhiyu Qian, Yueqing Gu*, Siwen Li*. Depletion of glioma stem cells by synergistic inhibition of mTOR and c-Myc with a biological camouflaged cascade brain-targeting nanosystem. *Biomaterials*, 2020, 268, 120564.
- [4] Yuying Ma, Yanqin Zhang, Ran Han, Ying Li, Yewen Zhai, Zhiyu Qian, Yueqing Gu*, Siwen Li*. A cascade synergistic strategy induced by photothermal effect based on platelet exosome nanoparticles for tumor therapy. *Biomaterials*, 2022, 282: 121384.
- [5] Ran Han, Luting Yu, Chenxuan Zhao, Ying Li, Yuying Ma, Yewen Zhai, Zhiyu Qian, Yueqing Gu*, Siwen Li*. Inhibition of SerpinB9 to enhance granzyme B-based tumor therapy by using a modified biomimetic nanoplatform with a cascade strategy. *Biomaterials*, 2022, 288 :121723.
- [6] Ying Li, Chunjiao Wu, Yewen Zhai, Ran Han, Ruoyu Gu, Yuying Ma, Peng Gao, Zhiyu Qian, Yueqing Gu*, Siwen Li*. Palliating the escalated post-PDT tumor hypoxia with a dual cascade oxygenation nanocomplex. *Applied Materials Today*, 2022, 26:101287.



B-I-32

Diffuse reflection based sapphire instruments for tissue characterization during ablation and resection

I.N. Dolganova^{1*}, A.K. Zotov¹, I.A. Shikunova¹, K.I. Zaytsev², V.N. Kurlov¹

1- Osipyan Institute of Solid State Physics RAS, Chernogolovka, Russia

2- Prokhorov General Physics Institute, Moscow, Russia

**e-mail: in.dolganova@gmail.com*

Combining remarkable properties, such as high hardness, mechanical strength, biocompatibility, chemical inertness, thermal resistance, high thermal conductivity at cryogenic temperatures, and high optical transparency in visible and near infrared ranges, sapphire can be applied for manufacturing of medical instruments for laser therapy and diagnosis, as well as for tissue resection and cryodestruction [1-4]. Different techniques for sapphire shaped crystal growth [5-7] provide significant expansion of opportunities of thus made instruments, since enable manufacturing of small crystals, with internal capillary channels, used for the accommodation of optical fibers, which can be connected with light sources and detectors. Therefore, such crystals allow performance of diffuse reflectance measurement, which opens perspectives for in situ diagnosis using compact sapphire medical instruments.

This work describes application of diffuse reflectance measurements made by sapphire scalpel and probes for cryosurgery and tissue condition monitoring. The scalpel combines analysis of fluorescence and diffuse reflectance intensities detected right on the scalpel blade [8]. This analysis allows for finding of tumorous tissue and estimate its margins with the resolution around 2 mm. Sapphire cryoprobe was developed enabling the modality of spatially resolved frequency-domain or stable-state diffuse reflectance measurements [9]. This probe can be applied for monitoring of tissue freezing depth during cryosurgery as well as for estimation of tissue optical properties that serves as a marker of cryo-necrosis. Another compact sapphire probe was tested for monitoring of circulatory disorder in muscle tissue. Using diffuse reflected intensity this probe can detect the alteration of the extinction coefficient of damaged tissue. This instrument can be further used for intraoperational noninvasive monitoring of tissue transplantation.

The problems of manufacturing of these instruments, theoretical aspects of estimation of tissue properties and particular examples of the applications of these instruments are discussed in the present work.

This work was supported by the Russian Science Foundation (RSF), research project # 19-79-10212.

- [1] G.M. Katyba, K.I. Zaytsev, I.N. Dolganova, et al., "Sapphire shaped crystals for waveguiding, sensing and exposure applications," *Prog. Cryst. Growth Charact. Mater.* 64, 133–151, (2018).
- [2] V. Kurlov, "Sapphire: Properties, growth, and applications," in *Encyclopedia of Materials: Science and Technology*. K.J. Buschow, R.W. Cahn, M.C. Flemings, B. Ilshner, E. J. Kramer, S. Mahajan, and P. Veyssi ere (Eds.), (Elsevier, Oxford), 8259–8264 (2001).
- [3] I.N. Dolganova, I.A. Shikunova, G.M. Katyba, et al., "Optimization of sapphire capillary needles for interstitial and percutaneous laser medicine," *J. Biomed. Opt.*, 24, 128001, (2019).
- [4] I.N. Dolganova, I.A. Shikunova, A.K. Zotov, et al., "Microfocusing sapphire capillary needle for laser surgery and therapy: Fabrication and characterization," *J. Biophotonics*, 13, e202000164, (2020).
- [5] H. LaBelle, "EFG, the invention and application to sapphire growth," *J. Cryst. Growth*, 50, 8-17, (1980).
- [6] V. N. Kurlov, S. N. Rossolenko, N. V. Abrosimov, K. Lebbou, *Shaped Crystal Growth* (John Wiley & Sons, Ltd, Wiltshire, UK), Ch. 5., (2010).
- [7] V. Kurlov, S. Rossolenko, "Growth of shaped sapphire crystals using automated weight control," *J. Cryst. Growth*, 173, 417-426, (1997).
- [8] I.N. Dolganova, D.A. Varvina, I.A. Shikunova, et al., "Proof of concept for the sapphire scalpel combining tissue dissection and optical diagnosis," *Lasers Surg. Med.*, 54, 611-622, (2022).
- [9] I.N. Dolganova, A.K. Zotov, L.P. Safonova, et al., "Feasibility test of a sapphire cryoprobe with optical monitoring of tissue freezing," *J. Biophotonics*, 16, e202200288, (2023).



B-I-33

Laser methods in the study of microrheological and microcirculation properties of blood during therapeutic plasmapheresis

**A.E. Lugovtsov¹, P.B. Ermolinskiy¹, Y.I. Gurfinkel², Ni.N. Kalinin², I.V. Tauson²,
M.A. Rudnitskaya², A.V. Priezzhev¹**

1- Physics Department, Lomonosov Moscow State University, Leninskie Gory 1-2, Moscow, 119991, Russia

2- Medical Research and Education Center, Lomonosov Moscow State University, Lomonosovskiy prosp. 27-10, Moscow, 119192, Russia

anlug@biomedphotonics.ru

Methods based on the use of diffuse elastic light scattering and diffractometry are widely used to measure several parameters that characterize the microrheological properties of blood [1]. The state of human organism essentially depends on the microrheological properties of red blood cells (RBC) and platelets aggregation as well as RBC deformability. The importance of monitoring these properties is determined by the need to correct them with the use of various drugs or with the help of drug plasmapheresis procedures. The procedure of therapeutic plasmapheresis is a method of extracorporeal hemocorrection aimed at changing the qualitative and quantitative composition, correcting the physicochemical state of the blood, removing pathogenic substances from the circulating bloodstream, normalizing the immune response. So far there is no information about the effect of plasmapheresis on blood microrheological properties. The paper demonstrates the physical foundations of the used laser-optical methods and their application for estimating the effect of the plasmapheresis procedure on the blood microrheology and microcirculation.

All measurements of deformability and aggregation of RBC were performed using the commercially available Rheoscan system (Rheomeditech, Korea). The essence of laser diffractometry is in obtaining and subsequent analysis of the obtained diffraction pattern from a highly diluted suspension of RBCs at rest and shear flow. Analysing the obtained diffraction patterns one can calculate the deformability index dependence on shear stress that characterise the ability of RBC to elastically deform in the flow. The light scattering (laser aggregometry) technique allows for assessing the parameters characterizing the ability of the RBCs to reversibly aggregate in large ensembles of the cells. It allows to register the kinetics of the spontaneous aggregation (time dependence of light intensity forward scattered from a sample of whole blood at rest) and shear-induced disaggregation (shear stress dependence of light intensity backscattered from a sample of whole blood under shear flow) of RBC for obtaining the characteristic time of aggregates formation (aggregation rate), aggregation index as well as hydrodynamic strength of aggregates. Platelet aggregation parameters were assessed using the laser aggregometer of platelets “Biola” (BIOLA LLC., Russia) implementing the turbidimetry technique. Light transmission kinetics and optical density fluctuation during the platelet aggregation process induced by adenosine diphosphate (ADP) was registered in platelet-rich plasma with subsequent calculations of the aggregation index and rate as well as the aggregate size. All these techniques are convenient, fast and relatively simple for *in vitro* measuring with EDTA- or sodium citrate-stabilized human blood samples drawn from patients before and after the procedure of plasmapheresis.

The results of *in vitro* measurements in blood of a group comprising 10 pregnant women, the indices of RBC deformability, aggregation of RBCs and platelets, hydrodynamic strength, characteristic time of RBC aggregates formation before and after the procedure of plasmapheresis are presented. A significant increase in platelet aggregation, a decrease in RBC aggregation, and a slight decrease in the deformability of RBCs were found.

This work was supported by the grant of Interdisciplinary Scientific and Educational School of Lomonosov Moscow State University «Photonic and Quantum technologies. Digital medicine» (grant No. 23-III06-03).

[1] A. E. Lugovtsov, Y. I. Gurfinkel, P. B. Ermolinskiy, A. I. Maslyanitsina, L. I. Dyachuk, A. V. Priezzhev, Optical assessment of alterations of microrheologic and microcirculation parameters in cardiovascular diseases, *Biomedical Optics Express*, v. 10(8), pp. 3974–3986 (2019).

[2] A.N. Yaroslavsky, A.V. Priezzhev, J. Rodrigues, I.V. Yaroslavsky, H. Battarbee, *Optics of Blood*, Chapter 2 in: *Handbook of Optical Biomedical Diagnostics*, V.V. Tuchin – editor, SPIE Press Bellingham, WA, United States (2002).



B-I-34

Multiphoton microscopy of intrinsic fluorophores in biological tissue

Wei Zheng

*Research Center for Biomedical Optics and Molecular Imaging, Shenzhen Key Laboratory for Molecular Imaging,
Shenzhen Institutes of Advanced Technology, Chinese Academy of Sciences,
1068Xueyuan Boulevard, Nanshan, Shenzhen 518055, China
zhengwei@siat.ac.cn*

Multiphoton microscopy (MPM) allows observation of cellular and subcellular dynamics and functions in deep live tissue within highly complex and heterogeneous environments, providing critical in situ and in vivo information for biological studies. In past decades, we have witnessed the striking development of MPM which has significantly revolutionized biomedical research. In this talk, I will first briefly review the recent advances of MPM and then focus on our new development of MPM techniques. A time- and spectral- resolved detection system was used in our home-made MPM system to provide the capability for detecting fluorescence lifetime and fluorescence spectra simultaneously. Furthermore, a short wavelength femtosecond fiber laser was used to extend the excitation source. To demonstrate the versatility of our novel MPM system, we carried out MPM imaging of endogenous fluorophores in live cells and tissues.

Metal clusters for biomedical application

Fu WANG¹

¹Med-X Research Institute and School of Biomedical Engineering, Shanghai Jiao Tong University, China
wangfu@sjtu.edu.cn

Fluorescent metal clusters, featured by their subnanometer size, good quantum yield and photostability, low toxicity, high extinction coefficients, large Stokes shift, tuneable emission spectrum, and unobtrusive blinking on all relevant time scales, fill a void between organic dye and much larger semiconductor-based probes. Herein, we prepared several kinds of metal clusters and used for superresolution microscopy, two-photon microscopy and correlated microscopy, respectively. Furthermore, the metal clusters were also been applied for ferroptosis Therapy.

First, we prepared an aptamer functionalized silver clusters for STED microscopy. Specifically, the aptamer functionalized silver clusters were constructed by linking the anti-proliferative G-rich aptamer AS1411 with a single stranded CCCTTAATCCC DNA oligomer. Figure 1 clearly shows that the AS1411 functionalized silver clusters can bind to the Hela cells. Nucleolin protein distribution in Hela cells demonstrated in STED microscopy with resolved resolution, proving that the aptamer functionalized Ag cluster is a promising probe for STED microscopy.

Further, near-infrared emitting bi-metallic gold/silver nanoclusters with an excellent large Stokes shift around 330 nm were manufactured through one-pot synthesis. The gold/silver nanoclusters exhibit strong NIR fluorescence due to the silver effect, and can be applied as a two-photon fluorescent contrast agent for in vivo imaging. Figure 2 showed the two-photon fluorescence imaging at different depths of the mouse rear paw.

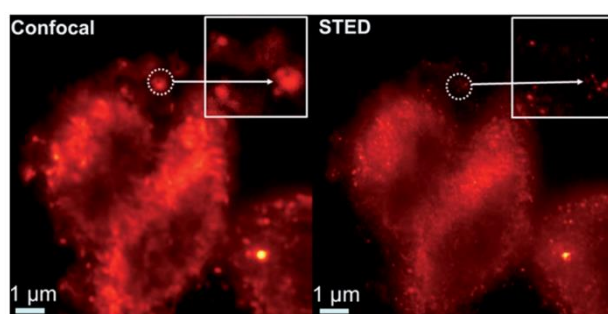


Figure 1: Confocal and STED images of AS1411-A5-AgNCs labeled Hela cells. STED power is 80 mW.

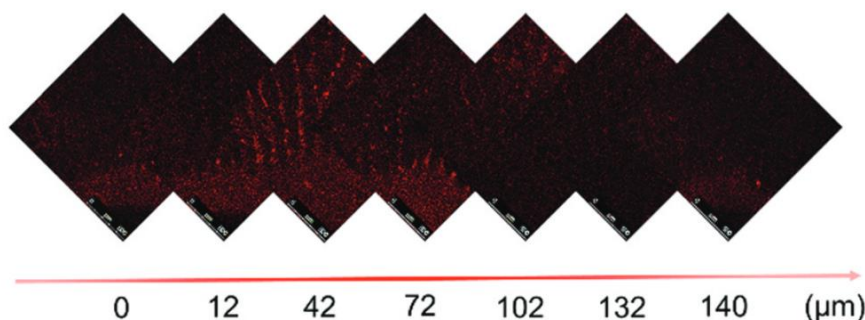


Figure 2: Two-photon confocal fluorescence images of the rear paw of a mouse at different depths.

- [1] Peng, Y.; Gao, L.; Pidamaimaiti, G.; Zhao, D.; Zhang, L.; Yin, G.; Wang, F. Facile Construction of Highly Luminescent and Biocompatible Gold Nanoclusters by Shell Rigidification for Two-Photon PH-Edited Cytoplasmic and in Vivo Imaging. *Nanoscale*, 14 (23), 8342–8348, 2022.
- [2] Peng, Y.; Huang, X.; Wang, F. Near-Infrared Emitting Gold–Silver Nanoclusters with Large Stokes Shifts for Two-Photon in Vivo Imaging. *Chem. Commun.*, 57 (96), 13012–13015, 2021.
- [3] Lan, J.; Feng, B.; Wu, X.; Yang, L.; Liu, J.; Shi, G.; Wang, F. Aptamer-Modified Silver Nanoclusters for Fluorescence Detection of Intracellular 8-Hydroxydeoxyguanosine. *ACS Appl. Nano Mater.*, 3 (2), 1332–1338, 2020.



B-I-36

Diagnostics of porous materials and biological tissues via diffusion-associated strain measurement with OCE

Yu.M. Alexandrovskaya¹, O.I. Baum², E.M. Kasianenko², A.A. Sovetsky¹, A.L. Matveyev¹,
L.A. Matveev¹, V.Y. Zaitsev¹

¹ Institute of Applied Physics of the Russian Academy of Sciences, 603950 Nizhny Novgorod, Russia

² Institute of Photon Technologies, Federal Scientific Research Centre 'Crystallography and Photonics' of Russian Academy of Sciences, Troitsk, 108840 Moscow, Russia

yu.alexandrovskaya@gmail.com

In this study we investigate diagnostic capabilities of optical coherent elastography (OCE) using visualization of osmotically induced slow deformations (tens of minutes) in porous water-saturated polymers and biological tissues [1,2]. Diffusion of hyperosmotic liquids and optical clearing agents through these materials is accompanied by subsurface strains, spatio-temporal evolution of which (amplitude, sign and rate) can be monitored in real time by OCE. It has been shown that the analysis of the dynamics of osmotically-induced deformation can be used to diagnose the presence of pathologies, such as the degradation of proteoglycans in cartilage tissue. The rate and amplitude of osmotically induced shrinkage and dilatation in polyacrylamide gels have been found to be dependent on the degree of their crosslinking [3]. Some possibilities of observing the development of crosslinks in tissues under the action of cross-linkers, such as glutaraldehyde, in real time have also been demonstrated. It is discussed how the formation of crosslinks depends on the initial composition and concentration of the used solution.

The study was supported by the Russian Science Foundation grant No. 22-12-00295

[1] Alexandrovskaya, Y.; Baum, O.; Sovetsky, A.; Matveyev, A.; Matveev, L.; Sobol, E.; Zaitsev, V. Optical Coherence Elastography as a Tool for Studying Deformations in Biomaterials: Spatially-Resolved Osmotic Strain Dynamics in Cartilaginous Samples. *Materials* **2022**, *15*, 904. <https://doi.org/10.3390/ma15030904>

[2] Yu. Alexandrovskaya, O. Baum, V. Zaitsev, A. Sovetsky, A. Matveyev, L. Matveev, K. Larin, E. Sobol, V. Tuchin, Optical and mechanical properties of the cartilage during optical clearing. In book *Tissue optical clearing: new prospects in optical imaging*, CRC Press (Dan Zhu, Elina Genina, and Valery Tuchin Eds.), **2021**, Boca Raton, Florida, United States.

[3] Alexandrovskaya, Y.M.; Kasianenko, E.M.; Sovetsky, A.A.; Matveyev, A.L.; Zaitsev, V.Y. Spatio-Temporal Dynamics of Diffusion-Associated Deformations of Biological Tissues and Polyacrylamide Gels Observed with Optical Coherence Elastography. *Materials* **2023**, *16*, 2036. <https://doi.org/10.3390/ma16052036>.

**B-I-37**

The peculiarities of photoacoustic signals from CTCs, tumors and blood vessels of immunocompetent mice

Daniil Bratashov¹, Olga Sindeeva², Oleg Grishin¹, Ekaterina Prikhozhenko¹, Olga Guslyakova¹, Olga Inozemtseva¹

1- Saratov State University, 410012 Saratov, Russian Federation

2- Skolkovo Institute of Science and Technology, 121205 Moscow, Russian Federation

bratashovdn@info.sgu.ru

Two *in vivo* flow cytometry systems were created - a photoacoustic flow cytometer with a tunable laser wavelength and a light sheet-based cytometer with the possibility of magnetic separation of objects from the bloodstream. For a minimally invasive analysis of the presence of circulating tumor cells in the bloodstream, a photoacoustic flow cytometer was mainly used. For circulating melanoma tumor cells, after inoculation of B16-F10 cells into the thigh of a C57BL/6 mouse and injection into internal organs (liver, kidney, spleen), the number of formed circulating tumor cells (CTCs) was studied in the large vessel of animal limb. At the same time, the spread of metastasis in internal organs was studied using photoacoustic tomography. Using the technique of photoacoustic flow cytometry, it was shown that these models form a large number of CTCs in large vessels of the limb of a laboratory animal. The complete study of the process of metastasis was carried out by *in vivo* flow cytometry, photoacoustic imaging, cryosection analysis, and histological analysis. The number of circulating objects in the bloodstream was obtained for several weeks of tumor growth.

This work was supported by RSF project 18-19-00354 and Russian government project (megagrant) number 075-15-2021-617.



B-I-39

Effect of local heating on cutaneous hemodynamics regulation of upper and lower extremities in type 2 diabetes mellitus

Irina Tikhonova¹, Irina Guseva², Andrey Grinevich¹, Arina Tankanag¹

1- Institute of Cell Biophysics of Russian Academy of Sciences, Pushchino, Russia
2- Hospital of Pushchino Scientific Centre of Russian Academy of Sciences, Pushchino, Russia
tav@icb.psn.ru

The functioning of large central and small peripheral vessels is regulated by different physiological factors that determine peripheral hemodynamics. There are various non-invasive methods for monitoring peripheral microvasculature, among which laser Doppler flowmetry (LDF) and photoplethysmography (PPG) are the most accessible and popular. It is known that in type 2 diabetes mellitus (T2DM) thermoregulation is impaired, which may lead to decreased skin vasodilation of extremities due to the development of neurovascular dysfunction. Analysis of changes in mechanisms of skin hemodynamics regulation in response to local heating in T2DM patients may be an indicator of early microvascular dysfunction in noninvasive diagnosis. The aim was to assess changes in spectral components and phase relationships between tissue blood volume dynamics and skin blood flow oscillations in upper and lower extremities of healthy volunteers and T2DM patients in response to local heating.

Twenty-two T2DM patients (5 males and 17 females) and twenty-two healthy volunteers (8 males and 14 females) participated in the study. Measurement procedures were conducted in a quiet room at $23 \pm 1^\circ\text{C}$ after a 15-minute adaptation period. All subjects were in supine position during registration. Four 35-minute records were recorded simultaneously for each subject - tissue blood volume dynamics of the right index finger pad (PPGfg) and the right second toe pad (PPGtoe), as well as skin blood flow dynamics from the outer surface of the right forearm (LDFfm) and of the right foot (LDFft). The local heating was performed by heating both skin sites from 32 to 38 °C in the area where LDF probes were placed. For each participant, two 15-minute fragments of the entire 35 min signals analyzed: the initial 15 minutes without heating (rest) and the last 15 minutes of probe (heating). Amplitude-frequency spectra were analyzed using adaptive wavelet transform, as well as phase interactions between pairs of analyzed signals were assessed by the value of wavelet phase coherence (WPC) function. Statistical analysis was performed using Wilcoxon tests for independent samples, significance differences were considered reliable at $p < 0.05$.

Amplitudes of respiratory oscillations (~ 0.3 Hz) of forearm blood flow (as measured by LDF) were higher at rest and during heating in patients versus healthy subjects. In comparison with controls the amplitudes of myogenic (~0.1 Hz) oscillations of foot blood flow were lower at rest and the amplitudes of cardiac (~1 Hz) oscillations - under local heating. No significant differences in spectral components of finger and toe tissue blood volume oscillations (as measured by PPG) were found between patients and healthy participants neither at rest nor under local heating. In patients WPC values for myogenic (~0.1 Hz) oscillations of LDFfm - LDFft and PPGfg - PPGtoe signal pairs were lower as compared to controls. The results obtained can provide the basis for development of methods for early noninvasive diagnosis of microvascular disorders and ways of their therapeutic correction in various socially significant diseases, including T2DM.

This study was supported by the Russian Science Foundation [grant number # 22-15-00215].

B-I-40**Optical visualization of biotissue microstructure and microvasculature in norm, pathology and after treatment**

Potapov A.L.¹, Moiseev A.A.², Sedova E.S.³, Gamayunov S.V.³, Radenska-Lopovok S.G.⁴, Gladkova N.D.¹, Sirotkina M.A.¹

1- Privolzhsky Research Medical University, 603950 - Nizhny Novgorod, Russia

2- Institute of Applied Physics of the Russian Academy of Sciences, 603950 – Nizhny Novgorod, Russia

3- Nizhny Novgorod Regional Oncologic Hospital, 603126 – Nizhny Novgorod, Russia

4- I.M. Sechenov First Moscow State Medical University (Sechenov University), 119991 – Moscow, Russia

sirotkina_m@mail.ru

Multimodal optical coherence tomography (OCT) is a modern biological tissues imaging method. OCT allows studying the structure, functional state, mechanical and optical properties of biological tissues. OCT technology can be used in routine clinical practice in neurosurgery, oncology, abdominal surgery, gynecology and other medical fields. OCT is a non-invasive real time and label free imaging that provides 3D images of subsurface tissues with a spatial resolution of 10-20 μm at a depth of 1-2 mm.

The multimodal OCT with the assessment of microstructure and microcirculation was used to diagnose and control photodynamic therapy of vulvar lichen sclerosis. Original algorithms for quantitative processing of OCT parameters were applied.

Unconditional OCT signs of normal vulva were formulated. At an early stage of lichen sclerosis, no changes were found in the connective tissue, but the number of blood and lymphatic vessels changed slightly. The severe stage of lichen sclerosis is characterized by the formation of sclerosis and hyalinosis of collagen fibers, which is manifested on OCT images by the absence of lymphatic vessels, a decrease in the number of blood vessels, and a change in their architectonics. A decrease in the density of the network of lymphatic vessels in the upper layer of the dermis was revealed at an early stage in the development of lichen sclerosis, which indicates that changes begin to develop directly under the epithelium. At a severe stage in the development of lichen sclerosis, the density of both the blood vessels and lymphatic vessels networks decreased to almost zero values in all layers of the dermis.

The restoration of the microstructure and microcirculation in the vulvar tissue for a period of 1-3 months after photodynamic therapy is shown to be almost to the level of normal tissue. This was accompanied by the absence of clinical manifestations of the disease and symptoms. In the case of partial recovery of vulvar parameters for a period of 3 months, all patients had a recurrence at 6 months after PDT.

This work was supported by the Russian Science Foundation grant 19-75-10084.



B-O-1

Study of the changes in the scattering properties of white matter under the influence of ionizing radiation

K.A. Achkasova¹, L.S. Kuhnina¹, A.A. Moiseev², A.Yu. Bogomolova¹, N.D. Gladkova¹

1- *Privolzhsky Research Medical University, 603005, N. Novgorod, Minin and Pozharsky sq., 10/1*

2- *Institute of Applied Physics of RAS, 603155, N. Novgorod, Ulyanova str., 46*

Main author email address: achkasova.k@bk.ru

Malignant neoplasms of the brain cause more than 250 000 deaths worldwide each year [1]. The combined treatment of brain tumors includes surgical resection, chemo- and radiotherapy. Intraoperative study of the white matter morphology in the perifocal zone of the tumor is necessary to accurately determine the boundaries of tumor resections. However, it must be understood that in the case of re-resection of the tumor, the white matter tissue can be damaged not only due to tumor growth, but also due to the use of radiation therapy [2], which causes more difficulties in distinguishing between tumor and normal brain tissues. Thus, there is a need to develop new methods for diagnosing white matter changes that occur during radiation therapy that could be used during surgical intervention. Optical coherence tomography (OCT) is a promising tool for study the white matter morphological features in brain tumors based on its scattering properties [3,4]. That is why the aim of the study was to evaluate the effect of ionizing radiation on the scattering properties of the white matter of the brain using OCT.

The study was performed on Wistar rats divided into control group and the group exposed to X-Rays (once at a dose of 15 Gy per region of the right hemisphere of the brain). At 7 time points since the experiment had started (each 2 weeks), the animals were euthanized, followed by an OCT study and an immunohistochemical study of the frontal sections of the brain. Numerical analysis of OCT data was carried out by calculating the attenuation coefficient and building of en-face color-coded optical maps. The corpus callosum was chosen as the region of interest.

As a result of the study, we discovered statistically significant decrease of attenuation coefficient values in corpus callosum at 3 time points. At 2 weeks after irradiation, we registered changes of attenuation coefficient values in the irradiated hemisphere, while at 6 and 12 weeks after the X-Rays exposure the attenuation coefficient values were decreased both in the irradiated and contralateral hemisphere. The detected changes were confirmed histologically: at the stage of 2 weeks after irradiation, a moderate edema occurred only in the area of the irradiated hemisphere, while at the stage of 6 and 12 weeks it was also found in the contralateral hemisphere and was characterized by significant severity, which indicates the spread of the process along the course of myelinated nerve fibers.

Thus, in the course of this study, morphological changes in the corpus callosum resulting from exposure to ionizing radiation were recorded, which were characterized by a decrease in its scattering properties, detected by OCT. The study was financially supported by the Russian Science Foundation, grant No. 23-25-00118.

[1] H. Sung, J. Ferlay, R.L. Siegel, et al., Global cancer statistics 2020: GLOBOCAN estimates of incidence and mortality worldwide for 36 cancers in 185 countries, *A Cancer Journal for Clinicians*, vol.73, pp. 209-249, (2021).

[2] D. Antoni, L. Feuvret, J. Biau, et al., Radiation guidelines for gliomas, *Cancer radiotherapie*, vol. 26, pp. 116-128, (2022).

[3] E. Kiseleva, K. Yashin, A. Moiseev, et al., Accurate detection of white matter tracts: mapping of human brain eloquent areas with cross-polarization optical coherence tomography, *Proceedings of SPIE*, vol. 11360, pp. 113600C, (2020).

[4] K. Achkasova, A. Moiseev, K. Yashin, et al., Nondestructive label-free detection of peritumoral white matter damage using cross-polarization optical coherence tomography, *Frontiers in Oncology*, vol. 13, pp. 1133074, (2023).

Feature analysis of OCT images for the diagnosis of brain glioma

**P.V. Aleksandrova^{1*}, K.I. Zaytsev¹, P.V. Nikitin², A.I. Alekseeva³, I.V. Reshetov⁴,
I.N. Dolganova⁵**

1- Prokhorov General Physics Institute of the Russian Academy of Sciences, Moscow 119991, Russia

2- University of Houston, Houston, Texas 77204, USA

3- Research Institute of Human Morphology, Moscow 117418, Russia

4 – Institute for Cluster Oncology, Sechenov University, Moscow 119991, Russia

5 – Institute of Solid State Physics of the Russian Academy of Sciences, Chernogolovka 142432, Russia

aleksandrovspolina98@gmail.com

Optical coherence tomography (OCT) is a fast non-invasive method which is used to visualize the internal structure of tissues [1]. OCT has found its application in various clinical fields, including neurosurgery [2-5]. An intraoperative diagnosis of brain tumors is one of the most urgent and challenging problem of modern neurosurgery [6-8]. Existing methods of the intraoperative neurodiagnosis of tumors are plagued with limited sensitivity or still rather expensive. Thus, a development of novel intraoperative diagnostic methods of brain gliomas, aimed at demarcation of tumor boundaries is one of the most important tasks of medicine, physics, and engineering sciences.

In our research, aimed at the application of OCT for the diagnosis of brain gliomas of different grades, we obtained OCT signals for *ex vivo* samples of brain glioma of various grades and intact brain tissue. In particular, we proposed a set of features for tissue differentiation, namely, the attenuation coefficient and its variance within the sample, and the local brightness fluctuations in OCT speckle patterns, obtained by means of the wavelet analysis. Then we applied the linear discriminant analysis to compare the advantages and weaknesses of particular features for distinguishing different tissue types. The results of this study confirmed the perspectives of combined attenuation-speckle signal analysis for neurosurgical purposes.

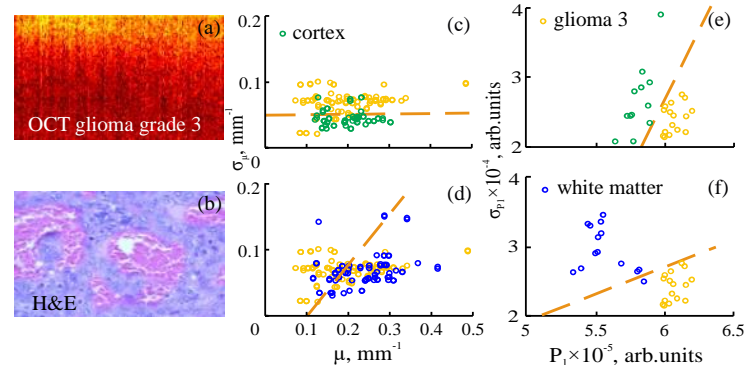


Fig. 2. An example of obtained results: (a) OCT images of glioma grade 3; (b) representative H&E-stained histological image; (c), (d) distribution of the attenuation properties μ and σ_μ for glioma grade 3, cortex and white matter, respectively; (e), (f) distribution of speckle properties P_a and σ_{P_a} for glioma grade 3, cortex and white matter, respectively.

This work was supported by the Russian Science Foundation (RSF), research project # 19-79-10212.

- [1] V. V. Tuchin Tissue Optics: Light Scattering Methods and Instruments for Medical Diagnostics, 3rd ed., SPIE Press, (2015).
- [2] F. Fercher, W. Drexler, C. K. Hitzenberger, Optical coherence tomography - principles and applications, T. Lasser, Reports on Progress in Physics, 66 (2), 239, (2003).
- [3] S. A. Boppart, Optical coherence tomography: technology and applications for neuroimaging, Psychophysiology, 40 (4), 529–541(2003).
- [4] W. Drexler, M. Liu, A. Kumar, et al., Optical coherence tomography today: speed, contrast, and multimodality, J. Biomed. Opt., 19 (7), 071412, (2014).
- [5] I.N. Dolganova, P.V. Aleksandrova, P.V. Nikitin, et al, Capability of physically reasonable OCT-based differentiation between intact brain tissues, human brain gliomas of different WHO grades, and glioma model 101.8 from rats, Biomed. Opt. Exp., 11, 6780-6798 (2020).
- [6] X. Yu, C. Hu, W. Zhang, et al., Feasibility evaluation of micro-optical coherence tomography μ OCT for rapid brain tumor type and grade discriminations: μ OCT images versus pathology, BMC Medical Imaging, 19, 102, (2019).
- [7] J. Wang, Y. Xu, S. A Boppart, Review of optical coherence tomography in oncology, J. Biomed. Opt., 22 (12), 1–23 (2017).
- [8] A. Majumdar, N. Allam, W.J. Zabel, et al., Binary dose level classification of tumour microvascular response to radiotherapy using artificial intelligence analysis of optical coherence tomography images, Scientific Reports, 12, 13995, (2022).

B-O-3

Assessment of endometrial tissue morphology by elastic properties using compression optical coherence elastography

**A.A. Plekhanov¹, M.M. Loginova^{1,2}, E.A. Avetisyan³, A.A. Sovetsky⁴, A.A. Shepeleva³,
A.M. Zaitseva¹, S.V. Gamayunov³, M.A. Sirotkina¹, G.O. Grechkanev¹, V.Y. Zaitsev⁴,
N.D. Gladkova¹**

1- Privolzhsky Research Medical University, Nizhny Novgorod, Russia

2- Lobachevsky State University, Nizhny Novgorod, Russia

3- Nizhny Novgorod Regional Oncologic Hospital, Nizhny Novgorod, Russia

4 - Institute of Applied Physics of the Russian Academy of Sciences, Nizhny Novgorod, Russia

strike_gor@mail.ru

Endometrial cancer ranks 5th among all oncopathology, and its affect the reproductive function of woman [1]. Different clinical diagnostic tools are used to identify endometrial cancer: ultrasound and magnetic resonance imaging make it possible to measure only the endometrium thickness, and hysteroscopic assess can visually determine localization of tissue area suspected of pathology. For morphological verification of endometrial cancer and differential diagnosis from other endometrial hyperplastic processes, diagnostic curettage of the uterine cavity is performed. This diagnostic procedure is characterized by high trauma and negatively affects the reproductive function. Therefore, there is a need for a new diagnostic tool for highly accurate and minimally invasive morphological assessment of endometrial tissue.

We present our study on the adaptation of Compression Optical Coherent Elastography (C-OCE) for the morphological diagnosis of endometrial pathologies. C-OCE allows label-free study of biological tissue heterogeneous structure based on differences in the elastic properties of morphological components with a resolution up to 40 μm [2]. The ability of C-OCE imaging of breast [3] and colon [4] tissue to determine the topography and morphomolecular status of pathology has been demonstrated previously. It has been shown that C-OCE can identify even small clusters of cancer cells [5], which can allow targeted biopsy sampling of endometrial cancerous tissue areas. Here, the main goal was to study the elastic properties of endometrial tissue in normal conditions and in various pathologies using C-OCE.

During *ex vivo* assessment of surgical samples, the elastic properties of tissue morphological components of the uterine cavity were determined in normal conditions (endometrium and myometrium); with typical endometrial hyperplastic processes; with low- and high-grade endometrial cancer (cancer cells and stroma). Higher stiffness values (more than 400 kPa) for cancerous tissues and lower stiffness values (less than 400 kPa) for non-cancerous tissues were established by C-OCE. The established differences in elastic properties indicate the possibility of endometrial pathologies diagnosis [6]. Future research will focus on developing an approach to *in vivo* C-OCE hysteroscopic assessment of endometrial tissue.

The study was funded by the Russian Science Foundation, grant No. 23-25-00405.

- [1] A. Ghoubara, M.J. Price, M.S.E. Fahmy, A.S. Ait-Allah, A. Ewies. Prevalence of hyperplasia and cancer in endometrial polyps in women with postmenopausal bleeding: A systematic review and meta-analysis. *Post Reproductive Health*: 25, 86-94, (2019).
- [2] V.Y. Zaitsev, A.L. Matveyev, L.A. Matveev, A.A. Sovetsky, M.S. Hepburn, A. Mowla, & B.F. Kennedy. Strain and elasticity imaging in compression optical coherence elastography: The two-decade perspective and recent advances. *Journal of Biophotonics*: 14(2), e202000257, (2021).
- [3] A.A. Plekhanov, E.V. Gubarkova, M.A. Sirotkina, A.A. Sovetsky, D.A. Vorontsov, L.A. Matveev, S.S. Kuznetsov, A.Y. Bogomolova, A.Y. Vorontsov, A.L. Matveyev, S.V. Gamayunov, E.V. Zagaynova, V.Y. Zaitsev, and N.D. Gladkova. Compression OCT-elastography combined with speckle-contrast analysis as an approach to the morphological assessment of breast cancer tissue. *Biomedical Optics Express*: 14(6), 3037-3056, (2023).
- [4] A.A. Plekhanov, M.A. Sirotkina, E.V. Gubarkova, E.B. Kiseleva, A.A. Sovetsky, M.M. Karabut, V.E. Zagainov, S.S. Kuznetsov, A.V. Maslennikova, E.V. Zagaynova, V.Y. Zaitsev, & N.D. Gladkova. Towards targeted colorectal cancer biopsy based on tissue morphology assessment by compression optical coherence elastography. *Frontiers in Oncology*: 13, 1121838, (2023).
- [5] A.A. Plekhanov, M.A. Sirotkina, A.A. Sovetsky, E.V. Gubarkova, S.S. Kuznetsov, A.L. Matveyev, L.A. Matveev, E.V. Zagaynova, N.D. Gladkova, V.Y. Zaitsev. Histological validation of *in vivo* assessment of cancer tissue inhomogeneity and automated morphological segmentation enabled by Optical Coherence Elastography. *Scientific Reports*, 10(1), 11781, (2020).
- [6] G.O. Grechkanev, A.A. Plekhanov, M.M. Loginova, E.A. Avetisyan, A.A. Shepeleva, A.M. Zaitseva, M.A. Sirotkina, V.Y. Zaitsev, S.V. Gamayunov, and Natalia D. Gladkova. The first experience of using multimodal optical coherence tomography for diagnosing endometrial hyperplastic processes. *Russian Bulletin of Obstetrician-Gynecologist*, (2023).

B-O-4

Gold nanostars with tunable optical properties for biomedical applications

V.A. Khanadeev¹, A.V. Simonenko¹, N.G. Khlebtsov^{1,2}

1- Institute of Biochemistry and Physiology of Plants and Microorganisms, Saratov Scientific Centre of the Russian Academy of Sciences (IBPPM RAS), 13 Prospect Entuziastov, Saratov 410049, Russia

2- Saratov State University of Genetics, Biotechnology and Engineering Named after N. I. Vavilov, 1 Teatralnaya pl., Saratov 410012, Russia

3- Saratov State University, 83 Ulitsa Astrakhanskaya, Saratov 410012, Russia

Khanadeev@gmail.com

Gold nanoparticles are widely used in laser-based biomedical applications due to the presence of localized surface plasmon resonance. Effective use in applications such as photothermal therapy, photoacoustic imaging, surface-enhanced Raman spectroscopy, etc. often requires spectral tuning of the plasmon resonance of nanoparticles to a given wavelength, usually coinciding with the wavelength of laser irradiation. In this case, gold nanostars compare favorably with particles of other shapes in that their plasmon resonance can be tuned in a wide wavelength range from 650 to 1900 nm. This range includes the so-called first, second and third biological penetration windows - spectral regions with the maximum depth of light penetration through biological tissues. Another feature of nanostars is sharp spikes on the surface, which can also be effectively used, for example, as "hot" spots for SERS applications.

The purpose of this work was to analyze the available literature data and perform an additional experimental study of the dependence of the morphological and optical properties of gold nanostars on the concentrations of reagents added during synthesis. Using transmission electron microscopy and extinction spectroscopy, we studied nanostars synthesized using two different seed-mediated methods: surfactant-free protocol developed by T. Vo-Dinh group [1] (Fig. 1a) and Triton-based protocol developed by P. Pallavicini [2] (Fig. 1b).

It was found that the main factors affecting the shape and optical properties of nanoparticles are the concentrations of silver nitrate, seeds and hydrochloric acid. The results obtained can be used to create gold nanostars with the necessary morphological and optical parameters for specific applications.

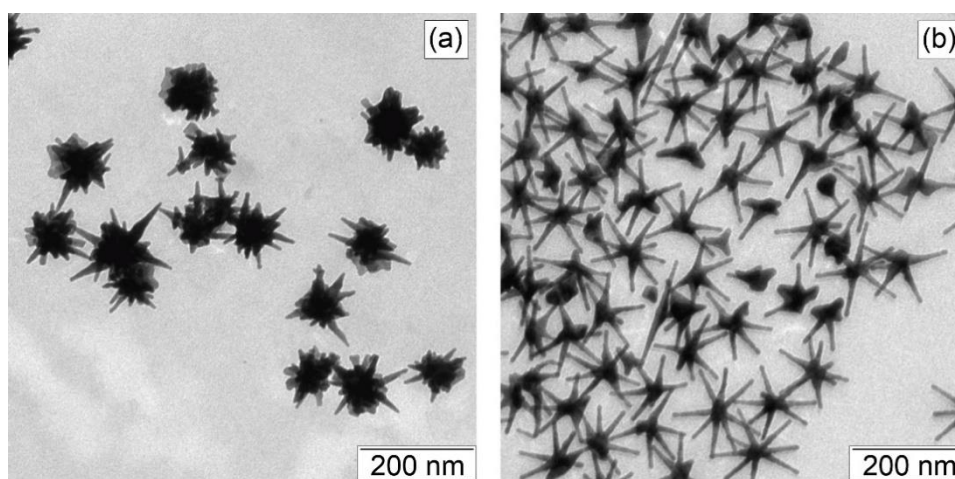


Fig. 1. TEM images of gold nanostars synthesized according to (a) surfactant-free and (b) triton-based protocols.

The work was supported by a grant from the Russian Science Foundation No. 23-22-00354, <https://rscf.ru/en/project/23-22-00354/>.

[1] H. Yuan, C.G. Khoury, H. Hwang, C.M. Wilson, G.A. Grant, T. Vo-Dinh, Gold nanostars: surfactant-free synthesis, 3D modelling, and two-photon photoluminescence imaging, *Nanotechnology*, vol. 23:075102, (2012).

[2] P. Pallavicini, A. Dona, A. Casu, G. Chirico, M. Collini, G. Dacarro, A. Falqui, C. Milanese, L. Sironi, A. Taglietti, Triton X-100 for three-plasmon gold nanostars with two photothermally active NIR (near IR) and SWIR (short-wavelength IR) channels, *Chem. Commun.*, vol. 49, pp. 6265–6267, (2013).

B-O-5

Treatment of neoplasm using of dielectric nanoparticles doped with Yb³⁺ ions and non-contact exposure to 970-nm radiation

S.A. Khrushchalina¹, I.A. Yurlov¹, P.A. Ryabochkina¹, O.A. Kulikov¹, V.I. Shlyapkina¹, V.P. Ageev¹, N.Yu. Tabachkova²

1- National Research Mordovia State University, 68 Bolshevistskaya Str., Saransk 430005, Republic of Mordovia, Russia

2- National University of Science and Technology "MISIS", Leninskiy Prospect, 4, Moscow 119049, Russia

Main author email address: *anabel-2005@yandex.ru*

Excitation of dielectric nanoparticles highly doped with rare-earth (RE) ions by intense laser radiation can lead to their significant heating and, as a consequence, "white" emission [1–3]. This effect can be used to enhance the thermal effect of laser radiation on biological tissue. In [3], by means of *in-vivo* experiments (on rats), we demonstrated the fundamental possibility of using particles based on ytterbium-doped zirconium dioxide to enhance the thermal effect of radiation with a wavelength of 980 nm. In [4], we studied the possibility of using particles based on zirconium dioxide doped with various RE ions (Ho³⁺, Tm³⁺, Yb³⁺, Er³⁺) to enhance the heating of biological tissue by laser radiation of various wavelengths (457, 532, 980, 1550, 1940 nm). *In-vivo* experiments have shown that the effect is most pronounced for ytterbium-containing particles and radiation with a wavelength of 980 nm.

The purpose of this work was to study the possibility of using ytterbium-containing particles when they are excited by laser radiation with a wavelength of 970/980 nm for the treatment of subcutaneous neoplasms. *In-vivo* experiments were carried out (on mice of the BALB/c line). The tumor strain of melanoma B16-F10 was used for the study. Tumor-bearing animals were divided into four groups of six each. In the first group, animals with a tumor did not receive any treatment. In the second group, on the seventh day from the moment of tumor implantation, the animals were intratumorally injected with a suspension of ZrO₂-30 mol.% Yb₂O₃. In the third group of animals, a thick suspension of ZrO₂-30 mol.% Yb₂O₃ powder in distilled water was applied to the skin covering the tumor site. Animals of the second and third groups twice with an interval of 48 hours were exposed to the tumor node and adjacent areas with a laser with a wavelength of 970 nm and a power of 1 W. Animals of the fourth experimental group received a double heating of the tumor node to 60°C using laser radiation with a wavelength of 970 nm. *In-vivo* experiments have shown that therapy with a suspension of ZrO₂-30 mol.% Yb₂O₃ particles (cutaneous or intratumoral location) has an antitumor effect against B16 melanoma cancer. In this case, a more effective therapeutic effect is achieved with intratumoral administration.

Experiments with the animals were carried out in accordance with the rules for working with animals formulated by Directive 2010/63/EU of the European Parliament and of the Council of the European Union on the protection of animals used for scientific purposes and were approved by the local ethics committee at the Medical Institute of National Research Mordovia State University, approval date: 9 May 2020, approval code: 88.

The transmission electron microscopy structural studies were conducted on equipment of the Materials Science and Metallurgy Joint Use Center with State financial support from the Ministry of Education and Science of the Russian Federation, Grant No. 075-15-2021-696. This work is financially supported by a grant from the Russian Science Foundation (Project 23-72-01099).

[1] P.A. Ryabochkina, S.A. Khrushchalina, I.A. Yurlov, A.V. Egorysheva, A.V. Atanova., V.O. Veselova, V.M. Kyashkin, Blackbody emission from CaF₂ and ZrO₂ nanosized dielectric particles doped with Er³⁺ ion, RSC Adv., vol. 10, pp. 26288 – 26297, (2020).

[2] S. Tabanlı, H. Cinkay Yılmaz, G. Bilir, M. Erdem, G. Eryurek, B. Di Bartolo, J. Collins, Broadband, White Light Emission from Doped and Undoped Insulators, ECS J. SolidState Sci. Technol., vol. 7, pp. R3199- R3210 (2018).

[3] P.A. Ryabochkina, S.A. Khrushchalina, A.N. Belyaev, O.S. Bushukina, I.A. Yurlov, S.V. Kostin, Use of dielectric nanoparticles doped with Yb³⁺ ions to enhance the thermal effect in a biological tissue exposed to near-IR laser radiation (in vivo experiments), Quant. Electron., vol. 51, pp. 1038–1043, (2021).

[4] .A. Khrushchalina, I.A. Yurlov, P.A. Ryabochkina, V.P. Ageev, O.A. Kulikov, V.I. Shlyapkina, M.N. Tremasov, M.N. Zharkov, A.N. Belyaev, O.S. Bushukina, The use of dielectric nanoparticles doped with rare-earth ions to increase the thermal effect of laser radiation of various wavelengths on biological tissues, 2022 Internat. Confer. Las. Opt. (ICLO), Saint Petersburg, Russian Federation, pp. 1-1, (2022).

B-O-6

Raman study of biodegradable poly(L-lactide-co- ϵ -caprolactone) materials

V.S. Novikov¹, S.O. Liubimovskii¹, E.A. Sagitova¹, S.M. Kuznetsov¹, N.G. Sedush², S.N. Chvalun², G.Yu. Nikolaeva¹

1- Prokhorov General Physics Institute of the Russian Academy of Sciences, Vavilov St. 38, 119991 Moscow, Russia

2- Enikolopov Institute of Synthetic Polymeric Materials of the Russian Academy of Sciences, Profsoyuznaya 70, 117393 Moscow, Russia

vs.novikov@kapella.gpi.ru

Poly(L-lactide) (PLLA) is biocompatible and biodegradable thermoplastic, which has the highest world consumption volume among bioplastics. PLLA has numerous applications, for example, as filament material in 3D printing, in production of ecologically friendly short-life consumer goods, including food wraps and disposable tableware. Also PLLA is widely used in medicine, in particular, as bioresorbable suture materials. PLLA-based copolymers, composites and blends have great potential for novel applications in production of bioresorbable medical implants, scaffolds and nanocarriers for targeted drug delivery with controlled release of active substances. Thus, analysis of the structure and degradation mechanism of various PLLA-based materials is of significant interest. In this work we applied Raman spectroscopy to study copolymers of L-lactide (LA) and ϵ -caprolactone (CL) with the aim to evaluate the relative contents of the comonomers and the degree of crystallinity.

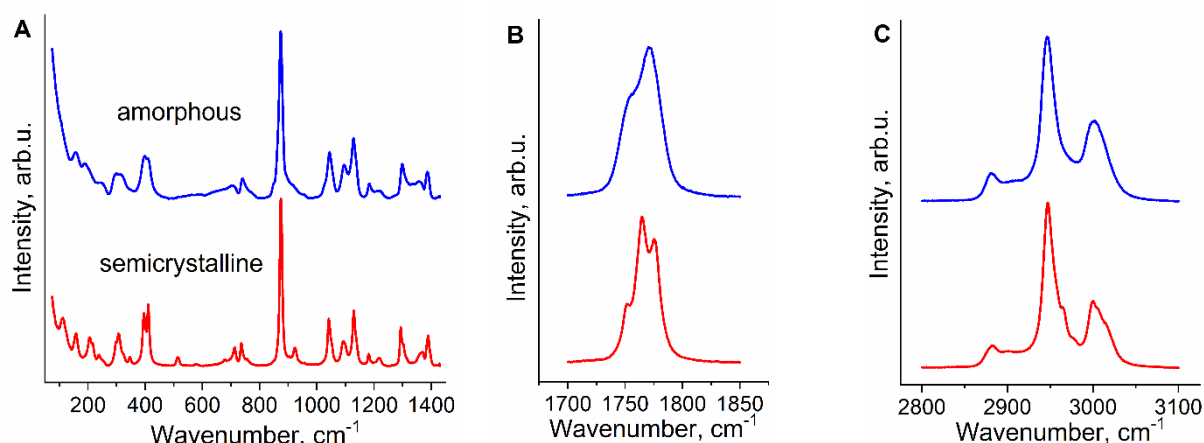


Fig. 1. Raman spectra of semicrystalline (the degree of crystallinity is 86%) and amorphous PLLA in the most informative spectral regions. In each region the intensity of the spectra was normalized to the intensity of the most intense band. The spectra were recorded using Bruker Senterra II Raman microscope with the spectral resolution of 1,5 cm^{-1} and laser excitation with wavelength of 532 nm.

We showed that the degree of crystallinity of PLLA areas in the LA/CL copolymers can be evaluated from measurements of the ratio of intensities of the PLLA bands at 411 and 874 cm^{-1} (Fig. 1A). These bands were assigned to the deformation vibrations of O-C(H)-C(H₃) groups and the symmetric stretching vibrations of C-O-C bonds on the base of quantum chemical calculations. The range of the C=O stretching vibrations (Fig. 1B) is not convenient to use in the analysis of the LA/CL copolymers because of the strong influence on this region of both copolymer chemical composition and the degree of crystallinity. The relative contents of comonomers in the LA/CL copolymers can be measured using the intensities ratio of the bands at 2947 and 2914 cm^{-1} , related to the symmetric stretching vibrations of CH₃ groups of PLLA monomeric units (Fig. 1C) and the symmetric stretching vibrations of CH₂ groups of poly(ϵ -caprolactone) monomeric units. Our Raman data on the contents of the comonomers and the degree of crystallinity of the PLLA areas are in good agreement with the results of X-ray diffraction study of these copolymers.

This study was supported by the Russian Science Foundation under the grant № 23-22-00347, <https://rscf.ru/en/project/23-22-00347/>.



B-O-7

Iron oxide nanoparticles coated with a photosensitizer for phototherapy: experimental study of local intracellular heating

A. Ryabova^{1,2}, D. Pominova^{1,2}, I. Markova², A. Nikitin³, P. Ostroverhov³, E. Plotnikova⁴, N. Morozova⁴, I. Romanishkin¹, M. Abakumov³, A. Pankratov⁴, R. Steiner², V. Loschenov^{1,2}

1- Prokhorov General Physics Institute of the Russian Academy of Sciences, 119991 Russia, Moscow, Vavilov-38

2- National research nuclear university MEPhI, Moscow, Russia

3- National University of Science and Technology "MISIS", Moscow, Russia

4- National University of Science and Technology "MISIS", Moscow, Russia

5- National Medical Research Radiological Centre of the Ministry of Health of the Russian Federation, P.A. Hertsen Moscow Oncology Research Institute, Moscow, Russia

nastya.ryabova@gmail.com

Iron oxide nanoparticles (IONPs) are promising for diagnosis and therapy: they can be coated with a photosensitizer for photodynamic therapy, laser or magnetic heating of IONPs can be used for controlled drug release or phototherapy [1]. Temperature measurement for cell organelles containing NPs during phototherapy is important, but complex and challenging. Fluorescent thermometers are reliable tools for measuring temperature fluctuations in nano-volumes, given their advantages such as fast response, high sensitivity and spatial resolution, ease of use and non-destructive detection [2].

In this work we performed an experimental study of the emergence of "hot spots" of IONPs ensembles of different sizes and shapes during laser scanning with the estimation of heat distribution over the cell volume using the fluorescence thermometry based on rhodamine B (RhB) lifetime measurement. In order to interpret the experimental data obtained, numerical simulations of the scattering and absorption cross sections of the studied IONPs and their ensembles, as well as the field enhancement and heating during the interaction with the excitation electromagnetic radiation were performed using the finite-difference time-domain method.

Depending on the IONPs shape and their location in space, a significant change in the spatial distribution of the EM field near the IONPs surface was observed. The local heating of IONPs in an ensemble reaches sufficiently high values; the relative change was about 35°C for Fe₂O₃ NPs. Nevertheless, all the studied IONPs water colloids showed heating by no more than 10°C. The heating temperature of the ensemble depends on the thermal conductivity of the medium, on which the heat dissipation depends.

When capturing IONPs inside the cell into lysosomes - lipid sacs with lower thermal conductivity, the situation was different. As a result, so-called "hot spots" with temperature over 100°C can appear inside cells around the accumulation of IONPs in vesicles. The distribution of "hot spots" determines the thermal response of the entire biosample. It should have a certain effect on the cell death mechanism through hyperthermia and the lysosomes destruction response.

The work was supported by the RFBR, grant 21-52-12030.

[1] S.K. Sharma, N. Shrivastava, F. Rossi, L.D. Tung, N.T.K. Thanh. Nanoparticles-Based Magnetic and Photo Induced Hyperthermia for Cancer Treatment, *Nano Today*, vol.29, p.100795 (2019).

[2] J. Zhou, B. del Rosal, D. Jaque, S. Uchiyama, D. Jin. Advances and Challenges for Fluorescence Nanothermometry. *Nat Methods* 2020, vol.17, pp. 967–980 (2020).

B-O-8**Formation of composite nanostructures by multiphoton lithography for biomedical applications****D. Murashko¹, E. Otsupko¹, U. Kurilova², A.Gerasimenko^{1,2}, S.Selishchev¹***1- National Research University of Electronic Technology MIET, Institute of Biomedical System, Bld. 1, Shokin Square, Zelenograd, Moscow 124498, Russia**2- I.M. Sechenov First Moscow State Medical University, 8 Trubetskay str., Moscow 119991, Russia**skorden@outlook.com*

Two-photon lithography, also known as multiphoton laser lithography, is a technique that allows direct laser writing in a volume with a resolution of less than 100 nm. When exposed to a near-infrared laser, the source material photopolymerises in the focal volume region to form complex micro- and nanostructures. Two-photon lithography is used in bioelectronics [1], labs-on-a-chip [2], and cell and tissue engineering [3,4].

Most synthetic photoresists and photoinitiators are not used in biological applications due to their cytotoxicity. To create a biocompatible structure, polysaccharides and proteins, which are the main elements of the extracellular matrix, are usually used. We chose bovine serum albumin (BSA) as a biopolymer because of its wide availability and well-studied properties, elasticity and enzymatic degradation. The organic dye riboflavin mononucleotide was used as the photoinitiator.

Despite their excellent biocompatibility and wide availability, natural polymers have inferior physical and chemical properties compared to synthetic photoresists. Therefore, single-walled carbon nanotubes (SWNTs) "TUBALL" were added to the material to improve the mechanical properties and provide electrical conductivity. The tubes have an average outer diameter of 16 nm and a length of more than 5 μm . The carbon nanotubes were dissolved in 5 g/l distilled water. BSA, riboflavin and SWNTs were dissolved in phosphate buffer saline (pH = 7.4) to avoid rapid aggregation of the protein.

The structure was formed using a femtosecond pulsed Ti:sapphire laser. The irradiation wavelength was 736 nm, the pulse duration was 140 fs, the repetition frequency was 80 MHz and the irradiation power was 30 mW. An OAGP-10-S optical attenuator with a Glan prism was used to control the irradiation power. The laser beam was focused on the sample using an optical microscope with 60x magnification (NA = 0.65). The samples were moved under the radiation using an XY 8MTF motorised scanning stage at a scanning speed of 5 $\mu\text{m/s}$. The average dimensions of the nanostructures formed were 40 μm x 40 μm , with a height of 15 μm . The mechanical properties of the nanostructures were investigated by indentation using a Nanoscan-4D Compact nanohardness tester. Measurements were made using a Berkovich trihedral pyramid indenter, with Poisson's ratio set at 0.3. The average modulus of elasticity of the BSA samples with SWNTs was 5.9 GPa and the hardness was 0.26 GPa. While for a BSA sample the value of Young's modulus was 0.86 MPa, the hardness was 75.16 MPa. The results showed that the addition of SWNTs improved the mechanical properties of the structures compared to the BSA material without filler. The nanotubes also ensured the electrical conductivity of the nanostructure. The addition of SWNTs reduced the resistance to 30 k Ω compared to BSA alone (1 G Ω). The studies were carried out using the Van der Pauw method.

[1] Dadras-Toussi O., Khorrani M., Abidian M. R., Femtosecond Laser 3D-printing of Conductive Microelectronics for Potential Biomedical Applications, 43rd Annual International Conference of the IEEE Engineering in Medicine & Biology Society (EMBC), pp. 1197-1200, (2021).

[2] Sima F. et al., Three-dimensional femtosecond laser processing for lab-on-a-chip applications, Nanophotonics, vol. 7, pp. 613-634, (2018).

[3] Maciulaitis J. et al., Customization of direct laser lithography-based 3D scaffolds for optimized in vivo outcome, Applied Surface Science, vol. 487, pp. 692-702, (2019).

[3] Ovsianikov A. et al., Two - photon polymerization technique for microfabrication of CAD - designed 3D scaffolds from commercially available photosensitive materials, Journal of tissue engineering and regenerative medicine, vol. 1, pp. 443-449, (2007).

B-O-9

Hybrids of carbon quantum dots and photoswitchable phosphonates - peculiarities of optical and biological properties

Gulia Bikbaeva^{1,4}, Anna Pilip², Anastasia Egorova^{2,3}, Ilya Kolesnikov⁴, Dmitry Pankin⁴, Kirill Laptinskii^{5,6}, Alexey Vervalde⁶, Tatiana Dolenko⁶ and Alina Manshina¹

1- Institute of Chemistry, St. Petersburg State University, St. Petersburg 198504, Russia

2- St. Petersburg Federal Research Center of the Russian Academy of Sciences (SPC RAS), Scientific Research Centre for Ecological Safety of the Russian Academy of Sciences, St. Petersburg 197110, Russia

3- St. Petersburg State Technological Institute (Technical University), St. Petersburg 190013, Russia

4- Center for Optical and Laser Materials Research, St. Petersburg State University, St. Petersburg, Russia

5- Faculty of Physics, M.V. Lomonosov Moscow State University, Moscow 119991, Russia

6- Skobeltsyn Institute of Nuclear Physics, M.V. Lomonosov Moscow State University (SINP MSU), Moscow 119991, Russia

**e-mail: BikbaevaGI@yandex.ru*

Nowadays the Photopharmacology is an urgent area of research. The main players of photopharmacology are ‘photoswitch-pharmacore’ couples that change biological activity because of light irradiation. Photopharmacological agents of a new generation can be used to treat various diseases, including Alzheimer's disease [1]. It is important, that practical implementation of photopharmacology is closely related with spatial control of medicinal treatment zone. Thus, demonstration of substances that meet all the listed requirements would determine the directions of breakthrough research in the coming years.

The purpose of this study is to develop photopharmacological agents that combine a number of functions – biological activity, the ability to change it under the influence of light and visualization of the zone of drug exposure.

In this study, we present for the first time CQDs@phosphonate nanohybrid that is conjunction of biocompatible and nontoxic luminescent carbon quantum dots (CQDs) with photoswitchable phosphonate compound possessing inhibition of butyrylcholinesterase (BChE) – prognostic marker of numerous diseases [2]. The study of the obtained nanohybrids using absorption spectroscopy, luminescence, FTIR spectroscopy and IPC –micro neurotoxins amperometric analysis revealed a pronounced effect of laser radiation on the optical and biological properties of new objects. CQDs@phosphonate hybrids demonstrate step increase of butyrylcholinesterase inhibition from 38% up to almost 100% and simultaneous luminescence decrease after laser irradiation with wavelength 266 nm. The all the listed Hybrids properties were demonstrated not only for in vitro experiments, but for complex biological sample – chicken breast. The uncovered photosensitivity and bioactivity of new phosphorylated phosphonates makes them promising compounds for clinical therapy as photopharmacological agents.

Acknowledgements

This work was supported by RSF project 22-13-00082. Authors are grateful to “Centre for Optical and Laser materials research”, Research Park of Saint Petersburg State University for technical support. Authors are grateful to Interdisciplinary Scientific and Educational School of Lomonosov Moscow State University “Photonic and Quantum technologies. Digital medicine”.

References

- [1] I. Kolesnikov, D. Mamonova, D. Pankin, G. Bikbaeva, A. Khokhlova, A. Pilip, A. Egorova, V. Zigel, A. Manshina, *Photochemistry and Photobiology*. 99(3), 929-935(2023)
- [2] I. Kolesnikov, A. Khokhlova, D. Pankin, A. Pilip, A. Egorova, V. Zigel, M. Gureev, G. Leuchs, A. Manshina, *New J. Chem.* 45, 15195–15199(2021)

B-O-10**Biomedical metabolic imaging revealed new criteria for reducing the regenerative potential of the liver**

S.A. Rodimova¹, V.V. Elagin¹, A.M. Mozherov¹, I.D. Shchekhin^{1,2}, D.P. Krylov^{1,2}, D.S. Kozlov^{1,2}, M.M. Karabut¹, A.I. Gavrina^{1,2}, N.V. Bobrov^{1,3}, V.E. Zagaynov^{1,4}, E.V. Zagaynova¹, D.S. Kuznetsova^{1,2}

1 - Privolzhsky research medical university, 603005, Nizhny Novgorod, Minin and Pozharsky sq. 10/1

2 - Lobachevsky Nizhny Novgorod National Research State University, 603022, Nizhny Novgorod, Gagarina 23

3 - The Volga District Medical Centre of Federal Medical and Biological Agency, 603000, Nizhny Novgorod, Ilinskaya st. 14

4 - Nizhny Novgorod Regional Clinical Oncologic Dispensary, Nizhny Novgorod, Delovaya St. 11/1

e-mail: daria.s.kuznetsova@gmail.com

Surgical liver resection remains the most effective treatment of liver tumors [1]. However, in the presence of hepatic pathologies, the regenerative potential of the liver is significantly reduced [2]. Standard clinical methods do not allow predicting the function of the liver remnant. Modern label-free methods of multiphoton microscopy with fluorescence lifetime imaging microscopy (FLIM) and second harmonic generation (SHG) allow to determine the criteria for reducing the regenerative potential of the liver with concomitant hepatic pathology.

A series of experiments were carried out on Wistar rats. Toxic liver fibrosis was induced by CCl₄ injections and steatosis was induced by 60% high-fat diet. At different stages of the pathology, we induced liver regeneration by 70% hepatectomy. Using multiphoton microscopy, we analysed the structure of the liver tissue on 3rd and 7th day after hepatectomy, and also determined the intensity of NAD(P)H autofluorescence in the zones of low and high signal. Using FLIM, we determined the fluorescence lifetime contributions of the free and bound forms of NADH and NADPH. Morphological analysis and a standard biochemical blood test were performed as controls.

As a result, we revealed the features of the structural and functional state at different stages of liver regeneration with steatosis and fibrosis. In case of steatosis, we identified zones with a reduced NADH autofluorescence intensity, corresponding to lipid infiltration or fibrosis. The area of zones with a reduced NAD(P)H autofluorescence intensity increased with the development of steatosis. We also showed a decrease in the contributions of the bound form of NADH and NADPH already in the early stages of steatosis. During regeneration with the presence of steatosis, there was no sharp increase in the contributions of the bound form of NADH and NADPH on the 3rd day after hepatectomy, due to mitochondrial dysfunction of hepatocytes. In case of fibrosis, we also identified zones with a reduced signal of NADH autofluorescence intensity, which corresponded to fibrosis. The area of zones with a reduced NAD(P)H autofluorescence intensity increased with the development of fibrosis. There was sharp a decrease in the contributions of the bound form of NADH and NADPH in the early stages of pathology, followed by an increase in these parameters in the later stages. Such changes are associated with mitochondrial dysfunction in the early stages and the progression of compensatory processes in the later stages of pathology.

The work was supported by the Grant from the Russian Science Foundation №19-15-00263.

[1] E. Ramos., J. Torras., L. Lladó. et al., The influence of steatosis on the short-and long-term results of resection of liver metastases from colorectal carcinoma, *Hpb*, 18(4), 389-396 (2016).

[2] V.E. De Meijer, B.T. Kalish, M., Puder, J.N.M. IJzermans, Systematic review and meta-analysis of steatosis as a risk factor in major hepatic resection, *Journal of British Surgery*, 97(9), 1331-1339, (2010).



B-O-11

Time-resolved fluorescence imaging of lipofuscin, incorporated *in vitro* into retinal pigment epithelial cells: Effects of photooxidation and protein-mediated antioxidant delivery

A.N. Semenov¹, E. G. Maksimov¹, A. M. Moysenovich¹, M. A. Yakovleva², G. V. Tsoraev¹, E. A. Shirshin^{1,3,4}, N. N. Sluchanko⁵, T. B. Feldman^{1,2}, A. B. Rubin¹, M. P. Kirpichnikov¹, Mikhail A. Ostrovsky^{1,2}

1- M.V. Lomonosov Moscow State University

2- Emanuel Institute of Biochemical Physics, Russian Academy of Sciences

3- World-Class Research Center "Digital Biodesign and Personalized Healthcare", Sechenov First Moscow State Medical University

4- Institute of Spectroscopy, Russian Academy of Sciences

5- Federal Research Center of Biotechnology, Russian Academy of Sciences

semenov@physics.msu.ru

Lipofuscin of retinal pigment epithelium (RPE) cells is a complex of chromophores accumulating as intracellular granules during the cell's lifespan. Being exposed to light, lipofuscin becomes a source of oxidative stress. It significantly complicates the course of various age-related eye diseases and without proper control may lead to the irreversible loss of the vision. Modern clinical routine utilizes fundus autofluorescence (FAF) imaging to assess the lipofuscin concentration in RPE. However, since FAF is based on the measurements of the intensity of lipofuscin fluorescence, very often this method does not allow to diagnose the pathology on the early stage. As a possibility to increase the sensitivity, the usage of the time-resolved measurements of lipofuscin fluorescence is being proposed. The aim of the work was to assess the lifetime of autofluorescence of lipofuscin, incorporated *in vitro* into RPE cells, with and without photooxidation in order to estimate lifetime as a diagnostic parameter. Additionally, we measured how administration of carotenoid antioxidant zeaxanthin via protein-mediated mechanisms affects lipofuscin fluorescence lifetime.

Lipofuscin granules (LG) were incorporated into RPE cell line culture ARPE-19 obtained from Koltzov Institute of Developmental Biology of RAS (Moscow, Russia). Fluorescence lifetime imaging (FLIM) was performed in the time-correlated single photon-counting (TCSPC) mode using the confocal system installed on the Eclipse Ti2 (Nikon, Tokyo, Japan) microscope. Excitation was performed by a 473 nm picosecond laser (30 ps impulse duration, 50 MHz repetition rate) synchronized with detector HMP-100-40 via board SPC-150 (Becker&Hickl, Germany). The detection was performed using a cutting-band filter at 530 nm with 40 nm band width (Thorlabs, USA). The photooxidation of cells enriched with LG was performed in CO₂-incubator by 18h-illumination with a custom LED array (light intensity 0.3 mW/cm²). Zeaxanthin was administered into ARPE-19 cells in complex with *Bombyx Mori* Carotenoid-Binding Protein (BmCBP-ZEA) at 200 nM concentration (calculated by the protein). The description of BmCBP production, as well as its abilities to bind various carotenoids, and demonstration of its antioxidant properties, are available in our previous work [1].

The analysis of the FLIM data of ARPE-19 cells, enriched with LG, revealed that autofluorescence of intact lipofuscin was characterized with mean lifetime $\tau_{\text{mean}} = 275 \pm 45$ ps. Irradiation of cells led to the massive photooxidation, and the significant increase in lipofuscin fluorescence lifetime (375 ± 37 ps) was detected. Supplement of cells with BmCBP-ZEA resulted in lower values of the lipofuscin fluorescence mean lifetime after illumination (310 ± 23 ps), demonstrating the suppression of the photooxidation due to the antioxidation effect. For more details please refer to our work [2].

Basing on the obtained results, we conclude that time-resolved diagnostics of lipofuscin autofluorescence is sensitive to the photooxidation processes, as well as to the effects of carotenoid antioxidants. Thus, it can be proposed as a part of fluorescence imaging ophthalmoscopy technique.

The present work was supported by Russian Scientific Foundation grant № 22-25-00183.

[1] N. Sluchanko, Y. Slonimskiy, E. Maksimov et al., Silkworm carotenoprotein as an efficient carotenoid extractor, solubilizer and transporter, International Journal of Biological Macromolecules, vol. 223, pp. 1381-1393 (2022).

[2] A. Semenov, E. Maksimov, N. Sluchanko et al., Protein-Mediated Carotenoid Delivery Suppresses the Photoinducible Oxidation of Lipofuscin in Retinal Pigment Epithelial Cells, IJMS, vol. 12 (413), pp. 1-19, (2023).

B-O-12**Studies on the structure and biocompatibility of multilayer laser formed material based on nanotubes and biopolymers for myocardial regeneration**

**U. Kurilova^{1,2}, D. Murashko², A. Kuksin², Yu. Vasilevskaya², K. Khorkov³,
A. Gerasimenko^{1,2}**

1 - Sechenov First Moscow State Medical University, 8 Trubetskaya str., Moscow 119991, Russia

2 - National Research University of Electronic Technology MIET, 1, Shokin Square, Zelenograd, Moscow 124498, Russia

3 - Vladimir State University, 87 Gorky str., Vladimir 600000, Russia

Main author email address: kurilova_10@mail.ru

Currently, cardiovascular diseases are the leading cause of mortality. Researchers efforts are focused on improving the regeneration of damaged cardiac tissue in coronary heart disease with tools of tissue engineering, where the patient's own cells form living tissue after cultivation on biocompatible scaffold of proper structure.

One of the promising classes of materials used for regeneration of damaged myocardium is composite materials with nanoparticles and biopolymers [1,2]. The multilayer biomaterial based on carbon nanotubes and proteins (collagen and albumin) and chitosan, obtained by layer-by-layer laser formation, is a good option for these purposes. Each of the biopolymer layers has specific properties for the best mechanical support and successful cell adhesion and proliferation. Laser treatment forms a strong electrically conductive scaffold of carbon nanotubes in the volume of the material, biopolymers ensure the necessary surface characteristics and high biocompatibility.

The obtained samples were analyzed using microscopy, vibrational spectroscopy and X-ray microtomography. The micro- and nanoarchitecture of the layers of the multicomponent structure for regeneration of myocardium tissue was evaluated with a scanning microscope. The albumin-based layer with single-walled nanotubes has a porous surface with the presence of elevations, which contributes to the adhesion of the cell culture. The chitosan and SWCNT layer is characterized by a porous grid, with nanotubes evenly distributed across the surface. Individual nanotubes and their bundles formed fine pores from 1 to 5 μm under the action of laser radiation. The layer based on collagen and SWCNT has a high degree of porosity, networks of individual nanotubes are observed inside the pores.

The X-ray microtomography data revealed that the samples had a homogeneous structure. The porosity of the layers increases with increasing power of laser radiation during formation process. Open pores prevail in all the experimental samples, which provides the possibility of blood vessels ingrowth into the material structure. Chitosan and SWCNT layer had the highest porosity. Vibrational spectroscopy made it possible to assess the influence of laser radiation on the organic components of the layers of the multicomponent structure for regeneration of myocardium tissue and prove the process of nanotube structurization, as it was seen on the microscopy images. Among the proteins, collagen was the most resistant to heating by radiation, because the characteristic bands were found on the spectra. Chitosan was the most laser-resistant of all the studied organic materials.

Cellular studies showed improved cell proliferation on the samples compared to the control. In the process of laser treatment, a grid was formed on the surface of the samples, the cells were aligned along the lines of laser structuring. The morphology of the cultured cells did not differ from the morphology of the cells in the control samples, which indicates the absence of toxicity.

This work was financed by the Ministry of Science and Higher Education of the Russian Federation within the framework of state support for the creation and development of World-Class Research Centers "Digital biodesign and personalized healthcare" № 075-15-2022-304.

[1] B. Huang, Carbon nanotubes and their polymeric composites: The applications in tissue engineering, *Bio manufacturing Reviews*, vol. 5, p.3, (2020).

[2] Y. Wu, L. Wang, B. Guo, P. X. Ma, Interwoven aligned conductive nanofiber yarn/hydrogel composite scaffolds for engineered 3D cardiac anisotropy. *Acs Nano*, vol. 11, pp. 5646-5659, (2017).

B-O-13

Quantum chemical modeling of structure and Raman spectra of L-lactide and ϵ -caprolactone oligomers

**S.O. Liubimovskii¹, V.S. Novikov¹, V.V. Kuzmin¹, D.D. Vasimov¹, N.G. Sedush²,
S.N. Chvalun², L.Yu. Ustynyuk³**

1- Prokhorov General Physics Institute of the Russian Academy of Sciences, Vavilov St. 38, 119991 Moscow, Russia

2- Enikolopov Institute of Synthetic Polymeric Materials of the Russian Academy of Sciences, Profsoyuznaya 70, 117393 Moscow, Russia

3- Chemistry Department, M.V. Lomonosov Moscow State University, Leninskie Gory 1(3), 119991 Moscow, Russia

liubimovskii@kapella.gpi.ru

Quantum chemical modeling is a powerful tool to study the conformational composition and the vibrational spectra of organic molecules. In particular, such modeling allows to identify the most probable molecular conformations, assign IR and Raman bands to the particular vibrations and determine the general regularities in dependences of the vibrational spectra on the chemical structure and the conformational composition of

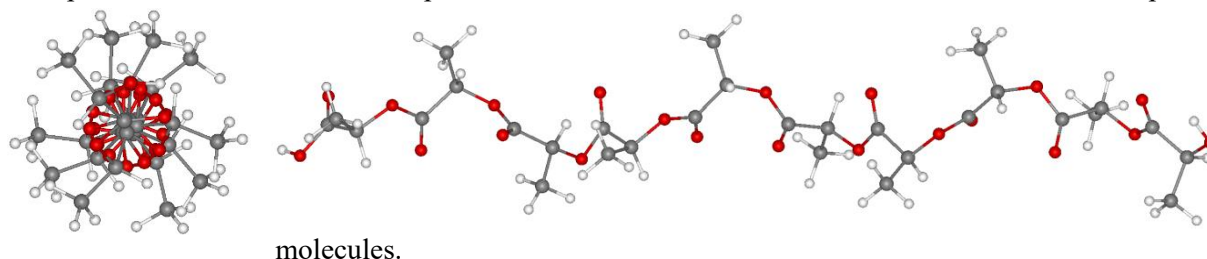


Fig. 1. Optimized structure of L-lactide decamer in the conformation of helix 10₃ (program PRIRODA, OLYP/4z).

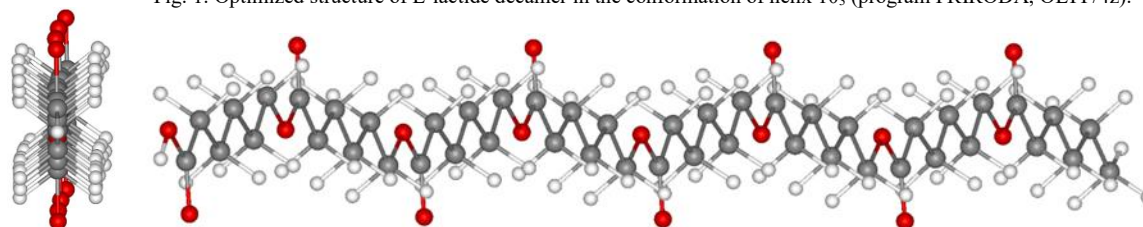


Fig. 2. Optimized structure of ϵ -caprolactone octamer in the *all-trans* conformation (program PRIRODA, OLYP/4z).

In this work, we used density functional theory (DFT) to study the structure and Raman spectra of L-lactide (LA) and ϵ -caprolactone (CL) oligomers with the aim to identify the Raman bands, which depend on the length and conformation of sequence of the monomeric units. This information is necessary for Raman evaluation of microstructure of LA/CL copolymers chains. These copolymers are very important as bioresorbable and biocompatible materials with adjustable degradation profile for novel applications in medicine.

We showed that the most probable conformation of LA oligomers is helix 10₃ (Fig. 1). The conformation of helix 3₁ is much less probable. If we do not apply any constraints during geometry optimization procedure, it easily transforms to the conformation of helix 10₃.

The DFT calculations showed that the most probable conformation of CL oligomers is *all-trans* conformation (Fig. 2). For both LA and CL oligomers the simulated Raman spectra describe well the main bands of poly(L-lactide) and poly(ϵ -caprolactone).

This study was supported by the Russian Science Foundation under the grant № 23-22-00347, <https://rscf.ru/en/project/23-22-00347/>. We are grateful to the Joint Supercomputer Center of the RAS for the possibility of using their computational resources for our calculations.

B-O-14

Diagnosing diseases in dentistry using Raman spectroscopy

P.E. Timchenko¹, E.V. Timchenko¹, L.T. Volova², I.V. Bazhutova², O.O. Frolov¹

1- Samara National Research University, Russia, Samara

2- Samara State Medical University, Russia, Samara

Main author email address: frolovaleh@gmail.com

Among the optical methods for studying biological tissues, the method of Raman spectroscopy is widely used in solving biomedical problems. This method can also be used to diagnose diseases and assess the course of the disease.

The main method of analysis was the Raman spectroscopy method implemented by the experimental stand that included Raman probe RPB-785, combined with the laser module Luxx Master LML-785.0RB-04 and the high-resolution digital spectrometer Shamrock sr-303i providing spectral resolution of 0,15 nm with the build in cooling camera DV420A-OE.

The spectra were normalized using the Extended multiplicative signal correction (EMSC) method [1]. Smoothing method - Maximum Likelihood Estimation Savitzky-Golay filter (MLE-SG) [2] with the parameter $\sigma = 4$.

To eliminate the contribution of autofluorescence in the Raman spectrum, was used a modified method of subtracting the fluorescence component by polynomial approximation Improved Modified Multi-Polynomial Fitting (I-ModPoly+) with a polynomial degree of 9.

To increase the information content of the obtained Raman spectra, we decomposed into the sum of spectral asymmetric Pseudo Voigt lines

- The possibility of using the method of Raman spectroscopy for non-invasive express evaluation of the effectiveness of treatment in periodontitis by changing the spectra of dental cement is shown.

The obtained results of the research will contribute to the adjustment of the treatment of patients with periodontitis and the exclusion of ineffective stages of the complex treatment of inflammatory periodontal diseases in dental practice.

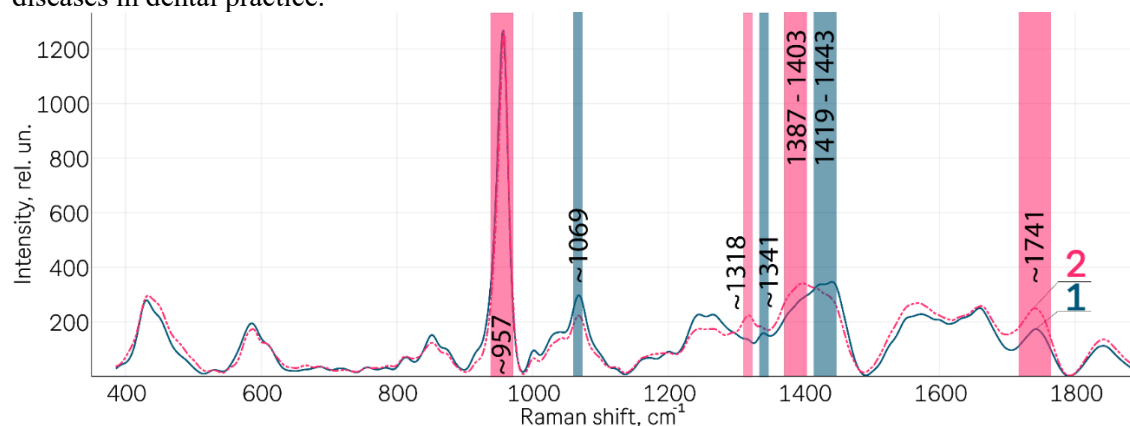


Fig. 1. Averaged Raman spectra of individual samples: 1 - normal bone tissue, 2 - bone tissue with periodontitis

It has been shown that the spectral characteristics of bone tissue samples in periodontitis differ significantly from the characteristics of the normal bone tissue spectra (fig.1). The greatest difference is seen in the Raman lines ~ 1741 (C=O ester group, phospholipids (Lipid assignment)), ~ 1419 , 1443 cm^{-1} (CH_2 deformation), ~ 1387 (CH_3 band), 1403 (Bending modes of methyl groups (one of vibrational modes of collagen)). Also, the spectra of group 2 (with periodontitis) are distinguished by the presence of a pronounced line ~ 1318 cm^{-1} Amide III (α -helix).

The cross-validated accuracy of the classifying model based on logistic regression was $84 \pm 9\%$.

[1] N.K. Afseth, A. Kohler, Extended multiplicative signal correction in vibrational spectroscopy, a tutorial, Chemometrics and Intelligent Laboratory Systems, 117., pp. 92–99, (2012).

[2] T. E. Ward, and B.M. Hennelly, Algorithm for optimal denoising of Raman spectra, Analytical Methods, 10.30, pp. 3759–3769 (2018).

B-O-15

Raman identification of carotenoid *cis*-isomers: DFT study

D. Vasimov¹, S. Kuznetsov¹, A. Ashikhmin², V. Kuzmin¹, V. Novikov¹

1- Prokhorov General Physics Institute of the Russian Academy of Sciences, 38 Vavilov St., 119991 Moscow, Russia

2- Pushchino Scientific Center for Biological Research of the Russian Academy of Sciences, Institute of Basic Biological Problems, 2 Institutskaya St., 142290 Pushchino, Moscow Region, Russia

vs.novikov@kapella.gpi.ru

Carotenoids are organic pigments, produced by plants, algae, a number of bacteria and fungi. They are involved in numerous vitally important biochemical processes in living nature, including crucial for humans provitamin, antioxidant and antiaging activities. Human organism cannot synthesize carotenoids and can get it only with food, dietary supplements and carotenoid-containing creams or ointments. Carotenoid properties strongly depend on both the chemical structure and isomeric composition. Thus, it is important to distinguish various types of carotenoids as well as various isomers of carotenoids in biological tissues and the sources of carotenoids for humans.

Due to very low photo-, thermal and oxidation stability of carotenoids in their pure form, density functional theory (DFT) analysis of these pigments is of great importance. In this work, we present DFT calculations of the structures and Raman spectra of *cis*-isomers with one *cis*-bond for *zeta*-carotene, neurosporene, spheroidene, lycopene, spirilloxanthin, *beta*-carotene, and lutein. All these carotenoids are involved in various branches of biosynthesis of carotenoids in plants and bacteria.

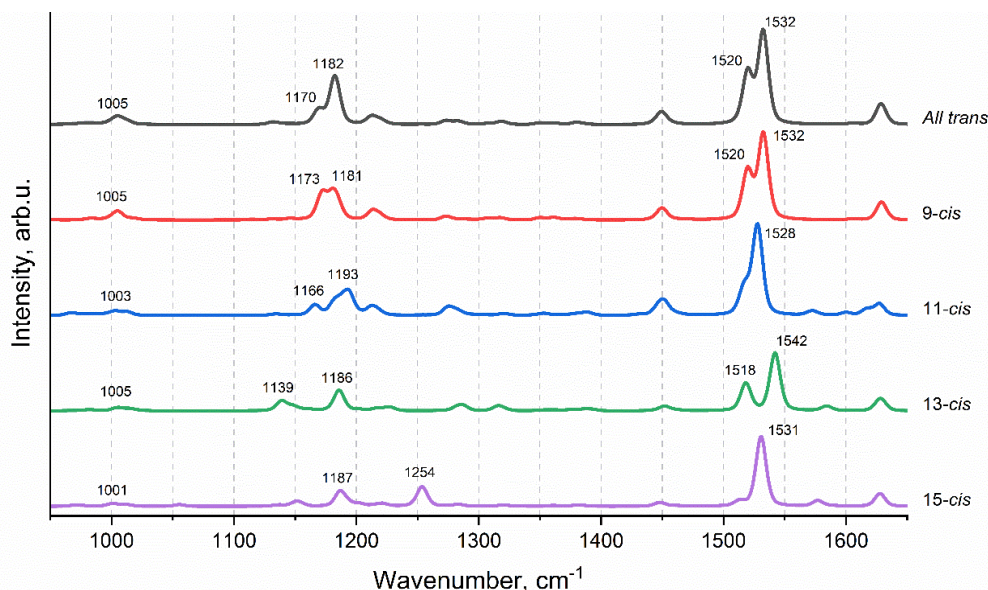


Fig. 1. Calculated Raman spectra of *zeta*-carotene molecule in *trans*-form and with one *cis*-bond at different positions in the polyene chain.

Analysis of this set of carotenoids allowed us to establish the dependence of Raman spectra, including the most informative C-C and C=C stretching bands, on the conjugation length (in the range from 7 to 13 conjugated C=C bonds), the structure of the end groups and position of *cis*-bond in the polyene chain. In particular, we have found a number of features in the Raman spectra that ambiguously relate to the vibrations of the *cis*-bond at a certain position in the carotenoid molecule. For example, Raman spectra of 15-*cis*-isomers of all the carotenoids under study contain a band near 1250 cm⁻¹, which refers to the stretching vibrations of C-C and C=C bonds around the *cis*-bond. As an example, Fig. 1 shows the calculated Raman spectra of various isomers of *zeta*-carotene, including 15-*cis*-isomer with the characteristic band at 1254 cm⁻¹. The results of our DFT analysis are in a good agreement with our spectra and published experimental Raman spectra of the carotenoids.

We are grateful to the Joint Supercomputer Center of the RAS for the possibility of using their computational resources for our calculations.

B-O-16

Efficacy of photodynamic therapy against uropathogenic bacteria

V. Elagin^{1*}, N. Ignatova², A. Antonyan³, I. Budruev⁴, P. Bureev⁴, O. Streltsova³, V. Kamensky^{1,5}

¹*Institute of Experimental Oncology and Biomedical Technologies, Privolzhsky Research Medical University, Russia*

²*Department of Epidemiology, Microbiology and Evidence-Based Medicine, Privolzhsky Research Medical University, Russia*

³*Department of Urology Named after E.V. Shakhov, Privolzhsky Research Medical University, Russia*

⁴*Institute of Biology and Biomedicine, Lobachevsky State University of Nizhny Novgorod, Russia*

⁵*Federal Research Center Institute of Applied Physics of the Russian Academy of Sciences, Russia*

elagin.vadim@gmail.com

It is well known that from 30% to 51% of urinary calculi are infected or have a bacterial origin. Modern lithotripsy approaches are based on crushing stones into small fragments that can be removed/washed out through small diameter accesses. In the case of infected stones, large amount of toxins and bacteria are inevitably released during fragmentation. Antimicrobial photodynamic therapy is considered to be an alternative to the antibiotic treatment of localized infectious processes. The purpose of the study was to evaluate the antibacterial efficacy of photodynamic therapy against human antibiotic-resistant bacterial uropathogens.

Uropathological microorganisms were isolated from renal calculi. It was found that 78.7±5.2 % of renal calculi were contaminated. Testing the sensitivity of the isolated strains to 10 antibiotics of different mechanisms of action showed that the studied strains have a high antibiotic resistance. The interaction between photosensitizer and uropathogenic microorganisms was analyzed. Since the samples were washed from free molecules of photosensitizer, the fluorescence was only detected from the photosensitizer that had penetrated into cells and/or was bound with cell wall. The photosensitizer accumulation was estimated to be dependent on both incubation time and concentration. The fluorescence intensity was found to be higher for Gram-negative strains than for the Gram-positive ones regardless of the photosensitizer concentration. The strains of *Enterococcus faecalis* and *Staphylococcus aureus* demonstrated the enhancement of the fluorescence intensity in a time-dependent manner with the maximal value at 60 min. *Escherichia coli* and *Proteus mirabilis* had the maximal value of fluorescence intensity after 30 min and that significantly decreased by 60 min. The optimal incubation time was found to be 30 minutes. However, this technique is planning to use during laser lithotripsy for sanitation, where the time is a limiting factor; therefore, 15 min of incubation was chosen. The concentration of the photosensitizer was selected to be 50 µg/mL. After 15 minutes of incubation in the dark followed by 15 minutes of manipulation (dilution, inoculation) at ambient light, no colony of *S. aureus* and *E. faecalis* was detected on the plates. The treatment of either Gram-positive or Gram-negative bacteria by laser light only did not induce significant reduction of CFUs. The survival rate of *P. mirabilis* for antimicrobial photodynamic therapy (aPDT) was power-dependent. The number of viable bacteria was decreasing from 65% to 10% with an increase in power from 50 mW to 150 mW. The maximal bactericidal effect was reached at 150 mW.

Next, the aPDT was adapted for Gram-negative species. The efficacy of aPDT of *E. coli* incubated with photosensitizer and Triton X-100 achieved 52.5%. It was found that washing of the extracellular photosensitizer led to loss of the aPDT efficacy. The high sensitivity of *P. aeruginosa* to aPDT with extracellular photosensitizer significantly reduced after washing of the photosensitizer. The efficacy of aPDT of *P. mirabilis* did not change after washing of the extracellular photosensitizer. It was demonstrated that the aPDT efficacy depended on laser power in all studied species, excluded *K. pneumoniae*. The efficacy of *K. pneumoniae* treatment did not exceed 93%. The irradiation of other bacteria species with a power of 450 mW provided an aPDT efficacy of 99.99%. To test the efficacy of the developed aPDT technique, urine cultures of the patients were incubated with a photosensitizer and Triton X-100 for 15 minutes in the dark. Then, the unwashed samples were illuminated by a continuous wave laser at 450 mW of output power. The efficacy of the aPDT of infected urine cultures was not less than 99.996%.

This work was supported by the Russian Science Foundation, project №21-15-00371.

B-O-17

Study of methylene blue interaction with cell membranes: influence on the mechanism of the photodynamic activity

Pominova D.V.^{1,2}, Ryabova A.V.^{1,2}, Romanishkin I.D.¹, Markova I.V.², Akhlustina E.V.², Skobeltsin A.S.^{1,2}

1- Prokhorov General Physics Institute of Russian Academy of Sciences, Moscow, Russia

2- National Research Nuclear University MEPhI (Moscow Engineering Physics Institute), Moscow, Russia

Main author email address: pominovadv@gmail.com

To date, there is an active search for new approaches for the treatment of oncological diseases, in particular, the development of methods for influencing tumors that are in a state of hypoxia, which are difficult to treat. A promising minimally invasive method of treating oncological diseases is photodynamic therapy. This method is based on use of photosensitizer (PS), which is selectively accumulated in tumor and irradiation with light. The PS absorbs the light and can then even transfer the energy to molecular oxygen and create singlet oxygen (type II photochemical reaction) or participate in electron-transfer reactions initiating formation of hydroxyl radicals and hydroperoxides and radical-induced damage in biomolecules (type I photochemical reaction) [1]. Most of clinically approved PS are prone to the type II photochemical reaction. However, the type I photochemical reaction may be preferable for therapy of hypoxic tumors [2].

One of the actively studied PS is methylene blue (MB). Depending on the environment (solvent, ionic strength, pH value, etc.), it can form both singlet oxygen and other reactive oxygen species [3]. In this work, we studied the interaction of MBs with cell membranes using spectroscopic methods and evaluated the efficiency of generation of singlet oxygen (by measuring the oxygen content in erythrocyte solution with MB by the hemoglobin oxygenation level) and reactive oxygen species (using fluorescent sensors) in order to determine which mechanism is prevalent under *in vitro* and *in vivo* conditions. In the investigated range of concentrations, the singlet oxygen generation efficiency was low, the existence of other reactive oxygen species in cells has been demonstrated. This indicates the tendency of MB to the type I photosensitization mechanism rather than to the type II mechanism, which is presumable attributed to MB binding to negatively charged cell membranes and aggregation.

The study was funded by a grant from the Russian Science Foundation (project N 22-72-10117).

[1] A.A. Krasnovsky, Photodynamic action and singlet oxygen, Biophysics, vol.49(2) pp. 289-306, (2004).

[2] M. S. Baptista, G. L. Indig, Effect of BSA Binding on Photophysical and Photochemical Properties of Triarylmethane Dyes, The Journal of Physical Chemistry B, vol. 23 (102), pp. 4678–4688, (1998).

[3] H.C. Junqueira, D. Severino, L.G. Dias, M.S. Gugliotti, M.S. Baptista, Modulation of methylene blue photochemical properties based on adsorption at aqueous micelle interfaces, Physical Chemistry Chemical Physics, vol. 11 (4), pp. 2320–2328, (2002).

B-O-18**Fluorescent analysis of photosynthetic organisms stress resistance in different conditions****V. Grishanov¹, A. Popov¹***1- Samara National Research University, Samara, Russia, 34, Moskovskoye shosse, Samara, 443086, Russia**Main author email address: hydroinvader@mail.ru*

Experiments aimed to create closed ecosystems for the purposes of both fundamental and applied science have been performed for many years. This kind of research is especially interesting for certain research including studying life in space and attempts to create fully or partially autonomous ecosystems that will be able to create and regenerate the environment suitable for existence of humans, animals or other organisms. The nature of such experiments implies long-term absolute isolation from the usual Earth conditions. We can collect data on the processes occurring in the isolated systems without any risks of losing of hermetic isolation either using data loggers put inside or using outer devices. In that case, we lose almost any possibility to repair, modify or replace the device without breaking the isolation of the ecosystem, besides we become limited by the size of the container and data gathering device.

We have performed a series of experiments that allowed us to get the information on the key members of the ecosystems such as photosynthetic organisms inside the intact hermetically sealed container, using the atomic excitation and registration of the fluorescence through its walls.

Spectrofluorometer with the excitation in the near-UV wavelength region of the electromagnetic spectrum (light-emitting diode, central wavelength 365 nm) was used [1]. The fluorescence was registered as a set of colored images, thus, the shape and color of the fluorescent areas could be observed.

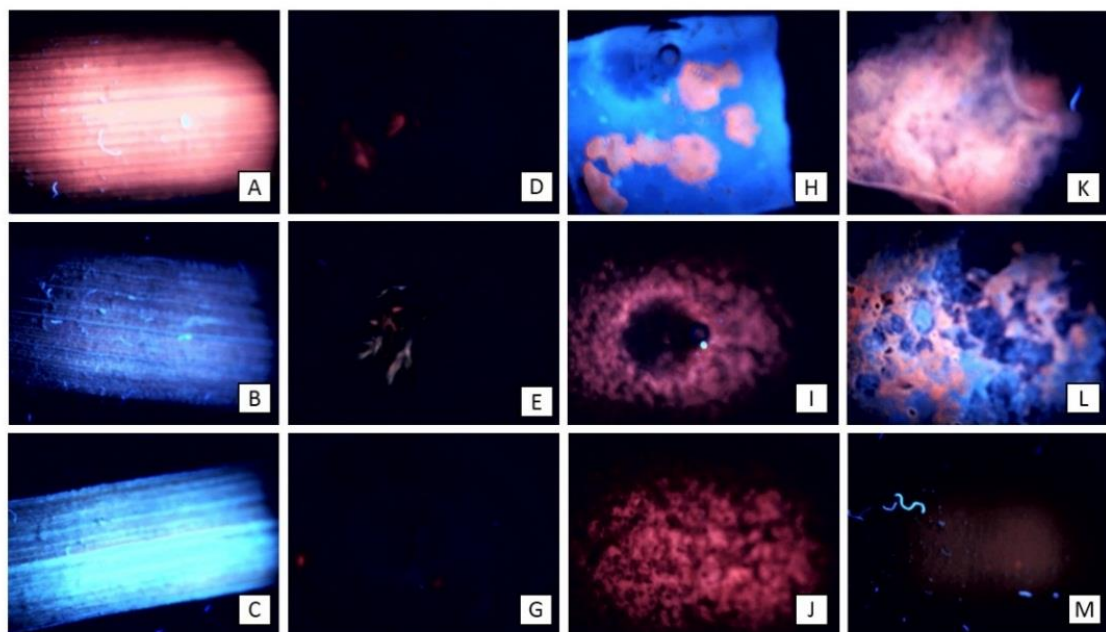


Fig 1. A – *Poa pratensis*, living leaf, B – *Poa pratensis*, dead leaf, 7 days, C – *Poa pratensis*, dead leaf, 10 days, D – Moss *Bryum* sp. living active plant, E – *Bryum* sp. living inactivated (dessicated) plant, G - *Bryum* sp. dead plant, H – Halophilic green algae *Dunaliella* (no cellulose cell wall), I, J – Living cyanobacteria, K – Cyanobacteria dead for a period of 12 months, L – Green algae *Trebouxia* sp. (cellulose cell wall), M - sea-buckthorn (*Hippophae* sp.) carotenoid oil extract

As a result, we can conclude that the method and the designed device can be applied for remote data gathering without any risk of breaking of the isolation of a closed ecosystem that includes oxygenic or anoxygenic photosynthetic organisms. It can be used for flexible long-term monitoring of condition of experimental semi-artificial ecosystems.

[1] Нигматулин, И.Р. Панорамный флуориметр [Текст] / И.Р. Нигматулин, В.Н. Гришанов - Актуальные проблемы радиоэлектроники и телекоммуникаций: материалы Всероссийской научно-технической конференции (г. Самара, 15.05 – 17.05.2018) / Под ред. А.И. Данилина. - Самара: Изд-во ООО «Офорт», 2018. – С. 194 – 195.



B-P-1

Intravital fluorescent imaging to test nanoparticles safety and distribution using liver slices

**V.V. Elagin¹, S.A. Rodimova¹, A.M. Mozherov¹, D.P. Krylov^{1,2}, D.S. Kozlov^{1,2},
M.V. Zyuzin³, D.S. Kuznetsova^{1,2}**

1 - Privolzhsky research medical university, 603005, Nizhny Novgorod, Minin and Pozharsky sq. 10/1

2 - Lobachevsky Nizhny Novgorod National Research State University, 603022, Nizhny Novgorod, Gagarina 23

3 - ITMO University, 191002, St. Petersburg, Lomonosova st., 9

e-mail: elagin.vadim@gmail.com

Despite the promising results currently achieved in stimulating liver regeneration using small bioactive molecules, there is still a problem of the lack of an effective method for their delivery with a controlled release period, their accumulation and excretion [1]. Such a technology based on complexes of nanoparticles and bioactive molecules is especially relevant due to the high risk of liver failure after liver surgery. The most promising methods for assessing the state of living liver cells seems to be multiphoton fluorescent microscopy with second harmonic generation (SHG) and time-resolved FLIM microscopy. These methods are non-invasive, label-free and allow intravital monitoring at the cellular level. In addition, the use of the model of precision-cut liver slices made it possible to screen several types of nanoparticles, excluding the individual contribution of the animal organism, simplifying the analysis and interpretation of the results.

Vibrating microtome 7000 cm3-2 was used to obtain liver slices using the protocol of Pearen et al. [2], and were placed in separate wells of a 12-well plate with a standard CO₂-conditioned form of DMEM supplemented with 0.1 μ m of dexamethasone and 10% FBS. Next, cultivation was carried out in DMEM medium with the addition of nanoparticles at a concentration of 50 and 100 mg/ml and incubated for 3, 24, and 48 hours. All obtained tissue explants were preincubated for 1 h in DMEM medium on an orbital shaker (90 rpm). Gold nanoparticles with a size of 100-120 nm in the form of nanorods were synthesized using a standard protocol based on seed mediated mechanism. The synthesis of SiO₂ nanoparticles with a size of 20-100 nm was carried out using the sol-gel method. Polylactide (PLA) nanoparticles with a size of 100 nm are tested by single-emulsion solvent extraction. All nanoparticles were modified with a Cy 5 fluorescent label. Liver slices were stained with LysoTracker Yellow HCK-123 and Phalloidin FITC. Using multiphoton microscopy, we assessed the tissue structure of liver slices. Using FLIM, we analyzed the metabolic state of hepatocytes based on fluorescence lifetime contributions of the free and bound forms of NADH and NADPH.

As a result, it was shown that SiO₂ nanoparticles were practically not accumulated by liver cells and show low cytotoxicity. Gold nanoparticles showed effective accumulation in liver cells, however, its had strong cytotoxic effect on liver cells. Finally, polylactide nanoparticles accumulated most effectively in liver cells, mainly in the cytoplasm of hepatocytes. Using FLIM, we revealed low cytotoxicity of PLA nanoparticles, due to the relative contributions of fluorescence lifetimes of bound form of NADH and NADPH did not differ significantly from control values. Thus, PLA nanoparticles seem to be the most promising for further development of a strategy for stimulating liver regeneration using nanoparticles modified by bioactive molecules. Based on the obtained data, we will select the appropriate miRNAs that stimulate liver regeneration.

The work was supported by the Grant from the Russian Science Foundation №23-15-00421.

[1] Liu Z., Li Y., Li W., et al. Multifunctional nanohybrid based on porous silicon nanoparticles, gold nanoparticles, and acetalated dextran for liver regeneration and acute liver failure theranostics. *Advanced Materials*, 30(24), 1703393, (2018).

[2] Pearen M. A., Lim H. K., Gratte F. D. et al. Murine precision-cut liver slices as an ex vivo model of liver biology. *JoVE*, (157), e60992, (2020).

B-P-2**FLIM reveals criteria for toxic liver damage in tissue slices**

**M.M. Karabut¹, D.P. Krylov^{1,2}, S.A. Rodimova¹, I.D. Shchechkin^{1,2},
D.S. Kozlov^{1,2}, A.M. Mozherov¹, D.S. Kuznetsova^{1,2}**

1 - Privolzhsky research medical university, 603005, Nizhny Novgorod, Minin and Pozharsky sq. 10/1

2 - Lobachevsky Nizhny Novgorod National Research State University, 603022, Nizhny Novgorod, Gagarina 23

e-mail: maria.karabut@gmail.com

Abuse with hepatotoxic agents is a major cause of acute liver failure. The search for new criteria indicating the acute or chronic pathological processes is still a challenging issue that requires the selection of effective tools and a research models. Modern label-free methods of multiphoton microscopy with fluorescence lifetime imaging microscopy (FLIM) and second harmonic generation (SHG) expand the possibilities of studying the structural and functional state of liver tissue at the cellular level [1]. Multiphoton microscopy with second harmonic generation (SHG) and fluorescence lifetime imaging microscopy (FLIM) are modern label-free methods of optical biomedical imaging for assessing the metabolic state of hepatocytes, therefore reflecting the functional state of the liver tissue. Using precision-cut liver slices model (PCLSs) allows to preserve of the key intercellular interactions and cellular components of pathological changes caused by most widely used hepatotoxic agents - acetaminophen (APAP), carbon tetrachloride (CCl₄), and ethanol.

Vibrating microtome 7000 cm3-2 was used to obtain liver slices using the protocol of Pearen et al. [2], and were placed in separate wells of a 12-well plate with a standard CO₂-conditioned form of DMEM supplemented with 0.1 μm of dexamethasone and 10% FBS, and incubated at 37 °C on orbital shaker (90 rpm). To induce APAP toxic damage, the liver slices were placed for 3 h in a 10 mM solution of APAP diluted in DMEM. To induce ethanol toxic damage, liver slices were placed for 3 h in 25 mM ethanol diluted in DMEM. For the CCl₄ model the liver slices were incubated for 3 h with 2 mL standard culture medium, and a piece of filter paper soaked in 10 μL of CCl₄ was attached to the lid of the 12-well plates. As a control, we used liver slices cultivated in DMEM without toxins. Monitoring were performed after 3 h, 24 h and 48 h of incubation. Using FLIM, we analyzed the metabolic state of hepatocytes based on fluorescence lifetime contributions of the free and bound forms of NADH and NADPH.

We have determined characteristic optical criteria for toxic liver damage, and these turn out to be specific for each toxic agent, reflecting the underlying pathological mechanisms of toxicity. Using multiphoton microscopy, we identified liver cells with both high and low NAD(P)H autofluorescence intensity, indicating cell damage. Interestingly, APAP-induced toxic damage was characterized by an increase in the contribution of the bound form of NAD(P)H, while exposure to ethanol and CCl₄ showed a significant decrease in the contribution of the bound form of NAD(P)H, which reflects differences in the mechanisms of damage by each toxic agent. The results obtained are consistent with standard methods of molecular and morphological analysis. Thus, our approach, based on optical biomedical imaging, is effective for intravital monitoring of the state of liver tissue in the case of toxic damage or even in cases of acute liver injury.

The work was supported by the Grant from the Russian Science Foundation №22-25-00098.

[1] M. S. Roberts, Y. Dancik, T.W. Prow, et al., Non-invasive imaging of skin physiology and percutaneous penetration using fluorescence spectral and lifetime imaging with multiphoton and confocal microscopy. *Eur J Pharm Biopharm*, 77(3), 469-488, (2011).

[2] Pearen M. A., Lim H. K., Gratte F. D. et al. Murine precision-cut liver slices as an ex vivo model of liver biology. *JoVE*, (157), e60992, (2020).

B-P-4

Study of *in vivo* optical clearing of the human oral cavity mucosa by Raman Spectroscopy

E. N. Lazareva^{1,2}, V. I. Kochubey^{1,2}, I. Yu. Yanina^{1,2}, Yu.V. Kistenev², V. V. Tuchin^{1,2}

1-Institute of Physics and Science Medical Center, Saratov State University (83 Astrakhanskaya st., 410012 Saratov, Russia)

2- Laboratory of Laser Molecular Imaging and Machine Learning, Tomsk State University (36 Lenin's av., 634050 Tomsk, Russia)
lazarevaen@list.ru

Optical methods are increasingly being used for new scientific developments in medicine due to a number of advantage [1]. One of these methods is Raman spectroscopy, which makes it possible to carry out a quantitative and qualitative chemical analysis and to evaluate changes in the conformation of molecules [1, 2]. However, the use of optical methods, in particular, Raman spectroscopy, for working with biological tissues has limitations, such as, the high power of the radiation used and the low probing depth. To increase the efficiency of these methods, the use of optical clearing can be prospective [3]. This pilot study demonstrates the use of optical clearing technology for the oral mucosa of volunteers in the study using Raman spectroscopy. The effect on tissue of optical clearing agents, such as a solution of 40% glucose and mixtures based on sorbitol, propylene glycol and water, on the tissue was investigated.

For example, the Raman spectra of the oral mucosa from the inner cheek before and after exposure to 40% glucose solutions are shown in Figure 1.

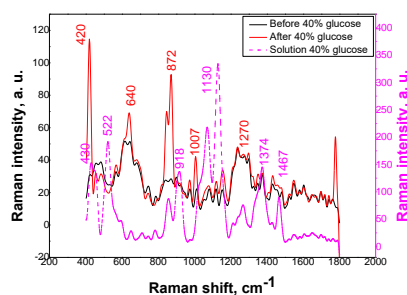


Fig. 1. Raman spectra of an area of the oral mucosa of a volunteer before and after exposure to a 40% glucose solution.

The effect of a 40% glucose solution on the oral mucosa shifted the lipid band from 786 cm^{-1} to 797 cm^{-1} and the amides/proteins band from 1661 cm^{-1} to 1671 cm^{-1} . A significant increase in intensity is observed for glucose at 420 cm^{-1} and the saccharide bands at 842 cm^{-1} and 872 cm^{-1} , which may indicate the interaction of proteins with glucose [4]. Glucose peaks at 1071 cm^{-1} and 857 cm^{-1} refer to C–O–H deformation stretching and C–C stretching vibrations and, according to the literature data, may indicate the interaction of glucose with tissue proteins and the formation of hydrogen bonds [5, 6].

The study was supported by RSF grant no. 23-14-00287, <https://rscf.ru/project/23-14-00287/>.

[1] V. V. Tuchin, J. Popp, V. Zakharov, Multimodal Optical Diagnostics of Cancer, Springer (2020)

[2] Q. Lin, E.N. Lazareva, V.I. Kochubey, Y. Duan, V.V. Tuchin, Kinetics of optical clearing of human skin studied *in vivo* using portable Raman spectroscopy, *Laser Phys. Lett.*, vol. 17(10), pp.:105601. (2020)

[3] V.V. Tuchin, D. Zhu, E.A. Genina, Handbook of Tissue Optical Clearing: New Prospects in Optical Imaging, 1st Edition. CRC Press, Boca Raton (2022).

[4] M. Saito Nogueira, V. Ribeiro, M. Pires, F. Peralta, L.F.dC.eS.d. Carvalho. Biochemical Profiles of *In Vivo* Oral Mucosa by Using a Portable Raman Spectroscopy System, *Optics*, vol. 2(3), pp.134-147 (2021).

[5] K.E.Shafer-Peltier, C.L.Haynes, M.R. Glucksberg, R.P. Van Duyne, Toward a Glucose Biosensor Based on Surface-Enhanced Raman Scattering, *Journal of the American Chemical Society*, vol. 125(2), pp. 588–593. (2003)

[6] L. Ouyang, L. Yao, R. Tang, X. Yang, L. Zhu, Biomimetic point-of-care testing of trace free bilirubin in serum by using glucose selective capture and surface-enhanced Raman spectroscopy, *Sensors and Actuators B: Chemical*, vol. 340, pp. 129941. (2021)

B-P-5

Laser tweezers technique in studies of impact of endothelium derived nitrogen oxide (NO) on red blood cell (RBC) aggregation

Maksimov M.K.¹, Ermolinskiy P.B.¹, Lugovtsov A.E.¹, Muravyov A.V.², Priezzhev A.V.¹

1- Lomonosov MSU, Faculty of Physics, Russia, 119991, Moscow, GSP-1, 1-2 Leninskiye Gory

2- Yaroslavl State Pedagogical University named after K.D.Ushinsky, Russia, 150000, Yaroslavl, Respublikanskaya street, 108/1

madoway@yandex.ru

Red blood cells (RBC) play a variety of roles in human body. Besides gas exchange function there are roles in immune response and hemostasis [1]. One of the important properties of RBC is their spontaneous aggregation, i.e. ability to reversibly form linear or more complex aggregates. RBC aggregation significantly impacts blood rheology by changing the blood viscosity and its alterations in some diseases may cause pathological complications [2]. RBC aggregation depends on different factors: from blood plasma osmolarity to protein concentration. One of these factors is the concentration of signaling molecules in the blood flow. Nitric oxide (NO) is a signaling molecule from gasotransmitters class. Its main target in blood flow are smooth muscle cells, NO causes vasorelaxation and systemic decrease in arterial pressure. The main sources of nitric oxide in the blood flow are endothelial cells, that produce NO from L-arginine by endothelial nitric oxide synthase (eNOS). There is evidence of NO changing RBC properties, in particular, their deformability and aggregability [3].

In this work, RBC aggregation in presence of endothelial cells monolayer was studied by laser tweezers technology. To stimulate NO production endothelial cells were treated with L-arginine solution. Measurements were taken in a microcuvette with the height of 300 μm and volume of 300 μl . On the bottom of the cuvette a monolayer of endothelial cells was placed, then cuvette was filled with human plasma containing a small number of RBC (0.1 % hematocrit). RBCs aggregation force is the minimal force needed to prevent spontaneous aggregation of two adjacent contacting RBC. RBC disaggregation force is the minimal force needed to disrupt the contact of two aggregated RBC. In order to decrease the data dispersion, the measured values were normalized by the mean value of the control (0 μM of L-arginine). Statistical significance of their alterations was calculated using the Mann-Whitney test.

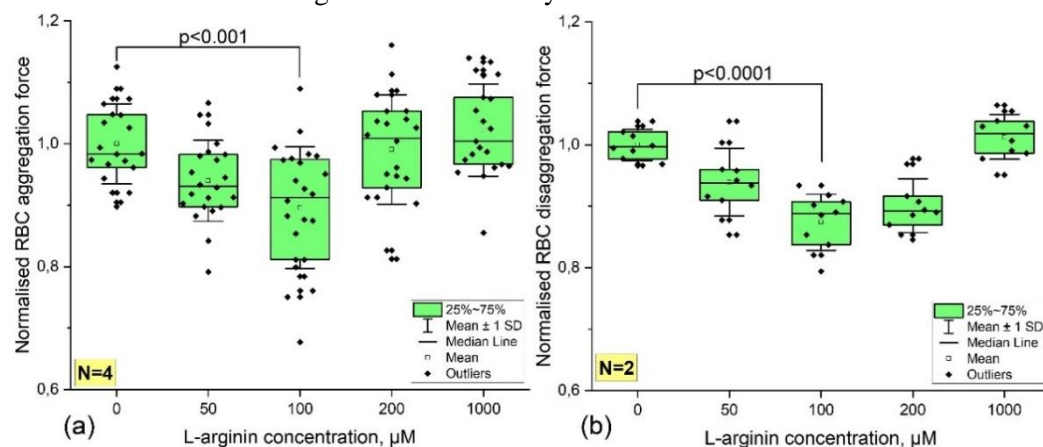


Figure 1. The dependence of RBC aggregation (a) and disaggregation (b) forces on L-arginine concentration

In our experiments, L-arginine caused a decrease in both RBC aggregation and disaggregation forces with a minimum at L-arginine concentration of 100 μM (Figure 1). In both cases, the dependence seems to be bell-shaped: the effect disappears at higher concentrations.

The study was financially supported by the Russian Science Foundation grant №. 22-15-00120.

[1] Pretini, V., Koenen, M. H., Kaestner, L., Fens, M. H., Schiffelers, R. M., Bartels, M., Van Wijk, R., Red blood cells: chasing interactions, *Frontiers in Physiology*, 10, 945, (2019).

[2] Maslianitsyna, A., Ermolinskiy, P., Lugovtsov, A., Figurenko, A., Sasonko, M., Gurfinkel, Y., Priezzhev, A., Multimodal diagnostics of micro-rheologic alterations in blood of coronary heart disease and diabetic patients, *Diagnostics*, 11(1), 76, (2021).

[3] Muravyov, A. V., Avdonin, P. V., Tikhomirova, I. A., Bulaeva, S. V., Malysheva, J. V., Effects of Gasotransmitters on Membrane Elasticity and Microrheology of Erythrocytes. *Biochemistry (Moscow), Supplement Series A: Membrane and Cell Biology*, 13, 225-232, (2019).



B-P-6

Multivariate analysis of Raman spectra and dermatoscopic images for the diagnosis of skin cancer

I. Matveeva¹, V. Derugina¹, L. Bratchenko¹, Y. Khristoforova¹, I. Bratchenko¹, V. Zakharov¹

1- Samara National Research University named after academician S.P. Korolev, 34, Moskovskoye shosse, Samara, 443086, Russia

m-irene-a@yandex.ru

The problems of diagnosing oncological diseases are associated with their wide distribution and a steady upward trend. Cancer research plays a vital role in the non-invasive diagnosis, staging and monitoring of various types of cancer and typically involves sophisticated instrumentation to provide detailed information about tumor size and location. Accurate diagnosis of the cancer type and early diagnosis are key factors in the successful treatment of neoplasms. Recently, for the diagnosis of skin cancer, it has been proposed to use dermatoscopy, which makes it possible to detect and visualize surface heterogeneities [2]. The modern trend in the development of optical diagnostics is also the use of Raman spectroscopy (RS) methods, which actually implement the tissue “optical biopsy” by identifying the chemical features of the tumor based on spectral data [1]. The application of machine learning methods makes it possible to ensure high accuracy of RS diagnostics of malignant neoplasms (more than 90%) [3], however, it has the same disadvantages of pinpoint biopsy (the possibility of an erroneous diagnosis if the optical biopsy site is chosen incorrectly) and reduced efficiency in multiclass diagnostics of the cancer type prevents real-time visualization of the tumor.

The paper is devoted to developing combined method for diagnosing skin cancer based on Raman spectra and dermatoscopic images of skin tissue. An *in vivo* study of skin tumors was carried out at the Samara Regional Clinical Oncology Center. The study involved 540 patients. Experimental skin Raman spectra were recorded using a portable setup that includes a laser source with a central wavelength of 785 nm [4]. The spectra were recorded with a spectral resolution of 0.2 nm in the range from 837 to 920 nm, which corresponds to 792-1874 cm⁻¹. Raman spectra of a healthy skin area and skin neoplasms were recorded in each patient. A total of 1000 spectra were used: 540 healthy skin, 113 keratosis, 122 basal cell carcinoma, 67 malignant melanoma, and 158 pigmented nevus spectra. Dermatoscopic images of this data set were obtained using a prototype multispectral digital dermatoscope [5]. The dataset consists of a total of 314 images: 104 malignant melanoma, 200 pigmented nevi.

Machine learning methods, in particular, convolutional neural networks, were used to analyze the registered data. Classification models for the main diagnostic cases have shown an increase in classification accuracy compared to the analysis of Raman spectra or dermatoscopic images alone. As a result, combined method for diagnosing skin cancer, which simultaneously takes into account both specific spectral features of tumors and spatial inhomogeneities in the distribution of optical density, has been proposed. The studied approaches to the analysis of spectral data can be further used as part of the software for automated screening diagnostics of skin pathologies in order to detect tumors at an early stage of development.

[1] J. Popp, C. Krafft and T. Mayerhöfer, Modern Raman spectroscopy for biomedical applications: A variety of Raman spectroscopical techniques on the threshold of biomedical applications, *Optik & Photonik*, vol. 6, №4, 24-28, (2011).

[2] V.A. Deryugina, I.A. Matveeva, I.A. Bratchenko, Neural network classification of dermatological images, *International scientific forum on control and engineering*, pp. 39-41, (2022).

[3] I.A. Bratchenko, L.A. Bratchenko, Y.A. Khristoforova, A.A. Moryatov, S.V. Kozlov and V.P. Zakharov, Classification of skin cancer using convolutional neural networks analysis of Raman spectra, *Computer Methods and Programs in Biomedicine*, vol. 219, pp. 106755, (2022).

[4] I.A. Bratchenko, L.A. Bratchenko, A.A. Moryatov, Y.A. Khristoforova, D.N. Artemyev, O.O. Myakinin, A.E. Orlov, S.V. Kozlov and V.P. Zakharov, In vivo diagnosis of skin cancer with a portable Raman spectroscopic device, *Experimental Dermatology*, vol. 30, №5, pp. 652-663, (2021).

[5] S.G. Konovalov, O.A. Melsitov, O.O. Myakinin, I. A. Bratchenko, A.A. Moryatov, S.V. Kozlov and V. P. Zakharov, Dermatoscopy software tool for in vivo automatic malignant lesions detection, *Journal of Biomedical Photonics & Engineering*, vol. 4, №4, pp. 040302, (2018).

B-P-7

Characterization of self-organized clusters of protein-coated Au nanoparticles in water

E. Molkova, B. Sarimov, S.Gudkov, V. Pustovoy, A.Semakin

Prokhorov General Physics Institute of the Russian Academy of Sciences, 38 Vavilova Str. Moscow, Russia

bronkos627@gmail.com

Nanoparticles trapped in the physiological fluid can be considered as systems that are formed as a result of successive interactions with the structures of the medium. The phenomenon of the formation of a "protein crown" on the surface of nanoparticles due to dynamic physicochemical interactions is known [1, 2].

Gold nanoparticles have important physical properties, such as surface plasmon resonance and the ability to quench fluorescence, which is successfully used in numerous test systems [3].

Lysozyme is widely used in the food industry. An increase in the content of lysozyme in biological fluids serves as a signal for certain diseases such as meningitis, blood and kidney diseases [4, 5]. Therefore, there is often a need for qualitative and quantitative characterization of lysozyme in liquid samples using biochemical test systems, including the use of nanoparticles. In this case, the question of the formation of protein–nanoparticle conjugates requires a detailed study.

The interactions of lysozyme protein with gold nanoparticles under different conditions of medium acidity were studied by optical methods, the results are shown in Fig.1. It was found that gold nanoparticles can act as stabilizers of lysozyme or interact with it, so that the degree of protein denaturation decreases at alkaline pH values, all other things being equal. And in turn, proteins prevent the aggregation of nanoparticles at acidic pH.

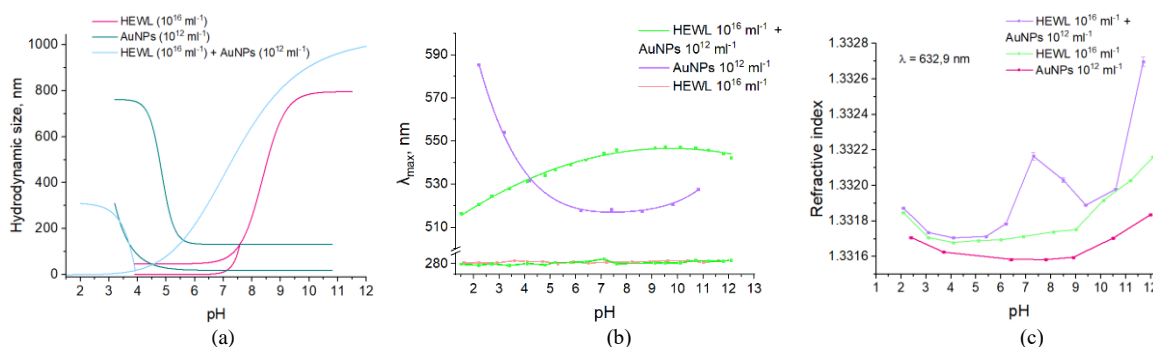


Fig.1. The effect of the acidity on the physical characteristics of colloids HEWL (10^{16} ml^{-1}), AuNPs (10^{12} mL^{-1}), HEWL (10^{16} ml^{-1}) + AuNPs (10^{12} mL^{-1}): (a) size distribution, (b) maximum absorption wavelength, (c) refractive index.

[1] T. Cedervall, I. Lynch, S. Lindman, T. Berggard, E. Thulin, H. Nilsson, K. Dawson, S. Linse. Understanding the nanoparticle-protein corona using methods to quantify exchange rates and affinities of proteins for nanoparticles. *Proceedings of the National Academy of Sciences*, 104(7), 2050–2055, (2007).

[2] S. Shanwar, L. Liang, A. Nechaev, D. Bausheva, I. Balalaeva, V. Vodeneev, I. Roy, A. Zvyagin, E. Guryev. Controlled Formation of a Protein Corona Composed of Denatured BSA on Upconversion Nanoparticles Improves Their Colloidal Stability. *Materials*, 14, 1657–1673, (2021).

[3] H. Khan, M. Sakharkar, A. Nayak, U. Kishore, A. Khan. Nanoparticles for biomedical applications: An overview. *Nanobiomaterials*, 357–384, (2018).

[4] P. Gu, X. Liu, Y. Tian, L. Zhang, Y. Huang, S. Su, W. Huang. A novel visible detection strategy for lysozyme based on gold nanoparticles and conjugated polymer brush. *Sensors and Actuators B: Chemical*, 246, 78–84, (2017).

[5] T. Jing, H. Xia, Q. Guan, W. Lu, Q. Dai, J. Niu, S. Mei. Rapid and selective determination of urinary lysozyme based on magnetic molecularly imprinted polymers extraction followed by chemiluminescence detection. *Analytica Chimica Acta*, 692(1-2), 73–79, (2011).



B-P-8

Cancer cells reaction to the exposure to UV-A and blue spectral regions radiation in the presence of antitumor drugs

V. Plavskii¹, O. Dudinova¹, L. Plavskaya¹, A. Svechko¹, A. Tretyakova¹, A. Mikulich¹, R. Nahorny¹, A. Sobchuk¹, T. Ananich¹, I. Leusenka¹, S. Yakimchuk¹, Le Hang Dang², Ngoc Quyen Tran²

1- B.I.Stepanov Institute of Physics of the National Academy of Sciences of Belarus, Minsk, Belarus

2- Institute of Applied Materials Science Vietnam Academy of Science and Technology, Ho Chi Minh City, Vietnam

v.plavskii@ifanbel.bas-net.by

The aim of this work is to study the response of cancer cells to the combined action of phytochromic anticancer drugs (curcumin, quercetin and apigenin), commonly used as chemotherapeutic agents in the treatment of cancer, and UV-A and blue radiation corresponding to their absorption spectrum.

Confocal fluorescence microscopy studies of a suspension of cancer cells (HeLa cervical epithelioid carcinoma cells and C6 rat brain glioma cells) showed the ability of antitumor chemotherapeutic drugs to penetrate through the cell membrane and localize in individual compartments of the cancer cell. It has been shown that curcumin is predominantly localized in the area of cell membrane; quercetin is distributed throughout the cell and its predominant localization in the area of the cell membrane is not observed; apigenin is selectively localized in individual intracellular organelles, which is confirmed by the bright localized luminescence of individual areas of cells.

It has been established that all studied anticancer chemotherapeutic drugs under dark conditions have an inhibitory cytotoxic effect, which manifests itself in a decrease in the metabolic activity of cells (colorimetric MTT-test). A decrease in the metabolic activity of HeLa and C6 cancer cells also is caused by exposure to their suspension to optical radiation with wavelengths of $\lambda = 365, 405, \text{ or } 440 \text{ nm}$ at energy dose of $D = 4.5\text{--}15 \text{ J/cm}^2$. Damage of the cells by radiation of this spectrum region is due to the sensitizing effect of endogenous porphyrins and flavins localized in cells. The damaging effect of light depends on the radiation wavelength, energy dose and is confirmed by MTT-test, flow cytometry and chemiluminescence studies.

It could be expected that with the combined action of anticancer drugs and light, a synergistic effect would be observed, which has been noted in a number of publications with other chemotherapeutic drugs. Indeed, the studies have shown that if under dark conditions curcumin in the concentration range of $1\text{--}5 \mu\text{M}$ has an insignificant inhibitory effect on the metabolic activity of cells, then under the action of light $\lambda = 440 \text{ nm}$, $D = 15 \text{ J/cm}^2$, inactivation increases by 5 times. According to flow cytometry data, such irradiation of cells increases their proportion by 4 times at the stage of necrosis and late apoptosis. Therefore, the main reason for the decrease in the metabolic activity of cells is a lethal outcome. The effect is realized due to photodynamic processes sensitized by curcumin. Moreover, in the studied photochemical process a decisive role is played by hydrogen peroxide, the formation of which is initiated by the generation of singlet oxygen by curcumin during its photoexcitation. Other results have been obtained when cells are exposed to $\lambda = 365 \text{ nm}$ radiation in the presence of apigenin and quercetin. It has been shown that these drugs do not have sensitizing properties; quercetin exhibits antioxidant properties even at low concentrations. This is confirmed by the data of chemiluminescent studies, as well as by a decrease in the rate of cell inactivation initiated by exposure to radiation $\lambda = 365 \text{ nm}$, when quercetin is added to their suspension before irradiation. During the chemiluminescence control, apigenin does not show antioxidant properties. However, it has turned out that the exposure to radiation with $\lambda = 365 \text{ nm}$, $D = 4.5 \text{ J/cm}^2$ on HeLa cells in the presence of $1\text{--}20 \mu\text{M}$ of apigenin almost protects them from the inactivating effect of the indicated phytochrome agent. Exposure to light of the same parameters on cells in the presence of quercetin leads to an evidential stimulation of the metabolic activity (survival) of tumor cells compared to the dark variant. Moreover, the magnitude of the stimulating effect increases with an increase in the concentration of the anticancer drug, which can be explained by its antioxidant properties. The protective role of phytochromic preparations photoproducts formed in the course of irradiation in respect to cells is also not excluded.

B-P-9**Fluorescence bioimaging for nanoparticles safety and biodistribution testing**

**S.A. Rodimova¹, A.M. Mozherov¹, D.P. Krylov^{1,2}, D.S. Kozlov^{1,2},
M.M. Karabut¹, M.V. Zyuzin³, D.S. Kuznetsova^{1,2}**

1 - Privolzhsky research medical university, 603005, Nizhny Novgorod, Minin and Pozharsky sq. 10/1

2 - Lobachevsky Nizhny Novgorod National Research State University, 603022, Nizhny Novgorod, Gagarina 23

3 - ITMO University, 191002, St. Petersburg, Lomonosova st., 9

e-mail: srodimova123@gmail.com

Despite the promising results currently achieved in stimulating liver regeneration using small bioactive molecules, there is still a problem of the lack of an effective method for their delivery with a controlled release period, their accumulation and excretion [1]. Such a technology based on complexes of nanoparticles and bioactive molecules is especially relevant due to the high risk of liver failure after liver surgery. The most promising methods for assessing the state of living liver cells seems to be multiphoton fluorescent microscopy with second harmonic generation (SHG) and time-resolved FLIM microscopy. These methods are non-invasive, label-free and allow intravital monitoring at the cellular level. In addition, the use of the model of precision-cut liver slices made it possible to screen several types of nanoparticles, excluding the individual contribution of the animal organism, simplifying the analysis and interpretation of the results.

Vibrating microtome 7000 cm3-2 was used to obtain liver slices using the protocol of Pearen et al. [2], and were placed in separate wells of a 12-well plate with a standard CO₂-conditioned form of DMEM supplemented with 0.1 μm of dexamethasone and 10% FBS. Next, cultivation was carried out in DMEM medium with the addition of nanoparticles at a concentration of 50 and 100 mg/ml and incubated for 3, 24, and 48 hours. All obtained tissue explants were preincubated for 1 h in DMEM medium on an orbital shaker (90 rpm). The average size of all nanoparticles was 100 nm. Gold nanoparticles were synthesized based on seed mediated mechanism. The synthesis of SiO₂ nanoparticles was carried out using the sol-gel method. Polylactide (PLA) nanoparticles were synthesized by single-emulsion solvent extraction. All nanoparticles were modified with a Cy 5 fluorescent label. Liver slices were stained with LysoTracker Yellow HCK-123 and Phalloidin FITC. Using multiphoton microscopy, we assessed the tissue structure of liver slices, and visualized cellular ultrastructures stained with fluorescent dyes. Additionally, the distribution of nanoparticles was analyzed using X-ray microtomography. Using FLIM, we analyzed the metabolic state of hepatocytes based on fluorescence lifetime contributions of the free and bound forms of NADH and NADPH.

As a result, SiO₂ and gold nanoparticles were practically not accumulated by liver cells and show high cytotoxicity. Wherein, polylactide nanoparticles accumulated most effectively in liver cells, mainly in the cytoplasm of hepatocytes. Using FLIM, we revealed low cytotoxicity of PLA nanoparticles, due to the relative contributions of fluorescence lifetimes of bound form of NADH and NADPH did not differ significantly from control values. Thus, PLA nanoparticles seem to be the most promising for further development of a strategy for stimulating liver regeneration using nanoparticles modified by bioactive molecules. The obtained results will become a basis for further development of a strategy to stimulate liver regeneration.

The work was supported by the Grant from the Russian Science Foundation №23-25-00100.

[1] Liu Z., Li Y., Li W., et al. Multifunctional nanohybrid based on porous silicon nanoparticles, gold nanoparticles, and acetalated dextran for liver regeneration and acute liver failure theranostics. *Advanced Materials*, 30(24), 1703393, (2018).

[2] Pearen M. A., Lim H. K., Gratte F. D. et al. Murine precision-cut liver slices as an ex vivo model of liver biology. *JoVE*, (157), e60992, (2020).

B-P-10

Sensitivity of clinical strain of *Staphylococcus aureus* to photodynamic action using pyridylporphyrins

T. V. Sharabarina¹, M. V. Korchenova¹, E. S. Tuchina¹, L. V. Mkrtchyan², A. A. Zakoyan², O. A. Inozemtseva¹, G. V. Gyulkhandanyan², V. V. Tuchin¹

¹Saratov State University, 410012, Russia, Saratov, Astrakhanskaya, 83

²Institute of Biochemistry, NAS of Armenia, 0014, Armenia, Yerevan, P. Sevak st., 5/1

kliany@rambler.ru

Currently, the problem of excessive and improper use of antibiotics for prevention and self-treatment is more acute than ever, which in turn leads to the emergence of new antibiotic-resistant strains of bacteria. Clinical strains of *Staphylococcus aureus* are most important pathogens causing severe nosocomial infections. In modern medicine, antimicrobial photodynamic action is an alternative way to combat diseases caused by both susceptible and resistant bacteria. In this regard, the main goal was to study new porphyrin compounds in low concentrations as promising photosensitizers in the antimicrobial photodynamic effect on staphylococci.

The clinical strain of *S. aureus* was used as the studied microorganisms and was grown at a temperature of 37°C on a universal nutrient medium.

An LED with a maximum emission spectrum of $\lambda=405$ nm and a power density of 80 mW/cm² was used as a radiation source. In all experiments, the radiation mode was continuous. Irradiation time varied from 5 to 30 min.

Water-soluble meso-substituted cationic pyridylporphyrins and their zinc derivatives (PPhI-TOEt4PyP; PPhII-Zn-TBut3PyP; PPhIII-Zn-TOEt4PyP) with various peripheral functional groups were used as a photosensitizer in concentration 0,03 μ g/ml.

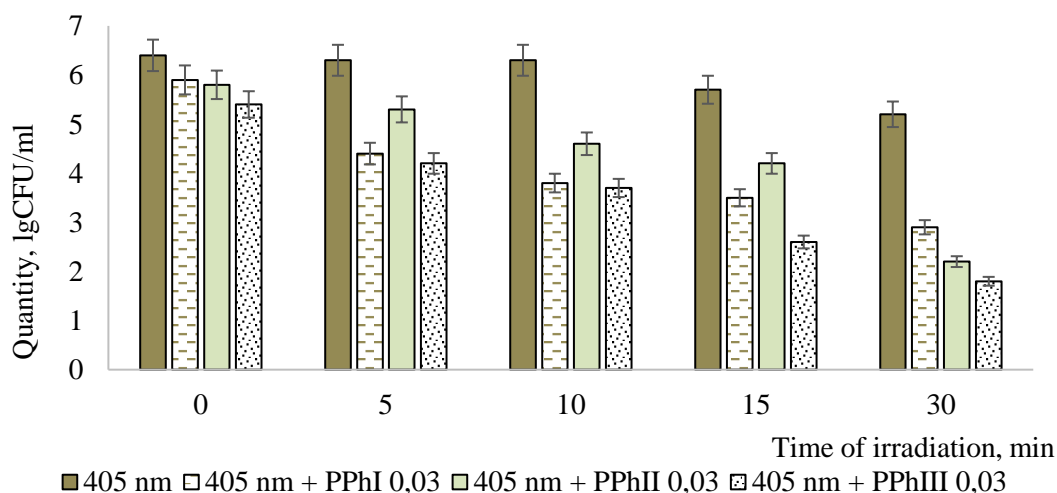


Fig.1. Change in quantity of clinical *S. aureus* strain under photodynamic action of blue (405 nm) LED radiation and pyridylporphyrins

Radiation with a wavelength of 405 nm did not affect the growth of tested *S. aureus* strain. After 30 minutes of exposure survival remained within 6,4-5,2 lgCFU/ml (Fig.1, black). After 10 min of irradiation there was a decrease in the bacterial population of *S. aureus* by 2,6 lgCFU/ml after treatment with PPhI (Fig.1, strips), by 1,8 lgCFU/ml after treatment with PPhII (Fig. 1, gray) and by 2,7 lgCFU/ml after treatment with PPhIII (Fig.1, dots). Increasing the irradiation time to 30 min led to the death of bacterial cells of *S. aureus* clinical strain by 3,5–4,6 lgCFU/ml. The maximum decrease in survival (by 4,6 lgCFU/ml) was demonstrated by the sample containing PPhIII.

Thus, it was found that the studied porphyrins at low concentrations are promising photosensitizers for antimicrobial photodynamic therapy of studied *S. aureus* clinical strain. Our studies revealed that PPhIII is the most effective of the studied porphyrins under 30 min 405 nm LED continuous radiation mode.

B-P-11

The effect of the gas transmitter NO on the parameters of platelet aggregation: measurement by laser-optical methods

Umerenkov D.A., Ermolinskiy P.B., Maksimov M.K., Lugovtsov A.E., Priezzhev A.V.

Faculty of Physics, M.V. Lomonosov Moscow State University,

Moscow, Russia, Leninskie Gory 1/2, 119991

umerenkov.da19@physics.msu.

Platelets are critical elements of the hemostasis system that prevent blood loss when the vascular wall is damaged. Nitric oxide (NO), secreted by endothelial cells, serves as a necessary physiological and regulatory biological mediator that modulates vascular wall tone and hemostatic-thrombotic balance [1]. Violation of the NO concentration in the human body leads to various kinds of cardiovascular diseases, including thrombosis, atherosclerosis, etc. It is known that nitric oxide inhibits the adhesion of platelets and leukocytes to the endothelium cell layer, inhibits the activation of platelets and leukocytes [2]. The aim of the work is to quantify the effect of sodium nitroprusside, which is a direct NO donor, on the aggregation properties of platelets by the turbidimetric method *in vitro*.

Measurements of platelet aggregation properties was performed by light transmission method. Venous blood for experiments was taken from healthy donors who had not taken any medication for at least 2 weeks before blood sampling. To prepare platelet-rich plasma (PRP), whole blood was centrifuged at 200g for 7 min. Before the start of the experiment, sodium nitroprusside (SNP) was added in a volume of 15 μl at concentrations of 1, 10, 25, 50, and 100 μM to the PRP. The required concentration of the SNS solution was achieved by adding distilled water to initial SNP. Incubation of PRP with SNP was carried out for 0, 5, 15, 25 and 40 minutes at 37 Celsius degrees.

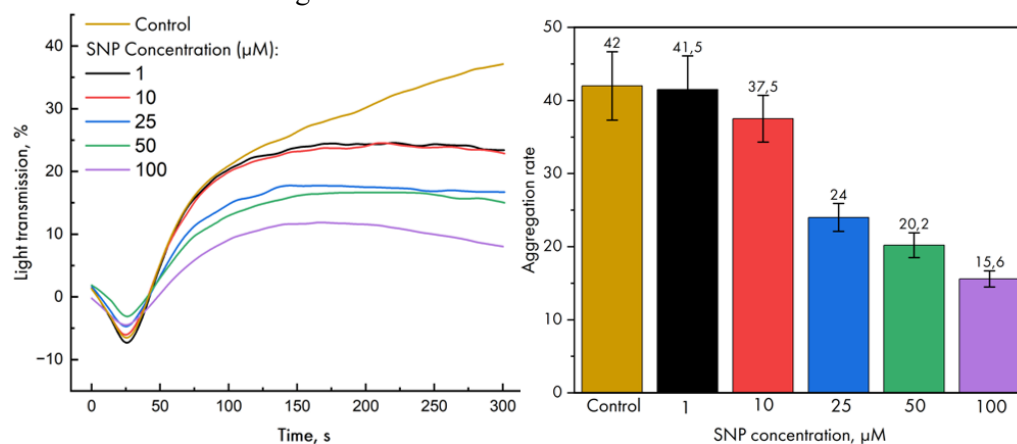


Fig. 1. Light transmission kinetics (left side) and platelet aggregation rate (right side): effect of SNP (NO) at various concentrations

The obtained results demonstrate that SNP, and hence the gas transmitter NO, significantly affect on the parameters of platelet aggregation *in vitro*. Note, that even at the lowest concentration of 1 μM of SNP, an inhibition effect of NO on the platelet aggregation is observed. The degree of aggregation in a sample incubated with SNP at a concentration of 1 μM decreases by $(37 \pm 7)\%$, but the aggregation rate does not change within the dispersion. At higher concentrations of SNP, an efficient inhibition of platelet aggregation is pronounced, and the rate of platelet aggregation also decreases. At SNP concentration of 100 μM , the degree of aggregation decreases by $(70 \pm 9)\%$, and the rate of aggregation decreases by $(27 \pm 5)\%$. A statistically significant decrease of the rate of platelet aggregation is observed at a concentration of 25 μM ($p < 0.05$). The incubation time also significantly affect the parameters of platelet aggregation. Longer incubation time leads to more effective inhibition of platelet aggregation

The study was financially supported by the Russian Science Foundation grant №. 22-15-00120.

[1] Muravyev A. V. The role of gas mediators (CO, NO and H₂S) in the regulation of blood circulation: analysis of the participation of microcirculation of blood cells // Regional blood circulation and microcirculation. V. 20. – №. 1. – P. 91-99. (2021)

[2] Hickey M. J., Kubes P. Role of nitric oxide in regulation of leucocyte-endothelial cell interactions //Experimental Physiology: Translation and Integration. V. 82. P. 339-348. (1997).



LASER SYSTEMS AND MATERIALS

LS-I-1**High-power mid-infrared quantum-cascade lasers and detectors****G.S. Sokolovskii***Ioffe Institute, St.Petersburg, Russia**gs@mail.ioffe.ru*

Quantum-cascade lasers (QCL) attract great attention of the research community since the first publication by Kazarinov and Suris proposing the principle in 1971 [1], and especially since the first realization in 1994 by Faist et al. [2]. due to numerous potential applications in spectroscopy, environmental monitoring, biomedicine, free-space optical communications and many other areas. The main QCL feature distinguishing them from the conventional semiconductor lasers is their unipolarity resulting in the photon emission in the transition of an electron in the conduction band from one quantum level to another instead of recombination of an electron-hole pair. Unfortunately, QCL structures are extremely complicated for practical implementation. The complication comes both from the number of layers that is two orders of magnitude larger than that in a “conventional” semiconductor laser (so-called laser diode) and from the need to maintain the layer homogeneity (i.e., identity of quantum cascades) during long-time epitaxial growth. However, thanks to over quarter of a century efforts of the international research community, QCLs became probably the most efficient sources of coherent radiation in the mid-infrared range. In addition to a review of the state of the art in mid-infrared quantum cascade lasers, this report will discuss the recent progress of QCLs at the Ioffe Institute, including demonstration of the high-power QCLs at 4.5 μm delivering above 14 W [3] as well as QCLs with record-high output power of over 16 W at 8 μm [4]. Also, we will discuss very unconventional turn-on dynamics recently revealed in mid-infrared QCLs [5] and quantum-cascade detectors (QCDs) fabricated from the structure of the record-high power quantum-cascade laser with measured sensitivity of 10-20 mA/W, which is comparable or better than that for similar detectors with a specially optimized structure.

This research is supported by the Russian Science Foundation (grant No. 21-72-30020)

[1] R.F. Kazarinov and R.A. Suris, *Semiconductors* 5, 797 (1971).

[2] J. Faist, et al., *Science* 264, 553 (1994).

[3] V.V. Dudelev et al., *International Conference Laser Optics*, St.Petersburg, Russia (2022).

[4] E.D. Cherotchenko et al., *Nanomaterials* 12, 3971 (2022)

[5] E.D. Cherotchenko et al., *Journal of Lightwave Technology* 40(7), 2104 (2022).

Current progress in the investigation of rare earth doped chalcogenide glass lasers

**S. Sverchkov¹, B. Denker¹, M. Frolov², B. Galagan¹, V. Koltashev³, V. Plotnichenko³,
G. Snopatin⁴, M. Sukhanov⁴, A. Velmuzhov⁴**

¹*Prokhorov General Physics Institute of RAS, Vavilov str.38, Moscow, Russia*

²*P. N. Lebedev Physical Institute of RAS, Leninskiy Prosp. 53, Moscow, Russia*

³*Prokhorov General Physics Institute of RAS, Dianov Fiber Optics Research Center, Vavilov str.38, Moscow, Russia*

⁴*Devyatykh Institute of Chemistry of High-Purity Substances of RAS, Tropinin str. 49, Nizhny Novgorod, Russia*

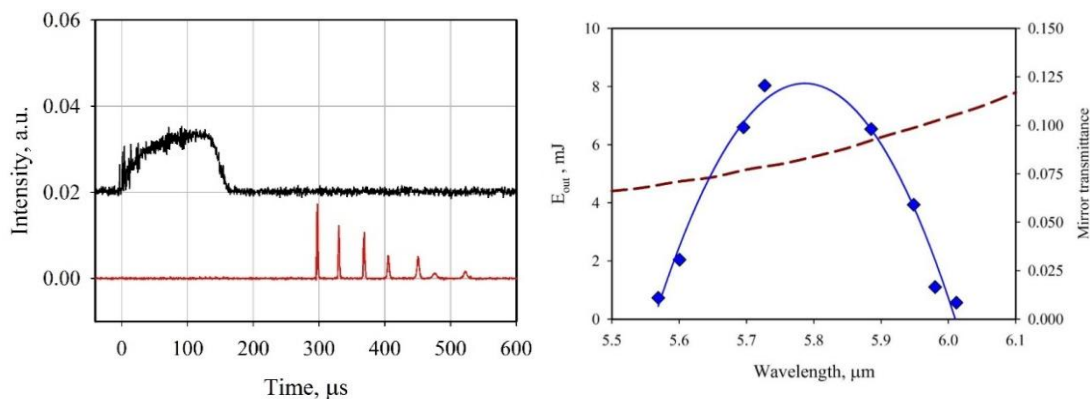
glasser@Lst.gpi.ru

In recent years, we have shown that rare earth doped chalcogenide glasses can serve as active materials for bulk and fiber mid-infrared lasers. Laser action in the spectral range from ~ 4.5 to ~ 5.5 μm was demonstrated at the transitions between the first excited and the ground states of Ce^{3+} , Pr^{3+} and Tb^{3+} ions [1, 2]. It was also shown, that in high purity selenide glasses even ~ 6 μm rare-earth ion transitions can have high luminescence quantum yield. Over the past year, we have been working both on improving the existing chalcogenide glass lasers and on the new rare earth laser transitions.

In particular, the CW Tb^{3+} fiber laser output has reached 150 mW and the gain in Tb-doped fibers has reached 40-50 dB/m. It was found that up-conversion process (${}^7\text{F}_5+{}^7\text{F}_5 \rightarrow {}^7\text{F}_3+{}^7\text{F}_6$) in heavily Tb-doped glasses may lead to the changeover from CW to non-relaxing spiky operation. Spiking can be suppressed by reducing the concentration of the active ion and/or by introduction of negative feedback into the laser cavity.

Ce^{3+} ions were made to generate CW laser radiation in chalcogenide fiber under pumping by a CW $\text{Fe}^{2+}:\text{ZnSe}$ laser. In contrast to Tb^{3+} -doped mid-infrared fiber lasers, Ce^{3+} -doped laser had no tendency to spike operation because the simple energy level structure of Ce^{3+} ions exclude up-conversion processes.

A novel sensitization scheme was proposed to excite 5-6 μm Nd^{3+} emission in selenide glasses with the help of Tb^{3+} ions. It was shown, that at room temperature the radiationless energy transfer from Tb^{3+} to Nd^{3+} is combined with the reverse process. At liquid nitrogen temperature the energy transfer from Tb^{3+} to Nd^{3+} becomes irreversible.



Laser action of Nd^{3+} ions corresponding to ${}^4\text{I}_{11/2} \rightarrow {}^4\text{I}_{9/2}$ transition was demonstrated for the first time. Up to 16 mJ output was obtained. The left Figure shows the oscillograms of the pump 2.93 μm Er:YAG laser pulse exciting Tb^{3+} ions (black) and Nd^{3+} ions lasing (red). Note the ~ 150 μs time delay between the pump and the lasing pulses due to the finite $\text{Tb} \rightarrow \text{Nd}$ energy transfer rate. The right Figure shows the tuning range of Nd^{3+} laser reaching 6 μm . It is the longest-wavelength glass laser for today.

[1] M.F. Churbanov et al., First demonstration of ~ 5 μm laser action in terbium-doped selenide glass, Applied Physics B, 126, 116(2020).

[2] M.F. Churbanov et al., Comparison of 4.5-6 μm luminescent and lasing properties of rare earth dopants in chalcogenide glasses, Journal of Luminescence, 245, 118756(2022).



Towards the gas-discharge fiber lasers

I.A. Bufetov, A.V. Gladyshev, A.P. Mineev, S.M. Nefedov, V.V. Velmiskin

*Prokhorov General Physics Institute of the Russian Academy of Sciences, 38 Vavilov St., Moscow, Russia
iabuf@fo.gpi.ru*

The advent of low-loss hollow-core optical fibers (HCFs) enabled the development of a new type of lasers—gas fiber lasers (GFLs). To date, various GFLs have already been demonstrated. An active medium of such lasers is some Raman-active or dipole-active gas that fills the hollow-core of a fiber. To excite the active medium, the GFLs rely on optical pumping by some solid-state laser. To fully realize the possibilities of hollow fibers (resistance to high-intensity radiation, wide spectral transmission range, etc.) in all-fiber optical schemes, it is necessary to solve the problem of generating laser radiation directly in HCF. Using an electric discharge to excite the active medium of a GFL can solve this problem. However, at small core diameters ($D_c \sim 100 \mu\text{m}$) of HCFs the researchers encountered the instability of the electric discharge.

To excite plasma in the core of a hollow fiber, a scheme like a slot antenna in the wall of a metal microwave waveguide was proposed by us and implemented [1]. Using the proposed scheme, the possibility of maintaining noble gases plasma in the core of a hollow fiber with a diameter as small as $100 \mu\text{m}$ was demonstrated (Fig.1). The total length of plasma column in the hollow-core fiber was up to 25 cm. The frequency of microwave radiation used was 2.4 GHz, the average generated power was below 20 W. The results obtained show that the microwave slot antenna is a promising pumping scheme for gas-discharge fiber lasers based on hollow-core fibers.

The minimum values of the electric microwave field ($\nu = 2.45 \text{ GHz}$), which are necessary to maintain discharge in several noble gases (Ar, Ne (see Fig.2), and He) in optical fibers with hollow cores of small diameter up to $100 \mu\text{m}$, have been measured for the first time [2]. The minimal electric field intensity values for all three gases are (2.5–2.8) kV/cm at a pressure of argon $p \sim 50 \text{ Torr}$, neon $p \sim 300 \text{ Torr}$, and helium $p \sim 500 \text{ Torr}$.

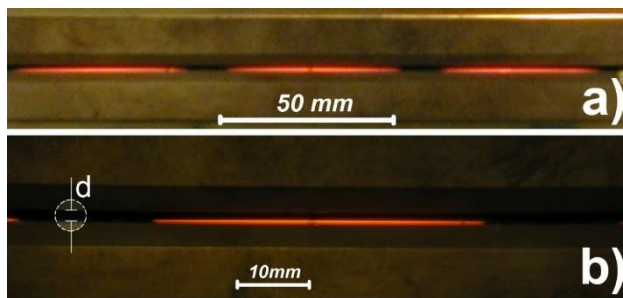


Fig.1. Picture of MW discharge in HCF ($D_c = 110 \mu\text{m}$, Ne, $p = 30 \text{ Torr}$) placed in the slot of MW guide wall. a) general view; b) improved spatial resolution. The HCF is located on the lower edge of the slot with a width of $d = 1.5 \text{ mm}$.

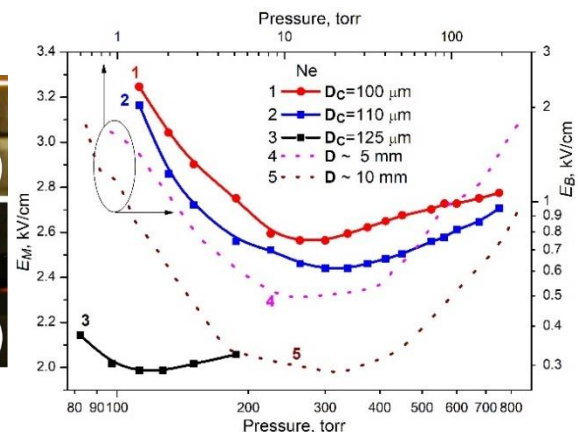


Fig.2. Threshold values of the electric field required to maintain (E_M) the discharge in Ne and for electrical breakdown (E_B) by the MW depending on the pressure. Lines 1-3 (refer to the left and bottom axes): dependences $E_M(p)$ for neon-filled HCFs for different D_c . Lines 4-5 (refer to the right and upper axes): the $E_B(p)$ dependences for neon given in [3] for much larger characteristic dimension of the discharge volume D .

The implementation of a stable MW discharge in a HCF filled with noble gases is a significant advance towards solving the problem of creating fiber gas lasers based on hollow-core fibers.

This research was supported by Russian Science Foundation (grant No. 22-19-00542), <https://rscf.ru/project/22-19-00542/>.

[1] A. Gladyshev, S. Nefedov, A. Kolyadin et al. Microwave Discharge in Hollow Optical Fibers as a Pump for Gas Fiber Lasers, *Photonics*, vol.9, p.752 (2022).

[2] I. Bufetov, A. Gladyshev, S. Nefedov et al. MW discharge maintaining in the hollow core fibers for gas fiber lasers, *Doklady RAS Physics*, vol.509, pp. 3-8, (2023) (in Russian).

[3] A.D. MacDonald, *Microwave Breakdown in Gases* (JohnWiley & Sons, Ink.: New York) Chapters 1, 5 (1966).



LS-I-4

Laser and sensor systems based on FBG arrays fs-inscribed in passive and active multicore fibers

A.A. Wolf, A.G. Kuznetsov, A.V. Dostovalov, S.A. Babin*

Institute of Automation and Electrometry SB RAS, Novosibirsk 630090, Russia

* *babin@iae.nsk.su*

Multicore fibers (MCFs) offer the involvement of multiple cores in optical signal generation, transmission and processing. Developments in this direction resulted in fiber-optic communication systems with increased capacity via spatial division multiplexing [1], an opportunity to use passive MCFs for multi-parameter sensing systems is also started to be explored [2]. Active MCFs also represent an attractive gain medium as an alternative to large-mode area (LMA) singlemode fibers for the development of compact laser systems with high-power output obtained by coherent combining of beams generated in individual cores [3], but they still have some lacks especially in terms of performance. The performance of MCF laser and sensor systems may be greatly improved with the use of in-fiber elements such as fiber Bragg gratings (FBGs) selectively inscribed in different cores. For that a point-by-point (PbP) femtosecond (fs) pulse inscription technology is the most promising for fabrication in passive and active MCFs the FBG arrays of arbitrary shape. Here we review our recent results on the PbP fs inscription of regular and random FBG arrays in active and passive MCFs and implementation of such structures in the advanced laser and sensor systems.

In passive 7-core MCFs, we fabricated 3D FBG arrays by the PbP fs inscription through polyimide protective coating. It is enough to involve in the array 3 side cores and central core for precise 2D and 3D fiber shape reconstruction with accuracy as high as ~1% [2,4] at curvature radii variation in the range from 2.6 mm to 500 mm. The temperature resistance of both the inscribed FBG structures and the protective coating, along with the high mechanical strength of the polyimide, makes it possible to use the sensor in harsh environments or in medical and composite material applications. Further, FBGs selectively inscribed in side cores of 7-core passive MCF were used as complex reflector of a MCF Raman laser with pumping and output coupling through the central core, which is able to generate singlemode output with narrow spectrum [6]. The narrowing occurs due to the suppression of nonlinear effects in the large effective area of 7-core fiber cavity and due to the interference of signals reflected from FBGs in different cores, which have sufficient optical coupling.

In active MCFs, we first studied an LD-pumped 4-core Yb-doped fiber with FBGs fs-inscribed in each core, where the core crosstalk is induced via strong bending, and have observed the fiber output power concentration in one core [5] that is different from the single-core out-coupling in 7-core fiber Raman laser [4]. We also perform similar study of an LD-pumped 7-core Yb-doped fiber with 3D FBG array [6]. Femtosecond inscription of highly-reflective FBGs in each core of 7-core Yb-doped fiber enables efficient (~70%) 1064-nm lasing in robust all-fiber scheme with ~33 W power, nearly the same for uncoupled and coupled cores. However, output spectrum is quite different: without coupling, 7 individual lines corresponding to the in-core FBG reflection spectra sum up into broad (>0.22 nm) total spectrum, whereas the multiline spectrum collapses into single narrow line at strong coupling. The developed model shows that the coupled-core laser generates coherent superposition of supermodes at the wavelength corresponding to the geometric mean of individual FBG spectra, whereas the generated laser line broadens with power (0.04-0.12nm) like single-core mode of 7-times larger effective area.

The details of these studies and potential application of devices will be presented at the conference.

This work is supported by Russian Science Foundation (№21-72-30024).

- [1] D. J. Richardson, J. M. Fini, & L. Nelson, Space-division multiplexing in optical fibres, *Nature Photonics*, vol. 7, pp. 354–362 (2013).
- [2] K. Bronnikov, A. Wolf, S. Yakushin, A. Dostovalov, O. Egorova, S. Zhuravlev, S. Semjonov, S. Wabnitz, and S. Babin, Durable shape sensor based on FBG array inscribed in polyimide-coated multicore optical fiber, *Opt. Express*, vol. 27, pp. 38421–38434 (2019).
- [3] C. Jaregui, J. Limpert, & A. Tünnermann, High-power fibre lasers, *Nature Photonics*, vol. 7, pp. 861–867 (2013).
- [4] A. Wolf, A. Dostovalov, K. Bronnikov, M. Skvortsov, S. Wabnitz, and S. Babin, Advances in femtosecond direct writing of fiber Bragg gratings in multicore fibers: technology, sensor and laser applications, *Opto-Electronic Advances*, vol. 5, 210055 (2022).
- [5] A. A. Wolf, M. I. Skvortsov, I. A. Lobach, A. V. Dostovalov, and S. A. Babin, Bending induced output power concentration in a core of a 4-core Yb-doped fiber laser, *Opt. Exp.*, vol. 30, pp. 7580–7590 (2022).
- [6] A. G. Kuznetsov, A. A. Wolf, A. V. Dostovalov, E. V. Podivilov, S.A. Babin. Spectrum collapse in a 7-core Yb-doped fiber laser with an array of fs-inscribed fiber Bragg gratings. *Opt. Lett.* (2023), in press.

Mid-infrared supercontinuum generation in hollow-core silica fibers

A.V. Gladyshev¹, D.S. Dubrovskii^{1,2}, Yu.P. Yatsenko¹, I.A. Bufetov¹

1 - Prokhorov General Physics Institute of the Russian Academy of Sciences, Dianov Fiber Optics Research Center, 38 Vavilov st., Moscow, Russia, 119991

2 – Faculty of Physics, Lomonosov Moscow State University, Leninskie Gory 1, str.2, Moscow, Russia, 119991

alexglad@fo.gpi.ru

Mid-infrared (mid-IR) supercontinuum (SC) sources are of great interest for many applications. Revolver-type hollow-core fibers (HCF) present an attractive platform to realize efficient fiber-based SC generation at wavelengths $\lambda > 2.4 \mu\text{m}$ in the mid-IR. In practice, however, mid-IR SC in HCFs has been experimentally achieved only in a few works [1-3], all of which used noble gases and demonstrated limited efficiency. Recently, we have proposed and demonstrated SC generation in a revolver HCF filled by molecular deuterium [4,5], in which the SC spectrum has reached the wavelength of $3.3 \mu\text{m}$ in the mid-IR due to cascaded stimulated Raman scattering (SRS) on deuterium molecules.

In this work, we investigate experimentally the way to extend the SC spectrum generated in a gas-filled revolver HCF further into the mid-IR. The revolver fiber was filled by a mixture of molecular hydrogen isotopes ($^1\text{H}_2$ and D_2) and pumped by chirped ultrashort pulses at the wavelength of $1.03 \mu\text{m}$. The transfer of pump energy into the mid-infrared range was initiated by cascade stimulated Raman scattering in the gas mixture, while Kerr nonlinearity was responsible for spectral broadening, thus giving rise to generation of a supercontinuum that covers the wavelength range of up to $4 \mu\text{m}$. The effect of Kerr nonlinearity was studied by controlling the amount of linear chirp introduced to the pump pulses. The influence of gas pressure and pump pulse energy on the supercontinuum generation was also investigated.

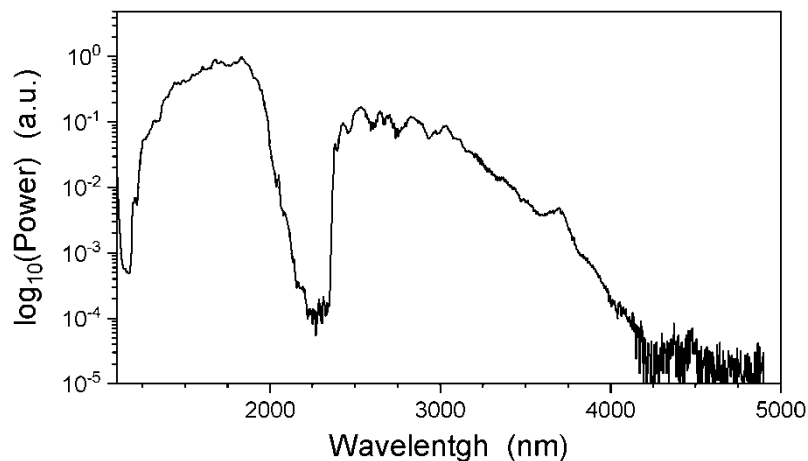


Fig. 1. Supercontinuum generation in the silica HCF that was filled by H_2/D_2 gas mixture and pumped by $82\text{-}\mu\text{J}$ 1-ps-long pulses at $1.03 \mu\text{m}$.

This work is supported by Russian Science Foundation (grant №19-12-00361).

- [1] F. Köttig, D. Novoa, F. Tani et al., Mid-infrared dispersive wave generation in gas-filled photonic crystal fibre by transient ionization-driven changes in dispersion, *Nat. Commun.*, vol.8, p.813 (2017).
- [2] M. Cassataro, D. Novoa, M.C. Günendi et al., Generation of broadband mid-IR and UV light in gas-filled single-ring hollow-core PCF, *Opt. Express*, vol.25, pp.7637-7644 (2017).
- [3] A.I. Adamu, M.S. Habib, C.R. Petersen et al., Deep-UV to Mid-IR Supercontinuum Generation driven by Mid-IR Ultrashort Pulses in a Gas-filled Hollow-core Fiber, *Sci. Rep.*, vol.9, p.1 (2019).
- [4] Yu.P. Yatsenko, A.V. Gladyshev, I.A. Bufetov, Mid-IR supercontinuum generation initiated by two-cascade stimulated Raman scattering in D_2 -filled revolver fibre, *Quantum Electron.*, vol.51, pp.1068–1075 (2021).
- [5] A. Gladyshev, Y. Yatsenko, A. Kolyadin, and I. Bufetov, Visible to Mid-Infrared Supercontinuum Initiated by Stimulated Raman Scattering of $1.03 \mu\text{m}$ Ultrashort Pulses in a Gas-Filled Silica Fiber, *Photonics*, vol.9, p.997 (2022).

Advances in bismuth-doped fiber lasers and amplifiers

M.A. Melkumov

Prokhorov General Physics Institute of the Russian Academy of Sciences, Dianov Fiber Optics Research Center, 38 Vavilov str., 119333 Moscow, Russia

Email: melkoumov@fo.gpi.ru

Bi-doped fiber is a new optical material providing possibilities of broadband optical amplification in the near IR range where other silica based active fibers doped with rare-earth elements are absent or inefficient. Variation of glass composition and pump wavelength allows one to obtain luminescence and gain of bismuth active centers (BAC) associated with Al, P, Si or Ge in several regions within 1.1-1.8 μm (see Fig. 1). Combination of different BACs and/or Er ions in separate fibers connected in chain or co-doped in one fiber (BDF or EBDF) allows one to significantly (up to 150 nm or larger) increase the available bandwidth for single optical amplifier [1,2] with acceptable noise figure (Fig. 1). One of important applications of such active fibers is ultrabroadband fiber telecom systems with the dense wavelength division multiplexing of optical channels where bismuth-doped fiber amplifiers (BDFA) help to increase fiber reach and capacity by several times in comparison with passive systems (without optical amplification) or active one based on erbium-doped fiber amplifiers (EDFA).

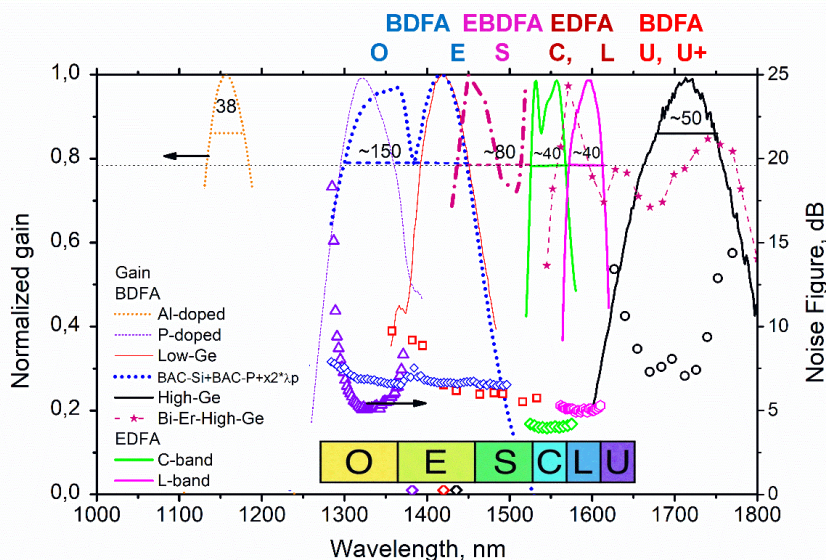


Fig. 1. Normalized gain (lines) and noise figure (symbols) of various BDFA, EDFA and EBDF

Starting from 2017 a successful BDFA assisted data transmission for in lab systems in O, E and S- telecom bands (for example see ref. [3]) as well as for deployed fiber links have been demonstrated. All these results were obtained for core-pumped scheme of BDFA and bismuth-doped fiber lasers (BDFL), which require complex and/or cost inefficient single-mode pump sources. Recently a significant progress towards cladding-pumped BDFL and BDFA have been demonstrated [4,5].

This talk aims to highlight latest results in the field of BDFL and BDFA and their possible applications.

This research was supported by the Russian Science Foundation (grant # 22-19-00708).

[1] Y. Ososkov, et al., Pump-efficient flattop O+E-bands bismuth-doped fiber amplifier with 116 nm –3 dB gain bandwidth, *Opt. Express*, vol.29, pp. 44138-44145, (2021).

[2] A. Khagai, et al., Gain Clamped Bi-Doped Fiber Amplifier With 150 nm Bandwidth for O-and E-Bands, *Journal of Lightwave Technology*, vol.40(4), pp. 1161-1166, (2022).

[3] M. Melkumov, et al., E - band data transmission over 80 km of non - zero dispersion fibre link using bismuth - doped fibre amplifier, *Electronics Letters*, vol.53(25), pp. 1661-1663, (2017).

[4] S. Firstov, et al., Cladding-Pumped Bismuth-Doped Fiber Laser, *Optics Letters*, vol.47(4), pp. 778-781, (2022).

[5] A. Vakhruşev, et al., Cladding pumped bismuth-doped fiber amplifiers operating in O-, E-, and S-telecom bands, *Optics Letters*, Vol.48(6), pp. 1339-1342, (2023).

LS-I-7

High peak power fiber lasers and its applications

M.E.Likhachev

Prokhorov General Physics Institute of the Russian Academy of Sciences, Dianov Fiber Optics Research Center, 38 Vavilov Street, 119333 Moscow, Russia

likhachev@fo.gpi.ru

In this report current state-of-art for high peak power fiber lasers operated and its applications is presented. Two types of fiber lasers – Yb-doped, operated near 1 μm and Er-doped operated near 1.55 μm are discussed. High peak power lasers with picoseconds pulse duration enables rapid and precise energy deposition into a processed material ensuring suppressed thermal diffusion and thus reduced a heat affected zone formation. Moreover, extremely high intensity of the pulses allows volume processing of materials, which are transparent at the wavelength of the pulses, via a nonlinear absorption process: one can utilize a two-photon polymerization and a three-dimensional processing of glasses and polymers to fabricate photonic devices and biochips. Moreover, high peak power fiber lasers are extremely useful for high harmonic generation in order to obtain a radiation in the vacuum ultraviolet wavelength range. The highest peak power could be obtained with Yb-doped fiber lasers. In particular chirped pulse amplifier with a final amplification stage based on a 108 μm ytterbium-doped core photonics crystal fiber (PCF) was enabling generation of 3.8 GW pulses with a duration of 480 fs and an energy of 2.2 mJ [1]. However, PCF-based systems contain a number of bulk elements and lose main advantages of all-fiber systems, such as compactness, reliability and high quality of an output beam. Thus, a great number of efforts is currently spent for development of alternative fiber design, which allow to built all-fiber high peak power. An alternative design of large-mode-area fibers is the so-called tapered fibers, in which a core diameter increases along the fiber length from a 6-10 μm (corresponding to single-mode operation) by several times (up to 100 μm core diameter). Few groups develop tapered Yb-doped fibers and a number of remarkable results (i.e. MW-peak power level directly from the final amplification stage, sub-kW average power and etc) were obtained by these groups [2-6].

Demonstrated output peak power of Er-doped fiber lasers is much lower than that of Yb-doped one. However, such lasers are of great demand as well. First of all, such lasers are used in different lidar applications - amplification spectral range of Er-ions falls into the transparency window of the atmosphere, also very important that 1.5 μm lasers are concerned to be “eye-safe” type of light sources (contrary to the lasers operated near 1 μm). Additionally, some applications require development of lasers, operated in a specific wavelength range, which could be covered by Er-doped fiber lasers only. Today the best results in term of peak power and pulse energy were achieved by Yb-free Er-doped fibers pumped through the cladding [7-8]. Even better results were obtained using tapered Er-doped fiber geometry [9]. However, the optimal configuration, which allows one to achieve simultaneously high peak power and a high pump-to-signal conversion efficiency is Yb-free Er-doped double clad fiber followed by Er-Yb large-mode-area fiber [10].

[1] T.Eidam, et al, “Fiber chirped-pulse amplification system emitting 3.8 GW peak power”, Optics Express, 19(1), 255-260 (2010).

[2] K.Bobkov, et al, “Sub-MW peak power diffraction-limited chirped-pulse monolithic Yb-doped tapered fiber amplifier”, Optics Express, 25(22), 26958-26972 (2017).

[3] V. Filippov, et al, “Highly efficient 750 W tapered double-clad ytterbium fiber laser”, Optics Express, 18(12), 12499-12512 (2010).

[4] K.Bobkov et al, “Scaling of average power in sub-MW peak power Yb-doped tapered fiber picosecond pulse amplifiers”, Optics Express, 29(2), 1722-1735 (2021).

[5] A. Petrov, et al, “Picosecond Yb-doped tapered fiber laser system with 1.26 MW peak power and 200 W average output power”, Sci. Rep., 10(1), 17781 (2020).

[6] K.K. Bobkov, et al, “All-fiber chirped-pulse amplifier emitting 670 fs pulses with 92 MW peak power”, IEEE Photonics Technology Letters, v34(18), pp.977-980 (2022).

[7] L.Kotov, et al, "Millijoule pulse energy 100-nanosecond Er-doped fiber laser", Opt. Lett., 40(7), p. 1189 (2015).

[8] L.V.Kotov, et al, "Record-peak-power all-fiber single-frequency 1550 nm laser", Laser Phys. Lett., 11(9), p.095102 (2014).

[9] M.M.Khudyakov, et al, "Narrow-Linewidth Diffraction-Limited Tapered Er-Doped Fiber Amplifier with 2 mJ Pulse Energy", Photonics, 9(12), p.933 (2022).

[10] M.M.Khudyakov, et al, "Highly efficient 3.7 kW peak-power single-frequency combined Er/Er-Yb fiber amplifier", Opt. Lett., 45(7), p.1782 (2020).

Dynamics of generation of polarization and longitudinal modes in short cavity fiber lasers based on composite ytterbium fibers

V.V. Vel'miskin¹, B.I. Denker², V.A. Kamynin^{2,*}, S.E. Sverchkov², A.A. Rybaltovskii²,
A.I. Trikshev², V.B. Tsvetkov²

1 - Prokhorov General Physics Institute of the Russian Academy of Sciences, Dianov Fiber Optics Research Center,
Moscow, Russia

2 - Prokhorov General Physics Institute of Russian Academy of Sciences, Moscow, Russia

*email address: kamyninva@gmail.com

Narrow-bandwidth laser sources are used in many fields of science and technology. The emission bandwidth of less than 10 kHz is required in systems for coherent reflectometry [1], hydrophones [2], gas analysis and high-resolution spectroscopy [3]. For a number of applications, however, there remains a need to implement radiation with a single longitudinal mode, where extreme narrowing of the line is unnecessary. Such quasi-single-frequency sources are in demand for the realization of high-power, kilowatt-level laser systems [4], coherent combining systems [5]. The bandwidth of these sources can be in the range from a few megahertz to a few gigahertz.

In our work, we investigated some lasers with a short Fabry-Perot cavity based on Bragg gratings directly UV-written into the active fiber core (Fig. 1 (a)). To realize a short cavity length (less than 2 cm), we have used a highly Yb-doped composite fiber. Absorption of a weak signal at a wavelength of 976 nm - 12.5 dB/cm. In the region of the generation wavelength, the background did not exceed 0.1 dB/cm.

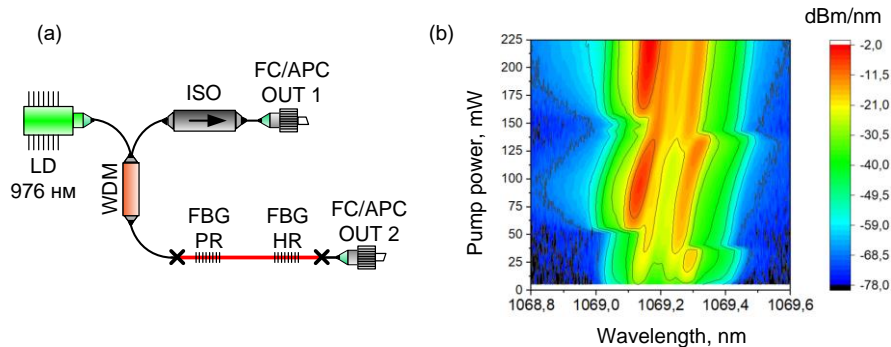


Fig. 1. (a) Experimental setup of the F-P Yb-doped fiber laser, (b) spectral power density depending on wavelength and pump power.

The spectral dynamics, linewidth dynamics, and polarization dynamics of lasers are studied as a function of pump power. Fig. 1 (b) shows the spectral power density as a function of wavelength and pump power. We observed spectral shifts and switching from the single-mode to multi-mode operation during pump power variation.

During laser operation, we observed a transition from narrow-bandwidth generation with a linewidth of about 2 MHz to the mode-beating regime. In addition, polarization mode dynamics with orthogonal polarization modes beating at the 300 MHz frequency have been registered.

We have demonstrated the applicability of Yb-doped phosphate core composite fibers in the fabrication of short cavity lasers with generation wavelengths up to 1070 nm based on direct UV FBG recording. It is shown that narrow bandwidth linear polarized laser generation requires accurate cavity design.

- [1] D. Uttam and B. Culshaw, Precision Time Domain Reflectometry in Optical Fiber Systems Using a Frequency Modulated Continuous Wave Ranging Technique, *J. Light. Technol.*, **3(5)**, 971–977, (1985).
- [2] X. Zhang *et al.*, Short cavity DFB fiber laser based vector hydrophone for low frequency signal detection, *Photonic Sensors*, **7(4)**, 325–328, (2017).
- [3] S. Persijn, F. Harren, and A. Van Der Veen, Quantitative gas measurements using a versatile OPO-based cavity ringdown spectrometer and the comparison with spectroscopic databases, *Appl. Phys. B Lasers Opt.*, **100(2)**, 383–390, (2010).
- [4] W. Li *et al.*, 694 W sub-GHz polarization-maintained tapered fiber amplifier based on spectral and pump wavelength optimization, *Opt. Express*, **30(15)**, 26875, (2022).
- [5] A.I. Trikshev, Yu.N. Pyrkov and V.B. Tsvetkov, Phasing of two amplifier channels for the coherent combining of laser beams with a total power of 60 W, *Quantum Electronics*, **47(11)**, 1045–1048 (2017).



LS-I-9

Characterisation of mid-IR light sources made of RE doped chalcogenide fibers on the base of modal approach

E. Romanova¹, N. Parshina¹, V. Shiryaev²

1- Saratov State University, Astrakhanskaya 83, 410012 Saratov, Russia

2- Devyatykh Institute of Chemistry of High-Purity Substances of RAS, 49 Tropinin Str., 603951 Nizhny Novgorod, Russia

romanovaelena@sgu.ru

Rare earth (RE) doped chalcogenide fibers are used in design of mid-IR lasers and luminescent sources [1]. Two systems of chalcogenide glasses (Ga-Ge-As-Se and Ga-Ge-Sb-Se) doped with RE elements (Pr^{3+} , Tb^{3+} , Dy^{3+}) have been mostly under investigation [2–4]. These glasses have small optical losses and high refractive indices of 2.5–3.5 magnitude in the range of wavelengths $\lambda = 2\text{--}15\ \mu\text{m}$ [5].

In accordance with the wave theory [6], when a pump beam is launched into an active fiber coaxially with the fiber axis (Fig.1), the guided modes, which do not have internal caustics (HE_{1m} modes) are mostly excited in the fiber. Each mode has its own wavelength-dependent intensity profile in the fiber transverse cross-section (TCS) and its own amplitude. However, in theoretical analysis of the luminescence excitation [2], pump and signal intensities are assumed constant over a TCS of a single-index fiber that is only feasible if the fiber is multimode.

In this work, the concepts of the wave theory of optical fibers that represent radiation propagating in a fiber as a set of modes, have been applied in the problem of luminescence excitation in a few-mode fiber. For a $20\ \mu\text{m}$ core made of Tb^{3+} doped $\text{Ga}_5\text{Ge}_{20}\text{Sb}_{10}\text{Se}_{65}$ glass with the refractive index $n_{\text{co}} = 2.55$ surrounded by a glass cladding with $n_{\text{cl}} = 2.35$ [4], the number of HE_{1m} modes at $\lambda > 3\ \mu\text{m}$ is less than 10. Propagation of the pump radiation (PR) at $\lambda_p = 2.95\ \mu\text{m}$ and luminescent radiation (LR) at $\lambda_l = 4.8\ \mu\text{m}$ in various modes has been investigated in a numerical model comprising kinetic equations for populations of three-level system of Tb^{3+} (Fig.2) and differential equations for PR and LR powers. Unlike the generally accepted theoretical model [2], the light intensity dependence on radial coordinate in the fiber TCS (Fig.3) has been taken into account.

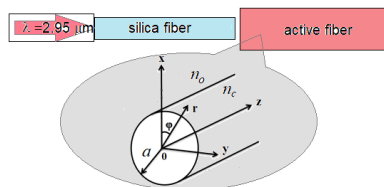


Fig.1. Schematic of light launching into an active fiber and the fiber TCS.

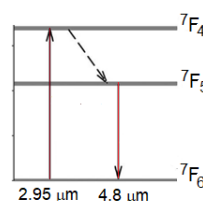


Fig.2. System of Tb^{3+} energy levels with pumping at $2.95\ \mu\text{m}$.

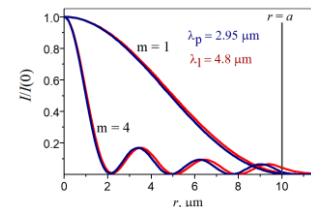


Fig.3. Radial profiles of HE_{1m} modes in the fiber TCS.

Results of the computer modeling reveal that population inversion is not distributed evenly over the fiber TCS and has a radial profile, which varies in time and along the fiber. The profile shape depends on an intensity profile of a given fiber mode. Due to the levels populations depend on radial coordinate, intensity profiles of PR and LR modes propagating in the fiber experience distortion. Consequently, some part of energy leaks out the fiber as a radiation field that is an additional source of optical losses.

This work was supported by the Russian Science Foundation (RSF) under Grant 21-13-00194.

[1] V. Nazabal, J.-L. Adam, Infrared luminescence of chalcogenide glasses doped with rare earth ions and their potential applications, *Opt. Mater.*: X, 15, 100168 (2022).

[2] L. Sójka, Z. Tang, D. Furniss, H. Sakr, Y. Fang, E. Bereś-Pawlik, T.M. Benson, A.B.S eddon, S.Sujecki, Mid-infrared emission in Tb^{3+} -doped selenide glass fiber JOSA B, 34, 70 (2017).

[3] F. Starecki, N. Abdellaoui, A. Braud, J.-L. Doualan, C. Boussard-Plédel, B. Bureau, P. Camy, and V. Nazabal, $8\ \mu\text{m}$ luminescence from a Tb^{3+} GaGeSbSe fiber, *Opt. Lett.*, 43, 1211 (2018).

[4] V.V. Koltashev, B.I. Denker, B.I. Galagan, G.E. Snopatin, M.V. Sukhanov, S.E. Sverchkov, A.P. Velmuzhov, V.G. Plotnichenko, 150 mW Tb^{3+} doped chalcogenide glass fiber laser emitting at $\lambda > 5\ \mu\text{m}$, *Opt. & Laser Technol.*, 161, 109233 (2023).

[5] M.V. Sukhanov, A.P. Velmuzhov, L.A. Ketkova, P.A. Otopkova, I.I. Evdokimov, A.E. Kurganova, V.S. Shiryaev, B.I. Denker, B.I. Galagan, V.V. Koltashev, V.G. Plotnichenko, S.E. Sverchkov, Method for preparing high-purity REE-doped chalcogenide glasses for bulk and fiber lasers operating at $\sim 5\ \mu\text{m}$ region, *J. of Non-Crystal. Solids* 608, 122256 (2023).

[6] A.W. Snyder, J.D. Love, *Optical waveguide theory*. Boston, MA, Springer (1983).



LS-I-10

Study of local structure and thermal properties in Ge-As-Se-S chalcogenide glass fiber optic materials

S.I. Mekhtiyeva¹, R.I. Alekberov^{1,2}, S. M. Mammadov¹

¹ The Ministry of Science and Education of the Republic of Azerbaijan, Institute of Physics G. Javid ave 13, AZ1143 Baku

² Azerbaijan State University of Economics (UNEC), st. Istiqlaliyyat 6, Baku, AZ 1001
e-mail: rahim-14@mail.ru

At present, scientific research is intensively growing in the field of local structure, optical spectroscopy and thermal properties of multicomponent chalcogenide glasses [1]. The main reason of these is related with high optical transparency of multi-component chalcogenide glasses in infrared region of the optical spectrum, as well as, with high optical nonlinearity and photostability, the broad glass-forming region and low energy phonons. Since these substances are obtained by the method of sharp cooling of melt practically remains in non-equilibrium state. The authors of other studies in this field show that the absence of long-range order and thermodynamic non-equilibrium the distinctive sign of glasses is the glass transition temperature T_g [2]. A phase changes does not occur at the temperature corresponding to the glass transition point [2].

The main purpose of this work is to study the relationship between the parameters of local structure and the glass transition temperatures (T_g) in the Ge-As-Se and Ge-As-Se-S chalcogenide glass systems according to theory of topological constraints [3], model the chemically ordered networks [4] and also idea of layered structures [5].

It was determined that partially good agreement exists between the experimental values of glass transition temperatures (T_g) and calculated for Ge-As-Se, Ge-As-Se-S chalcogenide glasses. The value of share of "zero" frequency oscillation modes (f) are equal about to $f \sim 0$ and average coordination number (Z) change in range of $Z=2.5 \div 2.7$ for studied glass compositions. The analysis of these results shows that $Ge_{24}As_{19}S_{20}Se_{37}$, $Ge_{25}As_{10}S_{25}Se_{40}$, $Ge_{26}As_{18}S_{30}Se_{26}$, $Ge_{33}As_{17}S_{35}Se_{15}$ compositions have high short range order and medium range order can be considered as more stable glasses compositions and prospective materials for fiber lasers. The glass transition temperature (T_g) in the mentioned compositions are higher and varies in the range of $589 \div 689$ K.

[1] Rongping Wang, Kunlun Yan, Zhiyong Yang, Barry Luther-Davies, Structural and physical properties of $Ge_{11.5}As_{24}S_{64.5}xSe_{64.5} \cdot (1-x)$ glasses//Journal of Non-Crystalline Solids 427 (2015) 16–19

[2] A. Popov Handbook of disordered semiconductors: Physics and Applications. Pan Stanford Publishing Pte. Ltd, 2011, 205p

[3] J.C. Phillips, M. F. Thorpe, Constraint Theory, Vector Percolation and Glass Formation// Solid State Communications, –1985, 53(8), –p.699-702, [https://doi.org/10.1016/0038-1098\(85\)90381-3](https://doi.org/10.1016/0038-1098(85)90381-3)

[4] Tichy, L., Ticha, H., (1995) Covalent bond approach to the glass transition temperature of chalcogenide glasses, J. Noncryst. Solids, 189, 141-146, [https://doi.org/10.1016/0022-3093\(95\)00202-2](https://doi.org/10.1016/0022-3093(95)00202-2)

[5] K. Tanaka, Structural phase transitions in chalcogenide glasses. Phys. Rev. B 39, 1270–1279 (1989), <https://doi.org/10.1103/PhysRevB.39.1270>

New spinel-based nanostructured glass-ceramics with broadband absorption of ferrous ions in the spectral range of 1.8-2.4 μm

O. Dymshits^{1,2}, V. Bukina³, K. Trukhanova¹, I. Alekseeva², M. Tsenter², A. Zhilin⁵

1- Ioffe Institute, Russian Academy of Sciences, 26 Politekhnicheskaya, 194021 St. Petersburg, Russia

2- S.I. Vavilov State Optical Institute, 36 Babushkina St., 192171 St. Petersburg, Russia

3- Saint Petersburg Mining University, 2 21st Line Vasil'yevski Ostrov, Saint Petersburg, Russia

4- D.V. Efremov Institute of Electrophysical Apparatus, Metallostroy, Doroga na Metallostroy, 3 Bld., 196641 Saint Petersburg, Russia

vodym1959@gmail.com

Crystals with ferrous ions doped in tetrahedral (T_d) sites are promising for saturable absorbers (SAs) of mid-IR lasers because of intense and broad absorption due to the ${}^5E \rightarrow {}^5T_2({}^5D)$ transition. ZnS and ZnSe based materials with T_d coordinated Fe^{2+} ions are used as such SAs. Spinel crystals are their good alternatives, as they are ecofriendly, have high hardness, low thermal expansion coefficient and high laser damage threshold. Transparent glass-ceramics (GCs) are multiphase materials in which nanocrystals are uniformly distributed in the residual glass. We present the results of a comparative study of the structure and spectral properties of new transparent GCs based on nanocrystals of $\gamma\text{-Al}_2\text{O}_3$, MgAl_2O_4 and ZnAl_2O_4 spinels doped with Fe^{2+} ions.

Initial iron doped glasses of lithium (LAS), magnesium (MAS), and zinc (ZAS) aluminosilicate systems containing TiO_2 as a nucleating agent were melted at 1580 $^\circ\text{C}$ under reducing conditions. GCs were obtained by heat-treatments in the temperature range of 680 - 1200 $^\circ\text{C}$. Their phase composition and structure were studied by X-ray diffraction analysis (XRD), differential scanning calorimetry (DSC), and Raman spectroscopy. The optical absorption spectra of glasses and GCs were recorded. The initial glasses are X-ray amorphous. During their secondary heat-treatments, lithium-(magnesium-, zinc-) aluminum-titanate regions and "low-silicate" regions enriched in magnesium (zinc) and aluminum are formed, in which crystals with a spinel structure are precipitated, Fig. 1a. Despite the similarity of the processes of phase transformations, the temperature intervals of crystallization of spinel nanocrystals and the character of the titanium-containing phase in these GCs are different, which is manifested in their absorption spectra, Fig. 1b. Absorption spectra are formed by absorption of Fe^{2+} ions in spinel crystals in O_h and T_d positions and by intervalent charge transfer transitions between Fe^{2+} , Fe^{3+} , Ti^{3+} , and Ti^{4+} ions in spinel and titanium-containing nanocrystals. The structuring of the spectrum of OH groups is due to their incorporation into spinel crystals.

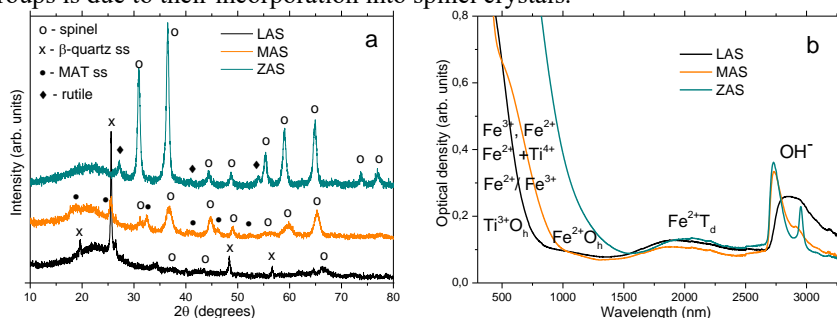


Fig. 1. XRD patterns and absorption spectra of spinel-based glass-ceramics of the LAS, MAS and ZAS systems.

The developed transparent glass-ceramics exhibit a broadband absorption in the spectral range of 1.8-2.4 μm due to the ${}^5E \rightarrow {}^5T_2({}^5D)$ transition of Fe^{2+} ions in tetrahedral sites in spinel nanocrystals. The glass-ceramics are promising as saturable absorbers of lasers emitting in this spectral range.

This work was partly supported by the Russian Science Foundation (Grant 23-23-00446).

[1] L. Basyrova, V. Bukina, S. Balabanov, *et al.* Synthesis, structure and spectroscopy of $\text{Fe}^{2+}:\text{MgAl}_2\text{O}_4$ transparent ceramics and glass-ceramics, *J. Lumin.*, vol. 236, pp. 118090 (1-17), (2021).

[2] O. Dymshits, V. Bukina, K. Ereemeev, *et al.*, Spectral properties and structure of transparent glass-ceramics based on $\text{Fe}:\text{MgAl}_2\text{O}_4$ and $\text{Fe}:\text{ZnAl}_2\text{O}_4$ crystals, *J. Opt. Technol.*, vol. 88, pp. 323-329 (2021).

[3] K. Ereemeev, L. Basyrova, O. Dymshits, Structure and spectral properties of $\text{Fe}:\text{ZnAl}_2\text{O}_4$ transparent glass-ceramics and ceramic, *J. Phys. Conf. Ser.*, vol. 2086, pp. 012138 (1-6), (2021).

LS-I-13

Fabrication of broad-band photodetectors based on two-dimensional materials

Nishant Tripathi¹

*1- Samara National Research University
443086, Samara, Russia, Moskovskoye Shosse 34;*

Main author email address: tripathi.n@ssau.ru; nishant.tripathi.11@gmail.com

Optical detectors are a very crucial part of many house appliances that are inseparable from our daily life. Photodetectors are very useful devices for light detection, imaging science, spectroscopies as well as for optical communication. Due to rapidly growing optical fiber based communication network, the development of high efficient and high speed photodetectors operating in the infra-red (IR) range are in huge demand. IR photodetectors are utilized for remote temperature sensing, night vision cameras, and astronomy.

Recently developed layered transition metal chalcogenides (TMCs) have been proven as the possible solution for the development of high performance and flexible optical detectors. TMCs show an appropriate and tunable band gap with a high carrier mobility (0.2 eV to 2 eV), which makes TMCs a favourite material for high-efficiency optoelectronic devices.

In recent years, we have analysed the photodetection properties of various types of TMCs such as TiS₃, TiS₂, MoS₂, etc. [1-4]. We also analysed the various types of heterostructures based on TMCs such as Ag-TiS₃, Ag-TiS₂, TiS₃-porous silicon and TiS₂-porous silicon. Photodetection properties of flexible nanocomposite materials based on ceramic-gel-TMCs have also been analysed. We also developed flexible photodetectors on the PET substrate. Various types of sample fabrication processes such as dielectrophoresis, drop-cast, gel-cast, etc. have been employed in order to develop high-performance photodetectors. The various effects of operating temperature have been investigated for the photodetector performance. Finally, ultra-sensitive, high-performance broadband photodetectors have been developed for a wide operating temperature range (77 K – 548 K).

References

- [1] M. Talib, N. Tripathi, S. Manzoor, P. Sharma, V. Pavelyev, V.S. Volkov, A.V. Arsenin, S.M. Novikov, P. Mishra, TiS₃- nanoribbon: a novel material for ultra-sensitive photodetection across extreme temperature ranges, *Sensors* [Just accepted].
- [2] M. Talib, S. Manzoor, P. Sharma, N. Tripathi, V. Platonov, V. Pavelyev, V.S. Volkov, A.V. Arsenin, A.V. Syuy, P.M.Z. Hasan, A.A. Melaibari, P. Mishra, Development of high-performance broadband optical detector for cryogenic to elevated operating temperature, *Materials Science in Semiconductor Processing*, 158, pp. 107364, (2023).
- [3] M. Talib, N. Tripathi, P. Sharma, P.M.Z. Hasan, A.A. Melaibari, R. Darwesh, A.V. Arsenin, V.S. Volkov, D.I. Yakubovsky, S. Kumar, V. Pavelyev, P. Mishra, Development of ultra-sensitive broadband photodetector: a detailed study on hidden photodetection-properties of TiS₂ nanosheets, *Journal of Materials Research and Technology*, 14, pp. 1243-1254, (2021).
- [4] A.R. Rymzhina, P. Sharma, V.V. Podlipnov, K.N. Tukmakov, V.S. Pavelyev, V.I. Platonov, P. Mishra, N. Tripathi, Ultrafast highly sensitive flexible infrared radiation detector, *Computer Optics*, (2023) (Just accepted).

LS-I-15

Transverse instabilities in wide-aperture semiconductor lasers with a vertical cavity and method for their suppression**A. A. Krents^{1,2}, N.E. Molevich^{1,2}, E.A. Yarunova^{1,2}***1- Department of Theoretical Physics, Lebedev Physical Institute, Novo-Sadovaya Str. 221, Samara, Russia**2- Department of Physics, Samara National Research University, Moskovskoye Shosse 34, Samara, Russia**krenz86@mail.ru*

Wide-aperture lasers are subject to various spatiotemporal instabilities. Modulation instability is characteristic of wide-aperture semiconductor surface-emitting lasers with a vertical cavity (VCSEL) [1]. In optics, this instability can lead to filamentation and beam quality degradation [2]. In this regard, it is relevant to investigate methods to improve the spatial and temporal quality of the radiation of such devices. This paper proposes to use coherent external optical injection to suppress the modulation instability arising in the VCSEL.

The dynamics of VCSEL can be described by a model that takes into account generation in a single longitudinal mode, presented in the [1]:

$$\begin{cases} \frac{\partial E}{\partial t} = -[1 + i\theta + 2C(i\alpha - 1)(N - 1)]E + i\Delta_{\perp}E + E_{inj}, \\ \frac{\partial N}{\partial t} = -\gamma \left[N - I + |E|^2 (N - 1) \right] + \gamma d\Delta_{\perp}N, \end{cases}$$

where E, N are dimensionless envelopes of the electric field and population inversion, respectively. The parameter E_{inj} is the normalized injected field. θ represents the detuning between the cavity and the injected field frequencies, α is the linewidth enhancement factor. As the basic parameters of the system, we chose the parameters given in the paper [1]: $\theta = -1.5$, $\alpha = 1.5$, $C = 0.6$, $d = 0.052$, $I = 1.85$, $\gamma = 0.1$.

A standard linear analysis was performed to investigate the stability of VCSEL generation. The aperture sizes at which the spatially homogeneous generation mode becomes unstable were determined ($L_{\min} \approx 115 \mu m$). The method of external optical injection was proposed to stabilize the generation. It is shown that coherent optical injection can suppress all unstable transverse modes. The stabilization effect has a threshold nature. The threshold value of injection can be calculated by the formula:

$$|E_{inj}| = \sqrt{-1 + \mu\beta/2 + \sqrt{\mu(\mu\beta^2 - 4(\beta - 1))}/2}, \text{ where } \mu = 2C(I - 1) \text{ and } \beta = \sqrt{1 + \alpha^2}.$$

An implicit Crank-Nicholson scheme with periodic boundary conditions, which is unconditionally stable, was used to numerically solve the system of equations (1). The spatially homogeneous laser generation regime with addition of Gaussian noise of small amplitude was chosen as initial conditions. As a result of numerical calculations, it was obtained that the system dynamics depends on the size of the spatial domain L . Simulation of spatiotemporal dynamics at $L < L_{\min}$, showed that the regime of spatiotemporal uniform generation is stable, despite the presence of unstable modes. Unstable modes arise only in the case of $L > L_{\min}$. Without injection, the instability of the homogeneous generation mode leads to spatiotemporal chaos and filamentation of the laser radiation. It is shown that for chosen parameters the injected amplitude is sufficient for stabilization to be of the order of 1% of the stationary field amplitude modulus. The proposed method of optical injection to suppress modulation instability is effective and can be used in this system. It was found that external optical radiation of low amplitude can completely suppress the modulation instability.

This work was supported by the Ministry of Science and Higher Education of the Russian Federation within the framework of the state assignment (project No. 0023–2019–0003, FSSS–2023–0009).

[1] W. Ahmed, S. Kumar, R. Herrero, M. Botey, M. Radziunas, K. Staliunas, Stabilization of flat-mirror vertical-external-cavity surface-emitting lasers by spatiotemporal modulation of the pump profile, *Physical Review A*, vol.92(4), p. 043829 (2015)

[2] W. Ahmed, S. Kumar, J. Medina, M. Botey, R. Herrero, K. Staliunas, Stabilization of broad-area semiconductor laser sources by simultaneous index and pump modulation, *Optics Letters*, vol. 43(11), pp. 2511-2514 (2018).



LS-I-16

Highly transient stimulated Raman scattering with combined frequency shifts in crystals

S.N. Smetanin, D.P. Tereshchenko, Yu.A. Kochukov, A.G. Papashvili, V.V. Bukin, V.E. Shukshin, E.E. Dunaeva, I.S. Voronina, L.I. Ivleva

Prokhorov General Physics Institute of the Russian Academy of Sciences, Moscow, Russia

Stimulated Raman scattering with combined frequency shifts on high- and low-frequency Raman modes in scheelite-type crystals at weakly chirped laser pulse duration shorter than a dephasing time of the Raman modes is experimentally investigated.

Development of Raman converters for ultrashort laser pulses shorter than a dephasing time of Raman medium is an important issue of laser physics because of a low Raman gain increment in such highly transient regime of conversion and its suppression due to competing nonlinear phenomena such as self-phase modulation. In this work, highly transient stimulated Raman scattering (SRS) in crystals under pumping by a sub-picosecond 1030-nm laser radiation with the pulse duration shorter than a dephasing time of the crystal Raman modes is experimentally investigated. For the scheelite-type Raman-active crystals (SrMoO_4 , CaMoO_4 , and others) owning two (primary, the stretching, and secondary, the bending) Raman modes with similar integral cross-sections, Stokes SRS radiation with not only a high-frequency shift on the primary Raman mode (at 888 cm^{-1} with the dephasing time of 4 ps for SrMoO_4), but also a low-frequency shift on the secondary Raman mode (at 327 cm^{-1} with the dephasing time of 1 ps for SrMoO_4) was obtained. A positive and negative weak chirp increasing the pump pulse duration from 0.24 ps up to 6.5 ps was used to optimize the Raman conversion preventing the issues of the pump pulse self-phase modulation and the Stokes pulse spectral narrowing. SRS generation threshold has been lowered relative to those for the competing nonlinear phenomena with a help of increasing the crystal length (a) up to a temporal walk-off length due to group-velocity mismatch between the pump and Stokes pulses, (b) up to a Rayleigh length of the focused pump beam, and (c) longer than coherence length of Stokes-anti-Stokes parametric coupling. Using the pump pulses with duration shorter than the secondary Raman mode dephasing time (1 ps in SrMoO_4) allowed obtaining higher intensity of the low-frequency-shift Stokes SRS component relative to the high-frequency-shift Stokes SRS component.

This research was funded by Russian Science Foundation—Project No 22-22-00708.

Laser-induced damage of Mid-IR high-purity nonlinear and laser crystals and glasses under 2- μ m laser irradiation

O.L. Antipov

*Institute of Applied Physics of the Russian Academy of Sciences, Nizhny Novgorod 603155, Russia
antipov@ipfran.ru*

High power and high efficiency coherent sources of mid-infrared (mid-IR) radiation have a wide variety of applications in areas such as materials processing, surgery and disease diagnostics, atmospheric remote sensing and environmental monitoring, among other applications [1,2]. The last decade has seen a notable progress in the design and development of high power solid-state lasers based on Cr²⁺- or Fe²⁺-doped chalcogenide crystals (ChCs) such as ZnSe, ZnS, CdSe and others, and solid-state laser systems based on optical parametric oscillators (OPOs). Recently, lasing in the 4.5–5.9 μ m wavelength range was demonstrated in glass samples and optical fibers based on chalcogenide glasses (ChGs) doped with rear-earth ions [3]. At the same time, the scaling of the average and peak power and the pulse energy of mid-IR solid-state laser systems is hindered by the laser induced damage (LID) [4].

This report gives an overview of the recent studies of LID of mid-IR nonlinear and laser crystals and glasses with high purity and different structural quality induced by the CW or repetitively-pulsed nanosecond lasers at 1900-2100 nm. LIDs of nonlinear crystals (ZnGeP₂, BaGa₄Se₇, BaGa₂GeSe₆ and GaSe) and ChCs (ZnSe, Cr²⁺:ZnSe and Fe²⁺:ZnSe) were analyzed [5-10]. The crystals grown in different conditions with the dissimilar crystal-lattice quality were examined. The effect of various crystal quality factors such as the impurity composition, lattice dislocations, and post-growth processing, surface treatments and polishing were discussed. The LID thresholds determined by both the pulse fluence and intensity were studied at various pulse repetition rates, pulse widths, and exposure durations. The thermo-optical lensing and LID of special pure Ge₃₅As₁₀S₅₅ and Ge₂₀As₂₂Se₅₈ glasses under the quasi-CW irradiation with the Tm-doped fiber laser at 1908 nm were also examined [11]. The LID mechanisms and prospects for the improvement of the LIDT threshold in mid-IR nonlinear and laser materials will be discussed in the presentation.

The reported study was financially supported by Russian Science Foundation (grant 22-12-20035, <https://rscf.ru/en/project/22-12-20035>).

- [1] K.L. Vodopyanov, *Laser-based Mid-infrared Sources and Applications* (Wiley, USA), 2020.
- [2] S. Mirov, I. Moskalev, S. Vasilyev, V. Smolski, V. Fedorov, D. Martyshekin, J. Peppers, M. Mirov, A. Dergachev, and V. Gapontsev, "Frontiers of Mid-IR Lasers Based on Transition Metal Doped Chalcogenides", *IEEE J. Sel. Top. Quantum Electron.*, vol. 24 (iss. 5), pp. 1-29 (2018).
- [3] M.F. Churbanov, B.I. Denker, B.I. Galagan, V.V. Koltashev, V.G. Plotnichenko, M.V. Sukhanov, S.E. Sverchkov, A.P. Velmuzhov, "Comparison of 4.5–6 μ m luminescent and lasing properties of rare earth dopants in chalcogenide glasses", *J. Lumin.* vol. 245, 118756 (2022).
- [4] D. Ristau (Ed.), "Laser-Induced Damage in Optical Materials (CRC Press Taylor & Francis Group: Boca Raton, FL, USA), 2015.
- [5] N.N. Yudin, O.L. Antipov, A.I. Gribenyukov, I.D. Eranov, S.N. Podzivalov, M.M. Zinoviev, L.A. Voronin, E.V. Zhuravleva, M.P. Zykova, "Effect of postgrowth processing technology and laser radiation parameters at wavelengths of 2091 and 1064 nm on the laser-induced damage threshold in ZnGeP₂ single crystal", *Quantum Electron.* Vol. 51, 306–316 (2021).
- [6] N. Yudin, O. Antipov, I. Eranov, A. Gribenyukov, G. Verozubova, Z. Lei, M. Zinoviev, S. Podzivalov, E. Slyunko, V. Voevodin, A. Zav'jalov, Ch. Yang, "Laser-induced damage threshold of single crystal ZnGeP₂ at 2.1 μ m: The effect of crystal lattice quality at various pulse widths and repetition rate", *Crystals* vol. 12, 652 (2022).
- [7] N. Yudin, A. Khudoley, M. Zinoviev, S. Podzivalov, E. Slyunko, E. Zhuravleva, M. Kulesh, G. Gorodkin, P. Kumeysya, O. Antipov, "The Influence of Angstrom-Scale Roughness on the Laser-Induced Damage Threshold of Single-Crystal ZnGeP₂", *Crystals* vol. 12, 83 (2022).
- [8] N.Yu. Kostyukova, A. A. Boyko, I.D. Eranov, O.L. Antipov, D.B. Kolker, A.I. Kostyukov, E.Yu. Erushin, I.B. Miroschnichenko, D.V. Badikov, V.V. Badikov "Laser-induced damage threshold of the nonlinear crystals BaGa₄Se₇ and BaGa₂GeSe₆ at 2091 nm in the nanosecond regime", *JOSA B*, vol. 37, No. 9, pp. 2655-2659 (2020).
- [9] Ch. Zhu, V. Dyomin, N. Yudin, O. Antipov, G. Verozubova, I. Eranov, M. Zinoviev, S. Podzivalov, Y. Zhuravlyova, Y. Slyunko, Ch. Yang, "Laser-induced damage threshold of nonlinear GaSe and GaSe:In crystals upon exposure to pulsed radiation at a wavelength of 2.1 μ m", *Applied Sciences*, vol. 11, 1208 - 10 (2021).
- [10] N. Yudin, O. Antipov, S. Balabanov, I. Eranov, Yu. Getmanovskiy, E. Slyun'ko, "Effects of Processing Technology of CVD-ZnSe, Cr²⁺: ZnSe, and Fe²⁺: ZnSe Polycrystalline Optical Elements on the Damage Threshold Induced by a Repetitively-Pulsed Laser at 2.1 μ m", *Ceramics* vol. 5, 459–471 (2022).
- [11] O. Antipov, A. Dobrynin, Yu. Getmanovskiy, E. Karaksina, V. Shiryaev, M. Sukhanov and T. Kotereva, "Thermal Lensing and Laser-Induced Damage in Special Pure Chalcogenide Ge₃₅As₁₀S₅₅ and Ge₂₀As₂₂Se₅₈ Glasses under Quasi-CW Fiber Laser Irradiation at 1908 nm", *Photonics* vol. 10, 252 – 13 (2023).



Prospective laser and optoelectronic components and their applications

**E. V. Borisov, A. A. Kozyrev, M. A. Kopenkin, O. V. Korenchenko, V. A. Panarin,
S.N. Sokolov, M. Yu. Starynin, L. I. Shestak**

Inject RME LLC, 410033 Saratov, Elmashevskaya st., 3a

Email address: s.sokolov@nppinject.ru

It is reported about fiber coupled laser diode (LD) modules, LD stacked arrays, micro-optical elements, and other products developed and manufactured by Inject RME LLC:

- LD module with an output power of CW 400 W, wavelength of 940 nm, an output fiber core diameter of 800 μm (NA=0.22) for pumping solid-state lasers and technological applications;
- fiber coupled LD modules:
 - 32 -976-90-CW - 975 nm, 105 μm , NA=0.22, 90 W and
 - 36-976-200-CW 200 μm , NA=0.22 , 975 nm, 200 W.
- QCW LD stacked arrays:
 - with a wide emission spectrum of 800-811 nm, with a peak output power of optical power of 1800 W, QCW operation mode: 300 μs , 10 Hz, for pumping DPSS lasers of an athermal design;
 - with a peak output optical power of 20 kW, wavelength of 940 nm, (operation mode: pulse duration - up to 1.5 ms, up to 20 Hz) for pumping high-energy Yb lasers;
 - SLM20-940-20000-QCW-L-263 with a peak output power of 20 kW at 940 nm (laser pulse energy density up to 3.75 J/cm², 1.5 ms, 20 Hz), collimated beam divergence – 14x2 degrees (FWHM);
 - SLM12-940-50000-Pulse-HD – 50 kW, 940 nm, 20 ns, 10 kHz.
 - laser beam homogenizer based on a two-sided array of perpendicularly arranged cylindrical microlenses made of optical quartz glass, with an aperture of 90x90 mm and a transmission of 99%;

A high-power diode laser is produced - PLD-6 type - provides an output optical power of laser up to 6 kW in CW mode on and a rectangular laser spot 22x2 mm in size at the focus, it is successfully used for laser thermal hardening, alloying and surfacing.

Experimental work has been carried out on the automated laying of a prepreg tape made of thermoplastic materials with local heating of the surface by a powerful diode laser, a technology that is promising for mass production of composite products.

LS-I-19

The role of rate constants measurement for the development of gas lasers

A. Torbin^{1,2}

1 – Lebedev Physical Institute, Samara Branch, Novo-Sadovaya str., 221, Samara, Russia, 443011

2 – Samara National Research University, Moskovskoye shosse, 34, Samara, Russia, 443086

Main author email address: torbin.ap@yandex.ru

To date, the most promising laser systems that would combine high power and diffraction quality of radiation are hybrid gas lasers with diode optical pumping. Systems of this type include, for example, diode pumped alkali metal vapor lasers (DPAL) and optically pumped metastable heavy rare gas lasers (OPRGL). The advantage of a gaseous active medium in comparison with a solid one is the lower influence of temperature that affect the output beam quality and the appearance of optical inhomogeneities. Due to this, a larger limiting energy output per volume unit of the active medium is achieved in a gas laser.

The photon source in gas lasers is an electronically or vibrationally excited particle Ex^* . The main parameters of the laser operation, such as the gain or specific energy output, are expressed in terms of the number densities of these excited particles. Accordingly, laser efficiency and its limiting parameters can only be calculated with exact knowledge of the rates of chemical and energy transfer processes in which Ex^* are produced and destroyed. In turn, the physical quantity that determines the rate of chemical reactions is the rate constant. Consequently, development of accurate mathematical models and the design of new gas laser systems is fundamentally impossible without experimentally measured rate constants of processes involving Ex^* . The measurement of these constants requires the use of modern research methods and precise scientific equipment.

For many years, our scientific group has been measuring the rate constants of processes occurring in the active medium of various lasers. In studies aimed at the development of DPAL [1,2], the rate constants of the deactivation processes of the electronically excited rubidium atoms in collisions with diluent gases H_2 , CH_4 , and C_2H_6 were measured, and a conclusion was made about the preferential use of methane in this role. We measured a number of kinetic constants of processes involving thermalized and vibrationally excited singlet oxygen $O_2(a, \nu)$, vibrationally excited ozone $O_3(\nu)$, and O atoms occurring in the active medium of an electric-discharge oxygen-iodine laser (EOIL) [3-5]. In [5] an explanation was given for the sharp drop in $O_2(a)$ number density at the output of an electric discharge generator of singlet oxygen in EOIL, based on the occurrence of the previously disregarded reaction $O_2(a) + O_3(\nu)$. Currently, the Samara branch of LPI is working on measuring the temperature dependences of the rate constants of energy transfer processes involving metastable argon atoms Ar^* in a mixture with helium He, which are necessary for the development of the OPRGL. Since Ar^* atoms in OPRGL are produced in the plasma of a repetitively pulsed discharge, knowledge of the temperature dependences of the rate constants becomes critical for the development of this new promising laser system.

[1] V. N. Azyazov, A. P. Torbin, A. M. Mebel, S. M. Bresler and M. C. Heaven, Product channels of the reactions of $Rb(6^2P)$ with H_2 , CH_4 and C_2H_6 , *Journal of Quantitative Spectroscopy & Radiative Transfer*, vol. 196, pp. 46-52, (2017).

[2] V. N. Azyazov, A. P. Torbin, S. M. Bresler, A. M. Mebel and M. C. Heaven, Removal of $Rb(6^2P)$ by H_2 , CH_4 and C_2H_6 , *Optics Letters*, vol. 41, pp. 669-672, (2016).

[3] A. P. Torbin, A. A. Pershin, A. M. Mebel, M. V. Zagidullin, M. C. Heaven and V. N. Azyazov, Collisional relaxation of $O_2(a^1\Delta, \nu = 1, 2, 3)$ by CO_2 , *Chemical Physics Letters*, vol. 691, pp. 456-461, (2018).

[4] A. A. Pershin, A. P. Torbin, M. V. Zagidullin, A. M. Mebel, P. A. Mikheyev and V. N. Azyazov, Rate constants for collision-induced emission of $O_2(a^1\Delta_g)$ with He, Ne, Ar, Kr, N_2 , CO_2 and SF_6 as collisional partners, *Physical Chemistry Chemical Physics*, vol. 20, pp. 29677-29683, (2018).

[5] V. N. Azyazov, A. P. Torbin, P. A. Mikheyev, A. A. Pershin and M. C. Heaven, Kinetics of Oxygen Species in an Electrically Driven Singlet Oxygen Generator, *Chem. Phys.*, vol. 463, pp. 65-69, (2015).



Laser on metastable atoms of inert gases with optical pumping

P. Mikheyev¹, A. Torbin^{1,2}, A. Chernyshov¹, M. Zagidullin^{1,2}, M. Svistun¹, N. Ufimtsev¹

1- P.N. Lebedev Physical Institute, Samara branch, 221 Novo-Sadovaya st. Samara, 443011, Russia

2- Samara National Research University, 34, Moskovskoye shosse, Samara, 443086, Russia

paulmikheyev@mail.ru

Optically pumped all-rare-gas laser (OPRGL) which was proposed recently [1], utilizes metastable atoms of Ne, Ar, Kr and Xe as lasing species and have a potential for scaling to a high-power system with good beam quality. Like alkali atoms, rare gas metastables host just one electron on the outer shell, making OPRGL kinetically analogous to the extensively studied diode pumped alkali laser (DPAL) [2]. However, OPRGL has a sound advantage – its active medium is chemically inert. Both DPAL and OPRGL are three-level systems where energy transfer from the optically pumped level is provided in collisions with a bath gas. However, in the most extensively studied cesium-based DPAL light hydrocarbons have to be used to provide efficient energy transfer at a moderate pressure. In that case, the presence of the excited alkali atoms leads to a complex chemistry that finally results in degradation of the laser medium. In OPRGL, energy transfer is efficient at an atmospheric pressure when He is the collisional partner. The pump wavelengths for the OPRGL's fall in a well-developed spectral region for laser diodes and the energy from large arrays of diodes can be combined to a high-power, high-quality beam. All lasing wavelengths fall in the atmospheric transparency window.

Rate coefficients for collisional energy transfer from pump to upper laser level are about $10^{-11} \text{ cm}^{-3} \text{ s}^{-1}$. Theoretical estimations [3] showed that the specific laser output in Ar:He mixture can be on the order of 10^2 W cm^{-3} with overall efficiency (including discharge requirements) more than 50%.

A discharge system should provide the metastables' number density about 10^{13} cm^{-3} or larger at near atmospheric pressure and this is the key problem for this class of lasers. Analysis of the discharge in Ar:He mixture [3] showed that efficient Ar(1s₅) production is possible when $E/N \approx 10 \text{ Td}$ or larger. That rules out cw discharges and leaves a repetitively pulsed nanosecond discharge as the most suitable for an OPRGL.

In this report the successful experiments with OPRGL lasing are reviewed and possible approaches for its further development and scaling are discussed.

[1] J. Han, M. Heaven, Gain and lasing of optically pumped metastable rare gas atoms, *Optics Letters*, vol. 37, pp. 2157-2159, (2012).

[2] W. Krupke, Diode pumped alkali lasers - A review, *Progress in Quantum Electronics*, vol. 36, pp. 4-28, (2012).

[3] A. Demyanov, I. Kochetov, P. Mikheyev, Kinetic study of a cw optically pumped laser with metastable rare gas atoms produced in an electric discharge, *Journal of Physics D: Applied Physics*, vol. 46, p. 375202, (2013).



Xe laser based on hollow-core fiber excited by microwave-discharge

A.V. Gladyshev, D.G. Komissarov, S.M. Nefedov, A.F. Kosolapov, V.V. Velmiskin, A.P. Mineev, I.A. Bufetov

*Prokhorov General Physics Institute of the Russian Academy of Sciences, 38 Vavilov St., Moscow, Russia
iabuf@fo.gpi.ru*

The attempts to create gas-discharge fiber lasers started about 15 years ago, shortly after the development of HCFs. The main problem here is the difficulty of maintaining plasma in a thin (about 100 μm in diameter) core. The HCF diameter of the order of $\sim 100 \mu\text{m}$ was used in almost all studies, since it provides an acceptable level of optical losses in a HCF. The most advanced result in this field so far was as follows. It was declared that optical amplification due to stimulated transitions in Xe atoms at wavelengths of 3.11, 3.37, and 3.51 μm was observed [1]. However, this result has not received further development so far.

In this work, a gas-discharge fiber laser based on a hollow-core fiber has been demonstrated for the first time. To pump it, we used the previously proposed scheme for excitation of a gas discharge in a hollow-core fiber using microwave radiation [2] and the results of microwave discharge stability investigation in noble gases under similar conditions [3].

The design of the gas-discharge fiber laser included a 100-cm-long segment of a revolver-type hollow-core fiber (RF, see Fig. 1b) filled with a He:Ar:Xe gas mixture in a ratio of 100:10:1 and a total pressure of 130 Torr. Both ends of the RF were hermetically sealed into miniature gas cells, which had inlets for gas injection and resonators windows to decouple the radiation. The highly reflective (HR) mirror was a polished aluminum plate. The output mirror with a multilayer interference coating had a high reflectivity ($\sim 90\%$) in a wide wavelength range from 2000 to 3500 nm. A section of the fiber 30 cm long was placed in a pulsed microwave field with a frequency of 2.45 GHz and a strength of about 1 kV/cm. The discharge in RF core was initiated by short-term UV irradiation of RF with a mercury lamp. The MW pulse duration was 20 μs with a repetition rate of 400 Hz. After alignment of the resonator mirrors, generation was observed at a wavelength of 2.027 μm . The lasing emission spectrum was monitored using band-pass filters and a Yokogawa 625 spectrum analyzer (see Fig. 2). Fig. 1a shows oscillograms of a MW pump pulse (curve 1), an oscillogram of a laser pulse obtained using a photodetector sensitive in the spectral range from 1 to 5 μm (curve 2). Curve 3 was obtained under conditions identical to curve 2, but with a misaligned HR mirror. The maximum peak generation power was $\sim 1 \text{ mW}$.

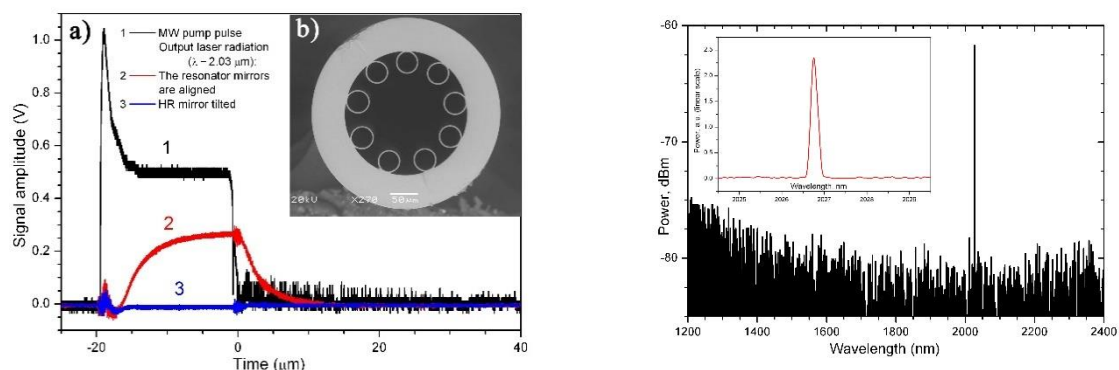


Fig.1. a) Oscillograms of MW pump pulse and Xe laser output at different conditions; b) cross-section of the revolver HCF used in experiments. Fig.2. Spectrum of Xe gas discharge fiber laser.

This research was supported by Russian Science Foundation (grant No. 22-19-00542), <https://rscf.ru/project/22-19-00542/>.

[1] S. A. Bateman, W. Belardi, F. Yu et al. Gain from Helium-Xenon Discharges in Hollow Optical Fibers at 3 to 3.5 μm ," in CLEO: 2014 Postdeadline Paper Digest, OSA Technical Digest (online) (Optica Publishing Group, 2014), paper STh5C.10.

[2] A. Gladyshev, S. Nefedov, A. Kolyadin et al. Microwave Discharge in Hollow Optical Fibers as a Pump for Gas Fiber Lasers, *Photonics*, vol.9, p.752 (2022).

[3] I. Bufetov, A. Gladyshev, S. Nefedov et al. MW discharge maintaining in the hollow core fibers for gas fiber lasers, *Doklady RAS Physics*, vol.509, pp. 3-8, (2023) (in Russian).



LS-O-2

Direct laser writing of high retardance structures in nanoporous glass

**S.I. Stopkin¹, A.S. Lipatiev¹, S.S. Fedotov¹, T.O. Lipatieva¹, Yu.V. Mikhailov¹, S.V. Lotarev²,
V.N. Sigaev¹**

1- Mendeleev University of Chemical Technology, Miusskaya sq. 9, Moscow 125047, Russia

2- Independent Researcher

e-mail: semenstopkin@gmail.com

Recent advances in femtosecond laser technology enables the possibility of space-selective nanostructuring of transparent materials due to nonlinear absorption mechanism. Tightly focused femtosecond laser pulses can induce nanoporous structures named as nanogratings with polarization-controlled form birefringence inside fused silica [1]. The possibility of precision control of the retardance and the slow axis orientation of birefringence paves the way to the fabrication of geometric phase optics [2] as well as polarization converters [3]. However, the formation of nanogratings in silica and other oxide glasses requires tens of laser pulses [1,4] and the search for novel birefringent structures which can be laser-induced by few laser pulses is still in progress. For example, recently, a new type of birefringent structures consisting of elongated nanopores or single nanoplanes were discovered in silica glass irradiated by femtosecond laser beam [3]. On the other hand, the rapid formation of the form birefringence by only 2-3 laser pulses was showed in high silica nanoporous glass (NPG) [5]. This paves the way to using the nanoporous glassy materials for the inscription of high retardance optical elements. In this work we study direct laser writing of phase elements in nanoporous glass.

We used the NPG glass samples, which synthesis was described previously [5] for laser writing experiments. For the inscription of phase elements in the form of squares 300x300 μm , we used femtosecond regenerative amplifier Pharos SP operating at the wavelength of 1030 nm. The pulse energy was varied from 300 to 800 nJ, at constant pulse repetition rate and pulse duration of 200 kHz and 180 fs respectively. The laser beam was focused inside the NPG by aspheric lens (N.A.=0.16). Measurements of retardance of birefringence was performed on laser-inscribed squares by raster scanning at 2 mm/s speed and interline separation of 1 μm . The birefringence dispersion of squares was estimated by means of the polarizing optical microscope Olympus BX51 equipped with CCD camera Olympus DP73, polarizers and the set of interference optical filters. Taking the birefringence dispersion into account, the value of retardance was calculated by spectroscopic method [6]. The fiber optic spectrometer Ocean Optics USB2000 connected to the microscope was used for registration of transmission spectra of birefringent squares which slow axis was oriented at 45° to parallel and crossed polarizers. The retardance dependency on laser pulse energy was derived by fitting the normalized transmission spectra. The higher the pulse energy, the higher the retardance of inscribed birefringent squares. It was shown that the retardance value can be as high as 908 nm. This allows the laser writing of single layer phase plate for NIR and Mid-IR lasers that is impossible in silica glass. Thus, NPG is a promising medium for the efficient fabrication of phase optical elements.

The work was supported by Russian Science Foundation (grant 22-79-10231).

- [1] Y. Shimotsuma et al., Self-Organized Nanogratings in Glass Irradiated by Ultrashort Light Pulses, *Phys. Rev. Lett.*, 91(24), pp. 247405, (2003).
- [2] R. Drevinskas and P.G. Kazansky, High-performance geometric phase elements in silica glass, *APL Photonics*, 2(6), pp. 066104, (2017)
- [3] Y. Lei et al., Ultrafast laser nanostructuring in transparent materials for beam shaping and data storage, *Opt. Mater. Express*, 12(9), pp. 3327-3355, (2022)
- [4] S.S. Fedotov et al., Direct writing of birefringent elements by ultrafast laser nanostructuring in multicomponent glass, *Appl. Phys. Lett.*, 108(7), pp. 071905, (2016)
- [5] S.S. Fedotov et al., 3-bit writing of information in nanoporous glass by a single sub-microsecond burst of femtosecond pulses *Opt. Lett.*, 43(4), pp. 851-854, (2018)
- [6] A. Messaadi et al., Optical system for measuring the spectral retardance function in an extended range, *J. Eur. Opt. Soc.-Rapid Publ.*, 12, pp. 1-9, (2016)

Infrared random laser based on artificial Rayleigh fiber

D.V. Ryakhovskii¹, S.M. Popov¹, A.A. Rybaltovskii^{2,3}, Yu. K. Chamorovskii², O.V. Butov²

1- Kotelnikov Institute of Radioengineering and Electronics of RAS, Vvedensky Sq. 1, 141190 Fryazino, Russia

2- Kotelnikov Institute of Radioengineering and Electronics of RAS, Mokhovaya 11-7 St, 125009 Moscow, Russia

3- Prokhorov General Physics Institute of the RAS, Vavilova 38 St., 119333 Moscow, Russia

dryh97@mail.ru

Optical fibers (OF) have their application in various fields of science and technology. In addition to the use of optical fibers in information systems (communication lines and fiber sensors), the use of optical fibers in laser systems is also developing. A new direction in the development of laser systems has become the so-called. “Random lasers” [1–2]. This direction has become a subject of great interest for researchers around the world due to the ability of random fiber lasers to generate light with unique performance characteristics without imposing strict requirements on the optical cavity. In such lasers, amplification is achieved due to the effects of Raman scattering [1] or SBS [2]. Due to the fact that the Rayleigh scattering coefficient is extremely small (it provides reflection), in such random lasers the cavity length is usually 10-100 km for SMF-28 type OF. New development trends are associated with the transition to lasers with a cavity based on short (5-20 meters) artificial Rayleigh OF [3] (OFs containing an array of fiber Bragg gratings - FBGs) inscribed during drawing process. This article is devoted the evolution of our previous works, including an optimization of random laser cavities, based on artificial Rayleigh fiber and adapted to the telecom conventional wavelength range (also known as “C-band” range). The main novelty is the development of artificial Rayleigh fiber on the basis of a special photosensitive Er-doped OF with a germanophosphosilicate core matrix.

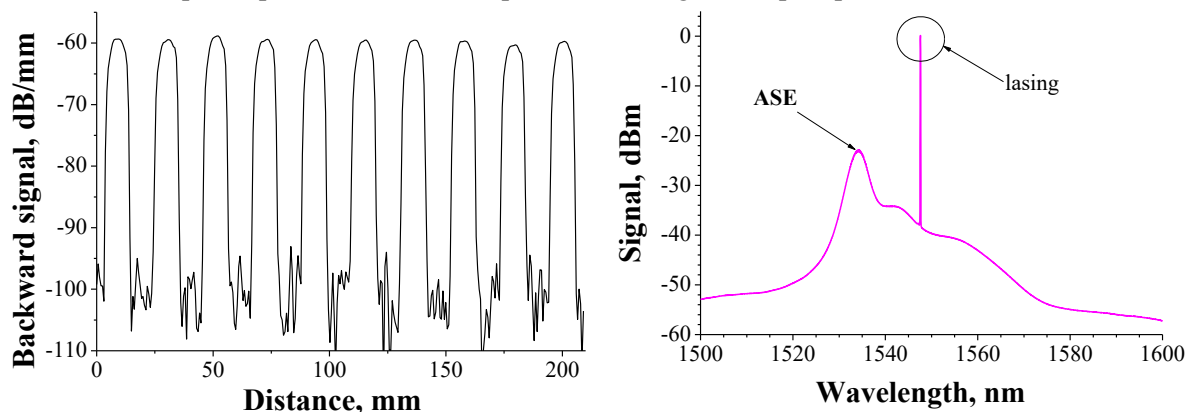


Fig. 1. Laser cavity structure – left. Laser emission spectrum at pumping on 976 nm (30 mW) - right.

The lasing cavity structure investigated by OFDR technique is shown in Fig 1 (left). The FBGs inscription contrast (excess of the return signal over the Rayleigh level) is 43 dB. The length of the laser’s cavity is 6 meters (600 FBGs). The phase mask period is 1070 nm. Core/cladding diameter – 5/125 μm . OF’s cutoff wavelength is 900 nm. The laser has a half-opened cavity extended by the wavelength-matched 90% FBG. The emission spectrum obtained under 976 nm “backward”-pumping is shown in Fig. 1 (right). The laser has a 1548 nm single emission peak and a slope efficiency of 33%. The operation mode is continuous-wave like showed previously [3]. The linewidth measured by self-heterodyne technique is less 1 kHz. These random fiber lasers can operate continuously at room temperature for a long time (at least tens of minutes), which is extremely important from the point of view of the prospects for its use as a compact source of high coherence optical radiation.

The work was carried out within the framework of the Kotelnikov IRE RAS state task. The work of A.A.R. is supported by RSF №22-19-00511 in part of producing preforms.

[1] S. Turitsyn, S. Babin, A. El-Taher, et al., Random distributed feedback fibre laser, *Nature Photonics* V.4, pp. 231–235 (2010).

[2] A. Fotiadi, An incoherent fibre laser, *Nature Photonics* 4, pp. 204–205 (2010).

[3] S.M. Popov, et al., Random lasing in a short Er-doped artificial Rayleigh fiber, *Results in Physics* 16, 102868 (2020).



LS-O-4

The features of sine operation regime in moderately erbium doped fiber lasers

Smirnov A.M.^{1,2}, Shikin A.S.¹, Przhialkovskii D.V.¹, Rybaltovsky A.A.^{1,3}, Dorofeenko A.V.^{1,4,5,6}, Butov O.V.¹

1- Kotelnikov Institute of Radioengineering and Electronics of RAS, Mokhovaya 11-7, Moscow 125009, Russia

2- Faculty of Physics of Lomonosov Moscow State University, Leninskie Gory 1-2, Moscow 119991, Russia

3- Prokhorov General Physics Institute of RAS, FORC, Vavilova 38 Moscow, 119991, Russia

4- Moscow Institute of Physics and Technology, 19 Institutskiy pereulok, Dolgoprudny 141700, Russia

5- Institute for Theoretical and Applied Electromagnetics RAS, 13 Izhorskaya, Moscow 125412, Russia

6- Dukhov Research Institute of Automatics, 22 Sushevskaya, Moscow 127055, Russia

*E-mail: alsmir1988@mail.ru

The paper presents the results of an experimental study of the moderately erbium doped fiber lasers with short resonators operation features. Operation regimes in the case of 976 nm wavelength pump have been investigated. The dependence of the parameters and regimes of operation on the cavity length and pump power, namely the transition from pulsed to CW lasing, is investigated.

The operation features study of single-frequency erbium fiber lasers of the 1.5 μm optical range is necessary to control and reduce the lasing linewidth which is required in modern fiber optics, allows them to be used for optical sensors, optical communication lines and spectroscopy.

The erbium doped fiber used in our work was made from a preform with a moderate concentration of erbium in the core (absorption at 1530 nm wavelength ≈ 17 dB/m, ≈ 0.03 mol.% Er_2O_3). Based on this fiber three erbium lasers were fabricated according to the classical Fabry-Perot scheme with two Bragg gratings (FP-EDFL) with a cavity length of 28 mm (Bragg gratings were inscribed using femtosecond point-by-point technology), 60 mm and 170 mm (Bragg gratings were inscribed by the UV technique by the radiation of an excimer ArF laser). The lasing wavelength of fiber lasers was determined by the period of the Bragg gratings and ranged from 1539 to 1551 nm.

The laser operation regime at low pump power corresponds to passive Q-switching, and when the pump power increases the operation switched to CW with sine modulation. The dependence of the pulse frequency and sine modulation on the cavity length and pump power at room temperature is established. The formation of a pulsed operation regime is characteristic of erbium heavily doped lasers due to accelerated depopulation of the excited erbium level in sight of the up-conversion at the lasing wavelength. Up-conversion proceeds most effectively when pairs of erbium ions (mini-clusters) are formed in the active fiber [1, 2]. The switching between pulsed and CW regimes at room temperature is achieved by reducing the doping level of the active fiber and increasing the pumping power, which together reduces the proportion of up-conversion in the process of the excited erbium level release [3,4].

[1] F. Sanchez, P. Le Boudec, P.-L. François and G. Stephan, Effects of ion pairs on the dynamics of erbium-doped fiber lasers, Phys. Rev. A, vol. 48, pp. 2220-2229 (1993).

[2] F. Sanchez and G. Stephan, General analysis of instabilities in erbium-doped fiber lasers, Phys. Rev. E, vol. 53, pp. 2110-2122 (1996).

[3] A.M. Smirnov, A.P. Bazakutsa, Y.K. Chamorovskiy, I.A. Nechepurenko, A.V. Dorofeenko and O.V. Butov, Thermal Switching of Lasing Regimes in Heavily Doped Er^{3+} Fiber Lasers, ACS Photonics, vol. 5, № 12, pp. 5038-5046 (2018).

[4] A. Smirnov and O. Butov, Pump and thermal impact on heavily erbium-doped fiber laser generation, Optics Letters 46, pp. 86-89 (2021).



Harmonic mode-locking and multi pulse generation of Holmium-doped fiber laser with the ring cavity

S.A. Filatova^{1,*}, V.A. Kamynin¹, A.D. Zverev¹, A.I. Lobanov¹, P.V. Balakin^{1,2}, Y.G. Gladush³,
D.V. Krasnikov³, A.G. Nasibulin³, V.B. Tsvetkov¹

1 - Prokhorov General Physics Institute of the Russian Academy of Sciences, 38 Vavilov Str., 119991 Moscow, Russia

2 - MIREA - Russian Technological University, 78 Vernadsky Avenue, 119454 Moscow, Russia

3 - Skolkovo Institute of Science and Technology, Nobel Str. 3, Moscow, 121205, Russia

*email address: filatova@kapella.gpi.ru

High repetition-rate mode-locked fiber lasers operating in the 2-3.5 μm spectral range are in demand for numerous applications in the fields of science and technology because of ultrashort pulse duration and compact size. Such sources are promising for burst-mode generation, polymer micromachining, medicine, free space optical communication, and etc [1]. Holmium-doped (Ho) fiber takes main advantages of longer gain wavelength up to 2.2 μm and larger emission cross-section. The simplest methods to increase repetition rate of passively mode-locked fiber laser are shortening cavity length and harmonic mode-locking (HML) [2].

This work focuses on the study of different types of passive mode-locking in a Ho-doped fiber laser with the ring cavity and the possibilities of obtaining harmonic mode-locking. Passive mode-locking was implemented based on the polymer-free single-walled carbon nanotubes (SWCNT) saturable absorber [3], nonlinear polarization evolution (NPE) and hybrid mode-locking [4].

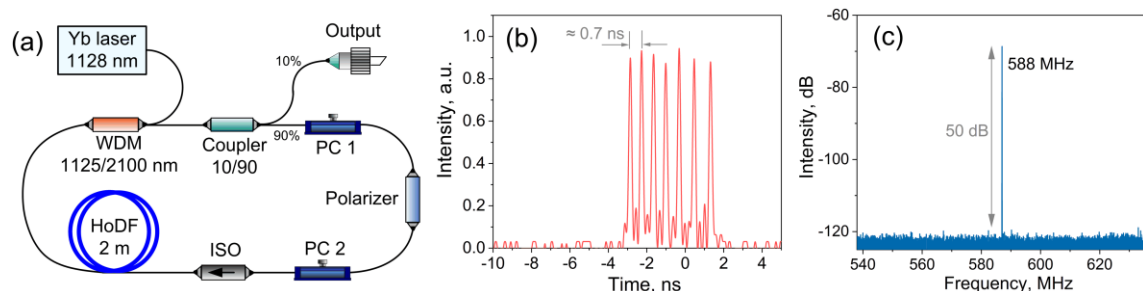


Fig. 1. (a) Experimental setup of the NPE mode-locked Ho-doped fiber laser, (b) oscillogram of the burst-mode generation with 7 ultrashort pulses in the burst, (c) radio frequency spectrum at the repetition rate of 588 MHz.

The cavity of Ho-doped fiber lasers consists of 2 m Ho-doped fiber pumped by the Yb-doped fiber laser at 1128 nm through a 1125/2100 nm wavelength division multiplexer (WDM), fiber coupler, polarization controllers (PC), isolator, polarizer in the case of NPE mode-locking as in Fig. 1(a), and FC/APC connectors with saturable absorber. In the case of hybrid mode-locking, NPE and SWCNT were combined in one cavity. The cavities length varied in the range of 7.5–8.8 m, depending on the mode-locking type.

In the case of NPE mode-locking, the burst-mode generation with a pulse repetition rate of ≈ 1.4 GHz and varying number of ultrashort pulses within a burst (up to 10 pulses) was obtained (Fig. 1(b)). The maximum pulse repetition rate obtained at a pump power of 2.9 W was 588 MHz with a signal-to-noise ratio (SNR) of ≈ 50 dB (Fig. 1(c)). In the case of hybrid mode-locking, the maximum pulse repetition rate obtained at a pump power of 3.2 W was 614 MHz with a SNR of ≈ 60 dB. In the case of mode-locking based on SWCNT, single- and dual-wavelength generation, as well as the unstable harmonic mode-locking with a maximum pulse repetition rate of ≈ 166 MHz, were obtained. The dependences of pulse repetition rate and average output power on the pump power were obtained.

This study was funded by a grant of the Russian Science Foundation № 22-72-00126 (development and study of fiber lasers characteristics).

[1] D.C. Kirsch, S. Chen, R. Sidharthan, Y. Chen, S. Yoo, M. Chernysheva, Short-wave IR ultrafast fiber laser systems: Current challenges and prospective applications, *Journal of Applied Physics*, **128**(18), 180906 (2020).

[2] X. Liu, M. Pang, Revealing the buildup dynamics of harmonic mode-locking states in ultrafast lasers, *Laser & Photonics Reviews*, **13**(9), 1800333 (2019).

[3] Y. Tian, A.G. Nasibulin, B. Aitchison, T. Nikitin, J.V. Pfaler, H. Jiang, Z. Zhu, L. Khriachtchev, D.P. Brown, E.I. Kauppinen, Controlled Synthesis of Single-Walled Carbon Nanotubes in an Aerosol Reactor, *J. Phys. Chem. C*, **115**(15), 7309–7318 (2011).

[4] S.A. Filatova, V.A. Kamynin, N.R. Arutyunyan, A.S. Pozharov, E.D. Obraztsova, P.A. Itrina, V.B. Tsvetkov, Comparison of mode-locking regimes in a holmium fibre laser, *Quantum Electronics*, **48**(12), 1113 (2018).

LS-O-6

Optimization of the length of the cavity of an erbium fiber laser with a sub-GHz repetition rate of ultrashort pulses

A. Zverev¹, V. Kamynin¹, V. Tsvetkov¹, S. Sverchkov¹, V. Velmiskin², B. Denker¹, Y. Gladush³, A. Nasibulin³

1- Prokhorov General Physics Institute of the Russian Academy of Sciences, Russia

2- Scientific Center for Fiber Optics, Russian Academy of Sciences, E.M.Dianova of the Russian Academy of Sciences, Russia

3- Skolkovo Institute of Science and Technology, Moscow, Russia

Main author email address: izverevad@gmail.com

Fiber sources of ultrashort pulses (USPs) with a sub-GHz repetition rate are in demand for various applications, including analog-to-digital converters[1], study of supercontinuum generation[2], and high-resolution microscopy[3]. The repetition frequency of the gigahertz level can be obtained by implementing harmonic mode locking or in lasers with an extremely short cavity based on heavily doped active fibers and hybrid components.

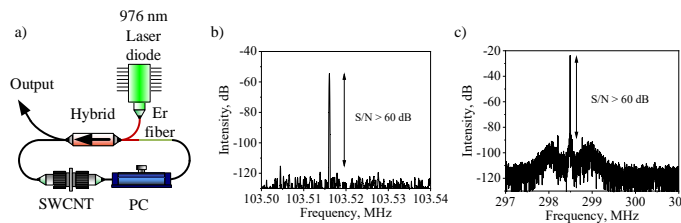


Fig. 1. a) Initial scheme of an erbium fiber laser (resonator length 1.93 m). SWCNT - connected ferrules, between which there are single-walled carbon nanotubes; A hybrid is a fiber element that combines the properties of a WDM, an insulator and coupler; PC - polarization controller. The pumping direction is shown in red. b) RF spectrum of initial signal; c) RF spectrum of final signal (resonator length 0.6 m).

In this work, we studied the possibility of increasing the repetition rate of ultrashort pulses by using a heavily doped active fiber and a hybrid (optical splitter (coupler), wavelength division multiplexer (WDM), insulator) in an erbium fiber laser with a ring cavity. The initial experimental setup is shown in Fig. 1 (a). As an active medium, we used a 12 cm the composite fiber with a phosphate glass core with a high concentration of erbium ions and a silica glass cladding. The composite fiber was pumped by the laser diode at a wavelength of 976 nm through a hybrid. The coupler split was 85/15 (15% yield). To be able to adjust the generation mode, the circuit included a polarization controller. Passive mode locking was provided by single-walled carbon nanotubes synthesized in an aerosol placed between two FC/APC optical connectors (SWCNT [4]). The resonator length in this case was exactly 1.93 m.

The laser generated ultrashort pulses with a repetition rate of 103.5 MHz (RF spectrum of the signal Fig. 1 (b)) and a duration of 5 ps at a central wavelength of 1535 nm. The spectrum width was 1 nm (Fig. 1 (b)). The output radiation power was 0.48 mW. With a decrease in the resonator length, stable modes were also obtained with ultrashort pulse repetition frequencies of 129 MHz (resonator length $L_r = 1.55$ m), 153 MHz ($L_r = 1.3$ m), 214 MHz ($L_r = 0.9$ m), 247 MHz ($L_r = 0.8$ m).

Next, we removed the polarization controller from the circuit and reduced the length of the resonator as much as possible (without changing the length of the active fiber) to 0.6 m.

In this case, we also managed to obtain a stable mode of single-pulse generation. The laser generated ultrashort pulses with a repetition rate of 298.5 MHz (RF spectrum of the signal Fig. 1 (c)) and a duration of 1.6 ps at a central wavelength of 1543 nm. The spectrum width was 1.3 nm. The output radiation power was 1.64 mW.

Thus, we have carried out an optimization of the ring laser circuit, as a result, sources with a repetition rate of ultrashort pulses from 100 to 300 MHz have been obtained.

The work is supported by the Russian Science Foundation (#23-79-30017)

[1] Valley, G. C. Photonic analog-to-digital converters. *Optics express*, 15(5), 1955-1982, (2007).

[2] Korobko, D., et al. "Control of supercontinuum generation due to soliton propagation in fibers with varying dispersion." *Optik*: 171032, (2023).

[3] Potma, Eric O., et al. "High-sensitivity coherent anti-Stokes Raman scattering microscopy with two tightly synchronized picosecond lasers." *Optics letters* 27.13,1168-1170, (2002).

[4] Kaskela, Antti, et al. "Aerosol-synthesized SWCNT networks with tunable conductivity and transparency by a dry transfer technique." *Nano letters* 10(11), 4349-4355 (2010).



Resonant loss reduction of high-order modes in all solid band gap fibers

G. Alagashev, A. Pryamikov

Prokhorov General Physics Institute of the Russian Academy of Sciences, 38 Vavilova Str. Moscow, Russia

alagashevgrigory@gmail.com

All solid band gap fiber (ASBGF) is a relatively simple waveguide micro - structure that can confine radiation in the solid core. The cladding of such fiber consist of the rods with larger refractive index than the surrounding glass matrix form a cladding of such a fiber. It was shown that in the case of ASBGF with even a small number of the cladding rods located on a some circle it is possible to obtain resonant low loss regime for the fundamental core mode for certain values of geometric parameters [1]. In this work we have studied ASBGF with the following parameters: number of rods is $N = 6, 9$, radius of the circle where rods are located is $R = 10\text{-}25 \mu\text{m}$, radius of a single rod is $r = 2 \mu\text{m}$, refractive index of glass matrix is $n_{\text{glass}} = 1.45$, refractive index contrast is $\Delta n = +0.05$, vacuum wavelength is $\lambda = 1 \mu\text{m}$. The cross section of the fiber is shown in Figure 1. Leakage loss of the fundamental core mode (HE_{11}) and high-order mode (HE_{21}) was calculated by multipole method (solid curves) and finite element method (markers) in COMSOL (Fig. 2). It is shown that when the number of rods in the cladding is increased the resonant loss reduction is observed for the high-order modes as well. Thus for $N = 9$ there are geometric parameters at which the HE_{21} mode has leakage loss lower than those of the fundamental core mode. The properties of such fibers with reduced high-order modes loss can be used for dispersion management and sensing [2,3]

The study was funded by Russian Science Foundation under project # 22 – 22 - 00575.

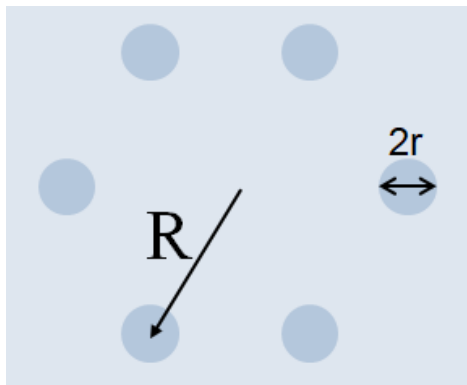


Fig. 1. Cross-section

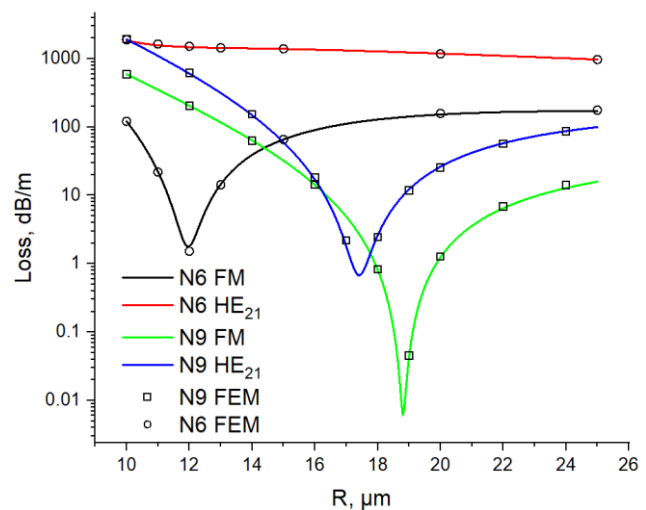


Fig. 2. Leakage loss

[1] A. Pryamikov, G. Alagashev, G. Falkovich, et al. Light transport and vortex-supported wave-guiding in micro-structured optical fibres, *Sci Rep*, 10, 2507 (2020).

[2] A. J. Verhoef, L. Zhu, S. M. Israelsen, L. Grüner-Nielsen, A. Unterhuber, W. Kautek, K. Rottwitz, A. Baltuška, and A. Fernández. Sub-100 fs pulses from an all-polarization maintaining yb-fiber oscillator with an anomalous dispersion higher-order-mode fiber. *Optics express*, 23(20):26139–26145 (2015).

[3] E. Li, X. L. Wang, and C. Zhang. Fiber-optic temperature sensor based on interference of selective higher-order modes. 2006.



LS-O-8

High-purity A^VB^{VI} chalcogenide glasses as a material for Mid-IR fiber optics

I. Skripachev¹, V. Pontnichenko², M. Churbanov¹

¹*G.G. Devyatikh Institute of Chemistry of High-Purity Substances, Russian Academy of Sciences, 603951, Nizhny Novgorod, Box-75, Tropinin st., 49,*

²*E.M. Dianov Fiber Optics Research Center, Moscow, Vavilov St., 38*

skripachev@ihps.nnov.ru

Chalcogenide glasses (ChG) consist of individual chalcogenides of III-V group elements (B, Ga, La, Ge, As, Sb) and of their mixtures. They consider as perspective optical materials since 1950 when high transparency of As₂S₃ glass in the middle infrared (IR) was obtained by purification of this compound [1].

In the 80's low optical losses were predicted for ChG, being at the level 0.1-0.05 dB/km at the 4-6 mkm wavelength region [2,3]. High non-linearity of the optical properties also have been observed. Optical fibers made of the glasses with such characteristics provided the new possibilities at solving of several problems in optics and optoelectronics.

The properties of ChG that are the most important for fiber optics application (optical transparency, laser beam energy threshold and mechanical strength) are very sensitive to impurities content in the ChG.

The content of some strongly absorbing impurities (hydrogenous and carboneous compounds, oxygen, carbon) must not exceed 10⁻²-10⁻³ ppm at. The content of particles with the size not larger than 100 nm is limited at the level 10¹-10³ cm⁻³ [4].

Due to efforts of researches high pure ChG were obtained, the content of limiting impurities did not exceed 10⁻²-10⁻³ ppm wt. in the best samples of the glasses. Optical fibers with minimum loss 12-14 dB/km in the 3-5 mkm wavelength region were fabricated from pure As-S glasses [4]. Optical fibers made of As-Se, Ge-As-S-Se and Ge-As-Se-Te glass have the minimum optical loss 40 – 150 dB/km in the 6-9 mkm wavelength region.

Chalcogenide glass optical fibers were tested as elements of various optical and optoelectronic devices [5].

The main goals of further developments in the field of high pure ChG and infrared optical fibers on its base are as follows:

- Search of the extrinsic loss sources that give contribution at the level 1-10 dB/km in the ChG of various systems. It means the evaluation of intrinsic contribution of the glass matrix as well as study of influence of defects in the fiber waveguide structure.
- Further decrease of the limiting impurities content in the ChG by 1-1.5 order in comparison with the level achieved as well as improvement of the glasses micro-homogeneity.
- Development of technologies that provide fabrication of ChG and optical fibers with reproducible set of exploitation parameters.
- Development of new kinds of optical fibers that use the unique properties of ChG. Among them are microstructured fibers, PCF, ChG fibers with the core doped by rare earth and transitional metals. Such kinds of ChG fibers are required for fabrication of IR fiber lasers, optical amplifiers and converters of IR radiation. Some brand new application of IR ChG fibers in the analytical systems of new generation will be shown.

The research was carried out with the support of the Russian Science Foundation, RSF grant No. 22-13-00226.

1. R. Frerichs, Phys. Rev., 1950, 78, p.643.

2. E.M.Dianov, M.Yu.Petrov, V.K. Sysoev and V.G. Plotnichenko. Quantum Electronics (Rus. Journ.), 1982, Vol.9, No. 4, 798.

3.M.E. Lines, J. Appl.Phys., 1984, v.55, No.11, p.4058.

4.G.E. Snopatin, M.F. Churbanov, A.A. Pushkin et.al. J. of Optoelectronics and Advanced Materials, 2009, v.3, No.7, p.889.

5.Chalcogenide glasses. Preparation, properties, applications, Edited by J.L. Adam and X. Zhang. Woodhead publishing Limited. 2014.

LS-O-9

Nonlinear absorption and refraction study of quaternary barium chalcogenide BaGa₂GeSe₆ crystal at 1053 nm in nanosecond regime**N. Kostyukova^{1,2,*}, E. Erushin^{1,2}, A. Boyko^{1,2}, A. Kostyukov¹, A. Kiryakova², D. Badikov³***1- Novosibirsk State University, Russia, 630090, Novosibirsk, 1, Pirogova str.**2- Institute of Laser Physics of the SB of the RAS, Russia, 630090, Novosibirsk, prosp. Ac. Lavrentiev, 15B**3- Kuban State University, 149 Stavropolskaya Str., 350040 Krasnodar, Russia*** n.duhovnikova@gmail.com*

Barium chalcogenide crystals are promising nonlinear media for efficient parametric down-conversion in the mid-IR range [1]. Nonlinear absorption and refraction that occur in crystals upon interaction with high-power laser radiation can lead to distortion of the transverse distribution of the laser beam intensity in the crystal and the occurrence of self-focusing effects and mismatch of the optical cavity, and thereby reduce the efficiency of conversion. Therefore, it is important to take them into account when designing optical set-ups of highly efficient mid-IR tunable optical parametric oscillators (OPOs). This work is devoted to an experimental study of the nonlinear optical characteristics of the BaGa₂GeSe₆ (BGGSe) crystal by Z-scan technique proposed in the work [2].

The radiation source was a diode-pumped Q-switched Nd:YLF laser produced pulses with a duration of 6 ns and energy up to 1 mJ at 1.053 μm with repetition rate varied from 0.1 to 4 kHz. The measured beam quality factor M^2 was around 1.4 and the radiation's linewidth was 227 pm (approximately 2 cm^{-1}). The BGGSe plate was cut at $\varphi=30^\circ$ and $\theta=30^\circ$ with wedge of all plates was no more than 10 arc seconds. The surface quality can be estimated as 60–40 scratch and dig, and surface flatness was $\lambda/6$ at 633 nm. The both sides of tested plate have an Al₂O₃ antireflection (AR) coating centered at 1053 nm. Measured β and n_2 -values in the BGGSe plate with nanosecond 1053 nm laser pulses at different intensity are presented in Table 1.

Table 1. Measured β and n_2 -values in the BGGSe plate with nanosecond 1053 nm laser pulses at 1 kHz

I, MW/cm ²	Pol.	β , cm/GW	$n_2 \times 10^{-13}$, cm ² /W	$n_2 \times 10^{-10}$, esu
49,3	e-wave	5,59	5,79	3,615
	o-wave	-	3,34	3,34
84	e-wave	6,58	9,37	5,85
	o-wave	4,7	7,53	4,55
117	e-wave	6,71	12,57	7,86
	o-wave	5,08	9,93	5,68

A strong dependence of nonlinear absorption and refraction on the radiation intensity is observed. This may be related to thermal effects, which are most appeared at nanosecond pulses [3].

This work was supported by the Russian Science Foundation (Project no. 23-22-00368).

[1] V. Petrov, V. Badikov, D. Badikov, K. Kato, G. Shevyrdyaeva, K. Miyata, M. Mero, L. Wang, Z. Heiner, V. Panyutin, Barium nonlinear optical crystals for the mid-IR: characterization and some applications, J. Opt. Soc. Am. B, vol. 38, pp. B46-B58, (2021).

[2] M. Sheik-Bahae, A. A. Said, E. W. Van Stryland. High-sensitivity, single-beam n_2 measurements, Opt. Lett., vol. 14, p. 955 (1989).

[3] T. Olivier, F. Billard, and H. Akhouayri, Z-scan theoretical and experimental studies for accurate measurements of the nonlinear refractive index and absorption of optical glasses near damage threshold, Proc. SPIE 5273, Laser-Induced Damage in Optical Materials: 2003, (10 June 2004).



Gyrotrons: impossible is nothing

G.Denisov, A.Litvak, E.Tai, M. Glyavin and IAP RAS/GYCOM team

Institute of Applied Physics RAS (IAP RAS), 46 Ul'yanov str., Nizhny Novgorod, Russia
GYCOM Ltd., 46 Ul'yanov str., Nizhny Novgorod, Russia

glyavin@ipfran.ru

There are a number of topical scientific problems that require the creation of powerful sources of microwave electromagnetic radiation in the frequency range 0.1-1 THz. Gyrotrons are the most powerful radiation sources in the sub-THz and THz wavelength ranges. Despite the difficulties with the generation of high-intensity magnetic fields required for resonant conditions of electron-wave interaction in volumes sufficient to accommodate electron-optical and electrodynamics systems of gyro devices, the problem of shaping high-power electron fluxes with a high fraction of rotational energy and low velocity spread, and the problem of selective excitation of high-order operating modes, harmonic excitation, etc., the gyrotrons continue to be the object of intense research and show a significant potential for improving the characteristics of the generated radiation [1,2].

Gyrotrons are in demand for the ECR of plasmas in controlled-fusion installations, the creation of systems for high-gradient acceleration of electrons by terahertz waves, energy transfer using narrow beams of microwave radiation, spectroscopy, and diagnostics of various media.

The years 2021-2022 were marked by an increase in the number of requests for megawatt (MW) gyrotrons both from representatives of large thermonuclear facilities well known to the gyrotron community (ITER, KSTAR, EAST) and from a number of new projects (F4E, MAST-U). An explosive growth in the number of commercial companies that focus on obtaining thermonuclear energy by 2025-2030 should be mentioned [3].

The purpose of this paper is to present a number of the most striking achievements of the IAP RAS and GYCOM in the development of gyro devices, which include: i) testing a prototype MW level gyrotrons with a frequency of 230-250 GHz in a pulsed generation mode, ii) development and experimental tests of frequency locked operation regime with narrow spectrum line at different tubes, including 1MW/170GHz gyrotron; iii) development of a pulse compressor circuit for a high-power gyrotron and preliminary analysis of its key elements for provision of microwave radiation with a power level of about 100 MW and a pulse duration of about 10 ns; v) development and experimental investigation of high power and efficiency gyrotron based technological systems with magnetically shield solenoid and vi) analysis of new schemes for broadband frequency tuning and excitation of higher harmonics.

The gyrotron development is supported by the IAP RAS projects FFUF-2021-0001, FFUF-2022-0007. Development, manufacturing and experimental test of ITER gyrotrons are supported by project 17706413348230000070/45-393 in the frame of the work "Development, pilot production and supply of 8 sets of gyrotrons with magnets and auxiliary equipment for the ITER plasma heating and current drive ECR system".

[1] A. G. Litvak, G. G. Denisov and M. Y. Glyavin, "Russian Gyrotrons: Achievements and Trends", *IEEE Journal of Microwaves*, 1, 1, 260 (2021) DOI: 10.1109/JMW.2020.3030917

[2] Sabchevski, S., Glyavin, M., Mitsudo, S. *et al.* Novel and Emerging Applications of the Gyrotrons Worldwide: Current Status and Prospects. *J Infrared Milli Terahz Waves* **42**, 715–741 (2021) DOI: 10.1007/s10762-021-00804-8

[3] "The global fusion industry in 2022" Fusion Industry Association <https://www.fusionindustryassociation.org/about-fusion-industry> (available online 10.12.2022)

LS-O-11

Realization of Thin-film transistors by using laser deposition technologies**Prachi Sharma***School of Electronics Engineering (SENSE), Vellore Institute of Technology (VIT), Vellore, India**Email: prachi.sharma@vit.ac.in;
er.prachi22@gmail.com*

Thin film technologies have already grown into a big industry that is centered on the new generation of displays such as organic light-emitting diode (OLED) and liquid crystal display (LCD). On these display panels, a thin film transistor (TFT) basically controls the operation of each pixel forming the image.

To produce new generation large displays, an active matrix addressing scheme is used for display panels where pixels are located at row and column intersections in order to minimize capacitive losses in column and row lines. This addressing scheme basically consists of two TFTs per pixel, of which one is operated under continuous gate bias and hence requiring a high stability

The nanocrystalline silicon (nc-Si) is widely used as an active layer in TFT. The electron beam physical vapor deposition (EBPVD) process is used for nc-Si film deposition over conventional Plasma-enhanced chemical vapor deposition (PECVD) process to avoid high RF-power and hydrogen dilution that are needed in PECVD to facilitate silicon nano-crystallization which leads to deteriorated quality of the nc-Si film.

Nowadays, Molybdenum disulfide (MoS₂) has proven as the best alternative material as an active layer of TFT. MoS₂ is known as one of the oldest representatives of the transition metal chalcogenides (TMCs) family. Researchers fabricated the MoS₂ layers using a catalysis-free, economical, and environment-friendly pulsed laser deposition (PLD) technique for the realization of TFTs with high mobility, good I_{ON}/I_{OFF}, and low power consumption.

References:

1. **P Sharma**, N Tripathi and N Gupta, "Nanocrystalline silicon thin film prepared by e- beam evaporation for display application" *Journal of Materials Science: Materials in Electronics*, Springer, pp. 3891–3896, vol. 28, issue 4, 2017.
2. **P Sharma** and N Gupta, "Model for threshold voltage instability in top-gated nanocrystalline silicon thin film transistor" *Journal of Computational Electronics*, Springer, pp. 666- 671, vol. 15, issue 2, 2016.
3. S Kumar, N Tripathi, **P Sharma**, V Pavelyev, V Podlipnov, S Stafeev, P Mishra, D Shishkina, V Platonov, A Rymzhina, "Development of transition metal dichalcogenides for modern photodetector devices," *2021 International Conference on Information Technology and Nanotechnology (ITNT)*, Samara, Russian Federation, 2021, pp. 1-4, doi: 10.1109/ITNT52450.2021.9649438.
4. V Pavelyev, **P Sharma**, A Rymzhina, P Mishra, N Tripathi, "Advances in transition metal dichalcogenides-based flexible photodetectors" *Journal of Materials Science: Materials in Electronics*, Springer, pp. 24397–24433, vol. 33, 2022.



LS-O-12

On the origin of radial and tangential cracks in optical fiber preforms

G. Bufetova¹, A. Kosolapov², M. Yashkov³, A. Umnikov³, V. Velmiskin², V. Tsvetkov¹, I. Bufetov²

1- Prokhorov General Physics Institute of the Russian Academy of Sciences, 38 Vavilov Str., 119991, Moscow, Russia

2- Prokhorov General Physics Institute of the R A S, Dianov Fiber Optics Research Center

3- Institute of Chemistry of High-Purity Substances of the R A S, Nizhny Novgorod, Russia

bufetova@lsk.gpi.ru

It is known that the difference in the coefficients of thermal expansion between the cladding glass (α_1) and the core material (α_2) during sample cooling leads to the formation of tangential cracks if $\alpha_2 > \alpha_1$ and to the formation of radial cracks if $\alpha_1 > \alpha_2$ [1]. We propose to pay attention to the well-known phenomenon—the formation of so-called "stars" in the cross sections of fiber preforms based on silica glass with cores doped with relatively high concentrations of germania or alumina. On many preforms the formation of perturbations at the core-cladding boundary, having the form of "needles" or narrow channels filled with the core substance, is observed.

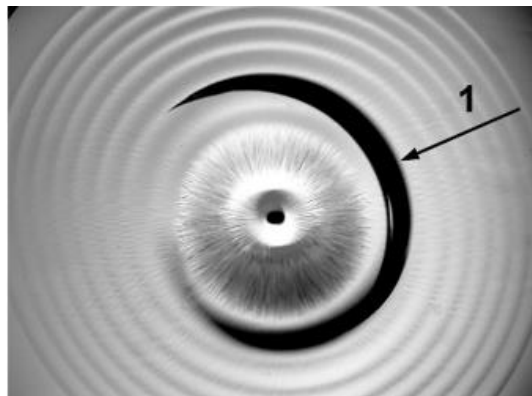


Fig.1. A cross section view with "star" and an annular crack around the core (1)

It is possible that mechanism of their formation could be as follows: in the cooling process due to high values of compressive stress in the still liquid core, cracks appear in a cladding (no longer liquid) directed mainly along the radius of the preform, which are immediately filled with the substance of the liquid core. It was shown [2] that refractive index of the core glass of the preform could increase up to ~ 1.75 in the visible spectral range at temperatures of $\sim 2000^\circ\text{C}$ (~ 1.46 at room temperature). This fact suggests that pressures close to or exceeding the ultimate strength of silica glass (~ 20 GPa) occur in the preform core region during the manufacturing process. Since the glass transition temperature of the core (silica glass with a high GeO_2 or Al_2O_3 doping level) is significantly lower than the glass transition temperature of SiO_2 , this may explain why the SiO_2 cladding cracks and the core material fills resulting cracks. The cross-section view of the preform (Fig. 1) testifies in favor of this assumption, since the star-shaped core (with rays along the radius) was formed during the manufacture of the preform at high temperature and indicates the compressive stress of the core material. At the same time, an annular crack along which the core is separated from the cladding, which appeared when cutting the cold preform, is a consequence of the tensile stress of the core at room temperature.

This work was carried out with the financial support of the Russian Science Foundation (grant № 19-12-00361)

[1] Von Kerkhof, F. Bruchentstehung und Bruchausbreitung im Glas. In Book *Glastechnische Fabrikationsfehler*, 4th ed.; p. 545 (2011).

[2] G. Bufetova, A. Kosolapov, M. Yashkov et al., Extra-High Pressure in the Core of Silica-Based Optical Fiber Preforms during the Manufacturing Process, *Photonics*, Vol. 10, No. 3, paper 335 (2023).



Influence of doping with lanthanides (Eu–Yb) on optical properties of samarium-scandium borate crystals

A.Y. Jamous^{1,2}, V.A. Svetlichnyi¹, A.B. Kuznetsov², A.E. Kokh²

1- Tomsk State University, Tomsk 634050, Russia

2- Sobolev Institute of Geology and Mineralogy SB RAS, Novosibirsk 630090, Russia

Email: ammarjamous2@gmail.com

Presently, borates, particularly rare-earth borates, are intensively investigated as potential functional materials for scintillators, phosphors, and nonlinear optical converters. This attention is due to their ease of preparation: chemical stability, short UV absorption edge, good optical and laser characteristics, as well as diversity of crystal structures. Owing to 5d-4f or 4f-4f transitions in several rare earth elements, it is possible to obtain light emission in different spectral regions. Especially, compounds containing Sm³⁺ are of interest for preparing red phosphors. Recently, we reported the optical properties of new two-cationic Sm_xSc_{4-x}(BO₃)₄ (SSB) solid solutions basing on the SmSc₃(BO₃)₄ compound [1]. In this work, lanthanides-doped samarium-scandium borates (RE:SSB) are presented. The effect of doping with various lanthanides both on the spectral properties of Sm³⁺, and on the efficiency of second harmonic generation (SHG) is determined.

Crystals with general formula RE_xSm_ySc_z(BO₃)₄ (x+y+z = 4, RE = Eu–Yb) were grown by TSSG method. XRD analyze showed that they are nonlinear biaxial monoclinic crystals. The absorption and photoluminescence (PL) were investigated in IR-Vis-UV regions. Additionally, the SHG of Nd:YAG laser radiation (1064 nm, 7 ns) was studied using the Kurtz-Perry powder technique [2].

All absorption bands that are corresponding to electron transitions from the ⁶H_{5/2} ground state to several excited states of Sm³⁺ were observed. The most intense absorption peak corresponding to the ⁶H_{5/2} → ⁴F_{7/2} transition was located at 405 nm. For various RE:SSB no spectral changes of Sm³⁺ absorption bands were observed. All characteristic absorption transitions for other RE³⁺ were also observed and labeled with their corresponding energy levels. In order to evaluate the emission caused clearly by Sm³⁺ ions, the PL excitation spectra were recorded for the 649 nm emission, hence the excitation wavelength 407 nm was chosen to record PL spectra. No shifts or spectral changes of Sm³⁺ emission peaks were observed for all RE:SSB, excepting Eu:SSB. It is due to the high luminescence of Eu³⁺ excited by 407 nm light. The two strongest Sm³⁺ fluorescence peaks are located at 605 and 649 nm, which correspond to relaxation from ⁴G_{5/2} to ⁶H_{7/2} and ⁶H_{5/2} respectively. Comparing Sm³⁺ fluorescence intensities for various RE:SSB one can conclude that doping with lanthanides with higher atomic number leads to lower Sm³⁺ fluorescence intensity (table 1).

The Kurtz-Perry powder test showed that in all grown crystals the phase matching is achieved, and all they have high SHG efficiencies (table 1) excepting Gd:SSB. The nonlinear susceptibility depends on the material density, and therefore on molar mass of constituents, RE/Sm/Sc ratio and the unit cell volume. The location and orientation of [BO₃] unites in crystals also effect. All RE:SSB compounds are monoclinic, but the point group still needs to be clarified. Furthermore, the composition and unit cell parameters have to be measured. Thus, at this stage, there is no enough information to explain the low d_{eff}(Gd:SSB). The relatively lower SHG efficiencies for Dy:SSB and Er:SSB could be explained by absorption at the pump and second harmonic wavelengths respectively.

Table 1 – Relative fluorescence intensity of Sm³⁺ (in percent with respect to the Eu:SSB) and d_{eff} values relative to LBO.

RE	Eu	Gd	Tb	Dy	Ho	Er	Tm	Yb	
λ _{em} (nm)	605 nm	100	73	78	32	23	27	21	14
	649 nm	100	82	92	39	22	30	25	16
d _{eff} /d _{eff} (LBO)	0,9541	0,4572	0,8416	0,7624	0,9201	0,7733	0,8575	0,8988	

This work was supported by the RSF project (№ 23-19-00617).

[1] A. B. Kuznetsov, K. A. Kokh, N. G. Kononova et. al. Polymorphism in SmSc₃(BO₃)₄: Crystal structure, luminescent and SHG properties, J. Alloys Compd, 851, Art. No. 156825, (2021).

[2] Kurtz S.K. and Perry T.T. A Powder Technique for the Evaluation of Nonlinear Optical Materials, J. Appl. Phys. 39, 3798–3813, (1968).

Spectroscopic properties of Cr²⁺ ions in Zn_{1-x}Mn_xSe solid solutions

M.E. Doroshenko¹, H. Jelinkova², A. Riha², K. Pierpoint¹

1- Prokhorov General Physics Institute of the Russian Academy of Sciences, Vavilov Street 38, Moscow Russia

2- Czech Technical University in Prague, Břehová 7, Prague, Czech Republic

Main author email address: kmartynova19@gmail.com

Over the last few decades, the development of ZnSe:Cr²⁺ tunable lasers that find a wide range of practical applications has made great progress. Maximum powers in excess of 140 W and efficiencies up to 60%, as well as the generation of ultrashort pulses (43 fs), have recently been demonstrated [1]. The benefits of Cr²⁺ ions in A^{II}B^{VI} materials (such as ZnS, CdSe, CdMnTe, e.t.c. [2–4]) include very broad absorption and emission spectra with a high cross-section, negligible excited-state absorption, and a relatively long lifetime that is only mildly dependent on temperature. The interest in the search for new A^{II}B^{VI} matrices and their solid solutions doped with Cr²⁺ is associated with the possibility to modify the chromium ions properties, thereby covering other spectral ranges. This work aims to investigate the Cr²⁺ ions spectroscopic properties in a range of cubic Zn_{1-x}Mn_xSe ($x = 0-0.4$) solid solutions.

The absorption and fluorescence spectra were measured at room temperature for a wide range of Zn_{1-x}Mn_xSe:Cr²⁺ ($x = 0-0.4$) samples. It was shown that with an increase in Mn content x , the maxima of both absorption and fluorescence spectra move practically linearly toward lower energies at a rate of roughly 30 cm⁻¹ for every 10% of Mn (see Fig. 1 for example). This shift is likely caused by the decrease in crystal field strength in Zn_{1-x}Mn_xSe solid solution with x due to the higher value of the lattice parameter and the lower position of the upper ⁵E Cr²⁺ ion level.

The temperature dependence of Cr²⁺ ions decay time was measured over a broad temperature range. Examples of the resulting curves for three samples with Mn content $x = 0.05, 0.3, \text{ and } 0.4$ are presented in Fig. 2. As can be seen, the decay rate of Cr²⁺ ions is almost independent of temperature for all samples up to about 240 K. The decrease in decay time with temperature starts earlier for samples with higher Mn content. The value of the ΔE_a gap between the bottom of the Cr²⁺ ion ⁵E configuration curve and the intersection of the ⁵T₂ and ⁵E curves was estimated, and the observed temperature dependence was associated with a ΔE_a gap decrease with Mn content (x) increase, resulting in stronger non-radiative quenching of Cr²⁺ ion fluorescence.

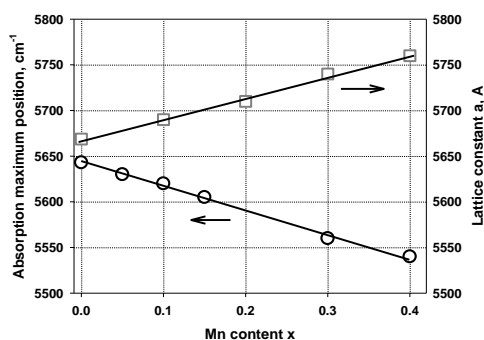


Fig. 1. Cr²⁺ ions absorption line maxima position (circles) and lattice constant a (squares) in Zn_{1-x}Mn_xSe crystal for various Mn content (x).

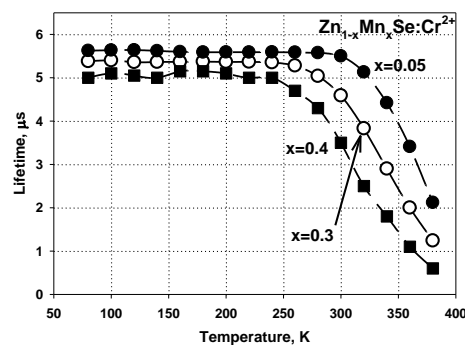


Fig. 2. Temperature dependence of Cr²⁺ ions fluorescence decay time in Zn_{1-x}Mn_xSe crystal for different Mn content x .

This work was supported by Russian Science Foundation Project № 23-22-00236.

[1] S. B. Mirov et al. Frontiers of Mid-IR Lasers Based on Transition Metal Doped Chalcogenides, IEEE Journal of Selected Topics in Quantum Electronics, vol. 24 (5), 1601829, (2018).

[2] L.D. DeLoach, R.H. Page, G.D. Wilke, S.A. Payne, and W.F. Krupke, Transition metal-doped zinc chalcogenides: spectroscopy and laser demonstration of a new class of gain media, IEEE Journal of Quantum Electronics, vol. 32 (6), pp. 885-895, (1996).

[3] V.I. Kozlovsky, Y.V. Korostelin, Y.P. Podmar'kov, Y.K. Skasyrsky, M.P. Frolov, Middle infrared Fe²⁺:ZnS, Fe²⁺:ZnSe and Cr²⁺:CdSe lasers: new results, Journal of Physics: Conference Series, vol. 740, 012006, (2016).

[4] M.E. Doroshenko, V.V. Osiko, H. Jelinkova, M. Jelinek, M. Nemeč, J. Sulc, N.O. Kovalenko, A.S. Gerasimenko, V.M. Puzikov, Spectroscopic and laser properties of Cr²⁺ ions in Zn_{1-x}Mg_xSe solid solutions, Optical Materials, vol. 47, pp. 185-189, (2015).

LS-O-15

The lifetime value of the terminal Nd:YAG laser level measured from direct gain saturation observations

V.B.Morozov, A.N.Olenin, D.V.Yakovlev

*Physics Faculty of M.V.Lomonosov Moscow State University, 119899 Leninskiye Gory, Moscow, Russia
morozov@phys.msu.ru*

Nd:YAG have been one of the most popular laser media for several decades due to the successful combination of useful properties of both the activator and the base crystal. Laser generation most often occurs between the Stark sublevels of the ${}^4F_{3/2} \rightarrow {}^4I_{11/2}$ transition with the strongest line at a wavelength of about 1.064 μm . Owing to relatively long radiation lifetime of the upper laser level ($\sim 230 \mu\text{s}$) Q-switching is the most commonly used regime in Nd:YAG lasers. This type lasers generate pulses of nanosecond duration (typically 10-30 ns), and are widely used in scientific research, technological, medical, pulse laser ranging and other applications.

Regarding the lifetime value of the lower laser level, there is no common consensus here and various considerations were discussed. Non-radiative transitions within the ${}^4I_{11/2}$ multiplet are characterized by times $\ll 10^{-8}\text{s}$, while for the transition between ${}^4I_{11/2}$ and the lower ${}^4I_{9/2}$ multiplet $\sim 10^{-8}\text{s}$ is suitable as a first approximation. This is much shorter than the lifetime of the upper laser level and usually does not exceed the pulse duration with Q-switching. That is, such an approximation is quite suitable in many practical cases for the characteristics of an ideal 4-level system. Indeed, this transition in Nd:YAG is usually regarded as a classic example of the 4-level system.

The transition linewidth of $\sim 4.5 \text{ cm}^{-1}$ at a temperature of 300K makes the Nd:YAG crystal suitable also for generating picosecond pulses. With use of passive or active mode locking in Nd:YAG lasers, pulses of from ~ 10 to ~ 100 ps durations can be produced. Typical applications of such lasers are scientific research, micromachining, remote precision laser ranging, cosmetology and others.

The generation and amplification of picosecond pulses shorter than the lower laser level lifetime are essentially nonstationary processes. In fact, on this time scale the system operates according to a three-level scheme. In the case of the arrival of an amplified pulse of energy close to the saturation energy, the populations of the upper and lower levels tend to equalize. The amplifying ability is partially restored only after a time corresponding to the lower level depopulation time. Thus, the problems of efficient amplification of ultrashort pulses in two-pass, multi-pass and regenerative amplifiers are essentially nonstationary if the time between successive passes of the amplified pulse through the amplifying medium is comparable to the lower level relaxation time.

Thus, the lifetime of the lower laser level refinement is of both fundamental and practical importance for common activating ions and various crystalline and glass matrices. The transition at 1.064 μm in Nd:YAG is of obvious interest in this respect, and quite a lot of papers have been published aimed its terminal level lifetime clarification. The results are distributed from 500 ns to 170 ps, with most of the results being significantly just the lower estimate. Such a broad scatter is obviously due to the use of estimate approaches based, typically, on indirect measurements. While the direct population diagnostics of the required multiplet component is an obvious problem.

We have carried out direct measurements based on the diagnostics of the gain recovery dynamics after the passage of a saturating pulse through the amplifying medium. In the experiments, we used a picosecond Nd:YAG laser generating a 25 ps pulses with an energy of 20 mJ and synchronized with it by pumping the side-diode-pumped Nd:YAG amplifier with a crystal aperture of 3 mm and a small-signal gain per pass of >10 . The main part of picosecond laser output was used as a pulse that saturates the laser transition in the preliminarily pumped active medium of the amplifier, and a small part was split off, passed through a controlled optical delay line, and passed through the amplifier with crossed polarization as a probe pulse diagnosing the gain. The dependence of the probe pulse amplification on the delay time with respect to the saturating pulse was measured.

Thus, the scheme used made it possible to test the gain magnitude defined by the population difference between precisely those components of the upper and lower multiplets which participate to the laser transition. A detailed description of experiments and results, their comparison with previous data and accounting in practical amplifying stages are planned to be discussed.



LS-O-16

High-power, high-efficiency Nd:YAG laser CW mode-locked with CVD-graphene

D.P. Tereshchenko (1), M.N. Ershkov (2), S.A. Solokhin (2), Slukhov S.A. (2),
S.N. Smetanin (1), A.G. Papashvili (1), M.G. Rybin (1,3), A. Ismaeel (3), E.D. Obraztsova (1,3)

1- Prokhorov General Physics Institute of the Russian Academy of Sciences, Moscow, Russia

2- Kovrov State Technological Academy named after V.A. Degtyarev, Kovrov, Russia

3- Moscow Institute of Physics and Technology, Dolgoprudny, Russia

High-power, high-efficiency diode-end-pumped Nd:YAG laser with CW mode-locking by single-layer CVD-graphene is experimentally investigated. Output radiation with average power of up to 1.7 W at optical-to-optical and slope efficiencies of 19.8% and 24% respectively is obtained.

Ultrafast mode-locked solid-state lasers have widespread applications in many different research fields, such as medical applications, microscopy, military, optical communication, material processing and so on. Passive techniques of mode-locking make the ultrafast lasers simpler and more compact. Recently, graphene based saturable absorbers are drawing more and more attention due to its unique properties, such as wideband tunability, fast saturable absorbability, and simple and low-cost fabrication. Usually graphene mode-locked solid-state lasers have low average power (< 1 W) or low optical efficiency (< 10 %). The highest output average power of Nd:YAG laser CW mode-locked with graphene was as high as 2.1 W, but optical efficiency was low (4.9 %) [L. Li et al, Opt. Commun. 315, 204 (2014)]. To date, the highest optical efficiency of a graphene-mode-locked solid-state laser with 1-W level output power is 16.2 % for Nd:YVO₄ [L. Zhang et al, Laser. Phys. 21, 2072 (2011)]. Further increase in power characteristics was limited by thermal load of the laser crystal. In present work, the laser design has been improved for high-power operation. The AR-coated, 8-mm long, 1 at. % Nd:YAG crystal with water cooling was chosen as the active medium for 808-nm diode end-pumping due to better thermo-optical characteristics. Internal losses of the Nd:YAG laser cavity were minimized by using a high-quality single-layer CVD-graphene applied directly on the end cavity mirror. Reflectivity of the output coupler, radii of curvature of the internal cavity mirrors, and the laser cavity length were optimized for input power of CW diode pumping of up to 9 W. The highest output average power of the laser was as high as 1.7 W (at 8.6 W pumping) in CW mode-locking regime at optical-to-optical and slope efficiencies of 19.8% and 24.0% respectively. The highest individual picosecond pulse energy was as high as 20.7 nJ for a repetition rate of 82 MHz at diffraction limited beam quality. Increasing the pump power higher than 9 W led to decreasing the optical efficiency due to a thermal lens in the Nd:YAG crystal.

The laser investigations were supported by Russian Science Foundation – Project No 22-22-20092. The graphene films preparation was supported by Russian Science Foundation – Project No 21-72-20050.

LS-O-17

Lasing on optically pumped metastable krypton atoms at 893 nm

Yu.A. Adamenkov, M.A. Gorbunov, V.A. Shaidulina, A.A. Kalacheva, A.V. Juriev

FSUE "RFNC – VNIIEF"

(Mira str, 37., Sarov, Russia, 607190)

E-mails: oefimova@otd13.vniief.ru

The optically pumped rare gas laser (OPRGL) is a new type of optically pumped gas laser with high quantum efficiency, which can convert the high output power of a diode laser into the output power of a gas laser with high beam quality. In [1], the first generation at a wavelength of 893.1 nm was demonstrated. According to published open sources, there has been a serious step in the world in studying the properties of the active medium on the model of a laser source based on a mixture of rare gases with optical pumping. The discharge was optimized and became stable at atmospheric pressure [2, 3].

A mixture of krypton (3%) and helium (97%) is used as the LONIG active medium. The main purpose of using helium is to increase the collisional relaxation from the pump level to the upper laser level in order to create the largest population inversion.

The results of an experiment on laser generation using metastable krypton atoms with optical pumping 893 nm are presented. An electric discharge was used to obtain metastable krypton atoms at atmospheric pressure. Optical pumping was performed using diode laser radiation. Kinetic model of the Ar-He and Kr-He plasmas were created. Efficiency of metastable atom production in these plasmas was compared.

- [1] J. Han, M.C. Heaven. Gain and lasing of optically pumped metastable rare gas atoms // Optics Letters. – 2012. - Vol. 37, No. 11, pp 2157-2159
[2] D. J. Emmons, D. E. Weeks. Kinetics of high pressure argon-helium pulsed gas discharge// Journal of Applied Physics. – 2017. – Vol. 121, No. 20.
[3] J. Han, L. Glebov, G. Venus, M.C. Heaven. Demonstration of diode-pumped metastable Ar laser // Optics Letters. – 2013. - Vol. 38, No. 24, pp 5458-5461

LS-P-1

Laser modification of optical properties of PbSe films by continuous radiation at a wavelength of 405 nm

M. A. Dubkova, A. A. Patrikeeva, A. A. Olkhova, M. M. Sergeev

National Research University ITMO, St. Petersburg, 197101, Russia

maria.dubkova@mail.ru

Chalcogenide PbSe films are widely used as a photosensitive element in gas analysis devices due to high absorption in the IR spectral range from 1 to 4 microns [1]. To increase the efficiency of detection of various toxic gases by these sensitive elements, the optical properties of PbSe films can be improved by laser exposure.

In this study, modification of the structure of PbSe films using continuous laser radiation at a wavelength of 405 nm is considered as an alternative to heat treatment in a furnace. Laser processing of the sample took place in the darkening mode and in the bleaching mode, which was observed when the film was scanned again in the darkening mode.

As a result of laser modification, the structure of the sample was changed, as well as the recrystallization of the material without the formation of an oxide crystal phase in the processing zone, in contrast to the processing in the furnace. This feature is an advantage, since the presence of oxide can contribute to the degradation of the film and reduce its service life. Laser treatment also led to a change in the reflection and transmission of the film in the IR region of the spectrum (Fig. 1) corresponding to the absorption peaks of toxic gases [2].

Thus, the use of laser irradiation makes it possible to carry out local modification of the structure and the predicted change in the optical characteristics of the films and can compete highly with heat treatment in the furnace.

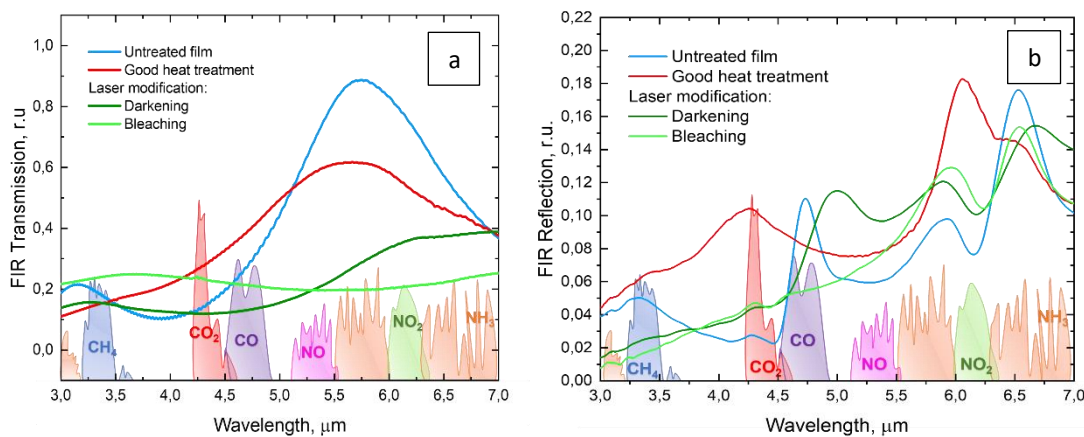


Fig. 1. Fourier spectra of (a) reflection (excluding the film substrate) and (b) transmission (taking into account the film substrate) obtained for samples subjected to various treatments: initial sample (blue curve), sample after heat treatment (red curve). Sample after laser modification in the darkening mode modified by continuous radiation (dark green curve), a sample after laser modification in the bleaching mode modified by continuous radiation (light green curve); Absorption spectra of various gases (CH₄, CO₂, CO, NO, NO₂, NH₃) [3].

- [1] C. L. Tan and H. Mohseni, Emerging technologies for high performance infrared detectors, *Nanophotonics*, 7.(1), pp.169-197, (2018).
 [2] M. Vainio and L. Halonen, Mid-infrared optical parametric oscillators and frequency combs for molecular spectroscopy, *Physical Chemistry Chemical Physics*, 18.(6), pp. 4266-4294, (2016).
 [3] A. A. Olkhova et al., Comparison of CW NUV and Pulse NIR Laser Influence on PbSe Films Photosensitivity, *Applied Sciences*, 13.(4), pp.2396, (2023)

Acknowledgment: this research was funded by the Russian Science Foundation grant (project no. 23-29-10081), grant UMNIK.PHOTONICS.



LS-P-3

Changes in the structure and functional parameters of the CVO optical medium doped with chromium

L.I.Ivleva¹, G.M.Kuzmicheva², M.E.Doroshenko¹

1-Prokhorov General Physics Institute, Russian Academy of Sciences, Vavilov str.38, Moscow, 119991, Russia

2- MIREA - Russian Technological University, 78 Vernadskogo pr., Moscow, 119454, Russia

ivleva@lst.gpi.ru

Calcium orthovanadate $\text{Ca}_3(\text{VO}_4)_2$ (CVO) is an optical material whose properties are defined by disordered whitlockite-like structure without an inversion center (sp.gr. $R3c$). Based on the structural features the crystal-chemical composition of stoichiometric CVO can be described as $[\text{Ca}_{18}\text{Ca}_{218}\text{Ca}_{318}\text{Ca}_{46}(\text{Ca}_5+\text{Ca}_5\text{A})_3](\text{V}_{18}\text{V}_{218}\text{V}_{36})\text{O}_{168}$, indicating the multiplicity of crystallographic sites. A change in the functional parameters of the optical medium is preceded by a change in the structure of the crystalline matrix, caused by the introduction of dopant ions. X-ray diffraction analysis and optical spectroscopy were used to study structural and spectroscopic parameters, actual composition, and point defects in CVO:Cr.

It was shown that chromium ions in various valence states can substitute Ca^{2+} ions in different positions (Ca_2 , Ca_3 , Ca_4) with appropriate excessive charge compensation formation vacancies in V-sites. Locations of Cr ions in the matrix and cell parameters were depended on Cr concentration. Real crystal compositions in the form of $(\text{Ca},\text{Cr})[(\text{V}^{5+}, \square)\text{O}_4]_2$ (\square - vacancies) were defined with Cr^{3+} ions with octahedral coordination for green colored crystals and Cr^{4+} ions with tetrahedral coordination for yellowish CVO:Cr.

Absorption spectra of chromium ions in CVO crystal and fluorescence measurements were carried out in visible and near IR spectral range. Absorption bands with maxima about 600, 700 nm and above 1100 nm were observed for investigated crystals. Time resolved excitation and fluorescence spectra measured for CVO:Cr crystal as-grown and after annealing were analyzed. In CVO:Cr (0.05 at%) as grown crystal the presence of Cr^{3+} , Cr^{4+} and Cr^{5+} ions was revealed. Annealing of the $\text{Ca}_3(\text{VO}_4)_2$:Cr crystal in the air was observed to result in an increase of chromium ions in $4+$ and a decrease in $3+$ valence state. This should obviously originate from sufficient decrease of Cr^{5+} ions amount which concentration looks to be nearly negligible in annealed sample. Some Cr^{5+} to Cr^{3+} ions charge exchange process ($\text{Cr}^{5+} \rightarrow \text{Cr}^{4+} + e^-$; $\text{Cr}^{3+} + e^- \rightarrow \text{Cr}^{4+}$) resulting in formation of two Cr^{4+} ions may take place which decrease both Cr^{5+} and Cr^{3+} ions concentration in the annealed sample. As a result, crystalline materials activated by chromium ions are very promising for laser media and are intensively studied at present.

The work was supported by Ministry of Science and Higher Education: grant № 075-15-2021-1362.

LS-P-4

Changing the spectrum of the arsenic sulfide fiber by X-ray radiation

V.V. Gerasimenko, A.N. Kachemtsev, I.V. Skripachev, G.E. Snopatin

*Institute of Chemistry of High-Purity Substances named after G.G. Deviatich of the Russian Academy of Sciences,
603951, Nizhny Novgorod, Box-75, ul. Tropinina, 49,*

kachemtcev@ihps-nnov.ru

Changes in the structure and properties of arsenic sulfide that occur as a result of irradiation with radiation of various nature have been studied for more than 60 years. The main results of studying the effect of radiation on the characteristics of both bulk samples and thin films of As_2S_3 are given, for example, [1,2]. The properties of light guides from As_2S_3 also change during and after radiation exposure, however, these processes have not been sufficiently studied. The work is devoted to the experimental determination of the spectral characteristics of an IR fiber made of high-purity arsenic sulfide after irradiation of samples with a source of continuous X-ray radiation. The maximum quantum energy is up to 100 keV, and the effective energy is 10 keV. The level of exposure was more than 12 kGy.

Two samples of a multimode fiber have been studied. Before and after irradiation, the transmission spectrum of the light guide was measured in the range of 2,0...6,0 microns. The measurements were carried out according to the procedure given in [3]. The measurement results are shown in Figure 1. Stationary irradiation with X-ray quanta of an arsenic sulfide fiber leads to a significant increase in the absorption of IR radiation in the entire studied range. In the region of 2.5 microns, the signal attenuation increased approximately 10 times. In addition, a change in the height of the impurity absorption peaks in the wavelength range of 4 – 4.5 microns in the irradiated samples was recorded in comparison with the initial spectrum. Figure 2 shows the spectral characteristics of the fiber normalized for minimum attenuation. Figure 2 allows us to qualitatively compare the obtained dependences and assess the presence of changes in the spectral characteristics of sulfide-arsenic light guides after radiation exposure, in particular, a significant broadening of the impurity absorption peak in the region of 3 microns with its significant expansion in the region of shorter wavelengths.

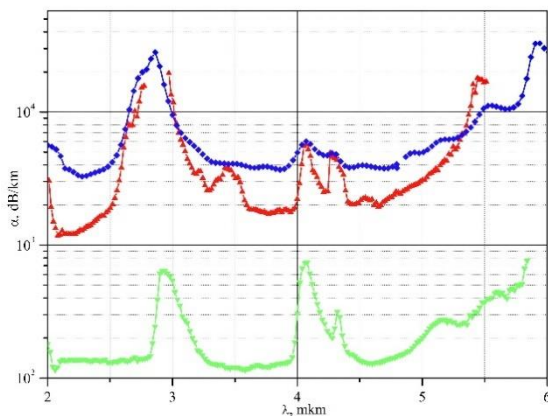


Fig. 1 Spectrum of As_2S_3 fiber before (green) and after (red and blue) irradiation

Absorbed dose of the X-ray fiber: sample No. 1 (red) – 416 G/m;
sample No. 2 (blue) - 388 Gy/m.

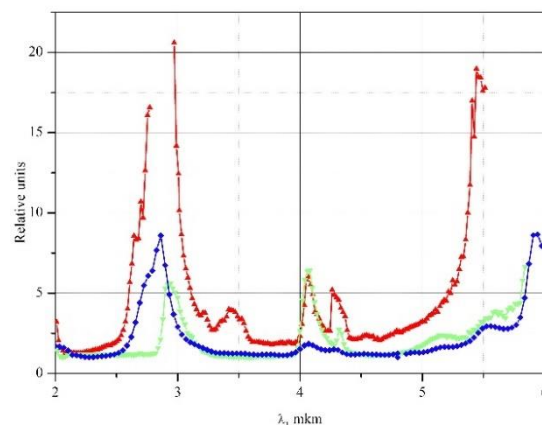


Fig. 2 Comparison of IR fiber spectra normalized to a minimum of losses before (green) and after (red and blue) irradiation

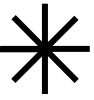
Absorbed dose of the X-ray fiber: sample No. 1 (red) – 416 G/m;
sample No. 2 (blue) - 388 Gy/m.

The research was carried out with the support of the Russian Science Foundation, RGNF grant No. 22-13-00226.

[1] O. Shpotyuk, M. Shpotyuk, S. Ubizskii, Radiation-induced optical effects in chalcogenide semiconductor glasses, *Radiation&Application*, vol. 2, issue 2, pp. 94–100, (2017).

[2] M. Shpotyuk, A. Kovalskiy, R. Golovchak, O. Shpotyuk, Phenomenology of γ -irradiation-induced changes in optical properties of chalcogenide semiconductor glasses: A case study of binary arsenic sulfides, *Journal of Non-Crystalline Solids*, vol. 498, pp. 315–322, (2018).

[3] V.G. Plotnichenko, V.K. Sysyoyev Measurement of total loss spectra in fiber optical fibers of the near and middle IR range, *Journal of Applied Spectroscopy*, vol. XXXVIII, issue 3, pp. 506-509, (1983).



Theoretical and experimental study of electronic properties of ZnIn₂Se₄ compound

I.A. Mamedova¹, Z.A. Jahangirli^{1,2}, E.G. Alizade¹, T.G. Mammadov¹, N.A. Abdullayev^{1,2}

1-Institute of Physics Ministry of science and education. Azerbaijan, Baku, Azerbaijan

2-Baku State University, Baku, Azerbaijan

E-mail: irada_mamedova@yahoo.com

ZnIn₂Se₄ belongs to the $A^2B_2^3C_4^6$ defective chalcopyrite family, attracting the attention of many researchers due to its potential application in semiconductor devices such as solar cells [1], memory devices [2], etc.

We have obtained and characterized by X-ray diffraction and Raman spectroscopy crystals of defective chalcopyrite ZnIn₂Se₄. Ab initio calculations of electronic, including optical, properties were carried out on the basis of DFT using the method of full-potential linearized augmented plane waves (FP-LAPW) implemented in the Wien2k code. Spectral ellipsometry was used to experimentally study the optical characteristics of ZnIn₂Se₄ semiconductor compounds. The calculated and experimental real and imaginary parts of dielectric function of ZnIn₂Se₄ are shown in Fig. 1. The main peaks of the calculated real and imaginary parts of dielectric function are located around 2.8 eV and 5.0 eV, respectively.

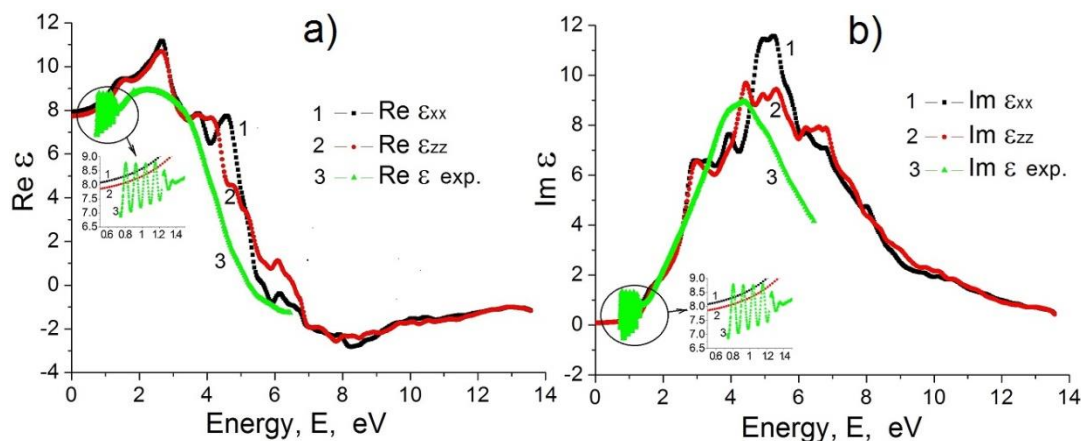


Fig. 1 Calculated and experimental real and imaginary parts of dielectric function of ZnIn₂Se₄

The absorption coefficient α , refractive n and extinction k indices were measured and calculated, the values of which are compared with the literature data.

The results of a study of photoluminescence in a wide temperature range from 10K to 300K of ZnIn₂Se₄ are presented. For the first time, a band with a maximum at 725 nm (1.71 eV) with a short-wavelength shoulder at 685 nm (1.81 eV) and a less intense infrared broad band with a maximum at 896 nm (1.39 eV) were found in the PL spectrum for the first time.

[1] F.J. Garcia and M.S. Tomar, n-CdS/p- ZnIn₂Se₄ thin film solar cell. Thin Solid Films. v. 69, pp. 137-139 (1980).

[2] J. Filipowicz, N. Romeo and L. Tarricone, Photoelectrical memory effect in ZnIn₂Se₄. Solid State Communications. v.38. pp. 619-62 (1980).



LS-P-8

Electronic properties of TlFeS₂ and TlFeSe₂ semiconductors. Theory and experiment

Z.I. Badalova, Z.A. Jahangirli, E.G. Alizade, T.G. Mammadov, N.A. Abdullayev

Institute of Physics of the Ministry of Science and Education of Azerbaijan, Baku

E-mail: abnadir@mail.ru

We have obtained and characterized by X-ray diffraction, Raman and infrared spectroscopy crystals of TlFeS₂ and TlFeSe₂ semiconductor compounds [1]. Ab initio calculations of electronic, including optical, properties were carried out on the basis of DFT using the method of full-potential linearized augmented plane waves (FP-LAPW) implemented in the Wien2k code. To experimentally study the optical characteristics of semiconductor compounds TlFeS₂ and TlFeSe₂, we carried out spectral ellipsometric studies based on determining the change in the polarization of light as a result of its interaction with the surface of crystals upon reflection. The measurements were carried out on an optical range ellipsometer M-2000 DI (J.A. Woollam Co, Inc., US). Figure 1 shows the values of the real $\text{Re } \epsilon$ (Fig. 1a) and imaginary $\text{Im } \epsilon$ (Fig. 1b) parts of the dielectric function at different energies for TlFeS₂ crystals. Curves 1 and 2 are the theoretically calculated values of the dielectric function for directions along the x and z axes, respectively. Curve 3 is the experimentally determined value of the dielectric function for a polycrystalline sample from ellipsometric measurements. Note the coincidence of critical points ($\partial\epsilon/\partial E = 0$) in the dependences $\epsilon(E)$. In the TlFeS₂ compound, for the real part of the dielectric function (Fig. 1a), this energy is 3.3 eV, and for the imaginary part of the dielectric function, the energies are 2.1, 2.8, and 3.5 eV. The dispersion of the refractive, extinction, and absorption coefficients is also determined. The width of the direct forbidden zone is estimated. Ab initio calculations determine the electronic band structure, the origin of energy states, and projected onto atoms partial densities of states (PDOS).

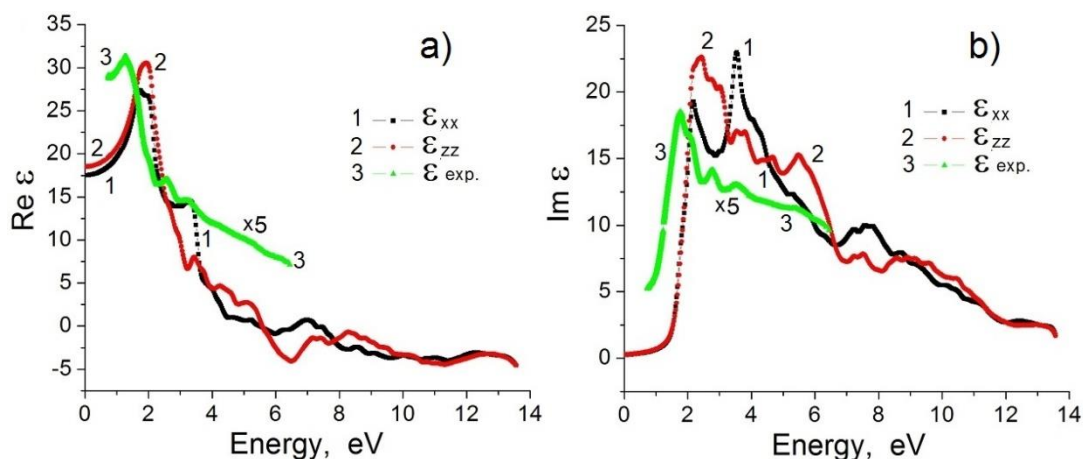


Fig.1. Real (a) and imaginary (b) parts of the dielectric function of TlFeS₂: (1, 2) result of theoretical calculation along the crystallographic directions x and z and (3) experimental data.

[1] R.G. Veliyev, N.A. Abdullaev, I.R. Amiraslanov, I.A. Mamedova, D.A. Mamedov, Z.I. Badalova, Sh.K. Qudavasov, S.A. Nemov, Optical Phonons in TlFeS₂ and TlFeSe₂ Semiconductor Compounds, Semiconductors, vol. 56, pp. 32–37, (2022).



LS-P-9

Peculiarities of titanium surface morphology after oxidation with the "Laser paintbrush" hand tool

Veiko V.P., Morozova A.A., Sinev D.A., Odintsova G.V.

*ITMO University, Saint-Petersburg, Russia
Main author email address: aamorozova@itmo.ru*

Local surface oxidation is a well-known method for imparting new functional properties to metals. This processing method can be used to protect products from external factors, increase antibacterial activity, change surface wettability, optical properties, etc. The last application is realized by color laser marking technology. Laser patterning, in addition to the usual methods, can be implemented using the "Laser paintbrush". However, when using this tool, we noticed that the surface morphology is different, which is investigated in this paper.

The fundamental difference between the "Laser paintbrush" tool under consideration and laser systems used in color laser marking technology is the manual type of control of the trajectory and scanning speed of the laser beam. The development of this device was aimed at integrating laser technologies into the field of artistic metal processing. It is of interest to compare the physical processes occurring during the transition from an electronic control method to an analogue (manual) one.

The objects of study were single laser tracks created by laser action with continuous laser sources with stationary and manual control. The surface morphology was studied by optical microscopy, spectrophotometry, scanning electron microscopy, and energy-dispersive X-ray microanalysis. The surface was studied perpendicular to the direction of the laser beam. Despite the similar principles of the formation of a colored oxide film on the surface, a comparative analysis of the surface morphology showed differences. On the surface modified with the "Laser Brush", periodic structures of the submicron order were found, as well as cellular structures presented in different sizes. In this work, we analyze each of the zones, which are different in morphological character, and put forward hypotheses about the reasons for their occurrence.

This research was supported by Priority 2030 Federal Academic Leadership Program

LS-P-10

Optical properties of Sm³⁺ doped chalcogenide glass samples irradiated with S polarized and P polarized light

Yu. Kuzyutkina¹, N. Parshina¹, V. Kochubey¹, E. Romanova¹, R. Blagin², V. Shiryaev²

1- Saratov State University, Astrakhanskaya 83, 410012 Saratov, Russia

2- Devyatykh Institute of Chemistry of High-Purity Substances of RAS,
49 Tropinin Str., 603951 Nizhny Novgorod, Russia

romanovaelena@sgu.ru

Design of rare earth (RE) doped chalcogenide glasses is a current trend towards creation of fiber lasers operating in mid-infrared spectral range. In this work, optical properties of chalcogenide glasses of the system Ge-Ge-As-Se doped with samarium ions (Sm³⁺) have been studied near their fundamental absorption band (FAB) edge. The glasses were obtained by direct melting of especially pure substances Ge, As, Se - 6N, Ga - 7N, Sm - 3N [1]. Content of Sm³⁺ in the glasses (0, 750, 1700 ppm) was determined by the Inductively Coupled Plasma - Atomic Emission Spectroscopy [2]. The presence of crystals and heterophase inclusions of micron size was analyzed by optical microscopy.

Transmittance and reflectance spectra of the glasses shaped as thin disks were measured by using the *Perkin Elmer Lambda 950* spectrometer in the wavelength range of 0.5–1.8 μm . The glass samples were irradiated by linearly polarized light of two orthogonal polarizations (P- polarized and S- polarized light). In accordance with the Fresnel equations, in the transmittance spectra (Fig.1a), the curves obtained with P- polarized light are located above the curves obtained with S- polarized light in the Sm³⁺ absorption bands and between the bands. Noises in the wavelength range of 0.8–0.9 μm are associated with switching the operation mode of the spectrophotometer.

Spectral dependencies of attenuation and refraction coefficients (Fig.1b,c), as well as optical bandgap energy (E_g) and Urbach energy (E_U) were calculated by using the approach described in [3].

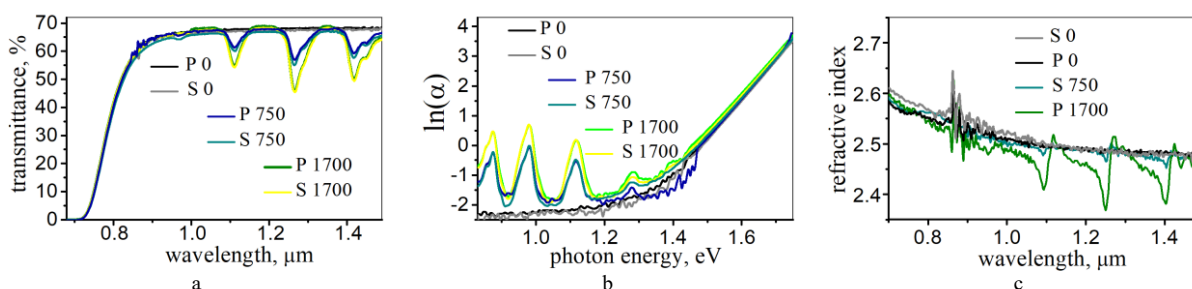


Fig.1 Spectral dependencies of glass samples transmittance (a) measured with an integrating sphere; logarithm of attenuation coefficient (b) obtained from measurements with an integrating sphere; refractive index (c) obtained from measurements with a collimated light beam.

Dependence of $\ln(\alpha)$ on the photon energy $h\nu$ (Fig.1b) shows that the absorption bands of Sm³⁺ are located at the weak absorption tail ($h\nu < 1.4$ eV) of the glass FAB edge. Magnitude of E_g corresponds to the high frequency edge of the linear part of the function $\ln(\alpha) = f(h\nu)$ at $\alpha = 10^3$ cm⁻¹. For E_U evaluation, the derivatives $S(h\nu) = d(\ln(\alpha))/d(h\nu)$ were calculated. For all the samples, the values $E_g \approx 1.93$ eV and $E_U \approx 0.073$ eV have been obtained. The ranges of anomalous dispersion within the Sm³⁺ absorption bands in Fig.1c are clearly seen.

In analysis of the results presented here, specific structural and electronic properties of chalcogenide glasses are to be taken into consideration.

This work was supported by the Russian Science Foundation (RSF) under Grant 21-13-00194.

[1] V.S. Shiryaev, E.V. Karaksina, A.P. Velmuzhov, et.al. Preparation and investigation of Ga_xGe₂₅As₁₅Se_{60-x} (x=1÷5) glasses, *Opt. Mat.* 67, 38-43 (2017)

[2] I.I. Evdokimov, D.A. Fadeeva, A.E. Kurganova, V.S. Shiryaev, V.G. Pimenov, E.V. Karaksina. *J. Analyt. Chem.*, 7 (7), 869–877 (2020).

[3] Yu.S. Kuzyutkina, E.A. Romanova, V.I. Kochubey, V.S. Shiryaev. *Opt. i spekt.*, 117 (1), 60–66 (2014). (in Russian).

Optimization of energy costs for the generation of metastable argon atoms in a repetitively pulsed discharge in an Ar-He mixture

M. Zagidullin^{1,2}, P. Mikheyev¹, A. Dvornikov²

1- P.N. Lebedev Physical Institute, Samara branch, 221 Novo-Sadovaya st. Samara, 443011, Russia

2- Samara National Research University, 34, Moskovskoye shosse, Samara, 443086, Russia

zagidullin_marsel@rambler.ru

In this work, the specific heat W , released in a nanosecond repetitively pulsed discharge (NRPD) in an Ar-He = 1:99 mixture at atmospheric pressure, when the produced number density of argon metastable atoms is 10^{13} cm^{-3} and water is present as the impurity, was calculated with the help of 0-D numerical model. The dependence of W on the reduced electric field E/N and repetition rate of applied discharge voltage pulses with triangular shape and 80 ns duration at their base was obtained for different water content. A repetitively pulsed discharge in a mixture of inert gases at an atmospheric pressure with a pulse duration from a few to hundreds of nanoseconds with a high pulse repetition rate ($\geq 100 \text{ kHz}$) is an effective way to produce a quasi-continuous weakly ionized homogeneous plasma, which is of interest for a number of applications [1,2]. Minimization of energy costs for the production of the required number density of metastable atoms of a noble gas plays an important role for scaling of the discharge volume and facilitating discharge stability. With a large pulse duty cycle and a repetition rate of $\sim 100 \text{ kHz}$, the kinetics during the afterglow stage plays an essential role in the NRPD, forming a decaying plasma where the next discharge pulse occurs. The model includes 10 electron impact processes and 31 plasma chemical processes during discharge pulse and afterglow. Initial condition was set as a large enough homogeneous ionization. Stable periodical solution appeared after 100-200 discharge pulses. For the triangular applied discharge voltage, the averaged over the discharge period number density $[\text{Ar}(s_5)]$ is a function of three parameters: water content, repetition rate of the discharge pulses f and amplitude of E/N .

Figure 1a represents the dependence of pulse repetition rate f on E/N for different water content, when $[\text{Ar}(s_5)] = 10^{13} \text{ cm}^{-3}$. Figure 1b represents the dependencies of W on E/N for these conditions, showing that there are pairs of $(f, E/N)$, when these dependencies exhibit minima. Evidently, there is a strong dependence of positions of these minima on the water content.

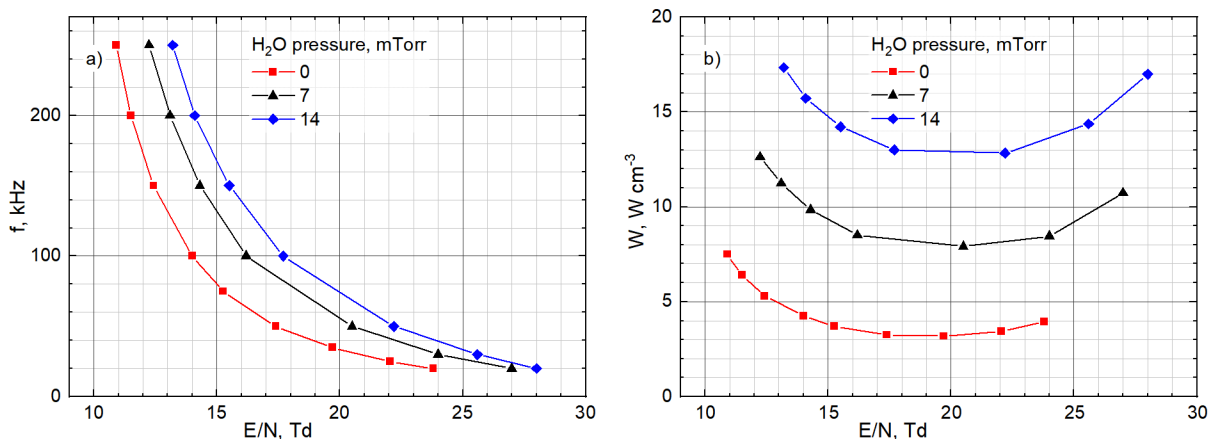


Fig. 1. Dependence of: a) – required for production of $[\text{Ar}(s_5)] = 10^{13} \text{ cm}^{-3}$ pulse repetition rate f on E/N , b) – heat release W on E/N for the repetition rates according to Fig. 1 a).

This work was supported by RSF grant № 23-22-10013, <https://rscf.ru/project/23-22-10013/>.

[1] J. Han, M. Heaven, P. Moran, A. Pitz, E. Guild, C. Sanderson, B. Hokr, Demonstration of a CW diode-pumped Ar metastable laser operating at 4 W, *Optics Letters*, vol.42, pp. 4627-4630, (2017).

[2] P. Mikheyev, A. Chernyshov, M. Svistun, N. Ufimtsev, O. Kartamysheva, M. Heaven, V. N. Azyazov, Transversely optically pumped Ar: He laser with a pulsed-periodic discharge, *Optics express*, vol. 27, pp. 38759-38767, (2019).

LS-P-13

Comparison compression methods of a strongly chirped signal from a pulsed Yb-doped fiber laser by diffraction gratings and CFBG compressors

I. Zhluktova¹, R. Okun¹, A. Kamynin¹, A. Wolf², V. Tsvetkov¹

1- Prokhorov General Physics Institute of Russian Academy of Sciences, Moscow 119991, Russia

2- Institute of Automation and Electrometry of the Siberian Branch of the RAS, Novosibirsk, 630090, Russia

Main author email address: zhluktova@kapella.gpi.ru

Pulse compression is necessary for high energy and ultra-short pulse (USP) generation, which has applications in various fields of science and technology, such as attosecond science [1], ultrafast spectroscopy [2], and terahertz generation [3]. Various compression methods are used to achieve shorter pulse durations. One such pulse compression method is the use of a diffraction grating or chirped fiber Bragg grating (CFBG). In this paper, we investigated the compression of a strongly frequency-modulated (chirped) amplified pulse from a ytterbium (Yb) doped fiber laser (MO) operating in a passive mode-locked regime. For this purpose, two different compressors were assembled to evaluate how compression of such complex pulses would occur. First, a Tracy compressor (TC) based on holographic diffraction gratings was assembled (recorded in Bayfol HX 200 photopolymer). The average MO output power after amplification in the Yb-doped fiber amplifier was 140 mW, after compression - 0.4 mW. This was enough to register autocorrelation traces (ACT), shown in Fig.1.a. Evaluating the ACT, we can see that a highly chirped pulse after the compressor produces compressed pulses with durations of less than 5 ps (approximated using the sech² form). The pulse also has wings, showing uncompressed higher order dispersion terms.

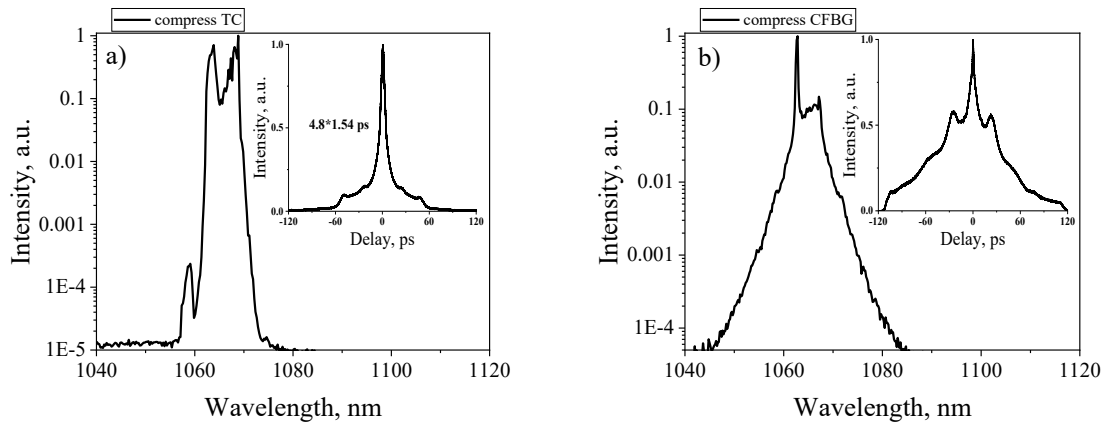


Fig.1. Pulse spectra after different compressors: a) after TC, b) after CFBG. The inserts in the figures are ACTs with a resolution of 0.3 ps.

In another case, a compressor based on CFBG (provided by IA&E SB RAS) was used. By using such a CFBG compressor, a pulse with a high uncompressed substrate was achieved. The output power was 17 mW at maximum amplifier pump power. Furthermore, a coherent structure of compressed pulses consisting of several pulses with a duration of less than 5 ps and a distance between them of about 35 ps was recorded, as shown in Fig. 1.b.

This research was funded with the financial support of the Ministry of Science and Higher Education of the Russian Federation, grant number 075-15-2022-315, and carried out on the basis of the World-Class Research Center «Photonics».

[1] F. Krausz and M. Ivanov, Attosecond physics, *Rev. Mod. Phys.* 81(1), 163–234 (2009)

[2] R. Berera, R. van Grondelle, and J. T. M. Kennis, Ultrafast transient absorption spectroscopy: principles and application to photosynthetic systems, *Photosynth. Res.* 101(2-3), 105–118 (2009).

[3] R. Piccoli, A. Rovere, Y.-G. Jeong, Yu. Jia, L. Zanonno, F. Légaré, B. E. Schmidt, R. Morandotti, and L. Razzari, Extremely broadband terahertz generation via pulse compression of an Ytterbium laser amplifier, *Opt. Express* 27, 32659–32665 (2019)



LS-P-14

Simulation of the operation of a phased radio antenna array using the Fourier transform in the visible wavelength range

V.S. Solovjev, S.P. Timoshenkov, A.S. Timoshenkov

Institute of Nano- and Microsystem Technology Moscow Institute of Electronic Technology

solov_06_v@mail.ru

Previously, the idea of transferring the radio frequency to the visible region using Mach-Zehnder modulators was put forward. Such an interferometer makes it possible to modulate coherent laser light with a high-frequency microwave signal. If each antenna element of a phased antenna array is used as a modulating element of a coherent laser beam, previously divided by an optical splitter into a number of channels equal to the number of phased antenna array elements, then further processing can be performed in the visible range of the electromagnetic wave. In this work, experimental modeling of the optical part of the idea of converting a radar signal into an optical spectrum is carried out. Using the inverse Fourier transform procedure, the amplitude image of the aircraft was converted into its pure phase function. The phase distribution of image elements with a dimension of $100 * 200$ was sent via a USB line to a space-time light modulator. As a result, a model of the phase distribution of light was obtained, simulating the phase distribution in the Phased Antenna Array (PAR) of the radio range. With the help of the direct Fourier transform (the lens standing after the PVMS), the image of the aircraft was restored. Target coordinates can also be restored. A 532 nm laser was used. It is shown that the use of the optical Fourier transform method makes it possible to increase the noise immunity of the received signal. It is proposed to use the method of converting radio-frequency signals of a phased antenna array into the visible optical range for direct observation of objects in the visible range. It is shown that when using Mach-Zehnder modulators and developing a photonic microcircuit, the optical Fourier transform rate can be of the order of one period of the carrier frequency.



LASER

DIAGNOSTICS AND

SPECTROSCOPY



LD-I-1

Nonlinear optical properties of doped MoS₂ for photonic applications

Mohd. Shahid Khan*

Department of Physics, Jamia Millia Islamia (Central University), New Delhi, India

* mskhan@jmi.ac.in

Lasers have been used for exciting applications more than any other scientific discovery of the last century. One important phenomenon intimately associated with lasers is the nonlinear optical characteristics of the materials which become pronounced and their realization seems realistic with intense laser sources. The nonlinear optical materials encompass a wide range of applications that create great impact on daily life. The fascinating applications of NLO include like 3D data storage devices, all optical switching devices, sensors, optical imaging, medicine, diversity of advanced lasers and coherent sources, military, and in scientific instrumentation etc. Due to their intriguing electrical and optical characteristics, two-dimensional (2D) materials have recently received a lot of attention. The non-linear optical properties of these materials could play a vital role in potential photonic applications, such as light modulation and optical limiting. Molybdenum disulfide (MoS₂), an example of a two-dimensional (2D) layered material, is one of most sought-after material for improved nonlinear optical coefficients in addition to the advantages which it offers as it has potential uses in optoelectronic fields like phototransistors, optical limiters, and ultra-fast photonic devices because of its distinct layered structure. The nonlinear optical properties of pure MoS₂, and its doped samples MoS₂/rGO, Al-MoS₂/rGO, and Co-MoS₂ etc are examined thoroughly by employing the Z-scan technique. The surface morphology, structure, and the laser intensity are further discussed as factors affecting the NLO characteristics of these nanohybrids employing various analytical techniques, including X-ray diffraction (XRD), Raman spectroscopy, field-emission scanning electron microscopy (FESEM), and UV-Visible spectroscopy. The NLO properties of doped MoS₂ nanohybrids are also compared with optical nonlinearity of multiferroic materials that attract a great attention of the researchers for fabricating new devices based on NLO materials and magneto electric coupling.

- [1] D Liu, C He, L Chen, W Li, Y Zu, The nonlinear absorption effects, and optical limiting properties of Bi₂Te₃/ rGO thin films, *Optical Materials* 111 (2021): 110634.
- [2] Prasad, Jagdees, Ashwani Kumar Singh, Monika Tomar, Vinay Gupta, and Kedar Singh. "Hydrothermal synthesis of micro-flower like morphology aluminum-doped MoS₂/rGO nanohybrids for high efficient electromagnetic wave shielding materials." *Ceramics International* 47, no. 11 (2021): 15648-15660.
- [3] Abith, M., and Sabari Girisun TC. "Excited state absorption induced optical limiting action of MoS₂-rGO nanocomposites." *Journal of Molecular Liquids* 341 (2021): 117337.
- [4] Jiang, Yaqin, Lili Miao, Guobao Jiang, Yu Chen, Xiang Qi, Xiao-fang Jiang, Han Zhang, and Shuangchun Wen, Broadband and enhanced nonlinear optical response of MoS₂/graphene nanocomposites for ultrafast photonics applications, *Scientific reports* 5, no. 1 (2015): 1-12.
- [5] Salmani, I. A., Khan, M. S., Ali, J., Hafiz, A. K., Mehkoom, M., Afzal, S. M., & Khan, M. S., Third-order optical nonlinearity and multiferroicity of nanoparticles thin films of isovalent rare earth Y³⁺ ion substituted BiFeO₃, *Physica B: Condensed Matter*, 655 (2023) 414750.
- [6] Imran Ahmad Salmani, Mohd Shahid Khan, Javid Ali, Aurangzeb Khurram Hafiz, Mohd Mehkoom, SM Afzal, Mohd Saleem Khan, Sol-gel synthesis of ZrFeO₃ nanoparticles and study of optical nonlinearity and multiferroicity of its nanocrystalline thin films, *Journal of Sol-Gel Science and Technology* (2023):

LD-I-2

Carrier-envelope phase control of sub-cycle dynamics of ultrashort pulses in anti-resonance hollow core fiberI.V.Saitsky¹, A.A.Voronin^{1,2}, E.A.Stepanov^{1,2}, A.A.Lanin^{1,2}, A.B.Fedotov^{1,2},*1 - Physics Department, M.V. Lomonosov Moscow State University, Moscow 119992, Russia**2 - Russian Quantum Center, Skolkovo, Moscow Region, 143025 Russia**a.b.fedotov@physics.msu.ru*

The carrier-envelope phase (CEP) of the laser pulse plays an extremely important role in variety of applications when the electric field strength is large enough for such phenomena as high-order harmonic and attosecond pulse generation [1–4], above-threshold ionization [5] and terahertz sub-cycle waveform formation [6]. The time duration of a near single-cycle pulse itself depends on the absolute value of CEP [7].

In our work we used Ti:Saaphire laser system and optical parametric amplifier to produce tunable pulses in idler wave with an energy of $E_0 \approx 180 \mu\text{J}$, central wavelength of $\lambda_0 \approx 2000 \text{ nm}$ and duration of $\tau_0 \approx 60 \text{ fs}$. These pulses couple into anti-resonant hollow-core fiber (AR HCF) filled with argon. The transverse structure of the fiber consists of a hollow core with a diameter of $D = 70 \mu\text{m}$, surrounded by six hollow tubes with diameters of $d = 36 \mu\text{m}$ and a wall thickness of $w \approx 590 \text{ nm}$ and allows to support radiation waveguiding in very wide spectral range. The sequence of nonlinear transformations of the femtosecond pump pulse in an AR HCF leads to spectral broadening (supercontinuum generation (SC)) and near single cycle waveform generation. The spectrum broadening follows the soliton self-compression (SSC) scenario, with additional enhancement from the self-steepening effect and parametric generation of four-wave components in the blue wing of the soliton spectrum [8,9]. In such condition it is possible to form very short pulses with the duration less than one cycle of the field, and for such pulses the influence of CEP could play noticeable role.

In our investigation we explore the signatures of phase dependence in the visible part of the SC generated during SSC down to single-cycle pulsewidth in an anti-resonant hollow-core fiber (AR HCF) filled with argon. This phenomenon is observed within the small parameter range, when the pulse reaches its maximum compression ratio, but there is still no strong ionization, leading to pulse decay. Theoretical analysis by means of the numerical solution of the generalized nonlinear Schrödinger equation (GNSE) reveals that the phase dependence arises from the broadband third harmonic generation (THG) in the range from 250 nm to 800 nm at the moment of a sub-cycle pulse composition and its spectral interference with the visible part of the SC. The CEP control of this ultrabroadband f-3f interference provides a signature of the sub-cycle pulse synthesis during SSC in the fiber with duration of 0.4 optical cycles and peak power more than 2 GW on the fiber output.

The work was supported by Russian Science Foundation grant # 22-12-00149.

- [1] P. B. Corkum and F. Krausz, "Attosecond science," *Nat. Phys.*, vol. 3, pp.381–387 (2007).
- [2] G. Vampa, T. J. Hammond, N. Thiré, B. E. Schmidt, F. Légaré, C. R. McDonald, T. Brabec, and P. B. Corkum, "Linking high harmonics from gases and solids," *Nature*, vol. 522, pp. 462–464 (2015).
- [3] O. Schubert, M. Hohenleutner, F. Langer, B. Urbanek, C. Lange, U. Huttner, D. Golde, T. Meier, M. Kira, S. W. Koch, and R. Huber, "Sub-cycle control of terahertz high-harmonic generation by dynamical Bloch oscillations," *Nat. Photonics*, vol. 8, pp.119–123 (2014).
- [4] A. Baltuška, T. Udem, M. Uiberacker, M. Hentschel, E. Goulielmakis, C. Gohle, R. Holzwarth, V. S. Yakovlev, A. Scrinzi, and T. W. Hänsch, "Attosecond control of electronic processes by intense light fields," *Nature*, vol.421, 611 (2003).
- [5] D. B. Milošević, G. G. Paulus, D. Bauer, and W. Becker, "Above-threshold ionization by few-cycle pulses," *J. Phys. B At. Mol. Opt. Phys.* vol.39, R203 (2006).
- [6] M. Kreß, T. Löffler, M. D. Thomson, R. Dörner, H. Gimpel, K. Zrost, T. Ergler, R. Moshhammer, U. Morgner, J. Ullrich, and H. G. Roskos, "Determination of the carrier-envelope phase of few-cycle laser pulses with terahertz-emission spectroscopy," *Nat. Phys.* vol.2, pp.327–331 (2006).
- [7] A. Wirth, M. T. Hassan, I. Grguraš, J. Gagnon, A. Moulet, T. T. Luu, S. Pabst, R. Santra, Z. A. Alahmed, A. M. Azezeer, V. S. Yakovlev, V. Pervak, F. Krausz, and E. Goulielmakis, "Synthesized Light Transients," *Science*, vol.334, pp. 195–200 (2011).
- [8] E. A. Stepanov, A. A. Voronin, F. Meng, A. V. Mitrofanov, D. A. Sidorov-Biryukov, M. V. Rozhko, P. B. Glek, Y. Li, A. B. Fedotov, A. Pugžlys, A. Baltuška, B. Liu, S. Gao, Y. Wang, P. Wang, M. Hu, and A. M. Zheltikov, "Multioctave supercontinua from shock-coupled soliton self-compression," *Phys. Rev. A*, vol. 99, p.033855 (2019).
- [9] I. V. Savitsky, E. A. Stepanov, A. A. Lanin, A. B. Fedotov, and A. M. Zheltikov, "Single-Cycle, Multigigawatt Carrier–Envelope-Phase-Tailored Near-to-Mid-Infrared Driver for Strong-Field Nonlinear Optics," *ACS Photonics*, vol. 9, pp. 1679–1690 (2022).



LD-I-3

Nonlinear light generation and emission control in nanophotonic structures combined with 2D materials

A.S. Shorokhov¹

1- Faculty of Physics, Lomonosov Moscow State University, Moscow 119991, Russia

shorokhov@nanolab.phys.msu.ru

Recently introduced Mie-resonant nanophotonics based on specially designed subwavelength dielectric or semiconductor particles has been proved to be a versatile tool both for flat optics and integrated photonics [1–3]. Combining such structures with 2D materials one can bring about functionality not available for such systems before [4]. Particularly, it has been shown that integrating monolayers of transition metal dichalcogenides (TMD) with high-Q resonant metasurfaces [5] it is possible to achieve efficient second-harmonic generation in such structures [6]. However, the interplay between optical resonances of the nanoantennas and intrinsic excitonic resonances of 2D materials [7] has not been systematically studied yet. In this work two different studies of Mie-resonant nanophotonic structures integrated with 2D materials are presented. The first one considers a high-Q resonant metasurface combined with a monolayer TMD film. The metasurface comprises a set of TiO₂ nanodisks arranged in a tightly spaced quadratic lattice on a silica substrate. MoSe₂ monolayer is transferred on top of the nanostructure by the mechanical exfoliation technique. Experimental SHG characterization conducted at room and cryogenic temperatures reveals non-trivial interplay between volumetric (associated with the metasurface) and material (associated with the TMD film) resonances in the structure leading to the multifold increase of the observed nonlinear effect. The second study considers integrated silicon waveguides composed of resonant nanoparticles and thin films of 2D materials. We demonstrate that excitation of magnetic Mie-type resonances in such waveguide chains of Si nanoparticles can increase on-chip light coupling efficiency for localized dipole sources in thin InSe films [8]. Particularly, we experimentally observe up to 2 times improvement in comparison with conventional silicon waveguides. Finally, we investigate a resonant waveguide system composed of SiN nanoparticles for effective optical coupling with localized interlayer exciton emitters in vertically stacked monolayer MoSe₂–WSe₂ heterostructures [9]. Numerically we demonstrate up to 8 times radiation coupling efficiency improvement and up to 12 times Purcell effect enhancement in comparison with the conventional silicon strip waveguide. Achieved results can be beneficial for development of on-chip light sources.

[1] A. Kuznetsov et al., “Optically resonant dielectric nanostructures,” *Science*, 354, aaf2472 (2016).

[2] R. Bakker et al., “Resonant Light Guiding Along a Chain of Silicon Nanoparticles”, *Nano Lett.*, 17, 3458–3464 (2017).

[3] Y. Sirmaci et al., “All-dielectric Huygens’ meta-waveguides for resonant integrated photonics”, *Laser Photonics Rev.*, 17, 2200860 (2023).

[4] R. Mupparapu et al., “Integration of two-dimensional transition metal dichalcogenides with Mie-resonant dielectric nanostructures”, *Adv. Phys.:* X, 5, 1734083 (2020).

[5] K. Koshelev et al., “Asymmetric Metasurfaces with High-Q Resonances Governed by Bound States in the Continuum”, *Phys. Rev. Lett.*, 121, 193903 (2018).

[6] N. Bernhardt et al., “Quasi-BIC Resonant Enhancement of Second-Harmonic Generation in WS₂ Monolayers”, *Nano Lett.*, 20, 5309–5314 (2020).

[7] G. Wang et al., “Giant Enhancement of the Optical Second-Harmonic Emission of WSe₂ Monolayers by Laser Excitation at Exciton Resonances”, *Phys. Rev. Lett.*, 114, 097403 (2015).

[8] A. Gartman et al., “Efficient integration of single-photon emitters in thin InSe films into resonance silicon waveguides”, *JETP Lett.*, 112, 693–698 (2020).

[9] A. Gartman et al., “Efficient Light Coupling and Purcell Effect Enhancement for Interlayer Exciton Emitters in 2D Heterostructures Combined with SiN Nanoparticles”, *Nanomaterials*, 13, 1821 (2023).



LD-I-5

Diode-laser spectroscopy of metastable atoms of heavy inert gases in high-frequency discharge plasma

A. Chernyshov, P. Mikheyev, E. Fomin

*Samara Branch of P.N. Lebedev Physical Institute of the Russian Academy of Sciences (SB LPI),
221, Novo-Sadovaya, Samara, 443011, Russian Federation*

chak@fian.smr.ru

Determination of gas-discharge plasma parameters, such as gas temperature, electron number density and population of levels, by noninvasive spectral methods is simplified if the collision broadening and shift coefficients of the relevant spectral lines of the plasma-forming inert (or rare) gas are known. In 2012, lasers with optical pumping of metastable atoms of heavy rare gases, which are produced in a low-power electric discharge (OPRGL), were proposed [1]. At present, OPRGL is extensively studied as a chemically inert alternative to powerful diode pumped alkali metal vapor lasers. The interest in OPRGL aroused the need for reliable determination of the collision broadening and shift coefficients of infrared lines of rare gases, and especially for those transitions that are included in the laser cycle.

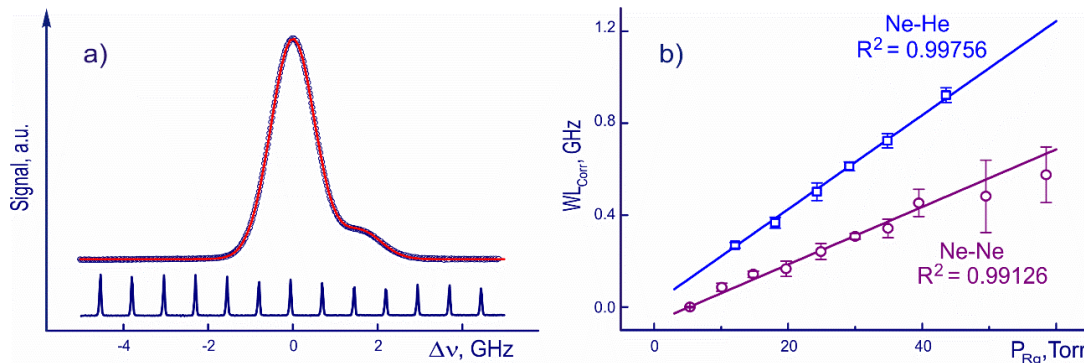


Fig. 1. Neon line 703.2 nm: a) Processed absorption signal for a natural mixture of isotopes and transmission resonances of the reference interferometer (FSR = 750 MHz); b) Dependence of the Lorentzian line width WL_{Corr} for the ^{20}Ne isotope on the partial pressure of the disturbing gases. The coefficient of determination R^2 close to unity confirms the linearity of the graphs.

The report discusses the technique for collisional broadening and shift coefficients measurements of the Ar^* , Ne^* and Kr^* IR lines by diode-laser absorption spectroscopy. In particular, inaccuracy due to temperature gradients that occur in the discharge region of the measuring cell with flowing gas is estimated. The possibility of reducing the Stark broadening to the line width to a negligibly low level when inert gas atoms are excited to a metastable state using an RF discharge is discussed [2]. A probing radiation source with a continuous tuning range up to 100 GHz is proposed, consisting of a quantum-well diode laser with an additional dual-plate external reflector [2-4]. The use of fluorescent lamp starters as reference cells for measuring of Ar^* and Ne^* line shifts is described [3]. The report also discusses a data processing technique [2-5] that accounts for the existence of Ne and Kr isotopes and their influence on the profiles of the studied lines Fig.1. The developed technique eliminates the need to use expensive isotopically enriched rare gases for spectroscopic measurements. The assessment of the reliability of the obtained collisional broadening and shift coefficients was made by comparing their values with relevant data from literature and calculations.

[1] P. Mikheyev. Optically pumped rare-gas lasers, *Quantum Electronics*, vol. 45, pp. 704-708, (2015).

[2] P. Mikheyev, A. Chernyshov, N. Ufimtsev et al. Pressure broadening of Ar and $\text{Kr} (n+1)s[3/2]_2 \rightarrow (n+1)p[5/2]_3$ transition in the parent gases and in He, *J. Quant. Spectrosc. Radiat. Transfer.*, vol. 164, pp. 1-7, (2015).

[3] A. Chernyshov, P. Mikheyev, N. Ufimtsev. Measurement of pressure shift and broadening for Ar and $\text{Kr} 4s[3/2]_2 \rightarrow 4p[5/2]_3$ transition in rare gases using diode-laser spectroscopy, *J. Quant. Spectrosc. Radiat. Transfer.*, vol. 222, pp. 84-88, (2019).

[4] A. Chernyshov, P. Mikheyev, N. Ufimtsev. Measurement of pressure shift and broadening coefficients for $\text{Ne} 3s[3/2]_2 \rightarrow 3p[5/2]_3$ transition in Ne and He using diode-laser absorption spectroscopy, *J. Quant. Spectrosc. Radiat. Transfer.*, vol. 258, pp. 107368, (2021).

[5] A. Chernyshov, P. Mikheyev, N. Ufimtsev. Collisional broadening and shift coefficients for $(n+1)s[3/2]_2 \rightarrow (n+1)p[1/2]_1$ argon and neon lines in parent and foreign rare gases, *J. Quant. Spectrosc. Radiat. Transfer.*, vol. 293, pp. 108381, (2022).



LD-I-6

Fast sensitive laser absorption spectroscopy

V.V. Lagunov, V.N. Ochkin, A.I. Volkova

P.N. Lebedev Physical Institute Russian Academy of Sciences 119991 Russia, Moscow, Leninskiy prosp., 53

ochkinvn@lebedev.ru

To achieve the high sensitivity of molecule densities measurements by means the optical absorption spectroscopy one needs to use the technique with fast frequency tuning and high resolution. The practice shows that for the real single-record low signal/noise ratios $\sim 10^{-2}$, absorption coefficient $k \sim 10^{-5} \text{ cm}^{-1}$, spectral resolution $R_s \sim 10^{-3} \text{ cm}^{-1}$ and time resolution of $\Delta t \sim 1 \text{ s}$ the frequency tuning rates have to be in the order of $r \sim (10^5 - 10^7) \text{ cm}^{-1} \text{ s}^{-1}$ for a free space single-pass schemes or $r \sim (10^2 - 10^4) \text{ cm}^{-1} \text{ s}^{-1}$ for multi-pass cavities [1]. Such kind of parameters can be implemented using conventional diode (DL) and/or quantum cascade (QCL) semiconductor lasers. But, as it was first shown in [2] in free space experiments with DL the limitations of fundamental nature appear. At such tuning rates it was observed that the non-harmonic oscillations disturb the classical spectral line profile and those were interpreted as a non-stationary coherent effect due to interference of the incident and induced radiation from matter. Much later (e.g. [3]) this effect was studied in more detail by many groups using fast-tuned QCL and it was related to those that were predicted [4] and observed [5] in radiofrequency spectral range for nuclear magnetic resonance NMR at variable magnetic field. Other spectra tuning rate dependent distortions of non-oscillatory type have been observed in recent experiments with high-quality optical cells and related to finite photon lifetime in intracell absorbing media [6].

Though the frequency tuning rate-dependent spectra distortions are now widely discussed the central question on the possibility to use the absorption as a quantitative technique is in a shadow. Some attempts [7] to measure the concentration of absorbing particles based on classic absorption losses in the fast frequency tuning mode failed. This situation was analyzed, and the main results are the following:

- in a single pass case the spectrum is not stationary since the recording time is comparable or shorter than the phase relaxation time of absorbing particle excitations. The non-perturbed stationary spectrum can be restored from the non-stationary one and the basic absorption laws can be applied for quantitative measurements within the processing scheme provided – (i) a single wing of the line profile is used in the frequency range corresponding to the onset of interaction between the probe radiation and the molecular resonance during the frequency tuning. This leads to the restoration of the convolution of static profile and instrumental function; (ii) to reconstruct the static Voigt profile after the deconvolution it is necessary to account for: *a*) Lorentz and Doppler broadening, *b*) the broadening by optical transition saturation, *c*) the broadening caused by finite time of light-matter interaction due to flight of particles across the laser beam.

- in case of measurements in high-quality external optical cells, the main mechanism of spectra distortion due to finite intracavity photon lifetime manifests itself at the frequency tuning times longer than the particles phase relaxation times. That is why even for strong spectra distortion the real line profile remains static and the problem of quantitative measurements is reduced to the exclusion of a single instrumental function in the experimental spectrum deconvolution procedure.

- if the integral version of absorption measurements is used, then for both of the abovementioned cases of tuning the spectra depending on the velocity the classic Kravetz integral relation is valid for the static component of the spectrum, which can be applied not only to real physical profile, but also to the experimentally observed one. It is shown that the result of measuring the particles density does not depend on the instrumental function form, so the profile deconvolution is not required.

This work was supported by a grant from the Russian Science Foundation (project No.19-12-00310, <https://rscf.ru/en/project/19-12-00310/>).

[1] V. Lagunov, V. Ochkin, A. Volkova Determination of particle concentrations from absorption spectra with fast frequency tuning. ALT-2022 conference abstracts, pp. 192-192 (2022).

[2] I. I. Zasavitskii, M. A. Kerimkulov, A. I. Nadezhdinskii, V. N. Ochkin, S. Yu. Savinov, M. V. Spiridonov, and A. P. Shotov, "Coherent nonstationary effects under quick recording of absorption-spectrum," *Opt.Spectrosc.* **65** (6), 706–709 (1988).

[3] G. Duxbury, et al., Rapid passage induced population transfer and coherences in the 8 micron spectrum of nitrous oxide, *Molecular Physics*, 105.5-7, 741-754, (2007).

[4] F. Bloch, "Nuclear induction," *Phys. Rev.* **70** (7-8), 460–474 (1946).

[5] N. Bloembergen, E. Parcell, and R. Pound, "Relaxation effects in nuclear magnetic resonance absorption," *Phys. Rev.* **73** (7), 679–712 (1948).

[6] V. V. Lagunov, I. V. Nikolaev, and V. N. Ochkin, "High-resolution and high-sensitivity absorption spectroscopy in external optical resonators with fast frequency tuning," *Spectrochim. Acta, Part A* **246**, 119060 (2021).

[7] J. H. Van Helden, S. J. Horrocks, G. A. D. Ritchie, Application of quantum cascade lasers in studies of low-pressure plasmas: Characterization of rapid passage effects on density and temperature measurements, *Applied Physics Letters*, 92(8), 081506, (2008).

LD-I-7

Structural coloring and information encryption via ablation-free femtosecond laser patterning

V. Lavidas¹, A. Zhizhchenko¹, A. Kuchmizhak^{1,2}

1- Institute of Automation and Control Processes, Far Eastern Branch, Russian Academy of Science, 5 Radio Str., Vladivostok 690041, Russia

2- Pacific Quantum Center, Far Eastern Federal University, Vladivostok, Russia

alex.iacp.dvo@mail.ru

Structural colors coming from light interaction with resonant nanostructures hold promise for optical filtering, displaying, color marking and anti-counterfeiting of valuable goods. In sharp contrast to pigments, these colors are non-fading and stable against UV radiation and thermal treatment. At the same time, state-of-the-art applications require controlling over the color tones/saturation at submicron lateral scale, thus expensive and nonscalable lithography-based technologies are to be applied for fabrication of the pixelated nanostructures and their proper arrangement. Direct laser technologies were suggested for more cheap fabrication of nanostructures supporting structural color effects. In particular, tightly focused laser exposure was found to cause local dewetting of the thin Au films coated above the Fabry-Perot filter to form randomly arranged plasmonic nanoparticles that absorb specific wavelength range and modulate the reflectance spectra of the surface [1]. Despite simplicity of the suggested approach, color tone and saturation can not be precisely controlled once the nanostructures are formed through random self-organization process, while their average size depends on the initial thickness of the top Au film.

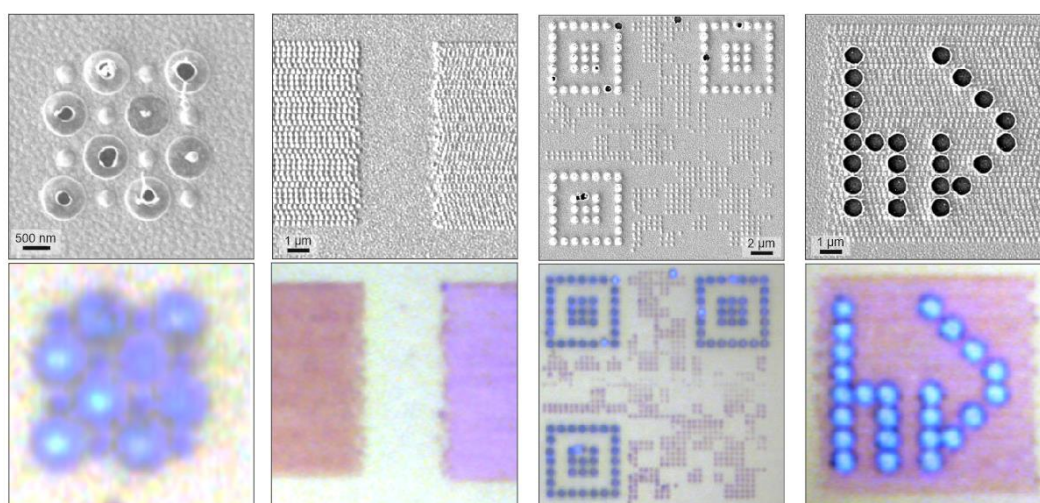


Fig. 1. Correlated scanning electron microscopy and optical images revealing the laser-printed nanostructures and their color appearance in the optical microscope (magnification 100x, numerical aperture of 0.95).

In our work, we suggested alternative approach providing control over the color tone and saturation at single-pixel level, expanded color gamut as well as fabrication resolution up to 50000 dpi. The approach is based on the femtosecond laser patterning of the metal-insulator-metal Fabry-Perot cavity with the layer thicknesses optimized to demonstrate pronounced reflectance dip in the visible spectral range. Variation of the applied pulse energy allowed to control geometry of the formed nanostructures spanning from 3D nanoprotusions and volcano-like nanoholes to micro-holes and random nanotextured surfaces that modulate the local surface reflectivity at single-pixel length scale (Fig. 1).

This work was supported by Russian Science Foundation (grant. 21-72-20122)

[1] A.S. Roberts, S.M. Novikov, Y. Yang, Y. Chen, S. Boroviks, J. Beermann, S. I. Bozhevolnyi, Laser writing of bright colors on near-percolation plasmonic reflector arrays, ACS nano vol. 13, 71-77 (2018).



LD-I-8

Optical and structural anisotropy induced in the thin amorphous films of chalcogenides and silicon by femtosecond laser action

D. Shuleiko¹, P. Danilov^{1,2}, E. Kuzmin^{1,2}, T. Kunkel^{1,3,4}, P. Lazarenko⁵, S. Zaboltnov¹, P. Kashkarov¹

1- Faculty of Physics, Lomonosov Moscow State University, 1/2 Leninskie Gory, Moscow, Russia;

2- Lebedev Physical Institute, the Russian Academy of Science, 53 Leninsky Avenue, Moscow, Russia

3- Moscow Institute of Physics and Technology, 9 Institutskiy Per., Dolgoprudny, Russia

4- Kurnakov Institute of General and Inorganic Chemistry of the Russian Academy of Sciences, 31 Leninsky Avenue, Moscow, Russia

5- Institute of Advanced Materials and Technologies, National Research University of Electronic Technology, 1 Shokina Sq., Zelenograd, Russia

shuleyko.dmitriy@physics.msu.ru

Femtosecond laser-induced periodic surface structures (LIPSS) on chalcogenide vitreous semiconductor (ChVS) films are of great interest owing to a possibility of optical and electrophysical anisotropy in them caused both by surface relief modulation and phase transformations [1, 2]. Currently, laser-induced surface relief formation accompanied by phase transformations has been well studied for GST225 ($\text{Ge}_2\text{Sb}_2\text{Te}_5$) films [3]. However, from the point of view of near and mid-infrared optics, arsenic sulfide (As_2S_3) and arsenic selenide (As_2Se_3) seem to be more suitable materials [2]. Therefore, this work was aimed to produce LIPSS of various types on the surface of abovementioned materials and analyze the possibility of simultaneous phase transformations in them.

To produce LIPSS, thin ChVS films ($\text{As}_2\text{S}_3 - 576 \pm 5$ nm; $\text{As}_2\text{Se}_3 - 842 \pm 5$ nm) on single-crystal silicon substrates with a chromium sublayer (100 nm) or on quartz glasses were irradiated with femtosecond laser pulses at the frequency of the second optical harmonic (515 nm, 300 fs, pulses energy and number $E = 0.1-0.4$ μJ , $N = 10-1200$) using a Satsuma laser system (Amplitude Systems) at normal incidence.

The LIPSS with wave- (~ 515 nm) and subwavelength (150–185 nm) periods, oriented, respectively, orthogonally or along the polarization vector, were formed on the surfaces of the films as a result of irradiation. The type of LIPSS formed varied depending on the number and energy of femtosecond laser pulses. The relief modulation reached 115 and 40 nm for wave- and subwavelength LIPSS, respectively. The numerical simulation within the framework of the plasmon-polariton mechanism for such LIPSS formation was consistent with experimental results: with an increase in the number of laser pulses or their energy, an evolution is observed from subwavelength to wavelength LIPSS. This effect is explained by a change in the mode of surface plasmon-polariton excited, caused by increased concentration of nonequilibrium charge carriers generated by femtosecond laser pulse. Additionally, during such evolution, the structures of both types can be observed simultaneously within the same crater formed by a femtosecond laser pulse impact, in the form of a hierarchical structure consisting of two orthogonal gratings with different periods.

Raman spectra analysis (Horiba HR800, 488 nm excitation) demonstrated no structural changes in As_2S_3 films. However, femtosecond laser-induced phase transformations are possible for As_2Se_3 films according to Raman data.

The obtained LIPSS on ChVS surfaces, possessing form anisotropy, can be used to create polarization-sensitive elements of infrared optics.

The work was supported by the Russian Science Foundation (grant 22-19-00035).

<https://rscf.ru/project/22-19-00035/>

[1] A. Kolchin, D. Shuleiko, M. Martyshov, A. Efimova, L. Golovan, D. Presnov, T. Kunkel, V. Glukhenkaya, P. Lazarenko, P. Kashkarov, S. Zaboltnov, S. Kozyukhin. Artificial anisotropy in $\text{Ge}_2\text{Sb}_2\text{Te}_5$ thin films after femtosecond laser irradiation. *Materials*, vol. 15, art. 3499 (2022)

[2] W. Ma, L. Wang, P. Zhang, W. Zhang, B. Song, S. Dai. Femtosecond laser direct writing of dif-fraction grating and its refractive index change in chalcogenide As_2Se_3 film. *Optics Express*, vol. 27, pp. 30090–30101 (2019)

[3] S. Zaboltnov, A. Kolchin, D. Shuleiko, D. Presnov, T. Kaminskaya, P. Lazarenko, V. Glukhenkaya, T. Kunkel, S. Kozyukhin, P. Kashkarov. Periodic relief fabrication and reversible phase transitions in amorphous $\text{Ge}_2\text{Sb}_2\text{Te}_5$ thin films upon mul-ti-pulse femtosecond irradiation. *Micro*, vol. 2, pp. 88–99 (2022)



LD-I-10

Laser heating of silicon and germanium nanostructures in Raman studies

A.V. Pavlikov

*Faculty of Physics, M.V. Lomonosov Moscow State University, Leninskie Gory, Moscow
119991, Russia*

E-mail: pavlikovav@my.msu.ru

The phenomenon of Raman scattering of light is a widespread research technique in which laser radiation is used for excitation. Continuous lasers with relatively low power are used for this purpose. However, when studying objects with a weak Raman scattering signal, in particular micro- and nanostructures, it is necessary to increase the intensity of excitation in order to obtain a recorded response.

Silicon nanostructures demonstrate reversible changes in the Raman spectra under intense laser excitation, which can manifest itself in a shift of peak positions additional to quantum confinement effect [1]. Unlike silicon, germanium has a stronger absorption of visible light; therefore, irreversible changes can occur during laser exposure. These changes lead to the appearance of a nanocrystalline peak in the Raman spectra (Fig.1) [2].

Electrochemically etched porous silicon nanostructures and vertically oriented silicon nanowires exhibit laser heating in two different ways. Porous silicon exhibits a gradual shift in the position of the peak and broadening of the line width. In addition to the manifestation of the heating effect described above, an additional peak can appear in the Raman spectra of vertically oriented silicon nanowires. By decreasing the laser intensity, one can obtain the original spectrum obtained at a low excitation intensity.

A comparison is made of germanium nanowires obtained by electrochemical deposition and ion implantation. Having a similar morphology, these two types of nanostructures also exhibit similar Raman spectra and similar irreversible changes associated with local heating of nanowires to temperatures sufficient for crystallization.

The effects of laser heating can be explained by the low thermal conductivity of nanostructures.

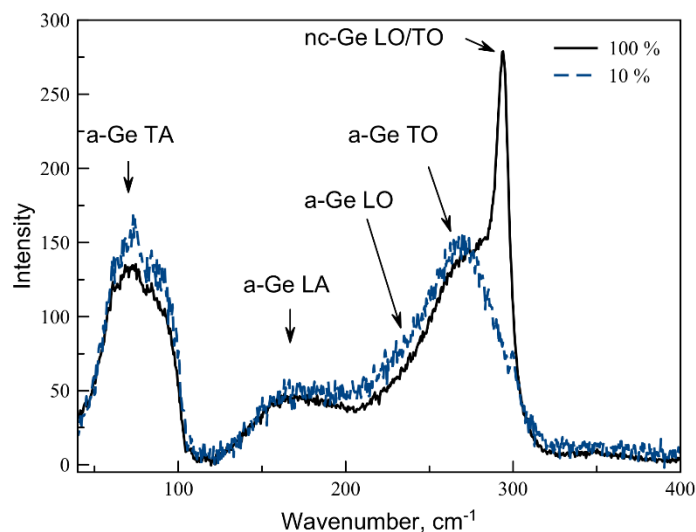


Figure 1. Raman spectra of implanted Ge obtained at low (10%) and high (100%) excitation laser intensity.

[1] S. Piscanec, M. Cantoro, A. C. Ferrari, J. A. Zapien, Y. Lifshitz, S. T. Lee, S. Hofmann, and J. Robertson, Raman spectroscopy of silicon nanowires, *Phys. Rev. B*, vol. 68, pp. 241312- 241316, (2003).

[2] A. M. Sharafutdinova, A. V. Pavlikov, A. M. Rogov, S. N. Bokova-Sirosh, E. D. Obraztsova, A. L. Stepanov, *J Raman Spectrosc*, vol. 53, p.p. 1055-1061, (2022).



LD-I-11

Metal nanostructures optimized for plasmonic enhancement of chemiluminescence yield of standard biocompatible chemiluminophores

A.V. Palekhova¹, D.R. Dadadzhanov¹, T.A. Vartanyan¹

1- International Research and Educational Center for Physics of Nanostructures, ITMO University, 49 Kronverksky pr., St. Petersburg 197101, Russia

Email: tavartanyan@itmo.ru, daler.dadadzhanov@gmail.com

Chemiluminescence phenomena has been widely used in the fields of medicine, chemistry and biology. It allows to detect extremely weak emission arising during chemical or biochemical reactions of chemiluminophores with reactive oxygen species [1]. The use of chemiluminescent research methods allows to successfully solve many theoretical and practical medical and biological problems. This method requires no special laboratory conditions and special preparation of the material for analysis, it is sensitive, reliable, and meets the requirements of express research methods. Unfortunately, the luminol chemiluminescence yield is large only in media with high pH levels, while its application in media with neutral, pH=7, and lower pH levels is also desirable [2]. To overcome this problem, the localized plasmon resonance in metal nanoparticles can be employed to speed up the radiative transitions and, in this way, to enlarge the chemiluminescence yield [3,4]. The enhancement factor is highly dependent on the nanoparticles size and shape that determines the spectral position of the localized plasmon resonance and its overlap with the luminol luminescent band as well as on their concentration that determines the mean distance between the luminol molecule and the nearest metal nanoparticle. Hence, a broad search for the optimum values of all these parameters is necessary to achieve the maximum enhancement factor.

The effect of the presence of silver nanoparticles on the luminol chemiluminescent intensity we measured in a specially designed microfluidic chip. The chemiluminescence spectra was measured by stationary spectrofluorometer with Xe-lamp-off, while the decay of luminol luminescence was measured with a home-made photon counter system. Silver nanoparticles were prepared by two different methods: laser ablation in water and chemical citrate-reduction method. The laser ablation method has a significant advantage over the chemical method, since the result is a colloidal solution of particles free from surfactants, while in the chemical method the surface of the nanoparticles is covered with the substances not always desirable. In the search for optimum conditions, we have studied the dependence of the luminol chemiluminescence on the pH of the medium, the nanoparticles concentration, the thickness of the shell around nanoparticles as well as on the extent of the spectral overlap between the silver nanoparticle plasmon band with the emission band of luminol. As a result of this search, about 5-fold enhancement of luminol chemiluminescence in the presence of silver nanoparticles fabricated by the laser ablation method was obtained in the media with the pH as low as 5.

This work was supported by the Russian Science Foundation (Project 23-72-00045).

[1] S. Bedouhène, F. Moulti-Mati, M. Hurtado-Nedelec, P. M. C. Dang, J. El-Benna, Luminol-amplified chemiluminescence detects mainly superoxide anion produced by human neutrophils, *Am. J. Blood Res.*, vol. 7, pp. 41 – 48, (2017).

[2] P. Khan, D. Idrees, M.A. Moxley, J.A. Corbett, F. Ahmad, G. von Figura, W.S. Sly, A. Waheed, M.I. Hassan, Luminol-based chemiluminescent signals: clinical and non-clinical application and future uses. *Appl. Biochem. Biotechnol.*, vol. 173, pp. 333-355, (2014), doi: 10.1007/s12010-014-0850-1.

[3] A. Karabchevsky, A. Mosayyebi, A. V. Kavokin, Tuning the chemiluminescence of a luminol flow using plasmonic nanoparticles, *Light: Sci. & Appl.*, vol. 5, pp. e16164-e16164, (2016), doi.org/10.1038/lsa.2016.164

[4] D. R. Dadadzhanov, I. A. Gladskikh, M. A. Baranov, T. A. Vartanyan, A. Karabchevsky, Self-organized plasmonic metasurfaces: The role of the Purcell effect in metal-enhanced chemiluminescence (MEC), *Sen. & Act. B: Chemical*, vol. 333, pp. 129453-1 - 129453-10, (2021), doi.org/10.1016/j.snb.2021.129453

LD-I-12

Laser synthesis for SERS

A. Manshina

Institute of Chemistry, Saint-Petersburg State University, 26 Universitetskii Prospect, 198504 Saint-Petersburg, Russia

email address: a.manshina@spbu.ru

Highly efficient, homogeneous, and reproducible substrates for surface enhanced Raman spectroscopy (SERS) are highly demanded for practical broadband sensing and various analytes detection. To date, there are huge number of different synthesis strategies allowing obtaining of SERS active substrates. However most of them give substrates with fixed characteristics – composition, morphology that requires using other methods for creation of SERS active structures with another properties.

Here we present universal and scalable approach for creation SERS active substrates with finely tuned parameters – composition, topology, spectral width of SERS sensing, etc. The approach is based on laser induced deposition method. It allows formation of plasmonic nanostructures directly on the substrate surface from simple solutions of metal precursors (metalorganic complexes or salts) under low intensity CW laser radiation [1-4]. Thus, variation of experimental parameters (kind of precursor, solvent, laser wavelength, laser irradiation time) allows precise variation of characteristics of plasmonic nanostructures (Figure 1). All the plasmonic nanostructures created by LID exhibit high SERS analytical enhancement factor in wide spectral range, and a linear response toward sensing in a wide concentration range as well as high reproducibility of SERS signal over substrate. As analytes, various substances from classical dyes to toxins and bioliquids were studied.

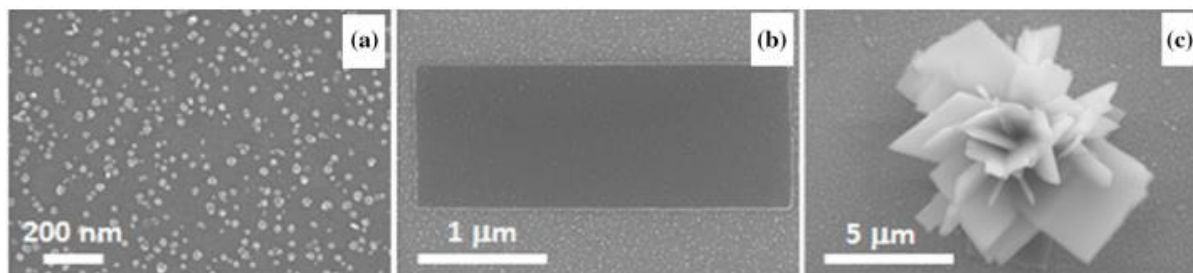


Figure 1 SEM images of typical nanostructures obtained by LID: a) nanoparticles, b) nanoflake, and c) nanoflower

Acknowledgements

This work was supported by RSF project 23-49-10044. Authors are grateful to “Centre for Optical and Laser materials research” and “Interdisciplinary Resource Centre for Nanotechnology” Research Park of Saint Petersburg State University for technical support.

References

- [1] A. Povolotckaia, D. Pankin, Yu. Petrov, A. Vasileva, I. Kolesnikov, G. Sarau, S. Christiansen, G. Leuchs, and A. Manshina, *J Mater Sci* 54:8177–8186,(2019)
- [2]. D. V. Mamonova, A. A. Vasileva, Y. V. Petrov, A. V. Koroleva, D. V. Danilov, I. E. Kolesnikov, G. I. Bikbaeva., J. Bachmann, and A. A. Manshina, *Nanomaterials* 12(1), (2022)
- [3] D.V Mamonova, A.A.Vasileva, Y.V.Petrov, ... J.Bachmann, A.A.Manshina, *Materials*, 14(1), p. 1–14, (2021)
- [4] G. Bikbaeva, A. Belhadi, D. Pankin, D. Mamonova, I. Kolesnikov, Yu. Petrov, T. Ivanova, D. Ivanov, A. Manshina, submitted to *Nano-Structures & Nano-Objects*.

Biodegradable luminescent porous silicon nanoparticles in cancer diagnosis and therapy

L.A. Osminkina^{1,2}

1- Lomonosov Moscow State University, Physics department, Leninskie gory 1, 119991, Moscow, Russia

2- Institute of Biological Instrumentation, Russian Academy of Sciences, Moscow oblast, Pushchino, 142290 Russia
 osminkina@physics.msu.ru

The development of new intelligent drug delivery systems to overcome unwanted side effects and maximize the therapeutic effectiveness of chemotherapy for cancer diseases is one of the main tasks of modern medicine. Active research is being conducted to explore various nanosized drug carriers (nanocarriers) for these purposes.

The use of porous silicon nanoparticles as the basis for nanocarriers is due to the unique properties of these solid-state nanomaterials, such as high biocompatibility [1] and complete biodegradability into non-toxic silicic acid [2]. The porous structure of the nanoparticles (with porosity values reaching up to 80% of their volume) provides a high drug-loading capacity for efficient drug delivery [3] (Figure 1). The simplicity of surface modification methods for the nanoparticles enables specific targeted delivery of various hydrophobic and hydrophilic drugs, radiopharmaceuticals, proteins, peptides, DNA, etc. into cells [4].

The presence of efficient luminescence in porous silicon nanoparticles allows their utilization as contrast agents for bioimaging of cells and tissues [5]. The properties of porous silicon nanoparticles, acting as photosensitizers [6], sensitizers of high-frequency electromagnetic fields [7] and therapeutic ultrasound [8], provide them with therapeutic functions and the potential for stimuli-triggered drug release from the nanopores of nanocarriers.

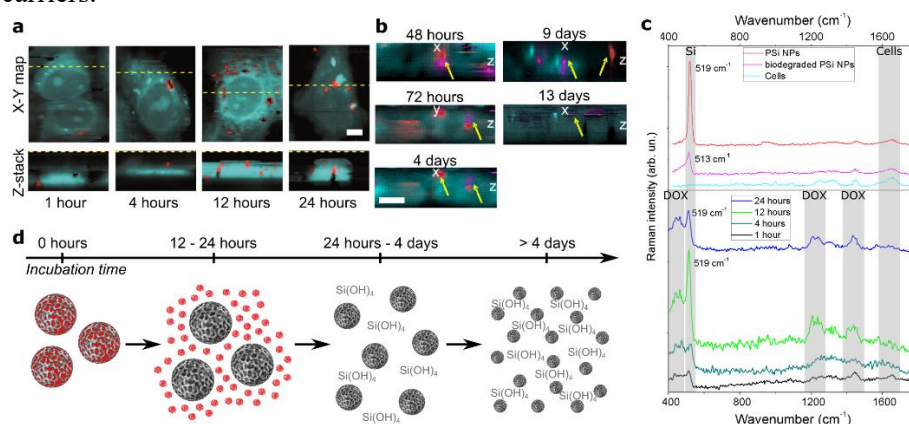


Figure 1. Study of doxorubicin delivery and biodegradation of porous silicon nanoparticles inside cancer cells by Raman spectroscopy [3]

The research is supported by Russian Science Foundation Grant No. 22-72-10062.

References:

- Low S.P., Voelcker N. H. "Biocompatibility of porous silicon." Handbook of porous silicon. Springer, 2014. 381-393.
- Qurrat. S. "Biodegradability of porous silicon." Handbook of Porous Silicon (2014): 395-401.
- Maximchik, Polina V., et al. "Biodegradable porous silicon nanocontainers as an effective drug carrier for regulation of the tumor cell death pathways." ACS Biomaterials Science & Engineering 5.11 (2019): 6063-6071.
- Tieu T., et al. "Advances in porous silicon-based nanomaterials for diagnostic and therapeutic applications." Advanced therapeutics 2.1 (2019): 1800095.
- Tolstik E., et al. "Linear and non-linear optical imaging of cancer cells with silicon nanoparticles." International journal of molecular sciences 17.9 (2016): 1536.
- Timoshenko V. Yu, et al. "Silicon nanocrystals as photosensitizers of active oxygen for biomedical applications." Jetp Letters 83 (2006): 423-426.
- Tamarov K.P., et al. "Radio frequency radiation-induced hyperthermia using Si nanoparticle-based sensitizers for mild cancer therapy." Scientific reports 4.1 (2014): 1-7.
- Osminkina L.A., et al. "Porous silicon nanoparticles as efficient sensitizers for sonodynamic therapy of cancer." Microporous and Mesoporous Materials 210 (2015): 169-175.

LD-I-14

Laser spectroscopy of carbon nanoparticles in creation of multimodal nanosensors

O. Sarmanova¹, S. Burikov¹, A. Vervald¹, K. Laptinskiy², T. Dolenko¹

1- Department of Physics, Lomonosov Moscow State University, Leninskiye Gory 1/2, 119991 Moscow, Russia

2- Skobeltsyn Institute of Nuclear Physics, Lomonosov Moscow State University, Leninskiye Gory 1/2, 119991 Moscow, Russia

tdolenko@mail.ru

The relevance of the development of optical nanosensors of environmental parameters is due to the active development of science and industry, where the problem of controlling the content of various substances in multicomponent media is becoming increasingly acute. At present, the development of such nanosensors is necessary for biomedicine, technological production, and ecology. One of the most promising bases for sensors are carbon dots (CD). According to the results of many publications, CD synthesized by certain methods have photoluminescence (PL) that is sensitive to environmental parameters, which makes it possible to develop sensors of these parameters based on CD.

In our study, the objects of the study were CD synthesized using the hydrothermal method of synthesis from citric acid and ethylenediamine. The effect of temperature, pH of the environment, as well as ions Fe^{3+} , Cr^{3+} , Al^{3+} , Co^{2+} , Cu^{2+} , Pb^{2+} , Zn^{2+} , Ni^{2+} , Mg^{2+} present in the medium, on the PL of our CD was found.

In this study, the mechanisms of the influence of pH and temperature on the CD PL were studied. It was shown that the influence of pH on the surface photoluminescence of nanoparticles with hydrogen-containing groups is due to the (de)protonation of surface carboxyl, hydroxyl, and amide groups. This conclusion is confirmed by quantum calculations of the behavior of surface groups at various pH and by the results of analysis of dependences of CD ζ -potentials on the pH. Using the artificial neural networks, CD-based nanosensors were developed that allow measuring the temperature and pH of the environment with an accuracy of 0.67°C and 0.005, respectively [1].

As a result of studying the interactions of CD with ions of the pointed metals, the sensitivity of CD PL to certain ions was discovered and confirmed by molecular dynamics calculations. It was found that all the studied metal ions quench the CD PL to some extent. Using the Stern-Volmer theory and measured PL decay kinetics, it was found that Cu^{2+} , Zn^{2+} , Ni^{2+} , Mg^{2+} are characterized by static photoluminescent CD-nanosensor was developed to determine the concentration of four ions Cu^{2+} , Cr^{3+} , Ni^{2+} , and NO_3^- in water simultaneously. The use of convolutional neural networks to solve the problem provided average absolute errors in determining the concentrations of Cu^{2+} , Cr^{3+} , Ni^{2+} и NO_3^- ions of 0.28 mM, 0.24 mM, 0.79 mM, and 1.15 mM, respectively [2]. The obtained errors in determining the concentrations of the investigated heavy metal cations fully satisfy the needs of monitoring the composition of waste and process waters [3].

The results were obtained using laser photoluminescence spectroscopy, laser time-resolved spectroscopy, laser correlation spectroscopy, IR absorption spectroscopy.

The research was carried out at the expense of the grant of the Russian Science Foundation No. 22-12-00138, <https://rscf.ru/en/project/22-12-00138/>

[1] O. Sarmanova, K. Laptinskiy, M. Khmeleva, S. Burikov, S. Dolenko, A. Tomskaya, T. Dolenko, Development of the fluorescent carbon nanosensor for pH and temperature of liquid media with artificial neural networks, *Spectrochimica Acta – Part A: Molecular and Biomolecular Spectroscopy*, vol.258, pp.119861-1 – 119861-2, (2023).

[2] O. Sarmanova, K. Laptinskiy, S. Burikov, G. Chugreeva, T. Dolenko, Implementing neural network approach to create carbon-based optical nanosensor of heavy metal ions in liquid media, *Spectrochimica Acta – Part A: Molecular and Biomolecular Spectroscopy*, vol.286, pp.122003-1 – 122003-8, (2023).

[3] F. Akbal, and S. Camc, Treatment of metal plating wastewater by electrocoagulation, *Environmental Progress & Sustainable Energy*, vol.31, pp.340–350, (2011).



LD-I-15

Near-field plasmon-enhanced spectroscopies of semiconductor nanostructures

**A.G. Milekhin¹, I.A. Milekhin², N.N. Kurus¹, L.S. Basalaeva¹, R.B. Vasiliev³, K.V. Anikin¹,
V.G. Mansurov¹, K.S. Zhuravlev¹, A.V. Latyshev^{1,4}, D.R.T. Zahn²**

1- A.V. Rzhhanov Institute of Semiconductor Physics, 630090, Novosibirsk, Lavrentjev av. 13, Russia

2- Semiconductor Physics, Chemnitz University of Technology, D-09107 Chemnitz, Germany

3- Department of Material Science, Moscow State University, Moscow, Russia

4- Novosibirsk State University, Novosibirsk, 630090, Pirogov str., 1, Russia

milekhin@isp.nsc.ru

Near-field plasmon-enhanced spectroscopies including Tip-Enhanced Raman scattering and photoluminescence (TERS and TEPL) were successfully applied to study the phonon and electron spectra of 2D, 1D, and 0D nanostructures with the spatial resolution much below diffraction limit.

TERS imaging by optical phonons in single 2D nanostructures including multi- and monolayer- graphene, 1D AlN nanocolumns, and 0D CdSe nanocrystals (NCs) placed in the gap between the TERS tip apex and plasmonic substrate allows determination of nanostructure size and shape, structural defects, mechanical strain, and local electromagnetic field enhancement.

The origin of ring-like TERS patterns with different diameters obtained for a single gold nanodisk with a monolayer coating of colloidal CdSe NCs excited with 638,2 and 785,3 nm wavelengths is discussed. TERS by surface optical (SO) phonons in AlN nanocolumns placed on an Au surface was observed. TERS taken for AlN nanocolumns with a diameter and height of about 200 and 50 nm, respectively, with different light polarizations with respect to the nanocolumn axes demonstrates different images. The origin of the changes in TERS images upon the light polarization is discussed.

TEPL from MoS₂ and WS₂ monolayer islands grown on a Si substrate reveals local variation of exciton PL energy and intensity depending on the number of monolayers and the presence of structural defects. The enhancement and quenching of TEPL originated from direct and indirect transitions in 1D and 0D single GaAs nanostructures is reported.

Acknowledgements

This work was supported by the Russian Science Foundation (project 22-12-00302).

LD-I-16

Exciton chirality of atomically thin AIBVI nanoplatelets with X-type stereoisomeric ligands

D.A. Kurtina, V.P. Grafova, A.I. Lebedev, R.B. Vasiliev

Lomonosov Moscow State University, 119991, Moscow, Russia

romvas@inorg.chem.msu.ru

Chirality refers to a geometrical property when an object cannot be superimposed onto its mirror image. In addition to its important role in biochemical and chemical processes, chirality leads to different interactions of molecules and structures with right- and left-handed circularly polarized light. Recently, chiral colloidal nanoparticles and nanostructures [1] have been of great interest, demonstrating different absorption of right- and left-handed circularly polarized light (circular dichroism, CD) or rotation of the light polarization plane (optical activity), as well as the emission of photons of a given circular polarization (circularly polarized luminescence). In this report, we present an analysis of 2D atomically thin nanostructures of cadmium and zinc chalcogenides hybridized with stereoisomeric L-/D-ligands and showed a distinctive CD in excitonic transitions.

We have developed a method for the growth of atomically thin nanosheets (nanoplatelets) of cadmium and zinc chalcogenides with a thickness of less than 1 nanometer (about 2-3 monolayers) in colloidal solutions. A system of cadmium (zinc) acetate/octadecene/oleic acid/oleylamine was used for the nanostructure growth in the temperature range of 110–250°C [2] and we achieved the formation of nanostructures with a precise (with an accuracy of 1 monolayer) thickness in the range of 0.6–0.9 nm. For the hybridization of nanostructures with chiral ligands, a protocol was developed for the exchange of native oleic acid ligand for stereoisomers of L-/D-cysteine and N-acetyl- L-/D- cysteine. A detailed study using HRTEM, HAADF-STEM, SAED, XRD methods showed zinc blende structure for CdTe and CdSe and wurtzite structure for ZnSe with the composition followed the ratio $[M_{n+1}E_nL_2]$ (M- zinc or cadmium, E - chalcogen, L - organic ligand, n - number of atomic planes) with integer coefficients.

Correlations between the size, composition, crystal structure of atomically thin nanosheets and their optical properties are established. Narrow (about 8-10 nm) exciton transitions involving the heavy hole HH, light hole LH, and spin-orbit hole SO were observed in the absorption spectrum of nanostructures at room temperatures together with exciton luminescence band in luminescence spectra. It was shown a bathochromic shift of all exciton bands up to 200 meV found for the thinnest nanostructures after ligand exchange supporting strong hybridization of ligand and semiconductor core.

The chiroptical properties of nanostructures hybridized with chiral ligands was studied by CD spectroscopy [3]. CD spectra showed distinct, sign-alternating bands correlated with the LH, HH, and SO transitions in the absorption spectra confirming the exciton nature of the induced CD bands. Change of L-stereoisomer of ligand to D-stereoisomer inverts the sign of the spectrum like mirror image with the same bands spectral position and intensity that supports the effect of the ligand on the induced preference in absorbance of right- or left-hand circularly polarized light. We found a maximum g-factor of dissymmetry of 0.01, which seems to be the highest value reported previously for AIBVI semiconductor nanoparticles. A model is proposed for induced chirality due to Wannier–Mott exciton in helicoidal potential of stereoisomeric ligands that was supported by analysis of effect of solvent polarity, optical rotation and modeling of ligand coordination. We believe that our work opens up new possibilities for creating artificial chiral nanostructures and will be useful for polarization-enabled applications in photonics.

This work was supported by the Russian Science Foundation (grant № 22-13-00101).

[1] Cho, N.H., Guerrero-Martínez, A., Ma, J. et al. Bioinspired chiral inorganic nanomaterials. *Nat Rev Bioeng* 1, 88–106 (2023).

[2] Kurtina D.A. et al., Atomically Thin Population of Colloidal CdSe Nanoplatelets: Growth of Rolled-up Nanosheets and Strong Circular Dichroism Induced by Ligand Exchange, *Chem. Mater.*, 31, 9652–9663, (2019).

[3] Kurtina, D.A.; Grafova, V.P.; et al. Induction of Chirality in Atomically Thin ZnSe and CdSe Nanoplatelets: Strengthening of Circular Dichroism via Different Coordination of Cysteine-Based Ligands on an Ultimate Thin Semiconductor Core. *Materials*, 16, 1073, (2023).



LD-I-18

Study of colloid nanoparticles in aqueous solutions by ultramicroscopy and dynamic light scattering

G.O. Silaev^{1,3}, F.V. Vereschagin¹, A.T. Shaydulin^{2,3}, Yu.V. Orlovskii²,
Yu.G. Vainer^{1,3}

1- Institute of Spectroscopy RAS, Moscow, Troitsk, 108840 Russia

2- Prokhorov General Physics Institute of RAS, Moscow, 119991 Russia

3- Higher School of Economics, National Research University, Moscow, 101000 Russia

E-mail: vainer@isan.troitsk.ru

The development of optical methods for studying colloidal nanoparticles in aqueous environments is one of the topical areas of nanophotonics. In particular, the development of methods that allow visualization and study of nanoparticles at the single particle level is highly relevant. Electron and probe microscopy methods, widely used for these purposes (tunneling, atomic force, optical near-field, etc.), have a number of fundamental drawbacks. They are characterized by a complex sample preparation and measurement procedure, are unsuitable for studying nanoparticles in aqueous environments, may have unwanted effects on the sample, and are not very accessible. Optical far-field microscopy methods are free from most of the listed drawbacks and are characterized by high efficiency, a significantly simpler measurement procedure, and a low effect on the sample.

In the overwhelming majority of cases, nanoparticles are studied in the form of powders or suspensions, which leads to distortion of information about the individual properties of the particles. Therefore, the development of methods for studying and visualizing nanoparticles at the single particle level is also one of the topical areas of modern science.

The talk reports the development of a highly sensitive laser ultramicroscope operating on the "light sheet" scheme, which allows visualization of single nanoparticles in aqueous solutions with sizes of up to 20 nanometers or less and determination of their individual sizes from the signals of light elastic scattering by analyzing the individual trajectories of their Brownian motion. The results of optical diagnostics of colloidal solutions of single dielectric nanocrystals of lanthanum fluoride - LaF₃ doped with europium (Eu³⁺) and neodymium (Nd³⁺) ions, with sizes within 10-30 nm, and their conglomerates using the developed microscope and developed methods are also reported. The results of comparative measurements of the sizes of the same nanoparticles using electronic and developed microscopes, as well as ensemble measurements of nanoparticles and their suspensions in water using the method of dynamic light scattering (DLS), are also presented.

Special attention is paid to the analysis of the experimental data obtained on the clusters formed on the basis of the studied colloidal nanoparticles, in order to gain a deeper understanding of the information about the properties of the particles obtained using the listed optical methods.

The research was supported by the Russian Science Foundation project No. 22-22-00998

LD-O-1

Determination of the concentration of metastable atoms of argon in the active medium of an optically pumped rare gas laser using one-dimensional model

A.V. Yuriev, Yu.A. Adamenkov, M.A. Gorbunov, V.A. Shaidulina, A.A. Kalacheva

*FSUE "RFNC – VNIIEF"
(Mira str, 37., Sarov, Russia 607190)*

E-mails: oefimova@otd13.vniief.ru

The optically pumped rare gas laser (OPRGL) is a new type of optically pumped gas laser with high quantum efficiency, which can convert the high output power of a diode laser into the output power of a gas laser with good beam quality. In [1], the first generation at a wavelength of 893.1 nm was demonstrated.

A mixture of argon (3%) and helium (97%) is used as the LONIG active medium. The main purpose of using helium is to increase the collisional relaxation from the pumping level to the upper laser level in order to create the largest population inversion [2, 3].

In this paper, a one-dimensional model of the LONIG active medium is presented. The model is necessary for the analysis of the discharge conditions.

The plasma kinetic model includes particles of argon (18 species) and helium (5 species). The model includes about 470 reactions describing the interaction of these particles.

The model was used to calculate the concentration of metastable argon atoms for different areas of the gap between electrodes. The concentration of metastable atoms was determined experimentally by diode laser spectroscopy. The experimental and calculated results are compared.

- [1] J. Han, M.C. Heaven. Gain and lasing of optically pumped metastable rare gas atoms // Optics Letters. – 2012. - Vol. 37, No. 11, pp 2157-2159
[2] D. J. Emmons, D. E. Weeks. Kinetics of high pressure argon-helium pulsed gas discharge// Journal of Applied Physics. – 2017. – Vol. 121, No. 20.
[3] J. Han, L. Glebov, G. Venus, M.C. Heaven. Demonstration of diode-pumped metastable Ar laser // Optics Letters. – 2013. - Vol. 38, No. 24, pp 5458-5461

Flexible infrared detector

**A.R. Rymzhina¹, P. Sharma^{1,2}, V.V. Podlipnov^{1,3}, V.S. Pavelyev^{1,3}, V. Platonov¹,
P. Mishra^{1,4}, N. Tripathi¹**

*1- Samara National Research University
443086, Samara, Russia, Moskovskoye Shosse 34;*

*2- School of Electronics Engineering (SENSE), Vellore Institute of Technology (VIT)
632014, Vellore, Tamil Nadu, India;*

*3- IPSI RAS – Branch of the FSRC “Crystallography and Photonics” RAS
443001, Samara, Russia, Molodogvardeyskaya 151;*

*4- Centre for Nanoscience and Nanotechnology, Jamia Millia Islamia (A Central University)
110025, Jamia Nagar, New Delhi, India.*

Main author email address: nishant.tripathi.11@gmail.com

Currently, e-textile is a popular area of research due to its ability to satisfy many needs of users [1]. Moreover, due to the rapid spread of fiber optic communication networks, it is necessary to develop highly efficient and fast photodetectors operating in the infrared (IR) range of radiation [2].

One of the main problems of the current IR detection technology is the low efficiency and the fact that the predominantly used sensing elements are based on crystalline epitaxial materials, which require rigid and brittle lattice-matched substrates such as CdZnTe, GaAs, InAs and InP. Therefore, these materials cannot be bent or compressed.

The TiS₂ band gap lies in the range from 0.2 to 0.9 eV, which indicates its dependence on the structure and the possibility of absorbing radiation in the IR spectral range [3]. TiS₂ in monolayer and few-layer forms is a transparent material that can be used in e-textiles [3]. In addition, the manufacturing process of devices based on transition metal dichalcogenides is mainly carried out by mechanical exfoliation.

The aim of this work is to solve the problems mentioned above by developing a flexible broadband IR photodetector based on a new promising TiS₂ material.

In this work, a comparative analysis of photodetectors based on TiS₂ nanosheets and on TiS₂ nanosheets functionalized with silver nitrate has been carried out. TiS₂ nanosheets were synthesized by chemical vapor transport technique following by 1 h ultrasonication treatment. The obtained solution was deposited between interdigitated electrodes fabricated on the surface of a flexible substrate using a dielectrophoresis process. Polyethylene terephthalate was used as the flexible substrate material. The characteristics of the fabricated photodetectors were determined by illuminating them with laser radiation with a wavelength of 1064 nm and a tunable power. A significant effect of silver nitrate particles scattered in the volume of the photodetector sensitive material on its efficiency is observed. The superiority of the photodetector based on TiS₂ nanosheets functionalized with silver nitrate is demonstrated. This photodetector demonstrates a significant response for the all used radiation powers (11.6, 19.6, 51, 100, and 150 mW), shows fast response (0.23 s) and recovery (0.49 s) times, coupled with high sensitivity (259840.34 A/W), quantum efficiency (303404.67 A/W·nm) and detectivity (3.1·10¹³ Jones) at an incident radiation power of 11.6 mW. The results obtained in this study can be used for the development and optimization of modern optoelectronic devices.

[1] Abid, P. Sehwat, C.M. Julien, S.S. Islam, WS₂ quantum dots on e-textile as a wearable UV photodetector: how well reduced graphene oxide can serve as a carrier transport medium, *ACS Applied Material Interfaces*, 12, pp. 39730–39744, (2020).

[2] L. Colace, G. Masini, F. Galluzzi, G. Assanto, G. Capellini, L.Di Gaspare, E. Palange, F. Evangelisti, Metal–semiconductor–metal near-infrared light detector based on epitaxial Ge/Si, *Applied Physics Letters*, 72, pp. 3175-3177, (1998).

[3] P.C. Sherrell, K. Sharda, C. Grotta, J. Ranalli, M.S. Sokolikova, F.M. Pesci, P. Palczynski, V.L. Bemmer, C. Mattevi, Thickness-dependent characterization of chemically exfoliated TiS₂ nanosheets, *ACS Omega*, 3, pp. 8655-8662, (2018).

Integration of data of various types of spectroscopy for determination of concentrations of ions in multi-component aqueous solutions

A. Guskov^{1,2}, I. Isaev², S. Burikov^{1,2}, T. Dolenko^{1,2}, K. Laptinskiy², O. Sarmanova^{1,2}, S. Dolenko²

1- Department of Physics, Lomonosov Moscow State University, Leninskiye Gory 1/2, 119991 Moscow, Russia

2- Skobeltsyn Institute of Nuclear Physics, Lomonosov Moscow State University, Leninskiye Gory 1/2, 119991 Moscow, Russia

dolenko@srd.sinp.msu.ru

The problem of simultaneous determination of concentrations of several types of ions in aqueous solutions is very topical in various subject areas, ranging from industry wastewater monitoring to environmental monitoring and quality control of beverages, e.g. mineral waters. Heavy metals are among the dangerous pollutants of water, therefore in many areas of industry and ecology there is a need to determine the concentration of heavy metal ions dissolved in water. Ions of various inorganic salts are simultaneously present in natural waters including those consumed by people, e.g. drinking or mineral waters.

The most accurate methods for determining the chemical composition of solutions are methods of conventional chemical analysis. However, this approach is time-consuming, it requires good sample preparation and consumption of expensive reagents. At the same time, most practical problems require easy-to-use, express and contactless methods. Optical spectroscopy (OS) techniques have the listed advantages; therefore, they make a promising alternative to chemical analysis. It should be also noted that different types of OS possess different properties, making them provide different information about the studied object. Therefore, integration of data of different OS types may result in more precise determination of the composition of the solution.

The most widely used types of OS are laser Raman spectroscopy, absorption spectroscopy and infrared spectroscopy. However, at present there is no analytical solution to the problem of determining the concentrations of each component in multicomponent solutions by their spectra for any of these methods. This problem is an inverse problem having properties that make solving it a hard task: it is non-linear, ill-conditioned or even ill-posed. Moreover, even the direct problem of modeling optical spectra cannot be adequately solved for spectra of liquids.

One of the few ways to solve such problems is the use of machine learning (ML) methods based on training ML models on experimental data. Here we present data integration of OS methods – simultaneous use of Raman, optical absorption and/or IR spectra to determine the types and concentrations of ions present in aqueous solutions.

In this paper, we report the results of solving two problems of the described type: determining the concentrations of 10 ions of inorganic salts by Raman and optical absorption spectra [1], and determining the concentrations of heavy metal ions in solutions by Raman absorption and infrared spectra [2]. The problems are solved using various ML methods. The results are compared with those obtained using data of each OS type separately.

The study was carried out at the expense of the grant from the Russian Science Foundation, project No. 19-11-00333, <https://rscf.ru/en/project/19-11-00333/>.

[1] I.Isaev, I.Gadzhiev, O.Sarmanova, S.Burikov, T.Dolenko, K.Laptinskiy, S.Dolenko. Using Method Integration Transfer Learning for Neural Network Solution of an Inverse Problem in Optical Spectroscopy. Proc.SPIE, 2022, V.12193, Laser Physics, Photonic Technologies, and Molecular Modeling, art.121930Y. DOI: 10.1117/12.2626358.

[2] A.Guskov, K.Laptinskiy, S.Burikov, I.Isaev. Integration of Data and Algorithms in Solving Inverse Problems of Spectroscopy of Solutions by Machine Learning Methods. In: Kryzhanovsky, B., Dunin-Barkowski, W., Redko, V., Tiumentsev, Y. (eds). Advances in Neural Computation, Machine Learning, and Cognitive Research VI. NEUROINFORMATICS 2022. Studies in Computational Intelligence, 2023, V.1064, pp. 395-405. Springer, Cham. DOI: 10.1007/978-3-031-19032-2_41.



LD-O-4

Features of the band structure in the luminescence response of 2D photonic crystals with Ge(Si) nanoislands

**A. Peretokin^{1,2}, M. Stepikhova¹, S. Dyakov³, D. Yurasov¹, M. Shaleev¹, D. Shengurov¹,
E. Rodyakina⁴, Sh. Smagina⁴, A. Novikov^{1,2}**

1- Institute of Physics of Microstructures RAS, st. Akademicheskaya, 7, 1 Afonino, Kstovsky district, Nizhny Novgorod region, Russia

2- UNN them N.I. Lobachevsky, Gagarin Ave., 27, Nizhny Novgorod, Russia

3- Institute of Semiconductor Physics A.V. Rzhanov SB RAS, 13 Lavrentiev Ave., Novosibirsk, Russia

4 - Skolkovo Institute of Science and Technology, st. Nobelya, 3, Moscow, Russia

aperetokin@ipmras.ru

To date, the problem associated with creation of effective silicon-based sources for the near-infrared range remains unresolved. One of the possible solutions to this problem are photonic crystals (PhC) with Ge(Si) nanoislands. In these structures, luminescence is observed in the wavelength range of 1.2-1.6 μm at room temperature [1]. The introduction of Ge(Si) nanoislands into PCs makes it possible to enhance their luminescent response by more than two orders of magnitude due to the interaction with distinct photonic modes [2]. A strong enhancement of the luminescence response is observed when the spectral position of PhC modes coincides with the maximum of nanoislands luminescence spectrum. In this work, we will show the possibilities to manage PhCs band structure depending on their parameters.

The luminescence response of PhCs that were fabricated on Si structures with self-assembled Ge(Si) nanoislands was analyzed depending on lattice period (a), r/a ratio, where r – is the hole radius, and hole depth (h) of PhCs. To analyze PhCs band structure, an original method for measuring the luminescence signal with angular resolution was used [3]. Measurements carried out with this technique allow us to restore the band structure of PhCs with good accuracy.

We will show the presence in luminescent response of PhCs of bound states in the continuum (BIC). The symmetry-protected BICs appear at the Γ point of Brillouin zone for both singlet and doublet photonic modes, and are manifested by thin lines in the luminescence spectra [2,4]. The quality factor of these lines (Q) can reach 2600. At certain parameters of PhCs, a flat zone with the symmetry-protected BIC can be formed. The latter is characterized by a near to zero group velocity [5]. Moreover, accidental BICs, modes anticrossing and so-called "hot-spots", which are related with the interaction of photonic modes in PhCs were also observed. Appearance of these phenomena in luminescence response of PhCs and their correlation with PhCs parameters will be discussed.

The features of the band structure of a PhC described above are of interest from both fundamental and applied points of view. For example, by selecting the parameters of the PhC, it is possible to achieve the combination of SP-BIC and parametric BIC. In this way, the "Super-BIC" state can be achieved, which makes it possible to obtain an extremely narrow lines in the PhC luminescence spectrum [6].

The work was funded by the Russian Science Foundation (grant #19-72-10011).

[1] V.Ya. Aleshkin, N.A. Bekin *et al.* Self-organization of germanium nanoislands obtained in silicon by molecular-beam epitaxy, JETP Letters, 67, p.48 (1998).

[2] S. Dyakov, M. Stepikhova *et al.*, Photonic bound states in the continuum in Si structures with the self-assembled Ge nanoislands, Laser & Photonics Reviews, 15, p. 2000242, (2021);

[3] A.V. Peretokin, M.V. Stepikhova *et al.* Photonic crystal band structure in luminescence response of samples with Ge/Si quantum dots grown on pit-patterned SOI substrates, Photonics Nanostructures: Fundam. Appl. 53, p. 101093 (2023).

[4] M. Stepikhova, S. Dyakov *et al.*, Interaction of Ge(Si) Self-Assembled Nanoislands with Different Modes of Two-Dimensional Photonic Crystal, Nanomaterials, 12, p. 2687, (2022);

[5] A. Peretokin, D. Yurasov *et al.*, Tuning the Luminescence Response of an Air-Hole Photonic Crystal Slab Using Etching Depth Variation, Nanomaterials, 13, p. 1678, (2023);

[6] M.-S. Hwang, H.-C. Lee *et al.*, Ultralow-threshold laser using super-bound states in the continuum, Nat Commun. 12, p. 4135, (2021).

SERS-active arrays of gold- and silver-coated porous silicon nanowires for bacterial identification and antibiotic susceptibility testing

D. Nazarovskaia¹, O. Giuppenen¹, P. Domnin^{2,3}, I. Tsiniakin¹, S. Ermolaeva³, K. Gonchar¹, L. Osminkina¹

1- Lomonosov Moscow State University, Physics department, Leninskie gory 1, 119991, Moscow, Russia

2- Lomonosov Moscow State University, Biology department, Leninskie gory 1, 119991, Moscow, Russia

3- N. F. Gamaleya Federal Research Center for Epidemiology & Microbiology, 123098, Moscow, Russia
nazarovskaia.da22@physics.msu.ru

Given the ever-growing threat of infectious diseases, it is crucial to respond promptly to bacterial contaminations. Although current microbiological methods for pathogen detection are reliable, they can be laborious and require laboratory equipment. Conversely, techniques utilizing the interaction of light with biomolecules offer the potential for ultrafast, specific, and reliable analysis.

Surface-enhanced Raman spectroscopy (SERS) is one such method that relies on the local surface plasmonic resonance generated by nanostructured noble metal surfaces like silver (Ag) and gold (Au). It is considered an alternative approach for biomolecule detection. Raman spectrometers can be designed to be portable, and conducting bacterial tests using this method is relatively simple.

Recently, numerous studies have focused on the application of surface-enhanced Raman spectroscopy (SERS) in biosensors. These studies have demonstrated the method's exceptional sensitivity in detecting both Gram-positive and Gram-negative bacterial strains, as well as their mutations. Furthermore, SERS has shown the potential to generate an optical signal from a single cell [1]. However, it has been observed that the choice of SERS-active substrate significantly affects the results, leading to ongoing debates regarding various enhancers of the SERS signal.

Porous silicon nanostructures, specifically porous silicon nanowires (pSi NWs), have immense potential in the advancement of SERS biosensors. These nanostructures have already demonstrated their capabilities in detecting bacterial metabolites [2], DNA [3], and various other molecules. The remarkable combination of a large surface area and high porosity in pSi NWs makes them highly suitable for functionalization with silver (Ag) and gold (Au) nanoparticles (AuAg@pSiNWs) for SERS applications. Furthermore, the porous structure of pSi NWs facilitates improved adsorption of bacterial samples onto the substrate, further enhancing the efficiency of the biosensor.

In this study, AuAg@pSi NWs substrates were developed for SERS diagnosis of *L. innocua* food bacteria (Fig. 1). It was shown that the bacteria were detected up to a concentration of 10⁶ CFU/ml. It is shown that SERS with the developed substrates can be used for rapid analysis of bacteria antibiotic resistance: the characteristic scattering lines of bacteria disappeared after 1 hour of incubation with gentamicin. The results presented can make a significant contribution to the field of diagnostics and the development of effective strategies for combating antibiotic resistance.

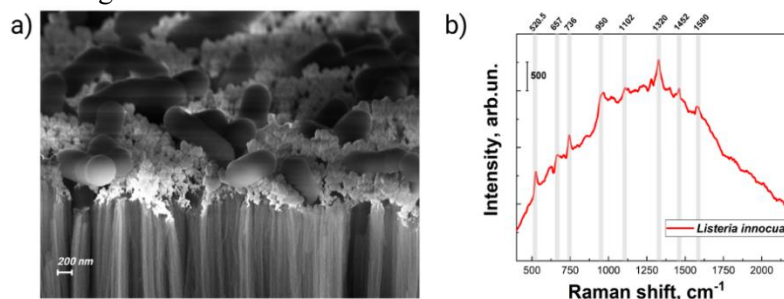


Fig. 1 a) SEM image of *L. innocua* adsorbed onto AuAg@pSiNWs surface; b) SERS spectra of *L. innocua* incubated with gentamycin.

The research is supported by Russian Science Foundation Grant No. 22-72-10062.

References:

- W. R. Premasiri, et al., Characterization of the Surface Enhanced Raman Scattering (SERS) of Bacteria, *Journal of Physical Chemistry*, 109, 312-320, (2005).
- O. Žukovskaja, et al., Rapid detection of the bacterial biomarker pyocyanin in artificial sputum using a SERS-active silicon nanowire matrix covered by bimetallic noble metal nanoparticles, *Talanta*, 202, 171-177, (2019).
- Y. He, et al., Silicon nanowires-based highly-efficient SERS-active platform for ultrasensitive DNA detection, *Nano Today* 6 (2), 122-130, (2011).

Stimulated Raman scattering in the ultrasound wave field – high conversion efficiency

A. A.Skrabatun, A.A.Matrokhin, A.D.Kudryavtseva, A.N.Maresev, T.V.Mironova,
M.A.Shevchenko, N.V.Tcherniega, S.F.Umanskaya

The P.N.Lebedev Physical Institute of the RAS, Leninskii pr., 53, Moscow 119991, Russia

akudr@sci.lebedev.ru

In numerous applications using the stimulated Raman scattering (SRS) process, the key issue is the energy efficiency of the process. One of actively applied ways to improve the efficiency of SRS is the use of distributed feedback, first considered in [1] and actively used at present [2]. SRS efficiency can be also significantly increased by a local increase in pressure caused by a shock wave [3].

This work presents the results of experimental studies of the effect of ultrasonic waves on the efficiency of the SRS process for a number of Raman-active liquids. SRS was excited by the second harmonic of a mode-locked Nd:YAG laser (532 nm, 30 ps, 10 mJ, 10 Hz). The experiments were carried out for two different geometries. In the first case, the radiation entered the sample from above, through the free surface. In this case, the SRS was registered in backward direction. In the second case, the exciting radiation was focused through the window of the cell and SRS was registered in forward and backward directions. The cell with the sample was placed in an ultrasonic bath (200 W, 40 kHz).

The experimental results showed that when the pump is focused into the open surface of the liquid, the backward SRS intensity increases in water by 1.5 times, in heavy water by more than 2 times, in ethanol for the first Stokes component by 15 times, and for the second Stokes component by 4 times (Fig. 1).

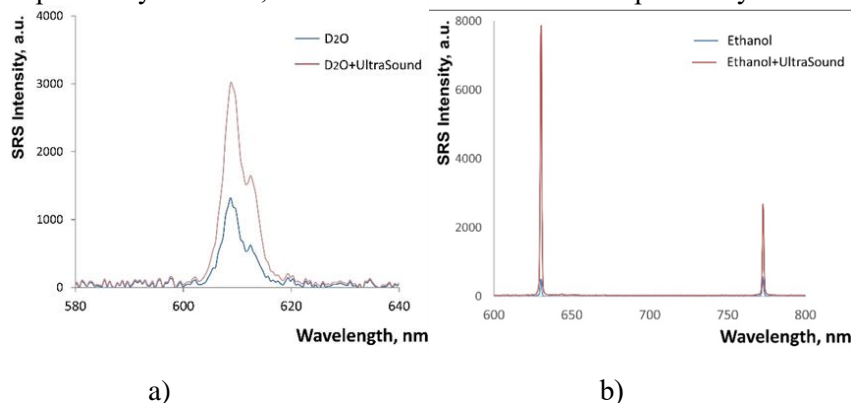


Fig. 1. SRS spectra when radiation is focused from above through the free surface of a liquid with ultrasonic impact switched off and on. a) in heavy water (pump energy 10 mJ), b) in alcohol (pump energy 2 mJ).

An increase in the power of ultrasound leads to a significant increase in the intensity of the scattered radiation. When the radiation was focused through the cell window into the bulk of the liquid, the forward SRS intensity also increased significantly when ultrasound was turned on. In water, the inclusion of ultrasound led to an increase in the SRS intensity by more than an order of magnitude.

An increase in the SRS intensity under ultrasonic impact is due to the arising of distributed random feedback caused by the phase inhomogeneities formation in the liquid. The reasons for the occurrence of these inhomogeneities are the acoustic currents of vortex flows that occur under the action of ultrasound, as well as cavitation - the formation and collapse of bubbles in a liquid.

[1] S.A.Akhmanov and G.A.Lyakhov, Effects of inhomogeneity of optical pumping in lasers and stimulated scattering. Self-excitation due to distributed feedback, JETP 66, 96-108 (1974).

[2] S. S. Loranger and R. Kashyap, Efficiency increase of distributed feedback Raman fiber lasers by dynamic control of the phase shift, Optics Letters 43, Issue 23, 5705-5708 (2018).

[3] C.Wang, Y.Wang, X.Cao, S.Wang, C.Sun, and Z.Men, Shock compression-induced enhancement of stimulated Raman scattering in heavy water, Optics Communications, 501, 127394 (2021).

LD-O-7

Symmetric C-C stretching mode as a universal characteristic of length of polymethylene chains: Experimental and DFT study

V.V. Kuzmin¹, A.B. Bermagambetov², S.M. Kuznetsov¹, G.Yu. Nikolaeva¹,
L.Yu. Ustynyuk³, E.A. Sagitova¹

1-Prokhorov General Physics Institute of the Russian Academy of Sciences,
Vavilov Str. 38, 119991 Moscow, Russia

2- Moscow Aviation Institute (National Research University), Volokolamskoye shosse 4, 125993 Moscow, Russia

3-Department of Chemistry, M.V. Lomonosov Moscow State University,
Leninskie Gory 1-3, 119991 Moscow, Russia

sagitova@kapella.gpi.ru

Substances, which molecules contain one or more polymethylene chains, are widely used in numerous fields of human activity, including petrochemical, pharmaceutical and food industries. Physical properties of these substances, such as viscosity, density, and dielectric constant, depend on both length and number of chains in molecule.

The band of the symmetric stretching vibrations of C-C bonds is observed in the spectral region 1100 -1160 cm^{-1} in Raman spectra of many substances, containing polymethylene chains. The wavenumber and intensity of this band depend not only on molecule length, but also on the chain conformation. At present, it is established that for normal alkanes this band corresponds to the most probable *all trans*-conformation, and its wavenumber directly relates to the molecule length. However, this dependence is still unknown for other substances with polymethylene chains.

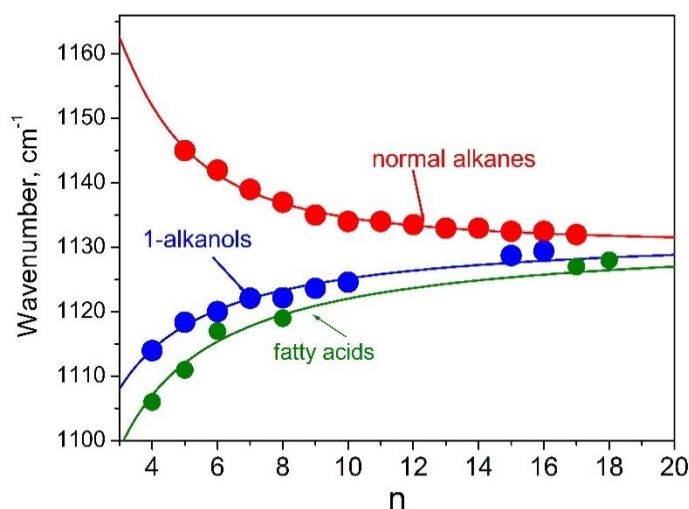


Figure 1. The symmetric C-C stretching mode wavenumbers *versus* the number of carbon atoms (n) in a molecule backbone, which is a measure of chain length, for normal alkanes ($\text{C}_n\text{H}_{2n+2}$), 1-alkanols ($\text{C}_n\text{H}_{2n+1}\text{OH}$), fatty acids $\text{C}_n\text{H}_{2n}\text{O}_2$

In our contribution, we present experimental study in conjunction with DFT calculations of a behavior of this mode in Raman spectra of a wide collection of substances with polymethylene chains. We determined the dependence of the symmetric C-C stretching mode wavenumber on the chain length for 1-alkanols and fatty acids (Fig. 1). For alkylammonium salts and branched alkanes we observed splitting of the C-C mode due to the presence of several polymethylene chains with various lengths. We showed that structure of terminal groups, chain branching, presence of strong intermolecular interactions dramatically influence the dependence of the symmetric C-C stretching mode wavenumber on the chain length. However, for all the substances under study the wavenumber of the C-C stretching mode is a universal characteristic of length of polymethylene chains.

We are grateful to the Joint Supercomputer Center of the RAS for the possibility of using their computational resources for our calculations.



LD-O-8

Raman spectroscopy as an effective tool for evaluating the iodine values and carotenoid content in vegetable oils

S. Kuznetsov¹, V. Novikov¹, P. Laptinskaya¹, O. Persidskaya¹, E. Sagitova¹

1- Prokhorov General Physics Institute of the Russian Academy of Sciences, 38 Vavilov St., 119991 Moscow, Russia

kuznetsovsm@kapella.gpi.ru

Vegetable oils are widely used in food industry, cosmetology, and medicine. Currently, the development of fast and efficient methods for monitoring their quality is relevant. For example, the thermal stability and shelf life of oils depend on the content of unsaturated fatty acids (UFA). The property of oils to increase the stability and bioavailability of carotenoids, that are vital for human health, is used in the creation of biologically active additives.

In this work, we apply Raman spectroscopy for assessing the iodine values (IV, the main measure of the number of C=C bonds in UFA) and carotenoid content in vegetable oils. Experimental Raman spectra of 35 various vegetable oils were recorded at the laser excitation with the wavelength of 532 nm. In addition, we used the Margoshes titrimetric method to obtain the exact IV of oils.

Figure 1 shows the Raman spectra of marula and tomato seed oils, which IV differ by about a factor of 1.5. The spectra of saturated triglyceride C8/C10 (a fraction of coconut oil which does not contain UFA), and of unsaturated sorbic acid are shown for comparison.

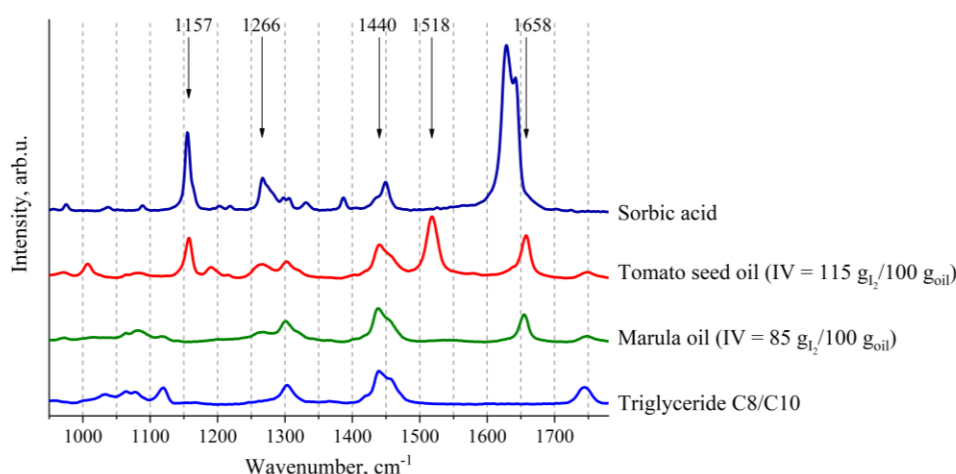


Figure 1. Raman spectra of marula and tomato seed oils, sorbic acid and triglyceride C8/C10 (a fraction of coconut oil).

As can be seen from Figure 1, an increase in iodine values leads to a growth of the peak intensities of Raman lines at about 1266 and 1658 cm^{-1} , assigned to the bending vibrations of C–H bonds and stretching vibrations of C=C bonds in UFA molecules, respectively. We found that the ratios of the intensity of each of these lines to the intensity of the line at about 1440 cm^{-1} (bending vibrations of C–H bonds) depend on the IV of oils. In this study, we showed that for oils with IV in the range of 60 – 165 $\text{g}_{\text{I}_2}/100 \text{ g}_{\text{oil}}$, these dependences are linear. We demonstrated that recording the Raman spectra at the excitation wavelength of 532 nm makes it possible not only to evaluate IV but also allows to carry out additional diagnostics of the carotenoid content at very low concentrations. This is due to the resonant enhancement of the lines assigned to the stretching vibrations of C–C (at 1155 cm^{-1}) and C=C (at 1525 cm^{-1}) bonds in carotenoid molecules in this case. We established that applying the Raman spectroscopy makes it possible to detect carotenoids in studied vegetable oils with the contents less than 0.4 mg/kg.

In this work, we also showed that the use of an excitation wavelength of 532 nm provides possibility to record Raman spectra with an insignificant fluorescence background (as it is in the case of excitation at 785 nm wavelength, traditionally used when analyzing oils).



Measurement of the absorption of waveguide layers using prismatic input radiation

V.V. Butuzov ¹, V.S. Solovyov ^{1,2}, A.S. Timoshenkov ²

1- JSC Research Institute "Ekran"

2-National Research University "MIET",

e-mail : solov_06_v@mail.ru

Currently, optoelectronics and photonics technologies are becoming very popular when it is necessary to combine electronics technologies and intensively developing optical technologies. One of the key, necessary directions for this is the creation of optical filters, both with a narrow bandwidth and with a wide one. A characteristic feature of optical materials is the low attenuation during the propagation of light in them compared to materials through which an electric current propagates. Therefore, the quality factor of optical filters can be orders of magnitude greater than electrical ones. Typical values of the quality factor of electrical filters are 10-50, while the quality factor of optical filters can be $10^5 - 10^{12}$. In order to know in advance what quality factor of the filter can be obtained when using one or another material, it is necessary to know the light losses during the propagation of light in it. In this article, we propose a measurement technique and its specific implementation using the example of measuring the attenuation of light in a layer of titanium dioxide. Layers of titanium dioxide with a thickness of 0.5 to 1 μm were fabricated by sputtering Ti_3O_5 onto a quartz substrate using electron beam sputtering technology. In the process of deposition, the layer was further oxidized and, as a result, a layer was formed. TiO_2 . For the work, a rutile prism with a refractive index of 2.6 was made. With its help, radiation from the waveguide layer was introduced. The measurements were carried out by fixing the beam track with a camera and processing it with the Gwyddion program. In our experiments, when photographing after processing, we obtained the loss of the waveguide layer 0.4 dB/cm, 0.41 dB/cm and 0.425 dB/cm.

LD-O-10

Laser ablation and fragmentation of nanoparticles in liquid, electrostatic and magnetic fields

A. Chernikov, D. Kochuev, A. Voznesenskaya, R. Chkalov, D. Abramov, K. Khorkov

Institute of Applied Mathematics, Physics and Computer Science, Vladimir State University, Gorky Street, 87, 600000, Vladimir, Russia

email address: khorkov@vlsu.ru

In this paper we present the results of various techniques for laser ablation and fragmentation of nanoparticles. Ablative synthesis was carried out on the developed experimental stands using liquid and gas media. During ablation in liquid media, the materials obtained were in the state of colloidal solutions. At the end of the ablation process, the target was removed from the resulting solution. If necessary, nanoparticles were selected, as well as fragmentation of the resulting material to achieve the necessary properties of the colloidal system (particle dispersion, chemical and phase composition) [1,2].

Materials obtained during ablation in a gas medium were deposited on the surface of the substrates under the action of an electrostatic or magnetic field [3]. To change the chemical composition of the compounds obtained, or to preserve the state of the initial substance, appropriate gas media were used, including with different percentages. The obtained nanoparticles MoS₂, WS₂, ZnS, ZnSe, Al₂O₃, Ti, Fe, Fe₂O₃ were analyzed using electron microscopy, Raman spectroscopy, X-ray diffraction analysis and other methods.

The experiments were carried out on a laser robotic complex based on the Yb:KGW femtosecond laser system (Avesta Ltd.), generating pulses with a duration of 280 fs at a wavelength of 1030 nm with a repetition frequency of 10 kHz and a maximum pulse energy of 150 μJ. This complex has a modular structure, which allows the use of various additional nodes included in the optical schemes of exposure and processing of materials by femtosecond laser radiation.

A complex of studies of the physicochemical properties of nanoparticles allowed us to evaluate their characteristics such as shape and size, morphology and surface composition. The optical properties of the obtained colloidal solutions were investigated by spectrophotometry. The obtained data are necessary to make a decision on the most appropriate ways of using nanoparticles and possible adjustment of the parameters of the method of production. Schemes for photothermal response of synthesized colloidal solutions have been developed. The dependences of temperature change on time during irradiation of colloidal solutions, as well as the change in the transmission of laser radiation by colloidal solutions during irradiation are presented.

The study of the processes of formation of nanoparticles was carried out at the expense of the grant of the Russian Science Foundation No. 22-79-10348. Preparation and analysis of samples was carried out within the framework of the state assignment of the Ministry of Science and Higher Education of the Russian Federation, subject FZUN-2020-0013.

[1] Kurilova, U.E., Chernikov A.S., Kochuev D.A. et al., Physical and Biological Properties of Layers with Nanoparticles Based on Metal Chalcogenides and Titanium Synthesized by Femtosecond Laser Ablation and Fragmentation in Liquid, *Journal of Biomedical Photonics & Engineering*, vol. 9(2), 020301, (2023)

[2] Chernikov A.S., Tselikov G.I., Gubin M.Y. et al. Tunable optical properties of transition metal dichalcogenide nanoparticles synthesized by femtosecond laser ablation and fragmentation, *Journal of Materials Chemistry C*, vol. 11(10), pp. 3493-3503 (2023).

[3] Chernikov A.S., Kochuev D.A., Voznesenskaya A.A. et al. Synthesis of spherical zinc sulfide nanoparticles produced by femtosecond laser ablation and deposited on a silicon substrate under the action of an electrostatic field, *Journal of Physics: Conference Series*, vol. 2077(1), 012002 (2021).

Ultrafast spectroscopy of tungsten disulfide nanotubes

M. Paukov¹, A. Goldt², A. Suyi¹, D. Yakubovsky¹, A. Melnikov³, G. Komandin⁴, M. Burdanova^{1,5}

1- Center for Photonics and 2D Materials, Moscow Institute of Physics and Technology, 9 Institutsky Lane, 141700 Dolgoprudny, Russia

2- Center for Photonic Science and Engineering, Skolkovo Institute of Science and Technology, 3 Nobel Str., 121205 Moscow, Russia

3- Institute of Solid State Physics, Russian Academy of Science, 5 Physicheskaya Str., 142092 Troitsk, Russia

4 - Prokhorov General Physics Institute of the Russian Academy of Sciences, 38 Vavilova Str., 119991 Moscow, Russia

5- Osypian Institute of Solid State Physics, Russian Academy of Sciences, 2 Osypiana Str., 142432 Chernogolovka, Russia

Paukov.MI@phystech.edu

Tungsten disulfide (WS₂) belongs to the class of transition metal dichalcogenides (TMDs), whose low-dimensional properties include strong photoluminescence [1], tunable bandgap [2] and etc. These properties provide various optoelectronic applications for this material [3],[4]. Here we study quantum confined WS₂ nanotubes (WS₂NT) on the subject of ultrafast processes emerging there. Their experimental research includes the creation of non-equilibrium state by means of photoexcitation in the experiments of optical pump – terahertz probe (OPTP) and transient absorption spectroscopy (TAS) in visible and near-infrared ranges. The obtained spectra combined with steady-state broadband absorbance spectrum (UV-Vis-NIR AS, FTIR, THz-TDS) and Raman spectrum reveal the presence of defects, trions, excitons, exciton polaritons and their evolution on picosecond timescale. Time constants of these processes are determined. Also, the photoconductivity in THz range is investigated and compared to the equilibrium THz conductivity. This research presents interest both in fundamental science, since it sheds more light on the processes in quasi-1D TMDs, and in practical applications of ultrafast optoelectronics.

This work was supported by the Russian Science Foundation (RSF), research project # 22-72-10033.

[1] A. Splendiani et al., “Emerging photoluminescence in monolayer MoS₂,” *Nano Letters*, vol. 10, no. 4, pp. 1271–1275, (2010).

[2] K. F. Mak, C. Lee, J. Hone, J. Shan, and T. F. Heinz, “Atomically thin MoS₂: A new direct-gap semiconductor,” *Physical Review Letters*, vol. 105, no. 13, (2010).

[3] B. Radisavljevic, A. Radenovic, J. Brivio, V. Giacometti, and A. Kis, “Single-layer MoS₂ transistors,” *Nature Nanotechnology*, vol. 6, no. 3, pp. 147–150, (2011).

[4] J. S. Ross et al., “Electrically tunable excitonic light-emitting diodes based on monolayer WSe₂ p–n junctions,” *Nature Nanotechnology*, vol. 9, no. 4, pp. 268–272, (2014)

LD-O-12

Up-Conversion in CdSe/ZnS quantum dots in liquid-crystal matrices

N.D. Presnov¹, V.Yu. Nesterov¹, V.B. Zaytsev¹, L.A. Golovan¹, A.S. Merekalov², Ya.I. Derikov²,
O.N. Karpov^{1,2}, G.A. Shandryuk^{1,2}, R.V. Talroze^{1,2}

1- Faculty of Physics, M.V.Lomonosov Moscow State University, Moscow 119991, Russia

2- A.V.Topchiev Institute of Petrochemical Synthesis RAS, Moscow 119991, Russia

Semiconductor quantum dots are of great interest for researchers and engineers due to their special properties, including high efficiency of photoluminescence (PL). The idea to form QD nanocomposite media based on of liquid-crystal polymers (LCP) is very promising since they allow formation of ordered QD arrays, high QD concentration, and ability to control QD distribution by means of light-induced order-disorder transitions.

We report on up-conversion in core/shell CdSe/ZnS QDs embedded into smectic BA-6PA LCP with various QD mass fractions (up to 60%). QD diameter was 4.1 nm.

Under excitation of both QDs toluene suspension and QDs in LCP by femtosecond infrared pulses of Cr:forsterite laser (1250 nm, 80 fs, 1 nJ, 80 MHz) visible PL was registered. The PL spectrum – a broad band 1.95-2.25 eV (550 – 640 nm) – coincides with one excited by picosecond pulses at wavelength of 532 nm. Analysis of the PL spectra reveals their saturating cubic dependence on the pumping laser power, which indicates three-photon absorption as a main mechanism of the up-conversion process.

This conclusion was supported by direct measurement of nonlinear absorption of femtosecond infrared pulses, which evidences square dependence of the absorption coefficient on laser power.

Excitation of the PL (584 nm) can be done by the second harmonic (SH) of the femtosecond infrared radiation (625 nm), with the linear dependence of the PL on the SH power.

This work was supported by Russian Science Foundation (grant 23-19-00246), synthesis of QDs and polymer matrices was carried out within the State Program of TIPS RAS.



Fluorescence amplification in laser-pumped random and homogeneous fluorescent media: the fundamental limitations

D.A. Zimnyakov¹, S.S. Volchkov¹, I.V. Mikhailov¹, D.V. Tsyplin¹, A.S. Tokarev¹, V.I. Kochubey²

1- Yury Gagarin State Technical University of Saratov, 77 Polytechnicheskaya St., Saratov, 410054, Russia

2- Saratov State University, 83 Astrakhanskaya St., Saratov, 410012, Russia

zimnykov@mail.ru

Fundamental features of the transition from spontaneous fluorescence to dominating stimulated emission in laser-pumped dye-based homogeneous and random media are considered. This transition, usually interpreted as overcoming the random lasing threshold [1,2] is analyzed in terms of kinetic equations for the relative population f of the excited state of dye molecules and the fluence rate of the fluorescence response in the pumped layer of the medium [3,4]. In the stationary mode of fluorescent emission at high pump intensities, the extreme value of f depends on the ratio of the wavelength-averaged cross section $\langle\sigma_{st}\rangle_{\lambda}$ of stimulated emission of fluorophore molecules and the average cross section $\langle\sigma_{rad}\rangle$ of radiation losses in the pumped layer. On the other hand, the effect of a significant narrowing of the fluorescence spectrum, which is characteristic of overcoming the random lasing threshold, is due to a significant increase in the dwell time τ_{dw} of fluorescence photons in the pumped layer in the threshold region. An analysis of the competitive influence of the key factors (pump intensity, concentration of dye molecules, their absorption and emission cross sections, transport mean free paths of pump and fluorescence propagation) that determine f and τ_{dw} was carried out using the above mentioned stationary solutions of kinetic equations and consideration of radiation transport in the pumped layer.

Experimental studies of the influence of $\langle\sigma_{rad}\rangle$, f and τ_{dw} in the pumped volume as the extinction mean free path l_{ext} of a pumping laser radiation (355 nm and 532 nm) decreases were carried out using 4-(dicyanomethylene)-2-methyl-6-(4-dimethylaminostyryl)-4H-pyran (DCM) solutions in ethylene glycol with various concentrations (from 1.2×10^{-3} M to 1.2×10^{-1} M). At high DCM concentrations, the optical transport properties of the studied system are largely controlled by the effect of homogeneous nucleation in a saturated DCM solution and, accordingly, by the formation of an ensemble of DCM crystallites as the scattering sites for the pump and fluorescence radiation. This feature made it possible to vary the pump and fluorescence extinction mean free paths over a wide range, with absorption dominating at low mass fractions of DCM in solutions and scattering at large values of the DCM mass fraction (more than 2.0×10^{-2} M). Structural and optical transport properties of randomly inhomogeneous fluorescent systems formed in this way were analyzed using spectroturbidimetry, scanning electron microscopy, and X-ray diffractometry. An analysis of the probability density functions of the dwell times of fluorescent photons in the pumped volume as a function of l_{ext} was performed using Monte Carlo simulations of the pump and fluorescence transport in the pumped layers of dye solutions.

Comparison of the obtained experimental data on the extreme conditions for the excitation of the fluorescent response in the studied systems at various l_{ext} values with the theoretical results based on the developed phenomenological model showed a fair agreement between them.

This research was funded by the Russian Science Foundation, grant number 22-29-00612.

[1] V.S. Letokhov, Generation of light by a scattering medium with negative resonance absorption, Soviet Physics JETP, 26, 835–840 (1968).

[2] D.S. Wiersma, The physics and applications of random lasers, Nature Physics, 4, 359–367 (2008).

[3] D.A. Zimnyakov, S.S. Volchkov, L.A. Kochkurov, A.F. Dorogov, On the minimum length of fluorescence enhancement upon laser pumping of randomly inhomogeneous media, JETP Letters, 116, 71–76 (2022).

[4] D. Zimnyakov, S. Volchkov, L. Kochkurov, A. Dorogov, Saturated emission states in fluorescent nanostructured media: the role of competition between the stimulated emission and radiation losses in the local emitters of fluorescence, Nanomaterials, 12, 2450–1 – 2450–19 (2022).

LD-O-14

Enhancement of Raman scattering efficiency in suspensions of submicron particles

O.I. Sokolovskaya, L.A. Golovan

Faculty of Physics, Lomonosov Moscow State University, 1/2 Leninskie Gory 119991 Moscow, Russia

oi.sokolovskaja@physics.msu.ru

Elastic light scattering in a disordered medium may result in an increase in the volume of light-matter interaction compared to a homogeneous medium [1]. As a result, an increase in the efficiency of various optical processes, e.g., Raman scattering (RS) can be observed. Therefore, it is necessary to establish scatterer parameters allowing RS efficiency to be enhanced and find its maximal possible increase due to elastic light scattering.

In this work, we have carried out both numerical simulation and experimental study of the light propagation and RS in scattering media. Suspensions of rutile particles with diameters of 350 and 500 nm and gallium phosphide particles with diameter of 3 μm in dimethyl sulfoxide (DMSO), which is Raman active liquid, were considered as a scattering medium. The volume fraction of particles in suspensions ranged from 10^{-4} to 10^{-1} . To record the dynamics of the radiation scattered by suspensions, the optical heterodyning method [2] employing laser pulses with a duration of 80 fs (wavelength 1250 nm) was used. Raman spectra were obtained with excitation wavelengths of 1064 and 532 nm.

Numerical simulation of light propagation in suspensions by the Monte Carlo method [3] showed that the dependence of the RS signal from DMSO on scatterer volume fraction is non-monotonic with the maximal 8-fold possible increase in the backscattered RS signal efficiency (see Fig. 1) When GaP powder is added to DMSO, the mean photon path length and the RS signal decreased significantly with an increase in the scatterer volume fraction due to light absorption in them.

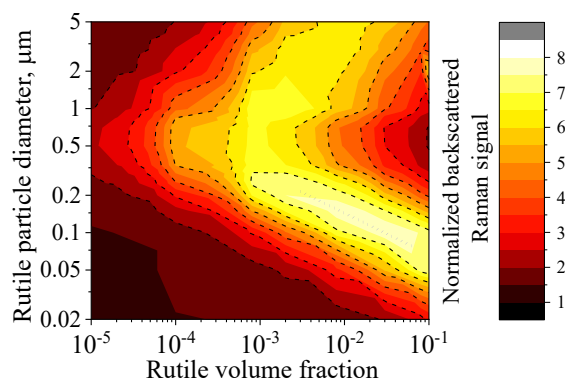


Fig. 1. Backscattered Raman signal enhancement in rutile suspensions for excitation wavelength of 1064 nm, simulation data.

The results of numerical simulation of the temporal dynamics of laser pulses propagation in suspensions are in good agreement with experimental data for the particle volume fraction not higher than 0.01. For denser suspensions, experimental data indicate non-diffusion light propagation caused probably by scattered waves interference. Experiments on RS in rutile particle suspensions demonstrate maximum 3-fold increase in the RS signal achieved at excitation wavelength of 1064 nm with a scatterer volume fraction of 0.006. A non-monotonic dependence of the RS signal on the scatterer volume fraction is shown: the monotonic increase of RS signal up to maximum, then decline and subsequent signal increase are observed. The found dependence is consistent with the experimentally observed increase in the photon dwelling time for relatively low scatterer volume fractions and possible appearance of coherent effects for higher scatterer concentrations.

[1] B.H. Hokr et al. Bright emission from a random Raman laser, *Nature Communications*, 5, 4356 (2014).

[2] K.P. Bestem'yanov, V.M. Gordienko, A.A. Ivanov, A.N. Konovalov, A.A. Podshivalov, Optical heterodyning study of the propagation dynamics of IR femtosecond laser pulses in a strongly scattering porous medium, *Quantum Electronics*, 34, 666 (2004).

[3] L. Wang, S.L. Jacques, L. Zheng, MCML—Monte Carlo modeling of light transport in multi-layered tissues, *Computer Methods and Programs in Biomedicine*, 47, 131-146 (1995).



LD-P-1

Influence of the input field of an array waveguide grating multiplexer on its spectrum

I.V. Babichek^{1,2}, A.A. Sapegin², E.S. Shamin^{1,2,3}, V.V. Svetikov^{3,4}

¹ *MIPT (NRU), Moscow, Russia*

² *JSC «MERI», Zelenograd, Russia*

³ *JCS «ZNTC», Zelenograd, Russia*

⁴ *Prokhorov General Physics Institute of the Russian Academy of Sciences*

Babichek.iv@phystech.edu

One of the key elements of integrated photonics, the optical (de)multiplexer, divides the signal along the wavelength or combines multiple signals with different wavelengths into a single signal. This device is widely used for optical communication and as an integral spectrometer. The arrayed waveguide grating (AWG) design is of a particular interest, because it has a good balance between the free spectral range and resolution. But further channel densification is problematic because lasers' instability starts to be noticeable within the spectral width of one channel [1], other spectrum shifting effects and error in wavelength matching. This is corrected by using the multiplexer's transmission characteristic's known as the flat-top peak shape. One approach of getting such a form in AWG is by adding MMIs (tapers) to input and/or output waveguides, which convert single mode input to multimode output and widen the amplitude profile. The width of input field determines one of the most important spectral characteristics of an AWG — the 3 dB bandwidth.

In this study the influence of the input field on the AWG spectrum is analyzed. Existing taper design techniques [2,3] are reviewed and the impact of the taper parameters on the input field is discussed.

[1] E. Wildermuth, Performance optimization of flat-top passband arrayed waveguide grating demultiplexers. Diss. ETH Zurich, (2000).

[2] D. Dai, W. Mei, S. He, Using a tapered MMI to flatten the passband of an AWG, Optics Communications, 219(1-6), 233-239, (2003).

[3] Y. Fu et al., Efficient adiabatic silicon-on-insulator waveguide taper, Photonics Research, 2(3), A41-A44, (2014).

LD-P-2

Simulation of oblique ray trajectories in an optical fiber with a step-index profile

A.A. Makovetskii, S.M. Popov, D.V. Ryakhovskii, A.A. Zamyatin

Kotelnikov Institute of Radioengineering and Electronics (Fryazino Branch), Russian Academy of Sciences, Vvedensky Sq. 1, 141190 Fryazino, Moscow region, Russia

maz226@ms.ire.rssi.ru

Within the framework of the geometric optics model, an algorithm for calculating the trajectories of oblique rays (hybrid modes) [1-3] in an optical fiber with a stepped refractive index profile has been developed. The first (three-dimensional) version of the algorithm is reduced to the sequential calculation of the coordinates of the ray reflection points in vector form. The second (two-dimensional) version of the algorithm is reduced to an independent calculation of the transverse coordinates of the reflection points, followed by the calculation of the longitudinal (axial) coordinates. The calculation results for the two variants of the algorithm are the same. Using the developed algorithm, the trajectories of oblique rays in an optical fiber with a core diameter of 400 μm were simulated under various excitation conditions. The projections of the ray trajectories onto the output end of the fiber are calculated. A characteristic topological form of projections is an envelope ring, the inner boundary of which determines the caustic. "Resonant" types of projections of ray trajectories are revealed. An experimental verification of the developed calculation algorithm was carried out in experiments on the excitation of oblique rays ($\lambda = 532 \text{ nm}$) in silica-polymer optical fibers with a core diameter of 400 and 600 μm .

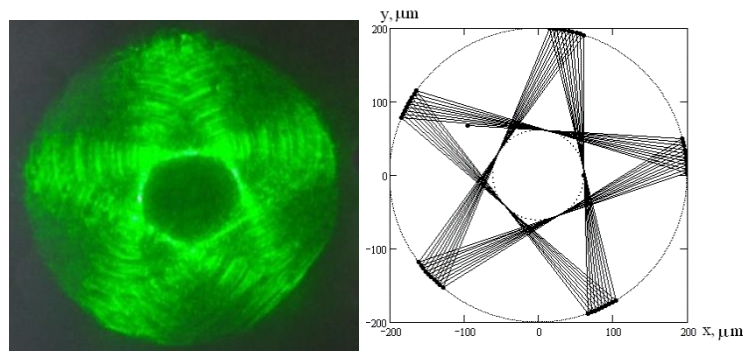


Figure 1. and experiment (left) and Simulation (right) of distribution of intensity.

Figure 1 shows photographs of the radiation intensity distributions of the hybrid modes obtained under some conditions of input of radiation, as well as their calculated analog (projections of trajectories). It can be seen that the experimentally recorded intensity distributions and their calculated analogues are topologically similar to each other.

Note that in works on the excitation of multimode OFs, close in subject matter to this work, the analysis of the features of the caustics of oblique rays was not carried out.

The work was carried out within the framework of the state task of the Kotelnikov IRE RAS.

[1] В.Б. Вейнберг, Д.К. Саттаров. Оптика световодов. Л.: Машиностроение, 1977.

[2] А. Снайдер, Д. Лав. Теория оптических волноводов. М.: Радио и связь, 1987.

[3] Д.В. Кизеветтер, Н.В. Ильин. Распределение интенсивности света вблизи выходного торца волоконного световода при наличии оптических вихрей. Научно-технические ведомости СПбГПУ. Физико-математические науки. № 3(177), С. 151-154, (2013).

Raman monitoring of structural evolution of glycols aqueous solutions on various substrates

S.O. Liubimovskii¹, V.S. Novikov¹, E.A. Sagitova¹, V.V. Kuzmin¹, P.V. Ivchenko^{2,3}, G.Yu. Nikolaeva¹

1- Prokhorov General Physics Institute of the Russian Academy of Sciences, Vavilov St. 38, 119991 Moscow, Russia

2- Chemistry Department, M.V. Lomonosov Moscow State University, Leninskie Gory 1(3), 119991 Moscow, Russia

3- A.V. Topchiev Institute of Petrochemical Synthesis of the Russian Academy of Sciences, Leninsky avenue 29, 119991 Moscow, Russia

liubimovskii@kapella.gpi.ru

Aqueous solutions of ethylene glycol (EG, HOCH₂CH₂OH) and 1,3-propylene glycol (1,3-PG, HOCH₂CH₂CH₂OH) are widely used as cryoprotectants and antifreezes, in particular as deicing fluids for ground deicing of aircrafts. The relative contents of the glycol and water determine the physicochemical properties of the solutions, including the freezing point, thermal conductivity and viscosity. Thus, development of effective methods of glycols aqueous solutions structural characterization is very much in demand for the fundamental researches and numerous applications.

At deposition on substrates, the polar and structurally flexible molecules of glycols can change their conformational states and form ordered structures on a surface. Besides, due to various rates of evaporation of the glycols and water, chemical composition of the solutions on substrates can change significantly with time.

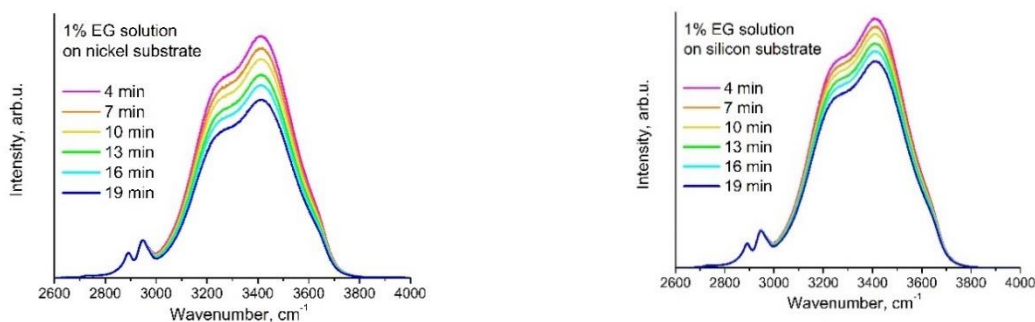


Fig. 1. Temporal evolution of Raman spectra of 1% EG solution on nickel and silicon substrates.

Recently, we developed Raman method for the glycol content evaluation in aqueous solutions, which can be used down to the glycol content of 1 mol.% [1]. In this work we used this method to study the structural evolution of 1% aqueous solutions of EG and 1,3-PG on various substrates as a function of period of time elapsed from the moment of casting of the solution on a substrate. We revealed that the conformational composition of the glycol molecules in the aqueous solutions on the substrates changes insignificantly compared with that of liquid glycols and glycol aqueous solutions. Analysis of the OH stretching band intensity in the Raman spectra of the solutions on the substrates showed that after application of the solution on the substrates the content of water in the solutions decreases fast. The change in relative contents of glycol and water on substrates depends on the chemical structure of glycol and material of the substrate. In particular, we revealed that the rate of water evaporation is greater on nickel substrate compared to silicon substrate (Fig. 1). We found out that some water remains in the solution on the substrate even an hour after the application of the solution.

1. Liubimovskii S.O., Novikov V.S., Ustynuk L.Yu., Ivchenko P.V., Prokhorov K.A., Kuzmin V.V., Sagitova E.A., Godyaeva M.M., Gudkov S.V., Darwin M.E., Nikolaeva G.Yu. Raman structural study of ethylene glycol and 1,3-propylene glycol aqueous solutions. // Spectrochimica Acta Part A: Molecular and Biomolecular Spectroscopy. – 2023. – V. 285. – Art № 121927.

LD-P-4

Photoluminescent porous silicon nanowires as bioimaging contrast agents

**M. Shatskaia¹, D. Nazarovskaia¹, Y. Evstratova², O. Shalygina¹, A. Kudryavtsev²,
K. Gonchar¹, L. Osminkina^{1,3}**

1 - Lomonosov Moscow State University, Physics department, Leninskie gory 1, 119991, Moscow, Russia

2 - Institute of Theoretical and Experimental Biophysics, Russian Academy of Sciences, 142290 Pushchino, Russia

3 - Institute of Biological Instrumentation, Russian Academy of Sciences, 142290 Pushchino, Russia

shatskaia.mg19@physics.msu.ru

Nowadays a lot of people are suffering from cancer diseases [1], so development of special bioimaging agents could be a breakthrough in oncology treatment. New approach implies a targeted impact on the tumor: directional drug delivery or different prospects of the sensitization help reduce hard consequences of chemo- and radiotherapy. Nanomaterials of porous silicon (pSi) have many useful properties for teranostics, such as biocompatibility, biodegradation, red and infrared luminescence. Due to this characteristic pSi could be detected in cancer cells or even in a whole living organism [2]. Tumors are tend to accumulate nanoparticles more active than health tissue, so pSi materials could be delivered into the tumor through the bloodstream. Bioimaging allows to trace metabolic ways of pSi and their degradation during the time.

In this work porous silicon nanowires were investigated. The most popular top-down method for the synthesis of porous silicon nanowires (pSiNWs) is the metal-assisted chemical etching (MACE) of crystalline silicon (c-Si) wafers. As a catalyst in MACE, silver nanoparticles are usually used [3,4]. However, the use of bioinert gold nanoparticles (Au-NPs) here can significantly improve the performance of pSiNWs for their biomedical applications. In the presented work, arrays of pSiNWs were obtained by the MACE method, where Au NPs were used as a catalyst. The scanning electron microscopy method showed that the etching of c-Si wafers with resistivity of 1-5 mOhm*cm produces arrays of porous nanowires with 50 nm in diameter consisting of small silicon nanocrystals (nc-Si) and pores. The size of nc-Si was calculated from the Raman scattering spectra and is about 4 nm. It was shown that due to the quantum confinement effect in small silicon nanocrystals, which are present in the porous structure of pSiNWs, the excitation of effective photoluminescence (PL) with a maximum in the red region of the spectrum is possible. At the same time pSiNWs are characterized by low toxicity to cancer MCF-7 cells and the PL properties of the pSiNWs allow their usage as contrast agents for bioimaging that was demonstrated (fig.1a).

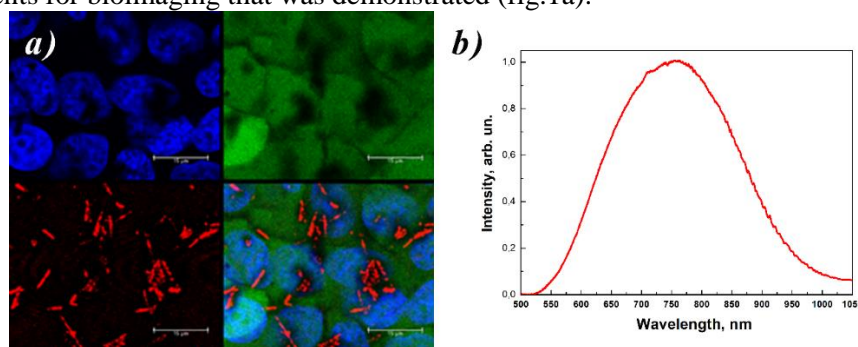


Figure 1 a) pSiNWs as contrast agents for imaging of MCF-7 cells, b) Photoluminescence spectra of pSiNWs.

The research is supported by Russian Science Foundation Grant No. 22-72-10062.

References:

- [1] Siegel R.L., et al., Cancer statistics, CA. Cancer J. Clin, vol. 73, pp. 17–48 (2023).
- [2] Park J.-H., et al., Biodegradable luminescent porous silicon nanoparticles for in vivo applications, Nat. Mater, vol. 8, pp. 331–336 (2009).
- [3] Chiappini C., et al., Biodegradable porous silicon barcode nanowires with defined geometry. Adv. Func. Mat, vol. 20, pp. 2231–2239 (2010).
- [4] Georgobiani, V. A., et al. "Structural and photoluminescent properties of nanowires formed by the metal-assisted chemical etching of monocrystalline silicon with different doping level." Semiconductors 49, pp. 1025-1029 (2015).

Polarization-sensitive infrared spectroscopy of thin amorphous silicon films with LIPSS

S. Zobotnov¹, D. Shuleiko¹, E. Kuzmin², P. Pakholchuk², L. Volkovoyanova³, A. Serdobintsev³, P. Kashkarov¹

1- Lomonosov Moscow State University, Faculty of Physics, 1/2 Leninskie Gory, Moscow, 119991, Russia

2- P.N. Lebedev Physical Institute of RAS, 53 Leninsky Ave., Moscow, 119991, Russia

3- Saratov State University, 83 Astrakhanskaya St., Saratov, 410012, Russia

zobotnov@physics.msu.ru

Modern challenges of photonics and nanoelectronics require designing new compact planar elements for integrated photonic circuits. Such systems usually are based on various thin semiconductor films. Therefore, fast and scalable techniques to make micro- and nanostructures in the thin films are actively developing now. Different multi-stage lithography techniques are widely used. Additionally, direct laser writing (DLW) approaches allow fabrication of photonic and electronic micro- and nanocomponents with desirable properties in one step. In particular, laser-induced periodic surface structures (LIPSS) can be created with femtosecond laser irradiation. One of the reasons of LIPSS arising is intensive photoexcitation of electron-hole plasma with following surface plasmon-polariton generation at semiconductor surface [1,2]. Such surface electromagnetic waves give a contribution to the relief modulation with the wavelength- and subwavelength periods.

Thin amorphous silicon films look promising for the DLW technique. So, LIPSS formation in them leads to noticeable optical [3] and electrophysical anisotropy [4] in plane of a sample.

Herein, we describe our experiment with thin amorphous silicon films (1.0 μm), including the films covered with a 10 nm aluminum layer, irradiated with femtosecond laser pulses (515 and 1030 nm, 300 fs). As a result, LIPSS were fabricated, and they covered areas up to $2 \times 2 \text{ mm}^2$. Structural features of irradiated surfaces were examined by optical and scanning electron microscopy. All LIPSS are gratings oriented perpendicular to the laser beam polarization and have periods close to the wavelength. The observed LIPSS formation is well explained with the plasmon-polariton mechanism and the so-called Sipe-Drude theory [1,5].

Surface periodicity may lead to artificial anisotropy according to the generalized Bruggeman model [6]. To examine the anisotropy, we studied our samples by Fourier-transform infrared spectroscopy in the range of 500–6500 cm^{-1} where silicon possesses relatively low absorption. The measured reflectance spectra are characterized by interference in the thin silicon films. The spectra are different for various polarization of the incident light. An analysis of the values of interference extremums and their spectral positions allowed to estimate the dichroism and birefringence values, respectively. The best results were obtained in the spectral region of 1.9–2.7 μm : the dichroism is 0.12 μm^{-1} (the difference between the absorption coefficients) and the birefringence is 0.2 (the difference between the refractive indices for the ordinary and extraordinary waves). These values look sufficient to further designing polarization-sensitive planar devices for the near infrared region.

The investigation was funded by the Russian Science Foundation grant # 22-19-00035, <https://rscf.ru/project/22-19-00035/>.

[1] J. Bonse and S. Gräf, Maxwell meets Marangoni—A review of theories on laser-induced periodic surface structures, *Laser Photonics Rev.*, 14, 2000215, (2020).

[2] J. Bonse, A. Rosenfeld, J. Krüger, On the role of surface plasmon polaritons in the formation of laser-induced periodic surface structures upon irradiation of silicon by femtosecond-laser pulses, *J. Appl. Phys.*, 106, 104910, (2009).

[3] R. Drevinskas, M. Beresna, M. Gecevičius, et al., Giant birefringence and dichroism induced by ultrafast laser pulses in hydrogenated amorphous silicon, *Appl. Phys. Lett.*, 106, 171106, (2015).

[4] D. Shuleiko, M. Martyshev, D. Amasev, et al., Fabricating femtosecond laser-induced periodic surface structures with electrophysical anisotropy on amorphous silicon, *Nanomaterials*, 11, 42, (2021).

[5] J. Sipe, J.F. Young, J. Preston, H. van Driel, Laser-induced periodic surface structure. I. Theory. *Phys. Rev. B*, 27, 1141–1154 (1983).

[6] V.I. Ponomarenko and I.M. Lagunov, Generalized formula for effective dielectric permeability of the medium with ellipsoidal inclusions, *J. Commun. Technol. El.*, 66(4), 403–407, (2021).

NONLINEAR AND TERAHERTZ PHOTONICS

Nano- and micro- size targets for generation of terahertz waves

A.V. Balakin¹, N.A. Kuzechkin², P.M. Solyankin², A.P. Shkurinov¹

1- Faculty of Physics, Lomonosov Moscow State University, Moscow 119991, Russia

2- Institute on Laser and Information Technologies of the Russian Academy of Sciences—Branch of the Federal Scientific Research Center “Crystallography and Photonics” of the Russian Academy of Sciences, Shatura, 140700, Russia

a.v.balakin@physics.msu.ru

Complex study of interaction of high intense femtosecond laser pulses with gas nanoclusters and single microdroplets aimed to providing fundamental and applied knowledge for development of effective pulsed sources of terahertz (THz) radiation is presented. High local density of the nano- and micro- targets in addition with high localization of the light wave's field near these subwavelength structures lead to appearance of strong nonlinear effects revealing, particularly, in efficient generation of new frequencies in an extremely wide spectral range: from X-ray to THz.

The nanocluster target in our experiments was formed by means of gas adiabatic expansion. In this method, the gas under high pressure expands through a special form nozzle into vacuum. Fast adiabatic cooling of the gas results in formation of nanometer scale clusters in the supersonic jet. Fig.1(a) illustrates the method and shows a distribution of the total atomic density in the cluster jet, studied in our experiments, and CCD-images of laser plasma filaments. The interaction of powerful femtosecond laser pulses with specially formed gas-cluster jet proceeds with high efficiency and is accompanied by the generation of directional beam of THz radiation [1]. Here we present and discuss the results of studies of THz generation from laser-excited nanocluster targets with various properties.

As a matter for the microdroplet targets a liquid metal eutectic alloy (48% Sn, 52% In) and dielectrics such as distilled water and isopropanol were used. The single free-falling microdroplets with a diameter of around 50 μm synchronized with laser pulses were produced with special high temperature dispenser device as described in our paper [2] and illustrated in Fig.1(b). We demonstrated that double-pulse excitation significantly enhances the yield of THz signal, which is accompanied with X-ray. The study of the THz signal dependence on laser excitation parameters together with its angular distribution allowed us to make some assumptions on origin of the THz radiation and the ways of the signal optimization.

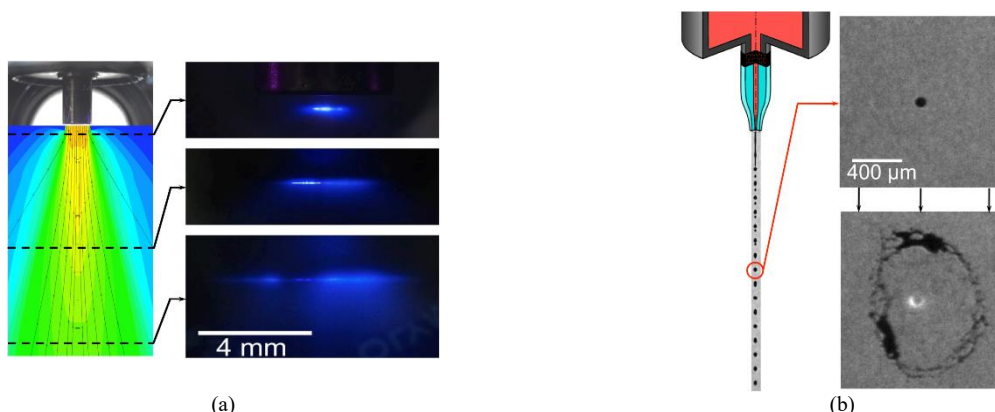


Fig. 1. Formation of nano- and micro- size targets for THz generation. (a) supersonic gas-cluster jet and photos of laser focus at 1.5, 18.3 and 32.3 mm below the nozzle output. (b) free-falling droplets and photos of single droplet before and 2 μs after laser excitation.

This work was funded partly by the Ministry of Science and Higher Education within the State assignment FSRC “Crystallography and Photonics” RAS and in part by the Ministry of Science and Higher Education of the Russian Federation in framework of Agreement № 075-15-2022-830 from 27 May 2022.

[1] Balakin A. V. et al. Directional terahertz beam generation under interaction of an intense femtosecond laser pulse with a cluster jet //JOSA B, vol. 38, №. 11, p.. 3515-3522 (2021)

[2] Solyankin P. M. et al. Single free-falling droplet of liquid metal as a source of directional terahertz radiation //Physical Review Applied, vol. 14, №. 3, p. 034033 (2020)



N-I-2

Nonlinear THz optics

Melnik M.¹, Nabilkova A.¹, Artser I.¹, Gusel'nikov M.¹, Zhukova M.¹, Ismagilov A.¹, Tsytkin A.¹, and Kozlov S.¹

*1- Research and Educational Center for Photonics and Optoinformatics, ITMO University, Russia.
mmelnik@itmo.ru*

Nonlinear optics of the THz frequency range is a rather young field of knowledge. This is due to the fact that high-power pulsed sources of THz radiation, which make it possible to observe nonlinear phenomena in various media without damaging them, appeared not so long ago [1]. The wide application of intense radiation in the THz range in various fields of knowledge elevates to the rank of topical the task of developing devices and technologies for controlling light by light, which can be based on nonlinear optics of this frequency range. Accordingly, the problem of systematic analysis of the mechanism of giant nonlinearity and study of the features of wave phenomena in media with such a nonlinearity has become urgent.

This work is devoted to a review of the achievements in the field of nonlinear optics of the THz frequency range over the past 5 years. For instance, it has been shown that for this spectral range the main low-inertia mechanism of the materials nonlinearity is the anharmonicity of molecular vibrations of optical media. Particularly large values of the nonlinear refractive index of crystals were predicted in the region of two-photon resonances with vibrational modes of crystals and in liquids [2]. The above theory has been modified to describe the nonlinear mechanisms of liquids with anisotropic molecules [3]. It has been shown theoretically and experimentally for the first time that the nonlinear refractive index of some liquids can be six orders of magnitude (million times) higher than that of the same liquids in the visible and near-IR spectral ranges [4].

In addition, the features of nonlinear wave phenomena in the field of THz radiation were studied. Such "surprises" of the nonlinear optics of pulsed THz radiation as the possibility of "disappearance" of self-focusing of radiation when its power exceeds the critical power of self-focusing due to the predominance of the phenomenon of their dispersion over diffraction in the field of few-cycle waves [5], or "disappearance" for single-cycle THz waves in media with cubic nonlinearity of another classical nonlinear phenomenon, third-harmonic generation, and the generation in the field of such an extremely short radiation pulse of quadruple frequencies with respect to the maximum of the main spectrum [6] have been shown theoretically and experimentally. It has been established that, due to the peculiarities of the spatiotemporal dynamics of single-cycle THz pulses, the use of known methods for estimating the nonlinear refractive index in this spectral range, for example, z-scan, requires their qualitative processing. Otherwise, the results obtained by the technique for quasi-monochromatic pulses may differ from the actual results for waves from a small number of oscillations by orders of magnitude [7].

The results obtained open up the possibility for detailed study of the nonlinear properties of materials caused by the interaction with intense THz pulses, which can help to reveal new features of nonlinear media, and to obtain the characteristics of the most promising materials for creating passive and active devices of THz photonics based on nonlinear phenomena.

[1] J. A. Fülöp, S. Tzortzakis, T. Kampfrath, Laser-driven strong-field terahertz sources, *Adv. Optical Materials*, vol. 8(3), pp. 1900681, (2020)

[2] K. Dolgaleva, D.V. Materikina, R.W. Boyd, S.A. Kozlov, Prediction of an extremely large nonlinear refractive index for crystals at terahertz frequencies. *Phys. Rev. A*, vol. 92, pp. 023809, (2015)

[3] A.N. Tsytkin, M.V. Melnik, M.O. Zhukova, I.O. Vorontsova, S.E. Putilin, S.A. Kozlov, X.C. Zhang, High Kerr nonlinearity of water in THz spectral range, *Optics express*, vol. 27(8), pp. 10419-10425, (2019)

[4] A.N. Tsytkin, M. Zhukova, M. Melnik, I. Vorontsova, M.S. Kulya, S.E. Putilin, S.A. Kozlov, S. Choudhary, R.W. Boyd, Giant Third-Order Nonlinear Response of Liquids at Terahertz Frequencies, *Phys. Rev. Applied*, vol. 15(5), pp. 054009, (2021)

[5] S. Kozlov, A. Drozdov, S. Choudhary, M. Kniazev, R. Boyd, Suppression of self-focusing for few-cycle pulses, *Journal of the Optical Society of America B*, vol. 36, pp. G68-G77, (2019)

[6] I. Artser, M. Melnik, A. Ismagilov, M. Guselnikov, A. Tsytkin, S. Kozlov, Radiation shift from triple to quadruple frequency caused by the interaction of terahertz pulses with a nonlinear Kerr medium, *Scientific Reports*, 12(1), 9019 9, (2022)

[7] M.V. Melnik, I.O. Vorontsova, S.E. Putilin, A.N. Tsytkin, S.A. Kozlov, Methodical inaccuracy of the Z-scan method for few-cycle terahertz pulses, *Scientific Reports*, vol. 9, pp. 9146, (2019)



On the opportunity of THz radiation detection using fluoride nanoparticles

**V.V. Semashko^{1,2}, G.S. Shakurov¹, A.S. Nizamutdinov², M.S. Pudovkin², S.S. Kharintsev²,
O.A. Morozov^{1,2}, S.L. Korableva², A.K. Dokudovskaja², A.R. Gazizov²**

1- Kazan E. K. Zavoisky Physical -Technical Institute (KPhTI), Sibirsky tract, 10/7, 420029 Kazan, Russia

2- Kazan Federal University, 18 Kremlyovskaya str., 420008 Kazan, Russia

Main author email address: ua4pcy@mail.ru

The development of physical principles for the designs of highly sensitive fast-response real-time detectors and visualizers of microwave and terahertz radiation is an urgent task [1]. Here the opportunity of implementing detectors and visualizers based on activated fluoride nanoparticles, which are efficient luminescent temperature sensors [2,3] is discussed.

Fluoride crystalline materials, having low values of heat capacity, thermal conductivity, and density [3, 4], allow to create composite nanoparticles of the "core-shell" type, where water clusters or metal inclusions can act as the core, providing efficient conversion of terahertz radiation into heat, followed by heating of the luminescent shells. It is proposed to use the dependence of the spectral-luminescent properties of nanoparticles on temperature. The features of the synthesis of rare earth ions doped fluoride nanoparticles of various compositions and morphology are presented, their absorption and fluorescent spectral-kinetic characteristics in THz and optical spectral and temperature ranges in which their maximum temperature sensitivity is realized are discussed. The detection thresholds for terahertz radiation and the inertial properties of temperature sensors based on fluoride nanoparticles are evaluated. A further prospects of nanosensoric are discussed.

[1] M. A. Medvedev and A. S. Oleynik, Devices for visualization of sources of terahertz radiation, *2016 International Conference on Actual Problems of Electron Devices Engineering (APEDE)*, Saratov, Russia, pp. 1-6, (2016)

[2] M. S. Pudovkin, O. A. Morozov, V. V. Pavlov, S. L. Korableva, E. V. Lukinova, Y. N. Osin, V. G. Evtugyn, R. A. Safiullin, V. V. Semashko, Physical Background for Luminescence Thermometry Sensors Based on Pr³⁺:LaF₃ Crystalline Particles, *J. of Nanomaterials*, vol. 2017, Art. ID 3108586, (2017)

[3] M. Dramićanin, Trends in luminescence thermometry, *Journal of Applied Physics*, vol. 128(4), Art. ID 040902, (2020).

[4] A. S. Okhotin, R. P. Borovikova, T. V. Nechaeva, A. S. Pushkarsky, *Teploprovodnost tverdikh tel (Energoatomizdat, Moskow)*, 321 p., (1984)

[5] P. A. Popov, P. P. Fedorov, *Teploprovodnost floridnikh opticheskikh materialov (in Russian) (Company group «Desjatochka», Brjansk)*, 210 p., (2012)

N-I-4

Coherent radiation generation by atomic systems in intense arbitrarily polarized laser fields

S.Yu. Stremoukhov

*Faculty of Physics, Lomonosov Moscow State University, Leninskie Gory, 1 /2, Moscow, 119991, Russia
National Research Centre "Kurchatov Institute", Akademika Kurchatova sq. 1, Moscow, 123182, Russia*

e-mail: sustrem@gmail.com

High-order harmonic generation (HHG) and generation of terahertz (THz) radiation in matter interacting with intense laser fields are the most actively studied phenomena in non-linear optics. Initially, it was assumed that the mechanisms of HHG and THz radiation are "located" on different spatial scales: HHG is a consequence of the response of a single atom [1], when discussing the mechanisms of generation of THz radiation in gaseous media, one mainly singles out the contributions of the macroscopic photocurrent generated by ionized electrons motion in the laser field, and a neutral medium by taking into account its non-linear susceptibility tensors [2]. At the same time, experimental studies demonstrate the common features of these two phenomena [3], therefore, at present, the concept of the unified nature of these phenomena is being developed: HHG and THz radiation generation are the result of a common process of electron motion in the superposition field of multicomponent multi-color arbitrarily polarized laser radiation and Coulomb potential of the atom [4, 5].

This work presents the results of recent theoretical studies on HHG and THz radiation by atomic systems interacting with two-color femtosecond laser fields. The calculations were carried out using a non-perturbative theoretical approach [5], which makes it possible to calculate the amplitudes and phases of radiation generated by a single atoms, as well as an interference model [6, 7], which makes it possible to calculate the angular-frequency spectra of radiation generated by an extended medium, which is an ensemble of space-distributed and non-interacting with each other atoms. The contribution of the effects of quasi-phase matching [8] during HHG and THz radiation by media, which are a set of gas jets separated by vacuum gaps, is discussed from the point of view of developing methods for increasing the generation efficiency and controlling the polarization state of the generated radiation.

The work was partially supported by the RFBR under Project No. 19-29-12030.

- [1] V. V. Strelkov, V. T. Platonenko, A. F. Sterzhantov, M. Yu. Ryabikin, Attosecond electromagnetic pulses: generation, measurement, and application. Generation of high-order harmonics of intense laser field for attosecond pulse production, *Physics Uspekhi*, V. 59, p.425–445, (2016).
- [2] A.V. Borodin, et al., Transformation of terahertz spectra emitted from dual-frequency femtosecond pulse interaction in gases, *Optics Letters*, V. 38, P. 1906-1908, (2013).
- [3] D.Zhang, et al., Synchronizing Terahertz Wave Generation with Attosecond Bursts, *Physics Review Letters*, V. 109, P. 243002, (2012).
- [4] A. V. Andreev, S.Yu. Stremoukhov, Terahertz-radiation generation in the ionization-free regime of light-atom interaction, *Physical Review A*, V. 87, p. 053416, (2013).
- [5] A.V. Andreev, S.Yu. Stremoukhov, O.A. Shoutova, Light-induced anisotropy of atomic response: prospects for emission spectrum control, *European Physical Journal D*, 66(16), (2012).
- [6] S. Stremoukhov, A. Andreev, Quantum-mechanical elaboration for the description of low- and high-order harmonics generated by extended gas media: prospects to the efficiency enhancement in spatially modulated media, *Laser Physics*, 28, 035403 (2018).
- [7] S. Yu. Stremoukhov, A. V. Andreev, Spatial variations of the intensity of THz radiation emitted by extended media in two-color laser fields, *Laser Physics Letters*, V. 12, p. 015402, (2015).
- [8] L.Hareli, G.Shoulga, A.Bahabad, Phase matching and quasi-phase matching of high-order harmonics generation – a tutorial. *Journal of Physics B: Atomic, Molecular and Optical Physics*, 53, 233001, (2020).



Controlling the polarization of THz radiation in spintron emitters

E. Mishina

MIREA - Russian Technological University, Vernadsky ave. 78, Moscow, Russia 119454

mishina_elen57@mail.ru

The generation of terahertz (THz) radiation is of great technological importance for many applications, such as non-destructive diagnostics, ultrafast computing, wireless communication, and direct control of material order parameters. Over the past decade, a lot of work has been done to find materials and mechanisms that provide terahertz radiation with the required characteristics. Spintron structures as terahertz emitters (SHEs) have special characteristics. First of all, this is a wide spectral range of radiation ($0.5 \div 15$ THz, two orders of magnitude of the dynamic range) with a signal amplitude comparable to that of a reference emitter, a ZnTe crystal. THz radiation is excited in the SHE by a femtosecond laser pulse due to the mechanism of the inverse spin Hall effect, where the ultrafast spin new photocurrent is converted into a transverse charge current. The highest efficiency of conversion to THz radiation was achieved with SHE in bi- and three-layer structures based on Co/Pt [1]. Polarization of THz radiation in SHE is perpendicular to its magnetization.

To work with THz radiation, as well as with optical, elements of THz optics are required, in particular, polarization rotators (analogues of a half-wave plate). The obvious way to rotate the polarization of the THz wave is to rotate the magnet around the SHE, which is extremely inconvenient. In this paper, we show the ways of polarization rotation upon changing only the magnitude of the external magnetic field in the spintron emitter and the magnitude of the voltage in the spintron emitter/piezoelectric structure.

Rotation of the plane of polarization without rotation of the magnet, but only by changing the strength of the external magnetic field, is possible in materials with a spin-reorientation transition (SRT) induced by a magnetic field. To do this, the structure must have an anisotropy of the “easy axis” type. In voltage controlled systems, energy consumption is usually lower than with current control. The use of a composite multiferroic is a way to combine the advantages of SHE and voltage control. The main problem of controlled spintron emitters is their low efficiency. In structures based on Co/Pt, which have the highest THz conversion efficiency, polarization control has not yet been demonstrated.

In this paper, a short review of current situation with achievements on THz emitters will be presented, both commonly used and polarization controlled ones. New results on magnetic-field controlled spintronic emitters will be shown.

The work is supported by Russian Science Foundation (Grant№ 23-19-00849).

[1] T. Seifert, S. Jaiswal, U. Martens, et al, Efficient metallic spintronic emitters of ultrabroadband terahertz radiation, *Nature Phot.* vol.10, pp. 483–488, (2016).

N-I-6

Terahertz stimulated emission from the molecular crystals

V.Kovalev¹, A.Sinko², A.Shkurinov³

1- Lebedev Physical Institute, Russian Academy of Sciences Leninskii Prospect 53, Moscow 119991, Russia

2- ILIT RAS-Branch of the FSRC "Crystallography and Photonics", RAS, 140700 Shatura, Moscow Region, Russia;

3- Faculty of Physics, Lomonosov Moscow State University, 119991 Moscow, Russia;

Main author email address: ashkurinov@physics.msu.ru

The growth in the number of methods and devices for generation terahertz (THz) radiation and improvement of their performance are essential for the progress of THz science and technology. In the recent years THz radiation below 3 THz realized with a reasonably high efficiency in the range of widegap solid crystals like GUHP, under the irradiation of femtosecond near-IR laser pulses. Typical for such sources is a single-cycle THz splash at the very beginning of generated pulse, and the prolonged oscillation radiation, the frequency of which corresponds to the frequency of a Raman active mode(s) in the samples. While the splash accounted for in terms of the optical rectification of pump radiation, the prolonged oscillation attributed to the dipole emission by coherent phonons generated in an optically transparent solid medium when a sufficiently short laser pulse passes through the phenomenon was called the impulsive stimulated Raman scattering (ISRS). Their THz radiation is possible because the correspondent phonon modes are both Raman and infrared active. The present talk studies narrow-band terahertz (THz) emission stimulated by femtosecond laser pulse in molecular crystal guanylurea hydrogen phosphite (GUHP). We demonstrate that this emission is closely connected with the excitement of high-quality phonon oscillations in the crystal, which is proved by the temperature dynamics of the spectra and DFT calculations. For the purposes of studying the origin of this stimulated THz emission and creation of the adequate model of the phenomenon, we analyzed the polarization sensitive spectra of spontaneous Raman scattering and THz transmission spectra while considering their polarization features in relation to crystallographic axes of GUHP crystal. In this paper we show that molecular crystals provide an effective means to convert vis-NIR laser light regardless of wavelength into the THz frequency range. This approach can lead to the creation of "laser-like" source with the desired THz frequency for a range of medical, scientific, and technological applications.



Terahertz imaging and spectroscopy for heritage science

Olga A. Smolyanskaya

*Heritage Science lab, ITMO University, Saint-Petersburg, 197101 Russia
heritage@itmo.ru*

Heritage science is a field of complex research, located at the junction of the humanities and the fine sciences: history, art history, archeology, sociology and urban studies, and at the same time - chemistry, physics and biology. In our country, a unique school of art history and restoration has been formed, combining the accuracy of the humanistic approach with the careful methods of preserving cultural heritage monuments. This was largely due to the emergence of technical and technological research laboratories at museums and restoration centers.

One of the most difficult problems for museum restorers and technologists is non-destructive studies of multilayer coatings. Traditional museum methods, such as x-ray radiography, infrared reflectography, give an integrated picture of all layers and it is almost impossible to determine the sequence of layers and highlight the layer of interest. For this purpose, the terahertz time-domain spectroscopy (THz-TDS-based) object visualization system can be useful. Due to non-invasive properties of THz radiation, such a system allows to be applied for investigation of an object of art.

The main goal of this study was to test the detecting capacity of such a system to identify layers of paint below the surface. We have used a unique test-object, mimicking the most common tasks for painting investigation. The image of paints on canvas was recorded using the TeraPulse LX (TeraView, UK) system with a spectral range 0.06 THz – 6.00 THz. Due to the high sensitivity of THz radiation to the distinction between the optical properties of painting materials, this experiment allowed us to obtain detailed information about the structure and spectroscopic data of layers of objects and pigments, and determine the shape of invisible elements without damaging the canvas. Thus, the THz imaging method can be very useful in restoration work designing, determining defects in the structure of paintings materials, as well as when searching for hidden objects under layers of paint.

Our research is dedicated as well to the investigation of image processing methods applied to THz images of painting. To our best knowledge, there is no comprehensive research on enhancement of THz images of art objects. Previous research in THz imaging concerned different image processing methods but were not applied to the objects of art. However, artworks appeared to be more complicated to reconstruct and process by means of THz imaging, which might be related to the specific structural data, unique for every object.

Algorithms of enhancement were created and applied to the images of painting's inner layer. The details on these images became sharper and more distinguishable. The results were quantified by PSNR value, which increased in every case. The intensity histograms and the intensity spectra before and after processing were compared. The obtained results can be regarded as positive and, therefore, these image processing methods can be interesting for the purposes of artworks investigation before restoration.



N-I-8

Conical emission from DC-biased filament at 10 THz

N.A. Panov^{1,2}, G.E. Rizaev², D.E. Shipilo^{1,2}, D.V. Pushkarev^{1,2}, I.A. Nikolaeva^{1,2},
D.V. Mokrousova^{1,2}, L.V. Seleznev^{1,2}, A.A. Ionin², O.G. Kosareva^{1,2}

1- Faculty of Physics, Lomonosov Moscow State University, 119991, Moscow, Russia

2- P.N. Lebedev Physical Institute of the RAS, 119991, Moscow, Russia

napanov@ilc.edu.ru

Femtosecond filament in the external electrostatic field (DC-biased filament) is a prominent source of terahertz (THz) radiation [1]. As the external field grows above ~ 3 kV/cm [2], the directional diagram of the THz emission from a DC-biased filament in air is unimodal with the maximum on the laser beam axis. This was confirmed by numerous experiments and numerous registration techniques, either narrowband detection [2], wideband detection [3, 4], or spectrally resolved [5, 6]. The excellent directionality of THz emission from DC-biased filament makes this THz source a promising tool for the measurements of low (10^{13} – 10^{15} cm⁻³) densities of free electrons [7]. The measurements of THz directional diagrams [2–6] were done in the low-frequency range below 2–3 THz. However, 3D + time simulations of THz generation in DC-biased filament performed in our recent work [6] predicted the appearance of THz conical emission in high-frequency THz range (for our 90-fs pulse at ~ 10 THz). In this work, we confirm this prediction experimentally.

In our experiment, we focused the 740-nm, 90-fs, 1.8-mJ pulse into the air gap between the electrodes biased by 15-kV/cm static electric field. The plasma filament between the electrodes was a source of THz radiation detected by a superconducting MoRe bolometer Scontel RS-CCR-1-12T-1+0.3-3T-0.1 sensitive in the spectral range of 0.3–10 THz. The bolometer with the bandpass filters (centered at the frequencies $\nu = 0.5, 1, 3$ and 10 THz) was fixed on the 40-cm-long horizontal board and rotated at the horizontal angle α around the vertical axis. The spherical mirror was fixed on the vertical 40-cm post. To vary the vertical angle β , we moved the focusing mirror along the post. So, the variation of the angles α and β allowed us to reconstruct the 2D distributions of the THz fluence $F(\alpha, \beta)$ at the frequency ν determined by the bandpass filter. We traced experimentally the transit from the on-axis unimodal angular distribution at 0.5–1 THz to the conical one at 10 THz, see Fig. 1.

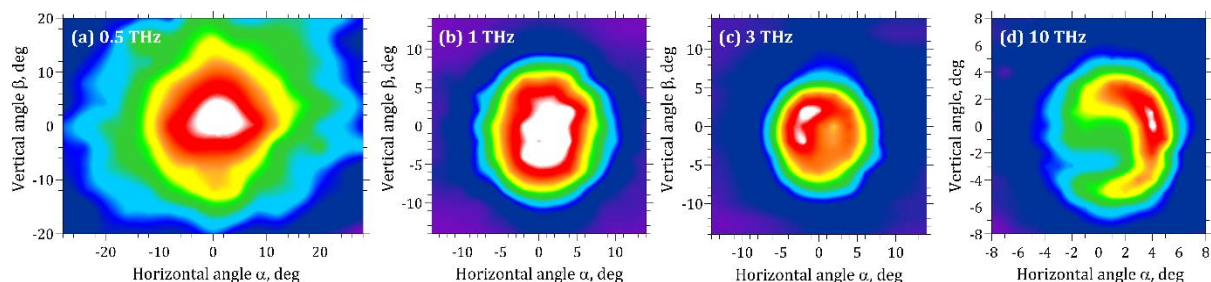


Fig. 1. 2D distributions of the fluence $F(\alpha, \beta)$ measured at frequencies (a) $\nu = 0.5$ THz, (b) 1 THz, (c) 3 THz, (d) 10 THz.

- [1] T. Löffler, F. Jacob, and H. Roskos, *Appl. Phys. Lett.* 77, 453 (2000).
 [2] A. Houard, Y. Liu, B. Prade, V. T. Tikhonchuk, and A. Mysyrowicz, *Phys. Rev. Lett.* 100, 255006 (2008).
 [3] R. Akhmedzhanov, I. Ilyakov, V. Mironov, E. Suvorov, D. Fadeev, and B. Shishkin, *Radiophys. Quantum Electron.* 52, 482 (2009).
 [4] D. Lubenko, V. Prokopen, S. Alekseev, M. Ivanov, and V. Losev, *Atmospheric Ocean. Opt.* 32, 430 (2019).
 [5] T. Fukuda, T. Otsuka, Y. Sentoku, H. Nagatomo, H. Sakagami, R. Kodama, and N. Yugami, *Jpn. J. Appl. Phys.* 59, 020902 (2020).
 [6] I. Nikolaeva, D. Shipilo, D. Pushkarev, G. Rizaev, D. Mokrousova, A. Koribut, Y. Grudtsyn, N. Panov, L. Seleznev, W. Liu, A. Ionin, and O. Kosareva, *Opt. Lett.* 46, 5497 (2021).
 [7] D. Jang, H. S. Uhm, D. Jang, M. S. Hur, and H. Suk, *Plasma Sources Sci. Technol.* 25, 065008 (2016).



Effect of magnetic field and injection current on spectral characteristics of multiple quantum well laser

Aurangzeb Khurram Hafiz

*Centre for Nanoscience and Nanotechnology, Jamia Millia Islamia, New Delhi – 110025, India
ahafiz@jmi.ac.in*

The spectral characteristics of MQW Laser is extremely sensitive to the presence of magnetic field as well as injection current density. The study on the effect of drive current on the spectral emission of the laser device in absence of magnetic field ($B = 0$ Tesla) typically results in the variation of the peak frequency of the spectrum as the drive current is increased from threshold and above. As the drive current increases, the number of longitudinal modes that are present, may compete with each other in the gain medium. This results in narrower spectral width and the average mode gain decreases. According to our laser model, the central mode (lasing mode) grows faster than the adjacent modes at current near threshold, and eventually the amplitudes of the adjacent modes effectively saturate. At a particular output level, additional increase in power is due to growth of a single primary mode. The output of the laser diode is shifted by two primary effects, current induced changes in the junction temperature, and charge carrier induced refractive index changes. Thermally induced changes are a result of thermal expansion of Fabry-Perot laser cavity and changes in the refractive index, which combine to increase the output wavelength with increasing junction current. As the single-mode power increases, a standard wave arises in the laser cavity. Carriers are depleted faster at the peaks of the standard wave than in the surrounding areas, which results in decrease in the average mode gain. This effect is known as 'spatial hole burning'. The depleted carriers have to be replenished by carrier diffusing into these regions. Thus, the amount of gain suppression of the lasing mode depends upon the diffusion rates of electrons and holes.

In presence of magnetic field, the response of the charge carriers in the active region is guided by the Hall effect dynamics. Several decades ago, the dynamics of the charge carriers in double-heterostructure (DH) lasers was studied under the condition of high magnetic field (about 10T) and very low temperature ($T \ll 100$ K) [1-2]. In the condition of strong magnetic field and very low temperature, a blue-shift in the DH laser spectral characteristics was observed. This was explained well with Landau level-based theory. The necessary condition for the formation of Landau levels is ($kT \ll \hbar\omega_c$) where (ω_c) is the angular frequency of the cyclotron orbit. This condition is only achieved at very low temperature ($T \ll 100$ K) and strong magnetic fields.

Around the room temperature, the thermal agitation is high enough to wash out Landau splitting. Also, contrary to the observed higher frequency side shifts of the oscillation wavelength of semiconductor lasers at low temperature and high magnetic fields, researcher have obtained shifts in the oscillating wavelength toward the lower frequency side, indicating device heating effects. In order to explain the observed effects at room temperature and low magnetic fields, researchers have propounded theory based on the heating of the active region of the device and longitudinal magneto-resistance effect [3-4].

In this work an attempt is made to correlate the charge carrier dynamics of MQW laser system under the following two conditions:

- a) Strong magnetic field (> 5 T) and very low temperature ($T \ll 100$ K).
- b) Low magnetic field (< 2 T) and room temperature (280K-300K) condition.

[1] Berendshcot, T. T. J. M., Reinen H. A. J. M., and Bluysen, H. J. A., Wavelength and threshold current of quantum well laser in a strong magnetic field, Appl. Phys. Lett., **54**, 1827-1829 (1989).

[2] Arakawa, y., Sakaki, H., Nishioka, M., Okamoto, M.m and Miura, N., Spontaneous emission characteristics of quantum well lasers in strong magnetic fields – an approach to quantum-well-box light source, Jpn. J. Appl. Phys., **22**, L804-L806 (1983).

[3] Sato, T., Magnetic field effect on oscillation characteristics of a semiconductor laser, Rev. of Laser Engineering, **22**, 91-99 (1994).

[4] Zaker, T. A., and Hafiz, A. K., Influence of Magnetic field on threshold current, temperature characteristics, and on the output power in AlGaInP Multiple Quantum well Laser, Appl. Phys. Res., **3**, 143-151 (2011).

N-I-11

Study of biofilms typical for ENT pathologies by THz high resolution spectroscopy

**V.Vaks^{1,2}, A.Ayzenshtadt^{1,3}, V.Anferte^{1,2}, E.Domracheva^{1,2}, M.Chernyaeva^{1,2},
P.Mokeeva³, D.Kryazhev⁴**

1- Institute for Physics of Microstructures RAS, 603950, Russia, Nizhny Novgorod, GSP-105, Russia

2- Lobachevsky University, 603022, Russia, Nizhny Novgorod, Gagarina av., 23, Russia

3- Children's Municipal Clinical Hospital No.1,603081, Russia, Nizhny Novgorod, Gagarina av., 76, Russia

*4 - Blokhina Scientific Research Institute of Epidemiology and Microbiology of Nizhny Novgorod,603950, Russia,
Nizhny Novgorod, Malaya Yamskaya str., 71, Russia*

Nowadays spectroscopic analytical methods, operating in the frequency ranges from microwave to ultra-violet as well as other physico-chemical methods (mass-spectrometry, microscopy etc.) are used for medical diagnostics. These methods allow to reveal the metabolites, typical for a specific disease. When compiling a metabolic profile one can diagnose a disease and its etiology, as well as predict treatment. One of the complicated problem is to identify a biofilm, being the main type of existence of bacterial associations, which has its spatial and metabolic structure and forms on the mucosa in a human body. The work is devoted to analyzing the metabolites composition of the biofilms, forming at chronic adenotonsillitis, by high-resolution THz spectroscopy and the comparison of the thermal decomposition products of biofilms formed by *Staphylococcus aureus*, *Streptococcus pyogenes*, *Klebsiella pneumoniae* and *Enterobacter coli*.

A THz spectroscopy based on nonstationary effects such as inducing and decaying the free dumping polarization in a gas sample at the interaction of radiation and gas molecules can be considered as a high sensitive method of investigating the multicomponent gas mixtures. The devices can be realized in phase switching or fast sweeping modes of the probing radiation. The spectrometers with phase switching or with fast frequency sweeping developed by the authors, operating in the range of 118-178 GHz, were used. The sensitivity of the recorded absorption coefficient for these spectrometers at a cell length of 1 m is from 10^{-7}cm^{-1} to $5 \cdot 10^{-8} \text{cm}^{-1}$. The THz gas spectroscopy method allows to detect volatile compounds in a multicomponent gas mixture, including ones of biological origin. Therefore, it is promising to study the volatile compounds (products of thermal decomposition of macromolecules) as secondary metabolites of films, that appear when the sample is heated. The main pathobionts and their ability to biofilm formation at chronic adenotonsillitis with the identification of tissue metabolites with using the THz high resolution gas spectroscopy methods were studied, at that the influence of the pathogen was analyzed.

The biofilms formed by such bacterial types as *Staphylococcus aureus*, *Streptococcus pyogenes*, *Klebsiella pneumoniae* and *Enterobacter coli* were studied. The compositions of their thermal decomposition products differ significantly. The results obtained can be used in the future to reveal the infection of ENT organs tissues with certain bacteria, as well as to detect the presence of biofilms in the microflora of ENT organs.

This research was funded by the Russian Science Foundation, grant No. 21-19-00357, <https://rscf.ru/en/project/21-19-00357/>.



THz optical elements based on the shaped sapphire crystals and porous opals

G. M. Katyba^{1,2}, V.E. Ulitko, A.S. Kucheryavenko^{1,2}, V.A. Zhelnov^{1,2}, N.V. Chernomyrdin^{2,3},
I.N. Dolganova¹, K. I. Zaytsev^{2,3}, and V. N. Kurlov¹

1- Institute of Solid State Physics of RAS, 2 Academician Osipyan str., Chernogolovka, 142432 Russia

2- Prokhorov General Physics Institute of RAS, 38 Vavilova str., Moscow, 119991, Russia

3-Bauman Moscow State Technical University, 2-nd Baumanskaya str., Moscow, 105005, Russia

email: katyba_gm@issp.ac.ru

During the past few years, we introduced various materials for THz optical elements designing. The sapphire shaped crystals which are characterized by the relatively low THz wave losses, high refractive index and high inertness to external environment. Waveguides, fibers and fiber bundles based on the shaped sapphire could be used both for low-loss radiation delivery and for superresolution imaging tasks [1-5]. Recently we developed the hollow-core THz waveguides with polymer cladding for managing the angular distribution of the two-color laser air plasma emitter [6]. Moreover, such waveguides with the combination of the sapphire solid immersion lens could be used for the endoscopic system development [7] with spatial resolution around 0.19λ . Artificial opals based on the colloidal SiO₂ nanoparticles also were considered as perspective THz material with manageable optical properties [8]. It was reported that variety of bulk THz optical elements, such as cylindrical and axicone lens, could be created from this material, while the optical properties are tuned by the annealing at different temperatures [9]. The investigation of the possible interactions between such a porous material and water vapors from the atmosphere has the significant interest for THz element designing. We report about the new results of the moisture adsorption studying by artificial SiO₂ opals using THz pulsed spectroscopy [10].

This work was supported by the Russian Science Foundation (RSF), research project # 22-72-10033.

- [1] K. I. Zaytsev, G. M. Katyba, V. N. Kurlov, I. A. Shikunova, V. E. Karasik, S. O. Yurchenko, Terahertz Photonic Crystal Waveguides Based on Sapphire Shaped Crystals, *IEEE Transactions on Terahertz Science and Technology*, **6**(4), 576 (2016).
- [2] G. M. Katyba, K. I. Zaytsev, N. V. Chernomyrdin, I. A. Shikunova, G. A. Komandin, V. B. Anzin, S. P. Lebedev, I. E. Spektor, V. E. Karasik, S. O. Yurchenko, I. V. Reshetov, V. N. Kurlov, M. Skorobogatiy, Sapphire Photonic Crystal Waveguides for Terahertz Sensing in Aggressive Environments, *Advanced Optical Materials*, **6**(22), 1800573 (2018).
- [3] G. M. Katyba, K. I. Zaytsev, I. N. Dolganova, N. V. Chernomyrdin, V. E. Ulitko, S. N. Rossolenko, I. A. Shikunova, V. N. Kurlov, Sapphire waveguides and fibers for terahertz applications, *Progress in Crystal Growth & Characterization of Materials* **67**(3), 100523 (2021).
- [4] I. V. Minin, O. V. Minin, G. M. Katyba, N. V. Chernomyrdin, V. N. Kurlov, K. I. Zaytsev, L. Yue, Z. Wang, D. N. Christodoulides, Experimental observation of a photonic hook *Applied Physics Letters*, **114**, 031105 (2019).
- [5] G. M. Katyba, M. Skorobogatiy, D. G. Melikyants, N. V. Chernomyrdin, A. N. Perov, E. V. Yakovlev, I. N. Dolganova, I. E. Spektor, V. V. Tuchin, V. N. Kurlov, K. I. Zaytsev, Superresolution Imaging Using a Tapered Bundle of High-Refractive-Index Optical Fibers, *Physical Review Applied*, **18**(3), 34069 (2022).
- [6] G. M. Katyba, P. A. Chizhov, V. N. Kurlov, I. N. Dolganova, S. V. Garnov, K. I. Zaytsev, V. V. Bukin, THz generation by two-color laser air plasma coupled to antiresonance hollow-core sapphire waveguides: THz-wave delivery and angular distribution management, *Optics Express*, **30**(3), 4215-4230 (2022).
- [7] A. S. Kucheryavenko, V. A. Zhelnov, D. G. Melikyants, N. V. Chernomyrdin, S. P. Lebedev, V. V. Bukin, S. V. Garnov, V. N. Kurlov, K. I. Zaytsev, G. M. Katyba, Super-resolution THz endoscope based on a hollow-core sapphire waveguide and a solid immersion lens, *Optics Express*, **31**(8), 13366-13373 (2023).
- [8] V. E. Ulitko, A. K. Zotov, A. A. Gavdush, G. M. Katyba, G. A. Komandin, I. E. Spektor, I. M. Shmytko, G. A. Emelchenko, I. N. Dolganova, M. Skorobogatiy, V. N. Kurlov, V. M. Masalov, K. I. Zaytsev, Nanoporous SiO₂ based on annealed artificial opals as a favorable material platform of terahertz optics, *Optical Materials Express*, **10**(9), 2100-2113 (2020).
- [9] V. E. Ulitko, G. M. Katyba, V. A. Zhelnov, I. M. Shmytko, G. A. Emelchenko, I. E. Spektor, V. M. Masalov, V. N. Kurlov, K. I. Zaytsev, M. Skorobogatiy, Opal-based terahertz optical elements fabricated by self-assembly of porous SiO₂ nanoparticles, *Optics Express*, **29**(9), 13764-13777 (2021).
- [10] V. E. Ulitko, G. R. Musina, V. M. Masalov, A. A. Gavdush, G. A. Emelchenko, V. V. Bukin, V. N. Kurlov, M. Skorobogatiy, G. M. Katyba, K. I. Zaytsev, Moisture adsorption by porous terahertz optical materials: a case study of artificial SiO₂ opals, *Optics Express*, **13**(4), 1163-1176 (2023).

N-I-13

Nonequilibrium transport in Hg_{1-x}Cd_xTe-based heterostructures induced by terahertz laser radiation

**A. Kazakov¹, A. Galeeva¹, A. Artamkin¹, A. Ikonnikov¹, S. Chmyr¹, S. Dvoretzkiy²,
N. Mikhailov², V. Bannikov³, S. Danilov⁴, L. Ryabova¹, D. Khokhlov^{1,3}**

1- *M.V. Lomonosov Moscow State University, Physics Department, Leninskiye Gory, 1-2, Moscow, 119991, Russia*
2- *Rzhanov Institute of Semiconductor Physics of the Siberian Branch of the RAS, Lavrentyev Avenue 13, Novosibirsk, 630090, Russia*

3- *The Lebedev Physical Institute of the RAS, 119991, 119991, Moscow, Leninsky Avenue, 53*

4- *Faculty of Physics, University of Regensburg, Regensburg D-93053, Germany*

Main author email address: askazakov@physics.msu.ru

Transport properties of topologically nontrivial materials are of a great applied and fundamental interest. Hg_{1-x}Cd_xTe solid solutions exhibit a composition-driven topological transition from the trivial semiconductor phase ($x > 0.16$), characterized by the direct energy band ordering, to the topological phase ($x < 0.16$) with the inverted energy spectrum. Terahertz optoelectrical probing may provide an experimental observation of topological conductive states in Hg_{1-x}Cd_xTe solid solutions due to relatively low bulk carrier concentration. In this work, we study terahertz photoconductivity in Hg_{1-x}Cd_xTe epitaxial films in a close vicinity to the alloy composition $x \sim 0.16$, which corresponds to the topological phase transition.

Hg_{1-x}Cd_xTe-based heterostructures ($0.12 < x < 0.16$) with active layer thickness $d \sim 4 \mu\text{m}$ were synthesized on a semi-insulating GaAs [013] substrate with ZnTe and CdTe buffer layers by means of molecular beam epitaxy. Transport properties of the structures were studied in the 4.2 - 300 K temperature range. All the samples were of the n -type. The typical bulk concentration was $\sim 10^{14} \text{ cm}^{-3}$ at $T = 4.2 \text{ K}$. Terahertz photoconductivity stimulated by 100 ns laser pulses was studied in the frequency range 0.6 - 3.9 THz in magnetic fields up to 4 T at $T = 4.2 \text{ K}$. The samples under study were prepared with both the standard Hall bar sample geometry and the nonlocal H-bar-like geometry with various geometrical parameters.

We show that the photoresponse in the topologically nontrivial phase ($x < 0.16$) demonstrates strong asymmetry in a magnetic field which is absent in the trivial phase samples ($x > 0.16$) [1]. Also, the photoresponse kinetics strongly depends on the position of potential probes on the sample which is not due to possible structure inhomogeneity. Moreover, the photoresponse in topological phase of Hg_{1-x}Cd_xTe-based heterostructures incorporates a chiral nonlocal contribution indicating the formation of edge conductive channels [2]. We discuss the photoconductivity features in terms of a qualitative model that takes into account the coexistence of bulk transport and boundary conductive channels.

The work was supported by the Russian Science Foundation, grant #19-12-00034.

[1] A.V. Galeeva, A.S. Kazakov, A.I. Artamkin, L.I. Ryabova, S.A. Dvoretzkiy, N.N. Mikhailov, M.I. Bannikov, S.N. Danilov, D.R. Khokhlov, *Sci. Rep.* 2020, 10, 2377.

[2] A.S. Kazakov, A.V. Galeeva, A.I. Artamkin, A.V. Ikonnikov, L.I. Ryabova, S.A. Dvoretzkiy, N.N. Mikhailov, M.I. Bannikov, S.N. Danilov, D.R. Khokhlov, *Sci. Rep.* 2021, 11(1), 1587.



Plasmonic-enhanced THz emission in high-aspect-ratio metal grating photoconductive antennas

**D. Ponomarev^{1,2}, D. Lavrukhin^{1,2}, A. Yachmenev¹, R. Khabibullin¹
Yu. Goncharov², I. Spektor², K. Zaytsev²**

*1- Institute of Ultra-High Frequency Semiconductor Electronics of the Russian Academy of Sciences,
117105 Moscow, Nagorny proezd 7, Russian Federation*

*2- Prokhorov General Physics Institute of the Russian Academy of Sciences,
119991 Moscow, 38 Vavilov st., Russian Federation*

email address: ponomarev_dmitr@mail.ru

Photoconductive antenna-emitters (PCAs) are intensively used in THz time-domain spectroscopic and imaging setups thanks to their reliability, cost-effectiveness, simplicity of fabrication, and their flexibility in the designing of antenna electrodes and topology, as well as the choice of photoconductive substrate. Compared with the existing THz devices [1,2], PCAs can efficiently work at room temperature demonstrating a broadband spectrum of 0.1–5.0 THz with a perfect dynamic range, i.e. signal-to-noise ratio exceeding even 100 dB [3]. Recently, the Ge-based PCA-emitters have demonstrated an unprecedented bandwidth reaching 70 THz thanks to an absence of polar phonons in Ge [4]. Moreover, an optical-to-THz conversion efficiency of the PCA-emitters is not limited by the Manley–Rowe relation [5-7], as the photoconductivity theoretically allows converting every single optical photon into one electron-hole pair. The drastic issue that limits the PCA-emitter performance is its low conversion efficiency, i.e. only the minor part of the laser radiation is transferred to the THz waves, limiting overall emitted THz power. Many approaches featuring seminal photoconductor designs and antenna topology have been predicted and demonstrated their efficiency, nevertheless the progress is still essential. The physical problem is due to low laser light confinement at the electrode/photoconductor interface, as only the photocarriers generated in vicinity to the electrodes can contribute to the THz emission.

We have proposed the design of the PCA-emitter with a plasmonic grating featuring a very high plasmonic Au electrode with a thickness of $h = 170$ nm. As we show numerically, the increase in h significantly changes the electric field distribution, owing to the excitation of higher-order plasmon guided modes in the Au slit waveguides, leading to an additional increase in the emitted THz power. We developed the plasmonic grating geometry with respect to maximal transmission of the incident optical light, so as to expect the excitation of higher-order plasmon guided Au modes. The bow-tie PCA was characterized via our laboratory THz-TDS [6,7], and compared to the same photoconductive emitter but featuring a 100 nm-thick grating [8]. The both PCAs were fabricated on LT-GaAs, while a wrapped-dipole PCA TERA-8 (by Menlo Systems) was used as a THz PCA-detector. We showed that the fabricated high aspect ratio plasmonic PCA efficiently work with low-power laser excitation, demonstrating an overall THz power of 5.3 μ W over an \sim 4.0 THz bandwidth, corresponding to a conversion efficiency of 0.2% [9].

The work was supported the Russian Science Foundation, project 18-79-10195.

- [1] P. U. Jepsen, D. G. Cooke, and M. Koch, *Las. Photon. Rev.* 5, 124 (2011).
- [2] D. S. Ponomarev, D. V. Lavrukhin, N. V. Zenchenko et al, *Opt. Lett.* 47(7), 1899 (2022).
- [3] R.B. Kohlhaas, S. Breuer, S. Mutschall et al, *Opt. Exp.* 30(13), 23896 (2022).
- [4] A. Singh, A. Pashkin, S. Winnerl et al, *Light: Sci. Appl.* 9, 30(2020).
- [5] A. Petukhov, V. Brudny, W. Mochàn et al, *Phys. Rev. Lett.* 81, 566 (1998).
- [6] D. V. Lavrukhin, A. E. Yachmenev, Yu. G. Goncharov et al, *IEEE Trans. THz. Sci. Technol.* 11(4), 417 (2021).
- [7] A. Gorodetsky, D. V. Lavrukhin, D. S. Ponomarev et al, *IEEE J. Sel. Top. Quant. Electron.*, 29(5), pp. 1-5 (2023).
- [8] D. V. Lavrukhin, A. E. Yachmenev, I. A. Glinskiy et al, *AIP Adv.* 9, 015112 (2019).
- [9] D. S. Ponomarev, D. V. Lavrukhin, I. A. Glinskiy et al, *Opt. Lett.* 48(5), 1220 (2023).



N-I-15

Drift-current-induced amplification and lasing of TE electromagnetic modes in graphene

I. Moiseenko¹, D. Fateev¹, V. Popov¹

1- Kotelnikov Institute of Radio Engineering and Electronics (Saratov Branch) of the Russian Academy of Sciences, Saratov, Russia

email address: popov_slava@yahoo.co.uk

The dispersion, excitation, and amplification of electromagnetic transverse electric (TE) modes at terahertz (THz) frequencies in graphene in the hydrodynamic (HD) regime, with a direct electric current flowing perpendicular to the TE mode wavevector, were theoretically investigated [1]. The expression for the nonlocal HD conductivity of graphene with a direct electric current (DC) flowing perpendicular to the TE mode wavevector was derived. The direct electric current in graphene leads to the capacitive nature of the graphene HD conductivity at THz frequencies, which makes TE modes exist in this frequency range [2]. The real part of graphene conductivity can be negative at THz frequencies due to DC in graphene which leads to amplification and lasing of THz radiation. The excitation of TE modes in graphene by an incident THz wave was modeled for the attenuated total reflection geometry. A new physical mechanism of TE mode amplification in graphene effective for a low value of carrier drift velocity was predicted. Terahertz lasing regimes with TE modes in graphene structure with direct electric current were found.

We study for the first time the interaction between the waveguide modes of graphene structure and freely propagating THz electromagnetic waves (this interaction takes place within the light cone) [3]. We revealed a new and rather unexpected physical phenomenon by showing that freely incident THz electromagnetic waves can resonate with the surface TE modes of the graphene waveguide in virtue of these modes having their dispersions in the vicinity of the light cone. The dispersion and amplification of surface TE modes in a dielectric waveguide covered with two graphene layers biased by DC, as well as the amplification and lasing of incident THz wave by excitation of TE mode resonances, are investigated. The results of this work can be used to create miniature technologically feasible sources and amplifiers of THz radiation. Such structure can be of great practical importance because an external THz wave can be amplified or generated in lasing process without using special coupling elements commonly needed for ensuring the interaction between external THz wave and surface waveguide modes. The use of a two-layer graphene structure makes it possible to reduce the charge-carrier drift velocity required for reaching the lasing threshold at those resonances, as compared to a structure with a single graphene layer.

This work was financially supported by the Russian Science Foundation (Project No. 22-19-00611).

[1] I.M. Moiseenko, V.V. Popov, D.V. Fateev, Terahertz transverse electric modes in graphene with DC current in hydrodynamic regime, *J. Phys.: Condens. Matter*, vol. 34, pp. 295301-1 – 295301-6, (2022).

[2] S.A. Mikhailov, K. Ziegler, New electromagnetic mode in graphene, *Phys. Rev. Lett.*, vol. 99, pp. 016803-1 – 016803-4 (2007).

[3] I.M. Moiseenko, V.V. Popov, D.V. Fateev, Terahertz amplification and lasing by using transverse electric modes in a two-layer-graphene-dielectric waveguide structure with direct current, *J. Phys.: Condens. Matter*, vol. 35, pp. 255301-1 – 255301-6, (2023).



Super-resolution THz imaging of biological tissues: Recent achievements and challenges

Kirill I. Zaytsev

Prokhorov General Physics Institute of the Russian Academy of Sciences, Moscow, Russia

E-mail: kirzay@gmail.com

Unique effects of THz-wave–matter interaction push rapid progress in THz optoelectronics aimed at bridging the problematic THz gap [1]. However, majority of the THz technology applications still suffers from low spatial resolution of common lens- or mirror-based THz optics [2]. In fact, such optics cannot overcome the $\sim 0.5\lambda$ Abbe limit and provides the resolution larger than a free-space wavelength λ (i.e., a few hundreds of micrometers or even a few millimeters) [3,4]. This hampers the use of THz technology in vigorously-exploded biomedical applications [5]: diagnosis of malignant and benign neoplasms [6–8], diabetes mellitus [9,10], cancer therapy [11], etc.

To mitigate this difficulty, super-resolution THz imaging modalities were recently introduced. Among them, we particularly underline different methods of the THz scanning-probe near-field optical microscopy. They rely on strong light confinement on sub-wavelength probes and provide the advanced resolution as high as $\sim 10^{-1}–10^{-3}\lambda$ [12]. Meanwhile, they suffer from small energy efficiency (or presume an interplay between resolution, energy efficiency, field of view, and operation rate), while the scanning probe may interact with an imaged sample and even perturb its structure.

In our research, we developed a novel super-resolution THz imaging modality – so-called, THz solid immersion (SI) microscopy [2,13–22]. The essence of a SI effect is a reduction in the electromagnetic beam caustic dimensions, when it is formed in free space, at small distance behind the high-refractive-index materials. We developed the THz SI lens, that is based on a wide-aperture aspherical singlet [3] and a near-focal composite silicon hemisphere, operates in reflection mode, and provides the resolution as high as 0.15λ (beyond the Abbe limit) [14]. It possesses advanced energy efficiency thanks to the absence of any near-field probes in an optical scheme, as well as adapted for imaging of soft biological tissues, thanks to the composite construction of the hemisphere [14]. We also studied capabilities of a bulk sapphire crystal [21], a bulk rutile crystal (with its impressive THz refractive index of ~ 10) [22], and a compound of rutile microparticles and polymer [17], as favourable material platforms of the THz SI optics.

All these modalities of super-resolution THz imaging were recently applied in biophotonics, where they allow for the highly-accurate delineation of the tumor margins, studying the tissue heterogeneity at the THz wavelengths scale and the related scattering effects [18–20]. In this talk, we discuss, recent achievements and challenging problems in super-resolution THz imaging of tissues.

This work was supported by the Russian Science Foundation, Project # 22-79-10099.

- [1] H. Guerboukha et al., *Advances in Optics & Photonics* **10**, 843 (2018).
- [2] N.V. Chernomyrdin et al., *Applied Physics Letters* **120**, 110501 (2022).
- [3] N.V. Chernomyrdin et al., *Review of Scientific Instruments* **88**, 014703 (2017).
- [4] G.M. Katyba et al., *Optica* **10**, 53 (2023).
- [5] O.A. Smolyanskaya et al., *Progress in Quantum Electronics* **62**, 1 (2018).
- [6] K.I. Zaytsev et al., *Journal of Optics* **22**, 013001 (2020).
- [7] H. Lindley-Hatcher et al., *Applied Physics Letters* **118**, 230501 (2021).
- [8] N.V. Chernomyrdin et al., *Opto-Electronics Advances* **6**, 220071 (2023).
- [9] G.G. Hernandez-Cardoso et al., *Scientific Reports* **12**, 3110 (2022).
- [10] A.A. Lykina et al., *Journal of Biomedical Optics* **26**, 043006 (2021).
- [11] O.P. Cherkasova et al., *Journal of Biomedical Optics* **26**, 090902 (2021).
- [12] H.-T. Chen et al., *Applied Physics Letters* **83**, 3009 (2003).
- [13] N.V. Chernomyrdin et al., *Applied Physics Letters* **110**, 221109 (2017).
- [14] N.V. Chernomyrdin et al., *Applied Physics Letters* **113**, 111102 (2018).
- [15] N.V. Chernomyrdin et al., *Optical Engineering* **59**, 061605 (2019).
- [16] V.A. Zhelnov et al., *Optics Express* **29**, 3553 (2021).
- [17] Q. Chapdelaine et al., *Optical Materials Express* **12**, 3015 (2022).
- [18] N.V. Chernomyrdin et al., *Optica* **8**, 1471 (2021).
- [19] A.S. Kucheryavenko et al., *Biomedical Optics Express* **12**, 5272 (2021).
- [20] G.R. Musina et al., *Biomedical Optics Express* **12**, 5368 (2021).
- [21] A.S. Kucheryavenko et al., *Optics Express* **31**, 13366 (2023).
- [22] V.A. Zhelnov et al., “Hemispherical rutile solid immersion lens for rerahertz microscopy with superior 0.06–0.11 λ resolution,” *Advanced Optical Materials* (2023), under review.





N-I-17

Photoresponse of a two-dimensional electron gas to structured terahertz radiation

S.A. Tarasenko

Ioffe Institute, 194021 St. Petersburg, Russia

tarasenko@coherent.ioffe.ru

Structured radiation, such as intensity and polarization gratings, and twisted beams carrying orbital angular momentum, has a variety of application in physics, chemistry, and biology [1]. The interaction of structured radiation with semiconductor systems is of particular interest from fundamental point of view and is crucial for the development of optoelectronics [2,3].

Here, we explore the photoresponse of a two-dimensional electron system to the terahertz radiation with structured intensity, polarization, and phase [4]. It is shown that, besides the photothermoelectric current associated with the intensity gradient, the photocurrent contains contributions driven by the gradients of the Stokes polarization parameters and the phase of the electromagnetic field. In particular, the photocurrents are induced by the radiation with a uniform intensity but spatially varying polarization, e.g., at the boundary between the domains excited by radiation with different polarizations. The total current emerging at the boundary of the domains excited by circularly polarized radiation with the opposite helicity flow along the boundary and does not depend on the boundary structure nor the electron gas mobility in the high-frequency limit. This current can be interpreted as the chiral edge current between the photo-induced topological phases with the opposite Floquet-Chern numbers. In the framework of the Boltzmann kinetic approach, we develop a microscopic theory of the non-linear non-local intraband transport of electrons induced by electromagnetic field of structured radiation and derive analytical expressions for all the photocurrent contributions.

The developed theory is also applied to study the photocurrents induced by the Bessel beams carrying orbital angular momentum. The emergent photocurrents have both radial and azimuthal (vortex-like) components which are controlled by the beam polarization and angular momentum. The radial photocurrents lead to a redistribution of electric charge in the two-dimensional plane and form the radial photovoltage. The azimuthal photocurrents induce a static magnetic field and the corresponding magnetization. The results suggest that the measurement of the photoresponse provides a useful experimental tool to determine the parameters of structured radiation, such as, e.g., the photon spin and orbital angular momentum.

This work was supported by the Russian Science Foundation (project No. 22-12-00211).

[1] A. Forbes, M. de Oliveira, and M. R. Dennis, Structured light, *Nat. Photonics*, 15, 253 (2021).

[2] Z. Ji, W. Liu, S. Krylyuk et al., Photocurrent detection of the orbital angular momentum of light, *Science*, 368, 763 (2020).

[3] S. Sederberg, F. Kong et al., Vectorized optoelectronic control and metrology in a semiconductor, *Nat. Photonics* 14, 680 (2020).

[4] A. A. Gunyaga, M. V. Durnev, S. A. Tarasenko, Photocurrents induced by structured light, arXiv:2306.08099 (2023).



Prism-lens couplers for efficient sideways Cherenkov terahertz wave generation in nonlinear crystals

N.V. Starkova¹, D.A. Safronkov¹, D.A. Markov¹, G.Kh. Kitaeva¹

¹Lomonosov Moscow State University, Leninskie Gory 1-2, Moscow 119991 Russia

gkitaeva@physics.msu.ru

The ways to increase the power efficiency of the sideways terahertz wave (THz) generation are studied considering Cherenkov optical rectification (OR) scheme in Mg:LiNbO₃ crystal. We propose to equip the generating nonlinear crystal with a prism-lens coupler made of high-resistance Si with a specially selected output surface curvature. Experimentally, about 4.5-fold increase in output THz field amplitude (Fig. 1a) and the 12-fold increase in the detected power at 0.5 THz have been achieved when a common flat-surface prism [1] was supplied by one of plano-convex lenses under investigation.

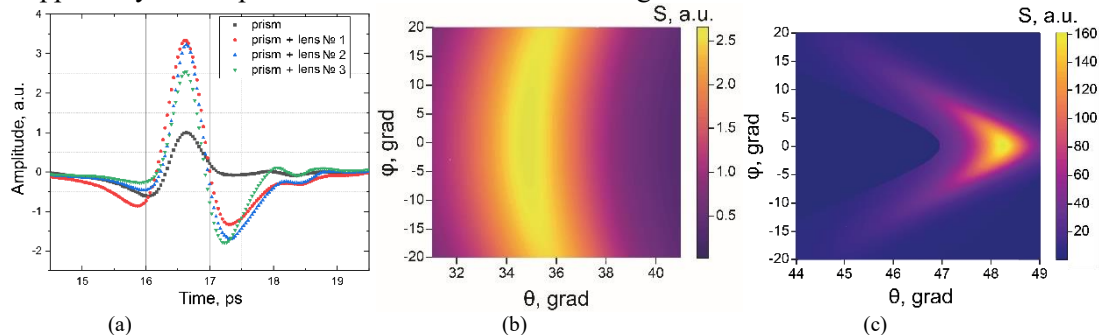


Fig. 1. THz waveforms detected experimentally with the flat Si prism (black dots) and with the same prism supplied by different Si plano-convex lenses (a); angular distributions of the output THz power calculated for the case of the flat Si prism (b) and the prism-lens coupler with optimal curvature of the output surface (c).

To explain the demonstrated advantage of the curved coupler's curvatures, we calculated the angular distributions of THz radiation power which are emitted by the crystal parts located at the lens axis (Figs. 1b,c). The calculations are based on the general approach, when the THz generation under OR of femtosecond laser pulses inside the nonlinear crystal is considered as a continuous set of simultaneous nonlinear three-wave processes of parametric difference frequency generation [2], and the subsequent transformation of differently directed planar THz components during their propagation through the crystal-Si and Si-air interfaces is taken into account [3]. The developed theoretical approach forecasts new perspective shapes of the Si-adaptor output surfaces and can be used for further design of optimal extraction elements.

The work was done under financial support of the Russian Science Foundation (Grant No. 22-12-00055).

[1] K. Kawase, J. Shikata, and H. Ito, Terahertz wave parametric source, *Journal of Physics D: Applied Physics* 35, R1 (2002).

[2] G.Kh. Kitaeva, V.V. Kornienko, A.A. Leontyev, and A.V. Shepelev, Generation of optical signal and terahertz idler photons by spontaneous parametric down-conversion, *Phys. Rev. A* 98, 063844 (2018).

[3] G.Kh. Kitaeva, D.A. Markov, D.A. Safronkov, N.V. Starkova, Prism couplers with convex output surfaces for nonlinear Cherenkov terahertz generation, *Photonics* 10, 450 (2023).



N-I-19

Terahertz HEB-based on-chip spectrometers for material and biomedical studies

A. Shurakov^{1,2}, A. Prikhodko^{1,2}, I. Belikov^{1,2}, G. Goltsman^{1,2}

1- Moscow Pedagogical State University, 1/1 Malaya Pirogovskaya St., Moscow 119991, Russia

2- National Research University Higher School of Economics, 20 Myasnitskaya St., Moscow 101000, Russia

Main author email address: alexander@rplab.ru

Terahertz (THz) electronics was a subject of numerous scientific studies for the last several decades. Efficient handling of THz radiation is vital for further enhancement of medical and security systems, meteorological and astronomical instruments, wireless communications, etc. Based on the requirements imposed by the application specifics, semi- or superconductor integrated circuits (ICs) are of interest in practical THz systems. In the upper part of the THz band, however, their ultimate performance can be achieved if electronic circuits are combined with photonic power distribution networks (PPDNs). Benefits of such an approach are investigated in number of studies published recently. Use of a hybrid electronic-photonic platform is meant to mitigate intrinsic losses in IC and to increase the integrability of nonlinear frequency conversion devices drastically [1].

In this paper, we report on the development of a THz on-chip spectrometer making use of an N-element linear array of nearly all-dielectric hot electron bolometers (HEBs) [2]. The spectrometer utilizes 2^N fixed frequency channels for processing of a wideband THz signal, whose interaction with a material under test (MUT) is followed by analog binning. The design relies on integrated Si photonic crystals merged with Si ribbon waveguide sections for frequency selective power splitting in the spectrometer PPDN. MUT is deposited on a single-mode Si ribbon waveguide at the spectrometer input or surrounds it if liquid samples are studied. In the latter case, the input waveguide section is implemented outside the cryostat used to cool down the PPDN with HEB sensors. Optical transition between cryogenic and room temperature parts is maintained by either a dielectric waveguide [3] or quasioptically [4]. The probing octave-wide THz signal, in turn, can be excited on-chip or inserted into it externally. Performance of the spectrometer is assessed and compared with alternative state-of-the-art designs. Our findings suggest that the proposed design of the spectrometer should find applications in material and biomedical studies.

The study was supported by the Russian Science Foundation grant No. 21-72-10119, <https://rscf.ru/project/21-72-10119/>.

[1] K. Sengupta, T. Nagatsuma, D.M. Mittleman, Terahertz integrated electronic and hybrid electronic-photonic systems, *Nature Electronics*, vol. 1, pp. 622–635, (2018).

[2] A. Shurakov, I. Belikov, A. Prikhodko, M. Ershova, G. Goltsman, Superconducting electronic-photonic platform for HEB-based terahertz spectrometers, *Applied Sciences*, vol. 13, no. 10, 5892, (2023).

[3] H.-T. Zhu, D. Liu, J. Hu, S. Li, S.-C. Shi, Q. Xue, W. Che, Low-loss, thermally insulating, and flexible rectangular dielectric waveguide for sub-THz-signal coupling in superconducting receivers, *Transactions on Terahertz Science and Technology*, vol. 10, no. 2, pp. 190–199, (2020).

[4] A. Endo, K. Karatsu, A. Pascual Laguna, B. Mirzaei, R. Huiting, D. Thoen, V. Murugesan, S.J.C. Yates, J. Bueno, N.V. Marrewijk, S. Bosma, O. Yurduseven, N. Llombart, J. Suzuki, M. Naruse, P.J. de Visser, P.P. van der Werf, T.M. Klapwijk, J.J.A. Baselmans, Wideband on-chip terahertz spectrometer based on a superconducting filterbank, *Journal of Astronomical Telescopes, Instruments, and Systems*, vol. 5, no. 3, 035004, (2019).

Electrical-field tunable diffraction optical elements based on lithium niobate single crystals

A. Akhmatkhanov¹, A. Esin¹, V. Shur¹, V. Pavelyev²

1- Institute of Natural Sciences and Mathematics, Ural Federal University 620002, Ekaterinburg, Russia

2- Samara National Research University, 443086, Samara, Russia

E-mail: andrey.akhmatkhanov@urfu.ru

Periodically poled lithium niobate (LN) single crystals are widely used for nonlinear optical applications for quasi-phase-matched laser light frequency conversion. The quasi-phases matching process in this case is realized due to opposite values of second order susceptibility tensors in neighboring domains of periodical domain structure. On the other hand, these domains possess opposite signs of electrooptic coefficient, which allows creation of electric field controllable diffraction optical elements (DOEs). The utilization of this effect led to demonstration of the following devices: optical beam deflectors [1-2], diffusers [3], Fresnel zone plates [4] and Shack-Hartmann sensors [5]. Creation of effective DOEs requires precise control of LN domain structure.

In this work we present the results of creation and characterization of various LN-based DOEs. The DOE creation process was based on deep study of the features of domain structure kinetics in LN. The dependence of domain wall velocity on field and orientation was analyzed. We have revealed that the walls oriented along Y crystallographic directions were more than four orders of magnitude slower than the X-oriented ones. This effect hampers creation of some types of DOEs as they require creation of domain structures with wide range of domain wall orientations. The methods of overcoming of this problem are discussed. We have designed the structure of 2D hexagonal zone plate, which represents the best approximation of circular zone plate by the set of hexagonal ferroelectric domains with Y-oriented walls. The creation of 2D hexagonal zone plate with minimal ferroelectric domain size down to 7 μm and period of 20 μm has been demonstrated. The obtained half-wave voltage of DOE was 2.9 kV. We have shown that additional heat treatment at temperature about 150°C allows to compensate built-in internal field and to decrease the zero-phase-shift voltage down to 0.4 kV.

The following DOEs were created and characterized: (1) 2D diffraction grating, (2) hexagonal zone plate, (3) bidomain element for TEM_{00} - TEM_{01} mode transformation [6], (4) DOE for generation of transformation of TEM_{00} mode into angular-momentum modes. The 2D diffraction grating allowed decreasing the zero-order diffraction maximum intensity by 80%. The hexagonal zone plate has focused up to 25% of the laser light into a spot of 0.13-mm-diameter. The measured response time of the bidomain element for TEM_{00} - TEM_{01} mode transformation was below 0.3 μs (limited by the photodiode bandwidth).

The possible applications of bidomain element for channel multiplexing in communication systems are discussed.

The research was made possible by Russian Science Foundation (Project №21-72-10160).

- [1] D. A. Scrymgeour, A. Sharan, V. Gopalan, K. T. Gahagan, J. L. Casson, R. Sander, J. M. Robinson, F. Muhammad, P. Chandramani, and F. Kiamilev, Cascaded electro-optic scanning of laser light over large angles using domain microengineered ferroelectrics, *Appl. Phys. Lett.*, vol.81, pp.3140-3142 (2002).
- [2] Y. Chiu, V. Gopalan, M. J. Kawas, T. E. Schlesinger, D. D. Stancil, and W. P. Risk, Integrated optical device with second-harmonic generator, electro-optic lens and electrooptic scanner in LiTaO_3 , *J. Lightwave Technol.*, vol.17, pp. 462-464 (1999).
- [3] R. Cudney, H. Escamilla, L. Ríos, Electrically controllable diffuser made from randomly-poled lithium niobate, *J. Opt. Soc. Am. B*, vol.21, pp.1797-1803, (2004).
- [4] R. Cudney, L. Ríos, H. Escamilla, Electrically controlled Fresnel zone plates made from ring-shaped 180° domains, *Opt. Express*, vol.12, pp.5783-5788, (2004).
- [5] J. Mávita, L. Ríos, C. Minor, R. Cudney, Switchable phase/intensity sensor made with ring-shaped and hexagonal ferroelectric domains, *Appl. Opt.*, vol.57, pp. 2208-2214, (2018).
- [6] A. Esin, A. Akhmatkhanov, V. Pavelyev, V. Shur, Tunable LiNbO_3 -based diffractive optical element for the control of transverse modes of a laser beam, *Comp. Opt.*, vol.45, pp. 222-226, (2021).



THz–IR dielectric spectroscopy of astrophysical ices: Recent achievements and challenges.

A.A. Gavdush¹, F. Kruczkiewicz^{2,3}, B. M. Giuliano², B. Müller², G. A. Komandin¹, K. I. Zaytsev¹, A. V. Ivlev², P. Caselli²

1- Prokhorov General Physics Institute of the Russian Academy of Sciences, Russia, 119991 Moscow, Russia

2- Max-Planck-Institut für Extraterrestrische Physik, Gießenbachstraße 1, Garching 85748, Germany

3- Aix-Marseille Univ, CNRS, CNES, LAM, Marseille, France

arsenii.a.gavdush@gmail.com

Understanding the chemical and physical properties of molecular clouds, in which the star and planet formation process takes place, is directly related to the correct estimation of the amount of gas contained in them. This problem is one of many in the list of relevant astrophysical problems [1-4] requiring the knowledge of broadband dielectric properties of interstellar and circumstellar laboratory ice analogues. The complex dielectric permittivity of ices is essential while modeling the dust continuum emission, radiative transfer in dense and cold University regions. Despite the importance of such parameters there is still a lack of data concerning dielectric properties of ices in terahertz (THz) and infrared (IR) ranges of spectra. Series of recent works from our scientific group [5, 6] is focused on solving such a problem. We developed original methods for processing the experimental data obtained by means of THz pulsed spectroscopy (TPS) and Fourier-transform infrared spectroscopy (FTIR). The possibility of direct reconstruction of the ices complex dielectric permittivity in the broad spectral range is a primary result of our studies. The algorithm of direct reconstruction takes into account the possibility of retrieving amplitude and phase information for TPS measurements and proposes an approach of merging TPS and FTIR data with the solution of the problem of eliminating uncertainties introduced by the Kramers-Kronig relations. Complex dielectric properties of several ices, including carbon monoxide and carbon dioxide ices, were studied in the THz-IR range. The obtained results are analyzed in terms of analytical Lorentz dielectric models with attribution to particular vibrational modes. The most promising areas for further research include ice structure investigation, study of the light scattering in ice, study of the regimes for producing ice samples, annealing of the ices. A review of the unanswered questions and promising results is a final part of the talk.

This work was supported by the Russian Science Foundation (RSF), Project # 22–72–00092.

[1] A.C.A. Boogert, P.A. Gerakines, D.C.B. Whittet, Observations of the Icy Universe, *Annual Review of Astronomy and Astrophysics*, vol. 53(1), pp. 541–581 (2015).

[2] S.L. Widicus Weaver, Millimeterwave and Submillimeterwave Laboratory Spectroscopy in Support of Observational Astronomy, *Annual Review of Astronomy and Astrophysics*, vol. 57(1), pp. 79–112 (2019).

[3] D.V. Mifsud et al., The Role of Terahertz and Far-IR Spectroscopy in Understanding the Formation and Evolution of Interstellar Prebiotic Molecules, *Frontiers in Astronomy and Space Sciences*, vol. 8 (2021).

[4] D.V. Mifsud et al., Sulfur Ice Astrochemistry: A Review of Laboratory Studies, *Space Science Reviews*, vol. 217(1), pp. 14 (2021).

[5] B.M. Giuliano et al., Broadband spectroscopy of astrophysical ice analogues: I. Direct measurement of the complex refractive index of CO ice using terahertz time-domain spectroscopy, *Astronomy & Astrophysics*, vol. 629, pp. A112 (2019).

[6] A.A. Gavdush et al., Broadband spectroscopy of astrophysical ice analogues: II. Optical constants of CO and CO₂ ices in the terahertz and infrared ranges, *Astronomy & Astrophysics*, vol. 667, pp. A49 (2022).

Terahertz surface plasmon refractometry of conducting surfaces and thin dielectric layers on the Novosibirsk free-electron laser

V. V. Gerasimov^{1,2}, V. D. Kukotenko¹, O. E. Kameshkov^{1,2}, A. G. Lemzyakov¹, V. P. Nazmov¹,
A. I. Ivanov³, I. A. Azarov³, I. Sh. Khasanov⁴, A. K. Nikitin⁴

1- Budker Institute of Nuclear Physics of SB RAS, 11, Lavrentiev prospect, 630090, Novosibirsk, Russia

2- Department of Physics, Novosibirsk State University, 630090 Novosibirsk, Russia

3- Rzhanov Institute of Semiconductor Physics SB RAS, 13 Lavrentiev Aven., Novosibirsk 630090, Russia

4- Scientific and Technological Centre of Unique Instrum. of RAS, 15, Butlerova str., 117342, Moscow, Russia

v.v.gerasimov3@gmail.com

Plasmon refractometry has found wide application in optical sensor devices in the visible range due to such features of surface plasmons (SPs) at these frequencies as short propagation length (which meets the requirement for miniaturization of sensors) and concentration of the SP field in the metal surface vicinity, that results in high sensitivity of SP devices to changes in optical characteristics of the sensor layer on the metal surface [1].

In the THz range, where the SPs propagation length on metals extends to tens of centimeters [2], plasmon refractometry based on plasmon interferometry [3] can be effectively used to control quality of the metal surface as well as to determine the effective permittivity of metal coatings used in plasmonic THz integrated circuits [4]. Besides, THz SP interferometers can be employed for investigations of thin dielectric films on metal surfaces, and for various sensor applications. The complementary experimental method that makes it possible to determine the effective permittivity of a conducting surface is the study of the attenuation of the evanescent field of the SPs over the conductor [5].

If semiconductors with a plasma frequency lying in the THz frequency range are used as the substrate on which the SPs propagate, then it is possible to implement the refractometry of semiconductor surfaces and dielectric (or weakly conductive) films deposited on them using the surface plasmon resonance (SPR) method [6]. If a dielectric film has an inhomogeneous relief on the semiconductor surface, then by taking images of the reflected radiation using a focal plane array under SPR conditions, it is possible to determine the inhomogeneous regions of the film. This method in the literature is called surface plasmon microscopy [7].

All the above methods of plasmon refractometry were tested on the THz radiation of the Novosibirsk free electron laser, which generates monochromatic linearly polarized coherent radiation, tunable in the wavelength range of 50 – 400 μm . Many of these methods have been implemented for the first time and will be presented in the talk.

The work was done at the shared research center SSTRC on the basis of the Novosibirsk FEL at BINP SB RAS.

[1] Y. Gao, Z. Xin, Q. Gan, X. Cheng, and F. Bartoli, Plasmonic interferometers for label-free multiplexed sensing, *Opt. Express.*, vol. 21, no 5, pp. 5859–5871 (2013).

[2] Vasily V. Gerasimov, Boris A. Knyazev, Alexey G. Lemzyakov, Alexey K. Nikitin, and Guerman N. Zhizhin. Growth of terahertz surface plasmon propagation length due to thin-layer dielectric coating, *Journal of Optical Society of America B*. V. 33, Is. 11, P. 2196-2203 (2016).

[3] V. V. Gerasimov, A. K. Nikitin, and A. G. Lemzyakov, Planar Michelson interferometer using terahertz surface plasmons, *Instruments and Experimental Techniques*, N. 3, pp. 67-79 (2023).

[4] S. Pandey, B. Gupta, A. Chanana, A. Nahata, Non-Drude like behaviour of metals in the terahertz spectral range, *Advances in Physics*, vol. 1, no 2, pp. 176-193 (2016).

[5] V. D. Kukotenko, V. V. Gerasimov, Approaches to studying the evanescent field of surface plasmons using THz radiation from the Novosibirsk free electron laser, Abstract book of the 5-th International Conference TERAHERTZ AND MICROWAVE RADIATION: GENERATION, DETECTION AND APPLICATIONS, 27 February — 2 March 2023, Moscow, Russia, p. 115.

[6] I. Sh. Khasanov, V. V. Gerasimov, O. E. Kameshkov, A. K. Nikitin, Observation of surface plasmon resonance in monochromatic terahertz radiation on indium antimonide, *Journal of Surface Investigation: X-ray, Synchrotron and Neutron Techniques*, to be published (2023).

[7] V. V. Gerasimov, O. E. Kameshkov, A. K. Nikitin, I. Sh. Khasanov, First experimental demonstration of the wide-field amplitude surface plasmon microscopy in the terahertz range, *Photonics*, to be published (2023).



Hierarchical multi-scale coupled periodical photonic nanopatterns inscribed in lithium niobate by femtosecond laser

M. Kosobokov¹, S. Kudryashov^{1,2}, A. Rupasov², A. Akhmatkhanov¹, G. Krasin², P. Danilov^{1,2}, B. Lisjikh¹, A. Turygin¹, A. Abramov¹, E. Greshnyakov¹, E. Kuzmin², M. Kovalev^{1,2}, A. Efimov¹, V. Shur¹

1- School of Natural Sciences and Mathematics, Ural Federal University, 620000 Ekaterinburg, Russia

2- Lebedev Physical Institute, 119991 Moscow, Russia

E-mail: mihail.kosobokov@urfu.ru

The ultrafast interaction of tightly focused femtosecond laser pulses with bulk ferroelectric media in direct laser writing (inscription) regimes is known to proceed via complex multi-scale light, plasma and material modification nanopatterns, which are challenging for exploration owing to their mesoscopic, transient and buried character.

In this study, we report on the experimental demonstration and analysis of hierarchical multi-period coupled longitudinal and transverse microtracks and nanogratings in bulk lithium niobate inscribed in the focal region by 1030 nm, 300 fs laser pulses in the recently proposed sub-filamentary laser inscription regime [1]. The longitudinal Bragg-like topography nanogratings, possessing the laser-intensity-dependent periods ≈ 400 nm, consist of transverse birefringent nanogratings, which are perpendicular to the laser polarization and exhibit much smaller periods ≈ 160 nm. The microtracks were imaged by optical microscopy. The nanoscale morphology of the microtracks was visualized at the sample cross-sections by atomic force microscopy (AFM).

Our analysis and modeling support the photonic origin of the longitudinal nanogratings, appearing as prompt electromagnetic and corresponding ionization standing waves in the pre-focal region due to interference of the incident and plasma-reflected laser pulse parts. The transverse nanogratings could be assigned to the nanoscale material modification by interfacial plasmons, excited and interfered in the resulting longitudinal array of the plasma sheets in the bulk dielectric material. Our experimental findings provide strong support for our previously proposed mechanism of such hierarchical laser nanopatterning in bulk dielectrics, giving important insights into its crucial parameters and opening the way for directional harnessing of this technology [2].

This research was funded by the Ministry of Science and Higher Education of the Russian Federation (Ural Federal University Program of Development within the Priority-2030 Program).

[1] S. Kudryashov, A. Rupasov, M. Kosobokov, A. Akhmatkhanov, G. Krasin, P. Danilov, B. Lisjikh, A. Abramov, E. Greshnyakov, E. Kuzmin, M. Kovalev, and V. Shur, Hierarchical multi-scale coupled periodical photonic and plasmonic nanopatterns inscribed by femtosecond laser pulses in lithium niobate, *Nanomaterials*, vol.12, p.4303 (2022).

[2] S. Kudryashov, A. Rupasov, R. Zakoldaev, M. Smaev, A. Kuchmizhak, A. Zolot'ko, M. Kosobokov, A. Akhmatkhanov, and V. Shur, Nanohydrodynamic Local compaction and nanoplasmonic form-birefringence inscription by ultrashort laser pulses in nanoporous fused silica. *Nanomaterials*, vol.12, p.3613 (2022).



Light frequency conversion by periodically poled ferroelectrics

**V. Shur¹, A. Akhmatkhanov¹, A. Esin¹, M. Chuvakova¹,
B. Slautin¹, D. Kolker^{2,3}, A. Boyko^{2,3}**

1- School of Natural Sciences and Mathematics, Ural Federal University, Ekaterinburg, Russia

2- Institute of Laser Physics SB RAS, 630090 Novosibirsk, Russia

3- Novosibirsk State University, Novosibirsk, Russia

E-mail: vladimir.shur@urfu.ru

We present the achievements in fabrication of effective nonlinear frequency converters by creation of the stable domain structure with precise period reproducibility by various methods of the domain engineering in single crystals of lithium niobate, lithium tantalate and potassium titanyl phosphate families. The promising applications of femtosecond laser irradiation for all-optical creation of the periodical domain structure in the crystal bulk are demonstrated [1-3].

The obtained achievements are based on complex study of the domain structure evolution in various uniaxial ferroelectrics with high spatial and temporal resolution. The realized methods of domain engineering are based on application of the electric field using: (1) periodical stripe electrodes [4], (2) biased tip of scanning probe microscope [5,6], (3) focused electron and ion beams [7], (4) pulse heating by IR laser irradiation [1]. The created precise tailored domain structures allowed to realize the highly effective optical parametric oscillation (OPO) and out-of-cavity second harmonics generation.

The periodical poling has been carried out also in thin single-crystalline ion sliced films of lithium niobate on SiO₂ isolation layer (LNOI) by conductive tip of the scanning probe microscope. The stable submicron-scale domain structures with period less than 200 nm have been created [5,6].

The creation of tunable mid-infrared pulsed optical parametric amplifier (OPA) based on periodically poled LN with fan-out domain structure pumped by 1.053 mm laser and tunable continuous-wave injection seeding have been demonstrated [8]. It was shown that injection seeding leads to four times decrease of the linewidth of output signal wave. The fan-out periodical domain structures allowed to obtain wide OPA tuning range from 2.5 to 4.5 mm [9]. The periodical domain structure in 1-mm-thick KTP single crystals with period 37.97 mm allowed to obtain OPO generation at wavelength 2.4 mm with average power 25 mW for 1300 mW pump.

The creation of the periodical domain structure both at the surface and in the bulk was demonstrated in the plates of single-domain MgO doped lithium niobate as a result of irradiation by femtosecond laser emitting pulses in TEM₀₀ mode at the 1030 nm wavelength with energies from 0.7 to 6.7 μJ in filamentation regime with duration 240 fs and repetition frequency 100 kHz [10].

The research was made possible by Russian Science Foundation (Grant No. 19-12-00210).

[1] B.I. Lisjikh, M.S. Kosobokov, A.V. Efimov, D.K. Kuznetsov, and V.Ya. Shur, Thermally assisted growth of bulk domains created by femtosecond laser in magnesium doped lithium niobate, *Ferroelectrics*, vol.604, pp.47-52 (2023).

[2] V. Shur, M. Kosobokov, A. Makaev, and D. Kuznetsov, Light-induced ordering of nanodomains in lithium tantalate as a result of multiple scanning by IR laser irradiation, *J. Appl. Phys.*, vol.133, p.014105 (2023).

[3] V.Ya. Shur, M.S. Kosobokov, A.V. Makaev, D.K. Kuznetsov, M.S. Nebogatikov, D.S. Chezganov, and E.A. Mingaliev, Dimensionality increase of ferroelectric domain shape by pulse laser irradiation, *Acta Materialia*, vol.219, p.117270 (2021).

[4] V.Ya. Shur, A.R. Akhmatkhanov, and I.S. Baturin, Micro- and nano-domain engineering in lithium niobate, *Appl. Phys. Rev.*, vol.2, p.040604 (2015).

[5] B.N. Slautin, A.P. Turygin, E.D. Greshnyakov, A.R. Akhmatkhanov, H. Zhu, and V.Ya. Shur, Domain structure formation by local switching in the ion sliced lithium niobate thin films, *Appl. Phys. Lett.*, vol.116, p.152904 (2020).

[6] B.N. Slautin, H. Zhu, and V.Ya. Shur, Submicron periodical poling by local switching in the ion sliced lithium niobate thin films with dielectric layer, *Ceramics International*, vol.47, pp.32900-32904 (2021).

[7] D.S. Chezganov, E.O. Vlasov, E.A. Pashmina, M.A. Chuvakova, A.A. Esin, E.D. Greshnyakov, and V.Ya. Shur, Domain structure formation by electron beam irradiation in lithium niobate crystals at elevated temperatures, *Appl. Phys. Lett.*, vol.115, p.092903 (2019).

[8] E. Erushin, B. Nyushkov, A. Ivanenko, A. Akhmatkhanov, V. Shur, A. Boyko, N. Kostyukova, and D. Kolker, Tunable injection-seeded fan-out-PPLN optical parametric oscillator for high-sensitivity gas detection, *Laser Phys. Lett.* vol.18, p.116201 (2021).

[9] O.L. Antipov, D.B. Kolker, A.A. Dobrynin, Yu.A. Getmanovskiy, V.V. Sharkov, M.A. Chuvakova, A.R. Akhmatkhanov, V.Ya. Shur, I.A. Shestakova, S.V. Larin, Mid-infrared optical parametric oscillation and second harmonic generation of repetitively-pulsed radiation of a fiber-laser pumped Tm³⁺:YAP laser in a fan-out periodically poled MgO:LiNbO₃ crystal, *Quantum Electronics*, vol.52, pp.254-261 (2022).

[10] S. Kudryashov, A. Rupasov, M. Kosobokov, A. Akhmatkhanov, G. Krasin, P. Danilov, B. Lisjikh, A. Turygin, E. Greshnyakov, M. Kovalev, A. Efimov, and V. Shur, Ferroelectric nanodomain engineering in bulk lithium niobate crystals in ultrashort-pulse laser nanopatterning regime, *Nanomaterials*, vol.12, p.4147 (2022).

Terahertz generation from a single-color filament: ponderomotive force versus light pressure

I.A. Nikolaeva^{1,2}, D.E. Shipilo^{1,2}, N.A. Panov^{1,2}, O.G. Kosareva^{1,2}

1-Faculty of Physics, Lomonosov Moscow State University, Moscow, Russia

2-P.N. Lebedev Physical Institute of the RAS, Moscow, Russia

nikolaevaia@lebedev.ru

Terahertz (THz) emission of a single-color femtosecond filament is presumed to originate from the free electrons motion driven either by ponderomotive force that pushes the electrons out of the filament core thereby providing a quadrupole source [1] or by the light pressure force that pushes plasma electrons along the beam axis thereby producing a longitudinal dipole source [2]. Both models of the local plasma response under the interference integral are able to successfully reproduce the conical spatial shape of the far-field distribution of THz radiation [3–6]. However, none of these models reproduces the THz spatial pattern at ~ 1 THz that was observed in 2D measurements [5,6], i.e. the two lobes separated by the driving laser pulse polarization plane and having the polarization almost orthogonal to the laser one.

In this work, we analyze the models of the filament plasma oscillations [7,8] so as to elucidate the quantitative relation between the ponderomotive and the light pressure sources. We show that the destructive interference of the THz waves driven by these sources can provide the two-lobe pattern observed in [5,6] on the condition of the $>\pi/2$ phase shift between the magnetic dipole and quadrupole contribution to the current. We note that the $\pi/2$ phase shift between the two sources corresponds to a ~ 250 fs delay for the frequency of ~ 1 THz. Since both sources develop within the laser pulse duration of <100 fs, such a phase shift should originate from the propagation effects including the plasma refraction. The simulations of such an effect require vectorial propagation equation in (t, x, y, z) geometry.

For the simulations we used Unidirectional Hertz vector propagation equation (UHPE, [9]) with the crossed domains for optical and terahertz radiation (XDOT, [10]) scheme. The latter allows us to simulate the propagation of the optical pulse on the moderate size numerical grids in the scalar axially-symmetric approximation using the Unidirectional pulse propagation equation (UPPE, [11]). The THz field is simulated with the account for all three vectorial components. Figure 1 shows the broken symmetry of the THz far field conical ring for the two selected phase shifts between the dipole and quadrupole contributions to the free electron current. In Fig. 1(b) the THz radiation reveals the two lobes and is polarized orthogonally to the laser pulse polarization direction in agreement with [5,6].

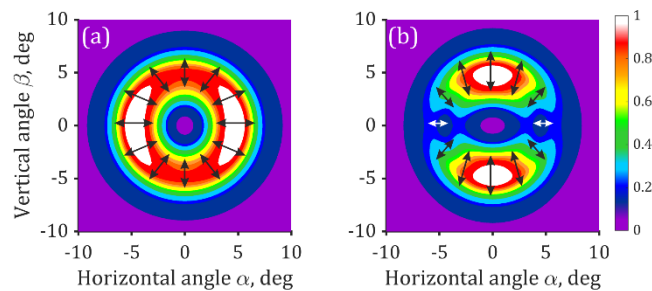


Fig. 1. Angular distribution of ~ 1 THz radiation emitted from single-color filament simulated using interference model with both ponderomotive force and light pressure accounted as emission sources. The laser polarization is horizontal. The results of simulations without (a) and with (b) artificial phase factor. The latter one (b) closely represents the experiments [5,6].

- [1] H. Hamster et al., Phys. Rev. Lett. 71, 2725 (1993).
- [2] C.C Cheng et al., Phys. Rev. Lett. 87, 213001 (2001).
- [3] C. D'Amico, Phys. Rev. Lett. 98, 235002, (2007).
- [4] A. P. Shkurinov et al., Phys. Rev. E 95, 043209 (2017).
- [5] R. Akhmedzhanov et al., Radiophys. Quantum Electron. 52, 482 (2009).
- [6] G. E. Rizaev et al., JETP Lett. 115, 657 (2022).
- [7] P. Sprangle et al., Phys. Rev. E 69, 066415 (2004).
- [8] I. Thiele et al., Phys. Rev. E 94, 063202 (2016).
- [9] A. Couairon et al., Opt. Express 23, 31240 (2015).
- [10] I. A. Nikolaeva et al., Opt. Lett. 46, 5497 (2021).
- [11] M. Kolesik and J. V. Moloney, Phys. Rev. E 70, 036604 (2004).

N-O-3

Periodical generation of sub-THz dissipative solitons based on passive mode-locking in helical-waveguide Gyro-TWTs

I.V. Zotova, N.S. Ginzburg, M.N. Vilkov, A.S. Sergeev

Institute of Applied Physics RAS, 46 Ul'yanov Street, Nizhny Novgorod, 603950, Russia

zotova@ipfran.ru

In laser physics, there exists a well-known principle for production of ultrashort optical pulses (USP), based on the effect of passive mode-locking [1, 2], which is achieved by incorporating a nonlinear element (for example, a Kerr lens) into the laser resonator that absorbs low-amplitude radiation and is transparent periodic trains of ultrashort pulses (USP) can appear at the laser output. From a general point of view, the generated pulses are considered as dissipative solitons [3], the formation of which is due to the balance of amplification, absorption, harmonic generation, and group velocity dispersion effects.

As shown theoretically in [4-6], this method of pulse generation can be developed in microwave electronics, where saturable absorber can be realized based on electron-wave interaction. Feasibility of such approach was confirmed in recent experiments [7], where we implemented the Ka-band pulse generator mode-locked by nonlinear cyclotron resonance absorber, providing periodical trains of 100 kW/ 0.4 ns with repetition rate of 400 MHz. As an active unit, a wide-band helical-waveguide gyro-TWT was used.

In this report, we present the result of a theoretical analysis of the possibility of realization of dissipative soliton generators in higher W and G frequency bands (0.1-0.25 THz), where the developed gyro-TWT mode-locked by saturable absorbers can also be used. In W-band, the cyclotron resonance absorber which is based on interaction with an initially rectilinear electron beam can be used. Generation of USP with peak power of 100 kW is possible (Fig. 1). In G-band, the non-linear absorber can be realized based on a helical gyro-TWT which operates in the Kompfner dip regime.

Note that short-wave USP generators may be of interest for a large number of physical and technical applications, including plasma and solid state diagnostics, spectroscopy, high-resolution communications and radar, etc.

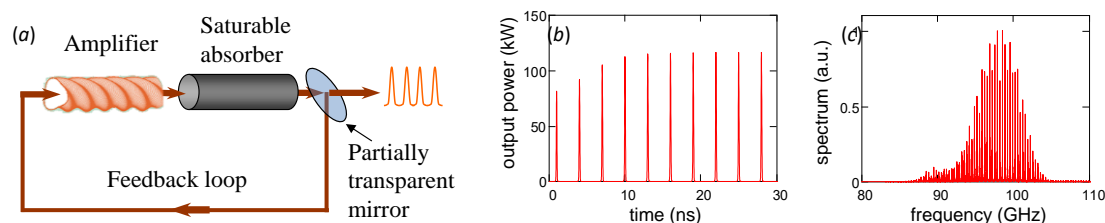


Fig.1. (a) scheme of a mode-locked microwave oscillator consisting of a helical gyro-TWT with cyclotron resonance absorber, (b) profiles of microwave pulses, and (c) radiation spectrum.

This work is supported by the Russian Scientific Foundation (RSCF), Grant No. 23-12-00291.

- [1] U. Keller, Recent developments in compact ultrafast lasers, *Nature*, 424, 831-838 (2003).
- [2] H.A. Haus, Mode-locking of lasers, *IEEE J. Quantum Electron.*, 6, 1173-1185 (2000).
- [3] E.V. Vanin, A.I. Korytin, A.M. Sergeev, et al. Dissipative optical solitons, *Phys. Rev. A* 49, 2806 (1994).
- [4] N.S. Ginzburg, G.G. Denisov, M.N. Vilkov, et al. Generation of "gigantic" ultra-short microwave pulses based on passive mode-locking effect in electron oscillators with saturable absorber in the feedback loop, *Phys. Plasmas*, 23, 050702 (2016).
- [5] N.S. Ginzburg, G.G. Denisov, E.B. Abubakirov, et al. Generators of high-power ultrashort microwave pulses with a saturable absorber in a feedback circuit, *Radiophys. Quantum Electron.*, 59, 613-628 (2017).
- [6] N.S. Ginzburg, G.G. Denisov, M.N. Vilkov, et al. Nonlinear Cyclotron Resonance Absorber for a Microwave Subnanosecond Pulse Generator Powered by a Helical-Waveguide Gyrotron Traveling-Wave Tube, *Phys. Rev. Applied*, 13, 044033 (2020).
- [7] N.S. Ginzburg, S.V. Samsonov, G.G. Denisov, et al. Experimental Realization of a Ka-band 100-kW subnanosecond pulse generator mode-locked by nonlinear cyclotron resonance absorber, *Phys. Rev. Applied*, 16, 054045 (2021).



N-O-4

Optical-pump terahertz-probe diagnostics of the ultrafast carrier dynamics in photoconductive materials

V. Bulgakova¹, V. Bukin¹, Yu. Goncharov¹, A. Ushakov¹, K. Zaitsev¹,
M. Burdanova^{2,3}, M. Paukov², D. Krasnikov⁴, A. Nasibulin⁴, S. Garnov¹

1- Prokhorov General Physics Institute of the Russian Academy of Sciences, 38 Vavilova Str., 119991 Moscow, Russia

2- Center for Photonics and 2D Materials, Moscow Institute of Physics and Technology, 9 Institutsky Lane, 141700 Dolgoprudny, Russia

3- Institute of Solid State Physics, Russian Academy of Sciences, 142432 Chernogolovka, Russia

4- Center for Photonic Science and Engineering, Skolkovo Institute of Science and Technology, 3 Nobel Str., 121205 Moscow, Russia

vbulgakova573@gmail.com

Optical pump - terahertz (THz) probe (OPTP) spectroscopy are currently used to obtain information about the ultrafast dynamics of photoexcited carriers in semiconductors. In an OPTP experiments, an ultrafast laser pulse create free charge carriers and a broadband THz pulses (most often in range 0.3-3 THz which corresponds to the photon energies from 1.2 meV to 12.4 meV) are used to probe of sample transmission. Unlike the usual optical pump-optical probe experiments, the OPTP technique allows measure the time dependence of the electrical field of probe pulse. Using Fourier analysis, the full complex absorption spectrum can be obtained, which describes amplitude change and a phase shift.

In this work, we utilized the OPTP spectroscopy to measure the carrier dynamics and charge transport in plasma-treated carbon nanotubes (CNTs) [1]. Impact of defects on the carrier dynamics and charge transport in carbon nanotubes remains undiscovered. In our study we established correlation between controllable number of defects and optoelectronic properties of CNTs. We used the OPTP spectroscopy to measure the carrier lifetimes governed by the trapping time at defect states and found out short and long lifetimes related to the defects. We carried out electron microscopy measurements in addition to absorption, Raman, Fourier-transform infrared spectroscopy (FTIR), THz and OPTP spectroscopy. The complementary nature of these methods allows us to evaluate the contributions of defects in photoconductivity of CNT networks. We find that the introduction of defects added by plasma-treatment leads to increased charge scattering along plasma-created segments and reduced consequently carrier mobility, photoconductivity, and lifetime.

[1] Tatiana N. Kurtukova, Daria S. Kopylova, Nikita I. Raginov, Eldar M. Khabushev, Ilya V. Novikov, Svetlana I. Serebrennikova, Dmitry V. Krasnikov, and Albert G. Nasibulin, Plasma-treated carbon nanotubes for fast infrared bolometers, *Appl. Phys. Lett.* 122, 093501 (2023)

Laser driven high power microwave compressor

G.Denisov, A.Palitsin, D.Sobolev, V.Parshin, S.Morozov, M. Glyavin

Institute of Applied Physics RAS (IAP RAS), 46 Ul'yanov str., Nizhny Novgorod, Russia

glyavin@ipfran.ru

Studies related to pulse shortening are currently becoming relevant for various promising applications of microwave and THz radiation, such as spectroscopy [1] and particle acceleration [2]. The shortening of the duration with simultaneous increase in the power of pulses makes it possible to increase accelerating gradients when sub-THz and THz sources are used. Active and passive pulse compressors are widely used for producing short microwave pulses [3,4] from continuous wave radiation or rather long pulses.

In experimental realizations of microwave pulse compressors based on ring resonator and semiconductor silicon switch the minimum duration of the compressed pulses cannot be less than the round-trip time in the resonator. In the report we present the experimental study of the pulse compressor [5] based on three-mirror ring resonator and GaAs switch with carrier relaxation time less than resonator round-trip time. It is especially important in the case of compression of high-power output radiation of gyrotrons. The minimum dimensions of the resonator and, accordingly, the round-trip time are limited by microwave breakdown on the resonator elements, primarily on the semiconductor switch. Thus, compared to compressors based on silicon switches, the developed GaAs based compressor is preferable for obtaining short sub-ns and ns pulses with maximum power.

It should be noted that for both silicon and GaAs switches, it is possible to shorten the compressed pulses by installing an additional switch, which is also activated by laser radiation and cuts off part of the generated compressed pulse after a given time interval. In this case, obviously, the compressor becomes more complicated due to the presence of the second switch and an additional laser pulse is required. This means the need for increasing the power of the laser used (or using an additional laser synchronized with sub-ns accuracy). Nevertheless, this method may be attractive especially of further pulse shortening to sub-ns durations when femtosecond lasers are used.

In the experiments we used a backward wave oscillator (BWO) as a microwave source and 532 nm laser with a pulse duration of about 100 ps and a pulse energy of about 50 mJ to activate the GaAs switch. BWO operated in CW mode with the power of about 10 mW; the frequency of BWO was stabilized by external generator. To form an input wave beam with the required parameters (transverse dimensions and waist located on a corrugated mirror), a quasi-optical system, consisting of a horn and two mirrors was used.

In fact, the switch "cuts" the part of radiation from the wave beam circulating in the resonator. The measured compression coefficient 25 is in a good agreement with its theoretical value calculated for the total measured losses and coupling coefficient. As the next project steps in 2023 we plan experiments with 170 GHz gyrotrons [6,7] as radiation source.

The work is supported by the RSI project #19-79-30071

- [1] K. O. Tan, C. Yang, R.T. Weber, G. Mathies, and R.G. Griffin, "Time-optimized pulsed dynamic nuclear polarization," *Sci. Adv.*, vol. 5, issue 1, eaav6909, January 2019.
- [2] M.A.K. Othman, J. Picard, S. Schaub, et al., "Experimental demonstration of externally driven millimeter-wave particle accelerator structure," *Appl. Phys. Lett.*, 117, 073502, August 2020.
- [3] S.C. Schaub, M.A. Franzi, and B.W. Hoff, "Low power demonstration of a W-band active pulse compressor for high power millimeter waves," *J Infrared Milli Terahz Waves*, vol. 43, pp. 819–828, November 2022.
- [4] J. Genouda, E.L. Claveau, S.K. Jawla, et al., "Generation of nanosecond THz pulses using a high gain ring resonator with a semiconductor switch," *Appl. Phys. Lett.*, vol. 121, 044101, July 2022.
- [5] G.G. Denisov, A.V. Palitsin, D.I. Sobolev, V.I. Belousov, I.A. Gorbunov, O.V. Kulagin, S.V. Morozov, A.A. Murzanev, A.N. Stepanov, M.Yu. Glyavin. Formation of short microwave pulses by laser-driven GaAs switch with sub-nanosecond transient response. 2021 46th International Conference on Infrared, Millimeter and Terahertz Waves (IRMMW-THz), 2021, pp. 1-2.
- [6] G.G. Denisov, A.N. Kufitin, V.N. Manuilov et al., "Development of master oscillator for frequency locking of a complex of megawatt level microwave sources". *Microwave and Optical Technology Letters* 62, 6, 2137, 2020
- [7] A. Litvak, G. Denisov, M. Glyavin, "Russian gyrotrons: achievements and trends". *IEEE Journal of Microwaves*, 1, 1, 260, 2021

N-O-5

Broadband conversion of multiline Q-switched CO laser emission under its double-pass through AR-coated ZnGeP₂ crystal

**I. O. Kinyaevskiy^{1,2}, Yu. M. Klimachev¹, M. V. Ionin¹, A. M. Sagitova¹, M. M. Zinovev^{2,3}, N.N.Yudin^{2,3},
A. A. Ionin¹**

1Lebedev Physical Institute of the Russian Academy of Sciences, 53 Leninskiy Ave., 119991 Moscow, Russia

2National Research Tomsk State University, 36 Lenin Ave, 634050 Tomsk, Russia

3LOC LLC, 28 Vysotsky Str., 634040 Tomsk, Russia

Main author email address: maximionin@gmail.com

To solve a number of problems (for example, environmental monitoring and air control of a working area, analysis of processed gases and gas mixtures composition, detection of leaks in main gas and oil pipelines), the development of broadband mid-IR laser sources is required. One of the most efficient amongst such laser sources is a CO laser. One of its advantages, for example, is that many spectral lines of a CO laser are in the spectral ranges of low atmospheric absorption [1]. However, to solve a number of problems, it is necessary to expand the spectral limits of CO laser radiation. One of the methods for expanding and enriching the spectrum of a CO laser is frequency conversion of its emission in nonlinear crystals.

The Gas Laser Laboratory of P.N. Lebedev Physical Institute of RAS has already implemented broadband sum-frequency generation (SFG) in several nonlinear crystals: ZnGeP₂ [2], AgGaSe₂ [3], BaGa₂GeSe₆, GaSe [4] with external conversion efficiency of 2.5%, 0.6%, 0.5% and 0.15%, respectively. Therefore, after comparing the obtained results, we can claim that just the ZnGeP₂ nonlinear crystal is the most efficient for this type of conversion. The CO laser SFG efficiency enhancement in nonlinear crystals ZnGeP₂ is possible by several procedures.

Firstly, an increase of the SFG efficiency is possible due to a sharper focusing. Secondly, it is potentially possible to increase the SFG efficiency by using an intracavity SFG scheme. Thirdly, conversion efficiency can be increased by an application of a double-pass scheme. The fourth option for increasing the conversion efficiency is application of a nonlinear crystal AR-coating which is the objective of the given research. This research became possible due to the development of new broadband multirange AR-coatings [5] for the ZnGeP₂ crystal with the high optical damage threshold both in the CO laser spectral range (5–7 μm) and in the sum-frequencies range (2.5–3.5 μm).

Broadband sum-frequency conversion of multiline (~60 spectral lines within ~5-6 μm) Q-switched CO laser emission in an AR-coated ZnGeP₂ crystal was experimentally studied by application of both single-pass and double-pass optical schemes. The maximum conversion efficiency in the double-pass scheme reached ~10% that is 2.5 times higher than one obtained in the same optical scheme with an uncoated ZnGeP₂ [6]. The spectrum control of frequency converted radiation by changing angles of incident and reversed CO laser beams in the ZnGeP₂ crystal was implemented within the wavelength range from 2.52 μm up to 2.92 μm. The maximum spectrum width of 0.35 μm was obtained with the double-pass scheme when the angle of the laser beam incident on the crystal and the angle of the deflected reversed laser beam were 4.0° and 3.0°, respectively, the spectral bandwidth being three times broader than one obtained with the single-pass scheme.

The research was supported from the Russian Science Foundation grant № 22-22-20103.

[1] A.A. Ionin, Yu.M. Klimachev, A.Yu. Kozlov, et al., Application of an overtone CO laser for remote gas analysis of the atmosphere, *Atmospheric and Oceanic Optics*, Volume 26, Issue 1, pp 68–73, (2013)

[2] I. Kinyaevskiy, A. Ionin, Yu. Klimachev, Yu. Andreev, and V. Mozhaeva, Three-stage frequency conversion of sub-microsecond multiline CO laser pulse in a single ZnGeP₂ crystal, *Optics letters*, Vol. 43, No. 13, 3184-3187 (2018).

[3] Budilova O.V., Ionin A.A., Kinyaevskiy I.O., et al., Broadband two-stage frequency conversion of CO laser in AgGaSe₂ crystal // *Optics Letters*, T. 41. C. 777, (2016)

[4] D. V. Badikov, V. V. Badikov, A. A. Ionin, et al., Sum-frequency generation of Q-switched CO laser radiation in BaGa₂GeSe₆ and GaSe nonlinear crystals, *Optical and Quantum Electronics*, 50, 243, (2018)

[5] M. Zinovev, N.N. Yudin; I. Kinyaevskiy; et al., Multispectral Anti-Reflection Coatings Based on YbF₃/ZnS Materials on ZnGeP₂ Substrate by the IBS Method for Mid-IR, *Laser Applications, Crystals*, 12(10), 1408; (2022)

[6] I.O. Kinyaevskiy, Yu.M. Klimachev, M.V. Ionin, et al., Broadband sum-frequency conversion of multiline Q-switched CO laser emission under its double-pass through uncoated ZnGeP₂ crystal, *Infrared Physics & Technology*, 104740, (2023)



N-O-6

Ultrafast spectroscopy and optoelectronic THz devices of nano-materials

M.Burdanova^{1,2}

1-Center for Photonics and 2D Materials, Moscow Institute of Physics and Technology, 9 Institutsky Lane, 141700 Dolgoprudny, Russia

2-Institute of Solid State Physics, Russian Academy of Sciences, 142432 Chernogolovka, Russia

burdanova.mg@mipt.ru

The existing and continuously growing THz technologies demand compact, fast, broadband high-performance devices. One-dimensional (1D) nanomaterials hold high potential for the implementation of efficient THz optoelectronics. By focusing on these applications, it is important to characterize the nature and dynamics of photoexcited states in these materials. By employing optical pump Terahertz (THz) probe spectroscopy, ultrafast photocarrier dynamics can be accessed. Therefore, we systematically studied the range of 1D nanomaterials such as carbon nanotubes (CNT), boron nitrate nanotubes (BNNT), MoS₂ nanotubes (MoS₂ NT), WS₂ nanotubes (WS₂ nanotubes) and their heterostructures. These materials have a unique terahertz photoconductivity that can be changed from anomalous (positive $\Delta T/T$, negative photoconductivity) to natural (positive photoconductivity) due to mobile free charges with charge carrier mobility comparable to their 2D counterparts. In addition, the presence of excitons and their dynamics in a given rarity when measured by the pump-probe method. Thus, in our work, we show the coexistence of charge carriers and excitons in these structures [1]. Such unique properties can be used in a wide range of applications [2-4]. This project was supported by the RSF project # 22-72-1003.

Velocity overshoot and terahertz generation in $\text{Al}_x\text{Ga}_{1-x}\text{As}/\text{GaAs}$ heterostructured p-i-n diodes

V. Trukhin¹, I. Mustafin¹, X. Fan^{1,2}, V. Kalinovskiy¹, E. Kontrash¹, K. Prudchenko¹, I. Tolkachev¹ and V. Malevich^{3,4}

1- Ioffe Institute, 19021, St Petersburg, Russia

2- ITMO University, 197101, St Petersburg, Russia

3- Belarusian State University of Informatics and Radioelectronics, Minsk, Belarus

4- Stepanov Institute of Physics, Belarusian Academy of Sciences, Minsk, Belarus

Main author email address: man-st@mail.ru

This paper presents the results of an experimental study of terahertz radiation generation in $\text{Al}_x\text{Ga}_{1-x}\text{As}/\text{GaAs}$ heterostructured p-i-n diodes under femtosecond optical pulse excitation. In a study of THz radiation excited from a p-i-n diode, it was found that the maximum efficiency of THz generation is observed at a reverse bias application above 8 V and an optical excitation level up to 10 mW (a linear dependence of the THz pulse amplitude on the average power is recorded). A comparative study of THz generation in p-InAs bulk semiconductor was carried out, which showed that the efficiency of THz generation in p-i-n diode is an order of magnitude higher than in p-InAs.

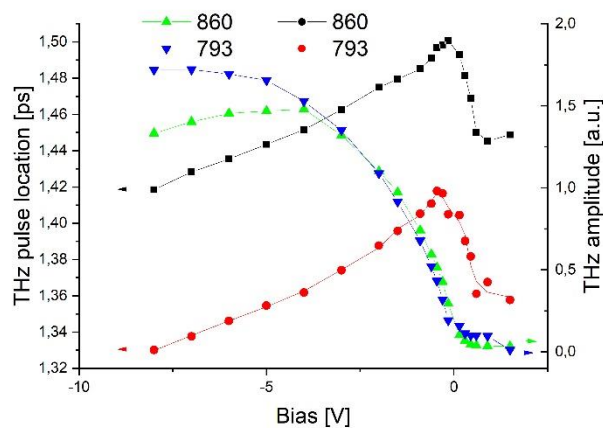


Fig. 1. Dependence of THz pulse amplitude and time location of THz pulse on the bias ($\lambda_{\text{opt.}} = 793, 860 \mu\text{m}$)

It was shown that the maximum pulse amplitude increases sharply as the magnitude of the reverse bias on the p-i-n diode grows, and the beginning of this growth depends on the energy of the excitation quantum of photon. Accordingly, the time position of THz pulse also changes with the change in the value of the reverse bias on the p-i-n diode, and when the value of the bias changes from positive values to the value of the diode voltage at which THz pulse amplitude begins to grow sharply, the THz pulse is delayed. With further increase in the reverse bias on the p-i-n diode, there is a reverse shift of the THz pulse on the time scale (Fig. 1). The Monte-Carlo simulation of the process of THz generation in the p-i-n diode performed by taking into account the ballistic motion of nonequilibrium carriers with the subsequent possible overshoot of the saturation speed confirmed the experimental results.

Thus, the results indicate that the mechanism of THz generation in the heterostructured p-i-n diode $\text{Al}_x\text{Ga}_{1-x}\text{As}/\text{GaAs}$ is due to the acceleration of electrons in the electric field to a speed significantly exceeding the saturation speed at times of hundreds of femtoseconds ("velocity overshoot"), and the subsequent sharp decline associated with the intervalley transition of electrons from the Γ -valley. It was shown that the THz generation efficiency in the $\text{Al}_x\text{Ga}_{1-x}\text{As}/\text{GaAs}$ heterostructure p-i-n diode at excitation levels, at which a linear dependence of the electric field amplitude on the optical radiation intensity is observed, is an order of magnitude higher than the THz generation efficiency in the p-InAs bulk semiconductor, which is now the most efficient coherent terahertz emitter [1].

[1] Adomavicius R., Urbanowicz A., Molis G., Krotkus A., Šatkovskis E., "Terahertz emission from p-InAs due to the instantaneous polarization," Appl. Phys. Lett., vol.85, p. 2463, 2004.

N-P-1

Optical parametric oscillation in periodically poled single crystals of titanyl-phosphate family

**M. Chuvakova¹, A. Akhmatkhanov¹, A.A. Esin¹, I.A. Kipenko¹, V. Shur¹,
A. Boyko^{2,3}, D. Kolker^{2,3}, L. Isaenko³, S. Zhurkov³**

1- School of Natural Sciences and Mathematics, Ural Federal University, 620000 Ekaterinburg, Russia

2- Institute of Laser Physics SB RAS, 630090 Novosibirsk, Russia

3- Novosibirsk State University, 630090 Novosibirsk, Russia

E-mail: m.a.chuvakova@urfu.ru

Potassium titanyl phosphate Rb:KTiOPO₄ (RKTP), potassium titanyl arsenate KTiOAsO₄ (KTA) and rubidium titanyl arsenate RbTiOAsO₄ (RTA) single crystals with periodical ferroelectric domain structure are one of the promising materials for nonlinear optical applications [1]. Despite the crucial importance of the *in situ* imaging of domain structure kinetics for creation of high quality periodical domain gratings, there are only a few works concerning potassium titanyl phosphate family.

We present the results of *in situ* imaging of domain kinetics in RKTP, KTA and RTA with the time resolution down to 12.5 μs. The wide range of wall velocities with two orders of magnitude difference was observed for switching in a uniform electric field [2]. The kinetic maps allowed analyzing the spatial distribution of wall motion velocities and classifying the walls by velocity. The distinguished slow, fast, and superfast domain walls differed by their orientation. The mobility and the threshold fields for all domain walls were estimated [3]. The revealed increase in the wall velocity with deviation from low-index crystallographic planes for slow and fast walls was considered in terms of determined step generation and anisotropic kink motion.

The domain kinetics and switching fields in RKTP and KTA were compared. It was shown that the more pronounced input of slow domain walls in KTA results in creation of narrow stripe domains important for periodical poling [4,5]. Spontaneous backswitching was revealed in RTA single crystals. It was shown that the time interval from the end of switching pulse to the start of spontaneous backswitching process (“domain structure stability time”) is proportional to the field applied during polarization reversal process. The periodical domain structure with period of 40 μm was created in 3-mm-thick RKTP single crystals for OPO generation at 2.326 μm using the 1.064 μm pulsed pump with 5.6 ns duration at 20 Hz. The single resonance double-pass optical scheme was used. The threshold power energy 630 μJ and generation efficiency 7% were obtained.

We investigated the characteristics of a PPKTA OPO with a period of 39.2 μm in the low-temperature-grown KTA sample. Under pumping at 1.053 μm, the signal and idler wavelengths were, 1.54 and 3.31 μm, respectively. The parametric generation threshold turned out to be 130 μJ (for a pump intensity of 14.4 MW cm⁻²), the quantum efficiency was 27%, and the differential efficiency was 12 % [6].

The obtained knowledge is important for further development of domain engineering in crystals of KTP family required for creation of high power, reliable, and effective coherent light sources.

The research was made possible by Russian Science Foundation (Grant No. 19-12-00210).

[1] V. Ya. Shur, E. V. Pelegova, A. R. Akhmatkhanov, and I. S. Baturin, Periodically poled crystals of KTP family: A review, *Ferroelectrics* vol.496, pp. 49–69, (2016).

[2] V. Ya. Shur, E. M. Vaskina, E. V. Pelegova, M. A. Chuvakova, A. R. Akhmatkhanov, O. V. Kizko, M. Ivanov, and A. L. Kholkin, Domain wall orientation and domain shape in KTiOPO₄ crystals, *Appl. Phys. Lett.* vol.109, p. 132901, (2016).

[3] V. Ya. Shur, A. A. Esin, M. A. Alam, and A. R. Akhmatkhanov, Superfast domain walls in KTP single crystals, *Appl. Phys. Lett.* vol.111, p. 152907, (2017).

[4] A. R. Akhmatkhanov, M. A. Chuvakova, N. A. Dolgushin, D. B. Kolker, V. N. Vedenyapin, L. I. Isaenko, V. Ya. Shur, Analysis of switching current data in KTA single crystals, *Ferroelectrics*, vol.559, pp. 1-7, (2020).

[5] A. R. Akhmatkhanov, M. A. Chuvakova, I. A. Kipenko, N. A. Dolgushin, D. B. Kolker, V. N. Vedenyapin, L. I. Isaenko, V. Ya. Shur, Abnormal kinetics of domain structure in KTA single crystals, *Appl. Phys. Lett.*, vol.115, p. 212901, (2019).

[6] L.I. Isaenko, A.P. Eliseev, D.B. Kolker, V.N. Vedenyapin, S.A. Zhurkov, E.Yu. Erushin, N.Yu. Kostyukova, A.A. Boiko, V.Ya. Shur, A.R. Akhmatkhanov, M.A. Chuvakova, Influence of growth temperature of KTiOAsO₄ single crystals on their physicochemical parameters and formation of domain structures, *Quantum Electronics*, vol.50(8), pp.788-792, (2020).

Analysis and research of nonlinear optical phenomena in silicon slot waveguide structures

S. M. Murzagalina^{1,2,3✉}, **I. D. Skuratov**^{1,2}

1- Moscow Institute of Physics and Technology (National Research University), Dolgoprudny, Russia

2- JSC « Molecular Electronics Research Institute», Moscow, Russia

3- JSC « Zelenograd Nanotechnology Center, Moscow », Moscow, Russia

✉murzagalina.sm@phystech.edu

The SOI platform provides integration of electronics, photonics and quantum technologies, and also offers a reliable solution for the expanding demands of the telecommunications. A substantial variety of devices, such as optical buffers, interconnections [1], and biological sensors, have already been implemented using linear optics. The second and third-order nonlinearities produce optical power losses, but in same time nonlinear optical phenomena may lead to new applications such as multiplexing and modulating signals. Therefore, researchers come across with the new challenge – to create the device with minimal losses and best functional qualities.

Due to silicon's centrosymmetric crystal structure, the second order nonlinear phenomena are weaker in the scope. However, the structure's borders is where their impact is more noticeable. The study takes into account two-photon absorption, second harmonic generation, four-wave mixing, which offers solution for electro-optical signal modulation. In this research, the structure of a slot waveguide with an OrmoCore polymer deposited is simulated. The figures below show model's cross-sectional parameters and mode characteristics.

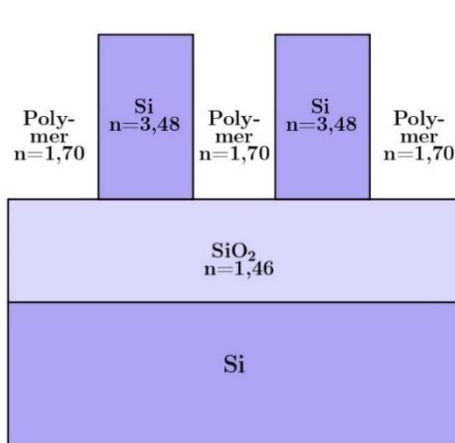


Fig.1. Planar overview of waveguide parameters

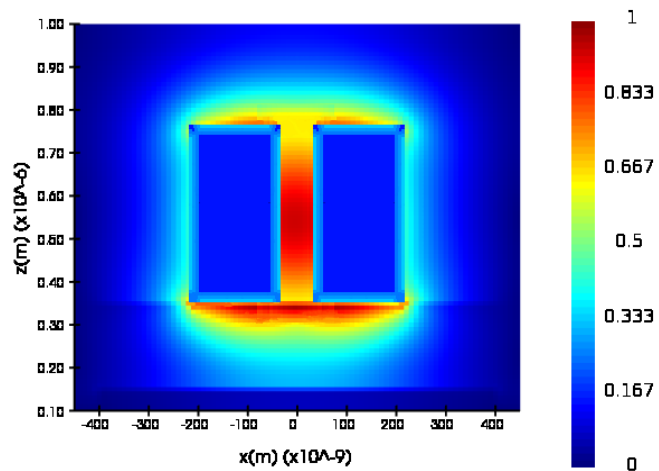


Fig.2. Mode profile

This structure is analyzed using modeling software based on the finite element method (FEM) and the finite difference method in the time domain (FDTD). To reduce optical losses, the geometric properties of the model were adjusted using machine learning approaches such as genetic algorithms. An analytical approach to obtain the parameters of a nonlinear slot waveguide using the singular perturbation method (SPT) is also investigated. SPT is used to study the behavior of waveguides with spatial perturbation and weak second- and third-order nonlinearities, to obtain solutions with appropriate accuracy [4,5]. The problem of a bent silicon slot waveguide is considered, which will solve the common issue of reducing rotation losses. It is also intended to develop insulin sensors based on that structure.

[1] Valeev A.S., Krasnikov G.Y. Manufacturing technology of intracrystal and intercrystal interconnections of modern ASIC// Microelectronics. 2015. vol. 44. No. 3. pp. 180-201.

[2] Leuthold J. [et al.], "Silicon Organic Hybrid Technology—A Platform for Practical Nonlinear Optics," in Proceedings of the IEEE, vol. 97, no. 7, pp. 1304-1316, July 2009.

[3] Lipson M. [et al.], "Guiding, modulating, and emitting light on Silicon-challenges and opportunities," in Journal of Lightwave Technology, vol. 23, no. 12, pp. 4222-4238, Dec. 2005.

[4] Nayfeh A.H., Asfar O.R. Parallel - plate waveguide with sinusoidally perturbed boundaries //Journal of Applied Physics. – 1974. – T. 45. – №. 11. – C. 4797-4800.

[5] Yokota M. [et al.], Guided transverse-magnetic waves supported by a weakly nonlinear slab waveguide //JOSA B. – 1993. – T. 10. – №. 6. – С. 1096-1101.



PHOTONICS IN QUANTUM TECHNOLOGIES

**P-I-1**

Cold atoms meet quantum technologies

V.I. Balykin*Institute of Spectroscopy, RAS, Moscow, Russia*

As a quantum mechanical system, the atom is characterized by two sets of degrees of freedom: internal (electron configurations and spin) and external (momentum and center-of-mass position), which can change in the interaction with laser radiation. Physics of ultracold atoms made their appearance due to successful investigations into the action of laser radiation on precisely the external degrees of freedom of the atom: its momentum and center- of-mass position. Laser cooling and the subsequent evaporative cooling allow obtaining both ultralow temperatures and ultrahigh atomic densities, which in turn permits realizing quantum Bose and Fermi gases.

Cooled and trapped atoms open the door of studies of the interaction of light with matter at the level of single atoms and photons that not only provide a deeper understanding of the quantum-mechanical nature of the light-matter interaction but also open up prospects for new quantum technologies. The possibility of achieving single-particle interaction is basic to the concept of quantum information processing and communication: atoms are treated as physical objects that can store and process information, and photons as objects for long-range data transmission through a quantum information network. The quantum information network can comprise, for instance, single atoms (ions, molecules, or quantum dots) representing addressable points of the quantum information network and optical (or other) waveguides providing photon- assisted effective connections among nodes of the quantum information network. We will review the work on the deterministic control of single atoms and single photons, and on establishing conditions for their efficient interaction.



P-I-2

Photon sources for quantum computing and communication systems**A.A. Toropov***Ioffe Institute, 26 Politekhnicheskaya, St Petersburg, 194021, Russian Federation**toropov@beam.ioffe.ru*

Sources of single photons are key elements of rapidly developing systems of quantum computing and quantum communications [1]. Currently, commercially available photon sources based on InAs/GaAs quantum dot (QD) microcavities operating around 920 nm provide excellent values of such critical parameters as the “purity” of single-photon radiation (more than 95%) and the degree of indistinguishability of emitted photons (more than 90%) [2]. Nevertheless, the achieved value of the third important parameter, the source brightness, defined as the probability of generating a photon per pump pulse, is still insufficient for the possibility of scaling such photonic devices to sizes of practical interest. At the same time, the functional capabilities of photon sources intended for the implementation of advanced photonic quantum computing systems should include the possibility of generating not only single indistinguishable photons, but also pairs of entangled photons and multiphoton cluster states, and the use of such devices in quantum secure communication systems is constrained by the lack of sufficiently efficient photon sources emitting in telecommunication spectral ranges.

In the Laboratory of Quantum Photonics, Ioffe Institute, a technology for manufacturing photon sources based on microcavities and nanoantennas with single QDs in the (Al, Ga, In)As system was developed to solve these problems, which made it possible to obtain single-photon sources with characteristics corresponding to the advanced world level [3-5]. In the talk, several approaches developed to increase the brightness of sources of indistinguishable photons will be presented, including the implementation of resonant coherent pumping of a trion state by a π -pulse in a QD placed in a dichroic optical microcavity and the use of quasi-resonant pumping of a QD in a microcavity by means of acoustic phonons. The prospects of manufacturing photon sources operating in telecommunication bands will be analyzed. Finally, studies of the spin dynamics of electrons and holes in a single charged QD, aimed at generation of photonic cluster states, will be presented.

This work was supported by Rosatom in the framework of the Roadmap for Quantum Computing (Contract No. 868-1.3-15/15-2021 dated 5 October 2021 and Contract No. R2152 dated 19 November 2021).

[1] C. Couteau, S. Barz, T. Durt, T. Gerrits, J. Huwer, R. Prevedel, J. Rarity, A. Shields, and G. Weihs, Applications of single photons to quantum communication and computing, *Nature Rev. Phys.* **5**, 326 (2023).

[2] <https://quandela.com>

[3] M. Rakhlin, G. Klimko, S. Sorokin, M. Kulagina, Y. Zadiranov, D. Kazanov, T. Shubina, S. Ivanov, A. Toropov, Bright single-photon sources for the telecommunication O-band based on an InAs quantum dot with (In)GaAs asymmetric barriers in a photonic nanoantenna, *Nanomaterials* **12**, 1562 (2022).

[4] M.V. Rakhlin, A.I. Galimov, I.V. Dyakonov, N.N. Skryabin, G.V. Klimko, M.M. Kulagina, Yu.M. Zadiranov, S.V. Sorokin, I.V. Sedova, Yu.A. Guseva, D.S. Berezina, Yu.M. Serov, N.A. Maleev, A.G. Kuzmenkov, S.I. Troshkov, K.V. Taratorin, A.K. Skalkin, S.S. Straupe, S.P. Kulik, T.V. Shubina, A.A. Toropov, Demultiplexed single-photon source with a quantum dot coupled to microresonator, *J. Lumines.* **253**, 119496 (2023).

[5] A. Galimov, M. Bobrov, M. Rakhlin, Yu. Serov, D. Kazanov, A. Veretennikov, G. Klimko, S. Sorokin, I. Sedova, N. Maleev, Yu. Zadiranov, M. Kulagina, Yu. Guseva, D. Berezina, E. Nikitina, and A. Toropov, Towards bright single-photon emission in elliptical micropillars, *Nanomaterials* **13**, 1572 (2023).



P-I-3

Bloch surface waves for integrated nanophotonics

A.A. Fedyanin

*Faculty of Physics, Lomonosov Moscow State University, Moscow 119991, Russia
fedyanin@nanolab.phys.msu.ru*

Modern integrated photonic platforms should combine low-loss guiding, spectral flexibility, high light confinement, and close packing of optical components. One of the prominent platforms represents dielectric nanostructures combined with photonic band gap media that manipulate low-loss Bloch surface waves (BSW). BSW platform is all-dielectric counterpart to surface plasmon-polariton one, but it has the advantages of long propagation length (up to cm in visible), ultrawide spectral range of operation (from UV to mid-IR and THz), and access to the confined electromagnetic field making BSW applicable for integrated photonics, sensing, and other fields. Here, we developed several ways for directed and highly efficient BSW excitation using dielectric nanostructures of various designs on the photonic crystal (PC) surface. First, we achieve color-selective directional excitation of BSW mediated by Mie resonances in a semiconductor nanoparticle printed on the PC surface using laser-induced backward transfer technique. We show that a single silicon nanoparticle can be used as a subwavelength multiplexer switching the BSW excitation direction from forward to backward within the 30 nm spectral range with its central wavelength governed by the nanoparticle size. Numerical simulation gives an estimate of 8% BSW excitation efficiency with a single nanoparticle. Second, we show a new concept of 3D out-of-plane coupler which is a microscale prism exploiting frustrated total internal reflection in the Otto configuration for unidirectional excitation of waveguide modes with efficiency up to 100%. Polymer micropisms are printed using two-photon laser lithography and allow transferring more than 40% of the incident light energy into BSWs. The couplers enable focusing BSWs simultaneously with their excitation. Finally, halide perovskite micro- and nanolasers were integrated with BSW platform and demonstrated directional BSW excitation with the efficiency of over 16%. A pronounced BSW beam steering effect is shown.



3D nanolithography for quantum technologies

A.G. Vitukhnovsky^{1,2}, D.A. Kolymagin², A.V. Gritsienko^{1,2}, A.M. Romshin³, I.I. Vlasov³

1- P.N. Lebedev Physical Institute, Russian Academy of Sciences, Leninsky Prospekt 53, 119991, Moscow, Russia,

2-Moscow Institute of Physics and Technology (National Research University), Institutskiy per., 9, 141700, Dolgoprudny, Russia,

3- A.M. Prokhorov Institute of General Physics Russian Academy of Sciences, st. Vavilova, 38, 119991, Moscow, Russia.

vitukhnovsky@mail.ru

At the moment, additive technologies are important for various fields of science and technology, such as nanophotonics, optoelectronics, optics, etc. DLW (Direct Laser Writing) technology, which allows you to create 3D objects of arbitrary shape and design with high spatial resolution. The DLW method is based on two-photon photopolymerization, a phenomenon in which focused femtosecond laser radiation initiates the polymerization reaction of the main component of a photosensitive composition, the monomer, in a small volume of the photocomposition (i.e. voxel) due to the effect of two-photon absorption in the photoinitiator.

Single photon sources (SPE-Single Photon Emitters) are in demand in many quantum technologies. However, for these sources to be used for practical applications, reliable single-photon detectors are required. In photonic integrated circuits, sources and detectors, as well as functional elements, require photonic "wires" (PWB-Photonic Wire Bonds) created by the DLW method.

The report assumes consideration of the DLW method for various optical applications: the creation of elements of photonic integrated circuits (PIC-Photonic Integrated Circuits) [1], the creation and study of photonic "wires" [2] in combination with sources of single (Fock) photons and optical cavities [3].

The presented results were obtained with the support of RSF projects 22-19-00324 and 22-79-10153, as well as Subsidy Agreement No. 075-02-2022-1672 of the Russian Ministry of Education and Science.

[1]. R.P. Matital, A.G. Vitukhnovsky et al// Luminescence confocal microscopy of 3D components of photonic integrated circuits fabricated by two-photon photopolymerization// *Journal of Science: Advanced Materials and Devices*, 7(2), 100413 (2022)

[2].A.V. Gritsienko, A.I. Duleba, A.G. Vitukhnovsky et al// Photodynamics of bright subnanosecond emission from pure single-photon sources in hexagonal boron nitride// *Nanomaterials* , 12(24), 4495; (2022)

[3]. D. A. Kolymagin, D. A. Chubich, D. A. Shcherbakov, R.M. Pattia, A. V. Gritsienko, A. V. Pisarenko, I. V. Dushkin, A. G. Vitukhnovskiy //Waveguide structures and photonic couplers created by direct (3+1) D laser writing // *Bulletin of the Russian Academy of Sciences: Physics*, in press (2023)

P-I-5

Modification of the luminescence response of Si-Ge materials in low-dimensional photonic structures

M. Stepikhova¹, S. Dyakov², M. Petrov³, V. Verbus¹, Zh. Smagina⁴, V. Zinoviev⁴, A. Peretokin¹, D. Yurasov¹, M. Shaleev¹, E. Rodyakina⁴, A. Novikov¹

1- Institute for Physics of Microstructures Russian Academy of Sciences, 603950, Nizhny Novgorod, Russia

2- Skolkovo Institute of Science and Technology, 143026 Moscow, Russia

3- ITMO University, St. Petersburg 197101, Russia

4- Rzhanov Institute of Semiconductor Physics, Siberian Branch of Russian Academy of Sciences, 630090 Novosibirsk, Russia

mst@ipmras.ru

The possibilities to control emitting properties of materials in low-dimensional photonic structures are among the most actively investigated topics to date. The development of technologies and, as a result, the opening up opportunities for creating photonic structures with dimensions comparable to or smaller than the emission wavelength gave impetus to the discovery of new phenomena and the creation of new emitting sources using low-dimensional effects. In particular, in this paper, we will consider light-emission phenomena in low-dimensional Mie resonators and arrays of such resonators, as well as in photonic crystals (PhCs) (Fig. 1), the features of the band structure of which can be controlled by changing the parameters. The studied low-dimensional resonators and photonic crystals were formed on silicon structures with Ge(Si) nanoislands emitting in the wavelength range of 1.2–1.6 μm . Interest in these structures is due, first of all, to the possibility of creating effective light-emission sources on their basis, technologically compatible and easily integrated into the circuits of modern micro- and optoelectronics. It will be shown that the embedding of Ge(Si) nanoislands into low-dimensional resonators and photonic crystals makes it possible to increase the emitting efficiency of structures by more than two orders of magnitude and to control their spectral response and radiation pattern. The paper discusses the observation conditions and features of manifestations in the studied photonic structures of bound states in the continuum (BIC) [1, 2], collective modes and modes with a flat dispersion characteristic [3], and the phenomenon of mode interaction in photonic crystals.

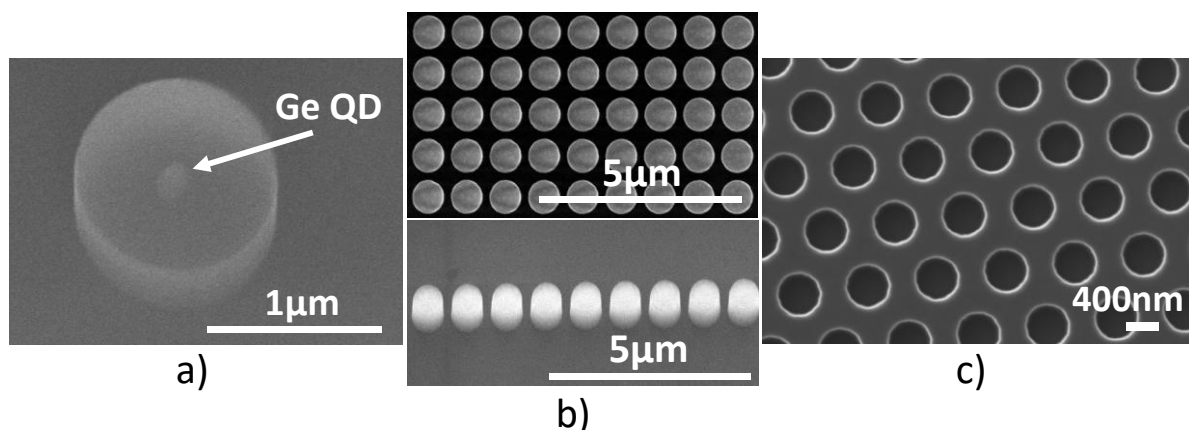


Fig. 1. Photonic structures realized on Si with Ge(Si) nanoislands: a) - single Mie resonator; b) – arrays of Mie resonators: square lattice and chain; c) – 2D photonic crystal.

The work was funded by the Russian Science Foundation (grant #19-72-10011).

[1] S. Dyakov, M. Stepikhova, A. Bogdanov *et al.*, Photonic bound states in the continuum in Si structures with the self-assembled Ge nanoislands, *Laser & Photonics Reviews*, 15, p. 2000242, (2021).

[2] M.V. Stepikhova, S.A. Dyakov, A.V. Peretokin *et al.*, Interaction of Ge(Si) Self-Assembled Nanoislands with Different Modes of Two-Dimensional Photonic Crystal, *Nanomaterials*, 12, p. 2687, (2022).

[3] A.V. Peretokin, D.V. Yurasov, M.V. Stepikhova *et al.*, Tuning the Luminescence Response of an Air-Hole Photonic Crystal Slab Using Etching Depth Variation, *Nanomaterials*, vol. 13, pp. 1678, (2023).



Efficient ultracold atoms source for quantum sensing

A. Afanasiev¹, P. Skakunenko^{1,2}, D. Bykova^{1,3}, A. Kalmykov¹, R. Kirtaev², D. Negrov²,
V. Balykin¹

1- Institute of Spectroscopy Russian Academy of Sciences, Fizicheskaya Str., 5, Moscow, Troitsk, 108840, Russia

2- Moscow Institute of Physics and Technology, 9 Institutskiy per., Dolgoprudny, Moscow Reg., 141700, Russia

3- National Research University Higher School of Economics, Myasnitskaya str., 20, Moscow, 101000, Russia

afanasiev@isan.troitsk.ru

Atom interferometry is considered as a new platform for development of quantum sensors. They can be used for high precision fundamental experiments and for solving numerous applied problems. Among the fundamental problems are the following: the detection of gravitational waves, the search for dark matter, tests of dark energy theories, tests of the equivalence principle and validity of quantum mechanics at macroscopic scale. Among the applied problems, the most important, are the study of the Earth's gravitational field, atomic clocks and applications to navigation. Obviously, the development of an atom interferometry approaches gives us the new stage of quantum metrology.

An important task in order to create efficient quantum sensors is the formation of an ensemble of ultracold atoms in a magneto-optical trap. Such an atomic ensemble is further used as a source of atoms in the construction of a quantum sensor. The number of atoms in an ensemble determines the accuracy of quantum sensors. For this reason, it is necessary to form ultracold atom source with as many atoms as possible.

This problem can be solved with using atom chip technology [1]. Atom chip is the combination of advanced industrial microelectronics technology and atom optical techniques to generate and control ultracold atomic ensembles. An atom chip can provide the ability to trap and manipulate atoms. The atom chip also enables Bose-Einstein condensation (BEC) of atoms.

The First Russian atom chip was developed in the Institute of spectroscopy [2]. For efficient loading of atom chip cold atom beam focusing was considered [3,4]. It was shown that the atomic flow can be gain up to 169 times. Because of such magnification it is possible to construct quantum sensors with high repetition rates. Also, a new design of atom chip was created for optimization of laser cooling. It makes atom chip as the efficient atom source for quantum sensors.

The study was supported by the Russian Science Foundation grant No. 23-22-00255, <https://rscf.ru/project/23-22-00255>

[1] M. Keil, et. al, "Fifteen years of cold matter on the atom chip: promise, realizations, and prospects", Journal of Modern Optics, 63, 1840, (2016).

[2] A.E. Afanasiev, et al., "Single-layer atom chip for continuous operation: Design, fabrication and performance", Optics & Laser Technology, 148, 107698 (2022).

[3] A.E. Afanasiev, et al., "Focusing of an Atomic Beam for the Efficient Loading of an Atom Chip". JETP Lett. 115, 509 (2022).

[4] D.V. Bykova, et al., "Sharp focusing of an atomic beam using Doppler and sub-Doppler laser cooling mechanisms in a two-dimensional magneto-optical trap". JETP Lett. 118, to be published (2023).

P-I-8

Quantum nano-plasmonics for biosensing and bioimaging on the level of single molecules and virions

P.N. Melentiev,¹ I.V. Doronin,^{2,3} A. A. Zyablovsky,^{2,3,4} E. S. Andrianov,^{2,3} D.S. Kudryavtsev,⁵ V. Mozhaeva,⁵ I. Ivanov,⁵ A. Siniavin,^{5,6} A. S. Kalmykov,¹ A.S. Gritchenko,¹ B.N. Khlebtsov,⁷ S.-P. Wang,⁸ B. Kang,⁹ V. I. Tsetlin,⁷ Victor I. Balykin¹

¹ Institute of Spectroscopy of Russian Academy of Sciences, Fizicheskaya str. 5, Troitsk, Moscow, 108840, Russia

² Moscow Institute of Physics and Technology, Institutskiy per. 9, Moscow, 141700, Russia

³ Institute for Theoretical and Applied Electromagnetics, Izhorskaya str. 13, Moscow, 125412, Russia

⁴ Kotelnikov Institute of Radioengineering and Electronics RAS, Mokhovaya str. 11-7, Moscow, 125009, Russia

⁵ Shemyakin-Ovchinnikov Institute of Bioorganic Chemistry of the RAS, Moscow 117997, Russia

⁶ N.F. Gamaleya National Research Center for Epidemiology and Microbiology, Ivanovsky Institute of Virology, Ministry of Health

⁷ Institute of Biochemistry and Physiology of Plants and Microorganisms, Saratov Scientific Centre of the Russian Academy of Sciences, Prospekt Entuziastov 13, Saratov, 410049, Russia

⁸ State Key Laboratory of Analytical Chemistry for Life Science and Collaborative Innovation Center of Chemistry for Life Sciences, School of Chemistry and Chemical Engineering, Nanjing University, 163 Xianlin Road, Nanjing, 210023, P. R. China

The detection and visualization of single atoms and molecules has always been one of the most important tasks of both fundamental scientific and practical importance: the study of the effects of quantum electrodynamics, the development of monatomic/single-molecule devices, the visualization of biological tissues, and much more. Recently, single molecule detection methods have been used to detect substances at very low concentrations: The molecules of an analyte are detected individually in a sample, which is known as the single-molecule counting method (SMCM).

Recent advances in quantum technology at the nanoscale have enabled the construction of nanoscale mesoscopic systems with quantum emitters, metal and dielectric nanostructures. These systems can exhibit profound quantum electrodynamic properties due to various physical mechanisms such as Foerster energy transfer, plasmonic field enhancement, and strong optical matter-wave coupling. In our study, we demonstrate the realization of ultrabright and optically stable plasmonic nanoemitters suitable for the detection and visualization of single biomolecules and virions.

In our study, we consider SMCM in sensing based on the use of ultrabright and optically stable plasmonic nanoemitters of light. The approach demonstrates sensitivity at the single-molecule level, enabling 5-minute-per-detection of practically important biomarkers of human diseases. As a practical implementation of SMCM, we demonstrate: (i) detection of biomolecules in ultralow concentrations of troponin in human blood - the most important biomarker for human cardiovascular disease - at a level of 10 - 20 fM, (ii) detection of SARS-COV -2 virus particles (human coronavirus). The fundamental limitations of the sensitivity of such approaches and the problems of their practical implementation are discussed.



P-I-9

Nanodiamond sensors as probes for local temperature variations in the neuron

E. Moreva, G. Petrini, G. Tomagra, E. Bernardi, P. Traina, A. Marcantoni, F. Picollo, K. Kvaková, P. Cígler, I.P. Degiovanni, V. Carabelli, M. Genovese

Italy

e.moreva@inrim.it

Temperature is one of the most relevant parameters for the regulation of intracellular processes. Measuring localized subcellular temperature gradients is fundamental for a deeper understanding of cell function, such as the genesis of action potentials, and cell metabolism. In this work we will review our latest progresses in NV-based thermometry ultimately leading to the first localized temperature increase detection in a firing neuronal network with precision under 0.1 K.

By exploiting ODMR techniques, temperature variations in cultured hippocampal neurons at the single-cell scale using NV color centers in nanodiamonds are probed. Our data show that, in the spontaneously firing network, 1K local temperature increases can be detected after picrotoxin administration, a selective blocker of the inhibitory GabaA receptors. Picrotoxin-induced temperature increases are associated to a significant potentiation of the firing rate, whereas ODMR stimulation protocols do not affect cell viability and functionality. Thus, for the first time, it is possible to unravel the firing activity of the network from the observed temperature increases.

In perspective, this technique will provide an extremely promising mean of indirect detection of the action potential and study of temperature variations in proximity of specific cell regions by functionalizing nanodiamonds in order to target specific cell components (e.g. ion channels, mitochondrions, ER).

P-I-10

Liquid crystals in quantum optics: Current experiments, applications and future prospects

S. Lukishova

Rochester, NY, USA

Email address: lukishova@hotmail.com

A review will be presented on using liquid crystal properties of molecular alignment and self-assembly into photonic bandgap structures, as well as their high thermo-optical coefficients and electro-optical properties in quantum and nano-photonics. The author's results on single-photon sources with definite polarizations¹⁻⁴ and collaborative research on using liquid crystals for modeling quantum mechanical tunneling phenomena^{2,5,6} will be overviewed. Future prospects of patterned liquid crystals⁷⁻⁸ will be discussed.

- [1] S.G. Lukishova and L.J. Bissell, "Nanophotonic advances for room-temperature single-photon sources", 103-178, in Quantum Photonics: Pioneering Advances and Emerging Applications, R.W. Boyd, S.G. Lukishova, V. Zadkov, Eds, Springer Series in Optical Sciences, Vol. 217, Springer NY, 2019.
- [2] S.G. Lukishova, A.C. Liapis, L.J. Bissell, G.M. Gehring, and R.W. Boyd, "Single-photon experiments with liquid crystals for quantum science and quantum engineering applications", Liquid Crystal Reviews, Vol. 2, No. 2, 111–129 (2014).
- [3] S.G. Lukishova, L.J. Bissell, J. Winkler, C.R. Stroud, Jr, "Resonance in quantum dot fluorescence in a photonic-bandgap liquid crystal host", Opt. Lett., Vol. 37 Iss. 7, 1259-1261 (2012).
- [4] S.G. Lukishova, A.C. Liapis, H. Zhu, E. Hebert, K. Kuyk, S. Choudhary, R.W. Boyd, Z. Wang, L.J. Bissell, "Plasmonic nanoantennas with liquid crystals for nanocrystal fluorescence enhancement and polarization selectivity of classical and quantum light sources", Mol. Cryst. Liq. Cryst. Vol. 657, 173-183 (2017).
- [5] G.M. Gehring, A.C. Liapis, S.G. Lukishova, and R.W. Boyd, "Time-domain measurements of reflection delay in frustrated total internal reflection", Phys. Rev. Lett. Vol. 111, 030404 (2013).
- [6] A.C. Liapis, G.M. Gehring, S.G. Lukishova, and R.W. Boyd, "Temporal reshaping of single photon wave packets using cholesteric liquid crystals", paper LTu4J.7, Technical Digest on CD, Frontiers in Optics/Laser Science Conference, 14-18 October, 2012, Rochester NY.
- [7] L. Marucci, E. Nagali, F. Sciarrino, L. Sansoni, F. De Martini, B. Piccirillo, E. Karimi, and E. Santamato, "Photonic quantum information applications of patterned liquid crystals", Mol. Cryst. Liq. Cryst., Vol. 526, 108–118 (2010).
- [8] M.V. Gorkunov, I.V. Kasyanova, V.V. Artemov, A.A. Ezhov, A.V. Mamonova, I.V. Simdyankin, S.P. Palto, "Liquid-crystal metasurfaces self-assembled on focused ion beam patterned polymer layers: electro-optical control of light diffraction and transmission", ACS Applied Materials & Interfaces, Vol. 12, 30815—30823 (2020).



P-I-11

Quantum computing with single trapped atoms in optical tweezers

I.B.Bobrov¹, G.I.Struchalin¹, M.Yu.Goloshchapov^{1,3}, A.Rosanov¹, D.A.Kuzmenok¹,
S.S.Straupe^{1,2}

1- Quantum Technology Centre, Faculty of Physics, M.V.Lomonosov Moscow State University, Moscow, Russia

2- Russian Quantum Center, Moscow, Russia

3- Moscow Institute of Physics and Technology, Moscow, Russia

straups@quantum.msu.ru

Single atoms trapped in dipole microtraps or optical tweezers are one of the most promising platforms for quantum computing. We will describe the system for digital gate-based quantum computing using hyperfine states of single Rubidium atoms as qubits. We will discuss the principles and methods for assembling the uniformly filled arrays of single atoms and the achievable parameters of atomic quantum registers. We will report our recent experimental results on characterizing the errors of single qubit gates with randomized benchmarking, achieving the error rate per gate below 10^{-3} and discuss the limitations related to single qubit addressing and gate time. We will also briefly describe our experimental progress towards implementation of two-qubit gates based on Rydberg excitation of single atoms with individual addressing and highlight the perspectives of improving the gate fidelity and scaling up the register size.



P-I-12

A photon computer. Optical logic gates

S.A. Stepanenko

Russian Federal Nuclear Center – All-Russia Research Institute of Experimental Physics, Sarov, Russia

The paper presents the structure of a general-purpose digital photon computer and principles of its implementation, as well as the logic gates required to create such computer.

The photon computer functionality is based on the effects of interacting coherent systems of light waves generated by a laser source. The efficiency of data processing in photon computers is achieved via application of

- passive optical logic gates;
- computation discipline based on the availability of operands (data flow);
- conflict-free algorithms of data processing by processors elements.

The classes of problems that can be solved on photon and electronic computers are the same (in contrast to quantum computers). The architectural and schematic design solutions found for electronic devices are acceptable. The interference-based logic gates proposed in the paper form a complete basic functional set. The identity requirements are met for the intensity values corresponding to logic constants «0» and «1» generated by various gates within fixed time intervals.

Estimates of the peak performance of a digital photon computer with a light wave length of 1.5 μm are 10^4 to 10^5 times higher than those of modern electronic devices with the same power consumption.

1. A Photon Computer: Implementation Principles and Performance Estimation. Doklady Akademii Nauk, 2017, Vol. 476, No. 4, pp. 389-394.
2. Interference-Based Logic Gates. Doklady Rossiyskoy Akademii Nauk, 2020, Vol. 493, pp. 64-69.



Thulium BEC as a diagnostic tool for a laser light with wavelength of 1064 nm

V.V. Tsyganok¹, D.A. Pershin^{1,2}, V.A. Khlebnikov¹, D.A. Kumpilov^{1,3}, I.A. Pyrkh^{1,4}, A.E. Rudnev^{1,3}, E.A. Fedotova^{1,3}, D.V. Gaifudinov^{1,3}, I.S. Cojocaru^{1,2}, K.A. Khoruzhii^{1,3}, P.A. Aksentsev^{1,4}, A.K. Zykova¹ and A.V. Akimov^{1,2,5}

¹Russian Quantum Center, Bolshoy Boulevard 30, building 1, Skolkovo, 143025, Russia

²PN Lebedev Institute RAS, Leninsky Prospekt 53, Moscow, 119991, Russia

³Moscow Institute of Physics and Technology, Institutskii pereulok 9, Dolgoprudny, Moscow Region 141701, Russia

⁴Bauman Moscow State Technical University, 2nd Baumanskaya, 5, Moscow, 105005, Russia

⁵National University of Science and Technology MISIS, Leninsky Prospekt 4, Moscow, 119049, Russia

The report is devoted to the use of thulium BEC to study the intensity distribution of optical lattice (OL) that is formed by two crossed laser beams with a wavelength of 1064 nm inside a vacuum chamber. Such configuration of beams create a periodic potential:

$$U(z) = U_0 \sin^2(k_L z), \quad (1)$$

where U_0 is the depth of the OL, $k_L = |\vec{k}_1 - \vec{k}_2|/2 = \pi/\lambda_L$ is one-half of the magnitude of the reciprocal lattice vector, \vec{k}_1 and \vec{k}_2 are wave-vectors of OL beams, $\lambda_L = \lambda/(2 \sin(\alpha))$ is a lattice period, $2\alpha = (\vec{k}_1; \vec{k}_2)$. The configuration of beams in the chamber could be imprinted on the matter wave of condensate in position space via the Kapitza-Dirac (or Raman-Nath) effect.

Analyzing the obtained results of the BEC expansion after a short-term exposure to a periodic potential, we found that the self-reflections of the lattice beams from the viewports of vacuum chamber create a significant parasitic potential. This effect helps us to reproduce the intensity distribution of the OL in region where BEC is located.

The work was supported by Rosatom in the framework of the Roadmap for Quantum computing (Contract No. 868-1.3-15/15-2021 dated October 5, 2021).



P-I-14

Optical coprocessor and diffraction neural networks

**N. Kazanskiy^{1,2}, L. Doskolovich^{1,2}, N. Ivliev^{1,2}, A. Nikonorov^{1,2}, V. Podlipnov^{1,2},
V. Protzenko^{1,2}, R. Skidanov^{1,2}, V. Soifer^{1,2}, D. Soshnikov^{1,2}**

1- IPSI RAS-Branch of the FSRC "Crystallography and Photonics" RAS, 443001 Samara, Russia

2- Samara National Research University, 443086 Samara, Russia

email: kazanskiy@ipsiras.ru

The exponential increase in the number of publications on Scopus data indicates the growing interest of scientists from different countries in the subject of optical computing [1]. The authors of the report present optical circuits with light modulators that implement matrix calculations, Fourier correlator circuits, including a volumetric holographic filter that provides parallel recognition of 7,500 objects. The presented results of designing one-dimensional photonic crystal resonators based on comb waveguides for differentiating and integrating optical signals justify the potentially achievable parameters of the corresponding photonic crystal devices. The calculated photonic crystal integrators and differentiators are tens of times more compact than the known solutions, the proposed devices are easily assembled into cascades, integrated on a crystal and interfaced with electronic components [2]. The authors of the report proposed a scheme of an optical coprocessor designed for analyzing video streams and implemented as a computer board (module) with which the computer exchanges data via a fast PCIe bus. The coprocessor implements a Fourier correlator circuit with an amplitude spatial light modulator at the input and a phase spatial modulator in the frequency plane. In this scheme, the external video stream coming to the camera is converted by an amplitude modulator into a coherent video stream, and then it is processed in a Fourier correlator with a phase spatial modulator in the frequency plane, which sets the mathematical core of processing. The transmission function of the modulator is determined by the phase function matrix transmitted to it from the computer. This allows you to perform exactly the processing that is necessary for a given video stream at a given time. An analysis of the progress in the performance of existing modulators and cameras that allow working with large data arrays shows that by 2025, the calculation speed with using the proposed system of 1.00×10^{19} bits/s is possible. The system turns out to be quite compact ($140 \times 80 \times 80$ mm) and relatively low-energy (no more than 100W - an order of magnitude smaller than a high-performance graphics card). The report shows experimental results of the selection of image contours using a created mock-up sample of such a coprocessor using a phase function implementing the Laplace operator on the modulator. Optical neural networks can also be implemented on such a system, while the phase function of the diffraction optical element (DOE) implementing the neural network layer is reproduced on the modulator. The report presents the results of a computational experiment for recognizing digitals and a number of symbols using one or more DOE. The authors show that with certain physical parameters, using only one DOE, it is possible to achieve recognition of handwritten digits with a probability higher than 0.91.

[1] N.L. Kazanskiy, M.A. Butt, S.N. Khonina, Optical Computing: Status and Perspectives, Nanomaterials, vol. 12, 2171 (2022).

[2] P. Serafimovich, N. Kazanskiy, Photonics Elements for Sensing and Optical Conversions (CRC Press), Chapter 2 Photonic crystal cavities in integrated on-chip optical signal processing components, (2023).



P-I-16

Investigation of the effect of a thermostat on the lifetime of entangled states of interacting qubits by path integration

M. Shleenkov¹, A. Biryukov²

1- Samara National Research University

2- Samara State Transport University

Main author email address: shleenkov@list.ru

We study the quantum entanglement of two identical superconducting qubits which interact with external electromagnetic fields and the thermostat. We develop the original method in path integral approach for numerical calculation of full density matrix. Then we calculate the Peres-Horodecki parameter (the measure of qubits entanglement). The results indicate the possibility of high-entanglement states excitation and long-time non-destructive control of them for certain parameters of the electromagnetic field and the thermostat parameters. It is shown that the measure and time of qubits entanglement can be effectively controlled by an external electromagnetic influence even in the case of decoherence in the thermostat field.



P-O-1

Dielectric microcavities as a platform for effective single photon emission of a color centers in nanodiamonds

A. Romshin¹, D. Pasternak¹, R. Bagramov², V. Filonenko², A. Zhivopistsev¹, I. Vlasov¹

1- Prokhorov General Physics Institute of the Russian Academy of Sciences, 119991, Moscow, Russia

2- Vereshchagin Institute of High Pressure Physics RAS, Moscow, Russia

alex_31r@mail.ru

A cavity quantum electrodynamics provides the platforms for implementation of effective single photon source (SPS) – a key node in realization of scalable quantum networks [1]. To maximize the efficiency and fidelity of operations at this node, the SPS' emission have to satisfy criteria of high brightness, radiation directivity and narrowness of spectral line. For these purposes, optical cavities with low energy loss and high emitter-cavity coupling strength are required to make use of the Purcell-enhancement of the radiative decay

by a factor $F_p = \frac{3}{4\pi^2} \cdot \left(\frac{\lambda}{n}\right)^3 \cdot \frac{Q}{V}$ (Q – quality factor, V – mode volume) into a cavity mode of interest and

thereby achieve a deterministic bit stream of single-photon pulses [2]. While there are many optical cavities, most of them suffer from excessive absorption and intrinsic mode mismatch between emitter and cavity.

In present work, we demonstrate an effective tunable coupling of the single photon emitter in nanodiamond (ND) placed in fully dielectric low-loss Fabry-Perot microcavity. The cavity consists from two macroscopic dielectric mirrors: the former (R>99.999%) is planar, the latter (R>99.95%) contains an array of concave holes with diameters of 4 and 16 μm . The finesse of the cavity is measured by transmission spectroscopy to be $F \sim 3000$ at 740 nm. As an emitter we use single negatively charged silicon-vacancy (SiV)-centers formed in ND. The SiV fluorescence is characterized by a narrow (1–7 nm) zero-phonon line (ZPL) at 738 nm, in which $\sim 70\%$ of the SiV emission is concentrated, and demonstrates high spectral and time stability [3]. NDs were deposited onto the surface of the planar mirror from the water droplet. By means of confocal spectroscopy and Hanbury-Brown-Twiss interferometry, the fluorescence spectra and saturation curves of individual SPS were measured and the results were quantitatively compared for the cases an emitter is in free space and inside cavity. An ability to change the distance between mirrors in microscale allowed us to spectrally overlap desirable cavity mode and ZPL of the SiV-center. So, such a dielectric microcavity revealed more than order enhancement of single photon emission accompanied with $F_p \sim 3$ and peak coupling efficiency of $\zeta \sim 75\%$.

The work was supported by the grant of the Russian Science Foundation No. 22-19-00324.

[1] N. Gisin, G. Ribordy, W. Tittel, and H. Zbinden, Quantum cryptography, Rev. Mod. Phys. 74, 145 (2002).

[2] E. Purcell, Spontaneous emission probabilities at radio frequencies, Phys. Rev. 69, 681 (1946).

[3] I. Vlasov, A. Barnard, V. Ralchenko, O. Lebedev, M. Kanzyuba, A. Saveliev, V. Konov and E. Goovaerts. Nanodiamond photoemitters based on strong narrow-band luminescence from silicon-vacancy defects Adv. Mater., 21, 808–12 (2009).



Low temperature single-photon SiV-luminescence in “bottom-up” grown nanodiamonds

**D. G. Pasternak¹, D. A. Kalashnikov², V. Leong², C. Chia²,
A. M. Romshin¹, O. S. Kudryavtsev¹, S. V. Kuznetsov¹, A. K. Martyanov¹,
V. S. Sedov¹, L. A. Krivitsky², R.H. Bagramov³, V.P. Filonenko³, I. I. Vlasov¹**

¹*Prokhorov General Physics Institute of the Russian Academy of Sciences, 38 Vavilova str,
Moscow, Russia*

²*Institute of Materials Research and Engineering Agency for Science Technology and Research (A*STAR), Singapore*

³*Vereshchagin Institute of High-Pressure Physics RAS, Kaluzhskoe shosse 14, Moscow,
Troitsk 108840, Russia*

e-mail address: dg.pasternak@physics.msu.ru

Negatively charged Silicon-Vacancy centers (SiV), are promising sources of both single-photon and classical radiation in the near-infrared spectral region, respectively, for quantum and biomedical technologies [1-3]. Chemical Vapor Deposition (CVD) and High Pressure High Temperature (HPHT) methods are mainly used for synthesis of SiV-containing diamonds. Here, we present a comparative low-temperatures (LT) analysis of the spectral characteristics of individual SiV centers in spontaneously nucleated CVD nanodiamonds (NDs) grown on germanium (Ge)/silicon (Si) substrates and HPHT NDs produced from adamantane in the presence of Si dopant.

First, we studied CVD diamond particles of less than 100 nm in size containing 10–20 centers per ND. These NDs were grown on a Si substrate. The SiV photoluminescence (PL) under off-resonant and resonant laser excitation at 15 K were investigated. The emission lines of SiVs of individual CVD NDs are well resolved and found to be spread in the range of 730–750 nm. The typical SiV linewidth is within 1–2 GHz for spontaneous CVD NDs, which is only a factor of 2.5–5 broader than the lifetime limited linewidth of the SiV at 15 K [5]. It was found that replacing the Si with Ge substrates does not affect the spectral characteristics of the SiV PL. A usage of Ge substrates with weak adhesion to diamond opens up opportunities for the controlled doping of NDs with Si, facilitates the transfer of diamond particles from the growth substrate into optical chips, microresonators and photonic crystals.

Then, we analyzed spectral characteristics of individual SiVs in spontaneously nucleated CVD NDs grown on Ge/Si substrates [7] and HPHT NDs doped with Si. Studied nanoparticles have a characteristic size of 300 nm. The SiV PL measured at LT was found to be localized in the range 730–750 nm for CVD and 735–739 nm for HPHT NDs. We attribute the narrowing of the SiV emission range for HPHT diamonds to their higher crystalline quality compared to CVD ones.

The work was supported by the Russian Science Foundation, Grant № 21-72-10153, <https://rscf.ru/project/21-72-10153/>

[1] F. Jelezko, J. Wrachtrup, Single defect centres in diamond: A review. *physica status solidi (a)* 203, 017402 (2006).

[2] O.A. Shenderova, A.I. Shames, N.A. Nunn, M.D. Torelli, I.I. Vlasov, A. Zaitsev, Review Article: Synthesis, properties, and applications of fluorescent diamond particles. *Journal of Vacuum Science and Technology B* 37, 030802 (2019).

[3] M. K. Bhaskar, R. Riedinger, B. Machielse, D. S. Levonian, C. T. Nguyen, E. N. Knall, H. Park, D. Englund, M. Lončar, D. D. Sukachev, M. D. Lukin, Experimental demonstration of memory-enhanced quantum communication. *Nature* 580, 60 (2020).

[4] M. Feudis, A. Tallaire, L. Nicolas, O. Brinza, P. Goldner, G. H'etet, F. B'en'edic, J. Achard, Large-Scale Fabrication of Highly Emissive Nanodiamonds by Chemical Vapor Deposition with Controlled Doping by SiV and GeV Centers from a Solid Source. *Advanced Materials Interfaces* 7, 1901408 (2019).

[5] D.G. Pasternak, D.A. Kalashnikov, V.S. Sedov, A.K. Martyanov, V.G. Ralchenko, L.A. Krivitsky, I.I. Vlasov, Low-Temperature Silicon-Vacancy Luminescence of Individual Chemical Vapor Deposition Nanodiamonds Grown by Seeding and Spontaneous Nucleation. *Physica status solidi (a)* 218, 2000274 (2018).

[6] B.V. Spitsyn, L.L. Bouilov, B.V. Derjaguin, Vapor growth of diamond on diamond and other surfaces. *Journal of Crystal Growth* 52, 219 (1981).

[7] Pasternak D. G., Kalashnikov D. A., Leong V., Chia K., Romshin A.M., Kuznetsov S. V., Martyanov A. K., Sedov V. S., Krivitsky L. A., Vlasov I. I. Luminescent properties of individual "Silicon-Vacancy" centers in CVD nanodiamonds grown on various substrates. *Optics and Spectroscopy*, 2, 218 (2023).



P-O-3

The polariton blockade in a microcavity dimer

T.A. Khudaiberganov¹, I.Yu. Chestnov², S.M. Arakelian¹

1- Department of Physics and Applied Mathematics, Vladimir State University named after A. G. and N. G. Stoletovs, 87 Gorkii st., 600000 Vladimir, Russia
 2- ITMO University, St. Petersburg, 197101, Russia
 Main author email address: thomasheisenberg@mail.ru

Exciton-polaritons are composite quasiparticles consisting of exciton and photon components. The quantum statistics of exciton polaritons is of interest in the sense that they using as a platform for the development of quantum computation [1]. The statistics of radiation from micropillar can be sub-Poisson, while the statistics of the polariton states themselves remain Poisson [2-3]. This is due to the weak nonlinearity $U/\gamma \ll 1$ (of the exciton fraction) in the exciton-polariton system [4]. The quantum blockade is effect of suppressing the probability of finding two polaritons in a certain state. The mechanism of unconventional quantum blockade, based on destructive interference ways $|00\rangle \rightarrow |10\rangle \rightarrow |20\rangle$ и $|00\rangle \rightarrow |10\rangle \leftrightarrow |01\rangle \rightarrow |11\rangle \leftrightarrow |20\rangle$ [5], see fig.1b, makes it possible to achieve the effect of polariton blockade in polariton dimer - a system of two coupled micropillars under conditions of resonant pumping, see fig.1a.

The following Hamiltonian describes system coupled anharmonic oscillators under laser pump energy (in the rotate wave approximation):

$$H = \Delta_1 \hat{a}_1^+ \hat{a}_1 + \Delta_2 \hat{a}_2^+ \hat{a}_2 + g_{12} \hat{a}_1^+ \hat{a}_2 + g_{21} \hat{a}_2^+ \hat{a}_1 + \frac{U}{2} \hat{a}_1^+ \hat{a}_1^+ \hat{a}_1 \hat{a}_1 + \frac{U}{2} \hat{a}_2^+ \hat{a}_2^+ \hat{a}_2 \hat{a}_2 \quad (1)$$

Here $\hat{a}(\hat{a}^+)$ annihilates (creates) bosons operators; $\Delta = \omega_i - \omega_L$ are the cavity detunings, ω_L - frequency driving fields F_i , which we will set equal to each other; ω_i amplitudes of the driving fields; U is the Kerr nonlinearity parameters (due to exciton-exciton scattering); $g_{ij} = g_{ji}$ are coupling constant between i - cavity and j - cavity (for polaritons is rabi energy, for coupled microcavity is hopping amplitude between the two cavities.)

Govern master equation by a matrix density for Hamiltonian (1),

$$\frac{d\rho}{dt} = -i[H_+^{eff}, \rho] + \gamma_1 D[\hat{a}_1] + \gamma_2 D[\hat{a}_2] \quad (2)$$

Where we introduce the follow dissipators: $D[\hat{a}_1] = \hat{a}_1 \rho \hat{a}_1^+ - \frac{1}{2} [\hat{a}_1^+ \hat{a}_1, \rho]_+$, $D[\hat{a}_2] = \hat{a}_2 \rho \hat{a}_2^+ - \frac{1}{2} [\hat{a}_2^+ \hat{a}_2, \rho]_+$.

The criterion for anticorrelations is the second moment of the correlation function. The second order correlation function we can define as,

$$g_1^{(2)} = \frac{\sum_{n,m} n(n-1) \rho_{n,n,m,m}}{(\sum_{n,m} n \rho_{n,n,m,m})^2} \approx \frac{\rho_{2,2,0,0}}{\rho_{1,1,0,0}^2} \quad (3)$$

Here $\rho_{n,n',m,m'} = \langle n'm' | \rho | nm \rangle$.

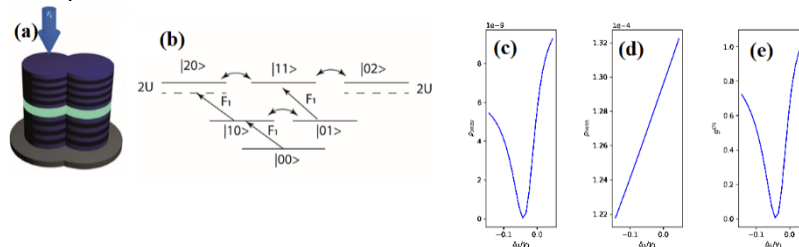


Figure 1 – (a) Sketh a polariton dimer; (b) the scheme of state population. (c-d) The matrix elements of the density matrix; (e) The second order correlation function of the lower-polaritons in dependency of detuning for the first micropillar. for $U = 0.01\gamma$, $g = 5.62\gamma$, $F_p = \gamma$.

The minimum value for the system under consideration is $g_{\min}^{(2)} \sim 10^{-3}$. The system of microresonators is asymmetric (pumped only first micropillar). In this case, the radiation statistics of the second microcavity remains coherent, and the statistics of the radiation of the first microcavity are nonclassicality.

[1] Ghosh S., Liew, T. C. Quantum computing with exciton-polariton condensates. npj Quantum Information, 6(1), 1-6. (2020).
 [2] Verger A., Ciuti C., Carusotto I. Polariton quantum blockade in a photonic dot. Physical Review B, 73(19), 193306. (2006).
 [3] Khudaiberganov T.A., Chestnov I.Yu., Arakelian S.M. Quantum statistics of light emitted from a pillar microcavity. Applied Physics B. v. 128. №. 7. P. 117. (2022).
 [4] Zubizarreta Casalengua E., et.al. Conventional and unconventional photon statistics. Laser & Photonics Reviews, 14(6), 1900279. (2020)
 [5] Flayac, H., Savona, V. Unconventional photon blockade. Physical Review A, 96(5), 053810. (2017).



P-O-4

Stochastic approach to describing non-Markovian dynamics of low-dimensional quantum systems

A. Pavelev¹, S. Kharitonov¹

*1- Samara University, 34, Moskovskoye shosse, Samara, 443086, Russia
Main author email address: 44dragon44@rambler.ru*

Low-dimensional quantum systems are of great interest from a research perspective as they serve as the physical foundation for quantum computing, quantum metrology, and quantum communication. Since low-dimensional quantum systems interact with the environment, they are essentially open quantum systems [1]. Interaction with the environment is commonly modeled using the simplified Markov approximation [2]. However, experimental evidence suggests that non-Markovian relaxation also occurs in open quantum systems and controlled transitions from Markovian to non-Markovian regimes can be observed [3].

In this report, we present a method for modeling non-Markovian dynamics of low-dimensional quantum systems by incorporating an Ornstein-Uhlenbeck process to modify the stochastic Schrödinger equation [4]. This approach enables numerical modeling of the non-Markovian relaxation dynamics of open quantum systems and their spectral characteristics. We provide modified equations, numerical solution schemes, and simulation results for specific environmental parameters.

Furthermore, we demonstrate how considering the non-Markovian nature of the environment can alter the equilibrium position for the probability of detecting the system in a certain energy state for a three-level system and dipole-dipole interacting qubits. We also illustrate the differences between the resonance fluorescence spectrum of a two-level atom in the Markovian and non-Markovian relaxation regimes.

The aim of this report is to discuss the advantages and disadvantages of the stochastic approach for describing relaxation of open quantum systems using numerical modeling of specific systems.

[1] H. Breuer et al. The theory of open quantum systems (Oxford University), (2002).

[2] G. Lindblad, On the generators of quantum dynamical semigroups. Communications in Mathematical Physics, 48., pp. 119-130, (1976).

[3] B. Liu et al., Experimental control of the transition from Markovian to non-Markovian dynamics of open quantum systems, Nature Physics 7(12), pp. 931-934, (2011).

[4] A Pavelev and V. Semin, Investigation of non-markovian dynamics of two dipole-dipole interacting qubits based on numerical solution of the non-linear stochastic Schrödinger equation. Computer Optics, 43(2), pp. 168-173, (2019).



P-O-5

Cascading of logic gates based on Y shaped photonic crystal waveguide

P. Mokshin¹, D. Golovashkin^{1,2}, V. Pavelyev^{1,2}

1- Samara National Research University, Samara, Russia

2- Image Processing Systems Institute, Branch of the Federal Scientific Research Centre "Crystallography and Photonics" of Russian Academy of Science, Samara, Russia

A further step in the development of photonic digital computing devices is the combination of interference logic gates into one circuit [1] using some serial connections. Sequential realization of logical operations imposes a significant limitation on the phase of the gate output signal. The phase has to be determined. Note, that the issue of phase uncertainty does not preclude the use of logic gates. However, there are limitations that arise when trying to cascade them. The problem of phase uncertainty lies in the dependence of the phase of the gate output signal corresponding to the value 1 on the values of the operands of the logic gate of the type "OR", "NOR", "XOR", etc. An uncertain value of the phase of the output signal makes it impossible to cascade such elements. The supply of different-phase signals corresponding to 1 to the input of the logic gate of the next stage will lead to different results.

To solve this problem authors propose to exploit the basic fact of Boolean logic. "AND" and "NOT" operations are enough to form a minimal complete basis [2]. Any other logical operation can be expressed as their combination. It should be noted that "AND" and "NO" gates do not have the problem of phase uncertainty, so it is possible to design a logic gate for any logical operation without this problem. The Figure 1 proposes the implementation of "NOR" on the base of "AND" and "NOT" gates cascading. Ports A and B are the "NOT" inputs. C and D are inputs of the second element associated with the realization of "NOT" operation. E is the output of the combined "NOR" logic gate.

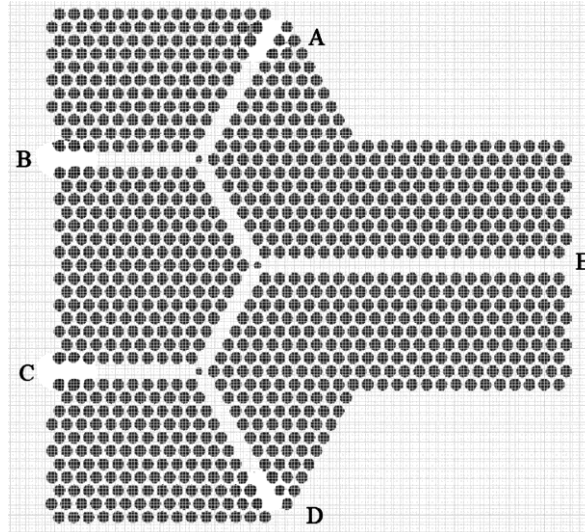


Fig. 1. Photonic crystal with three Y-shaped defects, which implements the logical operation «NOR». B and C are inputs for operand signals, A and D are inputs for reference signals, E is an output for the operation result signal

The proposed logic gate (Fig.1) was studied in a series of numerical experiments. The signal that corresponds to "true" value at the E output is always has the same phase. It should be noted that the implementation of the logic gate (Fig.1) demonstrates the possibility of logic gates cascading.

[1] Hussein M.E., Tamer A. Ali, Nadia H. Rafat, New designs of a complete set of Photonic Crystal logic gates, Optics Communications, vol. 411, pp. 175-181, (2018)

[2] S. V. Yablonski, Introduction to Discrete Mathematics, (1986, In Russian)



Genetic optimization of the Y-shaped photonic crystal logic element NOT

Y. Krivosheeva¹, D. Golovashkin^{1,2}, V. Pavelyev^{1,2}

1- Samara National Research University, Samara, Russia

*2 - IRSI RAS – Branch of the FSRC “Crystallography and Photonics” RAS, Samara, Russia
krivosheeva.yu.yu@gmail.com*

Optical logic gates based on photonic crystals have a number of advantages compared to traditional electronics: compactness, high data transfer rate, low power consumption and relatively low manufacturing costs. Therefore, their development seems to be an urgent task. The work [1] presents an interference logic gate AND based on a photonic crystal with a Y-shaped defect. This structure is characterized by manufacturability, efficiency and speed, due to which it can be considered promising.

In addition to the method of using the Y-shaped structure as an AND gate presented by the authors [1], it is proposed to implement the NOT gate on the same photonic crystal. If in a Y-shaped structure [1] signals with a phase difference π are applied to the input ports A and B, then negative interference will be observed in the center of the element and an intensity equal to 0 will be recorded at the output of the element. If, a signal is applied to only one of the ports, for example B, then some part of the signal will go to the output port, which can be interpreted as a logical 1.

Unfortunately, the efficiency (which is understood as the ratio of the intensity at the output port to the intensity at the input) of such an element is not high and amounts to 41.3%. However, optimization methods are known to be applied to photonic crystal structures. Thus, in [2], a genetic algorithm is used to optimize the 90° bend of a photonic-crystal waveguide with a square lattice and silicon rods. The efficiency obtained by the authors was 93%. Here, for the logical gate NOT, a similar approach is applied. In our work, we considered a maximum of 100 generations of the genetic algorithm, 10 individuals each, one individual consisted of eight variable parameters (“chromosomes”), the parents to create a new generation were selected by the roulette wheel method and subjected to single-point crossing, the resulting individuals mutated with a probability of 5%. To find the efficiency of each individual, the direct diffraction problem was solved using the FDTD method [3], which is implemented in the Ansys Lumerical R1 software package. As a result of genetic optimization, the output intensity was 0.949, which is 2.3 times higher than that of the gate without optimization.

The authors of this work suggest further use of the genetic algorithm for the development of logical gates on a photonic crystal basis that implement other logical operations.

[1] Preeti Rani, Yogita Kalra, R.K. Sinha Realization of AND gate in Y shaped photonic crystal waveguide Optics Communications 298–299, 227–231 (2013)

[2] Liyong Jiang, Hong Wu, Wei Jia Optimization of low-loss and wide-band sharp photonic crystal waveguide bends using the genetic algorithm Optik 124(14), 1721-1725 (2013)

[3] Taflove A., Hagness S.C. Computational Electrodynamics: The Finite-Difference Time-Domain Method, Third Edition (Artech House) (2005)

**P-O-7**

Super resolution virtual image models in a dielectric sphere

A.R. Bekirov

*Lomonosov Moscow State University
bekirov@nanolab.phys.msu.ru*

In the last decade, micrometer-sized lenses have been found to be able to resolve objects beyond the diffraction limit. Despite the fact that the possible nature of this phenomenon has been discussed in many works, a detailed theory of this phenomenon has not yet been developed. In this paper, two possible models of this phenomenon are discussed using the matrix formalism in imaging. The first model considers the transformation of the source field, with the real image unchanged. The second model is based on the search for the scattering matrix of a particle that gives over resolution in a virtual image. Both approaches convincingly demonstrate the required over resolution. Disadvantages of the proposed models and possible ways to solve them are discussed.

Investigation of the lifetime of entangled states of interacting qubits in an electromagnetic field by the path integration method

A. Biryukov¹, M. Shleenkov²

1- Samara State Transport University

2- Samara National Research University

Main author email address: biryukov_1@mail.ru

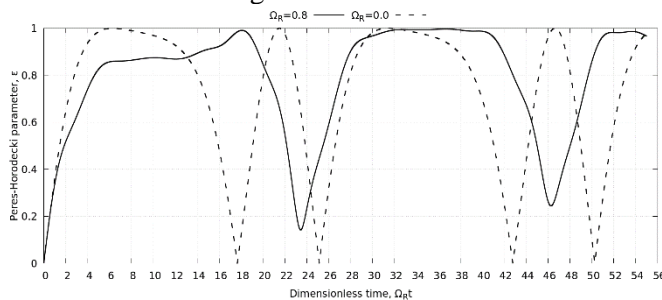
The entangled states of two identical qubits are super important in quantum informatics. They have lots of potential applications like quantum computers, cryptography, and quantum teleportation. But here's the catch: in real models, qubits can only stay highly entangled for a limited time. That's why there's been a ton of research, both theoretical and experimental, to understand and extend the duration of quantum entanglement for qubits over the last few decades.

In this case, we'll focus on a mathematical model where two qubits interact with an external electromagnetic field. The interaction between their dipole moments is described by a specific time-dependent function. Our goal is to study how the degree of entanglement depends on the parameters that characterize the qubit interaction and external electromagnetic field. By finding the most optimal values for these parameters, we can maximize the degree of entanglement for the qubits.

Hamiltonian of this model has the following form $\hat{H}_{full} = \hat{H}_Q + \hat{V}(\tau)$, $\hat{V}(\tau) = \hat{V}_{QF}(\tau) + \hat{V}_{QQ}(\tau)$, where \hat{H}_Q is hamiltonian of two non-interacting qubits; $\hat{V}_{QF}(\tau)$ is operator which describe interaction between qubits and one mode electromagnetic field; $\hat{V}_{QQ}(\tau)$ is operator which describe dipole-dipole interaction between qubits.

We describe the investigated system by statistical operator $\hat{\rho}(t)$ in the energy representation using the path integration [1]. To quantify the quantum entanglement of two qubits we use the Peres-Horodecki criterion [2,3] with the measure ε . The entanglement is maximal, when $\varepsilon = 1$, and minimal when $\varepsilon = 0$.

The proposed system of equations allows using numerical methods to construct graphs of dependence ε on system parameters and time. As an example of calculating the qubit entanglement parameter, let's consider the case when there is no external field and the qubits interact with each other. The graph of ε is represented by a dashed curve in Fig. 1.



The case is considered when the frequency of the external monochromatic field coincides with the transition frequency of the qubits. In the second numerical experiment, the qubits are affected by the field. The graph of the dependence of ε on the dimensionless time $\Omega_R t$ in Fig. 1 is represented by a solid curve. From the analysis of the graphs, it can be inferred that the external field stabilizes the entangled state of the qubits.

The proposed mathematical model allows investigating the qubit entanglement parameter ε under various system parameter changes within a wide range.

[1] A. Biryukov, V. Derbov and M. Shleenkov "Phase-difference-dependent laser-induced quantum entanglement in a pair of cubits," Proc. of SPIE 9448 (2015).

[2] A. Peres "Separability criterion for density matrices," Phys. Rev. Lett. 77, 1413–1415 (1996)

[3] M. Horodecki, P. Horodecki and R. Horodecki "Separability criterion for density matrices," Phys. Rev. A 232, 333–338 (1997).



P-P-1

Design features of optical splitters and their effect on output parameters

A.A. Krylov^{1,2,4}, I.D. Skuratov^{1,2,4}, V.V. Svetikov^{3,4}

1- JSC «Molecular Electronics Research Institute», Moscow, Russia

2- Moscow Institute of Physics and Technology, Dolgoprudny, Russia

3- Prokhorov General Physics Institute, RAS, Moscow, Russia

4- JSC «Zelenograd Nanotechnology Center», Moscow, Russia

Main author email address: krylov.aa@phystech.edu

In this work, we present a computational analysis of splitting ratio and insertion losses for four different designs of splitters. The designs of splitters were as follows: Y-branch splitter, MMI splitter, MMI-Y-branch hybrid splitter, and MMI-Y-branch hybrid splitter with optical leak reduction jumpers. The last splitter design is based on the MMI–Y-branch hybrid splitter with jumpers between branches in places of most prevalent optical leaks to preserve radiation in the structure (Fig. 1) [1]. This allows for a loss reduction in the splitter. Computational analysis proceeds as follows: topological parameters of the splitter, which include branch length, MMI width and length, and branch offset from center, are varied to build the dependence of output field power. Optimal topology is achieved when maximum field power is obtained. The example result of such a simulation for MMI width and branch starting offset selection of the optimal point could be seen in Figure 2. Based on the results of the computational analysis series, a comparison has been made between the four designs featured in the full work. In this comparison, the optimal design is selected and demonstrated.

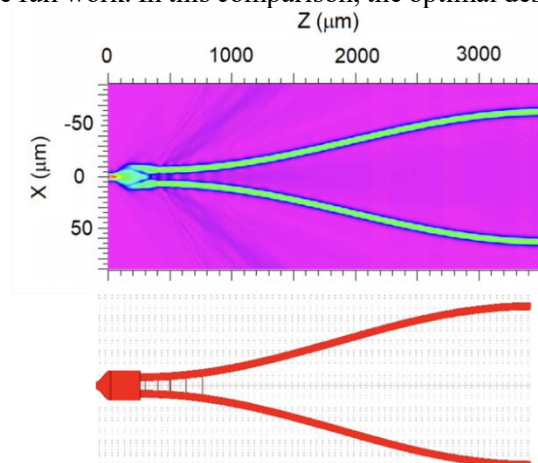


Figure 1. MMI - Y-branch hybrid splitter with optical jumpers view and field distribution

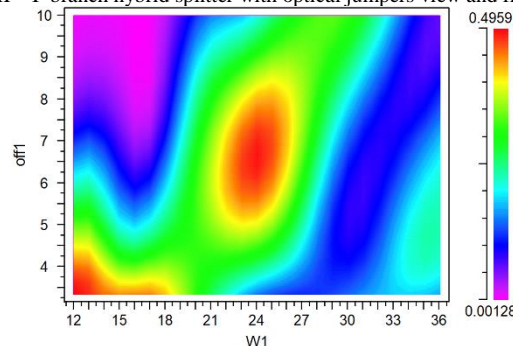


Figure 2. Result of the simulations series. Width of MMI and branch starting offset is variated and resulting field power from one brunch is obtained

[1] A.J Ticknor et al., Planar lightwave circuit optical splitter / mixer, U.S. Patent and Trademark Office, US 2018 / 0299617 A1 (2018)

[2] Y. Zhang, S. Yang, A.E.J. Lim, G.Q. Lo, C. Galland, T. Baehr-Jones, and M. Hochberg, A compact and low loss Y-junction for submicron silicon waveguide. Optics express, 21(1), pp.1310-1316, (2013)

[3] G. Y. Krasnikov, E.S. Gornev, I. V. Matushkin, General theory of technology and microelectronics: part 1. levels of technology, Electronnaya Technica, Seria 3: Microelectronika, 1(165), pp. 51-69, (2017).

Investigation of mode propagation in waveguide structures with chalcogenide glasses

A. E. Mitrofanova^{1,2,4}, I.D. Skuratov^{1,2}, V.V. Svetikov^{3,4}

1- JSC «Molecular Electronics Research Institute», Moscow, Russia

2- Moscow Institute of Physics and Technology, Dolgoprudny, Russia

3- Prokhorov General Physics Institute, RAS, Moscow, Russia

4- JSC «Zelenograd Nanotechnology Center», Moscow, Russia

mitrofanova.ae@phystech.edu

Currently, chalcogenide materials are widely used to create memory cells. Such devices are based on the principle of changing optical and electrical properties when the phase state of glass changes from amorphous to crystalline. The phase state is switched using heat from laser or electric pulses.

The research of Ge-Sb-Te (GST) glasses, which have a strong optical contrast [1] and a short phase state switching time (50 ms) [2], receives special attention. This opens up the option of using GST-225 (Ge₂Sb₂Te₅) thin films in optical switching devices. GST-225 has a high refractive index in both crystalline ($n=8.03$) and amorphous ($n=4.69$) phase states [3,4].

The possibility of creating a discrete phase shift using components that is based on GST-225 thin films was investigated in the work. Waveguide structures based on SOI were calculated.

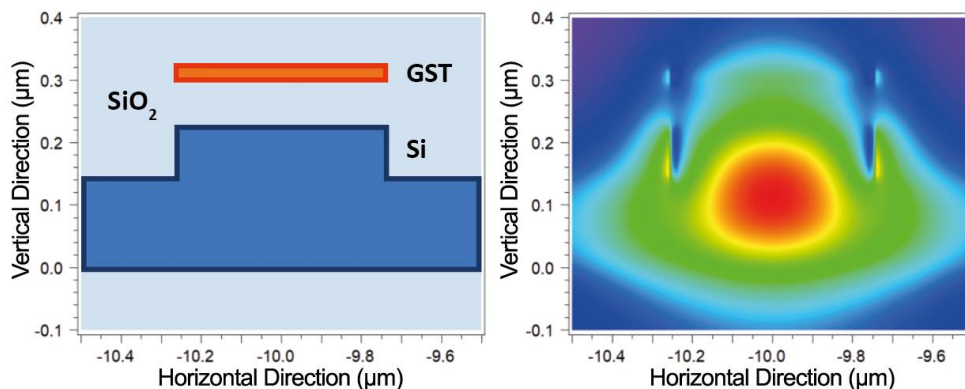


Figure 2. Waveguide geometry and field distribution in a waveguide

In the work presented computational analysis of the phase change of the waveguide mode and waveguide losses as variables of the phase state of the GST film and the geometric parameters of the structure: the thickness of the film (10-30 nm) and the thickness of the buffer layer (0-100 nm). Based on the results, an optimal model of a waveguide with a 75nm buffer layer and a 10nm GST film (Fig.1) is offered. A 5° phase shift on the length of a 1.94 micron GST segment is achieved, with losses of approximately 0.7 dB for a crystalline GST section and 0.1-0.2 dB for an amorphous GST section. Based on the results, a switch model based on the Mach-Zehnder interferometer has been constructed. The phase shift between signals passing in different arms must be 45 degrees. However, creating an optimal phase difference can be difficult because it requires a difference in the optical path between the two channels equal to $\lambda/8$. To make the correction, discrete sections of GST film were placed on both arms of the interferometer. By changing the phase state of the GST, it is possible to change the phase rotation by 1-15°, achieving the exact final phase shift of 45° required for the switch's operation.

[1] Guo P., Sarangan A. M., Agha I., A review of germanium-antimony-telluride phase change materials for non-volatile memories and optical modulators, Applied sciences. – 2019. – T. 9. – №. 3. – C. 530.

[2] Kozyukhin S. A. et al., Phase change memory materials and their applications //RUSSIAN CHEMICAL REVIEWS. – 2022. – T. 91. – №. 9.

[3] Bokarev V. P., Krasnikov G. Y., Estimation of the change in the physicochemical properties of Nanosized crystalline materials //Doklady Physical Chemistry. – SP MAIK Nauka/Interperiodica, 2008. – T. 420. – C. 96-99.

[4] Kim H. J. et al., PCM-net: a refractive index database of chalcogenide phase change materials for tunable nanophotonic device modelling //Journal of Physics: Photonics. – 2021. – T. 3. – №. 2. – C. 024008.



P-P-3

Investigation of volt-ampere characteristics of photosensitive structures based on porous silicon with WS₂ and MoS₂ quantum dots

D. Shishkina¹, **N. Poluektova**¹, **I. Shishkin**¹, **A. Rymzhina**¹, **N. Tripathi**¹

1- Samara National Research University, 34, Moskovskoye shosse, Samara, 443086, Russia

natapolivekt37@gmail.com

Currently, silicon-based solar cells are one of the most relevant types of alternative energy sources. The scope of their application is extensive: from the power supply of private homes or small enterprises on Earth to spacecraft in space [1, 2]. However, the efficiency of such elements, as a rule, does not exceed 30%, therefore, the task of increasing the efficiency of solar cells is relevant. There are many different methods to increase the efficiency of photosensitive structures, for example, applying coatings that reduce reflection, creating various nanostructured layers of silicon, carbon nanotubes, quantum dots from different materials on the surface of plates, etc. [3-5]. In addition, it is possible to increase the efficiency of solar cells by combining the above methods, for example, by creating multilayer photosensitive structures with a porous layer of quantum dots.

In this work, samples of photosensitive structures were made as follows. An n-type diffusant consisting of ethyl alcohol, tetraethoxysilane, nitric and orthophosphoric acids was applied to pre-purified silicon plates of the p-type. After drying, the plates were placed in a diffusion furnace for 40 minutes at a temperature of 1000°C to create a p – n junction. Then, after removing the oxide in hydrofluoric acid, a porous layer was created using liquid electrochemical etching for 5 and 10 minutes and a current density of $j = 10 \text{ mA/cm}^2$. Next, metallization was applied by thermal evaporation in vacuum. The final operation was the application of quantum dots. To do this, powders of tungsten and molybdenum disulfides weighing 50 mg were mixed with isopropyl alcohol, 50 ml in a glass container. Then these glass vessels were placed in an ultrasound bath for 4 hours.

The current-voltage characteristics were removed from the obtained samples before and after the application of quantum dots. Analysis of the data obtained showed that samples with an etching time of 5 minutes were practically not reacted to the introduction of quantum dots into the pores. While the data obtained from samples with an etching time of 10 minutes showed an increase in the saturation current. This can be explained by the deeper occurrence of quantum dots in the pores. However, quantum dots did not have a significant effect on dark currents.

[1] L. P. Andrianova, M. F. Tuktarov, A. E. Usmanova, V. G. Baynazarov, Assessment of the energy potential of a rooftop solar microelectric power plant with a photovoltaic module vst 10-12 for agricultural consumers, *Izvestiya Orenburg State Agrarian University*, vol. 4 (78), pp. 151-153, (2019).

[2] Z. A. Kazantsev, A.M. Eroshenko, L. A. Babkina, A.V. Lopatin, *Spacecraft and technologies, Spacecraft and Technologies*, vol. 5(3), pp. 121-136, (2021).

[3] N. V. Latukhina, D. A. Lizunkova, I. A. Shishkin, A. S. Erofeev, Photocurrent in structures with a layer of porous silicon, *Science of the present and the Future*, vol. 3, pp. 19-22, (2019).

[4] I. S. Shulgina, solar cells with graphene and carbon nanotubes on silicon, *Actual scientific research*, pp. 86-90, (2022).

[5] A.V. Wojciechowski, A. P. Kohanenko, K. A. Lozovoy, V. V. Dirko, R. Dukhan, Parameters of photodetectors and solar cells with Ge/Si quantum dots, *Proceedings of the XI International Conference "Fundamental Problems of Optics-2019"*, pp. 296-297, (2019).